10 - 13
MARCH
2019

7th INTERNATIONAL CONFERENCE
ON RENEWABLE FUELS
COMBUSTION AND FIRE

VII. INTERNATIONAL RENEWABLE FUELS COMBUSTION AND FIRE CONFERENCE IN ENGINEERING (FCE19)

BOOKS OF CONGRESS

ANTALYA, 2019

İÇİNDEKİLER / CONTENTS

Paper 1 **Bildiri 1**

OXY-FUEL COMBUSTION OF HYDROGEN CONTAINING LOW-CALORIFIC VALUE SYNGASES: AN EXPERIMENTAL AND NUMERICAL STUDY

Mustafa ILBAS[*], Abdulkadir BEKTAS[**], Serhat KARYEYEN[*]

[*] Gazi University, Technology Faculty, Department of Energy Systems Engineering, 06500, Teknikokullar, Ankara, Turkey

[**] Gazi University, Graduate School of Natural and Applied Science, 06500, Teknikokullar, Ankara, Turkey

Abstract

This study discusses the oxy-fuel combustion of low-calorific value syngases derived from Turkish coal. The effect of burner characteristics on combustion behaviours of the low-calorific value syngases due to high flame temperature arising from combustion with pure oxygen has also been investigated in the present work. This problem has been overcome by modifying the existing burner, which means that the oxidizer inlet section of the burner has been reduced approximately four times to be more suitable for pure oxygen. The modification enables to prevent overheating of the burner wall and to provide more stable flame for combusting of the low-calorific value syngases under oxy-fuel combustion conditions. In further modellings, it has been revealed that the predicted temperature distributions of the low-calorific value syngases have been more uniform due to increment of velocities of these gases.

Keywords: Combustion, Syngas, Burner, Modification, CFD

1. INTRODUCTION

It is very important to increase usage of local and/or renewable energy resources such as coal and biomass for energy supply security. Coal, which has the most reserves over the world and is not existed in a particular region, is the most used energy source and will remain strategic in the forthcoming years. Nevertheless, direct usage of coals brings about some challenges such as air pollution and higher emissions of greenhouse gas which impact upon on health (Habib et al. 2015). Consequently, it is more convenient to acquire gaseous fuels out of these resources and to use these fuels as alternative fuels.

Syngases are defined as by-product/products resulting from the coking of coal or directly obtained by gasification of coal and biomass. It may be more convenient to use as alternative fuels instead of natural gas (Huynh and S. Kong. 2012). However, the combustion performances of low-calorific value syngases are not suitable in any furnaces, combustors and etc. if they are combusted by air owing to their calorific values. In other words, air-combustion performances of these fuels are lower than that of natural gas. In view all these occasions, it is more reasonable to burn syngas with pure oxygen, and needs to research combustion and emission parameters of them under oxy-fuel combustion conditions.

It is known that there are some studies directly related to combustion of air-syngas, hydrogen and blending fuels (Ilbas and Karyeyen 2014; Ilbas and Karyeyen 2015; Yilmaz et al. 2013; Yilmaz and Ilbas 2008; Ilbas and Yilmaz 2012; Ilbas and Karyeyen 2017). It is, however, noted that studies related to combustion of syngases under oxy-fuel combustion conditions are still limited in the literature. For these reasons, the combustion performances and emission characteristics of the low-calorific value syngases have been investigated not only experimental but also numerical in the present study. Even so, overheating of the burner wall (the flame holder) has been determined during the experiments. This situation is not suitable for the burner material when any kind of fuelis combusted in any combustion process. Because of that, a modification meaning that has been reduced the oxidizer stream section of the burner has been implemented to provide movement of the flame into the combustor within the present study. Therefore, the modification and then generation of a burner has been performed and its effect has been studied numerically as well as the combustionbehaviours of the low-calorific value syngases have been investigated in the present study.

2. CFD MODELLING

3D CFD modellings have been performed by using the existing low-calorific value syngas burner in order to model combustion of low-calorific value syngases under oxy-fuel combustion conditions in the present study. Then, the burner has been modified and a new burner has been generated to provide more stable flame and uniform temperature distributions inside the combustor for oxy-fuel combustion of low calorific value syngases. This modification means that air stream zone has been reduced approximately four times to be more suitable for pure oxygen as volumetric flow rate of oxygen is lower than that of air under oxy-fuel combustion

conditions. The existing burner is shown in Figure 1(Karyeyen and Ilbas 2017).Air and oxygen stream regions and sections of the existing (the unmodified) and the modified burners are also given in Figure 2 and Figure 3, respectively.

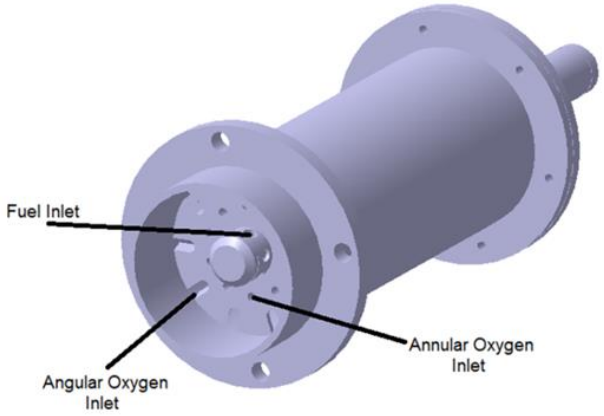

Figure 1. The existing low-calorific value syngas burner

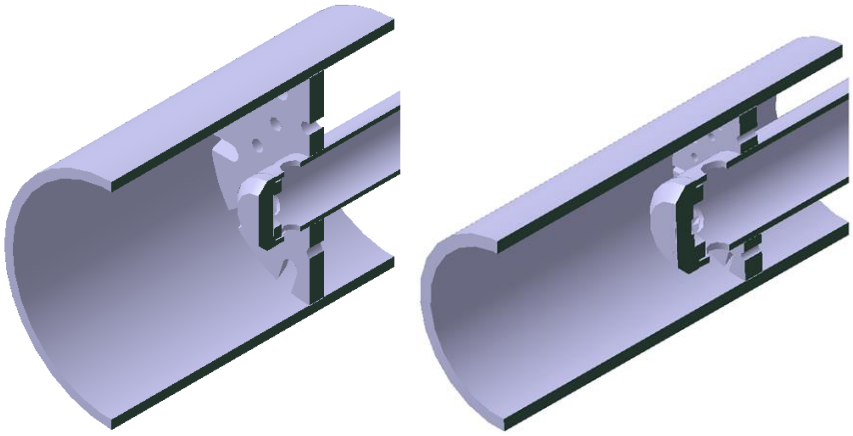

(a) (b)

Figure 2. Air (a) and oxygen (b) stream regions of the existing and the modified burners

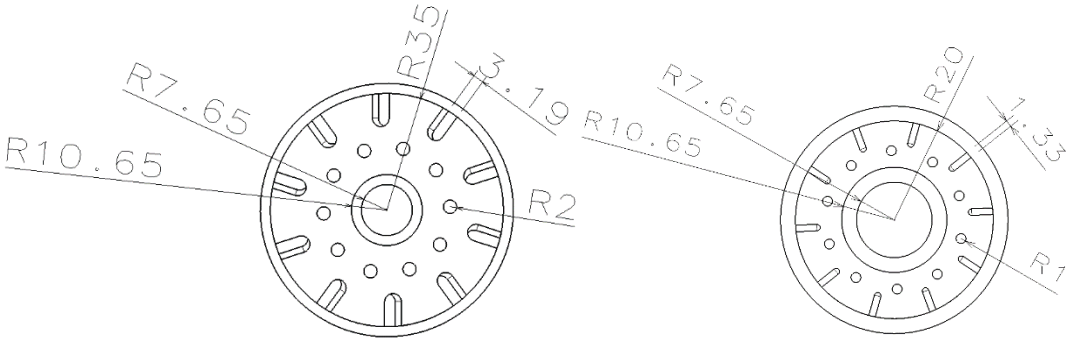

(a) (b)

Figure 3. Air (a) and oxygen (b) stream sections of the existing and the modified burners

Numerical simulation of the turbulence reacting flow in the existing and the modified burners and the combustor were carried out using Ansys Fluent code. Fluent uses the finite volume method in order to solve the basic equations. It enables usage of different physical models such as inviscid or viscous, laminar, turbulent and the other flow characteristics (Yilmaz 2013). The Simple scheme was used for the pressure–velocity coupling. For the spatial discretization, Second order upwind scheme was used for the convection terms in all transport equations. The convergence absolute criterias for all of the residuals parameters were limitedas 10^{-4} except energy and P-1 equations.

3. EXPERIMENTAL SETUP

The existing combustion system is schematically given in Figure 4. It includes low-calorific value syngas and the oxygen lines by which the fuel and the oxidizer are supplied into the combustor. The combustion chamber having five measuring ports located on the combustor wall length and diameter are of 100 cm and 40 cm, respectively. They enable measurement of temperatures and emissions of the low-calorific value syngases on different axial and radial positions inside the combustor. In order to determine temperature values of the low-calorific value syngases throughout the combustion chamber,ceramic coated R-type thermocouples capable of withstanding high temperatures up to 1700ºC have beenused in the experimental studies. The diameters of thermocouples are of 5 mm.

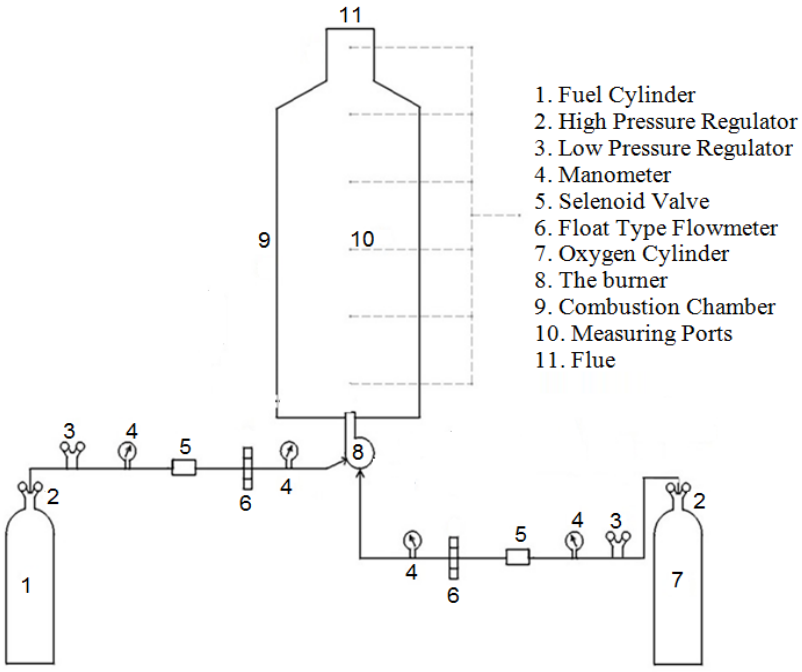

Figure 4. Layout of the combustion system

4. RESULTS AND DISCUSSION

Predicted results require to be validated in numerical studies. In this way, further results including temperature and emission distributions of the low-calorific value syngases for the modified burner are applicable. For this reason, the predicted temperature results of the low-calorific value syngaseshave been compared with the experimental results and are presented in Figure 5 and Figure 6 as axial distributions inside the combustor.

Figure 5 also involves the effect of the turbulence models in combusting of the generator gas. As can be seen in Figure 6, the predicted axial temperature profiles are in good agreement with the measured experimental data for all turbulence models. However, in particular, after the middle of the combustor, it may be said that there is more consistency between the measured data and the predicted temperature profiles for combustion conditions in which the k-Ɛ standard turbulence model has been used. Therefore, the k-Ɛ standard turbulence model has been selected as turbulence model for further modellings in the present study.

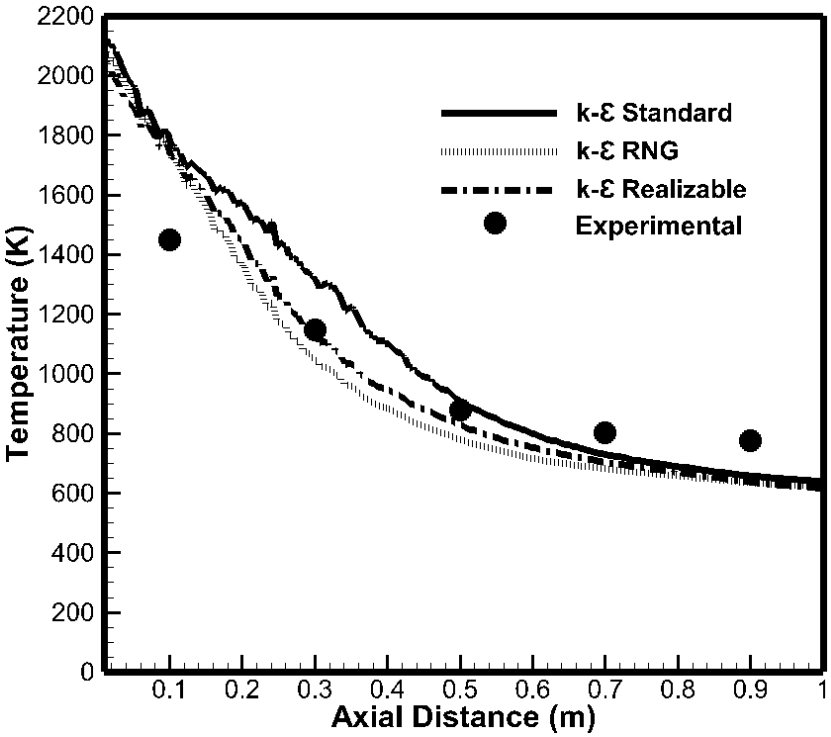

Figure 5. The effect of the turbulence models for generator gas

In this section of the present study, the temperature modelling results of generator and blast-furnace gases for the modified and the unmodified oxy-fuel combustion conditions are

presented. The present and the subsequent sections also cover comparison of the results regarding the combustion behaviours of generator and blast-furnace gases under air-fuel and oxy-fuel combustion conditions. The predicted axial temperature distributions of generator and blast-furnace gases for all combustion conditions are shown in Figure 6.

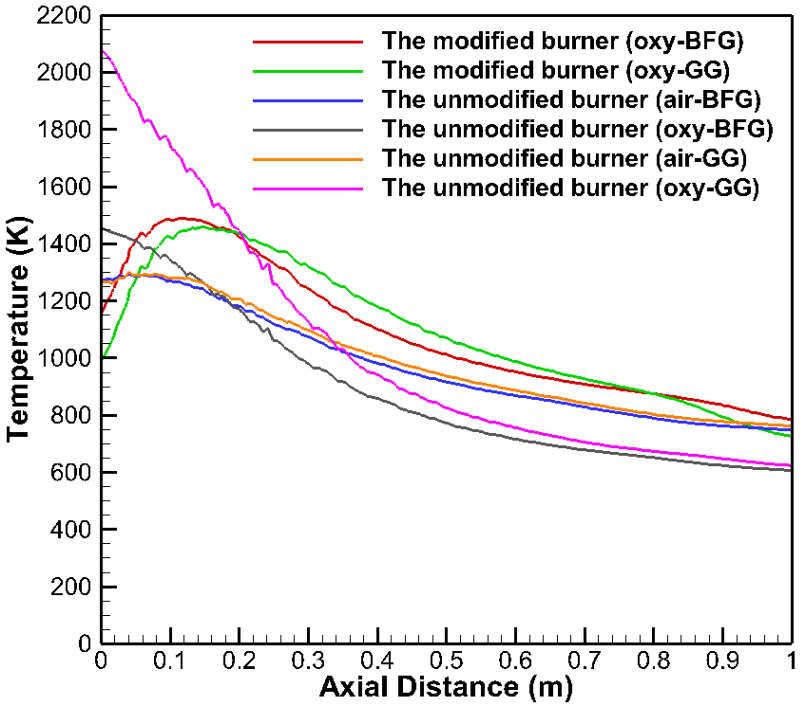

Figure 6. Axial temperature distributions of the low-calorific value syngases

When the combustion performances of these gases are firstly compared each other, it can be concluded that combustion performance of generator gas is higher than that of blast-furnace gas due to difference between their low calorific values. Because, generator gas includes higher amounts of hydrogen while blast-furnace gas contains higher amounts of nitrogen and lower amounts of hydrogen. When these gases are combusted by the existing burner,which means the unmodified burner, under oxy-fuel combustion conditions, it has been seen that the flame temperatures of the low-calorific value syngases increase rapidly in the flame region as oxidizer does not include nitrogen which prevents increase of temperature levels. Unless there is a limitation related to materials of the burner and the combustor due to overheating, this result is a rather suitable conclusion in terms of combustion performances of the low-calorific value syngases.

5. CONCLUSIONS

Combustion characteristics of the low-calorific value syngases have been investigated for the unmodified and the modified burners under oxy-fuel combustion the present study. 3D numerical modellings have been performed by a CFD code. Modelling results have been compared with the measured data obtained from the experimental part of this study firstly. This comparison has been made for the unmodified (the existing) burner under oxy-fuel combustion conditions. It can be firstly concluded that the predicted temperature distributions of the low-calorific value syngases are satisfactorily in good agreement with the measured data throughout the combustor. It has been consequently concluded that this overheating bring about the modification which means that the oxidizer stream of the burner has been reduced to be more appropriate to burn the low-calorific value syngases under oxy-fuel combustion conditions. Therefore, the oxidizer stream of the burner has been modified in order to prevent the overheating of the burner wall, to obtain more stable flame and its effect has been numerically investigated on the combustion characteristics of the low-calorific value syngases within the present study. In addition, the predicted oxy-fuel combustion results have been compared with the predicted air-fuel combustion results.

According to the modelling results, for the unmodified burner, it has been demonstrated that the flame temperatures of the low-calorific value syngases increase rapidly under oxy-fuel combustion conditions in the flame regions. Because, their flames move to the upstream of the burner and it leads to that their flame temperatures go up. The predicted axial velocity values support this result. For the modified burner combustion conditions, it has been revealed that the flames of the low-calorific value syngases move into the combustor uniformly and as a result of this, the overheating problem has been overcome. Therefore, it can be concluded that the modification facilitates uniform temperature distribution inside the combustor and enables improvement of their combustion performances.

In conclusion, the low calorific value syngases can be used as alternative fuels in furnaces, combustors, gas turbines and etc. under oxy-fuel combustion conditions. However, it is noted that the burner used in air-fuel combustion process requires a modification which means that the oxidizer stream section of the burner adapts to prevent overheating of the burner wall and to obtain more stable flame.

REFERENCES

Habib, M. A., Nemitallah, M. A., Ahmed,P.,Sharqawy, M. H.,Badr, H. M.,Muhammad, I. andM. Yaqub. 2015. Experimental analysis of oxygen-methane combustion inside a gas turbine reactor under various operating conditions. *Energy* 86:105-114.https://doi.org/10.1016/j.energy.2015.03.120.

Huynh, C. V. and S.Kong. 2012. Combustion and NO_X emissions of biomass-derived syngas under various gasification conditions utilizing oxygen-enriched-air and steam. *Fuel* 107:455-464.https://doi.org/10.1016/j.fuel.2012.12.016.

Ilbas, M. 1997. Studies of ultra low NO_X burner. PhD diss., University of Wales, College of Cardiff, UK.

Ilbas, M. and I. Yılmaz. 2012. Experimental analysis of the effects of hydrogen addition on methane combustion. *International Journal of Energy Research* 36(5):643-647. https://doi.org/10.1002/er.1822.

Ilbas, M. and S. Karyeyen. 2014. Modelling of combustion performances and emission characteristics of coal gases in a model gas turbine combustor. *International Journal of Energy Research* 38(9):1171-1180. https://doi.org/10.1002/er.3135.

Ilbas, M. and S. Karyeyen. 2015. A numerical study on combustion behaviours of hydrogen-enriched low calorific value coal gases. *International Journal of Hydrogen Energy* 40(44):15218-15226. https://doi.org/10.1016/j.ijhydene.2015.04.141.

Yılmaz, I. 2013. Effect of swirl number on combustion characteristics in a natural gas diffusion flame,*Journal of Energy Resources Technology* 135(4):1-8.https://doi.org/10.1115/1.4024222.

Paper 2 **Bildiri 2**

THE EFFECT OF SWIRL NUMBER ON COMBUSTION CHARACTERISTICS OF BIOGAS FUEL IN A COMBUSTOR

Mustafa İLBAŞ[*], Murat ŞAHİN[**],Serhat KARYEYEN[*]
[*]Gazi University, Faculty of Technology, Department of Energy Systems Engineering, Ankara
[**]Ahi Evran University, Faculty of Engineering, Department of Mechanical Engineering, Kırşehir

ABSTRACT

This study deals with the effect of the swirl number (0–0.8) on combustion characteristics of a biogas in a combustor. The present study is a numerical study that has been performed by using a commercial CFD (computational fluid dynamics) code. Selection of coherent combustion model is crucial for more accurate prediction in the reactive modelling. Because of this, the PDF/Mixture Fraction combustion model has been chosed. The other mathematical models applied in this study are k−Ɛ standard turbulence model of turbulent flow and P−1 radiation model. Methane as baseline fuel has been modelled to confirm the predictions. It is seen that predictions are in good agreement with the existing experimental data. In that case, biogas has been modelled to find out the effect of the swirl number on combustion characteristics of this fuel with three different swirl numbers from 0 to 0.8 at interval of 0.4. It is finalised that the flame temperatures are highly affected depending on changes of the swirl number. For why, tangential velocity of the air stream changes the temperature distributions in the combustor considerably. It is also displayed that changes in swirl number lead to position of the high NO_X regions.

Keywords: Biogas, Swirl number, Combustion, Modelling

1. INTRODUCTION

The importance of sustainable clean energy resources is increasing day by day. Energy is a key factor to maintain life and a significant part of the energy is produced by fossil fuels in the world. But, there are two problems during usage of fossil fuels. There are limitations related to the usage of fossil fuels due to pollutant effects and fossil fuels are running out all over the world. Scientists try to find out new resources to solve these problems. Biogas fuels are very attractive resources for scientists due to cleaner fuels.

2. MODELLING

2D CFD modelling has been performed by using the newly generated diffusion flame of burner in order to model the effect of the swirly number on combustion characteristics of the biogas in the present study. An axisymmetric natural gas-fired combustor, which is called as the Harwell furnace, has been chose as combustor in this study. This combustor is reported by Wilkes et al. and dimensions of the combustor have been exactly selected to be the same to validate our predictions before starting modelling. Radiuses of the fuel and air jets are from 0 to 6 mm and from 16.5 mm to 27.5 mm, respectively. Fig. 1 shows the
Physical domains of the combustor.

Grid and k-epsilon are showed that in the the Fig.3 and Fig.4, respectively. The combustor has been selected as an axisymmetric combustor. Because of that, modelling have been conducted in the half of the combustor due to the symmetry. The symmetry enables simpler grid generation and shorter computation time. Some assumptions and selected models related to modelling are as follows:

1) The flow is noted as steady state
2) Inlet temperatures of fuel and air streams are fixed at 293 K,
3) Heat inputs and equivalence ratios for all hydrogen containing fuels are considered as 60 kW and 0.83,
4) The PDF/Mixture Fraction model and P-1 radiation models have been selected as combustion and radiation models, respectively.

5) Conditions reported by Wilkes et al. are taken into account to validate the modellings in methane combustion case.

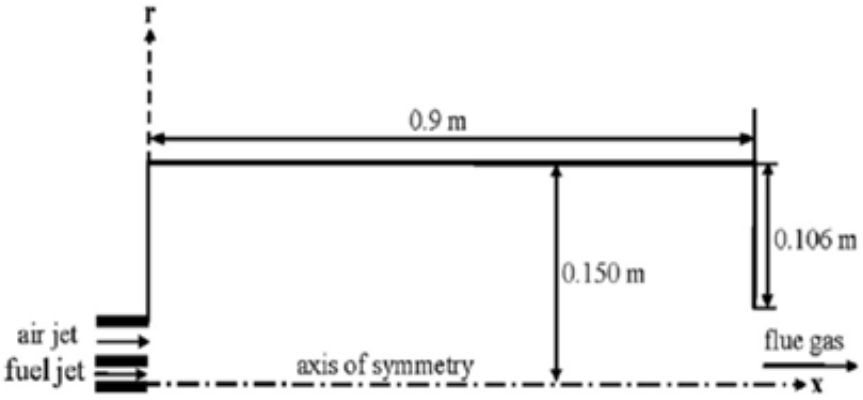

Figure 1. The physical domain of the combustor

The mathematical modelling described for the gas mixture combustion is based on the steady-state condition, 2D continuity, momentum, energy and speciese equations. It is showed that fuel and air intake in Fig.2.

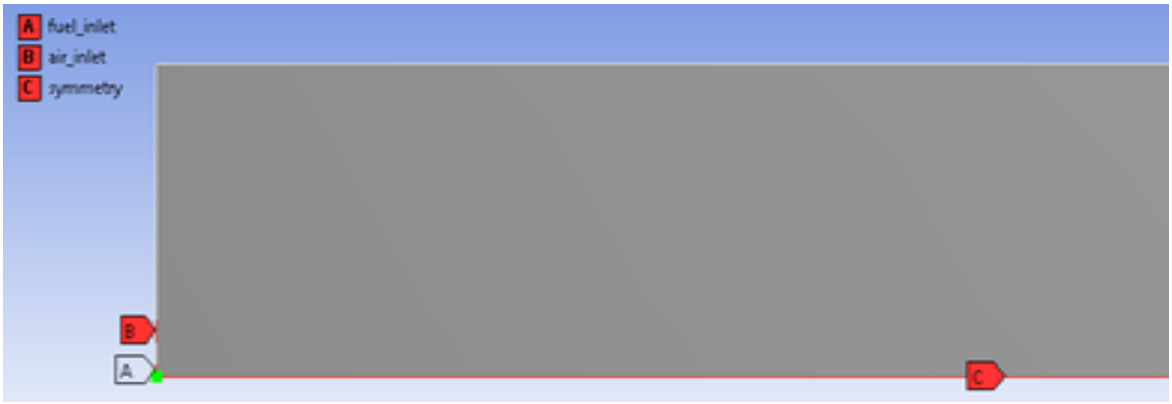

Figure 2. Display of fuel and air intake

The Mixture Fraction/PDF Model was used as combustion model in the present study (Ilbas,1997). The P-1 model can be easily applied to complicated geometries with curvilinear coordinates (Ilbas, 2005). Because of that, P-1 radiation model was used for a more accurate prediction of the biogas combustion in this study.

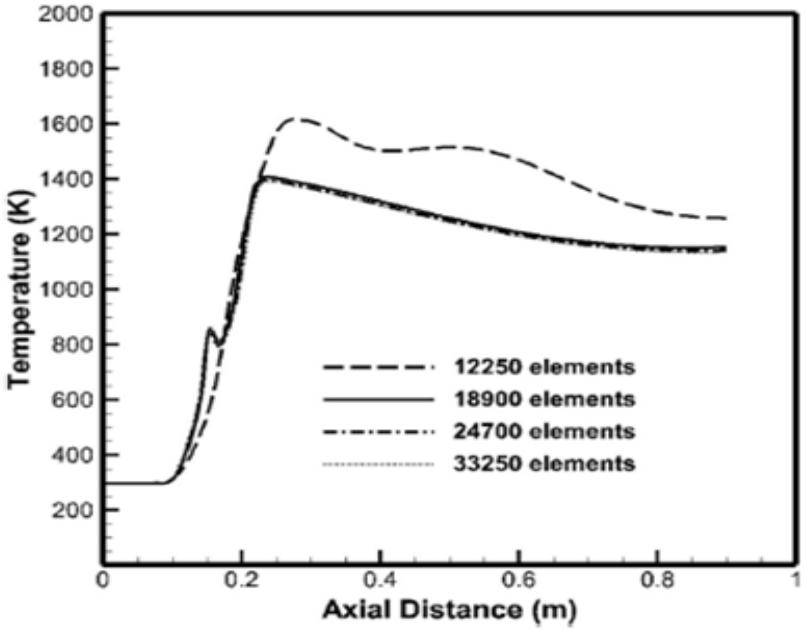

Figure 3. Grid independency solutions

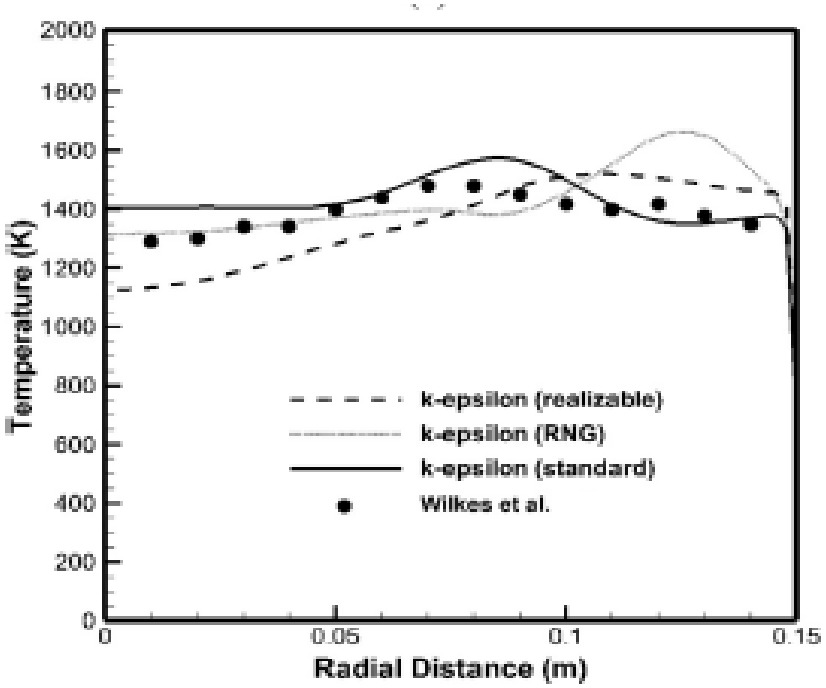

Figure 4. Comparison of temperature is tributions between the predictions and measurements

Components of the biogas consumed in this study are also presented in this section as can be seen in Table 1.

Table 1. The main properties of the biogas (by volume)

	Biogas (%)
CH_4	*55*
CO_2	*43,1*
N_2	*1,53*
H_2S	*10 ppm*
O_2	*0,3*
Calorific value (kcal/m^3)	*4422,06*

3. RESULTS AND DISCUSSION

The effect of the swirl number on combustion characteristics of biogas fuels have been numerically investigated in a Harwell furnace in this study. It is concluded that the flame temperatures are highly affected depending on changes of the swirl number. The range of the swirl numbers is from 0 to 0.8. Fig. 5 and Fig.6 give the effect of the swirl number on temperature levels of biogas flame at axial and radial directions. Under the effect of swirl number of the combustion chamber it is often observed along with an increase in combustion temperature.

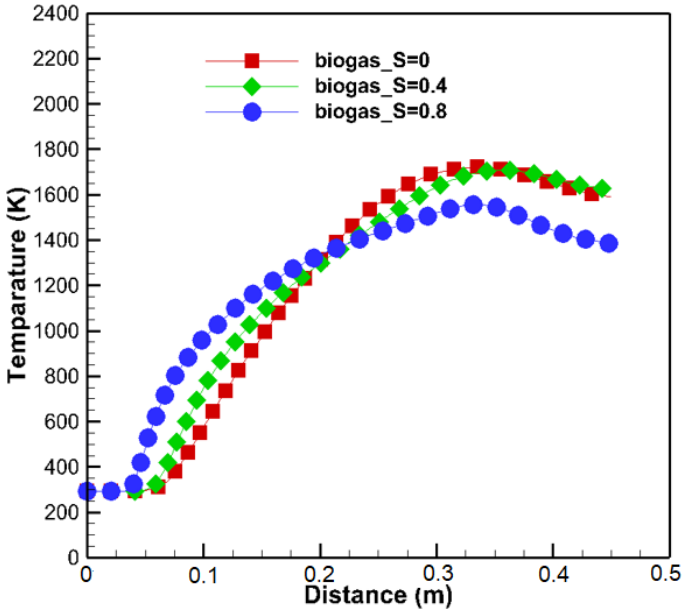

Figure 5. Axial temperature distributions

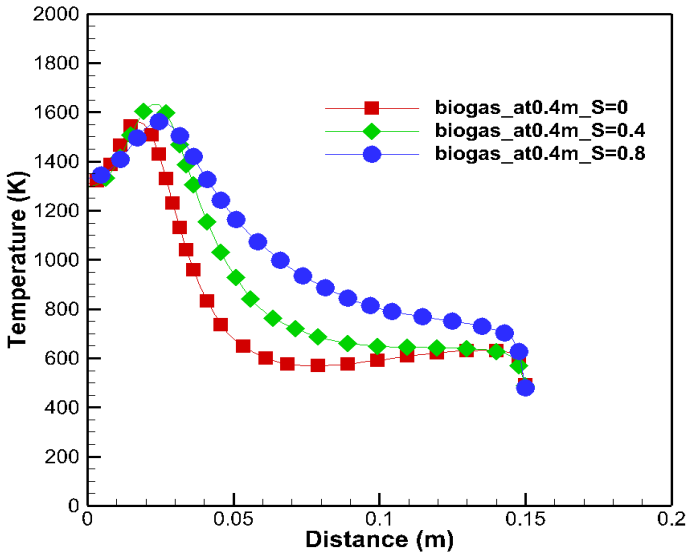

Figure 6. Radial temperature distributions at x=0.4 m

It is also showed that changes in swirl number lead to position of the NOx emissions. NOx values increase generally as the swirl number is changed from 0 to 0.8. Tangential velocity of the air stream changes the temperature distributions in the combustor considerably. This change is shown in Fig.7.

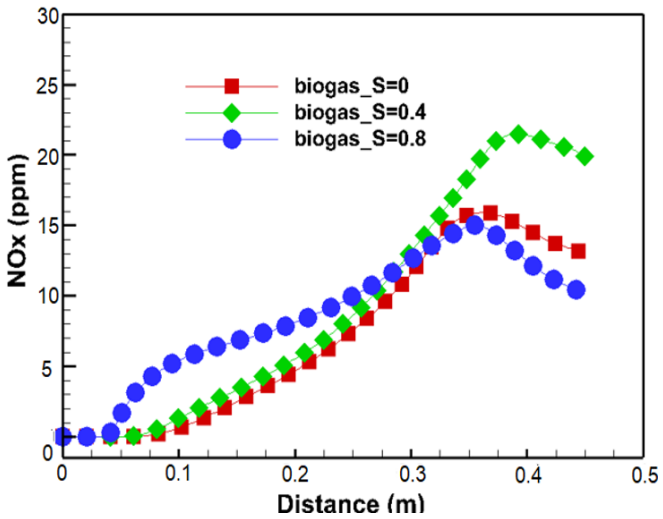

Figure 7. The effect of the swirl number on NOx gradients of biogas

4. CONCLUSIONS

The effect of swirl number on combustion characteristics of biogas fuel has been numerically investigated. Three different swirl numbers from 0 to 0.8 at interval of 0.4 have been used for modelling.

It is resulted that the flame temperatures are highly affected depending on changes of the swirl number. Because, tangential velocity of the air stream changes the temperature distributions in the combustor considerably. It is also showed that changes in swirl number lead to position of the NO_X emissions.

Acknowledgements

The authors thank to Gazi University for the support of this study.

REFERENCES

M. Ilbas, M. Sahin, S. Karyeyen, 3D numerical modelling of turbulent biogas combustion in a newly generated 10 KW burner, J. Energy Institute, 91 (2018) 87-99.

M. Ilbas, Studies of ultra low NO_X burner. PhD Thesis: University of Wales, College of Cardiff, UK, 1997.

M. Ilbas, The effect of thermal radiation and radiation models on hydrogen–hydrocarbon combustion modelling, Int. J. Hydrogen Energy 30 (2005) 1113-1126.

P. R. Bhoi and S. A. Channiwala, Emission characteristics and axial flame temperature distribution of producer gas fired premixed burner, *Biomass and Bioenergy*,Vol: 33, pp. 469-477, 2009.

S. E. Hosseini, G. Bagheri, M. A. Wahid, Numerical investigation of biogas flameless combustion, *Energy Conversion and Management*, Vol: 81, pp. 41-50, 2014.
Thermal Engineering, Vol: 66, pp. 181-190, 2014.

Wilkes N.S., Guilbert P.W., Shepherd C.M., Simeox S. The application of Harwell-Flow 3D to combustion models. Atomic Energy Authority Report, Harwell, UK, Paper No. AERE-R13508.

Paper 3 **Bildiri 3**

LARGE EDDY SIMULATION OF FLOW AROUND ENGINE-LIKE GEOMETRY

Murat ÖZKARA*, M. Zafer Gül

ABSTRACT

Nowadays, studies in the field of renewable energy cause pressure on the development of internal combustion engines due to increased fuel consumption and emission problems. Hence, in order to develop more efficient and environmental engine, the importance of combustion chamber design more and more increases. For this purpose, the precision of the heat transfer and flow calculations by using CFD software in the cylinder wall during the modeling phase of the combustion chamber has great importance. In this study, the accuracy of parameters such as in-cylinder flow and wall heat transfer in the design phase was compared with the results of Large Eddy Simulation by using Engine Like geometry. In this regard, the ways to get more accurate and effective results in the development of internal combustion engines together with the turbulence models that require less computational cost in the design phase were investigated. According to the obtained results, the variables data on the selected lines for comparison shows that the SST k-W and the Omega Based RSM turbulence models are more accurate.

Keywords: CFD, Large Eddy Simulation, Flow-Wall Interaction, Turbulence Modelling

* Corresponding Author

1. INTRODUCTION

Today, due to increased fuel consumption, high carbon emission, and emission problems, studies in the field of renewable energy cause pressure on the development of internal combustion engines. Therefore, in order to achieve more efficient and environmental engine, the importance of combustion chamber design gradually increases. To that end, the accuracy of the heat transfer and flow calculations by CFD software in the cylinder wall during the modeling phase of the combustion chamber has great importance. In this study, the precision of parameters such as in-cylinder flow and wall heat transfer in the design phase was compared with the results of Large Eddy Simulation by using Engine Like geometry. In this regard, the ways to get more accurate and effective results in the development of internal combustion engines together with the turbulence models that require a less computational cost in the design phase were investigated. Hence, SST **k - ω**, RNG **k - ε**, v2-f and omega based Reynolds stress turbulence models were used with the engine like geometry. As for that obtained results, the variables data on the selected lines for comparison shows that the SST k-W and the Omega Based RSM turbulence models are more precise. Schmitt[1] performed Direct Numerical Solution which solves all viscous stresses in finite volume over engine like geometry in his doctoral thesis. Buhl, Dietzsch et al.[2] et.al investigated a methodical comparative study of selected and well-structured scale-resolving turbulence models with regard to an IC engine flow focusing especially on the intake stroke. Giannakopoulos, Frouzakis et al.[3] et.al carried out incompressible flow solution over intake port geometry by using Direct Numerical Solution. Schmitt, Frouzakis et.al.[4] investigated evolution of the velocity and thermal boundary layers over in-cylinder flow by using Direct Numerical Solution. Schmitt, Frouzakis et.al.[5] performed Direct Numerical Solution for purpose of solving local wall heat flux and their study shows that accuracy of solution is strongly depending on wall distance. Plengsaard and Rutland[6] performed improved engine wall models for large eddy simulation by using the classical Werner-Wengle (WW) wall shear stress model. Schmitt, Frouzakis et.al.[7] investigated the effect of compression over flow and temperature variables by using Direct Numerical Simulation.

2. ENGINE LIKE GEOMETRY

Unlike other studies in this geometry, the valve is modeled as inward. In this way, the differences in the interaction of the flow with the wall are intended to be more comprehensible. Geometry was created by Ansys Design Modeller with following design parameter which shows in figure 1.

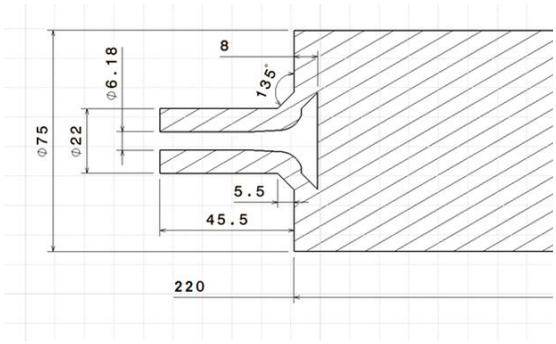

Figure 1. Geometrical parameters of Engine Valve flow computational domain. (Unit is mm)

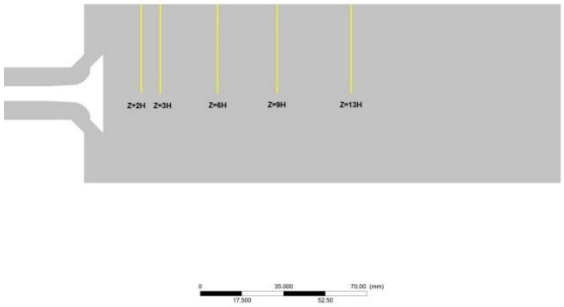

Figure 2. Sections of Probe location over z direction.

3. NUMERICAL MODELS AND BOUNDARY CONDITIONS

Segregated pressure based solver was preferred in this simulation. Velocity Inlet Boundary Condition specified with initial Static Pressure (1atm), Temperature (288.15K) and Velocity (6m/s) for inlet boundary condition. Pressure Outlet boundary condition specified with the ambient condition which requires static pressure and temperature for exit boundary. Incompressible Ideal Gas was selected as working fluid substance. Sutherland Law was applied for variable viscosity with Temperature.

Dynamic Smagorinsky model was preferred in Large Eddy Simulation. Simple Algorithm was used for solving pressure-velocity coupling. Node-

based green gauss theorem was chosen in order to reduce numerical diffusion error. The PRESTO! algorithm was preferred pressure discretization in order to capture pressure fluctuations properly. Bounded Central differencing schema was applied for momentum discretion. Third Order (MUSC) schema was preferred for energy discretization in order to solve accurately. Time step was chosen as 0.05sec with 200 time iteration which total flow time 10sec. Simulation was compleated about one week with Intel Xeon E3-1535M processor. Results of simulation were averaged statically at each time step.

3.1.Computational Domain

Computational domain was created by Ansys Meshing and it contains approximately 4.3 Milion nodes. Hexahedral mesh type was preferred due to it is capable to generate lower mesh count than tetra mesh and it is computational accuracy. Near-wall was modeled as y+<16 at the all face flow boundary as shown in figure 2.

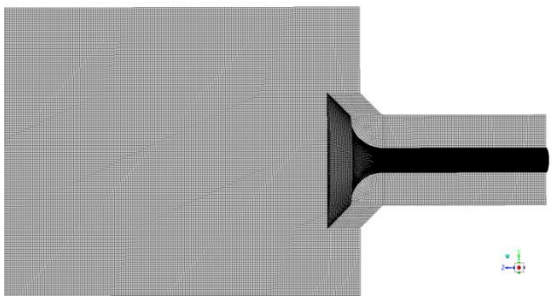

Figure 3. Mesh view of Engine Valve Computational Domain.

3.2.Mathematical Formulas

This section describes the general formulation of Ansys Fluent[8]. For solving the steady state RANS Equation, the general form of continuity, momentum and total energy equations are described in Equation 1 through Equation 4, and Equation 5, respectively.

Continuity Equation:

$$\frac{\partial \rho}{\partial t} + \nabla \cdot (\rho U) = 0 \quad (1)$$

Momentum Equation:

$$\frac{\partial (\rho U)}{\partial t} + \nabla \cdot (\rho U \otimes U) = -\nabla p + \nabla \cdot \tau + S_M \quad (2)$$

$$\tau = \mu \left(\nabla U + (\nabla U)^T - \frac{2}{3} \delta \nabla \cdot U \right) \quad (3)$$

Total Energy Equation:

$$\frac{\partial (\rho h_{tot})}{\partial t} - \frac{\partial p}{\partial t} + \nabla \cdot (\rho U h_{tot}) = \nabla \cdot (\lambda \nabla T) + \nabla \cdot (U \cdot \tau) + U \cdot S_M + S_E \quad (4)$$

$$h_{tot} = h + \frac{1}{2} U^2 \quad (5)$$

Where the relationship between the stress tensor, τ, and strain rate exists is defined in Equation (3). Where total enthalpy, h_{tot}, with respect to the static enthalpy $h(T, p)$ exists is defined in Equation (6). The viscous work term, $\nabla \cdot (U \cdot \tau)$, represents the work generated by viscous stresses in total energy equation.

Where the relationship between the stress tensor, τ, and strain rate exists is defined in Equation (3). Where total enthalpy, h_{tot}, with respect to the static enthalpy $h(T, p)$ exists is defined in Equation (6). The viscous work term, $\nabla \cdot (U \cdot \tau)$, represents the work generated by viscous stresses in total energy equation.

3.2.1. k - ε Turbulence Model

The turbulence kinetic energy, k, is the variance of the fluctuations in velocity and its dimensions are in the form of $L^2\ T^{-2}$ (for example, m2/s2). The symbol "ε" represents the turbulence eddy dissipation, which is the rate at which the velocity fluctuations dissipate, and its dimensions are in the form of k per unit time ($L^2\ T^{-3}$) (for example, m2/s3). The k-epsilon model introduces two variables into the system of equations and the continuity equation consequently assumes the form of following Equation (7).

$$\frac{\partial \rho}{\partial t} + \frac{\partial}{\partial x_j} \cdot \left(\rho U_j \right) = 0 \quad (7)$$

The momentum equation becomes in Equation (8).

$$\frac{\partial (\rho U_i)}{\partial t} + \frac{\partial}{\partial x_j} \cdot \left(\rho U_i U_j \right) = -\frac{\partial p'}{\partial x_i} + \frac{\partial}{\partial x_j} \left[\mu_{eff} \left(\frac{\partial U_i}{\partial x_j} + \frac{\partial U_j}{\partial x_i} \right) \right] + S_M \quad (8)$$

Where S_M represents the sum of body forces, μ_{eff} represents the effective viscosity explaining the turbulence, and p′ represents the modified pressure defined in Equation 9.

$$p' = p + \frac{2}{3}\rho k + \frac{2}{3}\mu_{ff}\frac{\partial U_k}{\partial x_k} \quad (9)$$

As it is in the case of the zero-equation model, the k-epsilon model is built upon the concept of eddy viscosity and hence turbulent viscosity becomes in Equation 10.

$$\mu_{eff} = \mu + \mu_t \quad (10)$$

Where μ_t represents the turbulence viscosity. The k-epsilon model considers the turbulence viscosity in association with the turbulence kinetic energy and dissipation through the relation in Equation (11).

$$\mu_t = C_\mu \rho \frac{k^2}{\varepsilon} \quad (11)$$

where C_μ is a constant. The values of k and ε are directly obtained from the differential transport equations for the turbulence kinetic energy and turbulence dissipation rate:

$$\frac{\partial(\rho k)}{\partial t} + \frac{\partial}{\partial x_j}(\rho U_j k) = \frac{\partial}{\partial x_j}\left[\left(\mu + \frac{\mu_t}{\sigma_k}\right)\frac{\partial \mathrm{k}}{\partial x_j}\right] + P_k - \rho\varepsilon + P_{kb} \quad (12)$$

$$\frac{\partial(\rho \varepsilon)}{\partial t} + \frac{\partial}{\partial x_j}(\rho U_j \varepsilon) = \frac{\partial}{\partial x_j}\left[\left(\mu + \frac{\mu_t}{\sigma_\varepsilon}\right)\frac{\partial \varepsilon}{\partial x_j}\right] + \frac{\varepsilon}{k}(C_{\varepsilon 1}P_k - C_{\varepsilon 2}\rho\varepsilon + C_{\varepsilon 1}P_{\varepsilon b}) \quad (13)$$

Where $C_{\varepsilon 1}$, $C_{\varepsilon 2}$, σ_k and σ_ε are constants.

P_{kb} and $P_{\varepsilon b}$ represent the influence of the below-described buoyancy forces. P_k is the turbulence production as a result of the below-modeled viscous forces that it becomes in Equation (14).

$$P_k = \mu_t\left(\frac{\partial U_i}{\partial x_j} + \frac{\partial U_j}{\partial x_i}\right)\frac{\partial U_i}{\partial x_j} - \frac{2}{3}\frac{\partial U_k}{\partial x_k}\left(3\mu_t\frac{\partial U_k}{\partial x_k} + \rho k\right) \quad (14)$$

For compressible flow, $\partial \mathrm{U_k}/\partial \mathrm{x_k}$ is only large in high-velocity divergence regions, (e.g., at the regions of shocks). The "frozen stress" assumption is adopted to obtain the $3\mu_t$ term. This prevents the excessive increase in the values of k and ε as a result of the shocks, which is a progressively aggravated situation by the refining of the mesh at shocks. In the model, the coefficients $\sigma_{\varepsilon 1} = 1.44$, $\sigma_{\varepsilon 2} = 1.92$, $\sigma_k = 1$, $\sigma_\varepsilon = 1.3$ and $C_\mu = 0.09$ required in the turbulence modeling were used.

4. RESULTS

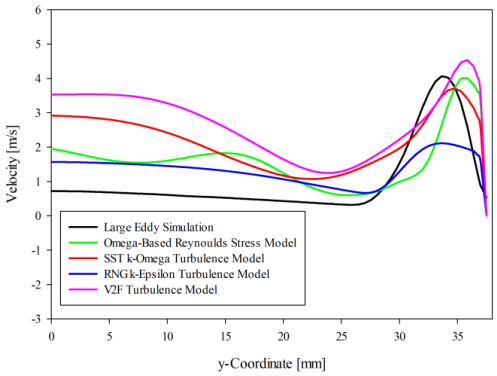

Figure 4. Absolute Velocity distribution along Z=2H line (H=8mm).

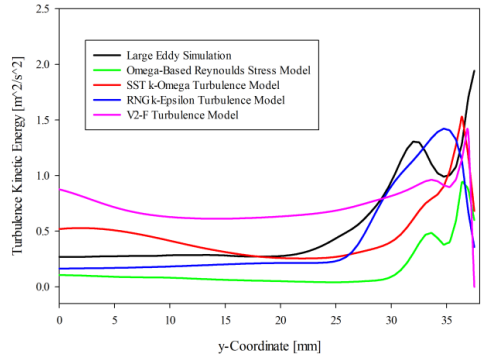

Figure 5. Turbulence Kinetic Energy along Z=2H line (H=8mm).

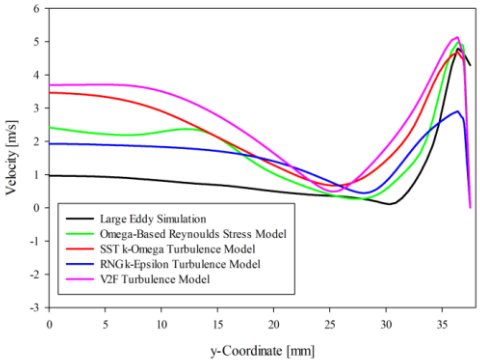

Figure 6. Absolute Velocity distribution along Z=3H line (H=8mm).

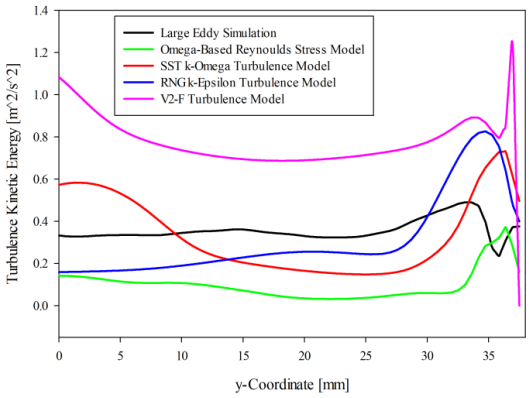

Figure 7. Turbulence Kinetic Energy along Z=3H line (H=8mm).

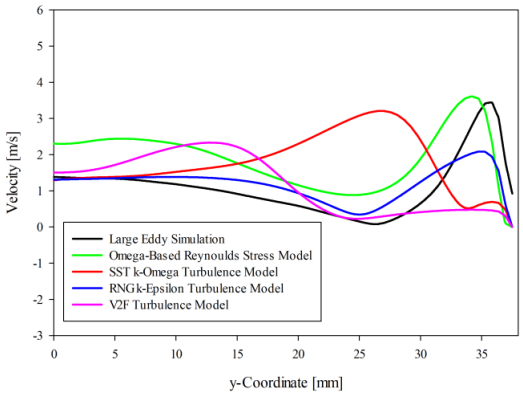

Figure 8. Absolute Velocity distribution along Z=6H line (H=8mm).

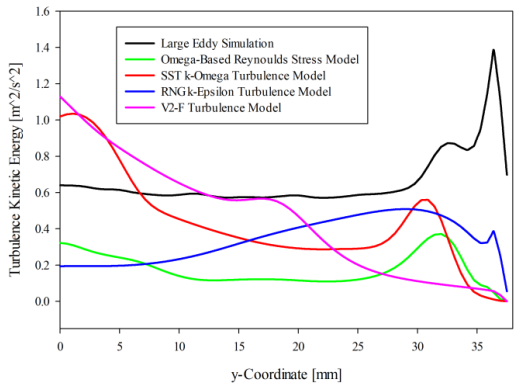

Figure 9. Turbulence Kinetic Energy along Z=6H line (H=8mm).

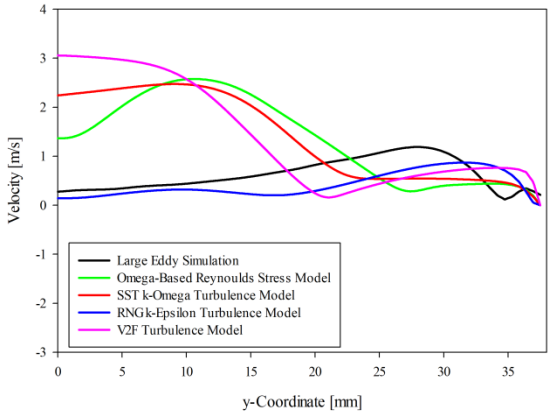

Figure 10. Absolute Velocity distribution along Z=9H line (H=8mm).

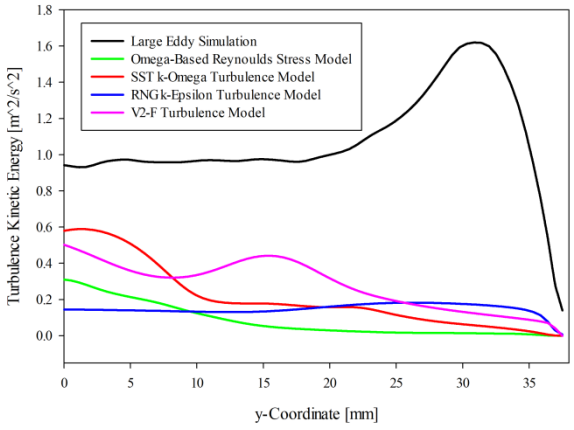

Figure 11. Turbulence Kinetic Energy along Z=9H line (H=8mm).

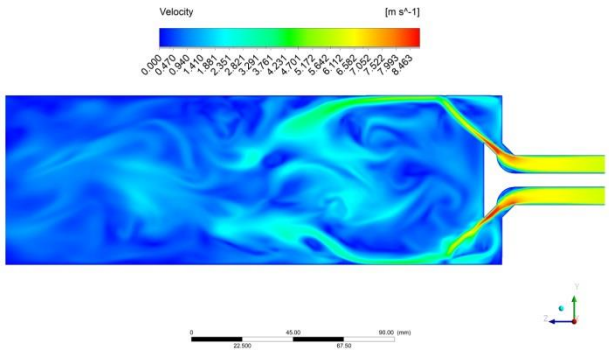

Figure 12. Velocity Contour of Large Eddy Simulation at the 10 sec.

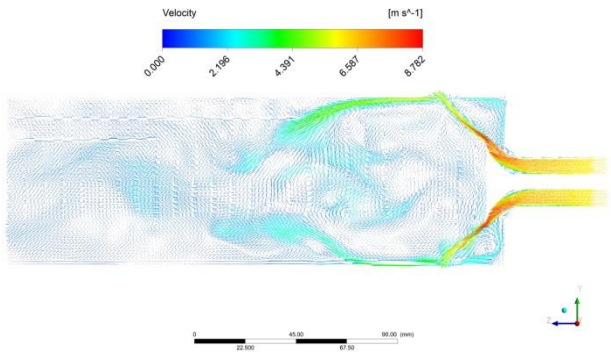

Figure 13. Velocity Vector of Large Eddy Simulation at the 10 sec.

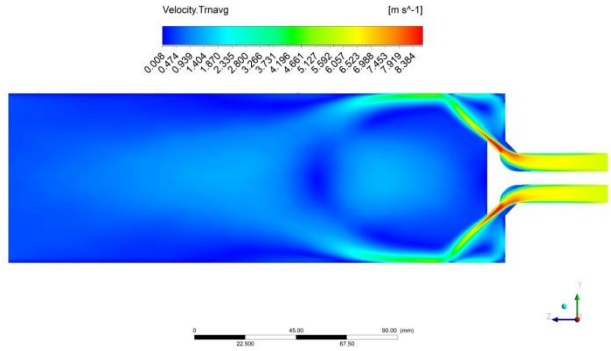

Figure 14. Statistical Averaged Velocity Contour of Large Eddy Simulation.

5. CONCLUSION

Figure 12 shows that some reverse flow along the centerline of the cylinder. This condition didn`t change each timestep but statistically gathered averaged velocity data clearly show that corner vorticity location is quite unstable along theta direction. Additionally, Reynolds stress component of flow was recalculated by statistically gathered data. Transient and statistically averaged Velocity component of velocity contours clearly prove that anisotropic flow characteristic at the around the valve and cylinder walls due to reflective flow condition. The velocity and turbulence kinetic energy distributions in the probe lines chosen for comparison show that the accuracy of the turbulence models is deteriorating as the probes move axially away. We can explain this situation as the flow becomes unstable as the flow progresses axially. However, in order to more accurately calculate the flow parameters in the cylinder wall, it is seen in the figures that it has critical importance in the near wall distance used during mesh modeling. This is because the y + value changes with the velocity fluctuations that occur during the flow interaction with the wall. Therefore, minimization of the near-wall distance is of critical importance in more accurate analysis of in-cylinder flow calculations, provided that they are compatible with turbulence models.

REFERENCES

[1] Schmitt, “Direct numerical simulations in engine-like geometries,” *Phd Thesis* , 2014.

[2] Buhl, Dietzsch et al., “Comparative study of turbulence models for scale-resolving simulations of internal combustion engine flows,” *Computers and Fluids*, 2017.

[3] Giannakopoulos, Frouzakis et al., “Direct numerical simulation of the flow in the intake pipe of an internal combustion engine,” *International Journal of Heat and Fluid Flow*, 2017.

[4] Schmitt, Frouzakis et al., “Direct numerical simulation of the compression stroke under engine-relevant conditions: Evolution of the velocity and thermal boundary layers,” *International Journal of Heat and Mass Transfer*, 2015.

[5] Schmitt, Frouzakis et al., “Direct numerical simulation of the compression stroke under engine relevant conditions: Local wall heat flux distribution,” *International Journal of Heat and Mass Transfer*, 2016.

[6] Plengsaard and Rutland, “Improved Engine Wall Models for Large Eddy Simulation (LES),” *Society of Automotive Engineering*, 2013.

[7] Schmitt, Frouzakis et al., “Direct numerical simulation of the effect compression on the flow, temperature and composition under engine-like condition,” *Proceedings of the Combustion Institute*, 2014.

Paper 4 **Bildiri 4**

DPF AGING TESTS ON COMMERCIAL AUTOMOTIVE CATALYST

İsmail Hakkı SAVCI*, Hande BEZCİ ZEREN**, Hasan ŞENER***

* Ford OTOSAN Flow Performance and Durability Laboratory

isavci@ford.com

** Ford OTOSAN Flow Performance and Durability Laboratory

hzeren@ford.com.tr

*** Ford OTOSAN Flow Performance and Durability Laboratory

hsener3@ford.com.tr

With stringent diesel engine emission regulations at recent years, the DPF systems have become the one of the main technology to remove soot particles from tailpipe of the diesel engines. Fresh catalyst parts become aged after certain miles and their characterization is decreased significantly. To understand emission performance of the catalyst aging is crucial due to emission legislation. One of the main characterization of the catalyst aging is thermal aging. To address this issue, flow burner systems may be used to increase exhaust temperature to get aged catalyst by the high temperature.

A burner-based aging system offers an alternative solution that provides higher exhaust temperatures, with lower fuel consumption compared to a diesel engine bench aging system. This paper presents a natural burner based aging system that addresses the technical challenges of using a burner to simulate diesel exhaust and the validation of aging equivalency between the burner-based system and a diesel engine dynamometer. The operational cost effectiveness of burner systems compared to diesel systems is also explored.

1. INTRODUCTION

In order to meet the increasingly tighter emission regulations, diesel particulate filters (DPF) have become serial standard in exhaust gas after treatment systems of diesel engines [1]. Soot particles form in the engine's combustion chamber as the result of incomplete combustion. Soot particles generated during the combustion process are trapped in the pores of the walls of ceramic filter monoliths. These soot particles increase the backpressure value of the exhaust system. This increase is a result of the soot loading in the filters, the pores get blocked by the

time. As a result of this, the flow of exhaust gases is obstructed and hence the backpressure increases. After that the exhaust system break down.

Exhaust systems not only have the back pressure problems but also the main problem encountered by diesel engines is the significant amount of soot particles emitted to the environment [2]. For this reason, the after-treatment devices such as Diesel Oxidation Catalyst (DOC), Diesel Particulate Filter (DPF) and Selective Catalyst Reduction (SCR), are invented to control the emission from diesel engines [4, 5]. The invention of DPF started in the last 20 years with various types of filter media and geometric configuration [2]. The compact arrangement without neglecting the filtration efficiency and back pressure drop, demonstrated by the wall-flow monolith honeycomb design, makes this type of DPF the best [1]. Usually, the cross section of the channel is square and the whole arrangement is like checkerboard with alternating blocked ends [2, 6]. Typical porous media used in DPF are either porous ceramic or sintered metal due to their high temperature resistance (~1200flC) [7] to withstand the temperature of exhaust gas [8] as seen in Figure 1.

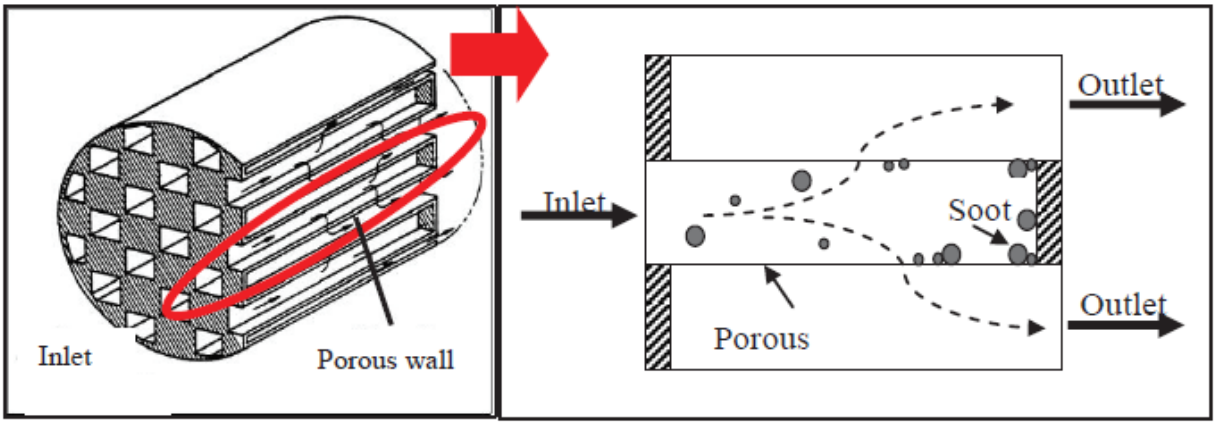

Figure 1. Soot Formation

The working principle of DPF can be explained in three steps [8]. First is the filtration process by depositing soot particles from exhaust gas when the gas passes through the porous wall. The collected soot particles can increase the back pressure since the soot plugged at the porous wall will block the flow of the exhaust gas. This phenomenon will result in increased fuel consumption and reduced engine power output [4, 5]. The second step is the regeneration process to oxidize the collected soot. The regeneration process will take place if the temperature inside the DPF exceeds 550°C [1, 8]. Therefore, the regeneration process can be achieved either actively using electric heating or passively using fuel-borne catalyst. The last process is the rearrangement of the ashes collected as to maintain the next filtration process and efficiency.

Better understanding on DPF is very essential to optimize its efficiency and design. Similarly, the reliability and durability of the DPF can be predicted by having detailed research from various approaches.

2. TEST

In ATS Flow Lab, thermal aging test is done with hot gas burner. Burner can run between 50-1200 °C temperature ranges. In this study, aging test is completed for both the DPF and pSCR in the same time. Test repeatability is important because soot production rate varies with DPF backpressure and ambient conditions.

The process includes a minimum 8 hour non-stop heating test duration. 12 hour aging process is also tested. The test must be unstoppable and continuous. During the test, temperature is controlled with 3 different thermocouple locations. First thermocouple is mounted on the burner exit, second one is on the inlet of sDPF and the last one is on pSCR inlet. Hot end inlet temperature is 870 C and pSCR temperature is 820 C during the aging process. After the test, ATS parts are tested in the dynamometer for the NOx legislation limits. Same test is repeated 11 times for decreasing the emission level taken from the tail pipe emission level.

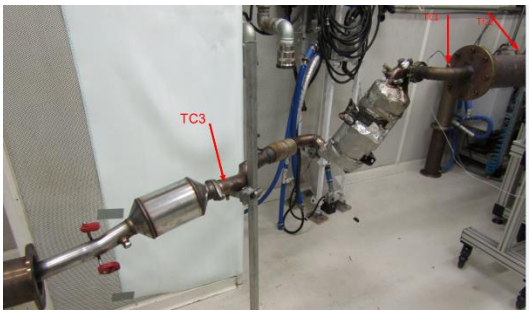

Figure 2. Test Rig

Test rig is given on Figure 2. Temperature is controlled on 3 different thermocouple locations. First thermocouple is mounted on the burner exit, second one is on the inlet of sDPF and the last one is on pSCR inlet.

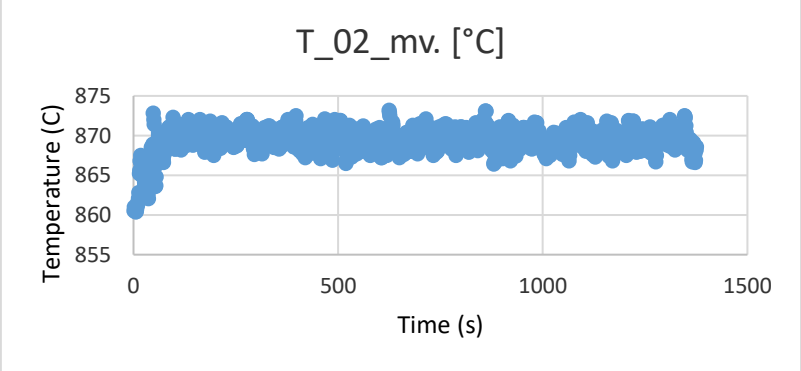

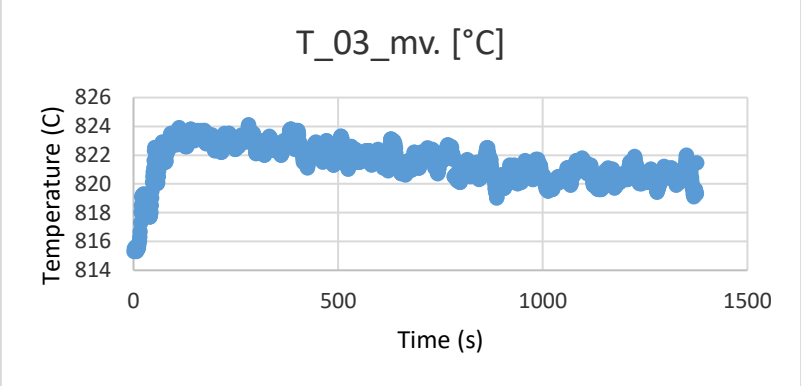

Figure 3. Temperature Control

Temperature oscillates over the target value over the test time. T_02 must be 870 C and T_03 (pSCR thermocouple) is 820 °C as seen in Figure 3.

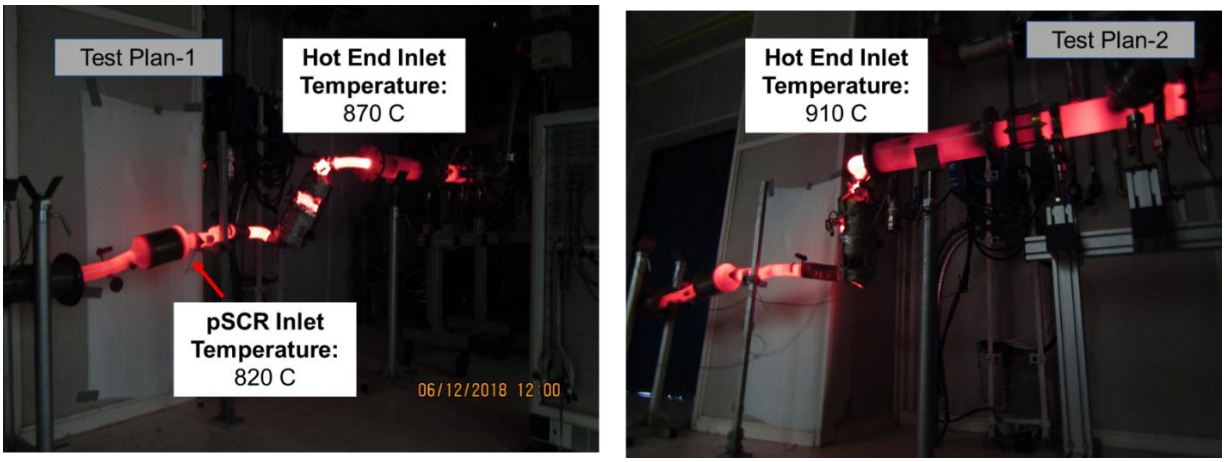

Figure 4. Test Image

There are 2 test plans. For the first plan, DPF temperature is 870 C for 8 hours. DPF temperature for second test plan is 910 C, 8 hours. Before each test 20 minutes regeneration is run in order to remove the deposits remaining from dynamometer and vehicle tests.

After the tests in Flow Lab, tests parts are taken to the dynamometer. WHTC tests are planned with hot and cold starting conditions. The WHTC test is a transient engine dynamometer schedule defined by the global technical regulations. The WHTC is a transient test of 1800 s duration, with several motoring segments. Normalized engine speed and torque values over the WHTC cycle are schematically shown in Figure below.

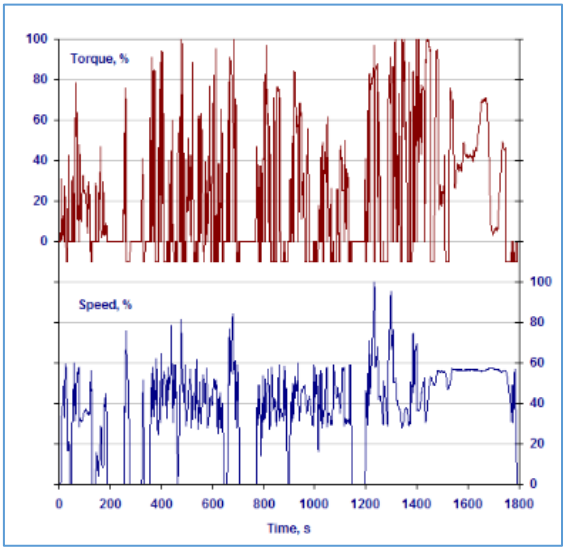

Figure 5. WHTC Transient Test Cycle

After the WHTC tests, emission levels are calculated on the Tail Pipe and compared with the target values. These values are given in Table 1. According to the tail pipe emission levels, aging tests repeated or ended.

Variant	OBD Emission Limits	Test Cycle
PC	140 mg/km	WLTC Cold
LDT (FWD / RWD)	220 mg/km	WLTC Cold
HDT (RWD)	1200 mg/kWh	WHTC Combined

Figure 6. Target Emission Test Values

3. RESULTS

Aging test is done 11 times in ATS Flow Lab Gölcük. The tests are done in order to design ATS parts under the NOx legislations limit values. Test temperature is 870 C for sDPF tests and 820 C pSCR tests. Test time is set as 8 hours and non-stop. For 9th and 11th Aging Test the test temperature is 910 C for DPF testing. The temperature control is done with 3 instrumented thermocouples. First thermocouple is mounted on the burner exit, second one is on the inlet of sDPF and the last one is on pSCR inlet. After the flow lab tests, parts are tested in dynamometer with WHTC cycle. Emission calculations are done on the tail pipe. The emission target values are reached and tests are finished.

4. REFERENCES

[1] Twigg M.V., Phillips P.R. Cleaning the air we breathe—controlling diesel particulate emissions from passenger cars. Platin. Met. Rev. 2009; 53:27–34. doi: 10.1595/147106709X390977.

[2] S. K. Hidemitsu Hayashi, "Computer Simulation Study on Filtration of Soot Particles in Diesel Particulate Filter," Computers & Mathematics with Applications, vol. 55, 2008.

[3] M. K. K. W. Addy Majewski, Diesel Emissions and Their Control. Warrendale: SAE International, 2006.

[4] M. N. Kazuhiro Yamamoto, "Simulation on Flow and Heat Transfer in Diesel Particulate Filter," Heat Transfer, vol. 133, 2011.

[5] K. S. M. K. Chen, D. Luss, "Transient Temperature Rise during Regeneration of Diesel PArticulate Filters," Chemical Engineering, vol. 176177, 2011.

[6] E. S. Margaritis Kostoglou, Eleni Papaioannou, Dimitrios Zarvalis and Evdoxia Kladopoulou, "Fundamental Studies of Diesel Particulate Filters: Transient Loading, Regeneration and Aging," Society of Automotive Engineers, Inc., vol. 2000-01-1016, 2000.

[7] S. K. Hidemitsu Hayashi, "Computer Simulation Study on Filtration of Soot Particles in Diesel Particulate Filter," Computers & Mathematics with Applications, vol. 55, 2008

[8] U. J. Timo Deuschle, Manfred Piesche, "A CFD-Model Describing Filtration, Regeneration and Deposit Rearrangement Effects in Gas Filter Systems," Chemical Engineering, vol. 135, 2007.

Paper 5 **Bildiri 5**

ONE-DIMENSIONAL MODELING AND PERFORMANCE ANALYSIS OF A V-12 HEAVY-DUTY DIESEL ENGINE

Emre ALTUĞ*, M. Zafer GÜL

ABSTRACT

This work is about one-dimensional modeling and performance analysis of a V-12 30 liter heavy-duty diesel overstroke engine. This engine is specifically designed for high RPM uses such as tanks. Since the performance and fuel consumption effects are more important in tanks, emissions are disregarded.In this work, the requirements are known, which is a V-12 30 liter engine with 1000-1500 preferred horsepower range. Bore, stroke and compression ratios are selected without exceeding piston velocity of 13 m/s at highest RPM, because of increased inertial forces. Then an initial zero dimensional model is created in Matlab to see the basic outputs. After the zero dimensional model is evaluated, one dimensional modeling has started in GT-Suite program. The initial intake and exhaust manifold geometries are created. Then, ports and valves are designed and 3-D drawings were performed in SolidWorks. 3-D drawings are imported into the Ansys Fluent ICE module to simulate port flow. The outputs are obtained and discharge coefficients for valves and ports are imported to GT-Suite. A cycloidal cam profile script is created in Matlab and imported to GT-Suite. The ignition timing and durations are adjusted, firing orders are selected. The simulation has run and with some modifications and adjustments in the geometries, the power range of the simulated engine met the requirements needed. The final simulation output is 1331 HP and brake specific fuel consumption is 239 g/kW.h @ 2750 RPM. Maximum torque is 3808 N.m and brake specific fuel consumption is 216 g/kW.h @ 1250 RPM.

Keywords: ENGINE, DIESEL, HEAVY-DUTY, PERFORMANCE

INTRODUCTION

Heat engine is a machine that converts thermal energy into mechanical energy. By combusting the required fuel (petrol, diesel, coal) thermal energy is created. This thermal energy causes expansion, which causes work. In internal combustion engine, the combustion of fuel takes place inside the engine. Modeling an engine is a time consuming hard work. In this work, starting from zero and one-dimensional models helps creating the basis of the engine and simulating to see the outputs. In the work of Montenegro, G. et al. [1], they applied an integration between a 1-D code (Gasdyn) with a CFD simulation code (OpenFOAM) to improve the performance of a Moto3 engine. Gurney, D. [2] worked on the design of turbocharged engines using 1-D simulation. Soid, S.N. et al [3] worked on the simulation analysis on the performance of hydrogen port fuel injection engine. Ordys, A. and Boretti, A. [4] has worked on super-turbocharging the dual fuel diesel injection ignition engine. Trindade, W.R. and Santos, R.G. [5] worked on an alternative fuel with its effect on 1-D engine simulation and experimental test results. They started a virtual engine model and they compared it with the test results until good agreement was done between them. In the work of Boccardi, S. et al [6], they focused on numerical and experimental study of a turbocharged GDI engine. They aimed CFD optimization.

METHODOLOGY

Zero-Dimensional Ideal Diesel Cycle Modeling

Zero-dimensional models include no air flow. They only depend on time. Because of these reasons, zero-dimensional models are ideal and basic methods to coarsely model an engine. First it is necessary to check the zero-dimensional outputs by loading the base inputs to the script created in Matlab. The codes used in the Matlab script are based on the thermodynamic relationships between pressure, temperature, volume and heat addition. The heat addition is a constant pressure process.

One-Dimensional Modeling

One-dimensional models are easier to use than higher-dimensional models and they generally are very accurately close to the experimental results. The computational effort and time is much lesser in one-dimensional models compared to the higher-dimensional models. GT-Suite is a user-friendly program which is a one-dimensional simulation program. In-cylinder processes

in the GT-Suite are zero-dimensional. Single or two-zone or multi-zone models are the subgroups of zero-dimensional models.

In GT-Suite, pipe friction losses are calculated normally, pipe bend losses are taken from a chart which is called Miller's chart [7] and embedded into the program. Also discharge coefficients may be introduced where it is not possible to create a coefficient, like orifices and contractions. Expansion losses are calculated by the program itself.

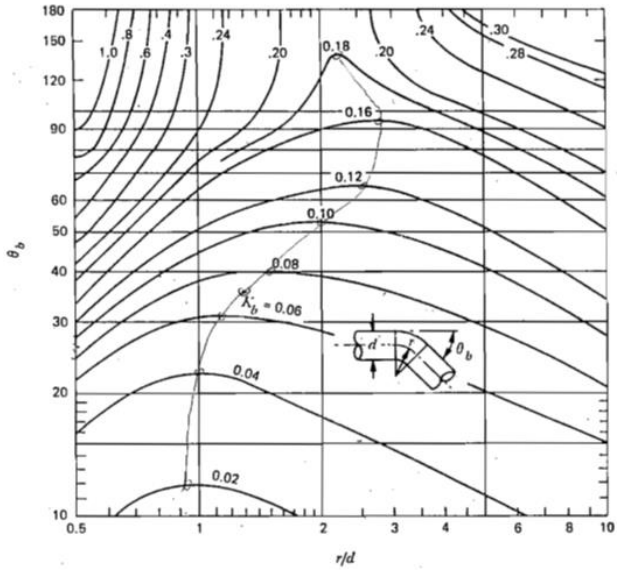

Figure 1. Miller's bend loss chart

Most one-dimensional models use the Wiebe burn function [8];

$$X_b(i) = 1 - \exp\left[-a_{wi} * \left(\frac{\theta(i) - \theta_0}{\theta_b} \right)^k \right] \tag{1}$$

θ_0 is advance, θ_b is burn duration in crank angles, k and a_{wi} are constants.

For single-zone model, following method is used;

$$\frac{dQ_c}{d\theta} - \frac{dQ_w}{d\theta} - \frac{dW}{d\theta} + \frac{dm_{f,i}}{d\theta} * h_{f,i} = \frac{dE}{d\theta} \tag{2}$$

For two-zone model, unburned zone equation is;

$$\frac{d(m_u * e_u)}{dt} = -P * \frac{dV_u}{dt} - \dot{Q}_u + \left(\frac{dm_f}{dt} * h_f + \frac{dm_a}{dt} * h_a \right) + \frac{dm_{f,i}}{dt} * h_{f,i} \tag{3}$$

Burned zone equation is;

$$\frac{d(m_b * e_b)}{dt} = -P * \frac{dV_b}{dt} - \dot{Q}_b - \left(\frac{dm_f}{dt} * h_f + \frac{dm_a}{dt} * h_a \right) \tag{4}$$

Subscripts are u for unburned zone, b for burned zone, f for fuel and f, i for fuel injected.

Conservation Equations

Continuity equation

$$\frac{dm}{dt} = \sum_{boundaries} \dot{m} \tag{5}$$

Energy equation (explicit method)

$$\frac{d(m*e)}{dt} = -P*\frac{dV}{dt} + \sum_{boundaries} (\dot{m}*h) - h_w * A_s * (T_{fluid} - T_w) \tag{6}$$

Enthalpy equation (implicit method)

$$\frac{d(\rho*H*V)}{dt} = V*\frac{dP}{dt} + \sum_{boundaries} (\dot{m}*h) - h_w * A_s * (T_{fluid} - T_w) \tag{7}$$

Momentum Equation

$$\frac{d\dot{m}}{dt} = \frac{dP*A + \sum_{boundaries} (\dot{m}*u) - 4*f*\frac{\rho*u*|u|}{2}*\frac{dx*A}{D_{eq}} - K_p*\left(\frac{1}{2}\rho*u*|u|\right)*A}{dx} \tag{8}$$

Where A is cross sectional area of flow and m is mass of control volume. u is velocity of fluid at boundary, e is internal energy, V is volume, P is pressure, A is cross sectional area, A_s is surface area for heat transfer, h is enthalpy, h_w is heat transfer coefficient,D_{eq} is equivalent diameter,K_P is loss coefficient, dx is discretization length and f is Fanning friction factor.

Intake Plenum

Plenum volume is important for tuning the intake system. When air is passes from intake pipe to plenum, the air expands into plenum and velocity decreases, pressure increases. It is easier for the cylinders to ingest the higher pressure, so the volumetric efficiency increases. For low RPM, one needs smaller plenum volume, and for high RPM, bigger volume is needed. For turbocharged engines, plenum volume is up to %150 of the engine volume. In the V-12 engine case with two plenums, the volumes are divided by 2.

Intake Pipe Diameter

The velocity in the intake pipe should be less than 180 ft/s (54,86 m/s).[9] For a V-12 engine, the half displacement should be taken for two plenum design.So the equation is;

$$D = \sqrt{\frac{\left(\frac{V_d}{2}*VE*N\right)}{180*18.5}}*0.0254 \tag{9}$$

VE is volumetric efficiency and N is engine speed.

Valves

For bowl-in piston engines, the valve head diameter, D_v is;

Inlet : 0.42*B – 0.44*B

Exhaust : 0.34*B – 0.37*B

B is bore diameter.

and max power with 14 m/s approximate mean piston speed [10]. Maximum intake valve lift is about 0.12*B - 0.15*B and maximum exhaust valve lift is about 0.2*B. With the advice of Prof.Dr. M. Zafer Gül, intake valve lift is taken 0.12*B and exhaust valve lift is taken 0.15*B. Below, intake and exhaust valves side views are represented, which were modeled in SolidWorks. Exhaust valve margin is 0.11 mm thicker compared to the intake and has a 30^o chamfer below. Intake valve head is 63.4 mm wide and exhaust valve head is 51.3 mm wide with 49.52 mm wide 30^o chamfer above.

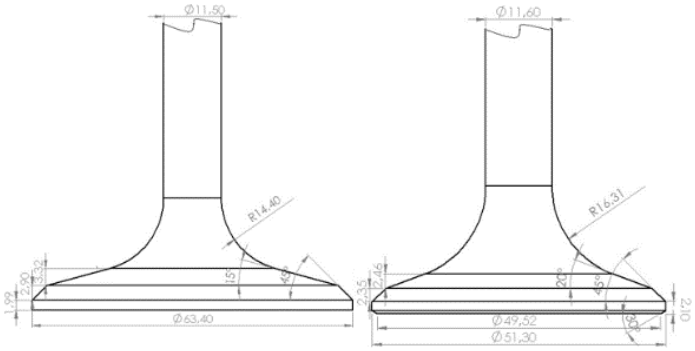

Figure 2. Side view of the intake(left) and exhaust(right) valves

Modeling Ports

When designing exhaust ports, the most important factor is the heating of the exhaust valve. The area exposed to the hot exhaust gases should be minimum. Because exhaust gases are at high pressure inside the cylinder, they can evacuate the cylinder easily, so exhaust ports can be narrower than the intake ports. They can have short and straight profile so there is less area exposed to the heat.

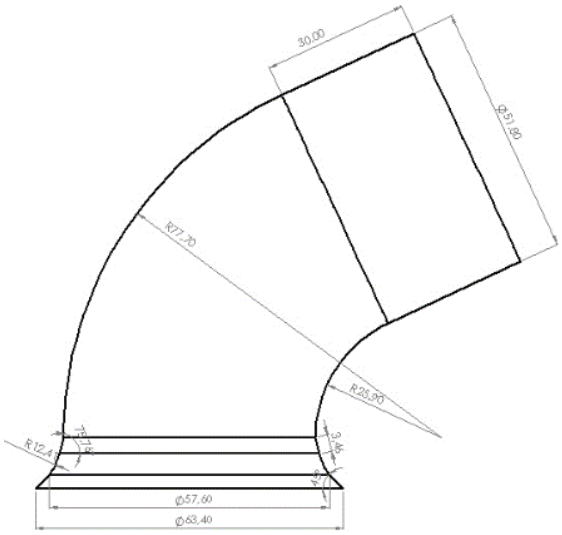

Figure 3. Intake port side view

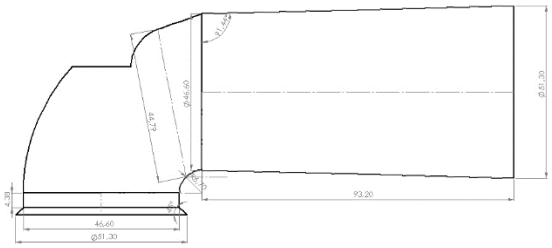

Figure 4. Exhaust port side view

Cam Profile

Cycloidal curves are good because they don't have discontinuities in the acceleration curve. So for high speed applications, cyclodial curves can be used. A cycloid is the locus of a point on a circle that is rolled on a straight line.

Following Rothbard's [11] definitions, the cam profiles for intake and exhaust valves can be obtained.

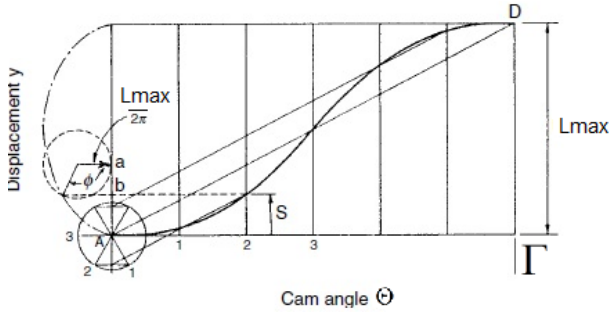

Figure 5. Cycloidal curve(Dwell-Rise-Dwell)

Whole cam motion is D-R-R-D. For D-R-D(dwell-rise-dwell) motion;

$$\text{Displacement } y = L_{\max} * \left(\frac{\Theta}{\Gamma} - \frac{1}{2*\pi} * \sin\left(\frac{2*\pi*\Theta}{\Gamma} \right) \right) \quad (9)$$

For the cam motion D-***R***-D (dwell-***return***-dwell), displacement is simply;

$$y = L_{\max} - L_{\max} * \left(\frac{\Theta}{\Gamma_2} - \frac{1}{2*\pi} * \sin\left(\frac{2*\pi*\Theta}{\Gamma_2} \right) \right) \tag{10}$$

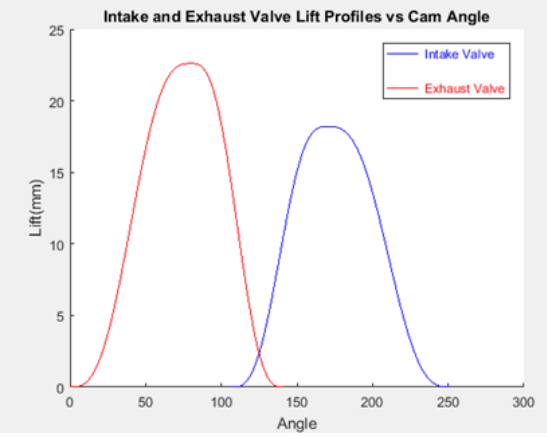

Figure 6. Cam lift profile

Obtaining Discharge Coefficients

Port and valve modelings are done with SolidWorks. In order to obtain the discharge coefficients of the ports and valves, port flow simulation is done in Ansys Fluent ICE. 10-28 inches of water column pressure is generally used for flow benches according to Vizard [12].

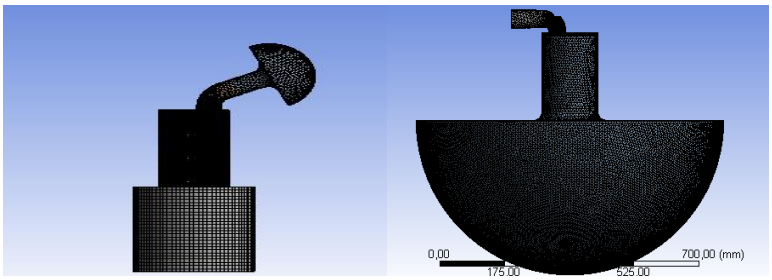

Figure 7. Meshing the port flow system for intake(up) and exhaust(down)

After simulating, the output variables are put into the GT-Suite's flow coefficient XLS file.

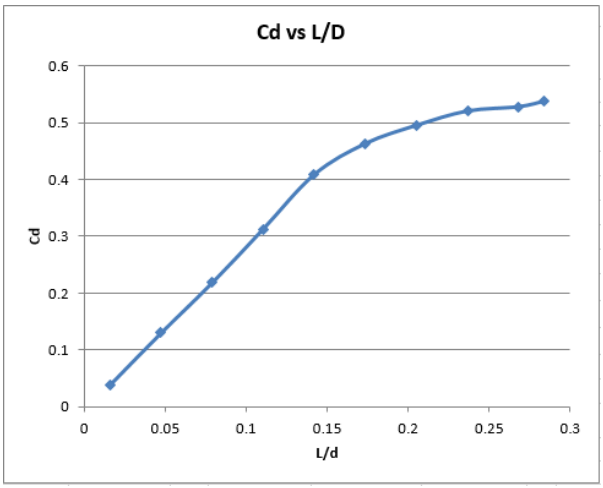

Figure 8. Intake system discharge coefficients

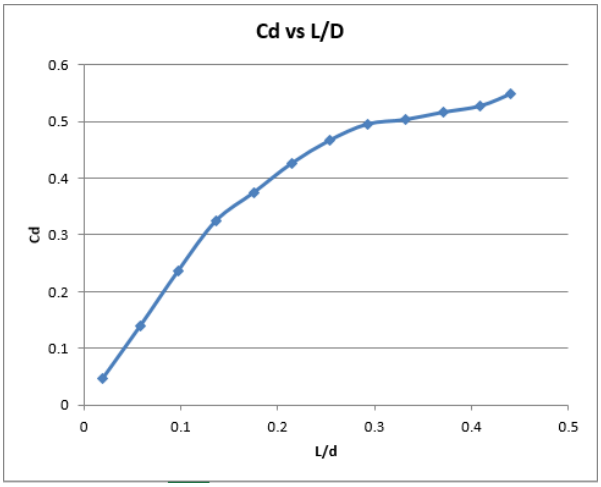

Figure 9. Exhaust system discharge coefficients

Modeling Manifolds

The intake manifold volume is taken the %150 of the volume of a single bank. Initial exhaust manifold has a constant diameter of 51.3 mm. If the final exhaust manifold is observed, it will be seen that it does not have a constant taper. Instead, it has stepped cross sectional area increases. That is because the GT-Suite program cannot count for losses in a tapered flowsplit. It needs discharge coefficients. So instead of calculating the discharge coefficients, simpler way is chosen so it has stepped cross sectional areas outside the manifold flowsplit length.

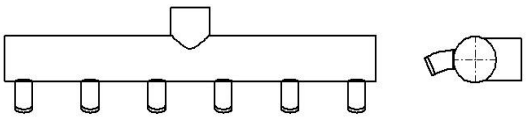

Figure 10. Intake manifold top and side view

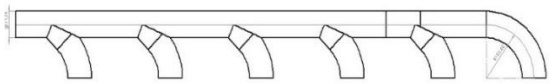

Figure 11. Initial exhaust manifold design with 51,3 mm constant diameter

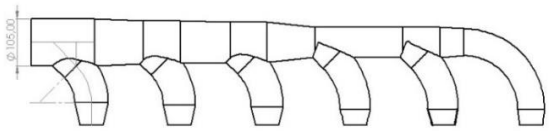

Figure 12. Latter exhaust manifold design with variable cross sectional areas

Injection Timing

Although the second case is selected for the simulations below, it is not the maximum power that the engine can obtain because of some limitations. During the simulation, many injection timing parameters are selected as cases and three good timing parameters are obtained. They are going to be compared by their advantages and disadvantages.

Table 1. Injection parameters

Case Number	Injection Timing(CA BTDC)	Injection duration (CA)
1	-20	6
2	-10	15
3	-8	15

The Engine RPM and Outputs

The engine outputs with final parameters are going to be checked in the RPM range of cases below.

Table 2. RPM cases

Case 1	850	Case 2	1000	Case 3	1250
Case 4	1500	Case 5	1750	Case 6	2000
Case 7	2250	Case 8	2500	Case 9	2750

Simulation Initialization

In the Table 3, the initial values for GT-Suite program are given. For the zero-dimensional modeling, only inlet pressure and temperature, atmospheric pressure, air-fuel ratio, which is

roughly 20, engine geometry parameters are important. Flow affecting parameters and timings are neglected.

Table 3. Engine parameters

Bore (mm)	151	Injected fluid temperature (K)	300
Stroke (mm)	139.6	Initial injection timing (BTDC CA)	-10
Number of cylinders	12	Initial injection duration (CA)	15
Con.rod length (mm)	350	Initial firing order	1-12-5-8-3-10-6-7-2-11-4-9
Compression ratio	16:1	Firing intervals (deg)	60º
TDC clearance height (mm)	9	IVO	22º BTDC
Injected fuel mass (mg)	240	IVC	54º ABDC
EVO	54º BBDC	Initial RPM	2500
EVC	19.7º ATDC	Exhaust lift (mm)	22.6
Intake lift (mm)	18.2	Absolute intercooler outlet total pressure (bar)	2.06
Absolute turbine inlet total pressure (bar)	2.2	Turbine inlet temperature (K)	800
Intercooler outlet temperature (K)	333		

RESULTS AND DISCUSSION

Ideal Zero-Dimensional Simulation

Table 4. Ideal cycle output

Thermal Efficiency %	77	IMEP (bar)	21.67
BMEP (bar)	19.51	Torque (N.m)	4655
Brake power	1218	BSFC (g/kW.h)	187.2

One-Dimensional Simulation

By simulating the system one-dimensionally, the effects of various parameters on performance are observed.

Initial Exhaust Manifold Geometry

Whole exhaust manifold is the same diameter as the exhaust port, 51.3 mm, the burned mass percentage at combustion start was also %6.65. The Mach number in the exhaust collector was 0.814. Maximum mass flow rate distribution difference was between exhaust runner 3 and 4, which was 11.1 g/s.

Table 5. Performance outputs for initial exhaust manifold geometry

Brake Power (kW)	787.4	PMEP (bar)	-3.39	Volumetric Efficiency %	150.7
Brake Power (HP)	1055	Air flow rate (kg/h)	3928	Volumetric Efficiency (M) %	150.7
Brake Torque (N.m)	3007	BSAC (g/kW.h)	4989	Trapping Ratio	1.000
IMEP (bar)	14.74	Fuel flow rate (kg/h)	216	A/F Ratio	18.19
FMEP (bar)	2.14	BSFC (g/kW.h)	274	Brake efficiency %	30.5

Modified exhaust manifold

Mach number at the exhaust collector was 0.358. The mass flow rate distribution between exhaust runner 3 and 4 was 3 g/s. Maximum difference occured between exhaust runners 2,5 being same compared to 3, was 5 g/s.

Table 6. Performance outputs for final exhaust manifold geometry

Brake Power (kW)	931.6	PMEP (bar)	-1.41	Volumetric Efficiency %	165.6
Brake Power (HP)	1249.4	Air flow rate (kg/h)	4318	Volumetric Efficiency (M) %	165.6
Brake Torque (N.m)	3558.6	BSAC (g/kW.h)	4635	Trapping Ratio	1.000
IMEP (bar)	17.06	Fuel flow rate (kg/h)	216	A/F Ratio	19.99
FMEP (bar)	2.15	BSFC (g/kW.h)	231.8	Brake efficiency %	36.1

Injection Timing Effects

Effects of different injection timings are observed. Second case is already given above.

Table 7. Ignition timing first case

Brake Power (kW)	963.3	PMEP (bar)	-1.36	Volumetric Efficiency %	165.8
Brake Power (HP)	1291.8	Air flow rate (kg/h)	4321	Volumetric Efficiency (M) %	165.8
Brake Torque (N.m)	3679.6	BSAC (g/kW.h)	4486	Trapping Ratio	1.000
IMEP (bar)	17.76	Fuel flow rate (kg/h)	216.0	A/F Ratio	20.01
FMEP (bar)	2.35	BSFC (g/kW.h)	224.2	Brake efficiency %	37.3

Table 8. Ignition timing third case

Brake Power (kW)	917.9	PMEP (bar)	-1.42	Volumetric Efficiency %	165.6
Brake Power (HP)	1231	Air flow rate (kg/h)	4317	Volumetric Efficiency (M) %	165.6
Brake Torque (N.m)	3506	BSAC (g/kW.h)	4703	Trapping Ratio	1.000
IMEP (bar)	16.8	Fuel flow rate (kg/h)	216.0	A/F Ratio	19.99
FMEP (bar)	2.11	BSFC (g/kW.h)	235.3	Brake efficiency %	35.6

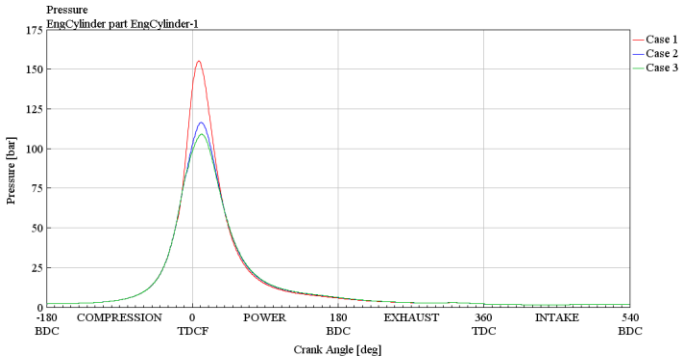

The Engine RPM and Outputs

The final cases are selected with the final intake and exhaust manifold geometries. Injection timing is selected as case 2.

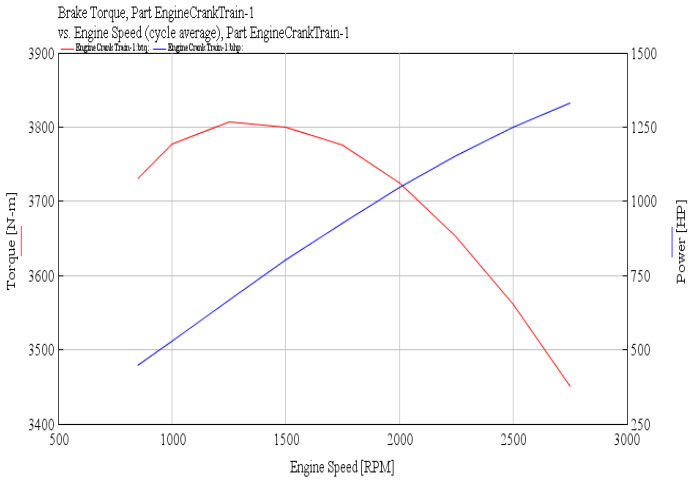

Figure 14. Torque-power curve vs RPM

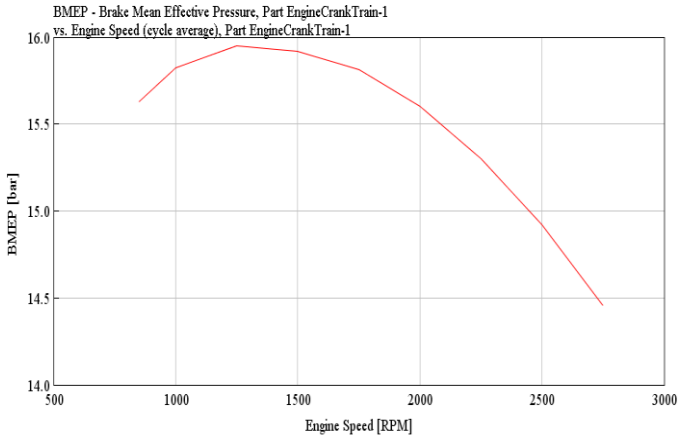

Figure 15. BMEP vs RPM

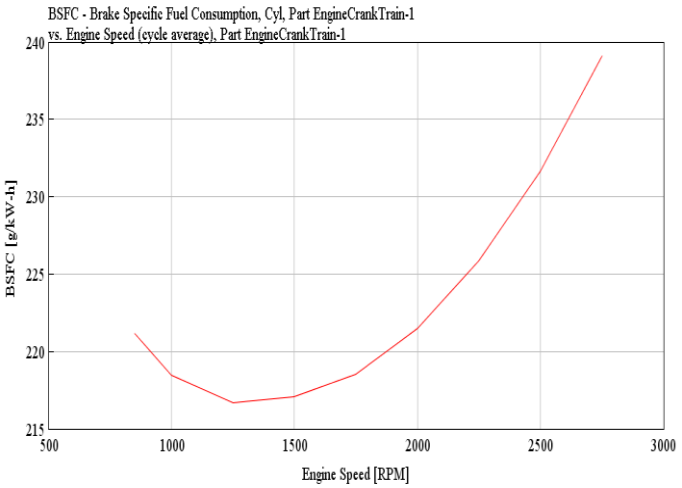

Figure 16. BSFC vs RPM

CONCLUSIONS

To model a 30 liter V-12 engine, first the bore and stroke are selected. With a fixed 30 liter displacement, If 150 mm of bore diameter is given, the mean velocity at maximum RPM would be 12.97 m/s. It is best to avoid high mean velocities so when 151 mm is taken, the piston mean velocity reduces to 12.8 m/s. Less than 13 m/s is ideal. Further increasing of bore diameter may cause higher pressure times piston surface area hence higher force acting on piston. But it may also increase the heat losses to the walls due to increased wall surface area of heat transfer. So 151 mm is thought ideal for starting. It is hard to go back on base engine dimensions, they should be decided at the very first moment.

In the initial exhaust manifold geometry, with the whole exhaust manifold being the same diameter as the exhaust port, 51.3 mm, the pumping losses were very high. Also mass flow rates in the exhaust runners were distributed very unevenly. The Mach numbers were high. With the modified exhaust manifold, the pumping losses are significantly lower than the initial manifold design. Many of the parameters have changed positively. Mass flow rate distributions in the runners were more evenly distributed than the initial manifold design. Maximum Mach numbers are lowered in the system.

Three cases in the injection timing and duration were observed. In the first case, maximum power and fuel economy is obtained. Friction losses were higher, as expected. Pumping losses were lower, volumetric and thermal efficiencies were higher. EVO losses were the lowest compared to the other cases. But the downside was the peak cylinder pressure was close to 160 bar. While this pressure is acceptable, the latter cases with lower peak pressures is expected to be more durable. Because of durability and longetivity, second case is taken into consideration for further simulation parameters.

As the engine is simulated at different RPM's between 850 and 2750, it is seen that peak brake torque, 3808 N.m is generated at 1250 RPM. After 1250 RPM the brake torque starts to decrease, minimum at 3448 N.m at 2750 RPM. At lowest engine speed simulated, 3730 N.m brake torque is generated. Maximum brake power, 1331 HP is generated at maximum engine speed, 2750 RPM. At peak torque, 1250 RPM, the generated brake power is 668 HP. At the lowest engine speed simulated, 850 RPM, 445 HP brake power is generated. BMEP and efficiencies were highest at 1250 RPM, as expected. Volumetric efficiency was the highest at

2250 RPM. Fuel consumption was the lowest,216 g/kW.h at 1250 RPM, where peak break torque is generated. At maximum engine speed, 2750 RPM, fuel consumption is observed 239 g/kW.h. Pumping and friction losses, combustion variations, differing air fuel ratios, valve timings, EVO losses, burned residuals all affect the engine performance differently at different engine speeds. These are the main causes of variations on engine performance at various engine speeds.

Further work is to do optimizations on the model. This work only contained an initialization and a conceptual modeling with basic optimizing. 4 valves per cylinder may have a positive impact on performance. Intake, exhaust manifold, port and valve geometries, valve and injection timings, firing orders, connecting rod length, compression ratio can be optimized to get a higher power output and lower fuel consumption. As stated before, emissions are not important for a military vehicle.

ACKNOWLEDGMENTS

Special thanks to my family for their support, to Marmara University and to Prof.Dr. M. Zafer GÜL for endless support and encouragement on my work.

REFERENCES

[1] : Montenegro, G., Cerri, T., Torre, A.G., Onorati, A., Fiocco, M., Borghesi, D., Fluid Dynamic Optimization of a Moto3™ Engine by Means of 1D and 1D-3D Simulations, SAE International Journal of Engines, Vol. 9, No. 1, pp. 588-600, April 2016

[2] : Gurney, D., "The Design of Turbocharged Engines Using 1D Simulation," SAE Technical Paper 2001-01-0576, 2001

[3] : Soid, S.N., Magalinggam, S., Hamid, M.N.A., Yusof, Z.N.M., Zahelem, M.N.M., ,Simulation analysis on the performance of hydrogen port fuel injection engine, Conference on Language, Education, Engineering and Technology, Kuala Lumpur, 2016

[4] : Bozza, F. and Torella, E., "The Employment of a 1D Simulation Model for A/F Ratio Control in a VVT Engine," SAE Technical Paper 2003-01-0027, 2003

[5] : Trindade, W.R., Santos, R.G., 1D modeling of SI engine using n-butanol as fuel: Adjust of fuel properties and comparison between measurements and simulation, Energy Conversion and Managament, Vol. 157, pp. 224-238, 2018

[6] : Boccardi, S., Catapano, F., Costa, M., Sementa, P., Sorge, U., Vaglieco, B.M., Optimization of a GDI engine operation in the absence of knocking through numerical 1D and 3D modeling, Advances in Engineering Software, Volume 95, pp. 38-50, May 2016

[7] : Miller, D.S, Internal Flow Systems, BHRA, 1978

[8] : Cuddihy, J.L. A User-Friendly, Two-Zone Heat Release Model for Predicting Spark-Ignition Engine Performance and Emissions. Master's Thesis, University of Idaho, Idaho, ID, USA, pp. 181-189, 2014

[9]: Grape Ape Racing, Induction Systems, http://grapeaperacing.weebly.com/uploads/4/1/2/0/41206275/inductionsystems.pdf, 14 November 2018

[10] : Barnes-Moss, H. W.,"A Designers Viewpoint" in Passenger Car Engines, Conference Proceedings, Institution of Mechanical Engineers, London, pp.133-147, 1975

[11] : Rothbart, H.A, Cam Design Handbook, 1st edition, McGraw-Hill, New Jersey, 2004

[12] : Vizard, D., David Vizard's How To Port & Flow Test Cylinder Heads, CarTech, Minnesota, USA, 2012

Paper 6 **Bildiri 6**

THERMOELECTRIC GENERATOR PROVIDING GAIN AS ELECTRIC ENERGY FROM THE WASTE HEAT ENERGY OF TRACTOR EXHAUST

Uğur Recep ŞAHİN, Gökhan COŞKUN, Hakan Serhad SOYHAN

Sakarya University, Engineering Faculty, Mechanical Engineering Department, Serdivan/Sakarya
ugurrecepsahin@gmail.com, gcoskun@sakarya.edu.tr, hsoyhan@sakarya.edu.tr

ABSTRACT

Today, the demand for energy is increasing each passing day with the rapid increase in human population. Depending these demands, the rapid rise in energy costs and changing climate conditions cause significant problems for countries. Especially in our country, there are incentives in many areas such as renewable energy, waste heat energy recovery in order to diversify energy production and to meet our own energy needs. In this study, thermoelectric generator design has been made to provide a clean, inexpensive and efficient energy production by providing the recovery of waste heat energy left to the nature without using a tractor exhaust. Firstly, a mathematical model was established by determining the system parameters. In addition, SolidWorks and ANSYS Workbench simulation programs are used for appropriate design depending on this model. This model has a thermoelectric power generator peltier module, a hexagonal frame and a wing cooling unit. The thermal, electricity-thermal analyzes of the designed model have been carried out and the current, voltage and power values to be obtained are examined and it has been observed that the thermal energy from the exhaust gas has an accurate distribution. Adjustable DC-DC voltage regulator board is used to increase current and voltage values.

Keywords: Thermoelektric Generator, Recovery of Waste Heat Energy. Heat-Electric

1. INTRODUCTION

Today, due to reasons such as global warming, increasing energy demand with increasing population, increasing economic problems due to fossil fuels and decreasing fossil fuels, mankind has started to look for different ways in energy production. Especially the renewable energy and the energy recovery left to the environment has importance. For example, an efficient energy can be obtained by using the heat energy of the exhaust gas that the internal combustion engines leave to the nature through the exhaust. Thus, by reducing the amount of wasted energy, both energy costs will be met and the need for fossil fuels will be reduced.

In addition to meeting the energy needs for most of the countries, providing environmental awareness, increasing the existing efficiency, also vital to ensure the diversity and continuity of the resources used. [1].

Thermoelectric devices are the most suitable devices for converting the waste heat energy resulting from the processes into electrical energy. With thermoelectric devices, as a result of a certain temperature difference, electric potential is produced through the Seebeck effect discovered by Thomas J. Seebeck. Also thermoelectric devices can be used for cooling or heating purposes with Peltier effect.

The first studies on thermoelectric power were carried out by German scientist Thomas Seebeck in 1821. In this study, in a closed circuit that two different metals were formed, electric current was circulated and the reaction of the metals used to two different temperature values was observed. But he had not realized the basis of the studies and the continuing temperature Seebeck production, has recognized that the impact of equal value has been circulating electric current [2].

In 1834, the French physicist Jean Peltier realized that while he was working on the Seebeck effect, the electric current was absorbed by the heat energy in one of the metals while the electric current was moving in a closed cycle and in the other [2].

After a while, the French physicist Jean Peltier published a statement about the effects of Thomson, Seebeck and Peltier, and explained the connection between these two thermoelectric effects [2].

Today's studies are examined, vehicle technologies, geothermal energy etc. in many areas studies have been done. For example, electricity is produced by utilizing the heat energy of the exhaust gas from the exhaust of an internal combustion diesel engine. In this study, flow analysis was performed and it was examined how much power the engine produced under different operating conditions in the experimental environment [3].

In another similar study, thermoelectric systems are used for the heating and cooling of vehicle seats. Recently, automobile companies are working on this subject. The clean energy obtained from thermoelectric systems can be used directly or stored.

Thermoelectric systems can be used in vehicle exhausts as well as other applications in the vehicle. In the studies, it is aimed to obtain electrical energy by using the heat energy released in the brake system depending on the sudden braking values at 30, 50 and 70 km / h speed. In the experiments carried out within the scope of this purpose, the energy recovery of the energy was provided [3].

Many other studies have been carried out to obtain electricity from flue gas, which is another area that thermoelectric systems can use. In a study, the experimental setup was prepared and it was aimed to change the

negative effects of the gas thrown out of the chimney to a positive direction by obtaining electrical energy from the waste heat generated. As a result, a 12.2% gain was observed in the calculations [4].

In a similar study, the hot surface of the thermoelectric generator was heated with waste gas and the cold surface was cooled at different water flows. The use of waste gas from the pipes of the stoves used in the houses for heating of the hot surface has been shown with the help of this representative mechanism that can generate energy from the waste gases occurring in the industrial establishments [5].

In this design, a thermoelectric generator suitable for a tractor exhaust system is designed. For this system, mathematical model was created and design parameters were determined. The system was designed according to the determined parameters and thermal analyzes were performed and suitable thermoelectric modules were selected. In order to obtain the temperature difference for the desired power value, heat sinks were used on the cold surface of the thermoelectric modules. As a result of the analyzes, it was aimed to obtain the power required to operate the electric parts of a tractor and tractor trailer.

2. THERMOELECTRIC GENERATIONS

Thermoelectric generators are thermoelectric elements that can produce direct current depending on the temperature difference between the two surfaces. Thanks to these thermoelectric elements, electrical energy can be easily obtained in all areas where temperature difference is present. In a closed circuit composed of two different metals, if different temperature values affect the connection points, Joule effect, Peltier effect and Seebeck effect are applied between these surfaces. The structure of the thermoelectric generator. As shown in Figure 1.

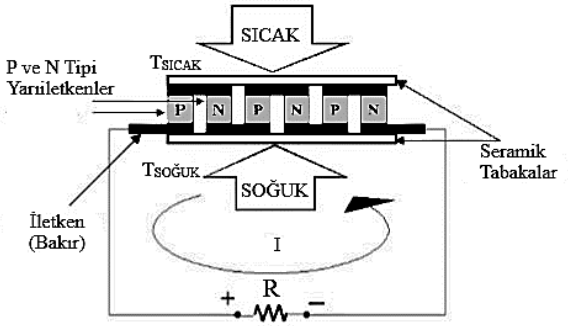

Figure 1. Structure of thermoelectric generator [7].

Thermoelectric generators convert the energy that is converted to heat into electrical energy for any reason. Thus, waste energy waste is avoided and the resulting energy losses are minimized [6].

Thermoelectric generators have many advantages. They are;

- They work quietly
- Reliable,
- Basic,
- Stable,
- Maintenance-free,
- They haven't moving parts,
- Long lived,
- They obtain electricity directly,
- They allow temperature control.

Thermoelectric generators have many advantages as well as disadvantages. The biggest disadvantage of thermoelectric generators is their low efficiency. The efficiency of thermoelectric generators is about 5-10%.

Both the increase in the costs of thermoelectric generators compared to the used areas and the lack of the desired amount of efficiency obtained due to their increasing costs reduce the number of areas they are applied. The yield amount of 5-10% can be considered very low, but it is seen that the yield amount is not low when the electricity obtained from the recovery of waste heat is made available [7].

The operating principle of thermoelectric generators is based on the Seebeck effect. Thermoelectric generators are thermoelectric modules composed of thermoelements. A thermoelectric module is an electrically series to increase the voltage generated from semiconductors p and n, .An electrical voltage is generated along with the temperature difference to be formed between the surfaces by connecting the electrical charge to the end parts of a thermoelectric generator and current flow from the load occurs. This is the working principle of thermoelectric generators in general.

3. MATERIAL AND METHOD

In this study, it is aimed to decrease the energy deficit by converting the heat energy which is left to the environment without being used efficiently to electrical energy. For this purpose, mathematical model has been formed in accordance with the principles of heat transfer and this model has been analyzed by using Thermal-Electric and Thermal modules in ANSYS Workbench 16.0 software program. Current, voltage and power values obtained as a result of these analyzes are recorded depending on certain temperature conditions.

3.1.Thermoelectric Generator Design

In this model designed to realize power production, ideal thermoelectric equations are used to determine the material properties of each piece used in accordance with the design parameters. The ideal thermoelectric equations used in this context depend on the Seebeck effect, the Joule heat and the conducting heat. Some assumptions have been made for the extraction of these ideal equations used in the design of the model:

- Exhaust gas temperature passing through the section where the thermoelectric generator is placed on the exhaust is 177 ^{0}C (450 K).
- The temperature distribution in the thermoelectric generator is homogeneous.
- The cold surface of the thermoelectric module contact a heat sink. The interaction between the heat sink and the environment is in a convective form.
- Thermal and electrical contact resistances have been neglected.
- Depending on the temperature, material properties do not change. Accordingly, the Thomson effect was neglected.
- Convection and radiation were neglected for the semiconductor thermoelectric leg in the thermoelectric module.
- The connection points in the model are perfect.

The basic heat transfer formulas have been used to determine the heat transmission coefficient and dimensions of the hexagonal block used in the design to convey the temperature of the exhaust gas to the hot surface of the thermoelectric module in the desired conditions. The heat transferred from the exhaust gas to the thermoelectric generator is calculated as in formula 1.

$$Q = m\, c\, \Delta T \quad (W) \qquad (1)$$

The thermophysical properties of the exhaust gas used in this formula are as in Table 1.

Table 1. Thermophysical properties of exhaust gas [9].

Temperature (K)	Specific Heat (c_p) (kJ/kgK)	Density (p) (kg/m^3)	Thermal Conductivity (W/mK)
400	1,106	0,912	23,6
450	1,114	0,810	29,1
500	1,126	0,729	35
550	1,140	0,662	36,6
600	1,070	0,607	48

To determine the size of the hexagonal block which is a part of the design according to the calculated amount of heat and the heat conduction coefficient of the material to be used

$$Q = K\,\Delta T \quad (W) \tag{2}$$

K is the total heat transmission coefficient. The unit is W / K. Calculated according to formula 3.

$$K = k\frac{A}{L} \quad (W/K) \tag{3}$$

In Figure 2, the voltage, current, resistance and power values of the thermoelectric power generator module, which is shown internally, depending on the design parameters and assumptions, are calculated according to the following relations.

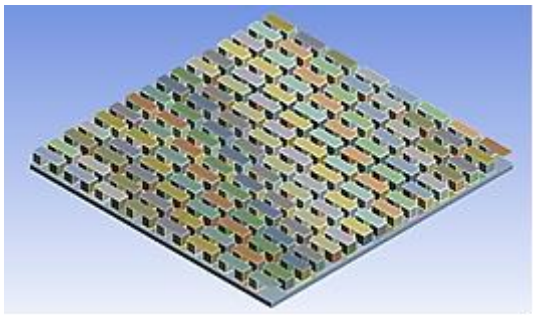

Figure 2. Internal structure of thermoelectric module

Voltage value;

$$V = \frac{N\,S\,(T_H - T_L)}{\frac{R_L}{R}+1}\left(\frac{R_L}{R}\right) \quad (V) \tag{4}$$

Internal resistance value;

$$R = \rho\frac{L}{A} \quad (\Omega) \tag{5}$$

Current Value ;

$$I = \frac{S\,(T_H - T_L)}{R_L + R} \quad (A) \tag{6}$$

Power value;

$$W = \frac{N\,S^2\,(T_H - T_L)^2}{R}\,\frac{\frac{R_L}{R}}{(1+\frac{R_L}{R})^2} \quad (W) \tag{7}$$

The efficiency of the thermoelectric power generator module selected according to these relations is as follows.

$$\eta = \frac{W}{Q_H} \tag{8}$$

The performance criterion (FoM) of the selected thermoelectric module is calculated as follows.

$$FoM = \frac{S^2}{\rho k} \quad (1/K) \tag{9}$$

3.2. Finite Element Method

The finite element method (FEM) is an important solution for many applications in engineering. FEM enable compound analysis in many analyzes such as thermal, flow and electromagnetic analysis. Also it includes solution of the analysis of the combined physics capabilities such as thermal-structural, fluid-structural, electromagnetic-thermal, thermal-electric.

The ANSYS analysis program enables a complete and effective analysis of thermoelectric devices. In addition to the Joule heating effect, Seebeck, Peltier and Thomson effects are used in the analysis according to FEM. These effects are used in the analysis of thermoelectric generators and thermoelectric coolers [10].

3.3.Thermoelectric Generator Modeling

Nowadays, simulations made in computer environment have enabled design in many areas with the development of technology. One of these simulation programs is the SolidWorks drawing program which is used for designing this model, for ease of use design efficiency etc. depending on the features of the design and assembly of parts is used in a program too. Also, ANSYS Workbench 16.0, which is another simulation program and which is used in part analysis in this project, enables the design of systems and analysis by simulations when combined with FEM based software. The ANSYS finite element program is a very preferred program because it has a very large archive and the analysis modules can be used interactively.

This model is designed as a one-to-one design and consists of 1 hexagonal block, 6 thermoelectric modules, 6 heat sinks and 6 aluminum plates. Also in the model shown in Figure 3, to ensure that the silicone part of the thermoelectric modules is not damaged in high temperature values, some glass wool is to be installed in the tractor exhaust system of the designed thermoelectric generator and two-piece outer casing to protect it from external environment and connection elements to keep the created design together.

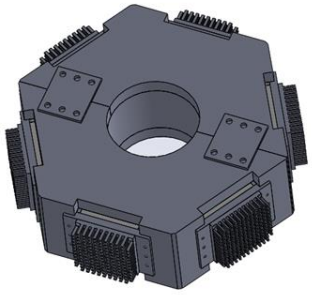

Figure 3. Design of Thermoelectric Generation

The use of stainless steel material is extremely common, as it is resistant to corrosion effects and high temperature effects caused by condensate water molecules in vehicle exhaust systems. As in Figure 4, extremely high temperature values start from the engine to the exhaust section.

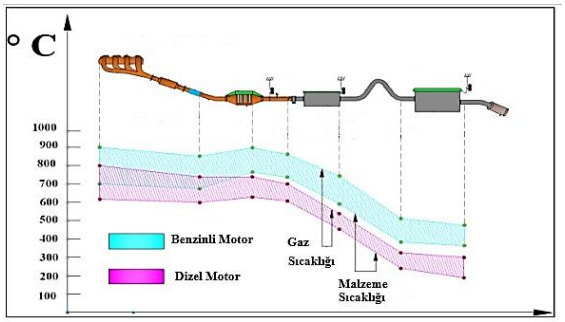

Figure 4. Temperature distribution of the exhaust system in diesel and gasoline engines [11].

One of the biggest problems that occur in thermoelectric generator design compatible with such a system is the high temperature factor. Thermoelectric modules that will be used in thermoelectric generator can work healthy until certain temperature values. Otherwise the thermoelectric modules break down and the designed system cannot achieve the desired efficiency. In this context, a hexagonal shaped block of heat-conducting low-ceramic material was designed to ensure that a temperature value lower than the exhaust gas temperature was

effected on the hot surface of the thermoelectric modules. This block, shown in Figure 5, is 18 cm wide, 4 cm thick, and as mentioned in Section 3.1, it allows the temperature value of 177 ^{0}C (450 K) to decrease the temperature value up to a temperature value which the thermoelectric module can work properly.

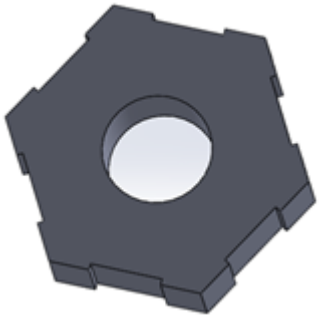

Figure 5. Hexagon Block

Thermoelectric modules which used in the design are located in hexagonal blocks. The reasons for this are to ensure that the temperature values acting on the hot surface of the thermoelectric modules act more uniformly, to efficiently use the limited working area and to keep the thermoelectric modules constant during the movement of the tractors. In addition, the heat transfer coefficient of these blocks is extremely low due to the glass wool, thermoelectric modules are not affected by the high temperature of the silicon parts.

Thermal analysis of hexagonal ceramic block was performed by using ANSYS Workbench 16.0 analysis program in order to obtain the desired voltage, current and power values by operating the thermoelectric modules properly. This model that was designed in SolidWorks program transferred to ANSYS Workbench 16.0. After these processes, all the features of the model are made dependent on each other by making mesh operation. During the formation of the mesh structure, the specific number of knots, the number of elements and the element size values are selected as the most suitable for the current, voltage and power values to be obtained depending on the performance characteristics of the computer and a uniform temperature distribution especially in the hexagonal block. The number of elements and the number of nodes vary according to the element size. Depending on the component dimensions are given total number of elements and nodes in Table 2.

Table 2. Bond created based on element size structure values

Size	Element Number	Number of Nodes
0,02	101586	443932

In the thermal analysis for the hexagonal ceramic block, the exhaust gas temperature was defined as 177 ^{0}C (450 K) and the air temperature value acting on the model was determined as 22 ^{0}C. Also the air convection coefficient is defined as 18 W / m^{2}K because of its natural convection. The results of the thermal analysis based on these parameters were observed.

The thermoelectric module that is showed the theoretical calculations in Section 3.1 is shown in Figure 6.

Figure 6. Properties of type SP1848-27145 thermoelectric power generation module [12].

The SP1848-27145 type thermoelectric module with dimensions 40 mm x 40 mm x 3.4 mm suitable for high power production in the design can withstand temperatures up to 150 ^{0}C. 6 piece of the SP1848-27145 type thermoelectric modules were used and all were connected in series. In thermoelectric

modules, a surface must be kept warm for power generation while the other surface needs to be cooled. In order to be able to cool the other surface of the thermoelectric module, 6 aluminum needle wing heat sink with 40 mm x 40 mm x 27 mm dimensions were used. The voltage and current values of the thermoelectric module used depending on the temperature difference are given in Table 3.

Table 3. Properties of type SP1848-27145 thermoelectric module [12].

Temperature Difference (ΔT)	Voltage (V)	Current (MA)
20	0,97	225
40	1,8	368
60	2,4	469
80	3,6	558
100	4,8	669

In thermoelectric modules, a surface must be kept warm for power generation while the other surface needs to be cooled. 6 aluminum needle wing heat sink with 40 mm x 40 mm x 27 mm dimensions were used in order to be able to cool the other surface of the thermoelectric module. The heat sink that designed to be easily manufactured, was assembled an aluminum plate with the screws. As shown in Figure 7, the reason for using the aluminum plate is to accelerate the cooling process. The plate can be preferred according to the outdoor temperature because the plate can be connected to the outer casing used in the heat sink and model.

Figure 7. Heat sink design

In this system which is carried out with natural convection, needle wing heat sink is preferred for increasing the air contact area and air flow direction.

Thermal analyzes were performed for low or high outdoor temperatures. In addition, as a result of the thermal-electric analysis performed for a pair of thermoelectric modules, the temperature value of the thermoelectric module to the ceramic base was determined and these values were used in the thermal analyzes for the heat sink. In the thermal analyzes for the heat sink, the air temperature values were accepted as 20 and 35 ^{0}C and the heat transfer coefficient of the air was accepted as 18 W / m^{2}K.

Shown in Figure 8, 70 mm x 38 mm x 30 mm dimensions K101 adjustable dc-dc voltage regulator card was used for voltage, current values can be adjusted in this modal which the mathematical model is formed and thermal and thermal-electrical analyzes are performed.

Figure 8. K101 200W adjustable dc-dc voltage regulator card [13]

For this card which known as dc dc voltage regulator, input and output voltage values and output current values are given in Table 4.

Table 4. Properties of dc dc voltage regulator card [13]

Voltage Value For Input	6 V - 35 V
Voltage Value For Output	6 V - 55 V
Current Value For Output	10 A

In the design, 2 outer crates are designed in order to protect the hexagonal ceramic block from the harsh outdoor conditions and to keep the thermoelectric generator constant in the tractor exhaust. These crates are connected to each other with screws. Also, screws and thermal paste were used for fixing other parts within the model.

The heat transfer coefficients of the materials used in the model are given in Table 5.

Table 5. Heat conduction coefficients of materials

Product name	Thermal Conductivity (W/mK)
Ceramic	4
Aluminium	237,5
Glass Wool	0,035
Thermal Paste	11

4. RESULTS

In this study, thermal analysis were performed for the hexagonal block and heat sink designed. Operating conditions of thermoelectric modules which were used according to the temperature values obtained as a result of these thermal analyzes were checked and the voltage, current and power values obtained from thermoelectric modules were found.

In the thermal analysis for the hexagonal block, the hot surface of the thermoelectric module and the temperature values affecting the silicon parts of the thermoelectric modules were found. In this context, the temperature values of the section in which the hexagonal block seen in Figure 9 comes into contact with the hot surface of the thermoelectric module were indicated. In the hexagonal model with a uniform temperature distribution as shown in Figure 10, temperature of about 113.51 ^{0}C was observed in the central part of the hot surface of the thermoelectric module. Also, this temperature value was observed to decrease slightly from the center of the hot surface of the thermoelectric module to the edge regions.

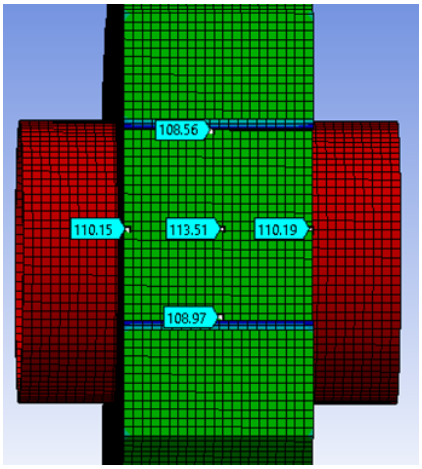

Figure 9. Temperature values on the hot surface of thermoelectric module

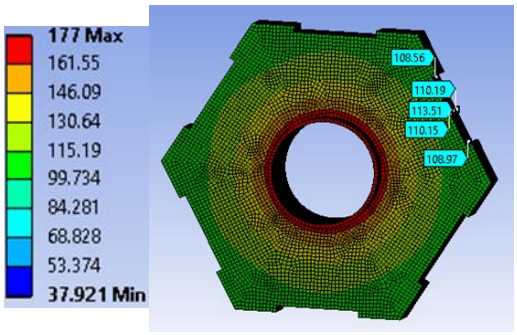

Figure 10. Temperature distribution in hexagonal block

The second thermal analysis for the hexagonal block was carried out to observe the effect of the glass wool used to prevent the silicon parts of the thermoelectric modules from being affected by the high temperature. As a result of the thermal analysis, the temperature value on the silicon sections is approximately 49,728 ^{0}C as seen in Figure 11. According to these results, the desired values of voltage, current and power were obtained and the designed hexagonal block was observed to be suitable for this purpose.

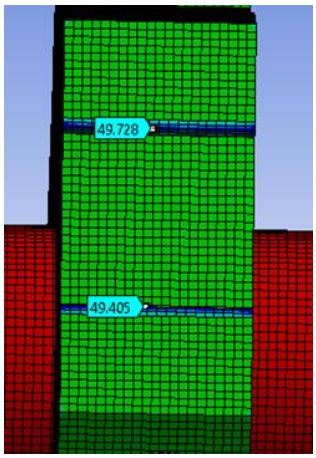

Figure 11. Temperature values affecting silicone surfaces

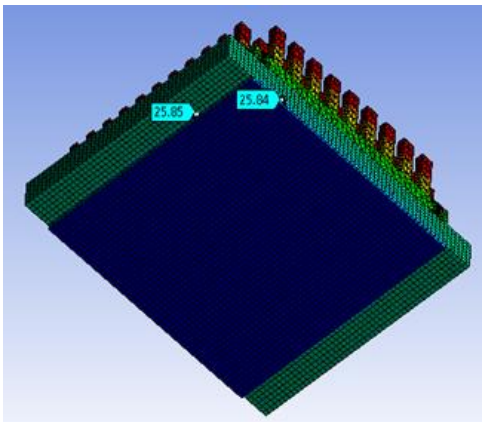

Şekil 13. Temperature at the cold surface of the thermoelectric module when the outdoor temperature is 35 ° C

The heat sink was used to cool the other surface of the thermoelectric module. It was aimed to perform natural convection cooling process depending on the outdoor temperature. In this context, 20 and 35 ^{0}C was indicated as the outdoor temperature. Also, the temperature of the bottom ceramic surface of the module has been determined as a result of the thermal-electric analysis for a pair leg of thermoelectric modules. In figure 12 and 13, thermal analysis was given for temperature values of 20 and 35 ^{0}C. According to the analysis process, the desired temperature values for the cold surface of the thermoelectric module were obtained.

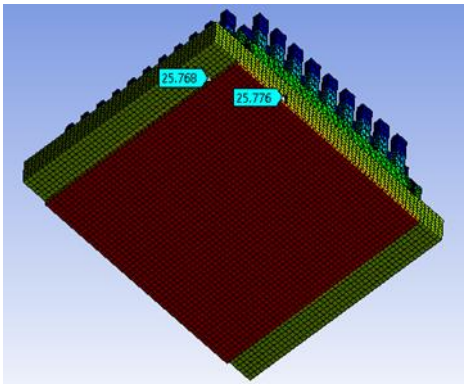

Şekil 12. Temperature at the cold surface of the thermoelectric module when the outdoor temperature is 20 ^{0}C

In the thermal analyzes performed for the heat sink design, the cooling process can be carried out without the use of the needle blade heat sink at the temperature values lower than the two temperature values used.

The working conditions of the outdoor environment, the conditions where the tractor is used, the temperature values of the exhaust gas etc. the temperature difference varies according to many variables. In this case, dc dc chopper card is used to adjust the current, voltage and power values. A total of 28,8 V voltage, 0,669 A current and 19,26 W power values were obtained from 6 thermoelectric modules. Thus, this power value which can be used either directly or by storage can be enabled to operate the electric parts of tractors and tractor trailers efficiently.

NOMENCLATURE

DC : Direct Current
FEM : Finite Element Method
FoM : Performance Criterion
K : Total Heat Conductivity Coefficient (W/K)
A : Cross Sectional Area, m^2
L : Length, m
V : Voltage, V
I : Current, A
W : Power, W

Q_H :The Amount of Heat Drawn From The Hot Surface of The Thermoelectric Generator
ΔT : Temperature Difference, ^{0}C
T_H : High Temperature, ^{0}C
T_L : Low Temperature, ^{0}C
S : Seebeck Coefficient, V/K
ρ : Resistivity , **Ω**m
k : Thermal Conductivity Coefficient, W/mK
R : Total Internal Resistance, **Ω**
R_L : Load Resistance, **Ω**
N : Number of Thermoelectric Leg Pair
η : Efficiency

REFERENCES

[1] İ. Temizer, Bir dizel motorunun performans ve emisyonları üzerine katkı maddelerinin etkisinin incelenmesi, *Yüksek Lisans Tezi*, *Fen Bilimleri Enstitüsü*, Elazığ, 2010.

[2] E. Dikmen, Fixing of factors what affects thermoelectric coolers working criteria and fields ofe use in industry, *Yüksek Lisans Tezi, Süleyman Demirel Üniversitesi Fen Bilimleri Enstitüsü*, Isparta, 2002.

[3] İ. Temizer, C. İlkılıç, C. Öner, Dizel motor egzoz sistemi için termoelektrik jeneratör uygulaması ve akış analizi, *Afyon Kocatepe University Journal of Science and Engineering*, 431-445, 2016.

[4] T. Kılıç, A study about recycling waste energy in buildings by using thermoelectric generators, *Yüksek Lisans Tezi, Mimar Sinan Güzel Sanatlar Üniversitesi Fen Bilimleri Enstitüsü*, İstanbul, 2010.

[5] B. Acar, M. Özkaymak, Ş. Baş, C. Yavuz, K. Boran, A.S. Tabak, H.İ. Varıyenli, Ö. Asal, Atık baca gazı kullanımı ile termoelektrik jeneratörlerde elektrik üretiminin faydalı kullanımının deneysel incelenmesi, *Gazi Üniversitesi Fen Bilimleri Dergisi*, 289-298, 2014.

[[6] M.M. Yaman, Güneş ısınımı ve termoelektrik malzemeler ile elektrik enerjisi üretimi, *Yüksek Lisans Tezi, Süleyman Demirel Üniversitesi Fen Bilimleri Enstitüsü*, Isparta, 2009.

[[7] R. Ahısta, H. Mamur, M. Uliş, Termoelektrik modülün jeneratör olarak modellenmesi ve deneysel çalışması, *Gazi Üniversitesi Mühendislik Mimarlık Fakültesi Dergisi*, 26, 4, 889-896, 2011.

[[8] Y. İslamoğlu, Termoelektrik enerji sistemleri: güç üretimi ve soğutma, *Termodinamik Dergisi*, 306, 66-70, 2018.

[9] A. Karabulut Kavaklı, Egzoz gazı ile çalışan absorbsiyonlu soğutma sisteminin otobüslerde kullanımı, *Yüksek Lisans Tezi, Balıkesir Üniversitesi Fen Bilimleri Enstitüsü*, Balıkesir, 2005.

[[10] E.E. Antonova, C.D. Looman, Finite Elements for Thermoelectric Device Analysis in ANSYS, *ANSYS Inc.* Southpointe, Technology Drive, Canonsburg, PA 15317, USA, 2005.

[[11] S. Rajadurai, M. Afnas, M. Ananth, S. Surendhar, Materials for automotive exhaust system, *International Journal of Recent Development in Engineering and Technology*, Volume 2, Issue 3, 82-89, 2014.

[[12] Url-1 https://robu.in/product/sp1848-27145-thermoelectric-power-generator-peltier-module-teg-120-degree/ (Accessed 31.12.2018).

[[13] Url-2 https://www.robolinkmarket.com/k101-200w-ayarlanabilir-dc-dc-voltaj-regulatoru.html (Accessed: 31.12.2018).

Paper 7 **Bildiri 7**

THE HEATING, EVAPORATION AND COMBUSTION OF KEROSENE DROPLETS IN A GAS-TURBINE COMBUSTOR: CFD MODELLING USING THE DISCRETE COMPONENT APPROACH

Mansour Al Qubeissi[1,2], Geng Wang[1], Nawar Al-Esawi[2], Oyuna Rybdylova[3], Sergei Sazhin[3]

[1]Faculty of Engineering, Environment and Computing, Coventry University, UK
[2]Institute for Future Transport and Cities, Coventry University, UK
[3]Advanced Engineering Centre, School of Computing, Environment and Mathematics, University of Brighton, UK

The modelling of heating, evaporation and combustion processes in a combustion system is crucial to its design and advancement [1,2], and essential to the assessment of the suitability of kerosene as an aviation fuel [3]. In this study, we have conducted a detailed analysis of kerosene fuel droplet heating and evaporation, using the previously developed discrete component model (DCM). Kerosene fuel composition (approximated by 44 components of the full composition reported in [4]) is replaced with 2 surrogate components to reduce the computational time. In contrast to the classical industrial analyses of aviation fuel (e.g. the distillation curve method [5]), the DCM takes into account gradients of species mass fractions in droplets. It is based on the analytical solutions to the heat transfer and species diffusion equations subject to appropriate boundary and initial conditions [6]. Numerical codes using these solutions were extensively verified and validated in [7–9]. The effective thermal conductivity and effective diffusivity approaches for moving droplets are used in the model.

The DCM was implemented in the commercial CFD software of ANSYS-Fluent which was applied to study the processes in a combustor. The computational domain is shown in Figure 1. A polyhedral mesh was used for the hydrodynamic model, as shown in Figure 2. This opened opportunities for the simulation of the full combustion cycle. The influence of droplet evaporation on the combustion process was investigated.

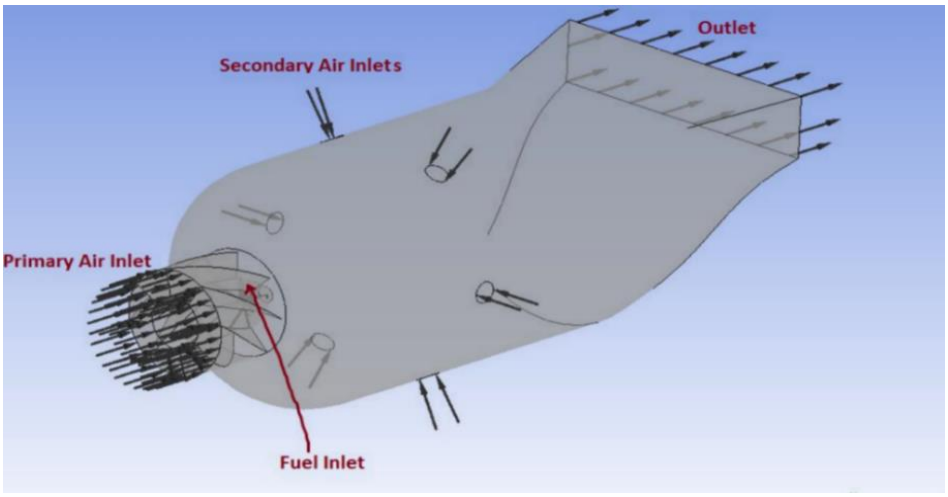

Figure 1. The can combustor geometry used in our CFD simulation.

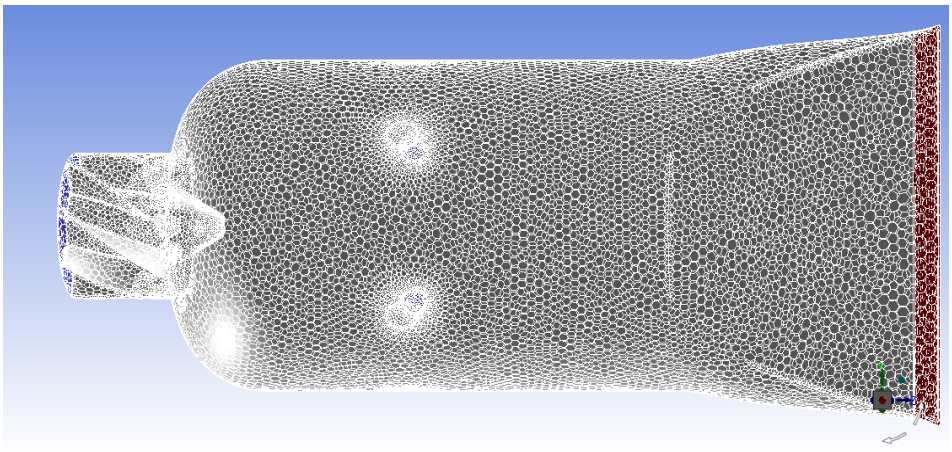

Figure 2. The mesh used for the combustor simulation.

The analysis was applied to a balanced mixture of kerosene and diesel fuels, represented in the ANSYS-Fluent database by $C_{12}H_{23}$ and $C_{10}H_{22}$, respectively. The initial droplet diameter and temperature were 100 µm and 375 K, respectively. The ambient gas temperature and pressure were 800 K and 4 bar, respectively. A co-axial air-blast atomizer was used with air and fuel mass flowrates of 0.175 kg/s and 0.003 kg/s, respectively, and an injection speed of 1 m/s. As shown in Figure 3, the evolution of droplet radii with time was predicted using three approaches, namely: 1) the results predicted by standard ANSYS Fluent software using constant properties; 2) the results predicted by ANSYS Fluent with the implementation of transient properties of fuel composition using the user defined function (udf), but without the DCM; and 3) ANSYS Fluent results with full implementation of the DCM and transient thermodynamic and transport properties.

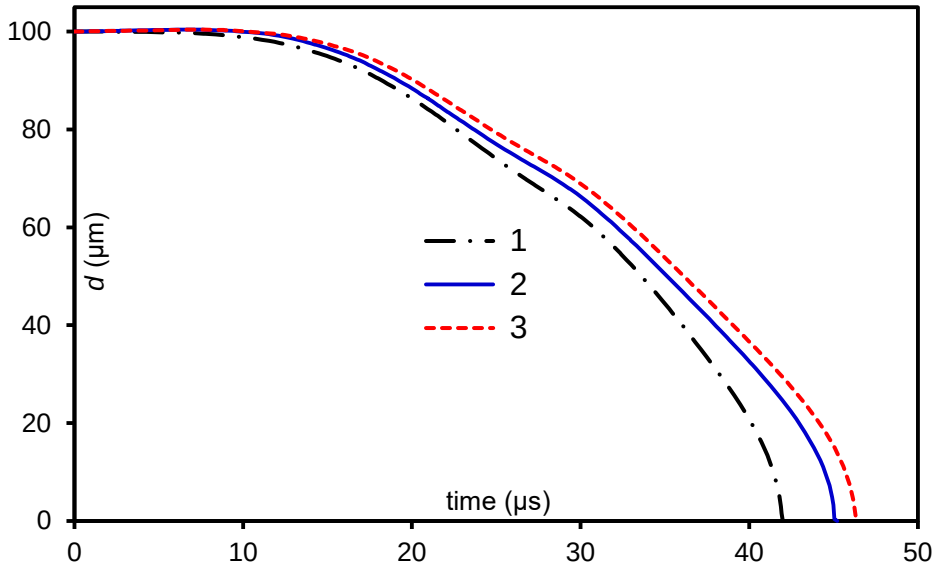

Figure 3. The evolutions of droplet diameter using the three modelling approaches: 1 refers to Standard ANSYS Fluent results, with constant properties, 2 refers to ANSYS Fluent results, with in-house properties using udf, and 3 refers to ANSYS fluent results with the in-house developed DCM using udf.

The preliminary results show that the maximal impact of incorporating the DCM into the ANSYS-Fluent prediction of droplet evaporation is up to 10.4% compared to the case when a standard ANSYS-Fluent model is used. Also, our results indicate that the fuel composition and temperature gradient inside droplets, which are ignored in the standard ANSYS Fluent model, can lead to noticeable impact on the spray formation and combustion processes. The new results have been compared with those reported in the literature [12] (see Figure 4) for kerosene droplets of 1.8 mm initial diameter.

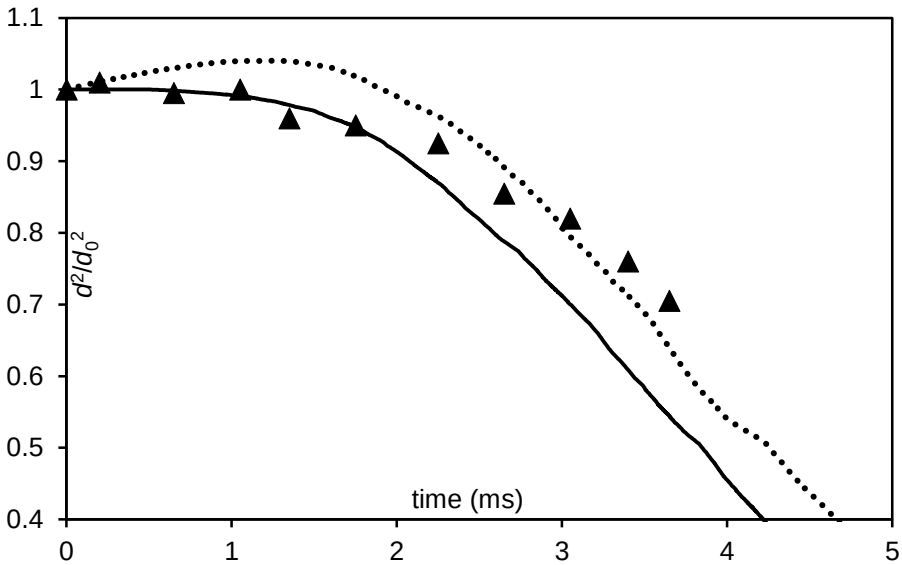

Figure 4. The validation of the models for the normalised droplet diameters squared predicted by the standard ANSYS-Fluent (solid curve), and ANSYS-Fluent with the DCM udf (dotted curve), using data reported in [12] (bold triangles) for kerosene fuel.

As can be seen from Figure 4, general agreement between the numerical results and experimental data was found. In our analyses, we considered the impact of thermal-swelling on droplet evaporation. Finally, the combustion of the blended fuel droplets was simulated, and the influence of fuel evaporation and species diffusion on flame properties was investigated and will be presented in the full paper.

Keywords: Aviation fuel, CFD model, Combustion, Droplet evaporation, Gas turbine, Kerosene

Acknowledgement

The authors are grateful to the Institute for Future Transport and Cities – Coventry University (Grant No. ECR019), and the EPSRC (Grant No. EP/R012024/1) for providing financial support for this project.

REFERENCES

[1] Al Qubeissi, M., 2018, "Predictions of Droplet Heating and Evaporation: An Application to Biodiesel, Diesel, Gasoline and Blended Fuels," Applied Thermal Engineering, 136(C), pp. 260–267.

[2] Sazhin, S. S., 2014, *Droplets and Sprays*, Springer, London.

[3] Jones, E. G., and Balster, L. M., 1997, "Impact of Additives on the Autoxidation of a Thermally Stable Aviation Fuel," Energy & Fuels, 11(3), pp. 610–614.

[4] Lissitsyna, K., Huertas, S., Quintero, L. C., and Polo, L. M., 2014, "PIONA Analysis of Kerosene by Comprehensive Two-Dimensional Gas Chromatography Coupled to Time of Flight Mass Spectrometry," Fuel, 116, pp. 716–722.

[5] Lovestead, T. M., and Bruno, T. J., 2009, "Application of the Advanced Distillation Curve Method to the Aviation Fuel Avgas 100LL," Energy & Fuels, 23(4), pp. 2176–2183.

[6] Sazhin, S. S., 2017, "Modelling of Fuel Droplet Heating and Evaporation: Recent Results and Unsolved Problems," Fuel, 196, pp. 69–101.

[7] Al Qubeissi, M., Al-Esawi, N., Sazhin, S. S., and Ghaleeh, M., 2018, "Ethanol/Gasoline Droplet Heating and Evaporation: Effects of Fuel Blends and Ambient Conditions," Energy & Fuels, 32(6), pp. 6498–6506.

[8] Sazhin, S. S., Elwardany, A. E., Krutitskii, P. A., Deprédurand, V., Castanet, G., Lemoine, F., Sazhina, E. M., and Heikal, M. R., 2011, "Multi-Component Droplet Heating and Evaporation:

Numerical Simulation versus Experimental Data," International Journal of Thermal Sciences, 50(7), pp. 1164–1180.

[9] Elwardany, A. E., Sazhin, S. S., and Im, H. G., 2016, "A New Formulation of Physical Surrogates of FACE A Gasoline Fuel Based on Heating and Evaporation Characteristics," Fuel, 176, pp. 56–62.

[10] Al Qubeissi, M., 2015, *Heating and Evaporation of Multi-Component Fuel Droplets*, WiSa, Stuttgart.

[11] Sazhin, S. S., Al Qubeissi, M., Kolodnytska, R., Elwardany, A. E., Nasiri, R., and Heikal, M. R., 2014, "Modelling of Biodiesel Fuel Droplet Heating and Evaporation," Fuel, 115, pp. 559–572.

[12] Wang, F., Liu, R., Li, M., Yao, J., and Jin, J., 2018, "Kerosene Evaporation Rate in High Temperature Air Stationary and Convective Environment," Fuel, 211, pp. 582–590.

Paper 8 **Bildiri 8**

BIOGAS TECHNOLOGY CONSIDERING ENERGY SECURITY AND SUSTAINABILITY

Cemil Koyunoglu[1,2*], Ece Polat[3]

[1]Energy Institute, Istanbul Technical University, Ayazaga Campus, 34469, Istanbul, Turkey

[2]Energy System Engineering Department, Yalova University, Çınarcik Campus, 77200, Yalova, Turkey

[2]Department of Environmental Engineering, Gebze Technical University, Gebze, 41400Turkey

Energy security for countries is today's topic for the availability of energy sources at an affordable price. Apart from the energy security, maintaining the sustainability on earth is important topic. More research on solar energy, wind energy, biogas and biofuels has been still stimulated by energy sector when environmental considerations are taken into account. Biogas energy is based on the principle of obtaining energy from organic wastes. Biogas technology is preferred technology when organic waste amount and energy production is taken into account. European Biogas Association (EBA) stated that energy produced from biogas has been on rise in the European markets. According to "The Biogas Report 2013", the total annual power consumption of households in Belgium and Slovenia was equal to the total amount of energy produced from European biogas plants. The report stated that more than 14,500 biogas plants are operational in Europe and the number is growing steadily. Hungary, the Czech Republic, Slovakia and Poland are the top European biogas markets. For Europe's energy security and decarbonisation, biogas-based energy is important. While Germany and Italy are among the biggest biogas contributors in Europe, the predictions are not too optimistic for them as well as some other European markets. In this part of review, the energy security and biogas technology in Turkey, Georgia and Bulgaria countries is expressed.

Keywords; Energy security, sustainability, decarbonisation, biogas

*Corresponding Author, Cemil Koyunoglu ckoyunoglu@itu.edu.tr

IMPORTANCE OF ENERGY SECURITY

Energy security is an important issue for the communities whose life depends on continuous energy supply. For the definition of energy security energy availability, prices, economic and social welfare of the society are taken into consideration [1].

The following seven themes represent the energy security: energy availability, infrastructure, energy prices, social effects, environment, governance and energy efficiency.

- **Energy availability** relies on geopolitical factors and heterogeneity of energy supply sources [1]. Especially, regional tensions tend to change the mode of the energy supply (oil supply, gas supply etc.) and transport of energy can change the availability of energy sources.
- **Infrastructure** represent the energy related transformation facilities such as pipelines, substations, oil refineries, thermal power plants. These facilities are important for continuous supply of energy with sufficient amount [1].
- **Energy prices** rule the affordability of energy supplies using energy market and price level of the energy supply [1].
- **Social effects** maintain the energy related living environment of the people [1].
- **Environment** concerns energy related carbon, nitrogen and other gas emissions in terms of global warming and especially focusing on the air pollution [1].
- **Governance** concerns the policies that protect the short-term energy breaks related to infrastructure problems and use taxes to overcome these concerns [1].
- **Energy efficiency** can lower the amount of required energy for energy utilization providing low energy intensity [1].

In addition to that, researchers are investigating risk of energy security to maintain the energy performance of countries [1]. The performance of energy can be measured using indicators and indexes by subjective manner [1]. For instance, Patlitzianas et al. [2] has investigated the security of energy supply, competitive energy market and environmental protection using 36 sustainable energy policy indicators mainly composed of dependence on imports of solid fuel, dependence on oil imports, dependence on natural gas imports and differentiation of primary fuel.

Specific focused areas (SFA) in index construction for energy security are taken into account while SFA-3 specifically concern the economic dimensions of the energy; SFA-5 is based on social dimensions [1]. For example, Sovacool and Brown [3] investigated 10 indicators using SFA-2, SFA-4 and SFA-6. In addition to that, normalization of indicators, weighting the normalized indicator and aggregating of the normalized indicators are required for construction of whole energy security index [1].

"Energy trilemma is defined as balancing the trade-offs between three major energy goals, namely energy security, economic competitiveness, and environmental sustainability" as stated by Ang et al. [1]. The schematic representation is shown in Figure 1. For countries that concern both energy security and economic competitiveness should take in to account the energy prices and infrastructure costs. However, when environmental sustainability and energy security are considered energy efficiency and clean and low carbon energy sources should be favored.

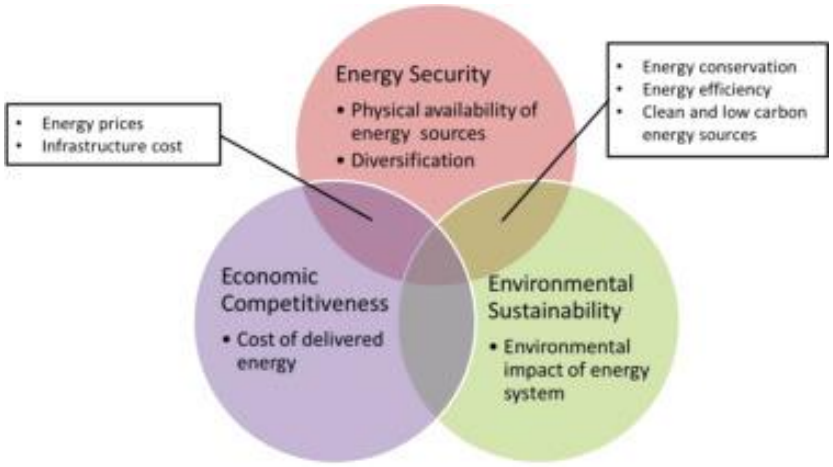

Figure 1. Energy security and relation with economy and sustainability [1]

ENERGY STRATEGIES OF SOME COUNTRIES

When energy security is considered, the energy strategies in countries are important topic for evaluating the energy performance and energy efficiency. The following 2.1 and 2.2 will maintain the current energy strategies of Turkey, Georgia and Bulgaria. Figure 2 shows the Turkey and Turkey's eight neighbor countries.

Figure 2. Energy security and relation with economy and sustainability [4]

Energy Strategy of Turkey

When we look at the geography, Turkey (we) as a part of Eurasia, have many natural gas routes and oil routes of Eurasia as shown in Figure 3a and Figure 3b. As it is known that around 70% of the world oil and natural gas reserves are found in East, Turkey stands as a bridge between the source donor and source acceptor countries [4] and these provide Turkey a geopolitical and geostrategic importance. Energy projects that involve Turkey can improve the employment status, also. For instance, in Baku–Tbilisi–Ceyhan project ten thousand people were employed and there are also huge number of employment for both Shah Deniz oil field and interconnector natural gas line Turkey-Greece-Italy. Whit these projects natural gas consumption amount in Turkey was increased up to 64% and gas pipeline length is increased up to 11000 kilometers [4].

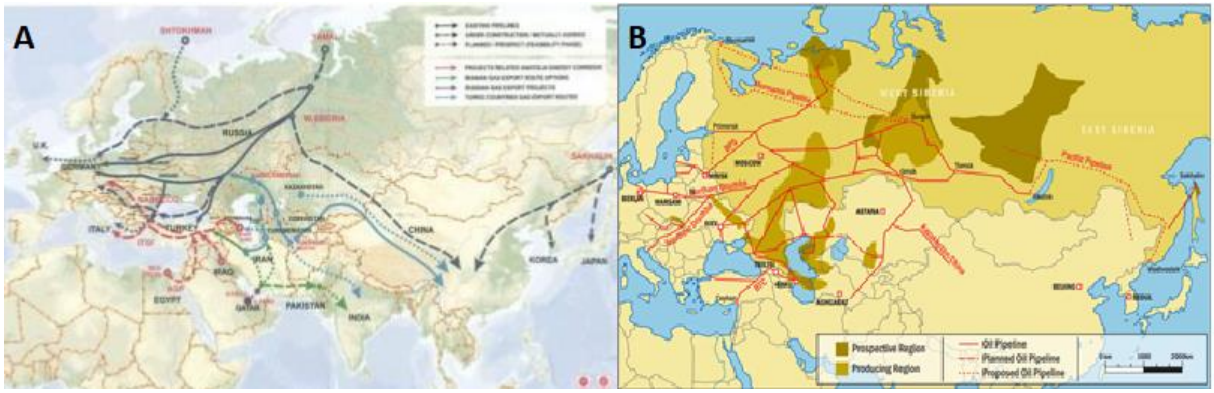

Figure 3. Natural gas and oil routes in Eurasia [5, 6]

Energy productivity has become important as taking into account both environment and depleting water sources. ENVER project become important for energy productivity issues and

as “enver” means “illumination” in Turkish, this project will maintain the efficient energy consumption considering even bulb changing in houses [4]. YERSAN is another project in which turbines, solar energy panels, drilling machines, and geo–thermal and geo–spring equipment are manufactured as a part of domestic industry [4]. Turkey’s new strategic goals are turning from energy corridor to energy terminal, changing the position of exporter to importer and switching from resource geography to transit geography [4].

Energy Strategy of Georgia and Bulgaria

Georgia is the country that enrolls the entire process of power generation in the Caucasus and Black See regions and use of the Caspian Sea oil and gas [4]. Their main aim is supplying full energy transition regarding to energy sustainability, competitive energy supply so they invested on energy market securities such as in 2007, Georgia spent 60 million USD for regeneration, and rehabilitation of the exiting gas pipelines [4]. Between 2009 and 2012, the project named High Voltage Interconnection Project provide the Black Sea Electricity Ring and strengthened East–West Power Bridge [4].

Bulgaria is the country that contribute the energy security of Balkans [4]. In 2009, Bulgaria and Greece signed Gas Interconnector Greece-Bulgaria project that covers the biflow pipeline between two countries, which may reduce the Bosphorus Straits, and risk of accidents in Bosphorus [4]. Bulgaria’s strategic role will provide more secure energy supply in the Balkan region and Bulgaria has also many investments on nuclear energy and hydroelectric power energy that has regional importance [4].

BIOGAS TECHNOLOGY

Composting and anaerobic digestion technologies are main Technologies that are used for waste management due to the constraints of land [7]. Anaerobic digestion is handled under anaerobic conditions and organic materials in the waste are transformed into another form biologically. The final products of anaerobic digestion process are biogas (mainly composed of methane and carbon dioxide) and other organic residues called digestate that may potential application on soils as a plant growth supporter [7]. The anaerobic digestion process is important for researchers as being supply 100–150 kWh energy per treated tons of waste [7].

Biogas production is a process involving complex microorganisms mainly composed of acetogenic bacteria and methanogenic bacteria. By the time acetogenic bacteria produce acids, methanogenic bacteria involves in methane production using either acetic acid or hydrogen [8].

There four main reactions in anaerobic digestion hydrolysis, acidogenesis, acetogenesis and methanogenesis [9]. Hydrolysis is the step in which fats, lipids, carbohydrates and proteins degraded into fatty acids, simple sugars and amino acids by using extracellular enzymes. These degradation products can be converted into alcohols or volatile organic acids by the active involvement of intracellular enzymes of acidogenic bacteria as part of acidogenesis. Acetogenesis is the third step of this digestion pathway and alcohol or volatile organic acids are converted into acetics or hydrogen and carbon dioxide by acetogenic bacteria or hydrogengenic bacteria. The final product of methane is generated using these products (acetics, hydrogen, carbondioxide) by methanogenic bacteria.

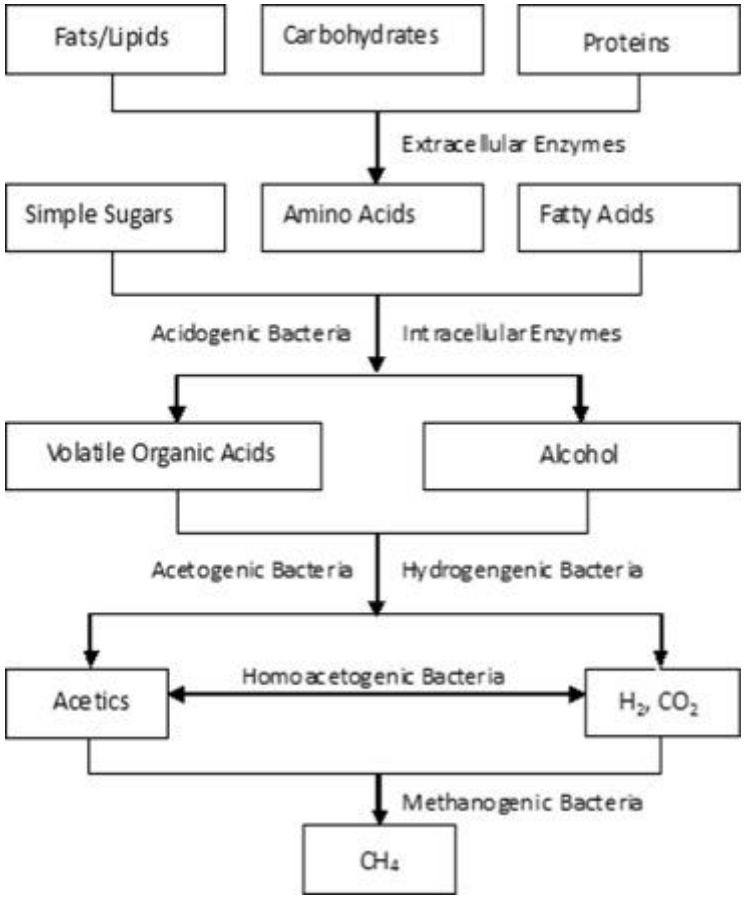

Figure 4. Anaerobic digestion reactions [9].

Operating temperature, reactor volume, solid content, organic loading rate, toxic compounds, nutrient balance, carbon to nitrogen ratio, microorganisms' degradation pattern can affect the biological activity of the microorganisms, biogas and methane yield of an anaerobic digestion reactor [8, 10].

Turkey's Biogas Technology

Biogas production potential in Turkey has been estimated at 1.0–1.5 million tonnes of equivalent petrol (MTEP) [11]. In 2010, 10 license biogas facility with 16.4 MW energy potential shared the %23 of the total bioenergy of Turkey [11]. It is also indicated that % 85 of the total biogas energy come from animal waste [11]. According to 2014 data, biomass energy in Turkey maintain only 4.9% of the total energy demand and only 0.09% of this energy come from biogas [11]. The Figure 5 shows the projected electricity generation form different sources in Turkey and the biomass and biogas sector is growing rapidly while hydropower based electricity generation is remained stable.

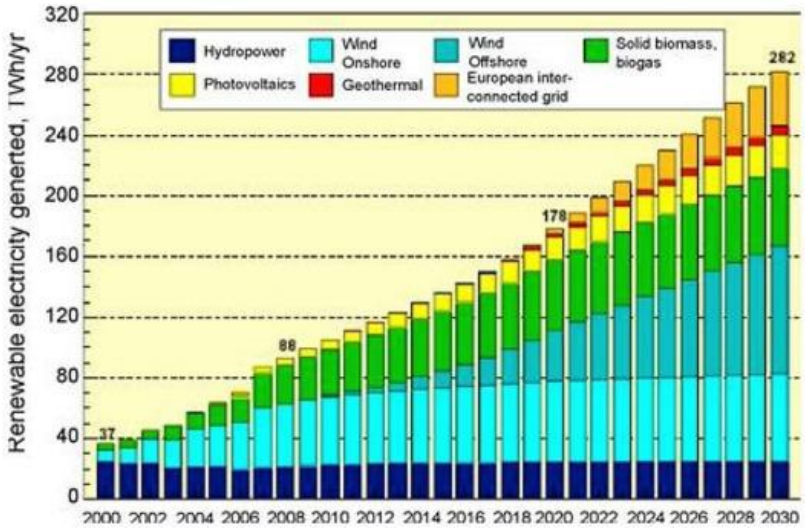

Figure 5. Installed bioenergy capacity of Turkey [11].

In addition to that, "It is estimated that the biomass potential in Turkey is about 8,6 million tonnes of equivalent petrol (MTEP), and biogas quantities that can be produced from this biomass is 1,5-2 MTEP [12]. It is also stated that in 2018, 216 GWh electricity was generated from biomass power plants with a total installed capacity of 811 MW [12].

Georgia's and Bulgaria's Biogas Technology

Georgia has great potential for biomass energy as having suitable geographical position and climate conditions [13]. Generally, residential waste in Georgia does not converted into energy generation processes and only the waste in Tbilisi and Kutaisi dumps which is equivalent to 900000 tons of waste and 2700 GWh of energy can produce 64 million m^3 natural gas and 90 million m^3 biogas [13]. The biogas potential of Georgia is estimated as 3-4 TWh and there approximately 400 biogas plants in Georgia [13].

By the time Bulgaria has great potential on biogas generation, the technology is not as common as the applications in Georgia. Bulgaria supports the use of renewable energy sources According to Directive 2009/28/EC [14]. Bulgaria's 2016 renewable energy based electricity production was only the 19% of the total energy demand [15]. In addition to that, while 66% of this energy was solid biomass for heat, 30% of this energy remain hydropower and wind energy.

Conclusions

Energy security is an urgent field for covering the global energy demand and energy policy. To maintain the efficient and affordable energy production many energy production technologies are being developed concerning the efficiency of conversion processes. Renewable energy sources are demanding energy production sources but not commonly used by countries based on prices and other installation limitations.

Biogas technology is the developing technology in which waste, even municipal solid waste can be used to obtain energy and minimizing the pollutants. Land application of the final solid products can also be important for providing fertilizer to soil. However, there are still some limitations and bottlenecks that the biogas technology is not commonly used in most of the Eurasia countries. Companies to widespread can promote biogas market and biogas projects to increase the number of biogas plants in countries.

REFERENCES

[1] Ang BW, Choong WL, Ng TS. Energy security: Definitions, dimensions and indexes. 2015.

[2] Patlitzianas KD, Doukas H, Kagiannas AG, Psarras J. Sustainable energy policy indicators: Review and recommendations. Renewable Energy 2008;33(5):966-73.

[3] Pasqualetti M. Energy and American Society: Thirteen Myths. 2008.

[4] drivingdirectionsandmaps. turkey map. drivingdirectionsandmaps; 2019.

[5] Çıngı İ. Seeking of common resolution for energy security. In: Sezgin O, ed. *Seeking of common resolution for energy security.* Istanbul: Mehmet Ali Çelik; 2009.

[6] korea-cbms.ethz.ch. Oil Pipelines. In: korea-cbms.ethz.ch, ed. Korea: korea-cbms.ethz.ch; 2019.

[7] Guven H, Akca MS, Iren E, Keles F, Ozturk I, Altinbas M. Co-digestion performance of organic fraction of municipal solid waste with leachate: Preliminary studies. Waste Management 2018;71:775-84.

[8] Halis Deviren Ci, Selman Aydın. Biyogaz Üretiminde Kullanılabilen Materyaller ve Biyogazın Kullanım Alanları. Batman University Journal of Life Sciences 2017;7(2):2.

[9] Mao C, Feng Y, Wang X, Ren G. Review on research achievements of biogas from anaerobic digestion. Renewable and Sustainable Energy Reviews 2015;45:540-55.

[10] Du Shin J, Won Park S, Lee S-I, Kim H, Lee S-R, Suk Kim M, et al. Effects of digestion temperatures and loading amounts on methane production from anaerobic digestion with crop residues. 2015.

[11] Toklu E. Biomass energy potential and utilization in Turkey. 2017.

[12] Turkey EGo. Bio-Fuels; 2018. Available from: https://enerji.gov.tr/en-US/Pages/Bio-Fuels. 2019].

[13] Elena Gvilava LG. Reinforcing cooperation with ENP countries on bridging the gap between energy research and energy innovation. Estonia: Energy Efficiency Centre Georgia (EEC); 2014.

[14] David Guentert DR, Libert Yavychev. Permitting procedures for biogas plants in Bulgaria, Croatia, Czech Republic, Greece, Latvia, Romania and Slovenia. *IEE Project.* WIP Renewable Energies; 2012.

[15] Mikalauskiene A, Streimikis J, Mikalauskas I, Stankūnienė G, Dapkus R. Comparative Assessment of Climate Change Mitigation Policies in Fuel Combustion Sector of Lithuania and Bulgaria. 2019.

Paper 9 **Bildiri 9**

NUMERICAL AND EXPERIMENTAL STUDY OF COLD EGR IMPACT ON THE PERFORMANCE AND EMISSIONS OF A BIODIESEL ENGINE

Alex de Oliveira,[1] Junfeng Yang,[2] and José Ricardo Sodré[3]

[1] Department of Mechanical Engineering, Pontifical Catholic University of Minas Gerais, Belo Horizonte, 30535-610, Brazil.
[2] School of Mechanical Engineering, Institute, University of Leeds, Leeds, LS2 9JT, UK.

[3] School of Engineering and the Built Environment, Birmingham City University, Birmingham, B4 7XG, UK.

Correspondence should be addressed to Junfeng Yang; J.Yang@leeds.ac.uk

Abstract

This work evaluated the effects of the application of the exhaust gas recirculation (EGR) on fuel consumption and pollutant emissions from a diesel engine fuelled by a blend of diesel oil (92%) and biodiesel (8%) (B8). The engine was adapted with an EGR system, including an EGR cooler and an electronic control system to control the EGR ratio. Experiments were carried out in a Diesel power generator with nominal power of 49 kW, with varying loads from 5 kW to 35 kW, B8 diesel fuel and 10% of cold EGR ratio. Carbon dioxide (CO_2), carbon monoxide (CO), oxygen (O_2), total unburned hydrocarbons (THC), nitric oxide (NO) and oxides of nitrogen (NO_X) emissions were evaluated. The results showed slight effects of EGR use in the engine specific fuel consumption, fuel conversion efficiency and in-cylinder pressure. THC and NO_X emissions were reduced up to 52% and 59%, respectively, on the other hand, CO_2 and CO emissions increased up to 19% and 155%, respectively. A numerical study, using *ANSYS Forte* software, on the effects of EGR use on NO formation was performed, for the load of 30 kW, and showed that the reduction of this component is obtained mainly by reducing the availability of oxygen and reducing the combustion temperature.

INTRODUCTION

Over the last decades, the allowable limits of internal combustion engine pollutant emissions has been reduced, as a consequence of continuous growth of environmental pollution and increasing concern for the environment and air quality [1,2]. Therefore, there are some challenges to ensure a sustainable economic growth. The use of biofuels in internal combustion engines has been encouraged by several researchers [3].

The biodiesel is a fuel derived from vegetable oil via transesterification reactions [3]. It is produced commercially all over the world as an alternative fuel that can replace conventional fossil diesel in many applications. The methyl or ethyl esters are referred to as biodiesel because their liquid and thermochemical properties are like those of conventional diesel, which allows it to be used without having to significantly modify an original diesel engine.

The advantages of using biodiesel include: it generates relatively low emissions of several key pollutants in the engine's exhaust [4–6], it is a renewable fuel, it has excellent lubricity properties and high flash point, making it safer to store [6,7]. Some current disadvantages of using biodiesel include relatively high emissions of nitrogen oxides exhaust [4–6,8] decreased oxidative stability, worse cold-flow performance than petroleum diesel [7], and dilution of lubricating fluids due to fuel impingement on in-cylinder surfaces when early- or late- injection strategies are employed [9].

In the last years, oxides of nitrogen (NO_X) and particulate matters (PM) emissions become more and more stringent and several technologies have been developed to reduce the emissions of these toxic components [10]. The NO_X mitigation technologies can be divided into two categories: pre-combustion and post-combustion technologies [11]. The main pre-combustion technologies are the addition of additives into fuel, exhaust gas recirculation (EGR), water injection, use of alternative fuel and injection timing retardation. Post-combustion technologies treatments are extensively used in diesel engines, as the NO_X absorber catalyst (NAC), selective catalytic reduction (SCR), selective non-catalytic reduction (SNCR) and DeNOX (lean NO_X) catalysts [11–13].

In the exhaust gas recirculation technique, a portion of the engine exhaust gas is added to the intake air via the intake system. The application of this technique has potential to reduce NO_X emission of spark ignition and compression ignition engines and to realize low temperature combustion (LTC) technique [14]. Several studies showed that this reduction results from thermal, chemical and dilution effects [11,15,16].

Ladommatos et al. [17–20] showed these effects simulating the application of EGR adding synthetic gases in the intake air. The main components of diesel engines exhaust gas are carbon dioxide (CO_2)

and water (H_2O), which have higher specific heat than the replaced oxygen (O_2) and nitrogen (N_2). The higher specific heat reduces the combustion temperature, representing the thermal effect. The reduction of oxygen content of the intake air, i.e., the dilution effect, also causes a reduction in the local flame temperature because of the spatial broadening of the flame. The dissociation of the recirculated H_2O and CO_2, during the combustion, occurs in an endothermic process and reduces the flame temperature. These processes modify the NO_X formation process. The use of cooled EGR reduces NO_X effectively compared to hot EGR but regarding brake thermal efficiency hot EGR is better than cold EGR [21] .

One of the main reported disadvantages of the use of EGR is the increase of particulate matter (PM) emissions, well-known as PM-NO_X trade-off. Asad et al. [13] suggested that this conflict can be reduced applying low temperature combustion techniques (LTC), where the event of the injection of diesel fuel is separated from the combustion, aiming to reduce NO_X emissions and soot simultaneously. Divekar et al. [22] suggested the use of diesel engine in dual fuel mode to reduce both NO_X and soot emissions.

Internal combustion engines simulation tools have become widely available due to the increase of the accuracy of turbulence, spray and chemistry models [23]. The numerical tools have been used to investigate different engine combustion characteristics, such as the effects of the use of EGR [24], knock resistance [25], soot formation [26], dual fuel operation [27–29], injection strategies [30] and study of the fuel sprays [31,32]. Yang et al. [33] studied methods for reduction of detailed reaction mechanism for the combustion of biodiesel fuels. The authors applied the reduced mechanism in the *ANSYS Forte* CFD simulation package and the modelling results demonstrate the effects of the start of injection (SOI) and exhaust gas recirculation (EGR) on a biodiesel engine performance.

Mardi et al. [34] investigated the effects of EGR on the emissions and performance of a spark ignition engine using a computational fluid dynamics method. The authors used the AVL FIRE CFD code to solve the flow field equations for the closed cycle of the engine. The numerical simulation with different fuels and EGR conditions allowed the understanding of the formation of different emissions components, such as NO_X and CO, and showed significant reduction of NO_X emissions. Galloni et al. [35] also presented numerical results using AVL FIRE exploring the potential of EGR in a spark-ignition engine under different operating points.

Accordingly to Shi et al. [10] Biodiesel and EGR have been studied in many researches, but the combination of these two technologies is relatively few. An improved understanding of the mechanisms responsible for the high NO_X emissions generated during biodiesel and diesel oil combustion could lead to inexpensive and effective mitigation strategies. Computational modelling of biodiesel and diesel oil spray combustion is an attractive tool for obtaining new insights into the origins of the NO_X emissions. Therefore, this work presents experimental results of a diesel a 49 kW stationary diesel engine operating with diesel fuel containing 8% biodiesel (B8) and 10% of cold EGR rate, including performance and

emissions data. A computational study based on a three-dimensional modelling, using the *ANSYS Forte*, code was conducted to better understand the formation of NO.

Materials and Methods

Experimental Methodology

The experimental and numerical studies were developed based in a production, naturally-aspirated, four-stroke, four-cylinder diesel engine, with the main characteristics present in Table 1.

Table 1. Diesel engine specifications

Manufacture/Type	MWM 229/4
Cycle	Four strokes
Diesel oil injection	Direct
Bore × stroke	102 mm × 120 mm
Number of cylinders	4, in line
Compression ratio	17:1
Total displacement	3.922 L
Rated Power	44 kW
Intake system	Naturally aspirated
Start of injection	23°BTDC

The engine diesel is equipped with a mechanically controlled injection system and the fuel injection settings were not changed during the studies. The diesel injector has four holes with diameter of 0.3 mm. For recirculation of the exhaust gas, an appropriate pipeline was installed with a water cooling heat exchanger. The EGR quantity was regulated by an electric valve installed in the EGR loop. An electronic system was developed to control the valve position, the EGR rate (%) fixed at 10% and the intake air temperature at 40°C, when using EGR.

The main measured parameters during the experiments were: temperature in different positions, fuel consumption, intake air mass flow rate and humidity, ambient conditions, engine load, CO_2, CO, O_2, total unburned hydrocarbons (THC), NO, NO_X emissions and in-cylinder pressure. All experimental data were acquired by a data and acquisition system built in LabVIEW platform. Figure 1 shows the test cell layout and the measurement device specifications are shown in the Appendix A.

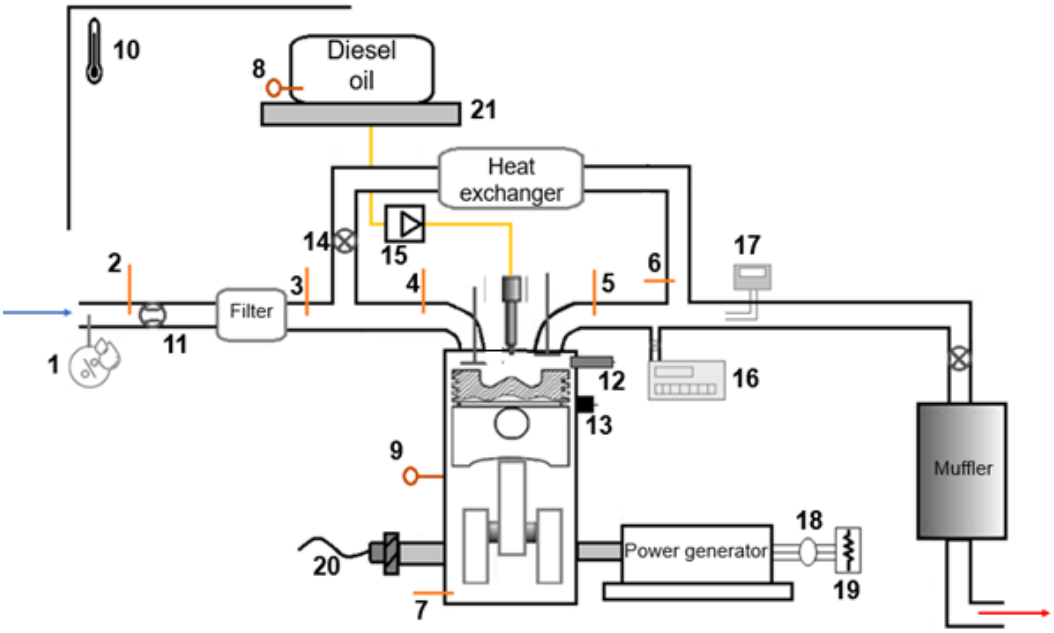

1	Thermohygrometer	8	Thermoresistor: diesel oil	15	Diesel oil mechanical pump
2	Thermocouple: fresh air	9	Thermoresistor: cooling water	16	Gas analyser
3	Thermocouple: fresh air	10	Barometer: atmospheric pressure	17	Opacimeter
4	Thermocouple: fresh air + exhaust gas	11	Mass airflow sensor	18	Power transducer
5	Thermocouple: exhaust gas	12	In-cylinder pressure sensor	19	Load bank
6	Thermocouple: recirculated gas	13	Knock sensor	20	Encoder
7	Thermocouple: crankcase oil	14	EGR valve	21	Platform balance

Figure 1. Schematics of the experimental apparatus

The tests were conducted using diesel oil containing 8% biodiesel (B8), due to the Brazilian government law No. 13263/2016 [36], which established the compulsory addition of biodiesel to diesel oil to 8% from March 2017. Common biodiesels include Rapeseed Methyl Ester (RME), Soybean Methyl Ester (SME), and Palm Methyl Ester (PME). At present, most of the biodiesel produced in Brazil is derived from soybeans. The tests were conducted without the EGR system (B8) and with 10% of EGR rate (B8 + EGR). Three tests were conducted for each engine condition, varying the engine loads from 5 kW to 35 kW and according to ISO 3046-1:2002 standard. The readings at each test were performed after the engine reached the steady-state condition, observing the exhaust gas and the cooling water temperatures. The load power and fuel consumption results were corrected to ambient standard conditions. The average results

are presented, and the combined standard uncertainty of the results is a combination of both the statistical spread and the instrument uncertainty.

NUMERICAL METHODOLOGY

The numerical simulation of the combustion phenomenon is a complex problem and it is constant development. In this work, the commercial code *ANSYS Forte* 18.1 was used to simulate the combustion process of a diesel engine. It is a computational software for three-dimensional modelling of internal combustion engines, which incorporates a technology to allow the use of multicomponent fuel models in a comprehensive study of liquid spray, without high computational time requirements. *ANSYS Forte* provides precise chemical models that allow good results without the need for specialized calibration.

When injecting a fuel into the stream, functions are included to account the iteration of the gas phase and the liquid droplets. The main considerations involving the derivation of the governing equations are the use of the ideal gas law for the gas phase state equation, the use of the Fick law for mass diffusion and the use of the Fourier law for thermal diffusion.

Essentially, three separated, but coupled, systems involve the combustion process: the fluid, described by the conservation equation of continuum mechanics; the iteration between the various fluid chemical species, which react kinetically and in equilibrium; and the iteration between the droplets of the injected fuel and the reactive fluid. The equations governing the coupled system are [37]:

a) The equations of compressible fluid dynamics: equations of conservation of mass, momentum and energy and the equations of state;

b) Kinetic and equilibrium chemical reactions: the reaction equations couple to the equations of the fluid by terms that describe the increase or reduction of the densities of the various chemical species while they react. Heat sources are added to the fluid energy equation for kinetic reactions;

c) Spray droplet interactions: source terms related to density are added to the fluid equations for the injected species. Heat source terms are added to the fluid energy equation for droplet iterations. A source of momentum related to the injection of droplets is also added;

d) Another system is coupled to the previous systems to capture the effects of flow turbulence.

The problem is modelled as a gas phase flow, including chemical reactions and liquid fuel droplets. Fluid dynamics is described by conservative equations. The basic fluid dynamics are governed by Navier-Stokes equations. The flow of reactive fluids in diesel engines is turbulent, which means that the inertial forces of the fluid are considerably larger than the viscous forces, identified by a high Reynolds number.

The thermodynamic properties required for the chemical formulation calculations are provided by tables available in the program library or given by the user. The *ANSYS Forte* theoretical manual [38] provides mores details about models used in the simulations, and the submodels embedded in the *Forte* code are listed in Table 2.

Table 2. The submodels employed in the *ANSYS Forte* software package

Turbulence model	**RNG κ-ϵ model**
Breakup model	KH-RT coupled with gas-jet model
Collision model	Collision radius of influence model
Spray/wall interaction model	Naber and Reitz model
Heat transfer model	Improved law-of-the-wall
Evaporation model	Discrete multi-component
Combustion model	Detailed chemistry
Turbulence/chemistry interaction	Mixing time scale model
Soot model	Hiroyasu soot formation and Nagle/ Strickland-Constable oxidation models
NO_X formation model	Thermal and prompt NO

Combustion Mechanisms

The real combustion of hydrocarbons involves hundreds of species and chemical reactions, and it is necessary to use validated detailed and reduced models to develop an accurate model. The model used in this work is based on mechanics of so-called surrogate fuel components, used to represent real fuels. In this work, the diesel oil was represented by the diesel oil surrogate (DOS) and the biodiesel by rapeseed methyl ester (RME), described by Golovitchev and Yang [39]. A summary of the main considerations of these mechanisms is shown below.

The diesel oil surrogate model used consists of a mixture of 70% n-heptane (C_7H_{16}), aliphatic component, and 30% toluene (C_7H_8), aromatic component, which provides the same ratio C/H

and cetane number of diesel oil #2. Both components can be formed by the pyrolysis of $C_{14}H_{28}$, which was considered as the real molecule of diesel oil. Therefore, an oxidizing pyrolysis process is used to consider the decomposition of this molecule into the components of the substitute fuel:

$$5C_{14}H_{28} + O_2 \rightarrow 7C_7H_{16} + 3C_7H_8 + 2H_2O \quad (1)$$

The combustion mechanism of the diesel surrogate involves 68 species participating in 280 reactions, validated through a shock tube and in studies involving in-cylinder combustion [40].

The biodiesel combustion process was represented by the RME, with physical and thermal properties represented by methyl oleate ($C_{19}H_{36}O_2$). The combustion mechanism was generated by combining the combustion submechanisms of DOS, reduced mb (methyl butanoate) and md (methyl decanoate). The methyl oleate compound is one of the main compounds of the real RME fuel, and its decomposition in md ($C_{11}H_{22}O_2$), mb ($C_5H_{10}O_2$) and alleno (C_3H_4) represents the first step of the combustion mechanism. The md is then decomposed into n-heptane and mp2d ($C_4H_6O_2$):

$$C_{19}H_{36}O_2 + O_2 \rightarrow C_{11}H_{22}O_2 + C_5H_{10}O_2 + C_3H_4 \quad (2)$$

$$C_{11}H_{22}O_2 \rightarrow C_7H_{16} + C_4H_6O_2 \quad (3)$$

The liquid properties of blended fuels were modelled using mixing rules, in the form of a virial equation of state as shown in Eq. (4), to extend the fuel library. Applying the rules involves calculating arithmetic means (Eq. (5)) to obtain energy parameters (e.g. temperature) or geometric means (Eq. (6)) to compute size parameters (e.g. volume).

$$Q_m = \sum_i \sum_j y_i \, y_j Q_{ij} \quad (4)$$

$$\text{If } Q_{ij} = \frac{Q_{ii} + Q_{jj}}{2}$$

$$Q_m = \sum_i y_i Q_i \quad (5)$$

$$\text{If } Q_{ij} = \left(Q_{ii} Q_{jj}\right)^{1/2}$$

$$Q_m = \left(\sum_i y_i Q_i^{\frac{1}{2}} \right)^2 \quad (6)$$

where Q_m is the property of the blend, Q_{ii} and Q_{jj} are the properties for pure component, and y_i and y_j are the volumetric ratios of each pure component.

Therefore, for the blended fuel B8, the extracted the property data from the library for the individual components, diesel oil and biodiesel, and calculated the blend's properties according to the volumetric ratios of the components.

Mechanism of NO_X formation

The four main mechanisms in the formation of nitrogen oxides can be summarized in: thermal mechanism, prompt mechanism, N_2O and fuel-bond nitrogen mechanism. The thermal mechanism, proposed by Zeldovich,[40] involves a series of elementary reactions with high activation energy, due to the strength of the triple bond of the N_2 molecule. It is considered as the main mechanism in NO_X formation in internal combustion engines. This mechanism is very sensitive to the combustion temperature, which in diesel engines is determined by the properties of the liquid fuel, such as cetane number and viscosity; by the thermal-physical properties of the vapor, such as enthalpy and head capacity; and by the rate of heat loss, which is primarily due to the radiation of the soot particles. The radical O may be derived from O_2 or from oxygenated fuel molecules.

In this work, the Zeldovich mechanism is one of the main factors for the determination of NO_X emissions. The main steps of the formation in these mechanisms are reactions 1-4 in Table 3, which were supplemented by reactions of N_2O pathways, represented by reactions 5-9, and steps corresponding to the catalytic interaction between NO and NO_2, represented by reactions 10-14.

The N_2O mechanism has a minor role in the overall generally formation of NO, being typically considered as part of the thermal mechanism, whose combination is considered as the thermal NO/N_2O route. The main step of the N_2O mechanism also involves an O atom attacking N_2 in the presence of a third component to form N_2O, which can subsequently react with O to produce NO.

In the prompt mechanism, the main characteristic is that the CH radical (methylidyne), which is formed exclusively in the flame front, reacts with the nitrogen of the air to form the hydrocyanic acid (HCN), which then reacts to form NO [41]. The NCN pathway of prompt NO formation, which involves 27 reactions, shown in Table 4, has been adopted and implemented in the current chemical kinetics Note that little was known about the impact of NO formation by this mechanism. Since the fuels studied have minimal amounts of nitrogen, NO formation by the fuel-bond nitrogen mechanism was not considered.

Table 3. Elementary steps in the thermal mechanism of NO and N_2O. The forward reaction rate is given by $\boldsymbol{k_f = A_f T^{n_f} exp(-\frac{E_f}{RT})}$ [40].

	Reactions	A_f	n_f	E_f
1	N+ NO = N2 + O	3.50E+13	0.00	330
2	N+ O2 = NO + O	2.65E+12	0.00	6400
3	N+ OH = NO + H	7.33E+13	0.00	1120
4	N+ CO2 = NO + CO	1.90E+11	0.00	3400
5	N2O+O= N2 + O2	1.40E+12	0.00	10810
6	N2O+O= NO + NO	2.90E+13	0.00	23150
7	N2O+H= N2 + OH	4.40E+14	0.00	18880
8	N2O+OH= N2 +HO2	2.00E+12	0.00	21060
9	N2O+M= N2 + O+M	1.30E+11	0.00	59820
10	NO +HO2 = NO2+ OH	2.11E+12	0.00	-480
11	NO2 +O = NO + O2	3.90E+12	0.00	-240
12	NO2 +H= NO + OH	1.32E+14	0.00	360
13	NO + O + M = NO2 +M	1.06E+20	-1.41	0
14	NO2 + CH3 = CH3O+NO	1.50E+13	0.00	0
15	NO + CH3O2 = NO2 + CH3O	2.53E+12	0.00	-358

Table 4. Elementary steps in the NCN pathway of prompt NO formation. The forward reaction rate is given by $\boldsymbol{k_f = A_f T^{n_f} exp(-\frac{E_f}{RT})}$ [41].

	Reactions	A_f	n_f	E_f
1	CH + N2 = NCN + H	3,00E+12	0	22155
2	CN + N2O = NCN + NO	6,00E+13	0	15360
3	CN + N2O = NCN + NO	1,80E+10	0	1450
4	CN + NCO = NCN + CO	1,80E+13	0	0
5	C2O+N2 = NCN + CO	7,00E+11	0	17000
6	CH + N2 = HNCN	1,65E+21	-3,62	14196
7	HNCN + M =H+NCN+M	1,79E+28	-3,44	64502

8	HNCN + O = NO + HCN	1,22E+14	0,05	73,5
9	HNCN + O = NH + NCO	5,60E+13	0,05	73,5
10	HNCN +O = CN + HNO	9,36E+12	0,05	73,5
11	HNCN + OH = NCN + H2O	8,28E+03	2,78	3135
12	HNCN + O2 = HO2 + NCN	1,26E+08	1,28	24240
13	NCN = N + CN	2,95E+30	-5,29	117090
14	NCN = C + N2	2,66E+28	-5,23	83110
15	NCN = CNN	3,69E+29	-5,84	78410
16	NCN + H = HCN + N	1,89E+14	0	8425
17	NCN + O = CN + NO	2,54E+13	0,15	-34
18	NCN + O = CO + N2	2,42E+02	2,32	-1135
19	NCN + O =N+NCO	2,20E+02	0,42	-157
20	NCN + N = N2 + CN	1,00E+13	0	0
21	NCN + C = CN + CN	1,00E+13	0	0
22	NCN + OH = HCN + NO	3,32E+10	-0,97	7290
23	NCN + OH = HCN + NO	4,69E+10	0,44	4000
24	NCN + O2 = NO + NCO	3,80E+09	0,51	24590
25	NCN + CH = HCNCN	3,21E+13	0	-860
26	NCN + CN = C2N2 + N	1,25E+14	0	8020
27	NCN + CH2 = H2CN + CN	7,99E+13	0	4630

NUMERICAL MODEL

The engine numerical model was constructed for a study focused on understanding the impact of the use of exhaust gas recirculation on NO_X emissions. The three-dimensional model of the engine combustion chamber was built in 360°. The diesel oil injector was positioned according to the experimental measurements. Figure 2 shows the cylinder two-dimensional model, indicating the piston bowl offset, and the three-dimensional model and the position of the injector through the fuel spray.

The closed cycle of combustion was simulated, that is, between 150°CA BTDC and 150°CA ATDC. Recirculation of the exhaust gases was considered by the inclusion of CO_2 and H_2O, the main components of the exhaust gases, in the initial composition of the air inside the cylinder. Table 5 shows the operating conditions used for the simulations.

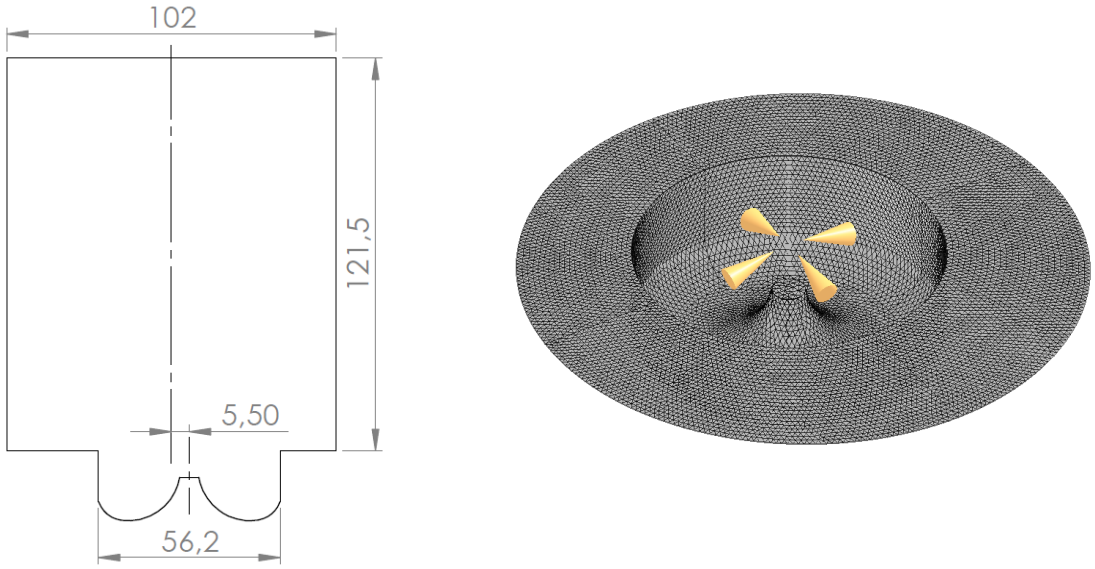

Figure 2. Combustion chamber model (dimensions in mm)

Table 5. Operating conditions of the engine simulation.

Parameter	**B8**	**B8 + EGR**
Nominal load	30	30
Engine speed (rpm)	1800	1800
Injector nozzle diameter (mm)	0.3	0.3
Included angle of spray (°)	151	151
Spray cone ½ angle (°)	12.5	12.5
Injected mass/stroke (B8)	35	36
Fuel temperature (K)	350	350
Start of injection (°CA BTDC)	20	20
Injection duration (°CA)	23	23
Walls temperature °C	~450	~450
Air initial composition	21% O_2	20.79% O_2
(mass fraction)	79% N_2	76.77% N_2
		1.73% CO_2
		0.71% H_2O
Initial pressure (kPa)	95	93
Initial temperature (K)	400	410

It was not possible to obtain the diesel injection profile experimentally, so that the profile provided by Singh, Reitz and Musculus [42] was used. The other parameters related to the numerical models, such as turbulence model, flame propagation model and chemical kinetics, were maintained with standard values, as recommended by the *ANSYS Forte* Theory Manual.

ANSYS Forte uses advanced control to adapt the convergence criteria according to the gradients found in the solution variables, guaranteeing the accuracy of the results.

The numerical grid was built by *ANSYS Forte*. A study on the effects of the numerical grid size on the results was carried out, seeking to verify the independence of solution in relation to the refinement of the numerical grid. The adaptive refinement technique was used to achieve a better numerical solution in the regions near the walls, where the remapping of the numerical mesh is determined according to the temperature and velocity gradient [43,44]. The final numerical grid was chosen according to the comparison with the experimental results and by the variation between the numerical results. There was a tendency of reduction of the pressure inside the cylinder with a greater refinement of the mesh, until stabilization of the results was identified, as also verified by Wei et al. [31]. The mesh used to present the results has about 440,000 elements at the beginning of the closed engine cycle, at 150 °CA BTDC, and 41,000 at the TDC. The time step of the solution was on average $1x10^{-5}$ s. The processing time was about 22 hours on a computer with Windows® 10 64-bit operating system, Intel® Core ™ i7-4790S processor, 8 cores, 16 GB RAM and 3.2 GHz clock.

RESULTS AND DISCUSSION

Numerical Validation

The numerical results were validated by direct comparison with experimental data of in-cylinder pressure and NO/NO_X emissions. Figure 3 shows the comparison between the numerical results and the experimental results for in-cylinder pressure, for 300 consecutive combustion cycles, for the cases B8 (a) and B8 + EGR (b), for an engine load of 30 kW. It is verified that the numerical solution shows a faster combustion in relation to the experimental data. The value of the numerical peak pressure presented a difference lower than 0.5% in relation to the experimental average value, in case B8, and of 1.5%, in case B8 + EGR. The moment of occurrence of the numerical pressure peaks were 4°CA BTDC for case B8 and 7°CA BTDC for the case B8 + EGR, with the experimental values of 9°CA for both cases. For a closer approximation between the results, a specific chemical model must be developed for the real diesel oil used.

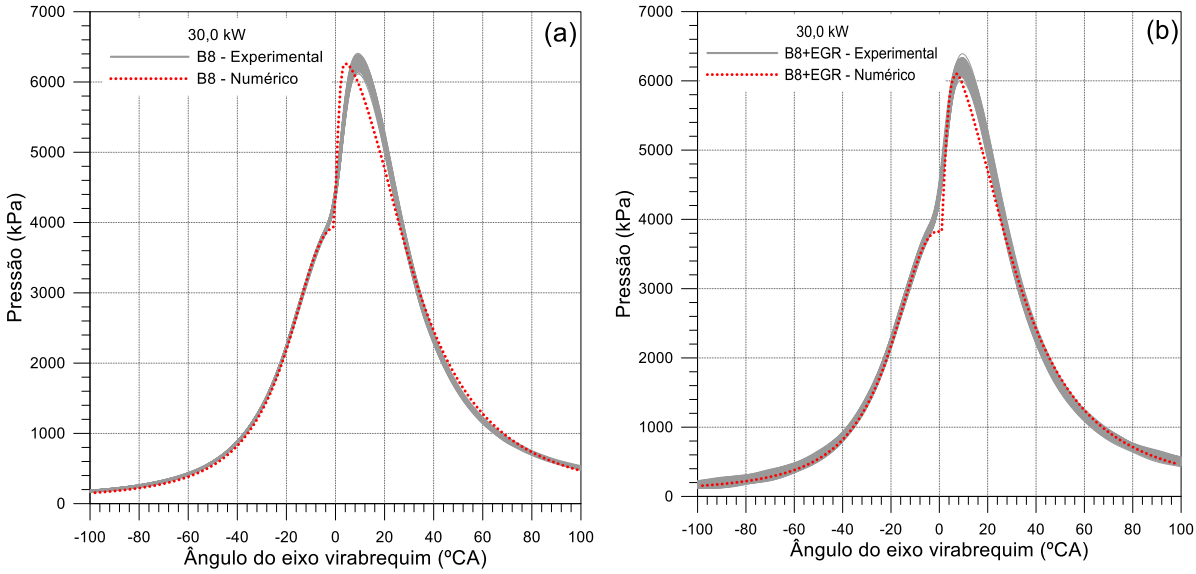

Figure 3. Comparison between numerical and experimental results – In-cylinder pressure.

Figure 4 shows the results obtained for NO (a) and NO_X (b) emissions for both simulated cases. The numerical values of case B8 are within the ranges of experimental uncertainties. For the B8 + EGR case, the numerical value of NO_X is also within the range of experimental uncertainties, but the numerical value of NO emissions is 10% lower than the mean experimental value and 5% lower than the lower limit of experimental uncertainty. These differences are associated with the displacement of the pressure curve, that changes the NO_X formation conditions. According to the results, it was considered that the numerical study showed good agreement with the experimental results, assuming, then, that the numerical behaviour of the gases inside the cylinder approaches the actual behaviour.

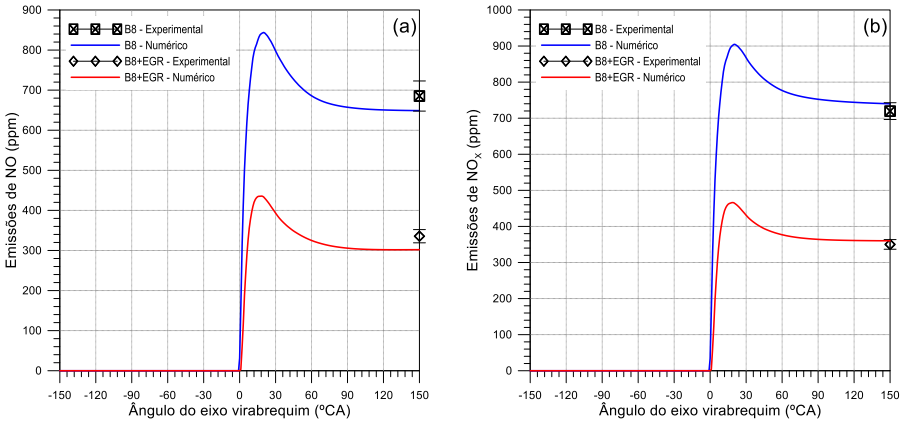

Figure 4. Comparison between numerical and experimental results – NO and NO_X emissions.

EXPERIMENTAL AND NUMERICAL RESULTS

Figure 5 shows the experimental engine specific fuel consumption (SFC) for the different operating conditions. There is a trend of increasing the SFC when using EGR for higher loads. Several factors can increase the fuel consumption when using the EGR technique, including the deterioration of combustion quality, by reducing the air/fuel ratio and the oxygen availability, and the longer ignition delay [22]. These factors also reduced the fuel conversion efficiency (Figure 6). The reduction of EGR temperature (EGR cooling) can mitigate the prejudicial EGR factors [45].

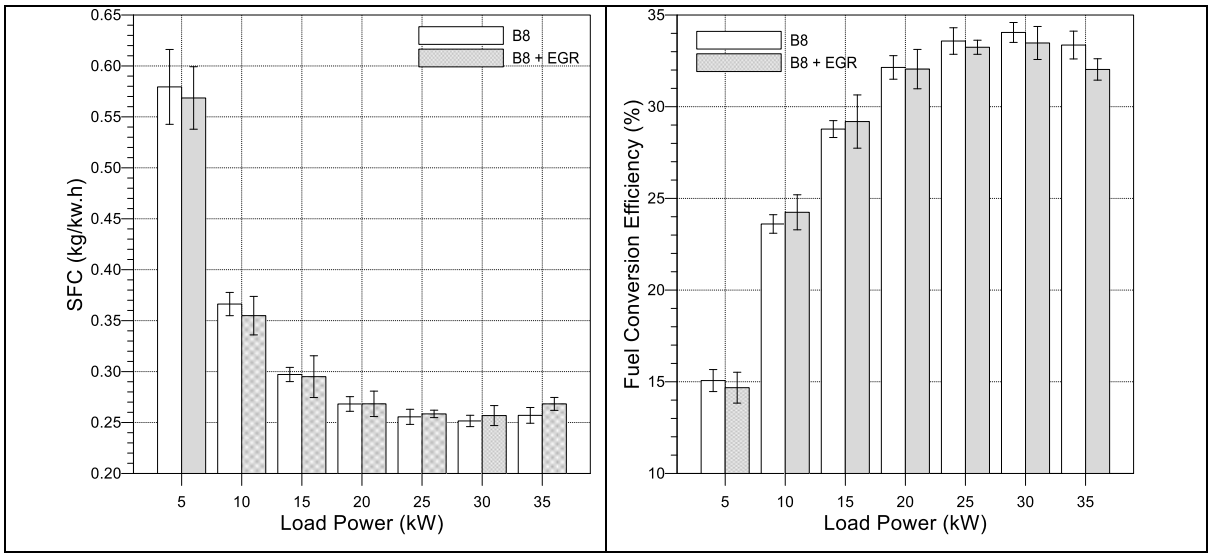

Figure 5. Specific fuel consumption and fuel conversion efficiency for different engine operating conditions

The EGR can lead to a slight reduction of the in-cylinder pressure during the compression stroke and a more intense reduction during the combustion and expansion strokes. The main effects that lead to this behaviour are the increase in the specific heat of the air-fuel mixture, due to the presence of the exhaust gases, the reduction of the O_2 availability, which has a negative effect on the combustion rate, and the CO_2 and H_2O dissociation. These effects slight affected the experimental in-cylinder pressure when using 10% exhaust gas recirculation in B8 + EGR mode, causing little reduction of the in-cylinder pressure and of the heat release rate, especially at higher loads, such as shown in Figure 6.

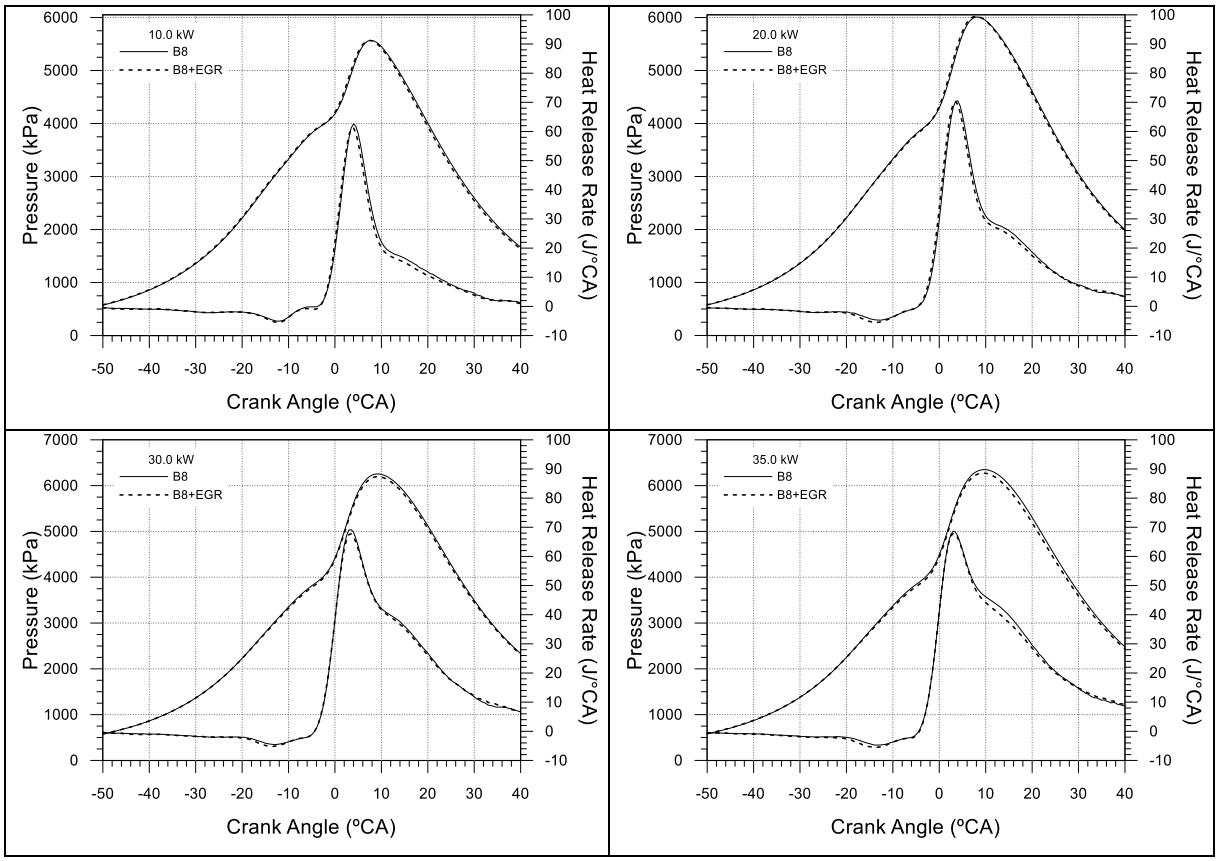

Figure 6. In-cylinder pressure and heat release rate for different engine operating conditions

The CO_2 specific emissions, shown in Figure 7, increased when using EGR, especially for the load of 5 kW, where an increase of 19% was identified. Zheng et al. [46] explains that there is a tendency to increase CO_2 emissions with the use of exhaust gas recirculation due to the exchange of fresh air, with negligible concentration of CO_2, by the exhaust gas with CO_2 concentration, in this work, varying between 4% and 12%.

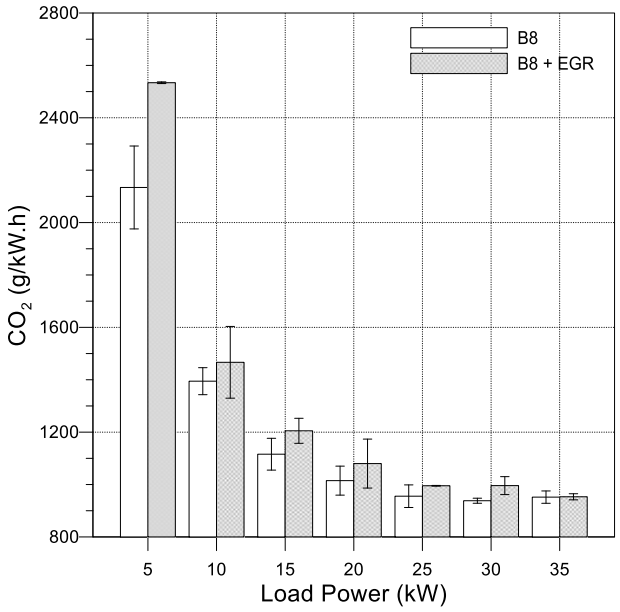

Figure 7. CO_2 emissions for different engine operating conditions

The use of EGR increased CO emissions for all the engine loads, as shown in Figure 8. Adding exhaust gas to the air-fuel mixture reduces the oxygen availability, slows the combustion reaction rates, and reduces the in-cylinder temperature. The temperature reduction may reduce the quality of combustion [47]. Comparing with the B8 mode, the largest increase when using EGR, of 155%, occurred at the load of 32.5 kW, and the smallest increase, of 90%, occurred at the load of 25 kW.

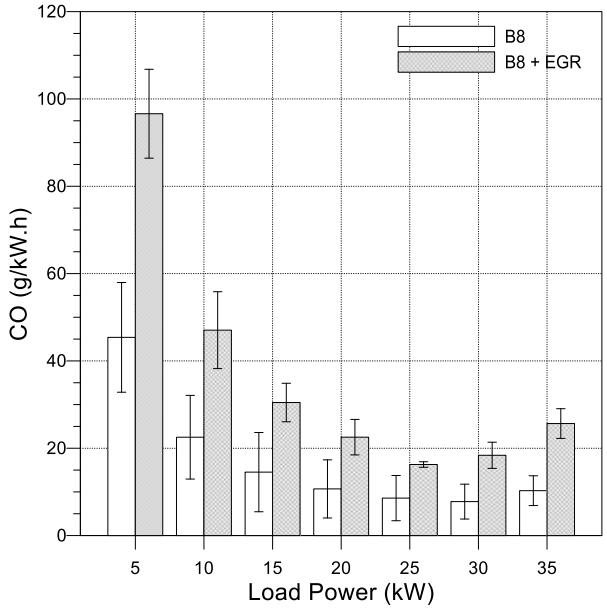

Figure 8. CO emissions for different engine operating conditions.

The reduction of oxygen availability when using the EGR technique is evidenced in O_2 emissions (Figure 9). Regarding the operation of the engine in mode B8, the mode B8 + EGR emitted between 17% (5 kW) and 36% (32.5 kW) less oxygen to the atmosphere.

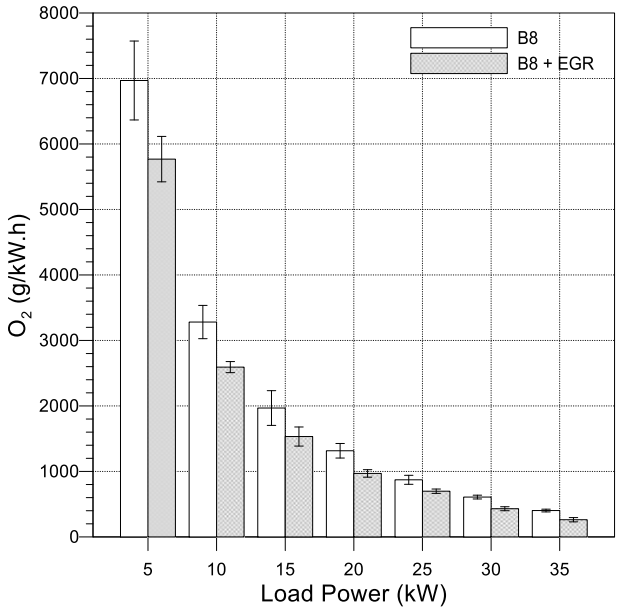

Figure 9. O_2 emissions for different engine operating conditions.

Figure 10. indicates a reduction of unburned hydrocarbon emissions when using the EGR technique, reaching reductions of up to 52% at the load of 20 kW. By using EGR, the heterogeneous mixture inside the cylinder hinders complete combustion and tends to increase THC emissions. This behaviour was not observed in this work and could be associated to the reburning of the hydrocarbons that returned to the combustion chamber by the exhaust gas recirculation [47], which also justifies the small effect of the EGR technique on the fuel conversion efficiency, shown in Figure 5.

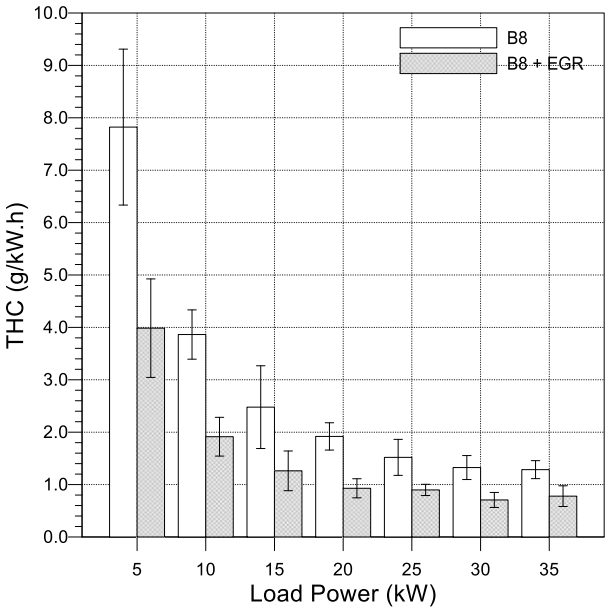

Figure 10. THC emissions for different engine operating conditions.

Figure 11. shows the specific emissions of NO and NO_X. In the B8 + EGR mode, NO and NO_X emissions were reduced for all engine load investigated, with maximum reduction of 59% and 56% at the load of 32.5 kW, respectively, and minimum of 34% at the load of 5 kW. The numerical analysis were performed focusing on understanding the effects of the use of EGR on NO formation.

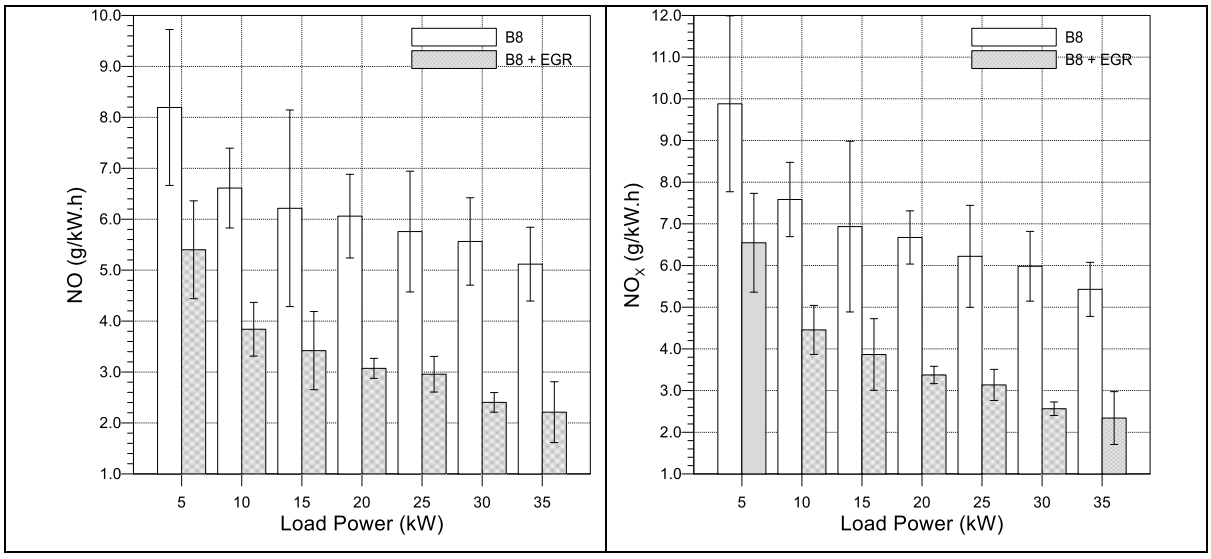

Figure 11. NO and NO_X emissions for different engine operating conditions.

Figure 12 shows the temperature distribution in the combustion chamber and the fuel spray when the cylinder is at TDC for the case B8. It is found that the fuel spray is directed towards

the walls of the cylinder and it is distributed to the combustion chamber when it collides the cylinder walls. The cylinder walls meet around 900K, while the cold fuel, around 400K, causes cooling of the stricken region.

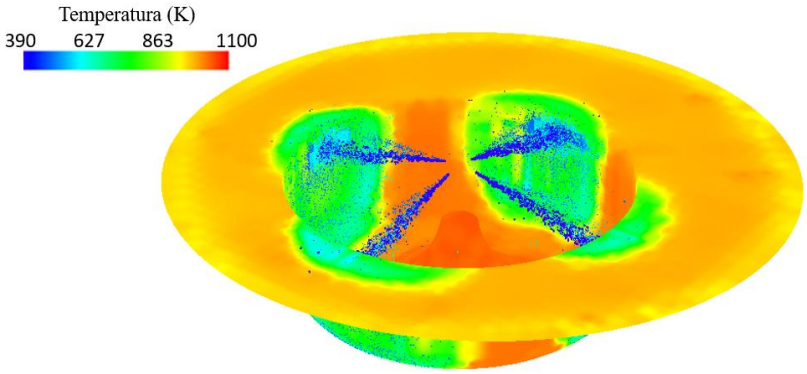

Figure 12. Temperature distribution of cylinder and diesel oil spray at TDC in case B8.

The NO/NO_X concentration in the cylinder as a function of the crank angle (Figure 4) shows that, in both cases, the NO/NO_X concentration increases rapidly after the start of combustion and that a large part of the NO/NO_X is formed during the initial stages of combustion.

Figure 13 shows a cross-section of the cylinder for different cylinder crank angles, with the contour images of the equivalence ratio of the fuel/air mixture, cylinder temperature and NO mass fraction of the engine in B8 mode. It is observed that the fuel is concentrated near the walls of the combustion chamber and near the region of the injector. NO emissions are formed in high-temperature and O2-rich local regions where the combustion temperature is above 2300 K. NO starts to form after TDC and the region of high NO concentration appears around the periphery of the reaction mixture. There is a high NO concentration in the region near the injector, which spreads along the cylinder due to the movement of the air.

The central region of the combustion chamber presents lower temperatures and, consequently, lower concentration of NO. There is no NO formation throughout the spray, since the start of combustion occurs at the end of the fuel injection. The results indicate, therefore, that a large part of the NO is formed in regions of high temperature, that is, by the thermal mechanism. The eccentricity of the combustion chamber of the cylinder causes asymmetry in the temperature distribution, especially during the expansion process.

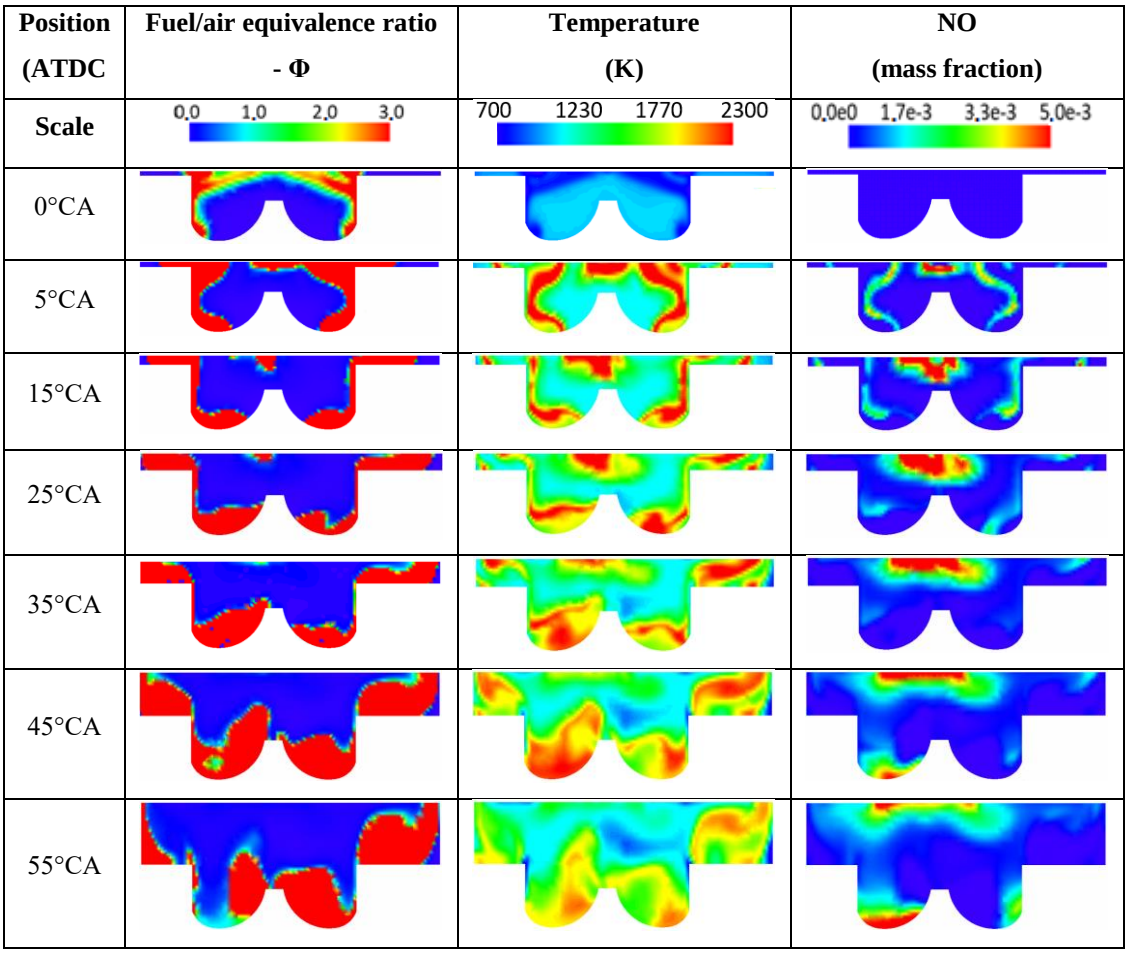

Figure 13. Contour images of the equivalence ratio of the fuel/air mixture, temperature in the cylinder and mass fraction of NO in mode B8.

Figures 14 and 15 show a comparison of the fuel/air equivalence ratio, temperature and mass fraction of NO in the combustion chamber for both cases, B8 and B8 + EGR. The results indicated a reduction of in-cylinder temperature when it is at TDC, associated to the increase of the heat capacity of the mixture, with the recirculation of CO_2. There is also a wider range of cylinder rich mixture with exhaust gas recirculation due to the reduction of the O_2 concentration in the air-fuel mixture.

The formation of NO is explicitly lower in the case B8 + EGR, since the main factors that influence the formation of this component have been reduced, that is, temperature and O_2 concentration. It is observed that the region of higher NO formation in the case B8 + EGR is in the upper face of the combustion chamber, where higher temperatures occurred in an environment of poorer mixtures.

Parameter	Φ		Temperature (K)	
Scale	0.0 1.0 2.0 3.0		700 1230 1770 2300	
Position (ATDC)	B8	B8 + EGR	B8	B8 + EGR
0°CA	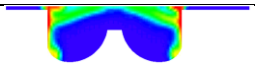	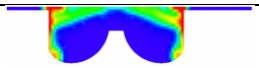	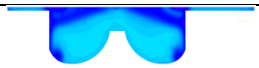	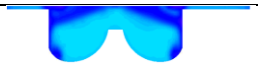
5°CA	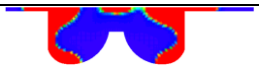	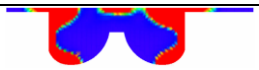	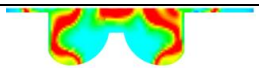	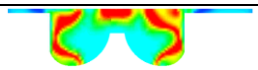
15°CA	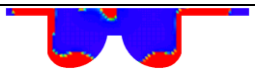	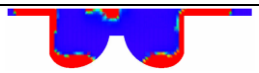	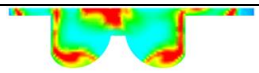	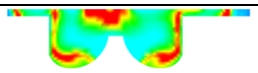
25°CA	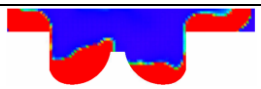	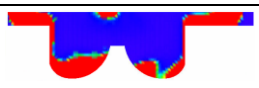	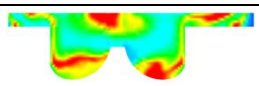	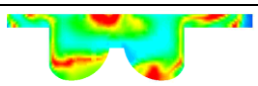
35°CA	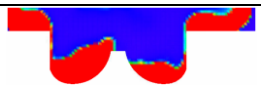	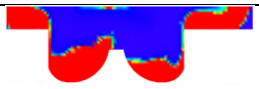	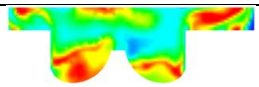	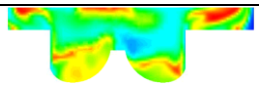
45°CA	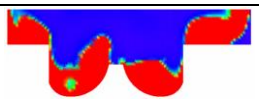	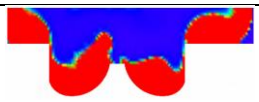	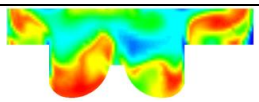	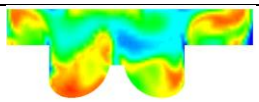
55°CA	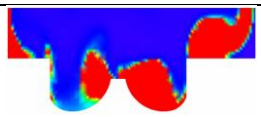	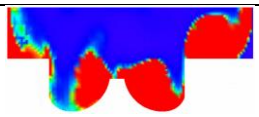	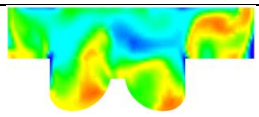	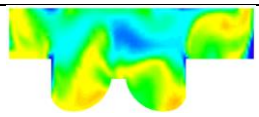

Figure 14. Contour images of the equivalence ratio of the fuel/air mixture and temperature in the cylinder in cases B8 and B8 + EGR

Parameter	NO (mass fraction)	
Scale	0.0e0 1.7e-3 3.3e-3 5.0e-3	
Position	B8	B8 + EGR
0°CA	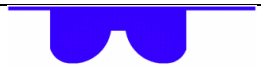	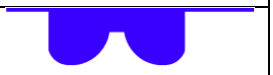
5°CA	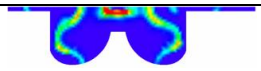	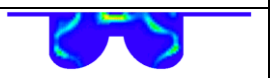
15°CA	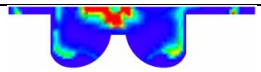	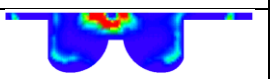
25°CA	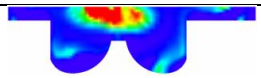	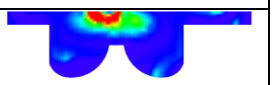
35°CA	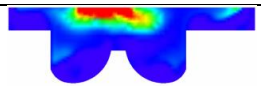	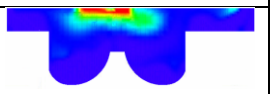
45°CA	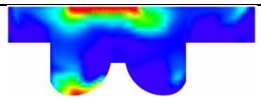	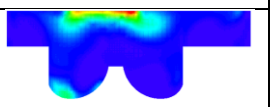
55°CA	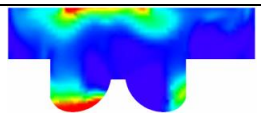	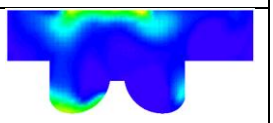

Figure 15. Contour images of the equivalence ratio of the fuel/air mixture and temperature in the cylinder in cases B8 and B8 + EGR

CONCLUSIONS

This study showed the effects of using cold EGR in a diesel power generator fuelled by B8. The recirculation of 10% of the exhaust gas slight affected the engine specific fuel consumption and fuel conversion efficiency and proved to be effective in reduce the NO_X emissions, reaching a reduction of up to 56%. The numerical study showed that the NO formation in the engine is mainly due to the thermal mechanism and that the EGR use inhibits the NO formation by the reduction of the in-cylinder temperature and O_2 concentration. The EGR use reduced THC emissions up to 52%. In contrast, CO_2 and CO emissions increased when using EGR, up to 19% and 155%, respectively.

Conflicts of Interest

The authors declare that there is no conflict of interest regarding the publication of this paper.

Funding Statement

CAPES – Brazilian Coordination for the Improvement of Higher Education Personnel

FAPEMIG - Minas Gerais Research Funding Foundation

CNPq - Brazilian National Council for Scientific and Technological Development

Acknowledgments

The authors thank CAPES, CNPq, and FAPEMIG for the financial support for this work.

REFERENCES

[1] de Oliveira A, de Morais AM, Valente OS, Sodr?? JR. Combustion, performance and emissions of a diesel power generator with direct injection of B7 and port injection of ethanol. J Brazilian Soc Mech Sci Eng 2017. doi:10.1007/s40430-016-0667-7.

[2] Hosseinzadeh-Bandbafha H, Tabatabaei M, Aghbashlo M, Khanali M, Demirbas A. A comprehensive review on the environmental impacts of diesel/biodiesel additives. Energy Convers Manag 2018;174:579–614. doi:10.1016/j.enconman.2018.08.050.

[3] Balamurugan T, Arun A, Sathishkumar GB. Biodiesel derived from corn oil – A fuel substitute for diesel. Renew Sustain Energy Rev 2018;94:772–8. doi:10.1016/j.rser.2018.06.048.

[4] States U. A Comprehensive Analysis of Biodiesel Impacts on Exhaust Emissions Draft Technical Report. United States Environ Prot Agency 2002:118. doi:EPA420-P-02-001.

[5] Graboski MS, McCormick RL. Combustion of fat and vegetable oil derived fuels in diesel engines. Prog Energy Combust Sci 1998;24:125–64. doi:10.1016/S0360-1285(97)00034-8.

[6] Knothe, G.; Krahl, J.; Van Gerpen J. Title :The Biodiesel Handbook. AOCS Press 2005. doi:10.1201/9781439822357.

[7] Knothe G. “Designer” biodiesel: Optimizing fatty ester composition to improve fuel properties. Energy and Fuels 2008. doi:10.1021/ef700639e.

[8] Lapuerta M, Armas O, Rodríguez-Fernández J. Effect of biodiesel fuels on diesel engine emissions. Prog Energy Combust Sci 2008. doi:10.1016/j.pecs.2007.07.001.

[9] Andreae M, Fang H, Bhandary K. Biodiesel and Fuel Dilution of Engine Oil, 2007. doi:10.4271/2007-01-4036.

[10] Shi X, Liu B, Zhang C, Hu J, Zeng Q. A study on combined effect of high EGR rate and biodiesel on combustion and emission performance of a diesel engine. Appl Therm Eng 2017;125:1272–9. doi:10.1016/j.applthermaleng.2017.07.083.

[11] Palash SM, Masjuki HH, Kalam MA, Masum BM, Sanjid A, Abedin MJ. State of the art

of NOx mitigation technologies and their effect on the performance and emission characteristics of biodiesel-fueled Compression Ignition engines. Energy Convers Manag 2013;76:400–20. doi:10.1016/j.enconman.2013.07.059.

[12] Shin B, Cho Y, Han D, Song S, Chun KM. Hydrogen effects on NOx emissions and brake thermal efficiency in a diesel engine under low-temperature and heavy-EGR conditions. Int J Hydrogen Energy 2011;36:6281–91. doi:10.1016/j.ijhydene.2011.02.059.

[13] Asad U, Kumar R, Zheng M, Tjong J. Ethanol-fueled low temperature combustion: A pathway to clean and efficient diesel engine cycles. Appl Energy 2015;157:838–50. doi:10.1016/j.apenergy.2015.01.057.

[14] Zheng Z, Xia M, Liu H, Shang R, Ma G, Yao M. Experimental study on combustion and emissions of n-butanol/biodiesel under both blended fuel mode and dual fuel RCCI mode. Fuel 2018;226:240–51. doi:10.1016/j.fuel.2018.03.151.

[15] Asad U, Zheng M. Exhaust gas recirculation for advanced diesel combustion cycles. Appl Energy 2014;123:242–52. doi:10.1016/j.apenergy.2014.02.073.

[16] Bozza F, De Bellis V, Teodosio L. Potentials of cooled EGR and water injection for knock resistance and fuel consumption improvements of gasoline engines. Appl Energy 2016;169:112–25. doi:10.1016/J.APENERGY.2016.01.129.

[17] Ladommatos N, Abdelhalim SM, Zhao H, Hu Z. The Dilution , Chemical , and Thermal Effects of Exhaust Gas Recirculation on Diesel Engine Emissions - Part 2 : Effects of Carbon Dioxide 1996.

[18] Ladommatos N, Abdelhalim SM, Zhao H, Hu Z. The Dilution, Chemical and Thermal Effects of Exhaust Gas Recirculation on Diesel Engine Emissions- Part 1: Effect of Reducing Inlet Charge Oxygen. SAE Tech Pap 961165 1996. doi:10.4271/961167.

[19] Ladommatos N, Abdelhalim SM, Zhao H HZ. The dilution, chemical and thermal effects of exhaust gas recirculation on diesel engine emissions- Part3: Effect of water vapor. SAE Pap 971659 1997.

[20] Ladommatos N, Abdelhalim SM, Zhao H, Hu Z. The Dilution , Chemical , and Thermal Effects of Exhaust Gas Recirculation on Diesel Engine Emissions - Part 4 : Effects of Carbon Dioxide and Water Vapour 1997.

[21] Edara G, Satyanarayana Murthy YVV, Srinivas P, Nayar J, Ramesh M. Effect of cooled EGR on modified light duty diesel engine for combustion, performance and emissions under high pressure split injection strategies. Case Stud Therm Eng 2018;12:188–202.

doi:10.1016/j.csite.2018.03.004.

[22] Divekar PS, Chen X, Tjong J, Zheng M. Energy efficiency impact of EGR on organizing clean combustion in diesel engines. Energy Convers Manag 2016;112:369–81. doi:10.1016/j.enconman.2016.01.042.

[23] Huang M, Gowdagiri S, Cesari XM, Oehlschlaeger MA. Diesel engine CFD simulations: Influence of fuel variability on ignition delay. Fuel 2016. doi:10.1016/j.fuel.2016.04.137.

[24] Kumar JTS, Sharma TK, Murthy KM, Rao GAP. Effect of reformed EGR on the performance and emissions of a diesel engine: A numerical study. Alexandria Eng J 2017. doi:10.1016/J.AEJ.2017.01.008.

[25] Boccardi S, Catapano F, Costa M, Sementa P, Sorge U, Vaglieco BM. Optimization of a GDI engine operation in the absence of knocking through numerical 1D and 3D modeling. Adv Eng Softw 2016. doi:10.1016/j.advengsoft.2016.01.023.

[26] Naik C V., Puduppakkam K, Meeks E. Simulation and Analysis of In-Cylinder Soot Formation in a Low Temperature Combustion Diesel Engine Using a Detailed Reaction Mechanism. SAE Int J Engines 2013. doi:10.4271/2013-01-1565.

[27] Fraioli V, Mancaruso E, Migliaccio M, Vaglieco BM. Ethanol effect as premixed fuel in dual-fuel CI engines: Experimental and numerical investigations. Appl Energy 2014. doi:10.1016/j.apenergy.2014.01.008.

[28] Huang Y, Hong G, Huang R. Numerical investigation to the dual-fuel spray combustion process in an ethanol direct injection plus gasoline port injection (EDI + GPI) engine. Energy Convers Manag 2015;92:275–86. doi:10.1016/j.enconman.2014.12.064.

[29] Dong S, Cheng X, Ou B, Liu T, Wang Z. Experimental and numerical investigations on the cyclic variability of an ethanol / diesel dual-fuel engine. Fuel 2016;186:665–73. doi:10.1016/j.fuel.2016.09.027.

[30] Cameretti MC, Tuccillo R, Simio L De, Iannaccone S, Ciaravola U. A numerical and experimental study of dual fuel diesel engine for different injection timings. Appl Therm Eng 2016. doi:10.1016/j.applthermaleng.2015.12.071.

[31] Wei S, Ji K, Leng X, Wang F, Liu X. Numerical simulation on effects of spray angle in a swirl chamber combustion system of DI (direct injection) diesel engines. Energy 2014;75:289–94. doi:10.1016/j.energy.2014.07.076.

[32] Das SK, Lim OT. Spray Simulation of n-heptane in a Constant Volume Combustion Chamber over a Wide Range of Ambient Gas Density and Fuel Temperature. Energy

Procedia, 2017. doi:10.1016/j.egypro.2017.03.526.

[33] Yang J, Golovitchev VI, Redón Lurbe P, López Sánchez JJ. Chemical kinetic study of nitrogen oxides formation trends in biodiesel combustion. Int J Chem Eng 2012;2012. doi:10.1155/2012/898742.

[34] Mardi K M, Khalilarya S, Nemati A. A numerical investigation on the influence of EGR in a supercharged SI engine fueled with gasoline and alternative fuels. Energy Convers Manag 2014. doi:10.1016/j.enconman.2014.03.031.

[35] Galloni E, Fontana G, Palmaccio R. Numerical analyses of EGR techniques in a turbocharged spark-ignition engine. Appl Therm Eng 2012. doi:10.1016/j.applthermaleng.2012.01.040.

[36] Brazil. Law Nr. 13033 - A adição obrigatória de biodiesel ao óleo diesel comercializado ao consumidor final. Brazil: http://www.planalto.gov.br/ccivil_03/_ato2015-2018/2016/lei/L13263.htm; 2014.

[37] Yang J. Biodiesel Spray Combustion Modeling Based on a Detailed Chemistry Approach. Chalmers University of Technology, 2012.

[38] ANSYS Forte ® Software 2017:1–110.

[39] Golovitchev VI, Yang J. Construction of combustion models for rapeseed methyl ester bio-diesel fuel for internal combustion engine applications. Biotechnol Adv 2009;27:641–55. doi:10.1016/j.biotechadv.2009.04.024.

[40] Zel'dovich Ya.B., Sadovnikov P.Ya., and Frank-Kamenetskii D.A. Oxidation of Nitrogen in Combustion. Academy of Sciences of the USSR, Moscow (1947).

[41] Konnov A.A. Implementation of the NCN Pathway of Prompt-NO Formation in the Detailed Reaction Mechanism. Combust. Flame 156 (2009), 2093{2115.

[42] Singh, S., Reitz, R., and Musculus M. Comparison of the Characteristic Time (CTC), Representative Interactive Flamelet (RIF), and Direct Integration with Detailed Chemistry Combustion Models against Optical Diagnostic Data for Multi-Mode Combustion in a Heavy-Duty DI Diesel Engine. SAE Tech Pap 2006;2006-1–0.

[43] Puduppakkam K V, Liang L, Shelburn A, Naik C V, Meeks E, Bunting B. Predicting Emissions Using CFD Simulations of an E30 Gasoline Surrogate in an HCCI Engine with Detailed Chemical Kinetics. SAE Int 2010. doi:10.4271/2010-01-0362.

[44] Battistoni M, Mariani F, Risi F, Poggiani C. Combustion CFD modeling of a spark ignited optical access engine fueled with gasoline and ethanol. Energy Procedia, 2015. doi:10.1016/j.egypro.2015.11.829.

[45] Hountalas DT, Mavropoulos GC, Binder KB. Effect of exhaust gas recirculation (EGR) temperature for various EGR rates on heavy duty DI diesel engine performance and emissions. Energy 2008;33:272–83. doi:10.1016/j.energy.2007.07.002.

[46] Zheng M, Reader GT, Hawley JG. Diesel engine exhaust gas recirculation - A review on advanced and novel concepts. Energy Convers Manag 2004;45:883–900. doi:10.1016/S0196-8904(03)00194-8.

[47] Agarwal D, Singh SK, Agarwal AK. Effect of Exhaust Gas Recirculation (EGR) on performance, emissions, deposits and durability of a constant speed compression ignition engine. Appl Energy 2011;88:2900–7. doi:10.1016/j.apenergy.2011.01.066.

[48] Agarwal D, Singh SK, Agarwal AK. Effect of Exhaust Gas Recirculation (EGR) on performance, emissions, deposits and durability of a constant speed compression ignition engine. Appl Energy 2011;88:2900–7. doi:10.1016/j.apenergy.2011.01.066.

Appendix A

1. Measurement device specifications

2. Measured parameter	3. Device	4. Uncertainty characteristics
5. Intake air mass flow rate	6. Orifice plate	7. Uncertainty of ±2.3 kg/h
8. Fuel consumption	9. Platform balance	10. Uncertainty of 0.1 kg/h
11. Temperature in the fuel tank, ambient air, inlet air, orifice plate inlet, exhaust gas	12. K-type thermocouples	13. Measured exhaust gas with maximum uncertainty of ±11 º 14. Other measured temperature with maximum uncertainty of ±5ºC
15. Cooling water temperature	16. PT-100 sensors	17. Uncertainty of ± 2ºC
18. Inlet air humidity	19. Thermo-hygrometer	20. Uncertainty of ± 2.5% of reading
21. Ambient pressure	22. Torricelli barometer	23. Resolution of ± 1.3 kPa
24. Engine load	25. Electric transducer	26. Uncertainty of ± 1%
27. Total HC emissions	28. Heated flame ionization	29. Resolution of ± 1 ppm
30. NO_x emissions	31. Heated chemiluminescent analyzer (HCLD)	32. Resolution of ± 1 ppm
33. CO emissions	34. Non-dispersive infrared	35. Resolution of ± 1 ppm
36. CO_2 emissions	37. Non-dispersive infrared	38. Resolution of ± 0.01 %
39. In-cylinder pressure	40. Piezoelectric pressure transducer – Kistler 6061B	41. Resolution of ± 0.5%

Paper 10 **Bildiri 10**

SCOOTER PROPULSION SYSTEM POWERED BY HYDROGEN FUEL CELL-PEM

Kenan Saka[1,*], Yaser Erar[2], Bashar Dadouch[3], Jamil Haddad[4], Abdullah Al-Qassab[5], Ibrahim Hag-Ali[6], Mehmet Fatih Orhan[7]

[1]Vocational School of Yenişehir Ibrahim Orhan, Bursa Uludağ University, PO Box: 16900, Yenişehir, Bursa, Turkey
[2-7]Department of Mechanical Engineering, American University of Sharjah, P.O. Box: 26666, Sharjah, UAE
*Corresponding author. Email: kenansaka@uludag.edu.tr

Abstract

The world has been increasingly weary of the changes happening to the climate. Global warming and its correlation with the release of hydrocarbons that are depleting the ozone layer is causing major concern about how society deals with its emissions. Of course, many steps have been taken to reduce our impact on the environment but we are still at the infancy stage of reducing harmful emissions. Our purpose in this study is to design a scooter that runs on fuel cells that releases no hydrocarbons to the atmosphere. We also plan to study its performance and find ways to optimize its power output in order for it to be a viable transportation method in the future.

In this regard, a fuel cell is optimized to enhance its performance and the range of the scooter is extended significantly by implementing a hybrid system with a Lead Acid Cell battery. The fuel cell would power the battery which would in turn drive a motor. Once the battery's power was around 60% charged the fuel cell would automatically start to charge it to about 99%, this was to ensure a longer battery life. The results show that a super capacitor implemented into the system would have improved performance and efficiency in areas of hills or where power demand was needed in cases of high acceleration.

Keywords: Hydrogen fuel cell, PEM, hybrid system, scooter

1. INTRODUCTION

About a third of the energy in the United States is used for transportation. More than 60% of the energy used in transportation is used for personal vehicles that run on burning petroleum-based fuels. This has become a defining component not only for the citizens in the US but for many around the world. A study shows that in 2007, about 3 trillion miles have been travelled by vehicles in the US, equivalent to driving towards the sun and back 13,440 times [1]. The problem for this is that the energy demand in vehicles is not going to decrease and alternatives must be made to reduce the harmful hydrocarbons released into the atmosphere. Our motivation lies in reducing largely/removing harmful emissions by designing and building a fuel cell scooter. The purpose of this project is not study how fuel cells work but to see in what ways can a fuel cell system be optimized to produce the most power and get the most range from it.

Our first step in this project, since fuel cells were a relatively new concept for us was to invest as much time as possible into initial research. We looked at fuel cells in every possible way and studied its mechanisms in order to find out which configuration was suitable for our project. We looked at how fuel cells work, which type of fuel cell configuration was suitable and fuel cell systems and other components to see how we could optimize our scooter.

A typical fuel cell for a Proton Exchange Membrane looks like the one shown in figure 1. It is composed of three active components:

- A fuel electrode (anode).
- Oxidant electrode (cathode).
- Electrolyte sandwiched between the electrodes. [2]

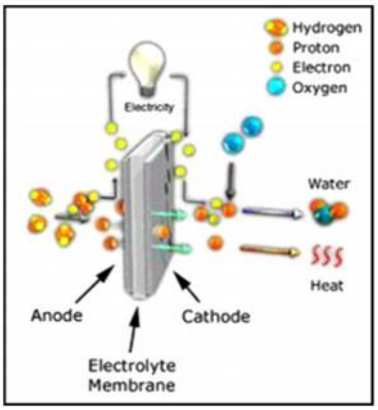

Figure 1. Fuel Cell Schematic

To understand how electricity is generated let's look at this from a basic chemical reaction. First, molecular hydrogen H_2 is supplied to the anode where it reacts electrochemically inside it. The hydrogen is oxidized and breaks down as shown by this reaction equation:

$$H_2 \rightarrow 2H^+ + 2e^-$$

The hydrogen electrons ($2e^-$) are forced through an external circuit where the electricity can be transferred to a load and the hydrogen ions react with the oxidizer which is oxygen flowing the cathode. The hydrogen ions travel through the electrolyte and the resulting byproduct are,

$$\frac{1}{2}O_2 + 2H^+ + 2e^- \rightarrow H_2O$$

By looking at the reaction as a whole we can come to this final equation,

$$H_2 + \frac{1}{2}O_2 \rightarrow H_2O + W_{ele} + Q_{heat}$$

What this means is very important. By the reactions happening in this system we can effectively convert these chemical reactions into electricity and the byproduct is heat and water only. This device can effectively operate without releasing any harmful emissions into the atmosphere.

This analysis just scratches the surface because this is the basic fundamental reaction in fuel cells, the catalyst and electrodes can be different and have different operating conditions and even different fuels. We had to decide on a configuration that was portable enough and the criteria met our operating conditions. After some more research we stumbled upon 3 types of fuel cells and their specifications are listed below in table.

Fuel cell type	Typical electrolyte	Typical anode/ cathode catalysts[a]	Typical interconnect material	Typical fuel	Charge carrier[a]	Major contaminants[a]	Operation temperature (°C)	Specific advantages	Specific disadvantages	Electrical efficiency (%)	Technological maturity[b]	Research activity[c]
Low-temperature proton exchange membrane	• Solid Nafion®	• Anode: Platinum supported on carbon • Cathode: Platinum supported on carbon	Graphite	Hydrogen	H^+	• Carbon monoxide (CO) • Hydrogen sulfide (H_2S)	60–80	• Highly modular for most applications • High power density • Compact structure • Rapid start-up due to low temperature operation • Excellent dynamic response	• Complex water and thermal management • Low-grade heat • High sensitivity to contaminants • Expensive catalyst	40–60	4	H
Direct methanol	• Solid Nafion®	• Anode: Platinum–Ruthenium supported on carbon • Cathode: Platinum supported on carbon	Graphite	Liquid methanol–water solution	H^+	• Carbon monoxide (CO)	Ambient-110	• Compact size • Simple system • High fuel volumetric energy density • Easy fuel storage and delivery • Simple thermal management for liquid methanol systems	• Low cell voltage and efficiency due to poor anode kinetics • Low power density • Lack of efficient catalysts for direct oxidation of methanol • Fuel and water crossover • Complex water management • High catalyst loading • High cost • Carbon dioxide (CO_2) removal system • Fuel toxicity	35–60	3	H
Direct ethanol	• Solid Nafion® • Alkaline media • Alkaline-Acid media	• Anode: Platinum–Ruthenium supported on carbon • Cathode: Platinum	Graphite	Liquid ethanol–water solution	H^+	• Carbon monoxide (CO)	Ambient-120	• Compact size • Environmentally-friendly fuel • High fuel volumetric energy density • Relatively low	• Low power density • High sensitivity to carbon monoxide (CO) • Low cell voltage and efficiency due to poor anode kinetics	20–40	2	L

Figure 2. Comparing and Contrasting Different Membranes

We landed on three choices but we ultimately narrowed it down to the Proton Exchange Membrane due to its specific advantages and the availability of hydrogen in AUS. It also had an operating temperature that was good and did not vary allowing thermal stresses to be reduced and with its high research activity it would be less difficult to implement this system with the more resources available.

The purpose of our project is to optimize the fuel cell's power output in order to drive a scooter with the maximum range possible and efficiency. This requires an energy management system that exposes the fuel cell's capabilities and allows us to harness the maximum from a fixed supply of hydrogen. According a study by P. Thuonthong and S. Rael, one way to do this was to have the fuel cell for supplying energy to the battery and load at the dc bus. This means the structure plans to have a fuel cell that supplies energy to the battery and the battery discharges by supplying energy to the load (motor) [4]. This idea is what shaped our objectives into choosing a hybrid structure. Another study showed that a hybrid fuel cell battery scooter gave better efficiencies and speeds compared to battery and petrol powered scooters alone. The component diagram as simple and similar to the one shown in Figure 3 [5].

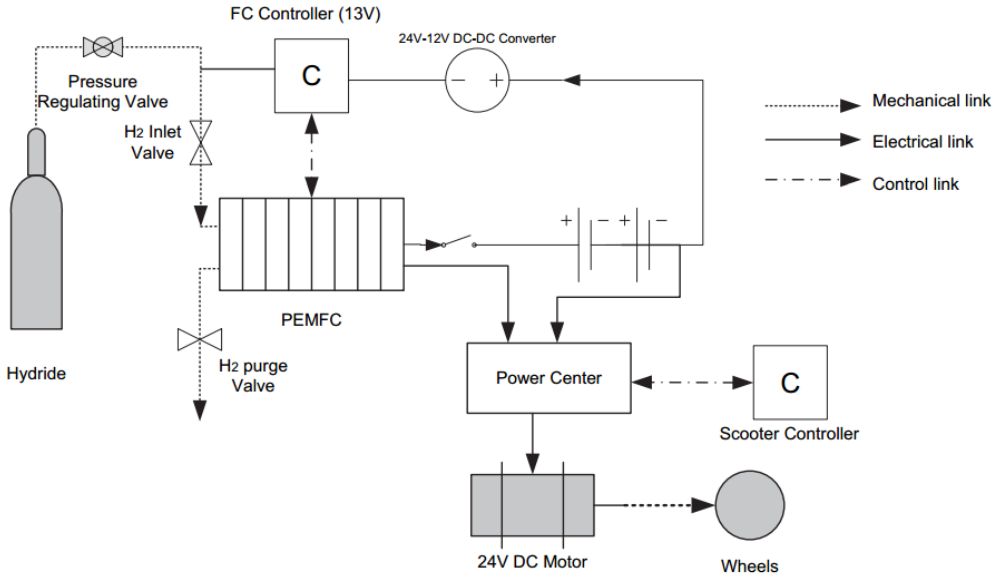

Figure 3. Component diagram of hybrid fuel cell structure and drive system.

Among the following sources above, a literature review of other aspects of the project was conducted. These range from sustainability of the fuel cell system, the future mass production and proposed delivery systems as well as recycling initiatives to further reduce impact on the environment. The following sources with their summaries are listed below.

Some researchers discuss the assessment of hybrid fuel cell/supercapacitor system for scooters by analyzing the propulsion system as well as the fuel cell/supercapacitor system in comparison to the fuel cell/battery system. In conclusion the paper shows that the supercapacitor holds comparative advantage over the battery system in terms of maintenance, weight, more flexibility in packaging and orientation setup which is important in a limited space project such as the scooter, and it also has a longer life time [2].

Hwang et al. [3] report the design, testing results, and fabrication of a fuel cell powered bicycle. The system design specifications are illustrated as well as explained briefly. In addition to that the management of the sub-systems of the bicycle such as the cooling turbofans is explained. Furthermore, the main goal of the paper is to develop a single-chip microcontroller to operate the fuel cell.

Kulikovsky et al. [4] provide a clear picture of the inside of the fuel cell distribution of performance related to the reactant consumption, thus helping justify the modes of optimal fueling. Furthermore, understanding these pictures help increase the fuel cell efficiency through

the maximum utilization of the reactants (oxygen and hydrogen) where before the fuel cells were run at high stoichiometric ratios of feed gases which are not necessary according to this paper. These pictures and models are justified using the laws of feed gas consumption and then the results are interpreted under various conditions and justified simplifying realistic approximations.

In this paper the assembly of a fuel cell is modeled as a stiffness model of several springs in either parallel or series connections and studied in depth. The model is first studied as a single fuel cell model and then developed into a larger stack model. Based on the model the paper finds the various parameters such as temperature on the internal stress of the components and the contact resistances. Furthermore, a 3D finite-element analysis is performed and the results are compared with the results obtained from the equivalent stiffness model. The models are then introduced to variations in parameters such as temperature to acquire a relationship between these parameters and the stresses developed in the element .This is needed because the clamping load applied to the fuel cell stack directly affects its performance, a very high clamping load will result in a reduction of the permeability as well as the power density of the fuel cell and a plastic deformation that could lead to cracks in the cell. On the other hand a low clamping load can cause a high contact electrical resistance which is undesirable as well as leakages [5].

Hwang [6] gives a brief explanation about the components that can make a fuel cell scooter better. Then he clarifies why fuel cell scooters are better than ICE and battery operated scooters. Finally, he gives a detailed analysis of how Taiwan has been developing fuel cell scooters. This is a useful paper because it explains the components of the fuel scooter, the advantages and disadvantages of fuel cells, and what a country needs to do in order to succeed in the fuel cell market.

By Hwang and Chang [7], a description of the different ways in which different types of fuels can make ready for scooters is given. Furthermore, a comparison between the well-to-wheels, well-to-tank, and tank-to-wheels efficiencies of ICE scooters, electric battery scooters and fuel cell scooters is done. This is an important paper because it helps us recognize which type of fuel cell is the most energy efficient and environment friendly.

Some researches give an overview of the most important applications of PEM fuel cells. Next, they give an explanation about the importance of energy management in fuel cells and then introduce the newest energy management methods. This is a very important paper because it helps us differentiate which energy management approach is the best for our system [8].

Sharaf and Orhan [9] gave a thorough explanation of how fuel cells work, and the different types. Next, they provided us with a summary of the different characteristics of the fuel cells. Moreover, the different types of applications were all described. Then the authors discussed the research and development that is currently under progress. Finally, they described the thermodynamic reactions that are involved. In conclusion, this paper is extremely helpful because it provides a complete overview about everything that has to do with fuel cells.

Lin [10] focused on a conceptual design and modeling of a fuel cell scooter. It discusses the relevant challenges that we face when designing a scooter for our project. Areas of design like the fuel cell stack and its size are given treatment. Depending on the power required, the stack size is determined through a graph. It gives the best viable option of metal hydride canisters as the source of storage of the fuel (hydrogen). Also, some insight is given on parasitic load requirement such as the blower, intake of hydrogen, etc. Advice is given on using a battery hybrid system to run these components as well as for use in instants of peak power.

Jiao and Li [11] emphasize on the importance of water management in a polymer exchange membrane fuel cell, the one most suited for transportation purposes. It describes what is needed in order to produce a well hydrated membrane without causing blockage in the flow fields. This is an important part of any fuel cell system because the system and its components can degrade quickly if proper water management has not been issued. It also describes methods and techniques to be able to solve for this problem.

In an article, the writer compared the battery and hydrogen fuel cells as an alternative source for an ICE. He compares them across various factors, like the cost, size, running life, running cost, safety, emissions, operation easiness and storage. At the end with all the factors stated the hydrogen fuel cell was the best alternative when compared to the battery when assuming the range needed for operation is more than 160km. If the range is lower the 160 km then the battery is better at one factor which is the running cost [12].

Hwang et al. [13] describe the way to assemble the hydrogen fuel cell in detail, and explain what the use of each component is. In addition the author emphasis what affects each component like the distance between the membranes. This article also talks about the best condition the fuel cell must be maintained at and what are the best factors the fuel cell must be assembled at. For example the best optimum coupling must be 90kgfcm, this value will assure the best distance and the best pressure in the cell to get the best outcome and avoid any risks like water flooding and not efficient output.

A research talks about the emissions that internal combustion engines produce these days and what are the major effects these emission have on earth. It also talks about those types of emissions that are produced from using fossil fuels, like carbon dioxide and carbon monoxide. The affects that were discussed were the ozone layer and the carbon footprint. Then the hydrogen fuel cells were introduced as the zero emission technology where the only product from the hydrogen fuel cell is energy, heat and water vapor, and these are not harmful at all. However, there is one risk that gets introduced in hydrogen fuel cells, and it is the hydrogen leakage. Lastly, this paper predicts that using hydrogen fuel cells will reduce the carbon foot print and save the plant and avoid killing human lives because of the harmful emissions that Ice vehicles produce [14].

The main purpose of the article is consecrated to the thermodynamic analyses of fuel cells. Moreover, the thermodynamic approach also specifies the irreversibility in the thermodynamic process occurring in the fuel cells, with and without impurities in the reactants. The article then goes on to demonstrate the irreversibility evaluation in fuel cells. In conclusion, the main point of this article is to efficiently calculate the second law efficiency of fuel cells, as the article has demonstrated in its many sections. Therefore, this article will be of more help to our project over the calculation and thermodynamic analysis segment of the project [15].

The high cost of production of fuel cells is mainly due to the cost of the electrolyte membrane, which is itself expensive as a result of the expensive platinum catalyst used. A research concentrates on recycling these platinum corroded and inactive catalysts in order to render the cost of maintaining the PEM fuel cells cheaper. The process suggested to reclaim the platinum is chemical reduction of the inactivated catalyst. The article proposes two methods to control

the concentration of the chemical reduction solution. The first involves controlling the pH value of the solution, and the second consist on controlling the mass of the obtained solid. This article is useful to the project in analyzing the sustainability of fuel cells as sustainability is considered a pitfall of fuel cells [16].

The article includes useful information explaining why fuel cells are not to be ignored when planning the sustainable future. The article then mentions a very crucial aspect to the scooter project: safety. The most significant part of the article, significant specifically to our project, is presented towards the end of the article and consists of proposing ameliorations for future studies. The main improvements that are to be done on fuel cells, and which are not extensively attended to, include improving the feeble acceleration of fuel cell-powered scooters, as well as the scooters' ability to climb, and ultimately permitting a wider range of speeds [17].

Huang et al. [18] showed the type of microcontroller that is needed to control the PEM fuel cell scooter, the components controlled by the microcontroller as well as a useful flow chart is also presented by the article and explained briefly in terms of voltage for shut down and operation.

Some researches demonstrated the basic functions of the microcontroller as well as the fail-safe shut-down operation that can be a result of low fuel cell voltage output, low stack voltage, high temperature in the stacks or low hydrogen flow pressure. Fixing these conditions through the microcontroller would be through the control of the air pump flow rate as well as the solenoids [19].

With the problem statement in mind our objective is to complete the hybridization of a fuel cell system to allow to achieve specified ranges, speeds, and efficiencies. We hope to have a range of 20 km distance on a single supply of hydrogen stored in metal hydride canisters. Achieve a speed of 15 km/hr with a weight capacity of 120 kgs. Our efficiency target for this early stage of development is 35-50%. We plan to reduce noise levels associated with 2 stroke engines in scooters down to 70dB.

CONCEPTUAL DESIGN AND SIMULATION

As with any other product in the industry, the main goal while designing our product is to satisfy the customer's needs. On the other hand, try to achieve these demands while min-maxing the

various engineering elements regarding the product at the same time becomes a challenge and a goal at the same time.

Four main alternative designs were put into study based on the various factors that were introduced based on many factors such as complexity. Each provide a number of disadvantages and advantages that were cross checked in order to choose the best possible design that will be implemented.

Alternative designs:

1- Fuel-Cell Scooter: Having a fuel-cell as the only source of electricity would make the scooter simple, however the fuel efficiency would be lacking due to the fact that the entire load of the system would be carried by the fuel cell only. This will either lead to low fuel efficiency or a low performance scooter depending on several factors.

2- Hybrid Fuel-Cell and Ultracapacitor Scooter: In order to solve this problem, the team researched possible alternatives to that problem, and hybrid systems came to surface. The idea is that the Ultracapacitor would be a secondary source of electricity in order to share the load with the fuel cell. Where the fuel cell would supply the power needed to drive the scooter, and the Ultracapacitor would supply the power to run the blower, microcontroller, et cetera. This however would make the system very complex and hard to control in terms of managing the different scenarios that would happen through the microcontroller.

3- Fuel-Cell Scooter with hydrogen reactor: One of the main issues of the fuel cell systems is the supply of hydrogen, and in order to solve that problem one of our members suggested the use of a mini hydrogen reactor that would supply hydrogen to the system though small hydrogen cores thus creating a charger for the system. After researching the market, we found hydrogen cores that were manufactured by Brunton for only 19.99$, however the supply of these cores is very small and we would need multiple cores to run the system. After further research was done we found a product called h2o hydrolyzer manufactured by the same company and costs 249.99$, where the cores can be recharged using only water. However, this system is very expensive and has low efficiency; furthermore in order to make the system run on water only

to produce hydrogen the team would have to redesign the hydrolyzer to make it more efficient and capable of providing the hydrogen directly to the fuel cell.

4- Electric Scooter with Fuel Cell generator: Another idea was to use a battery as the main power provider to the system while using the fuel cell as a recharger to the battery, this idea would decrease the supply of hydrogen needed for the system as well as make the system start up process easier. However, the system would become heavier and the range acquired by the scooter and the life expectancy would drop.

The following figure demonstrates the internal system of the scooter that supply power to the load, where the load is the motor and battery used to run the scooter, and their connections.

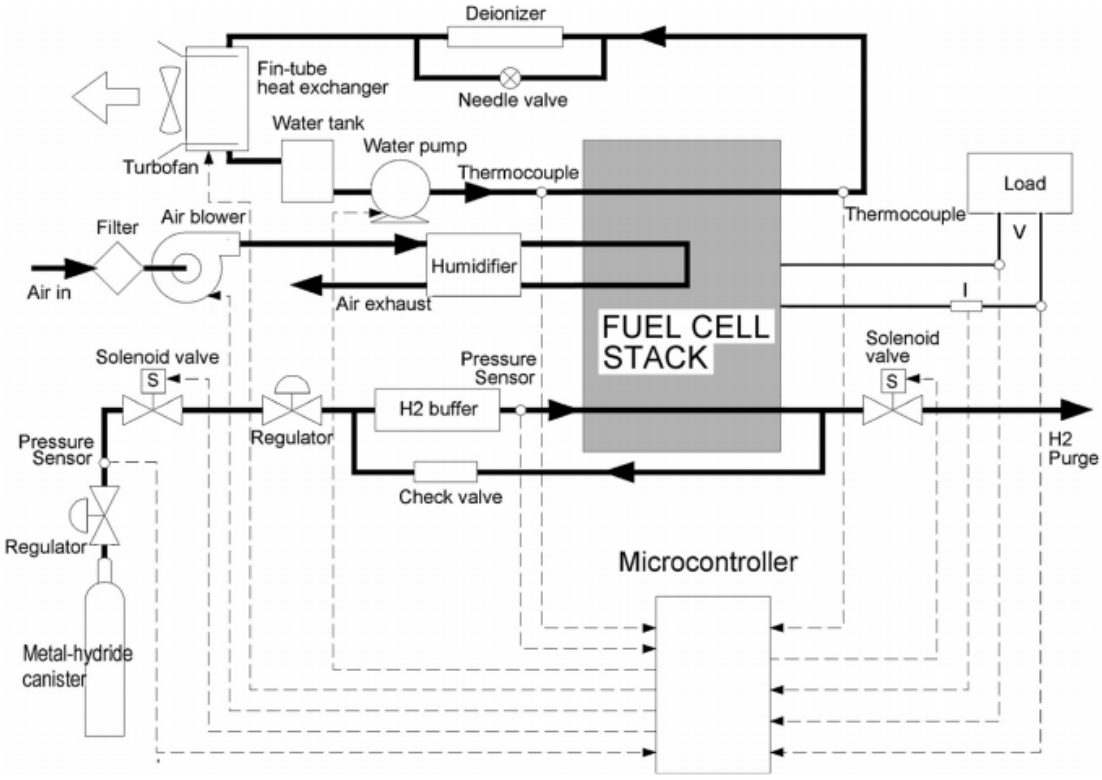

Figure 4. Initial Proposed System [6]

As seen from the figure above, each component carries a significant role in the functionality of the scooter. The fuel cell converts the hydrogen chemical energy into electrical energy that is then supplied to the load whether it is a battery or a super capacitor that then run the motor hence providing the mechanical power to make the scooter move. Some of the other key components are the microcontroller, the metal hydride canister, sensors, valve, and air pump.

ANALYSIS

A preliminary step in our designing process is finding the load applied on the system itself; in other words, finding the required power to move the scooter. There are many forces exerted on the scooter due to the nature of nature itself, these force must be taken into account since they illustrate the required power necessary to move the scooter at said given conditions. This step in the fuel cell powered scooter is foundational as it permits to unveil the required load that will be applied on the fuel cell based in the battery selection which itself will be done as per the required load necessary to power the scooter.

This analysis will be conducted on the basis of finding the inertial force of the scooter (F_I), the resistive force of the rolling motion of the tires due to friction (F_F), the aerodynamic force exerted on the scooter due to drag (F_D), and finally, the extra force exerted/gained while claiming/descending an incline (F_A). From there, the total required power at given circumstances for a give speed can be calculated by multiplying the sum of the forces calculated by the speed of the scooter at said required moment.

In this context, there is an important note to make. There is an additional force that is usually included in such calculations, that is the resistive rolling force due to the deformation of the tire itself, which is mainly due to the heat increase of the tire. However, since the scooter has small tires, and since the temperature of the tires would not be too high due to the low speeds of the scooter, this force is assumed to be zero.

Once the forces are uncovered in terms of symbolic algebraic equations, they will be entered in the system simulation in order to be able to play and tweak the conditions. This will permit to discover the overall performance of the designed system and of the scooter itself. Moreover, based on these calculations, the limitations on the scooter itself is illustrated. This is crucial to the design process. For instance, based on these calculations, the maximum mass of the scooter will be illustrated. The same could be said for the type of wheels, the mass of wheels, et cetera. In order to do so, however, multiple iterations are required, hence the importance of the later simulation.

Due to the nature of the two different forces acting on the scooter as a result of two different accelerations, the inertial forces must be segregated into two: linear acceleration exerted force

and rotational acceleration exerted force. Both are derived from Newton's infamous second law.

For linear acceleration, it is simply the mass of the entire scoter multiplied by its linear acceleration, $F_{il} = m_{scooter} * a_{linear}$.

For the rotational acceleration, rotational acceleration of the wheels that is, the force the ratio of the angular moment variation (M_i) and the radius of the wheels, $F_{ir} = M_i/r$. However, the angular moment variation must first be found in order to find F_{ir}.

$$M_i = J * \frac{d\omega}{dt} = J * \frac{a}{r} \ [Nm] \quad (1)$$

where, J, ω, a and r are moment of inertia (m^2*kg), angular speed ($1/s^2$), acceleration of scooter (m/s^2) and radius of wheel (m), respectively. Therefore,

$$F_{ir} = J * \frac{a}{r\text{^}2} \ [N] \quad (2)$$

To calculate J, it is the sum of the moment of inertia of tire and the rotational moment of inertia of the rim. This distinction is important not only because the mass of each is different, but more importantly, because their radii are interdependent.

$$J = J_r + J_t = \frac{1}{2} m_r r_r^2 + \frac{1}{2} m_t (r_r^2 + r_t^2) \ [m^2*kg] \quad (3)$$

Finally, assuming full transfer ration of the wheels, and assuming the scooter has two wheels, the total inertial force (F_I) of the scooter is,

$$F_I = (m_{scooter} + \frac{2[\frac{1}{2}mrrr2 + \frac{1}{2}mt(rr2+rt2)]}{r\text{^}2}) * a_{scooter} = (m_{scooter} + \frac{2J}{r\text{^}2}) * a_{scooter} \ [N] \quad (4)$$

The resistive rolling force is the friction between the tires and the ground itself; therefore, it is very dependent on the material of the ground; the rougher the surface, asphalt for instance, the greater resistive frictional force (F_F) is.

F_F is dependent on two foundational parameters: coefficient of friction which differs with material and motion, and the normal force applied on the object, usually the weight of the object, which is highly dependent on the inclination of the ground. The equation is as follows,

$$F_F = \mu_{k/s} * N \ [N] \quad (5)$$

The coefficient of friction could be programmed to enter different values based on the criteria of static conditions or kinetic conditions. As for the normal force, though the above equations is correct for a 0^o slope, it would be safer to formulate the following equation that takes inclination into account; moreover, it would reduce to the above equation if the inclination were to be 0^o since cos(0) is 1. The safer equation is,

$$F_F = \mu_{k/s} * N * \cos(\alpha) \ [N] \quad (6)$$

where, $\mu_{k/s}$, N and α are coefficient of friction (unitless, usually less than 1), normal push of the ground on the scooter (N) and angle of inclination (degrees), respectively.

Aerodynamic drag force (F_D), though often neglected, is crucial to determine the push exerted by the air on the scooter which should not be ignored in the case of the scooter as the scooter is not necessarily designed for aerodynamic efficiency; therefore, the force would be significant enough to be taken into account. Moreover, based on this force the terminal velocity of the scooter could be calculated if needed in further design processes.

The main parameters required to calculate this force are the density of air, which differs based on the conditions of location, the frontal cross-sectional area of the scooter, the velocity of the scooter, and the coefficient of drag of the design of the scooter itself.

$$F_D = \tfrac{1}{2}(\rho_{air} * A_{FCS} * C_D * v^2_{scooter}) \ [N] \quad (7)$$

where, ρ_{air}, A_{FCS}, C_D and $v_{scooter}$ are density of air (kg/m^3), frontal cross-sectional area of scooter (m^2), coefficient of drag (untiless) and velocity of scooter (m/s), respectively.

Inclination force (F_A) is crucial to the final power calculation; perhaps the most important after the foundational inertial forces since a slight inclination could increase the consumption of power very significantly. Moreover, not only does it permit to design the scooter propulsion system for an upper-slope, but also energy conservation designs for a downward inclination slope. Note that tis force could have been added and included in the inertial forces calculations; however, by adding it by itself it could be more easily manipulated. Moreover, if there is no slope, it would not be taken into account since sin(0) is none other than 0 itself.

The main parameters to finding this force are the weight of the scooter and the inclination of the slope.

$$F_A = m_{scooter} * g * \sin(\alpha) \ [N] \quad (8)$$

where, $m_{scooter}$, g and α are mass of scooter (kg), gravitational acceleration (m/s^2) and angle of inclination (degrees), respectively.

These equations all represent the resistive forces acting on the scooter itself; therefore, it provides a clear indication of the load the scooter would exert on the battery, and hence, on the fuel cell. Furthermore, from these equations, a more precise, accurate, and efficient propulsion system for the scooter could be designed.

In order to figure out the power required to move the scooter, all these forces must be summed up and multiplied by the velocity of the scooter at said instant. The power equation goes as follows,

$$P = (F_I + F_F + F_D + F_A) * v_{scooter} \ [W] \quad (9)$$

where, F_I, F_F, F_D, F_A and $v_{scooter}$ are inertial force (N), resistive frictional forces (N), aerodynamic drag force (N), inclination force (N) and velocity of scooter (m/s), respectively. Additionally, from these parameters, the resistive torque of the entire system itself can be calculated. This, however, is not a paramount calculation for the design process, merely a number on the specifications sheet.

$$T = ([F_I + F_A] * y_{cg}) + (F_D * y_{stag}) + (F_R * r) \ [Nm] \quad (10)$$

where, F_I, F_F, F_D, F_A, y_{cg}, y_{stag} and r are inertial force (N), resistive frictional forces (N), aerodynamic drag force (N), inclination force (N), vertical distance from bottom of scooter to the center of gravity of structure (m), vertical distance from bottom of scooter to the stagnation of air resistance (m) and radius of wheel (m), respectively.

RESULTS & DISCUSSION

The section begins with the simulation of the fuel cell, followed by that of resistance forces, finally, illustrating the entire proposed system simulation.

Fuel cell simulation is a more than crucial foundation to the entire design process. The fuel cell simulation was designed based on the polarization curves provided by the manufacturer of the fuel cell: Horizon Fuel Cell Technologies.

The fuel cell simulation was simulated in static fashion and modeled as per the polarization curves provided by the manufacturer. A significant difficulty faced was to incorporate these graphs in Simulink. This was overcome by re-graphing the graphs on Excel, utilizing several points, and modeling the fuel cell based on the best fit curves. Moreover, due to the designed simulation later presented, two of the graphs are re-graphed in inverted function. The errors are taken into consideration in the graph. The Excel graphs obtained are demonstrated in Figures 5-7.

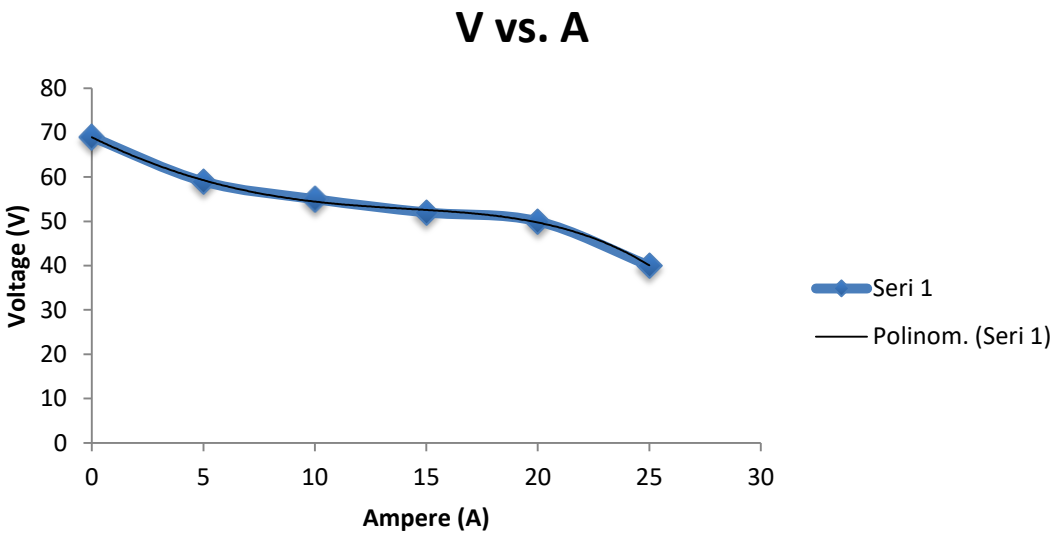

Figure 5. U-I Polarization Curve of 1000W Fuel Cell

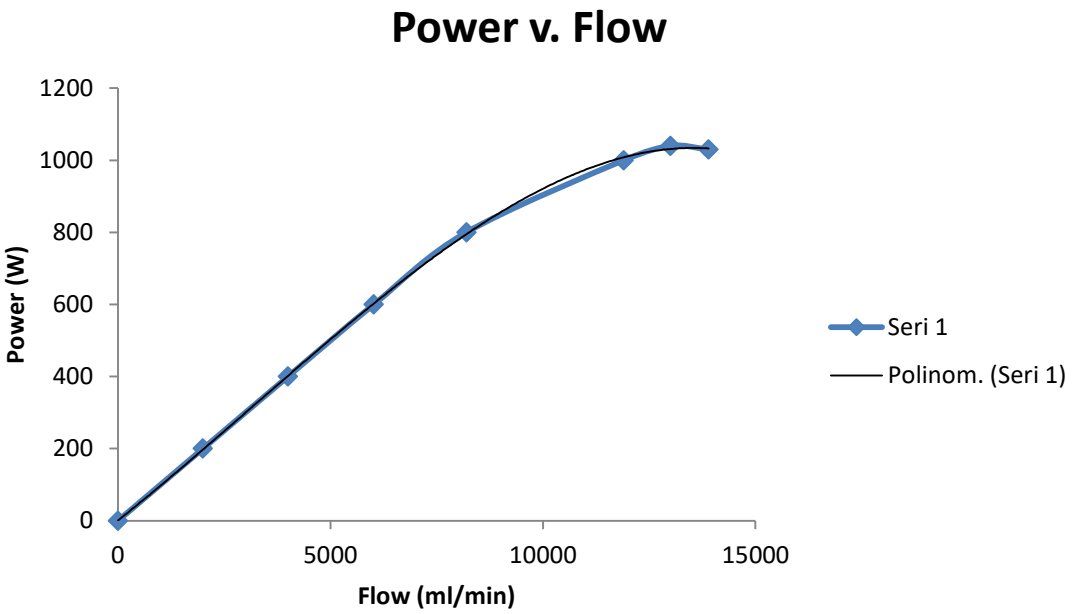

Figure 6. Inverted H_2 Flow-P Polarization Curve of 1000W Fuel Cell

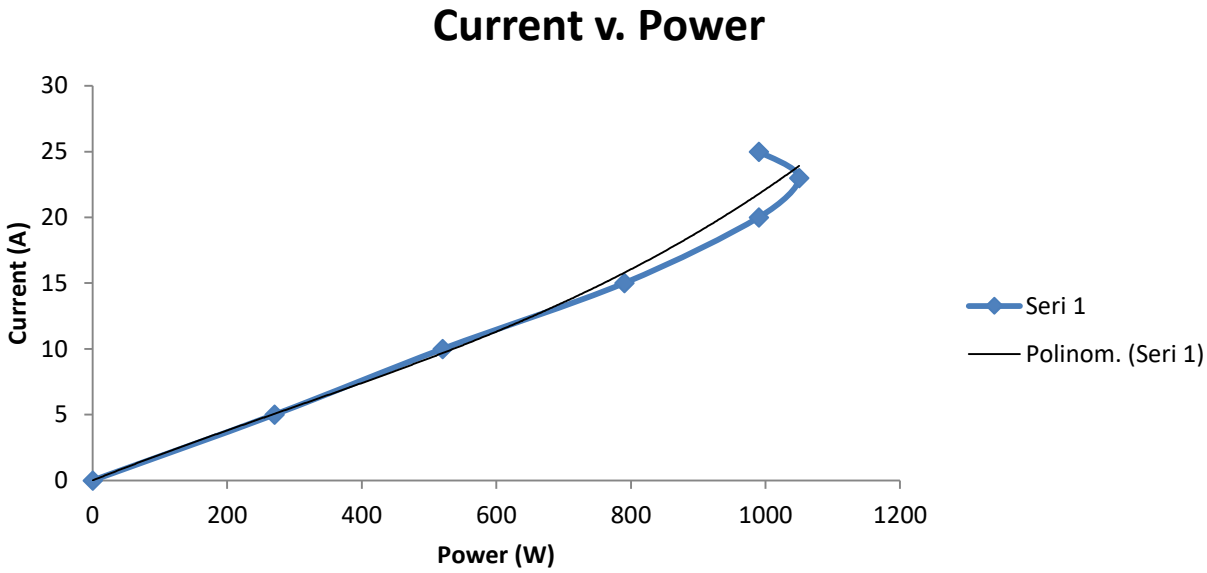

Figure 7. Inverted P-I Polarization Curve of 1000W Fuel Cell

Two Simulink models were created. The first, which is demonstrated here, is based on a scalar constant value. This is made in order to be able to check the different outputs at different H_2 flow inputs. The values were cross-checked. The simulation is presented in Figure 8.

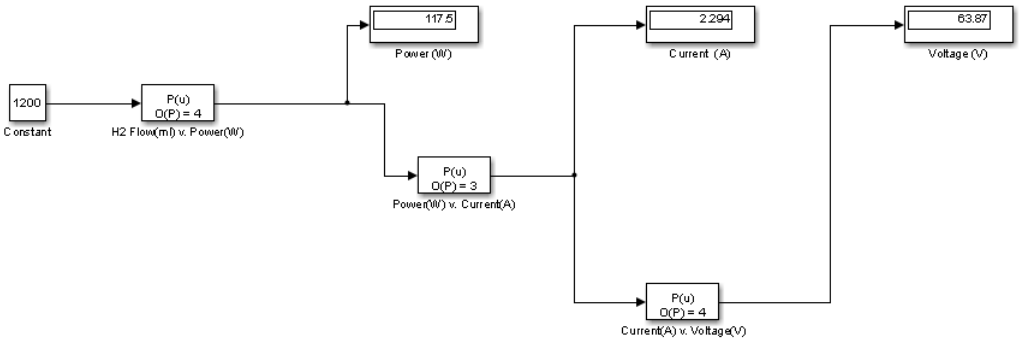

Figure 8. Constant Scalar Input Simulink Model

This second simulation seeks to illustrate the relationship between input and outputs in a graph format. A vector of an array of numbers is inputted into the system and then the vector output are taken to the workspace and graphed with the initial input. These results are demonstrated in Figure 9.

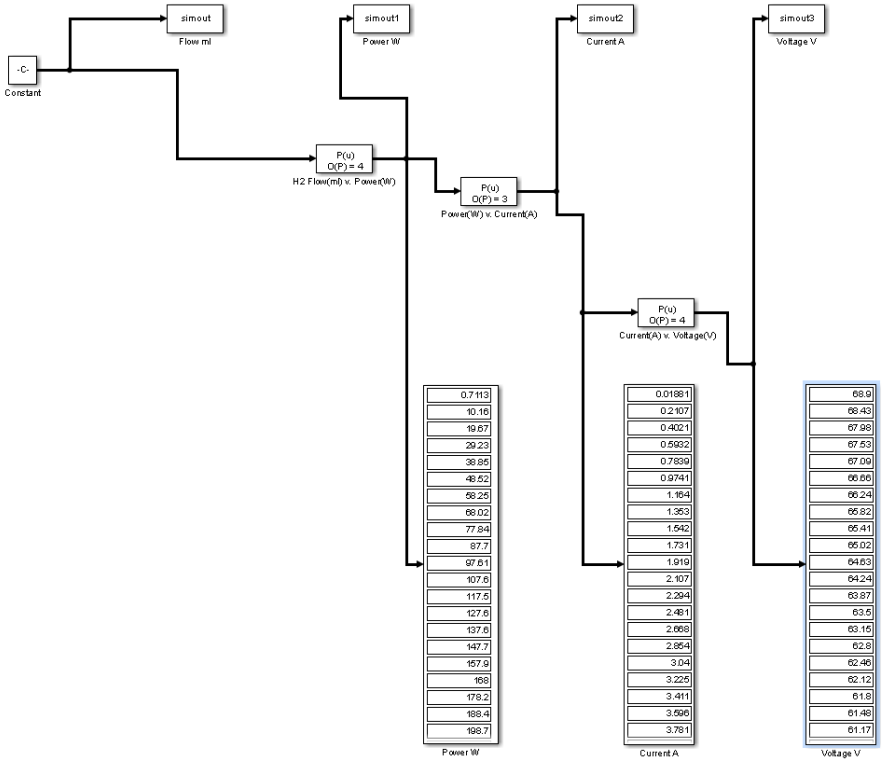

Figure 9. Constant Vector Input Simulink Model

Having accomplished the fuel cell simulation, the next important simulation to accomplish is that of the resistive forces calculated previously.

The next step in this report is to, as previously mentioned, simulate the resistive forces acting on the scooter. This is important as it gives a set program from which different values could be inputted. By doing so, the optimum conditions for the fuel cell propulsion system could be obtained.

Since the Simulink model is too big to be observed in one image, it will be segregated into the four resistive forces and reassembled in Figures 10-13.

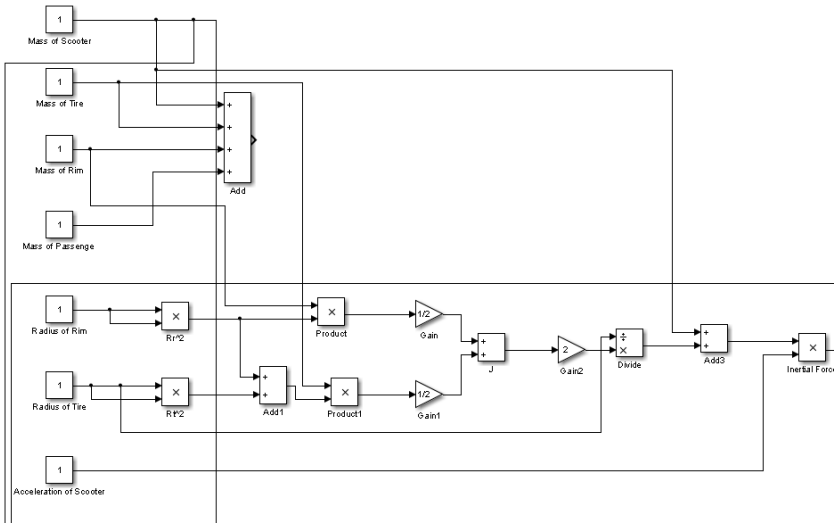

Figure 10. Inertial Force Simulation

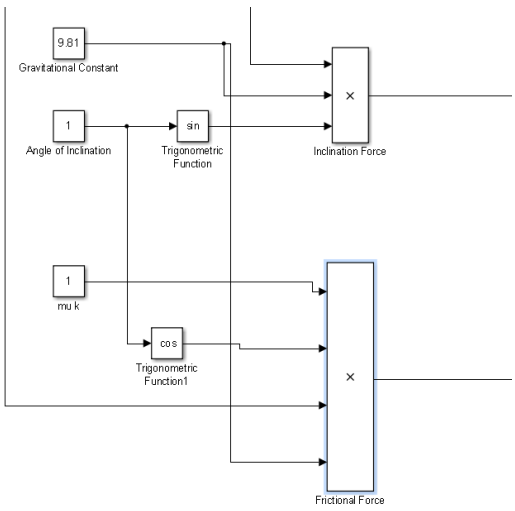

Figure 11. Resistive Frictional Force (F_F) and Inclination Force (F_A) Simulation

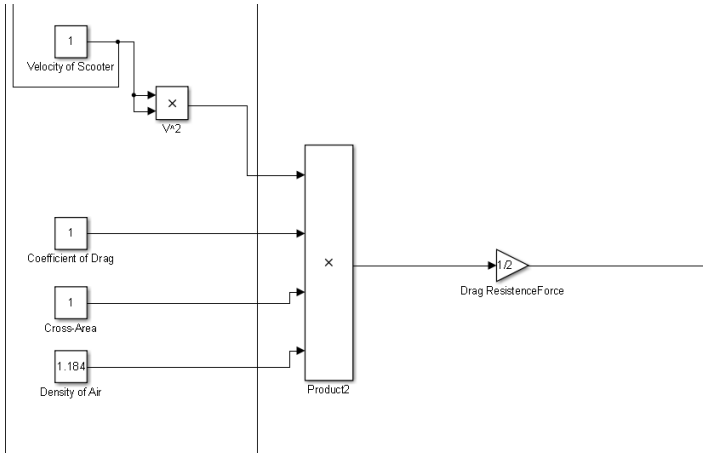

Figure 12. Aerodynamic Force (F_D) Simulation

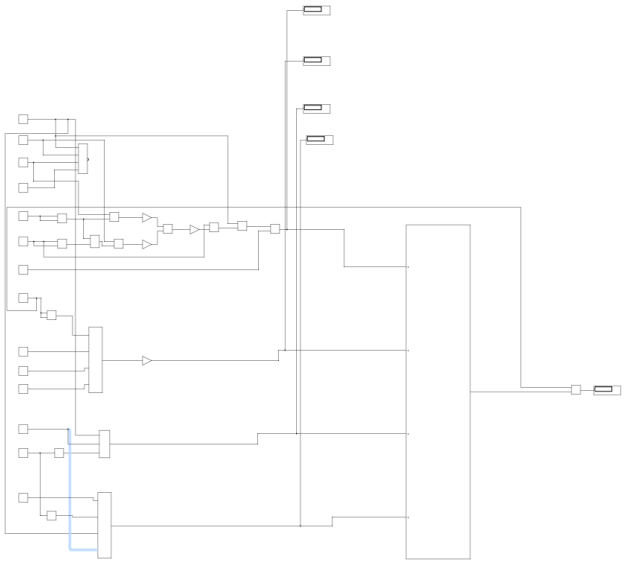

Figure 13. Entire Resistive Forces Simulation

The final single output of the entire simulation is the power load in watts. Based on the maximum current and voltage output of the fuel cell, and most importantly, based on the desired load the selected battery must be rated at 70V and must be capable of supporting 25Ah. The Simulink program will be programed in such a way that if the power output of the battery is less than 300W, then the fuel cell turns on and the battery will charge, if the power outage of the battery reaches 990W then the fuel cell turns off. Moreover, it is significant to note that the chosen battery is Lead Acid Cell Battery in large part due to its low cost and low self-discharge. However, it is important to note that the most suitable choice would have been the Li-ion Cell Battery mainly due to high energy density, hence low weight; however, the cost of a 70V 25Ah Li-ion battery would be too much to bear.

The simulation of the battery is included in the final simulation of the entire system represented in Figure 14. The simulation of the battery takes into account the characteristics of Lead Acid Cell battery.

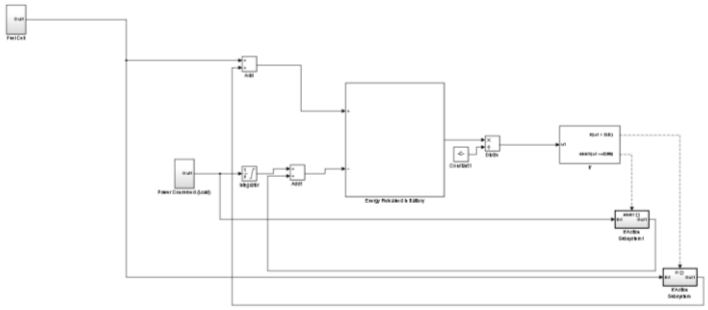

Figure 14. Entire Proposed System Simulation

There are two subsystems in the system itself, the first represents the fuel cell simulation and the second represents the power consumed (load) simulation. They are illustrated in Figure 15 and 16, respectively.

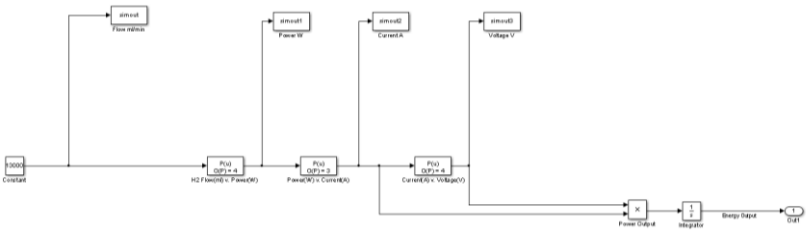

Figure 15. Fuel Cell Simulation Subsystem

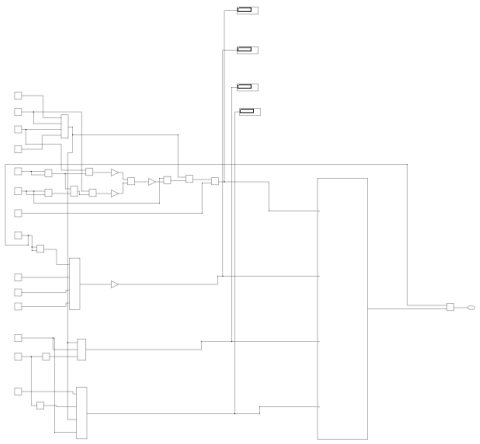

Figure 16. Resistive Forces Simulation Subsystem

The simulation was a success and it provided us with a lot of insight regarding the performance of our fuel cell system. From the simulation, we were able to acquire different graphs such as Current vs. H_2 Flow (Figure 17), Voltage vs. H_2 Flow (Figure 18) and Power vs. H_2 Flow (Figure 19). From these graphs, we were able to get the ranges of the possible outputs. The ranges possible are presented in Table 1.

Table 1. Output v. Range

Output Type	Range
Voltage	40-70 (V)
Current	0-25 (A)
Power	0-1040 (W)
Flow of hydrogen	0-13000 (ml)

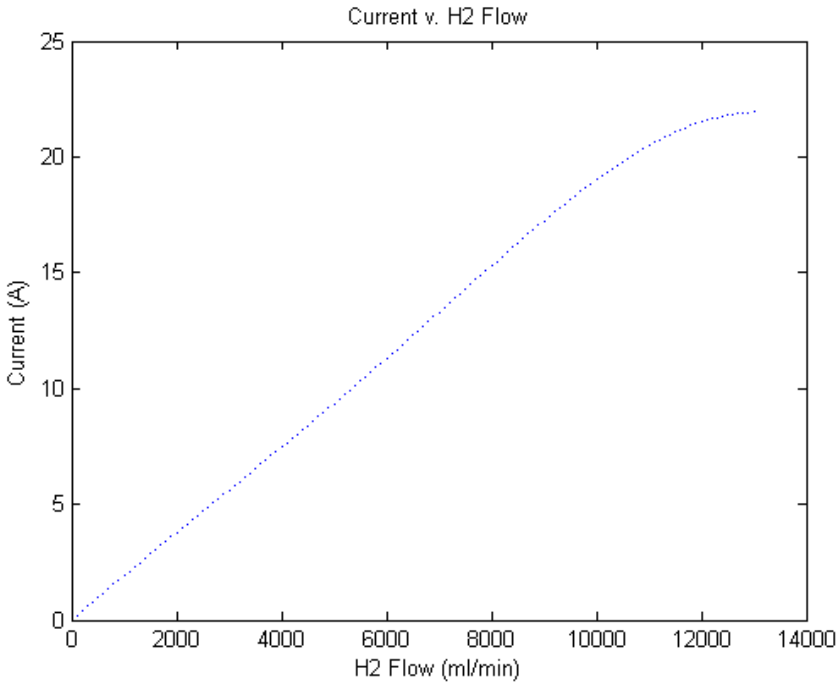

Figure 17. Current v. H_2 Flow

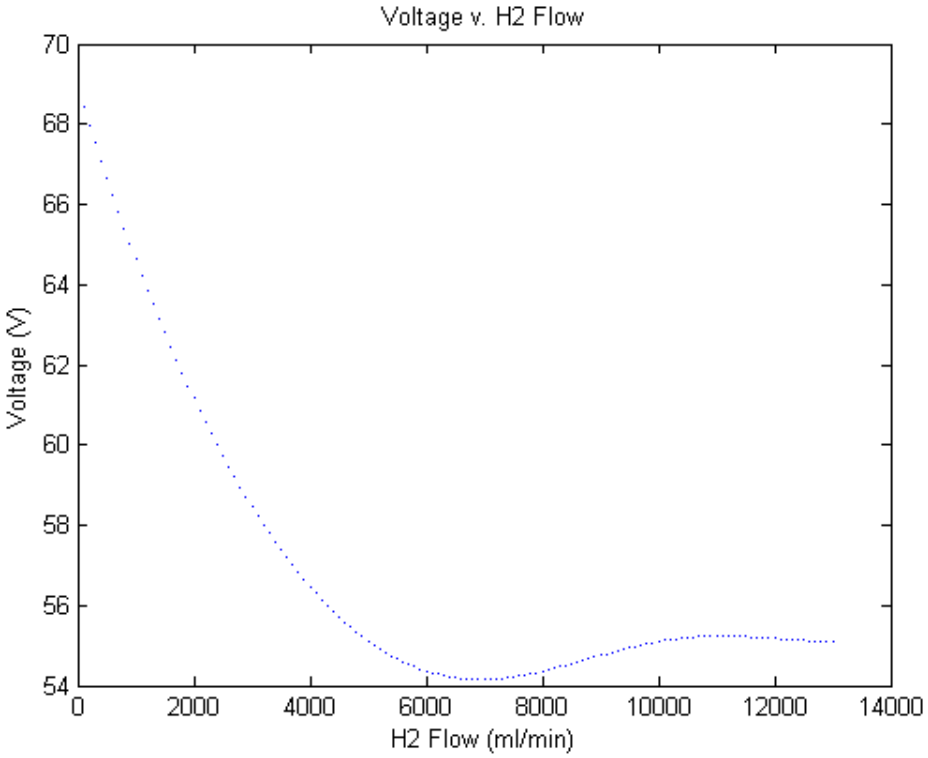

Figure 18. Variation of Voltage with H_2 Flow

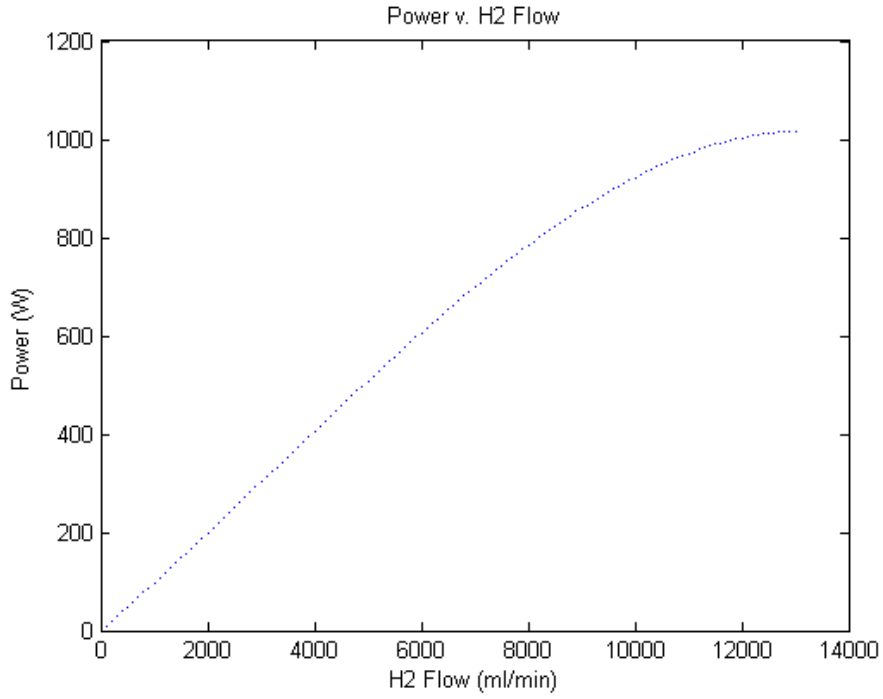

Figure 19. Power v. H_2 Flow

From the graphs and table it is clear that voltage is inversely proportional to the current. As the voltage decreases from 70 to 40 V, the current increases from 0 to 25 A. However, from Ohm's Law we know that current is directly proportional to the voltage. Thus, we can deduce that the

reason the voltage decreased as the current increased is that the resistance of the fuel cell changed. Hence, we can use Ohm's Law to calculate the equivalent resistance of the fuel cell at different currents and voltages (Table 2).

Table 2. Resistance at Different Voltages and Currents

Voltage (V)	Current (A)	Resistance (Ω)
60	5	12
56	10	5.6
52	15	3.5
50	20	2.5
40	25	1.6

The table clearly demonstrates how the resistance decreases as the current increases. That decrease of resistance is what leads to the decrease in the voltage. If the resistance was a fixed constant, then the graph of voltage versus current would have demonstrated a directly proportional relation between them. As a result, it is clear that the fuel cell follows Ohm's Law as expected.

From the power versus flow graph (Figure 19), it can be observed that as the flow of hydrogen increases, the power output increases. Between the ranges of 0-8,000 milliliters of hydrogen flow, the power output increases linearly. For every 1,000 milliliters increase in flow, the power output increases by 100 Watts. This relation holds true up until the flow of hydrogen exceeds 8,000 milliliters. Then between the ranges of 8,000-13,000 milliliters, the increases in the power output starts to decrease, until finally, the power output starts to decrease once the hydrogen flow exceeds 13,000 milliliters.

From these relations, a few statements can be made. The first is that the most efficient range of operation for our fuel cell is between 0-8,000 milliliters of hydrogen flow because the power increases linearly at a rate of 10:1. After that the efficiency starts to decreases gradually. Last but not least, the maximum power output possible is 1,040 Watts at a flow of 13,000 milliliters of hydrogen.

From the results, it can be clearly observed that the current is directly proportional to the power output; the greater the current, the greater the power output. This culminates in the end to a final current of 25 A, providing us with 1,000 W. Moreover, as stated before, the voltage and the resistance of the fuel cell decrease as the current increases. Thus, it can be said that the voltage and resistance have an indirectly proportional relation to the power output. In other words, as the voltage and resistance decrease, the power output increases. This can be explained using the different variations of Ohm's Law. Since the voltage decreases as the current increases, different combinations of voltage and current can give the same power output. For instance, from the voltage versus ampere graph, we can get two possible points of (50 V, 20 A) and (40 V, 25 A) as in Table 3.

Table 3. Different Variations of Voltage and Current

Voltage (V)	Current (A)	Power (W)
50	20	1,000
40	25	1,000

This table clearly demonstrates how different combinations of voltage and current can produce the same power output, and as a result, proving our fuel cell abides Ohm's Law. Furthermore, the same can be said about the relation between the resistance and current, as shown Table 4. Once again, the table shows proves that our fuel cell follows Ohm's Law, which validate our model and analyses.

Table 4. Different Variations of Resistance and Current

Resistance (Ω)	Current (A)	Power (W)
2.5	20	1,000
1.6	25	1,000

CONCLUSIONS

The study above conclude that hydrogen fuel cell projects are vital since oil will come to an end eventually leaving the humans with useless vehicles. In addition, to the harm that the oil running vehicles create extending from global warming, climate change and hazardous emissions to dreadful products that negatively affect the human being. All of these points meant that a new renewable source must be found to replace this current system. The fuel cell system itself isn't the renewable part in the project, instead it's the way that hydrogen is produced from and meaning if the hydrogen is produced using oil combustion then there is no use of the shift between the systems. The hydrogen should be produced using renewable energy sources. Through our research we found that there are various types of fuel cells, however, the best type that would fit the transportation uses is the proton exchange membrane hydrogen fuel cell.

In conclusion, the results acquired prove that our fuel cell works as expected of any electrical device by abiding to Ohm's Law. It produces a maximum current of 25 A, a maximum voltage of 70 V, and a maximum power output of 1,040 W. Meanwhile, the maximum flow of hydrogen recommended is 14,000 ml.

The PEMFC Scooter can be a very useful product due to its impact on the economics of countries, the benefits on the environment, the effects on society and the overall global impact such a product can achieve. It is already being used in Asian countries, such as Tokyo, and a lot of the impacts can already be observed there.

From an economical point of view, the PEMFC Scooter can be relatively cheap, especially on the long run due to the low cost of hydrogen and maintenance required. Moreover, having a PEMFC Scooter oriented market can lead to huge changes in any country. For example, the country can invest in hydrogen production factories, which can boost the economy by increasing income and increasing job opportunities for the public. Moreover, hydrogen-refueling stations can be built all around the country and that will also improve the economy. Therefore, it is clear that PEMFC Scooters can greatly boost the economy of any country that decides to implement them.

Meanwhile, from an environmental point of view, fuel cells are environment friendly due to their low carbon footprint. Unlike fossil fuels, they do not produce any harmful gases that can harm the environment. Consequently, PEMFC Scooters would significantly improve the environment of any country.

Likewise, from society's point of view, PEMFC Scooters have a very positive impact. They offer a cheap alternative to cars and are even cheaper in the long run due to the low cost of fuel and maintenance. In addition, since they are small, they can impressively reduce traffic jams because drivers can easily weave in and out of traffic. As a result, people would leave to their jobs later than usual because they don't have to worry about traffic, and that would lead to happier people with less stress and worries. Undoubtedly, this proves that PEMFC Scooters would help societies greatly, both economically and mentally.

Last but not least, the culmination of economical, environmental and societal impact can lead to a huge global impact. These three aspects are crucial to any country, and having all three of them improved in many different countries can have a significant impact on the world. Governments would have more money because they don't have to pay excessive amounts of money for gas and oil. While, the environment would greatly improve and global warming would be less of a global phenomenon. Finally, societies in general would be happier, thus leading to a more peaceful existence between people.

REFERENCES

[1] "A vehicle running on hydrogen" Mar. 3, 2014. [Online]. Available: http://www.toyotaglobal.com/innovation/environmental_technology/fuelcell_vehicle/. [Accessed: Oct. 12, 2014].

[2] Angkee Sripakagorn, Nartnarong Limwuthigraijirat, Experimental assessment of fuel cell/supercapacitor hybrid system for scooters, International Journal of Hydrogen Energy, Volume 34, Issue 15, August 2009, Pages 6036-6044.

[3] J.J Hwang, D.Y Wang, N.C Shih, D.Y Lai, C.K Chen, Development of fuel-cell-powered electric bicycle, Journal of Power Sources, Volume 133, Issue 2, 4 June 2004, Pages 223-228.

[4] A.A. Kulikovsky, A. Kucernak, A.A. Kornyshev, Feeding PEM fuel cells, Electrochimica Acta, Volume 50, Issue 6, 30 January 2005, Pages 1323-1333.

[5] P. Lin, P. Zhou, C.W. Wu, A high efficient assembly technique for large PEMFC stacks: Part I. Theory, Journal of Power Sources, Volume 194, Issue 1, 20 October 2009, Pages 381-390.

[6] Jenn Jiang Hwang, Review on development and demonstration of hydrogen fuel cell scooters, Renewable and Sustainable Energy Reviews, Volume 16, Issue 6, August 2012, Pages 3803-3815.

[7] Jenn Jiang Hwang, Wei Ru Chang, Life-cycle analysis of greenhouse gas emission and energy efficiency of hydrogen fuel cell scooters, International Journal of Hydrogen Energy, Volume 35, Issue 21, November 2010, Pages 11947-11956.

[8] O. Erdinc, M. Uzunoglu, Recent trends in PEM fuel cell-powered hybrid systems: Investigation of application areas, design architectures and energy management approaches, Renewable and Sustainable Energy Reviews, Volume 14, Issue 9, December 2010, Pages 2874-2884.

[9] Omar Z. Sharaf, Mehmet F. Orhan, An overview of fuel cell technology: Fundamentals and applications, Renewable and Sustainable Energy Reviews, Volume 32, April 2014.

[10] Bruce Lin, Conceptual design and modeling of a fuel cell scooter for urban Asia, Journal of Power Sources, Volume 86, Issues 1–2, March 2000, Pages 202-213.

[11] Kui Jiao, Xianguo Li, Water transport in polymer electrolyte membrane fuel cells, Progress in Energy and Combustion Science, Volume 37, Issue 3, June 2011, Pages 221-291.

[12] C.E. Thomas, Fuel cell and battery electric vehicles compared, International Journal of Hydrogen Energy, Volume 34, Issue 15, August 2009, Pages 6005-6020.

[13] J.J. Hwang, W.R. Chang, F.B. Weng, A. Su, C.K. Chen, Development of a small vehicular PEM fuel cell system, International Journal of Hydrogen Energy, Volume 33, Issue 14, July 2008, Pages 3801-3807.

[14] Cleaning the Air and Improving Health with Hydrogen Fuel-Cell Vehicles M. Z. Jacobson, W. G. Colella and D. M. Golden Science New Series, Vol. 308, No. 5730 (Jun. 24, 2005) , pp. 1901-1905

[15] Umberto Lucia, Overview on fuel cells, Renewable and Sustainable Energy Reviews, Volume 30, February 2014, Pages 164-169

[16] Jishi Zhao, Xiangming He, Jianhua Tian, Chunrong Wan, Changyin Jiang, Reclaim/recycle of Pt/C catalysts for PEMFC, Energy Conversion and Management, Volume 48, Issue 2, February 2007, Pages 450-453.

[17] “Case Study: Taiwan Hydrogen Fuel Cell Scooter Fleet Demonstration,” Jan. 14, 2013. [Online]. Available: http://www.fuelcells.org/pdfs/TaiwanScooterCaseStudy.pdf. Accessed: Oct. 12, 2014

[18] P. Huang et al., “Design and Implementation of 8051 Single-Chip Microcontroller for Stationary 1.0 kW PEM Fuel Cell System”, Journal of Chemistry, vol. 2014, Article ID 762954, 8 pages, 2014, http://dx.doi.org/10.1155/2014/762954.

[19] J.J Hwang et al., "Development of fuel-cell-powered electric bicycle", Journal of Power Sources, vol. 133, no. 2, pp. 223-228, June 2004.

Paper 11 **Bildiri 11**

EXPERIMENTAL INVESTIGATION OF THE EFFECT OF SWIRL NUMBER ON THE BURNING OF SYNTHETIC GASES IN A BURNER

Buğrahan ALABAŞ[1], Güven TUNÇ [2], Murat TAŞTAN [1*], İlker YILMAZ [1]

[*1]Faculty of Aeronautics and Astronautics, Department of Airframe-Powerplant, Erciyes University, 38039 Kayseri, TURKEY

[2] Faculty of Aeronautics and Astronautics, Department of Aeronautical Engineering, Erciyes University, Kayseri, TURKEY

Corresponding Author e-mail: mrt@erciyes.edu.tr

Abstract

Today, there are many different studies on increasing combustion efficiency and reducing flue gas emission values. In this study, H_2 and CO were added to 30% methane gas in a premixed laboratory scale model burner with high H_2 / CO ratio (3) and medium (1,5). Swirl numbers (s = 0,6 and 1) have been changed by keeping the equivalent ratios constant. The experiments have been carried out at a constant burner power (3 kW), regardless of the fuel composition. The effect of swirl number on the temperature distribution and emission values of radial and axial directions in the combustion chamber. While the number of swirl has been low, CO emissions have increased, NO and O_2 emissions have decreased with the decrease of H_2 / CO ratio. When the number of swirls has been increased, CO emissions are decreased, and NO emissions are increased with the decrease of H_2 / CO ratio. As a result of the experiments, the swirl number and the rate of H_2/CO has a great effect on combustion characteristics and emissions of flames.

1. INTRODUCTION

Nowadays, energy consumption has increased due to the increase in industrialization in order to meet the increasing needs of the human population. This increase in energy consumption has led to the intensification of studies on combustion efficiency of fuels used in energy production. On the other hand, the increase in energy production has revealed the problem of flue gas emissions, which is as important as efficiency. Products such as CO, CO_2 and NO_x, which are present in the flue gases as combustion products, damage humans, animals and plants. The H_2

and CO synthetic gas fuel mixture which is produced by wood and organic wastes is an alternative and renewable fuel that meets the energy demand of the synthetic gas fuel mixture [1].

Especially hydrogen is a renewable synthetic fuel that has recently attracted attention and required more field-tested and can be used as an alternative fuel for many areas. Unlike fossil fuels, due to containing only water vapour as combustion emission while burned with oxygen, hydrogen is known as environment-friendly and zero emission future green fuel. Therefore, the use of hydrogen fuel instead of carbon-based fuels can be considered as the most effective way to prevent hazardous emissions such as CO_2, CO, Sulphur oxide and organic acids when faced up increasing power requirements.

These synthetic gases vary in terms of flame temperature and flue gas emissions according to different combustion chamber conditions and mixing ratios. Hence, nowadays many researchers have studied the combustion characteristics of H_2/CO synthetic gas mixture and have been obtained numerical and experimental data for different working conditions. Some of these studies have been mentioned below.

Lee at al. have been performed experiments in a gas turbine burner with a burning power of 60 kW. In these experiments, they have been observed flame stability, dynamic pressure, NO_x, CO emissions and temperatures in the combustion chamber. First, they tested the mixture of real synthetic gases used in two different power plants in Korea (Taean) and the Netherlands (Buggenum). In these gases have been tested without dilution, the gas used at the Buggenum plant had higher flame stability than the Taean plants. This is thought to be caused by higher hydrogen content. In dilution, the stability of the gas used in the Buggenum plant has been higher than that of Taean because of the higher nitrogen dilution rate. As a result of the experiments, it has been revealed that nitrogen dilution caused partial differences in emission and flame stability values because of the different H_2/CO ratio in the gases used in two separate power plants [2]. Hagos at al. have been examined air/fuel ratio and they have been tested from the possible lowest excess air ratio to the poor operating conditions. As a result, the NO_x emission of H_2/CO combustion was higher than natural gas combustion. On the other hand, it has been observed that the combustion process with the synthetic gas mixture can occur in a wider range of air/fuel ratio [3]. Samiran et al. have been set H_2/CO ratios of tested gas mixtures as 3.0 (high) and 1.2 (moderate) and diluted each mixture with CH_4 and CO_2. They have been reported that as the CO amount in gas mixture increases, more luminous flames arise, indicating

increased sooting tendency. Hydrogen has been found to make flame more compact and more resistant to the blowout. On the contrary, flames of high CO content mixtures have been found to the blowout at higher equivalence ratio, which poses stability issues. It was also shown that while CO_2 and CH_4 dilution increases blowout equivalence ratio, CH_4 dilution promotes flame stability; high CO content results with high NO_x emissions [4]. İlbas and Karyeyen have been simulated flames under the same physical and atmospheric conditions and achieved a good consistency between measured and predicted temperature values. Later, they have been set turbulator angle of their burner as 15, 30 and 45°, and numerically evaluated effects of these variations on combustion characteristics of studied flames. It has been found that as the turbulator angle increases, the flame base moves upstream and flame temperature increases based on the tangential velocity component entrainment to flow and better mixing between reactants, respectively. Consistently; CO emissions decrease and CO_2 emissions increase, as the turbulator angle increases [5]. Cellek and Pınarbası, have been investigated the natural gas combustion in a burner with low swirl value. Four different gas contents have been tested to evaluate the combustion emissions of hydrogen-enriched natural gas and pure hydrogen (% 75 NG % 25 H_2, % 50 NG % 50 H_2, % 25 NG % 75 H_2, % 100 H_2). As a result of the investigation, the combustion behavior of natural gas and methane have been found to be close to each other but the NO_x and O_2 emissions have been different. In addition, NO_x emissions increased as the hydrogen ratio increased compared to pure natural gas combustion [6]. Yu et al. have been investigated that the addition of hydrogen to hydrocarbon fuels increases combustion performance (combustion ignition and stability) and reduces pollutant emission [7]. Choudhuri et al. have been found that the addition of hydrogen to natural gas resulted in shortening of the flame length and reduced CO emission. However, NO_x emissions have been increased due to the increase in flame temperature [8]. Wu et al. have been studied that the emission and heat transfer characteristics of methane-hydrogen mixtures. CO and CO_2 emissions were reduced by the addition of hydrogen. Oxidation from CO to CO_2 has been more efficient in high hydrogen additions. Reducing the amount of carbon in the fuel was the dominant factor in the reduction of CO_2 emissions. They have determined that NOx is caused by the NNH mechanism (NNH is formed by the reaction of nitrogen with the H atom) [9]. Zhen et al. have been studied pre-mixed LPG - hydrogen mixtures. They have been found that the addition of hydrogen increased the flame temperature and the CO emissions decreased and NO_x emissions increased [10]. Yilmaz et al. have been showed that the effect of flame characteristics (temperature and pollutant emission distributions) on the number of swirls has not been monotonous and the

flame behavior due to the equivalence ratio has been changed differently in the different vortex numbers [11]. Lee has been investigated that the flame structures have greatly changed by the fuel composition and heat input, and they have been subjected to key affecting parameters of the temperatures of the flames and the liners. NO_x and CO emissions also largely varied according to fuel composition and heat input. When fuel has been changed from natural gas to syngas to minimize NO_x and CO emissions with stable combustion, it could contribute to the optimal selection of the fuel supply condition [12].

As can be seen in the literature, current studies on H_2/CO synthetic gas fuel mixtures have an important place in the field of energy. The combustion instability and emission values of these fuels are a field of study where researchers frequently study experimentally and numerically. In this study, unlike the previous ones, experiments have been carried out at high (3) and moderate (1.5) H_2/CO ratios in a pre-mixed gas turbine burner with 3 kW burning power. In addition, the effect of two different swirl numbers (0.6 and 1) on the emission values of these gas mixtures have been examined. The emission values resulting from the combustion process have been taken from the points at different axial and radial distance to the burner inside the combustion chamber and these values have been compared, respectively.

2. EXPERIMENTAL SETUP

2.1. Operating Conditions

Tested gas compositions have been tabulated in Table 1. Irrespective of the gas composition, thermal power has been kept constant and mass flow rate of each mixture has been specified based on thermal power. Equivalence ratio has been set as 0.7 while the swirl number has been as 0.6 and 1. All experiments have been carried out at room temperature and 20 mbar

Table 1. Tested gas mixture

Synthetic Gas	CH_4 (%)	H_2 (%)	CO (%)	Swirl Number	H_2 /CO
Exp 1	30	52.5	17.5	0.6	3
Exp 2	30	42	28	0.6	1.5
Exp 3	30	52.5	17.5	1	3
Exp 4	30	42	28	1	1.5

2.2. Burner

A burner should comply with the combustor to be used to better meet emissions and fuel efficiency requirements. In burner design, parameters such as the dimensions of the combustion device, thermal power and the properties of the fuel to be used are important. At the same time, a burner should be able to provide complete combustion through the entire operating range with at least excess air and even heat dissipation. With these considerations, a pre-mixed burner balanced with a vortex generator has been used in a laboratory scale combustor.

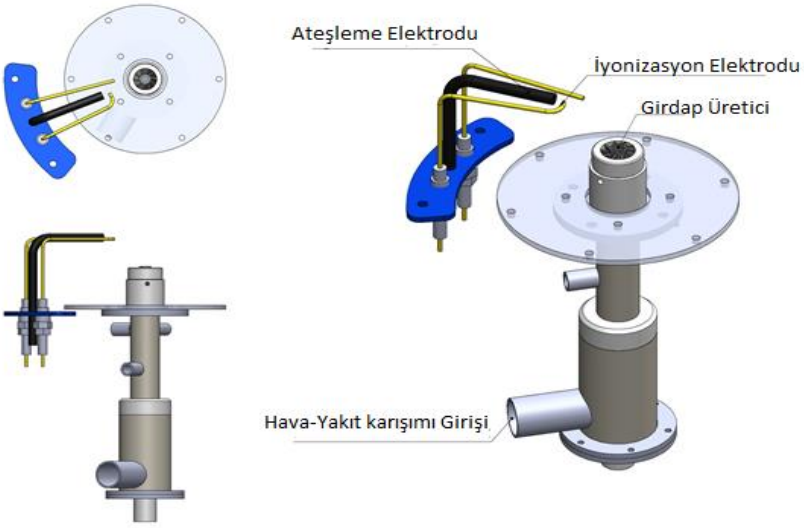

Figure 1. Burner Design

This burner has been designed to operate at 10 kW power and 20 mbar pressure. Since the flame-tightening position is difficult to control and at higher pressures complex and expensive flow control equipment is required, the working pressure is kept relatively low to the maximum pressure that can be exited. The burner model can be seen in Figure 1.

2.3. Fuel Supply Lines

The diameter of the fuel supply lines has been determined by the density and the heating value of each synthetic gas component as well as the thermal power depending on the mass flow rate ratio. Each gas pressure has been supplied from an external gas tank and has been measured by a mass flow controller controlled by the vacuum system controller. The gas pressure of the tank has been reduced from 200 - 300 bar to 0 – 1.5 bar with a gas regulator mounted on the gas tank. These relatively high-pressure values are necessary for the operation of the mass flow controller. Since the burner has been designed to operate at 20 mbar, pressure regulators have been mounted on gas supply lines to reduce the pressure at this value. Manometers have also

been used to monitor the pressure. For the purpose of inspection, float type mechanical flow meters have been mounted on each gas supply line.

2.4. Combustor

The length of the burner is 1650 mm. It has an outside diameter of 330 mm and an internal diameter of 320 mm but has a wall thickness of 5 mm. In order to make axial and radial temperature and emission measurements, a lot of space is formed in the walls, side arms and chimneys of the combustion wheel. There is also a cooling receptacle which is supplied by air via an external air turbine around the periphery of the combustion chamber. Tempered glasses on the front and side walls of the burner make the flame optically accessible. It also makes it possible to change the vortex manufacturer without removing the burner. All metal parts of the combustion device are made of stainless steel. In order to ignite gas mixtures, flame stability was maintained in all operating conditions, a reliable operation process was achieved, and pilot ignition system was fabricated. This system consists of a fuel supply line, solenoid valve, air fan and burner. Other equipment not covered in the figure has been mounted on the combustion system for flame stability studies. The combustor model measuring port has been shown in Figure 2.

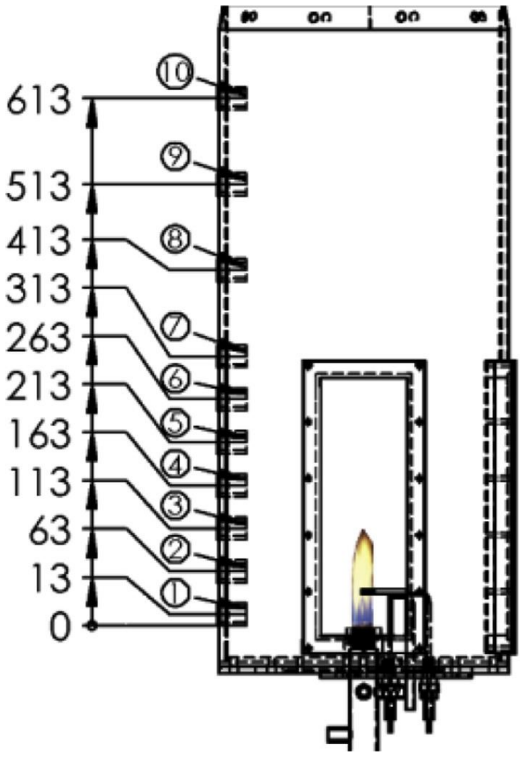

Figure 2. Measuring ports.

2.5. Air Supply Lines

Combustion air is supplied from a piston type air compressor with a storage capacity of 1500 m^3. After that, filtered to remove oil and steam. The amount of air (depending on the equivalence ratio) is regulated by a digital (thermal) mass flow controller (MKS-1579A). The other equipment's of the air supply line are a manometer and a mechanical flowmeter. For safety purposes, solenoid valves have been installed to each gas supply line to electromechanically cut fuel supply in the absence of flame, which is detected by an ionization electrode. The schematic view of the combustion system and the test equipment is shown in Figure 3. All fuel gases and combustion air are delivered to a gas collector then fully mixed in a static pre-mixer, which is equipped with a mechanical flashback arrestor, before entering burner.

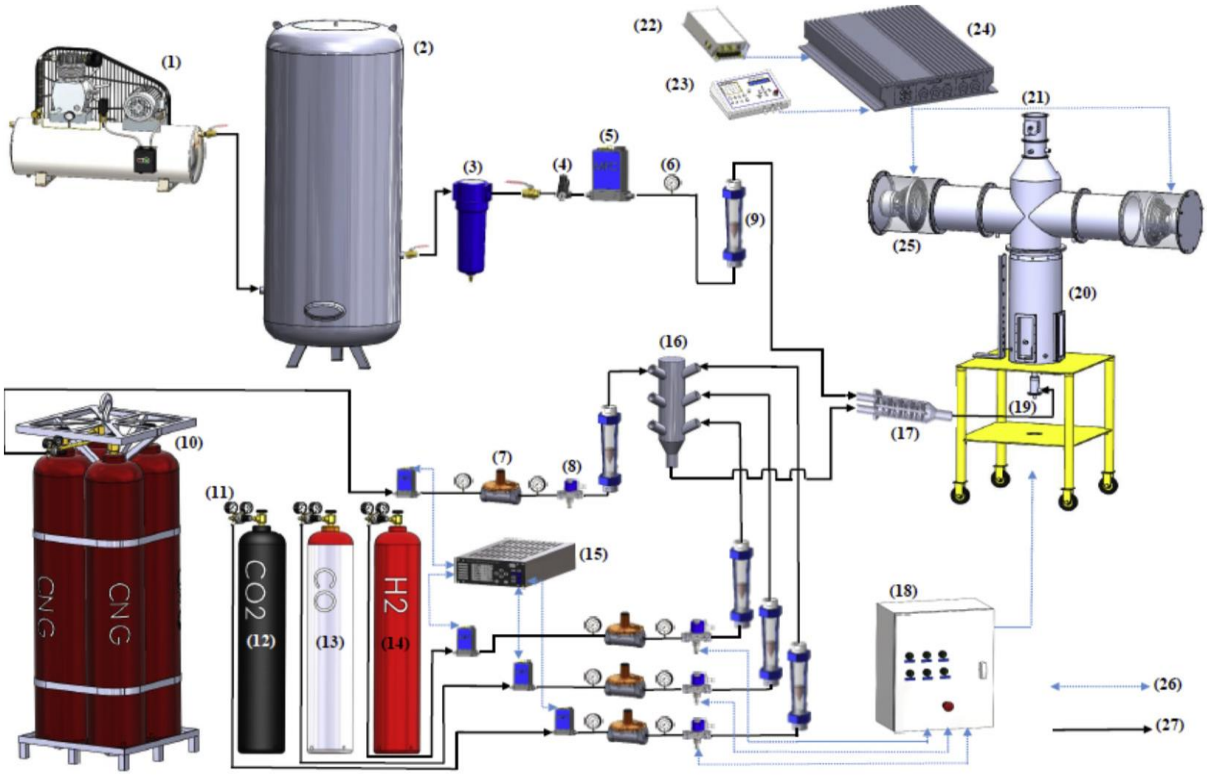

1. Air compressor (5.5 hp, 500 lt)	10. CNG tank	19. Burner
2. External air tank (1 m^3)	11. Pressure regulator	20. Combustion chamber
3. Filter (for steam and oil removal)	12. CO_2 tank	21. Flue
4. Pressure regulator (1 MPa to 0.3 MPa)	13. CO tank	22. Power source
5. Mass Flow Controller	14. H_2 tank	23. Function generator
6. Manometer	15. Vacuum system controller	24. Audio amplifier
7. Pressure Regulator	16. Gas collector	25. Loudspeaker
8. Solenoid Valve	17. Fuel/air pre-mixer (static)	26. Electrical connections
9. Float type flowmeter	18. Control panel	27. Gas supply lines

Figure 3. Layout of the overall combustion system

2.6. Measurement Equipment

Temperature measurements have been conducted with ceramic coated NiCreNi alloy K (Temperature range: 200 - 1200 °C) and Pt13%Rh-Pt alloy B-type (Temperature range: 0-1800 °C) thermocouples. Data from these thermocouples have been converted into quantifiable parametric information through a 28-channel data logger with a sampling rate of 100 kS / s and stored in a computer. The setting of each channel to the sampling rate, selecting the channel input value and monitoring of the measured data during the experiments have been carried out with ProfiSingal Go software. In addition, emission measurements have been performed with a flue gas analyzer.

3. RESULTS AND DISCUSSION

It can be seen that in Figure 4, the H_2 / CO ratio has not been changed too much the maximum flame temperature independently of the gas mixture. The temperature values in the post-flame region have decreased and the highest amount of reduction has been seen in the Exp.-3 (30% CNG- 52.5% H_2-17.5% CO, S/N:1, H_2 / CO:3). In the mixture gases, the presence of H_2 accelerates the chemical reactions and shortens the turbulent flow time due to the high flame velocity and the good diffusion capability of hydrogen [13]. Carbon monoxide oxidation kinetics are much slower than hydrogen [14], [15]. In the combustion zone, hydrogen gas and other components of the synthetic gas mixtures are burning firstly. As the amount of hydrogen in the mixtures increases, the flame goes upstream. In the case of a high CO contented mixture, long flames with low burning intensity form seen. In the light of the above, one could be concluded that in the mixtures with a high amount of hydrogen (Exp 1 and Exp 3) create higher temperature distributions in the middle of the combustion chamber and in the outlet area than in the other mixtures. As the number of swirl increases, the mixing state of air and fuel improves, the residence time of the resulting mixture in the high-temperature zone may increase and so the heat could spread in the radial direction better. The resulting flame may expand radially towards the burner walls, thus it burns more stable and intense.

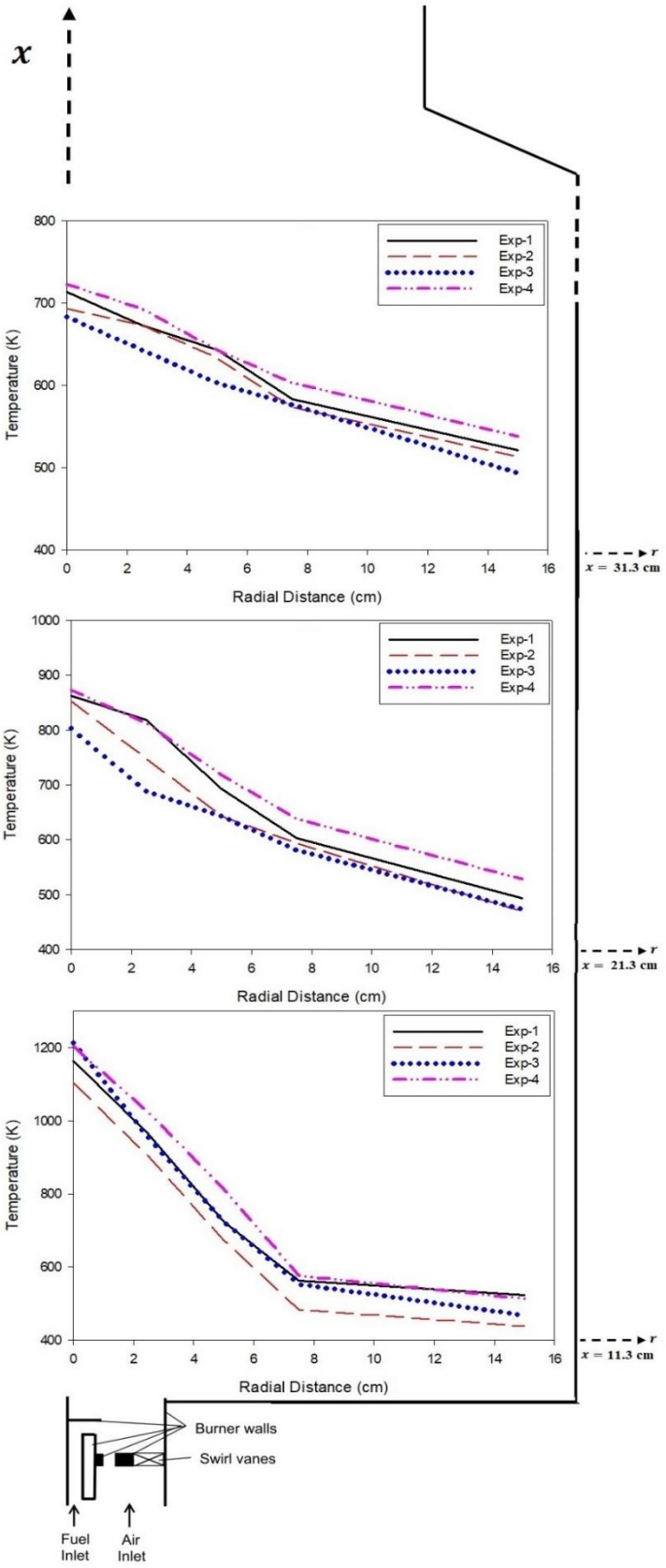

Figure 4. Temperature distribution in the combustion chamber

The increase in swirl number has resulted in a decrease in axial temperatures after the flame zone (~11 cm). As the swirl number increases, the place that the chemical reactions take place radially may slip outward and the temperature in the centre of the flame decrease. It is has been thought that high-temperature values in low swirl numbers are caused by this situation. The temperature profiles tend to be similar but differ in value. Relatively short flames have been formed as the burning power is kept low. For this reason, the number of swirls could affect the temperature values in the flame and combustion chamber exit zones too much.

The emission measurements of the gases have been carried out in different radial (2.5, 5, 7.5, 10 and 15 cm away from the combustion chamber center) and in the axial (11, 21 and 31 cm) position. The effect of H_2 / CO ratio and swirl number on CO emissions can clearly be seen in Fig.-5. Looking at the comparison of the Exp.-1 and Exp.-3 which both have high H_2 / CO (3) ratio, it can be seen the Exp 1 with a low Swirl number has a lower CO emission at the axial distance. The CO emission values of the Exp.-1 mixture are approximately three times lower in axial distance compared to the Exp.-3 mixtures. If both Exp.-2 and Exp.-4 mixtures that have with a medium H_2 / CO (1.5) ratio have compared, it could be seen the Exp.-4 that has high swirl number has lower CO emissions at the axial distance.

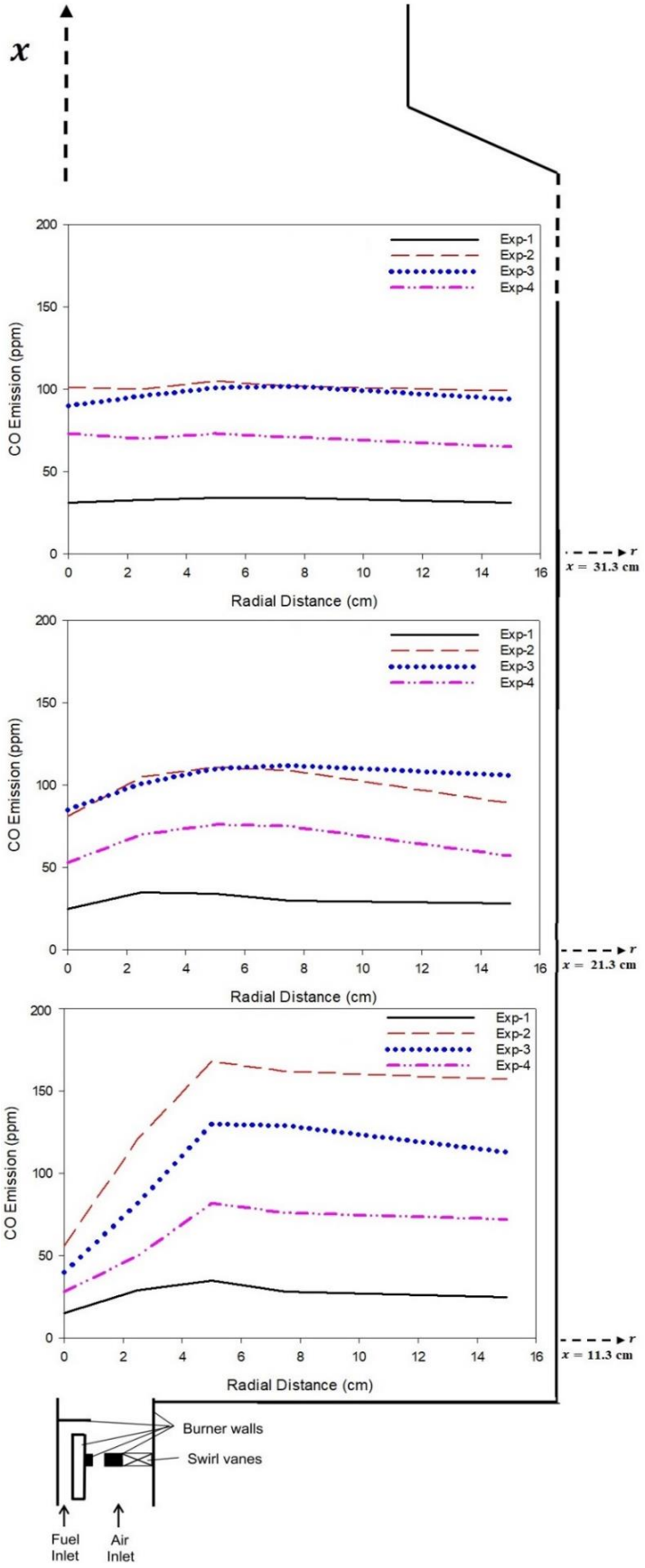

Figure 5. CO emission distribution in the combustion chamber

The CO emission values of the mixture of Exp.-4 are approximately two times lower than in each position at the axial distance compared to the mixtures of Exp.-2. The increase of CO emission in the flame zone at the radial distance may be due to the decrease in temperature. There has been no significant change in the distribution of CO emissions in the radial direction over distances from the flame zone. High CO emission values in the mixture of Exp1 and Exp 3 are due to low combustion temperature. The cause of this situation may be the high H_2 and low CO content of the respective mixture. Thus, it could conclude that hydrogen improves the oxidation kinetics of carbon monoxide.

When the NO_x emissions have considered, it can be seen at the Fig.-6, the changes have been related to depending on the temperature. The NO_x increase due to the combustion temperature shows that the thermal Zeldovich mechanism is effective in NO_x formation [16]. If both Exp.-1 and Exp.-3 mixtures that have with a high H_2 / CO (3) ratio have compared, it could be seen the Exp.-1 which has low swirl number produces higher NO_x emissions at the axial distance. As it moves away from the flame zone, the NO_x emission decreases. If both Exp.-2 and Exp.-4 mixtures that have with a medium H_2 / CO (1.5) ratio have compared, it could be seen the Exp.-2 which has high swirl number produces lower NO_x emissions at the axial distance.

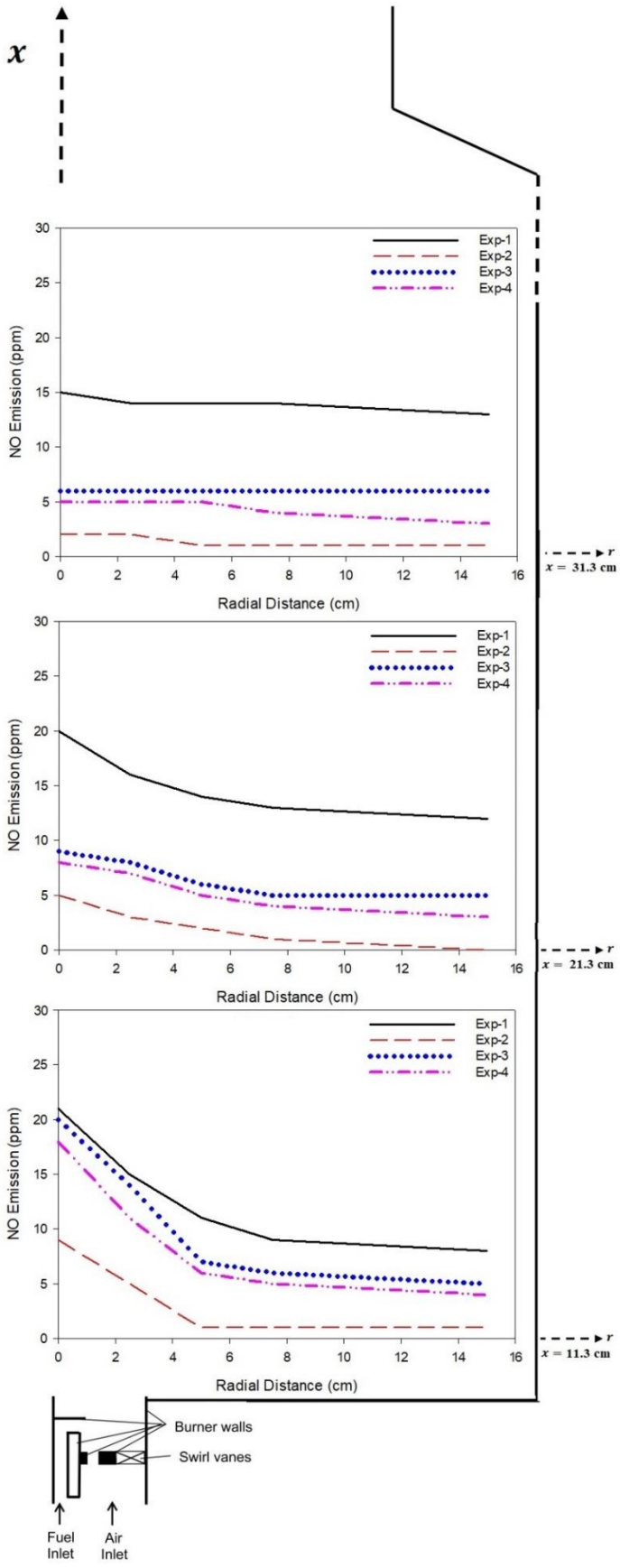

Figure 6. NO_x emission distribution in the combustion chamber

The high H_2 / CO ratio increased NOx emissions compared to the medium H_2 / CO ratio. NNH mechanism is effective in NOx formation in low levels of hydrocarbon and high concentrations of H_2 gas. NNH is caused by the reaction of nitrogen with the H atom [17]. The difference between the numbers of Swirl has affected NO_x emissions. Mixtures with a swirl number 1 have achieved more stable combustion. As a result of this stable combustion, NO_x emissions have been measured as more stable values. It could be concluded that NO_x formation mechanisms are more effective than changes in NO_x values in mixtures with Swirl number 0.6. It can be thought that when we consider, Exp.-1 and Exp.-2 that have equal swirl number, NNH mechanism is more effective in the Exp.-1 which has high H_2/CO and Zeldovich mechanism is more effective in the Exp.-2 which has medium H_2/CO.

The O_2 emissions as a percentage of the total exhaust gases of the mixtures are given in Figure 7. It could be seen the effect of the swirl number is noticeable in O_2 emissions. It is concluded that mixtures with a swirl number 1 have more stable combustion than mixtures with a Swirl number of 0.6 so they produce lower O_2 emission. The effect of H2 / CO ratio could not be determined significantly. Reduction of NOx emissions in the flame zone at radial distances may be due to a decrease in temperature. No significant change has been observed in the radial direction in the distribution of NOx emissions over distances from the flame zone.

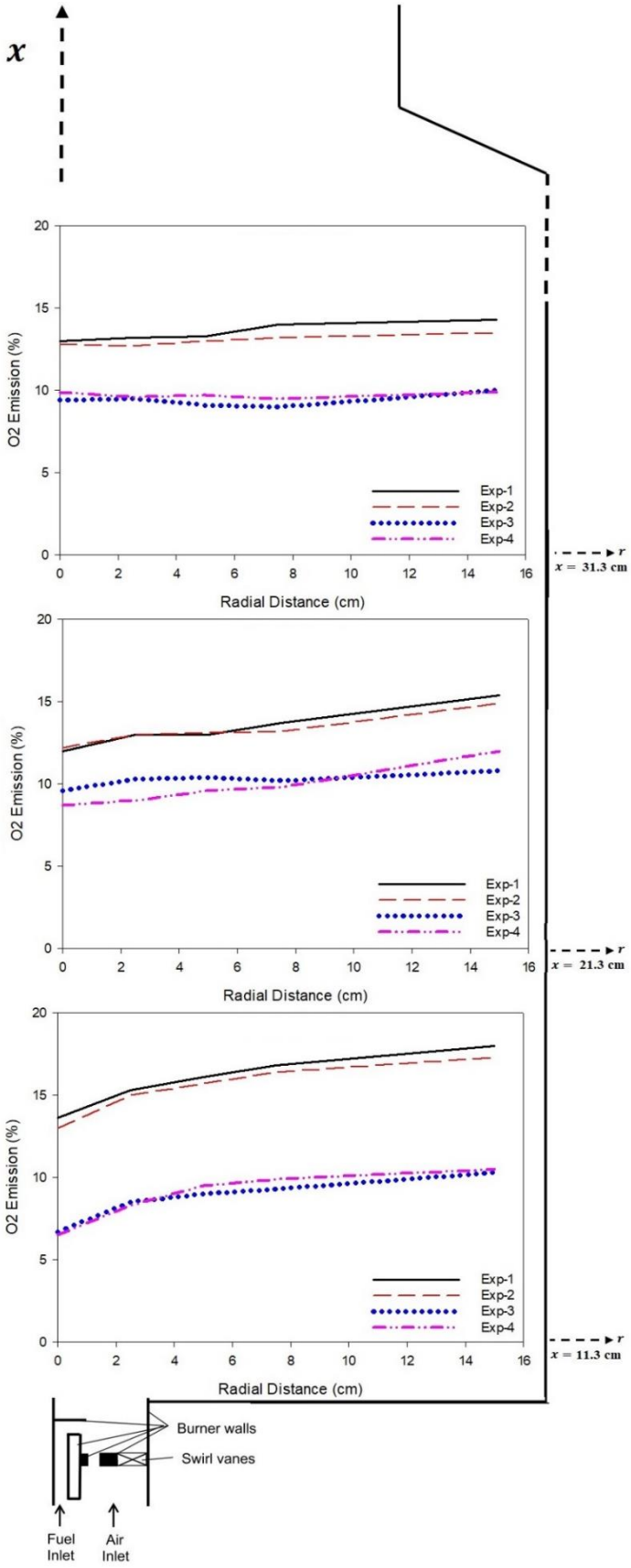

Figure 7. O_2 emission distribution in the combustion chamber

4. CONCLUSIONS

In this study, the effect of gas composition and swirl number on combustion and emission behavior of premixed syngas mixtures has been experimentally investigated in a burner. Results have obtained from this study are:

- From the temperature distributions in the combustion chamber have been obtained consistent results regardless of the number of swirl and the mixing ratios.
- It has been observed that the H_2 ratio in the mixtures has a positive effect on the temperature, the decrease in the number of swirls decreases the temperature in the axial direction and increases the radial direction slightly.
- It is found that mixtures are sensitive to CO emissions. It has been also found that the low Swirl number in mixtures with high H_2 / CO (3) ratio leads to lower CO emissions with relatively high Swirl number in mixtures with medium H_2 / CO (1.5) ratio.
- It is thought that NO_x formation mechanisms are different in mixtures with high H_2 / CO ratio and medium H_2 / CO (1.5).

REFERENCES

[1] H. Yilmaz and I. Yilmaz, "Effects of synthetic gas constituents on combustion and emission behavior of premixed H2/CO/CO2/CNG mixture flames," *Journal of the Energy Institute*, Elsevier, 18-Jun-2018.

[2] M. C. Lee, J. Yoon, S. Joo, and Y. Yoon, "Gas turbine combustion characteristics of H2/CO synthetic gas for coal integrated gasification combined cycle applications," *Int. J. Hydrogen Energy*, vol. 40, no. 34, pp. 11032–11045, Sep. 2015.

[3] F. Y. Hagos, A. R. A. Aziz, and S. A. Sulaiman, "Syngas (H2/CO) in a spark-ignition direct-injection engine. Part 1: Combustion, performance and emissions comparison with CNG," *Int. J. Hydrogen Energy*, vol. 39, no. 31, pp. 17884–17895, Oct. 2014.

[4] N. A. Samiran, J.-H. Ng, M. N. Mohd Jaafar, A. Valera-Medina, and C. T. Chong, "H2-rich syngas strategy to reduce NOx and CO emissions and improve stability limits under premixed swirl combustion mode," *Int. J. Hydrogen Energy*, vol. 41, no. 42, pp. 19243–19255, Nov. 2016.

[5] M. Ilbas and S. Karyeyen, "Turbulent diffusion flames of a low-calorific value syngas

under varying turbulator angles," *Energy*, vol. 138, pp. 383–393, 2017.

[6] M. S. Cellek and A. Pınarbaşı, "Investigations on performance and emission characteristics of an industrial low swirl burner while burning natural gas, methane, hydrogen-enriched natural gas and hydrogen as fuels," *Int. J. Hydrogen Energy*, vol. 43, no. 2, pp. 1194–1207, Jan. 2018.

[7] G. Yu, C. K. Law, and C. K. Wu, "Laminar flame speeds of hydrocarbon + air mixtures with hydrogen addition," *Combust. Flame*, vol. 63, no. 3, pp. 339–347, Mar. 1986.

[8] A. R. Choudhuri and S. . Gollahalli, "Combustion characteristics of hydrogen–hydrocarbon hybrid fuels," *Int. J. Hydrogen Energy*, vol. 25, no. 5, pp. 451–462, May 2000.

[9] L. Wu, N. Kobayashi, Z. Li, H. Huang, and J. Li, "Emission and heat transfer characteristics of methane–hydrogen hybrid fuel laminar diffusion flame," *Int. J. Hydrogen Energy*, vol. 40, no. 30, pp. 9579–9589, Aug. 2015.

[10] H. S. Zhen, C. S. Cheung, C. W. Leung, and Y. S. Choy, "Effects of hydrogen concentration on the emission and heat transfer of a premixed LPG-hydrogen flame," *Int. J. Hydrogen Energy*, vol. 37, no. 7, pp. 6097–6105, Apr. 2012.

[11] H. Yilmaz and I. Yilmaz, "Combustion and emission characteristics of premixed CNG/H2/CO/CO2 blending synthetic gas flames in a combustor with variable geometric swirl number," *Energy*, vol. 172, pp. 117–133, Apr. 2019.

[12] M. C. Lee, "Effects of H2/CO/CH4 syngas composition variation on the NO x and CO emission characteristics in a partially-premixed gas turbine combustor," *Sci. China Technol. Sci.*, vol. 59, no. 12, pp. 1804–1813, Dec. 2016.

[13] "Flammability limits and laminar flame speed of hydrogen–air mixtures at sub-atmospheric pressures," *Int. J. Hydrogen Energy*, vol. 37, no. 22, pp. 17580–17588, Nov. 2012.

[14] "Experimental study on the laminar flame speed of hydrogen/carbon monoxide/air mixtures," *Fuel*, vol. 88, no. 10, pp. 1858–1863, Oct. 2009.

[15] D. P. S. Abam, " Carbon monoxide oxidation in laminar diffusion flames," *Combust. Flame*, vol. 68, no. 2, pp. 95–107, May 1987.

[16] Glassman, I., Yetter, R. A., Glumac, N. G., “Combustion” , Fourth Edition. Elsevier, USA, 773 pp. 2014.

[17] Lefebvre, A. H., “Gas Turbine Combustion: Alternative Fuels and Emissions”, Third Edition. CRC Press, USA, 537 pp. 2010.

Paper 12 **Bildiri 12**

USE OF LOW COST WASTE EGG SHELL AS A CATALYST IN BIODIESEL PRODUCTION, INVESTIGATION OF YIELD, DENSITY AND VISCOSITY PARAMETERS OF BIODIESEL OBTAINED IN DIFFERENT METHANOL / OIL MOLAR RATIOS AND COMPARISON WITH CAO CATALYST

Fevzi Yaşar

Batman University Vocational School of Chemistry and Chemical Process Technology Department,

72100, Batman, Turkey

yasarf75@gmail.com

Abstract:

Most of the world's energy needs are met by oil, and many countries import a large portion of their oil demand. This causes a very critical problem, such as energy dependence. Nowadays, petroleum, which is the raw material of mining, construction and chemical industry, has the biggest share in energy consumption, especially in transportation, construction machinery, automotive, marine, electricity production. For these sectors, the development of alternative fuels other than oil is vital issue for a possible oil crisis. On the other hand, as a result of the increase in consumption of petroleum products, they cause global climate changes that can cause harms to environment, human health and dangerous developments globally due to harmful and toxic gases such as CO_2, SO_2 and NOx. In this respect, research and development of alternative fuels has become a very crucial issue. It is necessary that alternative fuel sources be human-oriented, renewable, feasible and easily available, with local resources for sustainable economic development and a cleaner environment. One of the alternative fuels is biodiesel. Catalysts used in biodiesel production are the most important parameters affecting the production efficiency in the production process by biodiesel transesterification. Homogenous and heterogeneous catalysts are used in biodiesel production. Although the yield in homogeneous catalysts is high, many factors such as saponification, excess reagent consumption and extra separation cost negatively affect production costs. Therefore, efforts to develop high-efficiency and highly usable heterogeneous catalysts that prevent saponification have gained a great speed and importance today. In this study, the use of cheap and domestic waste egg shell as a catalyst and the efficiency, density and viscosity parameters of biodiesel

obtained in different methanol / oil molar ratios were investigated. The study was detailed by means of XRD, P-XRF analysis methods. The results showed that the waste egg shell can be used as a catalyst, it has a significant effect on the biodiesel efficiency, the waste egg shell catalyst can be used repeatedly, and the cost of biodiesel production can be reduced significantly.

Keywords: Waste egg Shell, Catalyst, Biodiesel, Methanol/oil molar ratio

1. INTRODUCTION

Energy is one of the most fundamental and accelerating requirements of a country's economic and social development. For this reason, the phenomenon “energy security” is one of the vital elements of economic security and national security. Energy is an indispensable input for almost all processes necessary for sustaining our social lives; and is used in sub-sectors of industry, transportation, housing and commerce. Today, the energy consumed in the world is obtained from many energy sources; and fossil sources such as oil, natural gas and coal account for 87% of these resources [1]. Energy efficiency policies should be the foremost issue to be taken into the consideration since on the one hand, they are directly related to the sustainability of economic growth and social development targets, on the other hand, they play the key role they play in reducing total greenhouse gas emissions. Within the framework of sustainable development goals, countries should be determined to use their energy resources effectively, efficiently and with minimal impact on the environment. We are fulfilling our responsibilities for the environment and providing our energy supply security by giving the necessary importance to renewable resources in energy production which is the basic input of development and evaluating our mines in accordance with environmental standards [2]. Existing petroleum, natural gas, coal etc. fossil resources are expected to decline rapidly due to future population growth and increased use of fuel run vehicles used in everyday life [3]. Therefore, the use of renewable energy resources, which are local and renewable, are of great importance in terms of meeting the energy needs in our country and in other countries. Therefore, the use renewable energy sources around the world both in terms of technological research as well as utilizing the energy produced from these sources has been directed. It is essential that renewable energy sources be human-centred, feasible, and easily available for sustainable economic development and a cleaner environment [4-5]. One of these energy sources is biodiesel. The most important feature of biodiesel that separates biodiesel from other types of energy sources is that it renews itself and can be extinct naturally. Besides, biodiesel

is very important in terms of reducing the carbon emissions that harm the environment, reducing the dependence on foreign sources in terms of energy and not being required to be imported because they are domestic sources [6]. One of the most important parameters affecting the production yield of biodiesel in the production process by transesterification is the used catalysts and the methanol / oil molar ratios [7-9]. Homogeneous and heterogeneous catalysts are used in biodiesel production [10]. Although the yield in homogeneous catalysts is high, many factors such as saponification, excess reagent expenditure and extra separation cost negatively affect the cost of production [11]. Therefore, efforts to develop a highly efficient and highly usable heterogeneous catalyst, which prevents saponification, have gained speed and importance today [12].

1.1. Material Method

1.2. Catalyst Preparation

Canola oil used in the experiments was obtained from a local market. A 99.8% purity methyl alcohol from Sigma-Aldrich, a commercial company, was purchased from in order to produce the fuel appropriate for the standard. Waste eggs shells were carefully cleaned with clean water before removing dice and other wastes. The cleaned eggshell was dried in an oven at 120°C for one hour. The inner lining and other impurities containing in the dried shell were removed and then milled on the electric milling machine and milled to approximately 70mm. The resulting powder was baked in the shell oven at 950°C for 24 hours and calcined for conversion of $CaCO_3$ into CaO. The product obtained was used as heterogeneous base catalyst in methyl ester production.

1.3. Catalyst Characterisation

The product obtained as a result of 24 hours calcination at 950°C of organic material (eggshell) was exposed to XRD investigations. XRD analyses were carried out in Batman University Geology engineering Department Research Laboratory with Rigaku brand Miniflex-II model X-ray diffractometer (Anode = Cu (CuK_α= 1.541871 Å), Filter = Ni, Voltage = 35 kV, Current = 15 mA, Goniometer velocity 2°/ Min., Paper speed = 2cm / min., Time constant = 1 sec, Slits = 1° = 0.15 mm 1° second 0.30 mm, Paper spacing = = 2θ = 20-80°). The peaks observed at 3.03 Å and 3.78 Å, which correspond to the surface of the calcite minerals (104), indicate that the calcite crystal phase still continues despite calcination. Figure 1 shows that the best catalytic conversion performance is obtained at 950°C. Similar studies showed that the best conversion

yields were in the range of 800-900°C. Tshizanga et al. found that the best conversion efficiency was obtained by calcination at 800°C for 24 hours in the optimization of biodiesel production from waste vegetable oils and eggshell ashes [13]. Jazıe et al. reported that egg shell was as an environmentally friendly catalyst for transesterification of rapeseed oil: They stated that they achieved optimum yield in the optimization studies for biodiesel production at 200-1000°C and for 2 hours calcination [14].

Niju et al., in their study of modification of egg shell and its use in biodiesel production, examined the calcination time of 2,5 hours at 900°C; and reported that they achieved the best conversion efficiency [15]. Wong et al. stated that they obtained optimum yield in 2 hours calcination time and at 1000°C temperature in their study of calcined eggshell as a potential catalyst in converting waste frying oils into biodiesel [16]. Jazie et al. stated that optimal efficiency was achieved in 2-hour calcination time at 900°C temperature using waste eggshell waste for transesterification of mustard oil by employing the Response Surface Methodology (RSM) [17].

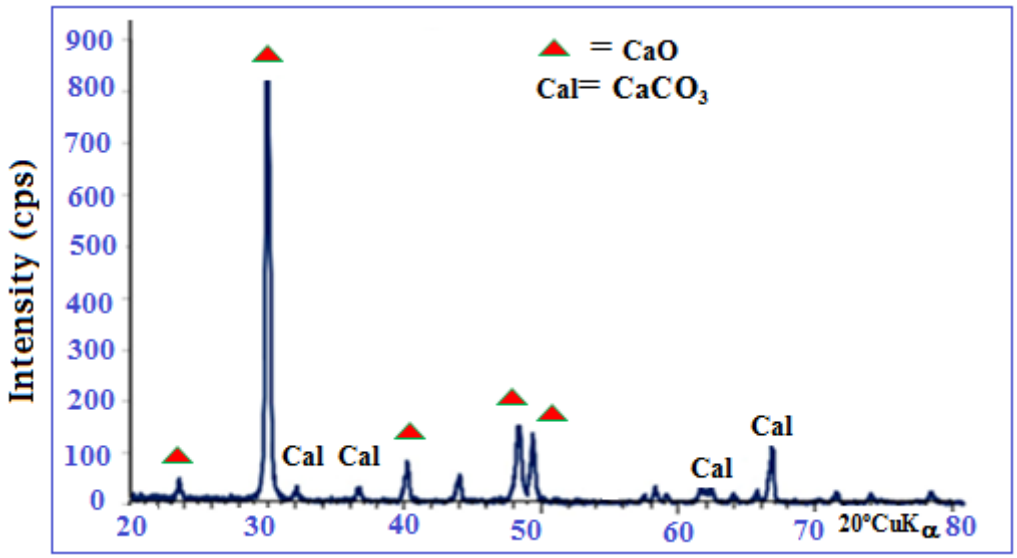

Figure 1. XRD patterns belonging to calcination of egg shell at 950°C

Calcined and uncalcined eggshells were analysed chemically by means of Portable X-ray Fluorescent Spectrometry (P-XRF) device in Batman University Archaeology Department Research Laboratory. According to the results of analyses, it is possible to witness that almost all of the egg shell is composed of CaO. It can be easily observed that the results obtained in similar studies in the literature are very close to those of ours [18-20]. Table 1 gives the results of P-XRF analysis of calcined and uncalcined egg shells.

Table 1. P-XRF analysis results of calcined and uncalcined egg shells

Compound	Commercial CaO	Uncalcined Egg Shell	Calcined Egg shell
MgO	---	0,301	---
Al_2O_3	---	0,222	---
SiO_2	---	0,942	0,1042
P_2O_5	---	0,3175	1,283
SO_3	---	0,3463	0,1338
K_2O	---	0,11	---
CaO	**99,230**	**97,6389**	**98,505**
Mn_2O_5	---	0,006	
Fe_2O_3	0,110	0,022	--
SrO	0,120	0,1776	0,0208
ZrO_2	0,010	--	--
BaO	0,240	--	--
La_2O_4	0,130	--	--
CeO_2	0,040	--	--
Pr_2O_3	0,040	--	--
Yb_2O_3	0,050	--	--

The experiments were planned to determine the effects of the reaction time on biodiesel yield, density and kinematic viscosity. According to the results obtained, the most appropriate conditions were determined and the biodiesel produced under optimized conditions was tried to be evaluated as a diesel fuel in terms of both its compatibility and fuel properties. This catalyst was then washed with ionized water and dried at about 100°C; and reused under the same reaction conditions in biodiesel production; and then the above-mentioned parameters (yield, viscosity and density) were measured. The same catalysts were washed for the second time and the same processes were repeated and the values of the working parameters were determined.

1.4. Methanol/Oil Molar Ratio effect

One of the most important parameters having an effect on the yield of oil acid methyl ester (OAME) in addition to its direct effect on biodiesel production cost is the methanol / oil molar ratio [21]. The quality of the oil molar ratio of alcohol and alcohol alone plays an important role in the biodiesel production method [22]. The reaction of three moles of methanol and one mole of triglyceride in a stoichiometric manner yields three moles of OAME. Due to the fact that it is an equilibrium reaction, the equilibrium is progressed in the direction of products using more methanol than the stoichiometric amount to increase OAME yield [21]. As demonstrated in Figure 2, by stoichiometric reaction of three moles of methanol with one mole of triglyceride, three moles of OAME are formed.

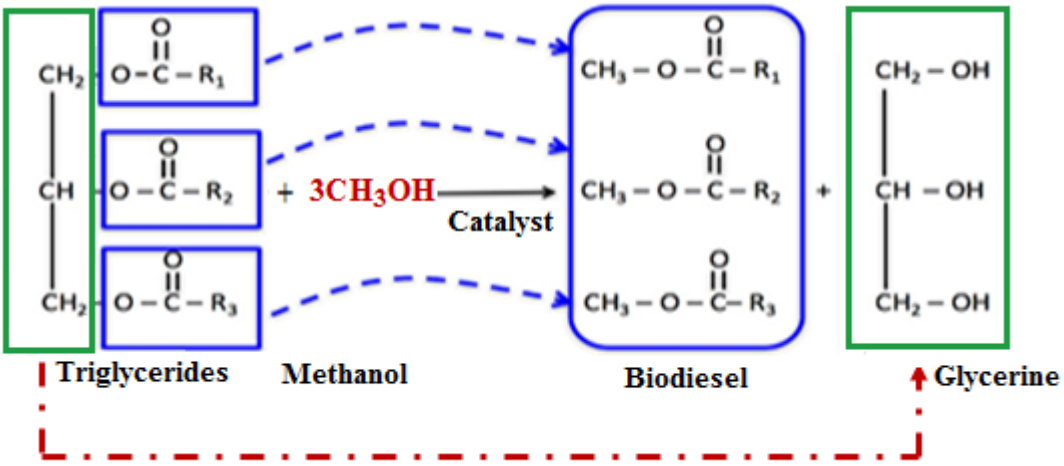

Figure 2. Stockymetric transesterification reaction

Since the amount of alcohol used in the biodiesel production process is directly related to the cost, it is very important to determine this amount. In this study, it was aimed to determine the best methanol / oil molar ratio; and for this, CaO and eggshell catalysts, with an amount of 4% catalyst were used at 60°C temperature under 1 hour constant reaction conditions in 7: 1, 8: 1, 9: 1 and 10: 1 methanol / oil molar ratios. In the end of these experiments, parameters such as product yield, density and viscosity were determined. These catalysts were then washed with ionized water and dried at about 110°C and used again under the same reaction conditions for biodiesel production; and the above mentioned parameters (yield, density and viscosity) were measured. The catalysts we used in the study were washed for the second time and the same processes were repeated and the values of the working parameters were determined as a result

of reaction. Table 2 shows the effects of methanol / oil molar ratio on biodiesel yield, density and viscosity as a result of optimization experiments.

Table 2. Effects of methanol/oil molar ratio on biodiesel yield, density and viscosity

Catalyst Use	Methanol/Oil (mol)	CaO			Egg Shell		
		Biodiesel Yield (%)	Density (kg/m³)	Viscosity (mm²/s)	Biodiesel Yield (%)	Density (kg/m³)	Viscosity (mm²/s)
1st Use	7	95.56	895	4,965	94.24	897	4,974
	8	95.78	890	4,958	94.63	894	4,968
	9	96.81	888	4,946	95.12	890	4,954
	10	95.22	889	4,952	94.34	892	4,962
2nd Use	7	94.34	897	4,974	93.43	898	4,982
	8	94.86	895	4,962	93.67	895	4,978
	9	95.43	891	4,951	94.08	892	4,972
	10	94.18	893	4,957	93.22	894	4,974
3rd Use	7	93.54	898	4,984	92.21	899	4,991
	8	93.78	896	4,978	92.65	897	4,988
	9	94.08	893	4,964	93.30	895	4,982
	10	93.24	895	4,972	92.14	896	4,985

The methanol / oil molar ratio effect was investigated by keeping the 4% catalysts, 1 hour and 60ºC reaction conditions constant. As exhibited in Figure 3, the increase in methanol / oil molar ratios up to 9: 1 showed that biodiesel yields (for 1st use) increased by 96.81% (CaO), 95.12% (egg shell), while density and viscosities decreased. However, when the molar ratio was increased to 10: 1, a partial decrease in biodiesel yields, but small increases in density and viscosities were observed. It was determined that there occurred an expected partial decrease in biodiesel yields when the catalysts were used for the 2nd and 3rd times, whereas there observed some increase in density and viscosities. In all three uses, when the methanol / oil molar ratio was increased to 9: 1, this affected the reaction efficiency in decreasing trend. When Figure 3 is examined, it can be clearly seen that the biodiesel obtained as a result of the experiment meets the density and viscosity values of biodiesels mentioned in EN 14214. Similar studies using

CaO and eggshell catalysts in literature demonstrated that the most suitable methanol / fat ratio ranges from 6: 1-14: 1 [23-30].

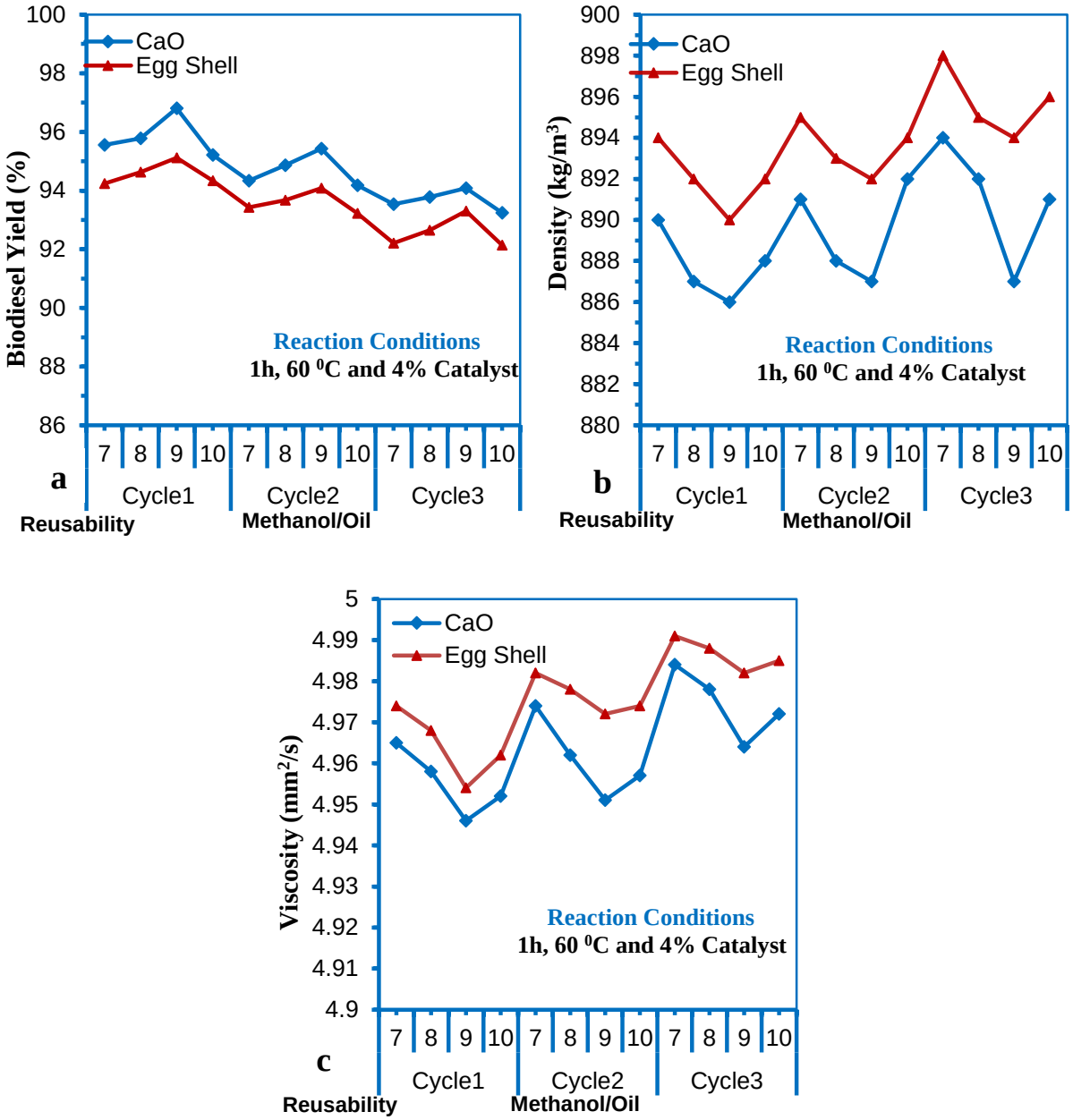

Figure 3. Change in biodiesel yield (**a**), density (**b**), and viscosity with methanol/oil ratio

RESULTS

In the production of biodiesel, the parameters having an influence on transesterification reaction of methanol with canola oil and low-cost waste egg shell and CaO catalysts were investigated. The most appropriate reaction conditions for the transesterification reaction were investigated by keeping the 4% catalysts, 1 hour reaction time and 60ºC reaction conditions constant. The highest OAME yields under the above conditions (For 1st Use) were obtained as 96.81% (CaO),

95.12% (egg shell). The density and viscosity values of the biodiesel obtained in these conditions were determined as CaO: 888kg / m³, 4,946mm² / s, eggshell: 890kg / m³, 4,954mm² / s, respectively. The density and viscosity values of the biodiesel obtained from all operating parameters were found to be between 860-900 kg / m3 and 3.5-5.0 mm2 / s, which are within the accepted limits of EN 14214. The results obtained are very important that the waste egg shell can be used as an environmentally friendly catalyst, and that it has a significant effect on the biodiesel efficiency, and that the catalyst can be used again, and the cost of biodiesel production can significantly be reduced.

REFERENCES

The report of crude oil and natural gas, May 2016. https://www.enerji.gov.tr/tr-TR/Anasayfa (15 Şubat 2019).

Owusu P A., Sarkodie S A., A review of renewable energy sources, sustainability issues and climate change mitigation, *Cogent Engineering* (2016), 3: 1167990.

Chela A., Kaushik G., Renewable energy technologies for sustainable development of energy efficient building, *Alexandria Engineering Journal* (2018) 57, 655–669

Dinçer I., Renewable energy and sustainable development: a crucial review, *Renewable and Sustainable Energy Reviews*, 4, (2000) 157-175.

Popa V.I., Biomass for fuels and biomaterials, Biomass as Renewable Raw Material to Obtain Bioproducts of High-Tech Value, (2018), 1-37.

Kolhe N S., Gupta A R., Rathod V K., Production and purification of biodiesel produced from used frying oil using hydrodynamic cavitation, *Resource-Efficient Technologies*, 3 (2017) 198–203.

Musa I A., The effects of alcohol to oil molar ratios and the type of alcohol on biodiesel production using transesterification process, *Egyptian Journal of Petroleum*, (2016), 25, 21–31.

Narasimharao K., Lee A., Wilson A., Catalysts in production of biodiesel: A Review, *Journal of Biobased Materials and Bioenergy*, (2007), Vol.1, 1–12.

Di Serio M., Cozzolino M., Giordano M., Tesser R., Patrono P., Santacesaria E., From homogeneous to heterogeneous catalysts in biodiesel production, Industrial & Engineering Chemistry Research, (2007), 46, 20, 6379-6384.

Talha N S., Sulaiman S., Overview of catalysts in biodiesel production, *ARPN Journal of Engineering and Applied Sciences*, Vol. 11, No. 1, 2016 .

Aras Servan M., Preparation, characterization of basıc alkali catalysts and biodiesel production with transesterification of oils with the existence of these catalysts, Master Thesis, Gazi University, Science Institute, 2011.

Tshizanga N., Aransiola E F., Oyekola O., Optimisation of biodiesel production from wastevegetable oil and eggshell ash, South African Journal Of Chemical Engineering, 23 (2017) 145-156.

Jazıe A A., Pramanık H., Sınha A S K., Egg Shell as Eco-Friendly Catalyst for Transesterification of Rapeseed Oil: Optimization for Biodiesel Production, *Special Issue of International Journal of Sustainable Development and Green Economics (IJSDGE)*, V-2, I-1, 2, 2013.

Niju S, Meera S. Begum K M., Anantharaman N., Modification of egg shell and its application in biodiesel production, *Journal of Saudi Chemical Society*, (2014) 18, 702–706.

Wong Y C., Ang R X., Study of calcined eggshell as potential catalyst for biodiesel formation using used cooking oil, Open Chem., 2018; 16: 1166–1175.

Jazie A A. , Pramanik H., Sinha A S K., Egg shell waste-catalyzed transesterification of mustard oil: optimization using response surface methodology (RSM), *2012 2nd International Conference on Power and Energy Systems (ICPES 2012).*

Haroon H I., Elbadawi A A., Siddig M A., Abuelhassan H H., Sabah Elkhair M K., Studying the physical characters of eggshell and recycling hen's egg waste as powder for cleaning used in household wares, *Nova Journal of Medical and Biological Sciences*, Vol. 4(1) 2015:1-5.

Ayodeji A A., Modupe O E., Rasheed B., Ayodele J M.,Data on CaO and egg Shell catalysts used for biodiesel production, Data in Brief, 19, 1466–1473, 2018.

Elabbas S., Mandi L., Berrekhis F., Pons M N., Leclerc J P., Ouazzani N., Removal of Cr(III) from chrome tanning wastewater by adsorption using two natural carbonaceous materials: Eggshell and powdered marble,

İlgen O., Biodiesel production from canola oil and methanol with dolomite catalyst loaded with calcium aesthete, *Anadolu University Journal of Science and Technology A- Applied Sciences and Engineering*, 2016, 17, 2, 413 – 421. *(İlgen O.,)*

Musa I.A., The effects of alcohol to oil molar ratios and the type of alcohol on biodiesel production using transesterification process, *Egyptian Journal of Petroleum*, 25, 21–31,2016.

Viriya-empikul N., Krasae P., Puttasawat B., Yoosuk B., Chollacoop N., Faungnawakij K., Waste shells of mollusk and egg as biodiesel production catalysts, *Bioresource Technology,* 101 (2010) 3765–3767.

Boroa J., Dekaa D., Thakur A J., A review on solid oxide derived from waste shells as catalyst for biodiesel production, Renewable and Sustainable Energy Reviews, 16 (2012) 904–910.

Khemthong P., Luadthong C., Nualpaeng W., Changsuwan P., Tongprem P., Viriya-empikul N., Faungnawakij K., Industrial eggshell wastes as the heterogeneous catalysts for microwave-assisted biodiesel production, *Catalysis Today,* 190 (2012) 112–116.

Chen G., Shan R., Shi J., Yan B., Ultrasonic-assisted production of biodiesel from transesterification of palm oil over ostrich eggshell-derived CaO catalysts, *Bioresource Technology*, 171 (2014) 428–432.

Oğuz H., Çelik Tolu M., A review on biodiesel production using eggshell as catalyst, *International Journal of Energy Applications and Technologies*,5(3) [2018] 147-152.

Buasri A., Chaiyut N., Loryuenyong V., Wongweang C., Khamsrisuk S., Application of eggshell wastes as a heterogeneous catalyst for biodiesel production, *Sustainable Energy*, 2013, Vol. 1, No. 2, 7-13

Anastopoulos G., Zannikou Y., Stournas S., Kalligeros S., Transesterification of vegetable oils with ethanol and characterization of the key fuel properties of ethyl esters, *Energies*, 2009, 2, 362-376.

Koohi Kamali S., Tan C P., Ling T C., Optimization of sunflower oil transesterification process using sodium methoxide, *The Scientific World Journal*, 2012.

Paper 13 **Bildiri 13**

EVALUATION OF CYCLE ANALYSIS IN WANKEL AND RECIPROCATING ENGINE

Ömer Cihan[a], Osman Akın Kutlar[b], Abdurrahman Demirci[c], Hüseyin Emre Doğan[b], Majid Javadzadehkalkhoran[b]

[a]Hakkari University, Engineering Faculty, Department of Mechanical Engineering, Hakkari, Turkey, E-mail: omercihan@hakkari.edu.tr
[b]Istanbul Technical University, Mechanical Faculty, Department of Mechanical Engineering, Istanbul, Turkey, E-mail: kutlar@itu.edu.tr, edogan@itu.edu.tr, javadzadehkalkh@itu.edu.tr
[c]Karamanoğlu Mehmetbey University, Engineering Faculty, Department of Mechanical Engineering, Karaman, Turkey, E-mail: arahmandemirci@kmu.edu.tr

Abstract

In this study, a single-rotor 13B-MSP (Multi Side Port) Wankel-type port fuel injection, 4-stroke and research engine and a single cylinder Antor 3LD 450, port fuel injection SI engine with three different type combustion chamber were used. Both engines were compared in same load, speed and excess air coefficient conditions. The indicator diagrams and cycle analysis were compared at 3 bar P_{me} load and 2000 rpm engine speed.

As a result; maximum pressure values were close to each other for the three combustion chamber geometries in reciprocating engine. The difference between them was due to flow and flame formation in the combustion chamber. In the Wankel engine, the maximum pressure value is lower than the others in test results and far away from the TDC. The reason for this is that the combustion speed is lower and it shifts toward the expansion stroke. This is due to low turbulence intensity during the compression process.

Keywords: Rotary engine, Wankel engine, SI engine, Indicator diagram, Cycle analysis

1. INTRODUCTION

The Wankel engines which are in the class of rotary engine, operate according to the four-stroke operating principle. Its operation is different in structure and principle compared to reciprocating engines. Only rotor and eccentric shaft act as moving parts in the Wankel engine. Compared to conventional piston engine; there is no valve assembly for intake and exhaust process. Also, the Wankel engine is provided with charge change through the ports on the side housing. The opening and closing times of the ports in side surfaces is limited by the moving rotor. The rotor

provides rotational motion due to the pressure generated by the burning gases. By the way, the power is transmitted directly to the output shaft. Wankel engines can reach high rotational speeds. In addition, in evaluation of engine parts, it does not have a slider-crank mechanism compared to the reciprocating engine, therefore it has a simpler structure and less parts.

Other advantages of the Wankel engine can be listed as lighter weight, lower NOx emissions and more power production than reciprocating engine with same weight. In addition, it operates with lower vibration due to absence of reciprocating masses such as pistons and connecting rods [1-7].

2. EXPERIMENTAL STUDY

Antor 3LD 450 engine is used in reciprocating engine experiments [8-10]. General information about the engine is shown in Table 1. The engine is a single-cylinder direct-injection diesel engine in original. The process of converting the compression ignition engine to the spark ignition engine was carried out by Kutlar [9].

The pistons with three combustion geometries (MR, cylindrical bowl, Flat) were assembled and tested in conventional piston engine (Figure 1).

a) **b)** **c)**

Figure 1. Produced MR type (a), cylindrical bowl (b) and flat (c) combustion chamber geometries.

The other engine is Mazda 13B - MSP (Multi-Side Port) Wankel engine which wwas used in the experiments. The engine is originally twin-rotor. After conversion, it was transformed into a single rotor test engine [7]. The basic and geometrical properties of the engine are given in Table 2. Cylinder pressure measurement in reciprocating engine is done with AVL brand GU13Z-24 piezoelectric sensor, which was adapted to the spark plug. In Wankel engine, Kistler brand 6118BF107Q01 piezoelectric sensor has been used with a spark plug.

Table 1: General characteristics of piston engine [8].

Term	Value	Unit
Engine name	Antor 3LD 450	-
Number of cylinders	1	-
Stroke X Dimension	80X85	mm
Compression ratio	10,5	-
Stroke volume	454	cm^3
Connecting rod length	145	mm
Ratio of crank radius to connecting rod length	0,275	-
Intake valve opening advance	16	KMA
Intake valve closing delay	40	KMA
Exhaust valve opening advance	40	KMA
Exhaust valve closing delay	16	KMA

Table 2. Basic and geometric datas related to 13B MSP Wankel engine.

Term	Value	Unit
R (Rotor corner-center length)	105	mm
e (Eccentricity)	15	mm
b (Rotor width)	80	mm
ε (Compression ratio)	10	-

3. Experimental Results

The indicator diagrams and the cycle analysis of the Wankel test engine were compared with the test results of different combustion chamber geometries in the reciprocating engine. This engine has single cylinder and port fuel injection system. In the reciprocating engine experiments, different combustion chamber geometries (MR, Cylindrical bowl, Flat) with a compression ratio of 10.5 were used. The comparison was made in terms of the load and speed of the two types of engine and the selected point is the 3 bars break mean average effective pressure and 2000 rpm engine speed.

In conventional piston engine, maximum pressure values are close to each other in all three types of combustion chamber geometry. The difference in the combustion chamber geometry affects the flow and flame formation.

The maximum pressure of the Wankel test engine is much lower and is more distant from the TDC (Figure 2). This indicates that the combustion speed of the Wankel engine is lower than the conventional piston engine and shifts towards the expansion stroke. Previously, Cold flow models by Taşkıran showed that the turbulence intensity in the combustion chamber is very low during compression [11].

When the charge change processes of engines are examined, the effect of load level was investigated on pumping losses. The pressure level remained relatively constant due to constant start of the intake after the TDC in the Wankel engine and the

intake port remained fully open in most of the intake times (Figure 3).

Heat release rate is shown cumulatively for the engines at average effective pressure of 3 bar (Figure 4). The cumulative heat release rate of the three combustion chamber geometries is close to each other. The combustion velocity is lower than the others in the Wankel engine. Due to larger stroke volume of the Wankel engine, the cumulative heat release rate is by far the highest.

In order to eliminate this difference rising from the difference of the stroke volume, all engine types are normalized by converting to 1 liter stroke volume and cumulative heat release is shown in Figure 5. The Wankel engine has a significantly lower burning velocity and a cumulative amount of heat is 15-20% higher than conventional piston engines.

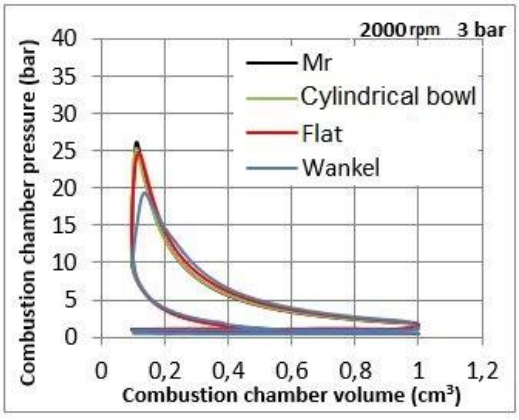

Figure 2. Comparison of p-V diagrams for Wankel engine and different combustion chamber geometries.

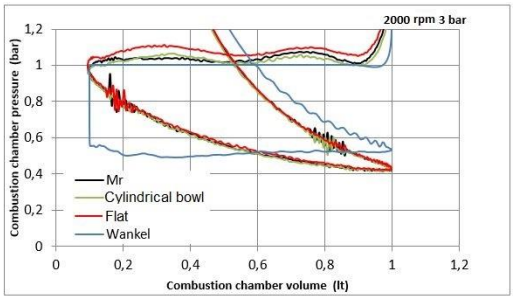

Figure 3. Comparison of charge change process for Wankel engine and different combustion chamber geometries.

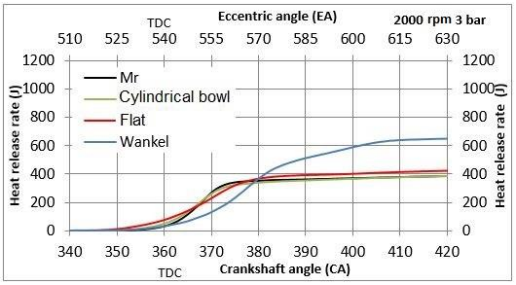

Figure 4. Comparison of cumulative heat release quantities at 3 bar load.

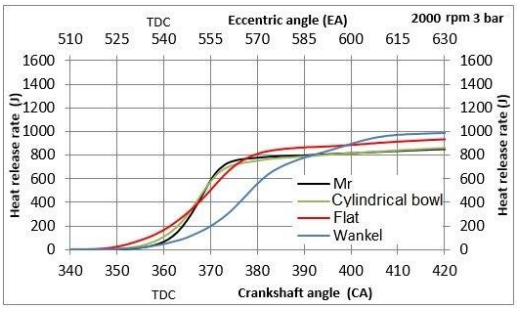

Figure 5. Comparison of the normalized amount of cumulated heat release at 3 bar load.

4. CONCLUSIONS

Three different combustion chamber geometries (MR, Cylindrical bowl, Flat) of 3LD 450 conventional piston engine with 13B MSP single rotor Wankel engine is tested and compared. Experiments are made at engine speed of 2000 rpm, 3 bar BMEP load and $\lambda = 1$ condition.

The maximum pressure values of the three different combustion chamber geometries were close to each other. The difference between these results was due to the geometry affecting the flow and flame formation.

In the Wankel test engine, the maximum pressure values were lower than the others and more distant from the TDC. This is because of the lower combustion velocity and as a result, the process shifts toward the expansion stroke. On the other hand, the lower turbulence intensity in compression is another factor.

The pressure level remains relatively constant due to the greater opening time of the intake port in the Wankel engine.

The cumulative heat release amount for each of the three combustion chamber geometries was close to each other. Due to larger stroke volume of the Wankel engine, the cumulative heat release rate is by far the highest.

When the stroke volumes are 1 liter in both engines, the burning velocity of the Wankel engine is lower and the cumulative heat release is about 15 - 20% higher than the others.

REFERENCES

[1] Ansdale, R. F., The Wankel RC Engine (1. Basım), London: Iliffe Books Ltd, p. 158, 1968.

[2] Yamamoto, K., Rotary Engine (1. Basım), Toyo Kogyo Co., Ltd, p. 147, 1971

[3] Yamamoto, K., Rotary Engine (6. Basım), Japan: Sankaido Co., Ltd, p. 67, 1981.

[4] Warner, M., Street Rotary (1. Basım), Penguin Group, p. 170, 2009.

[5] Ohkubo, M., Tashima, S. ve Shimizu, R. Developed Technologies of the New Rotary Engine (RENESIS), SAE Technical Paper Series, 2004-01-1790, p. 1-13, 2004.

[6] Froede, W. G. The Nsu-Wankel rotating combustion engine, SAE paper, 610017, p. 179-203, 1961.

[7] Cihan, Ö., Wankel motoru ve çevrim atlatma sisteminin deneysel ve sayısal olarak incelenmesi, (Doktora tezi). İstanbul Teknik Üniversitesi Fen Bilimleri Enstitüsü, İstanbul, 2017.

[8] Demirci, A., İçten yanmalı motorlarda farklı yanma odası geometrilerinin performans ve emisyonlara etkisi, (Doktora tezi). İstanbul Teknik Üniversitesi Fen Bilimleri Enstitüsü, İstanbul, 2017.

[9] Kutlar, O. A., Dört Zamanlı Otto (Rochas) Çevrimli Motorlarda Kısmi Yükte Yakıt Tüketimini Azaltmak İçin Yeni Bir Yöntem (Periyot Atlatmalı Motor). (Doktora tezi). İstanbul Teknik Üniversitesi Fen Bilimleri Enstitüsü, İstanbul, 1999.

[10] Doğru, B., Buji Ateşlemeli Motorlarda Çevrim Atlatma Yönteminin Kısmi Yüklerde İncelenmesi (Doktora tezi). İstanbul Teknik Üniversitesi Fen Bilimleri Enstitüsü, İstanbul, 2013.

[11]Taşkıran, Ö., Çalık, A.T. ve Kutlar, O.A. Effect of side ports on the flow field of a rotary engine, Sixth Conference Renewable Fuels, Fires and Combustion, in Kayseri

Paper 14 **Bildiri 14**

SIMULATION OF NANOPARTICLE FORMATION IN FLAME SPRAY PYROLYSIS PROCESS

Mustafi. A. Alhaleeb[1], Nesrin. E. Machin[1,]*

[1]Department of Chemical Engineering and Applied Chemistry

Atılım University, Ankara, Turkey

**nesrin.machin@atilim.edu.tr*

A B S T RA C T

The gas dispersion flow rate in the flame spray pyrolysis (FSP) process is one of its most important process parameters, which must be adjusted according to the liquid flow rate and process requirements. Generally, the FSP process employs an external-mixing gas-assisted atomiser. In this study, we developed an equation to adjust the gap exit for any dispersion gas flow rate at a constant pressure drop, based on the external measurable quantities of the nozzle. The equation was validated by comparing the results with the data given in the nozzle supplier charts. Using the developed equation, the nozzle geometry was built and a simulation study was performed using the commercial ANSYS FLUENT v.19 software coupled with a MATLAB code to predict the multicomponent droplet evaporation, temperature, velocity, gas density and the particle growth in the flame spray pyrolysis process. The simulation results were tested and verified.

Keywords: flame spray pyrolysis, air cap, nozzle gap, nanoparticle production

1. Introduction

In an FSP process, the flow rate of the dispersion gas is an important operation parameter that ensures the appropriate dispersion gas velocity required for the atomisation process and controls the pressure drop across the nozzle tip. This can be achieved by changing the cross-sectional area of the nozzle throat. This study employs the commercially available external mixing two-phase nozzles (Düsen-Schlick GmbH, Germany) with a convergent-divergent configuration. This allows the maximum possible mass flow to pass through a duct when its throat is at the critical or sonic condition. The duct then becomes choked and cannot carry any additional mass flow unless the throat is widened [1].

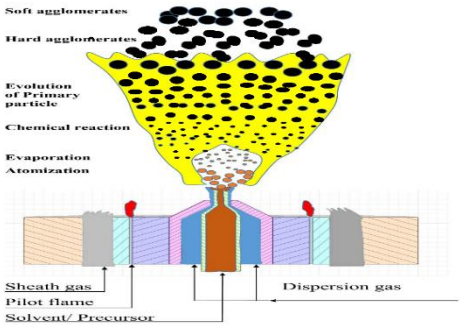

Figure 1. Nozzle configuration H. Torabmostaedi et. al. [2].

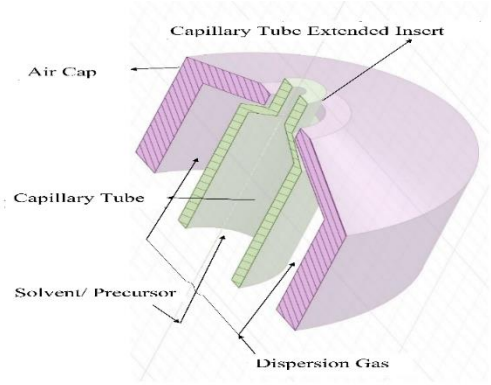

Figure 2. Schematic of the external- mixing gas-assisted atomiser apparatus

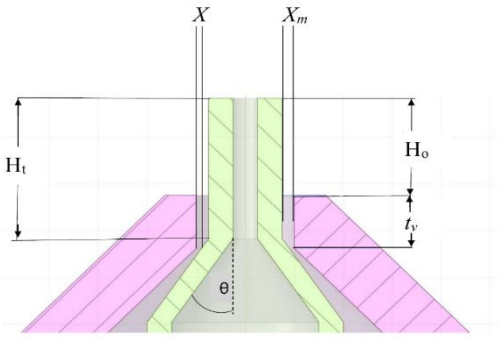

Figure 3. Side view of the nozzle. *symbols*: gap between the air cap and outer capillary tube diameter (X), maximum gap available (X_m), angle of inclination(θ), measurable length (H_o), maximum liquid insert length (H_t), and wall thickness of the air cap (t_v)

The mathematical relationship between the measurable external parts and the internal gap at the nozzle throat was developed to calculate exit gap area, and precisely set the nozzle throat as:

$$H_o = \left(X_m - \frac{Do}{2} + \frac{\sqrt[2]{Do^2 - \frac{4}{\pi}Amin}}{2}\right) / \tan\theta + H_t - t_v - \left(\frac{\boldsymbol{Do}}{\boldsymbol{2}} - \frac{\sqrt[2]{\boldsymbol{Do}^2 - \frac{4}{\pi}\mathrm{Amin}}}{\boldsymbol{2}}\right) cos\ \theta\ \ cos\ (90\text{-}\theta) \qquad (1)$$

A validation study on commercially available nozzles (Düsen-Schlick GmbH, Germany, Series 940-943 and 970 Form 4 S32) was conducted to check the accuracy of the above equation. The required air flow was calculated as a function of the applied upstream pressure to remain below sonic conditions and was subsequently compared to the data for air provided in the supplier charts [3,4]. Figure 1-a and b suggest a good match between the calculated and measured air flowrates. The average percentage errors for all the cases are small and no more than 2.63 %.

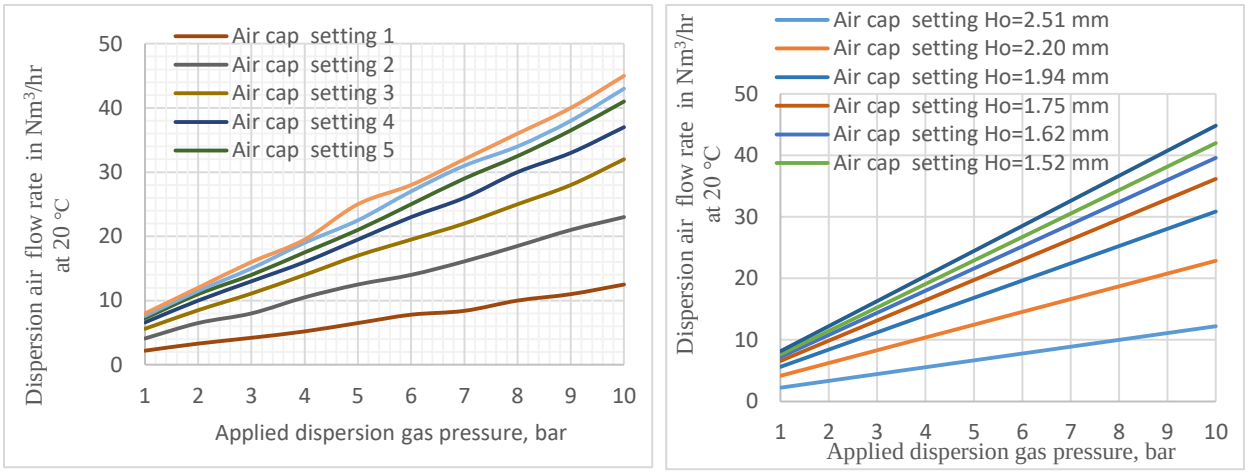

Figure 4: Dispersion air flow rate (a) measured experimentally by the nozzle supplier at different air cap settings, as a function of applied dispersion gas pressures for the Series 940-943 [3].

Dispersion air flow rate (b) predicted by the equation at different air cap setting H_o, as a function of applied dispersion gas pressures for the Series 940-943.

2. Application of the equation in the simulation of FSP

Equation 1 was applied to provide the air cap position to set up FSP with external-mixing stainless-steel gas-assisted nozzle (Düsen-Schlick GmbH, Germany, 970/4-S32) [4] at four different oxygen dispersion flows. The nozzle was used with dimensions X_m (maximum gap)= 0.325 mm (ID/OD 1.7/2.35 mm) , θ (the angle of inclination)= 35°, Sl (the straight length)= 3 mm, and τ (wall thickness of the air cap)=1 mm. The nozzle air cap position was calculated using the equation and the results are presented in Table 1. The geometry drawn by Ansys Design Modeller is shown in Figure 4.

Table 1. Air cap position at different dispersion gas flow rate calculated by using the equation

Flame configuration	F1	F2	F3	F4
Measurable length (mm) H_o	2.33	2.28	2.23	2.17
Dispersion gas flow rate (LPM)	11	15	19	23

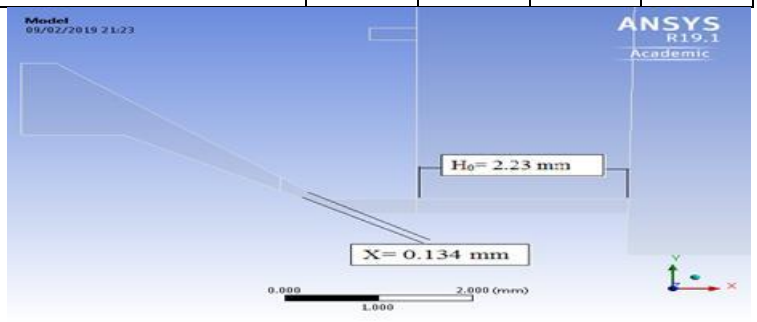

Figure 5. Geometry

ANSYS FLUENT v.19 software coupled with Matlab are used to predict the multicomponent droplet evaporation, temperature, velocity, gas density and the particle growth in the flame spray pyrolysis process. Experimental data was taken from the published literature data by H. Torabmostaedi *et al.* for ZrO_2 formation [2]. The Euler model was used to simulate the continuous phase using the realizable K-ε to describe the turbulence. The droplet flow field was modelled using Discrete Phase Model (DPM) Lagrangian. The discrete phase trajectories of multi-component injection defined according to the injection point properties which consist of the initial value of droplet velocity, mass flow rate of liquid injection, liquid temperature, and the initial droplet diameter. The axisymmetric model can represent the FSP system well via a 2-D simulation rectangular domain 300 mm length and 100 mm width which was adopted in this study. The mesh comprises of 146520 nodes. The grid around the capillary tube and atomizer was progressively refined in a grid. A constant pressure condition was used at the exit (atmospheric pressure). The control volume based numerical method was used to solve the governing equations sequentially. In order to ensure the accuracy, stability, and convergence, a second order upwind discretization scheme was used. SIMPLEC algorithm (SIMPLE-Consistent) is used for coupling pressure and velocity. Temperature, velocity, spray droplet size are shown in Figure 6-8.

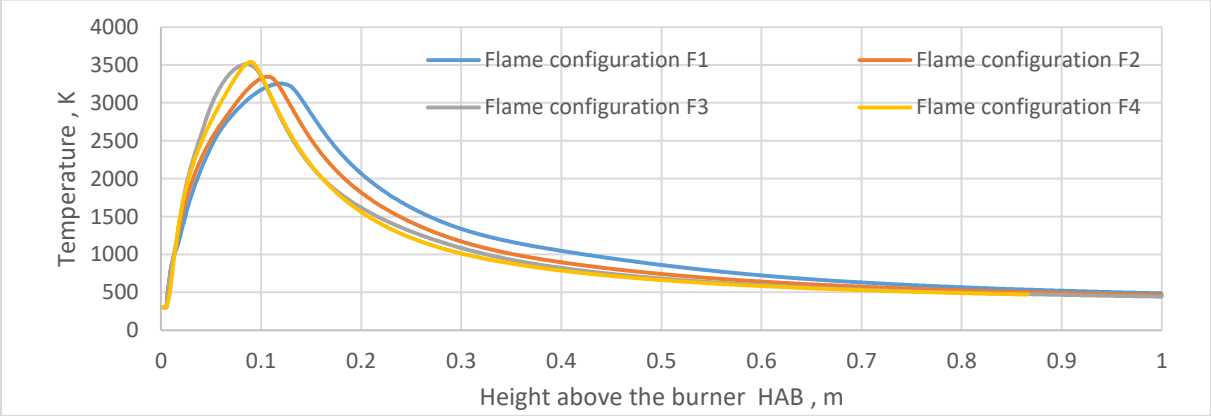

Figure 6. Temperature profile as a function of dispersion oxygen flowrate

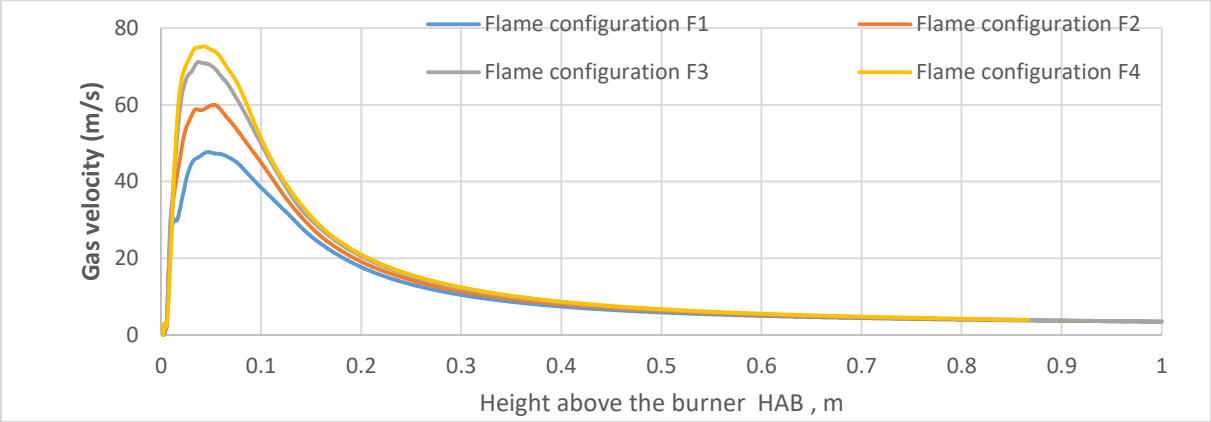

Figure 7. Velocity profile as a function of dispersion oxygen flowrate

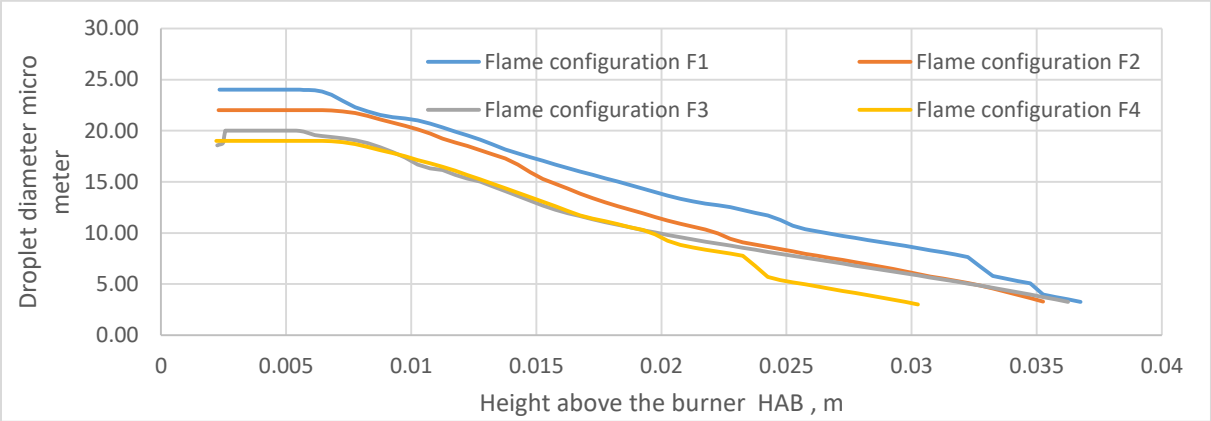

Figure 8. Spray droplet diameter as a function of dispersion oxygen flowrate

MATLAB code for the prediction of the particle diameter consisted of two part; one is the main code and the other is ode23s function as subroutine to solve stiff differential equations. Other subroutines have been tested, and ode 15s provided the fastest and more accurate results compared to the experimental data. Results are shown in Figure 9 to 11.

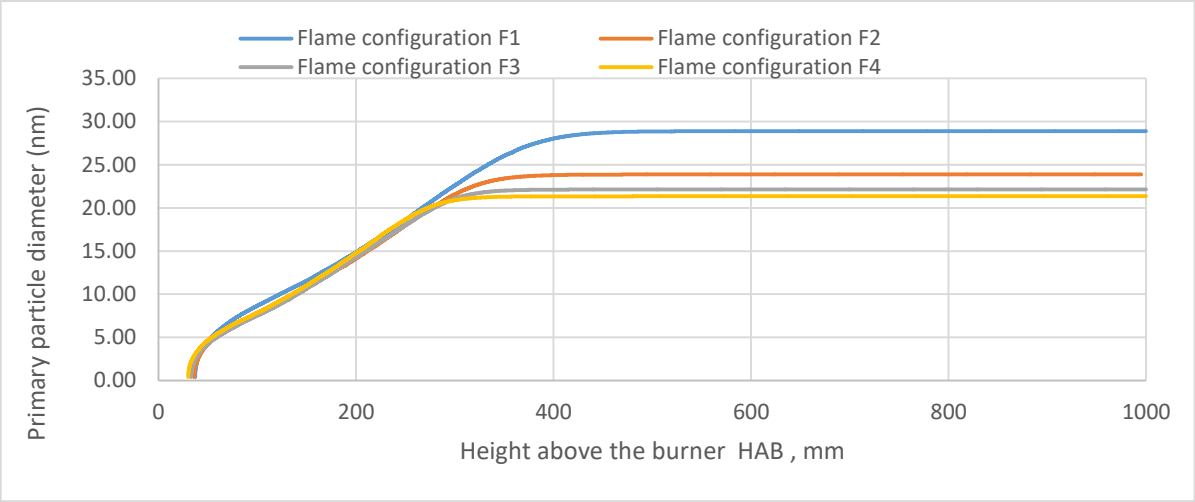

Figure 9. Primary particle diameter predicted at the centreline

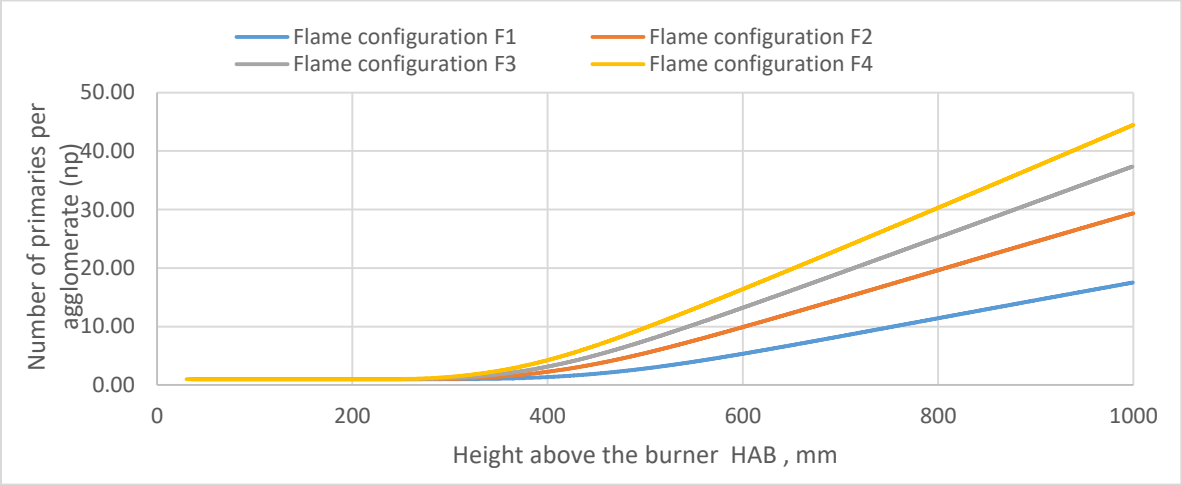

Figure 10. Number of primary particles per agglomerate predicted at the centerline

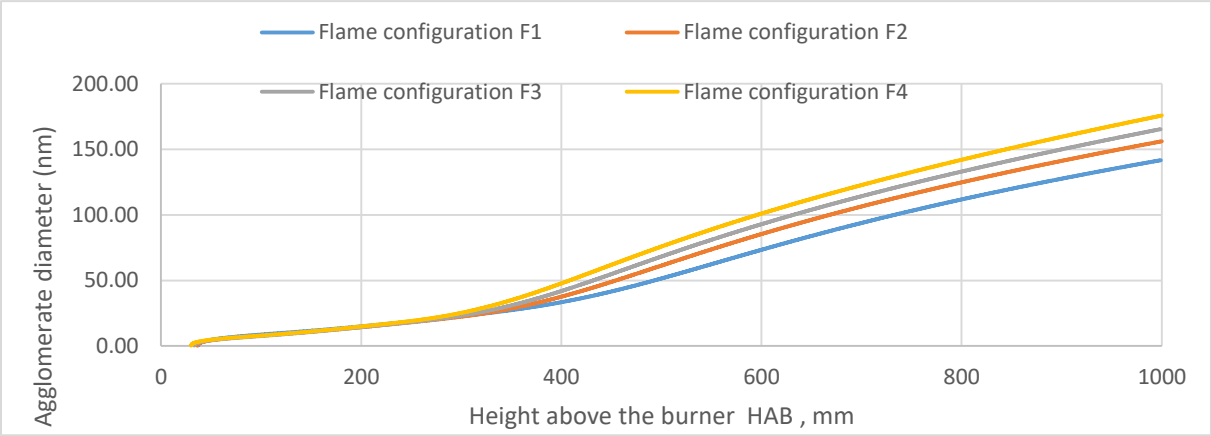

Figure 11. Agglomerate collision diameter predicted at the centerline

3. CONCLUSIONS

To adjust the air cap settings of external-mixing, gas-assisted atomisers at any dispersion gas flow rate, a simple mathematical expression was developed using the external measurable dimensions. The results revealed that the equation provides accurate settings for dispersion gas

applied pressures ≤10 bar. The equation was applied in a case study to observe the effect on the operating conditions of changing the air cap position using academic CFD code, FLUENT v 19. The simulation results were input into a numerical model as MATLAB code to solve the coagulation and sintering equations to predict the formation of nanoparticles The case study was carried out to apply the equation at the applied pressure of 2 bars and low dispersion gas that was needed to adjust the air cap position to less than the minimum position. The calculated measurable length H_o using the equation were 2.35, 2.30, 2.25 and 2.21mm at F1, F2,F3 and F4, respectively. Modelling results showed the growth rate of primary particles depends on the velocity and temperature. As the velocity decrease or the temperature increase, the primary particle sizes also increase. This is due to the increased sintering rate at high temperatures, and increased residence time at low velocities. As the flame configuration changes from F1 to F4, the growth rate of the particles decreases from 28 nm to 21 nm. The results also showed that the equation is suitable for adjusting the required air cap position for each dispersion gas flow rate up to 10 bars in the experimental run and during FPS simulation.

Acknowledgement:

The authors are grateful for the financial support from TUBITAK (Grant no:117M165).

REFERENCES

[1] Frank M. White, Fluid Mechanics, Seventh Edition, McGraw-Hill, 2009.

[2] H. Torabmostaedi, T. Zhang, P. Foot, S. Dembele, C. Fernandez, Process control for the synthesis of ZrO2nanoparticles using FSP at high production rate, Powder Technology 246 (2013) 419–433. http://dx.doi.org/10.1016/j.powtec.2013.05.006

[3] Schlick Atomizing Technologies, Operating Instructions for Schlick Two-Substance Nozzle series-940-943. https://www.yumpu.com/en/document/view/24172705/schlick-series-940-943-two-substance-nozzles-da-1-4-sen-schlick-/3.

[4] Schlick Atomizing Technologies, Operating Instructions for Schlick Two-Substance Nozzle Model 970 Form 4 S32. http://www.myschlick.com/fileadmin/user_upload/Downloads/Informationsmaterial/04_Two Substance_970.pdf.

Paper 15 **Bildiri 15**

NUMERICAL ANALYSIS OF AN EARLY DIRECT INJECTION IN A WANKEL ENGINE

Ozgur Oguz TAŞKIRAN[1], Seçkin Burak KURT[2], Alper Tolga CALIK[3], Osman Akın KUTLAR[3]

[1] Design Project Office, Turkish Naval Forces, Pendik, Istanbul
[2] Faculty of Aeronautics and Astronautics Istanbul Technical University, Istanbul, Turkey
[3] Automotive Division, Faculty of Mechanical Engineering, Istanbul Technical University, Istanbul, Turkey
Corresponding author, taskiranoz@itu.edu.tr

ABSTRACT

The emphasis on the recent studies of Wankel type rotary engines is related to decreasing its fuel consumption to a level that is compatible with reciprocating engines. Especially at part loads, it is possible that if the fuel is injected directly to the combustion chamber rather than port injection, a stratified fuel air mixture can be obtained enabling more efficient engine. However, rotary engines counter some limitations on direct injection strategies for a stratified charge. Though a late direct injection, near TDC is needed for a stratified charge, it is restricted by rotor movement because the edges of triangular shaped rotor sweep housing inner surface during their rotational movement. Furthermore as the rotor moves to TDC, wide and long shape of the volume between rotor and housing does not allow spray to penetrate longer as it does in reciprocating engines. Successful implementation of a direct injection method can be achieved by making numerical investigation on injection location and its timing before making expensive experimental tests on rotary engines. In this study we will discuss the potential of direct injection method by making an early injection at the beginning of compression stroke.

In numerical calculations, geometrical model of rotary engine that has 654 cc displacement and 10 compression ratio was used. Numerical model represents the experimental single rotor test engine that was constructed from a Mazda 13B-Renesis engine in the Automotive Laboratory of ITU. In order to obtain a realistic numerical model of the engine, all three chambers are included in the model as seen in Fig 1. The eccentric motion of the rotor were simulated by using User Defined Function (UDF) of ANSYS-Fluent that enables dynamic mesh motion in the fluid region.

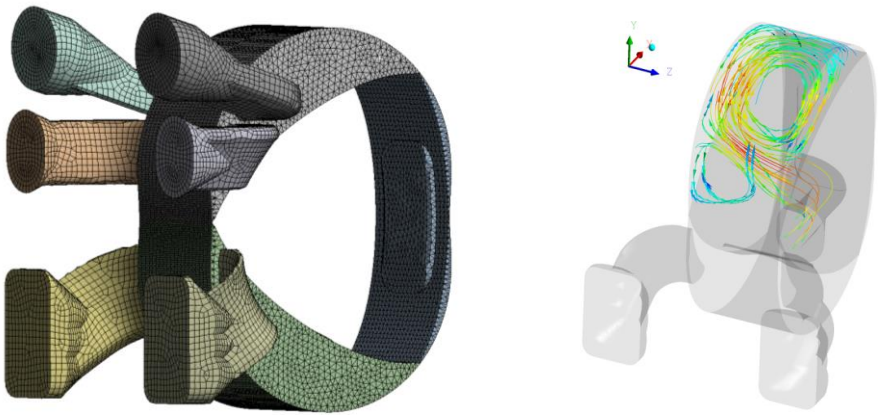

Figure 1. Numerical model of the single rotor 13B- Renesis engine (right side), air motion during intake from single side port (left side)

A series of validation processes were performed during simulation studies. First, flow field data of the numerical results using RNG turbulence model was validated by experimental data presented in the literature [1] as shown in Fig 2. Second, spray injection shown in Fig. 3 was validated by using data given in Engine Combustion Network and the study of Manin et al [2]. After obtaining validated result, the same methodology were applied to numerical modeling of this study. The injection location was chosen at a point that is available to install an injector on the experimental studies of 13B-Renesis single rotor test engine.

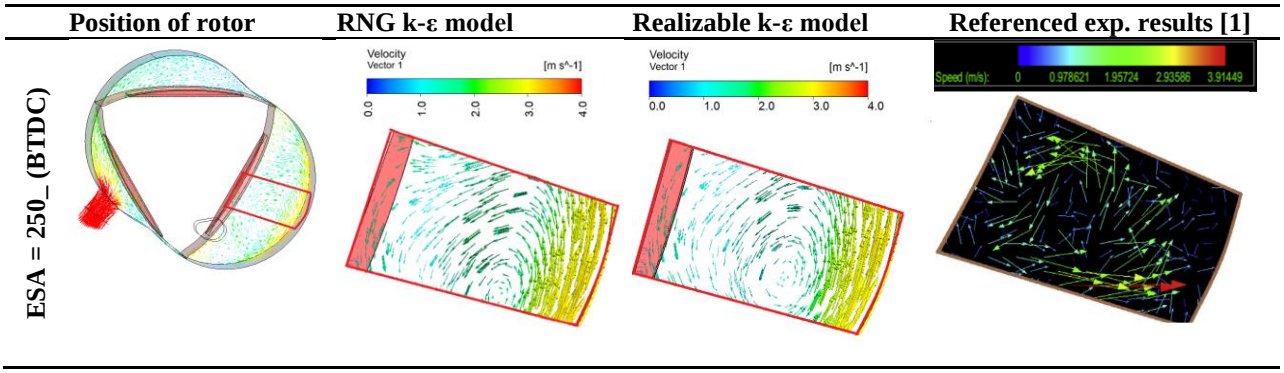

Figure 2. Comparison of RNG and Realizable k-ε models. Numerical results of 160cc engine are calculated in this study and experimental results are taken from Fan and colleagues [1].

Gasoline fuel was represented by gasoline surrogate (PRF-85) that has 85% iso-octane (C_8H_{18}) and 15% n-heptane (C_7H_{16}). Reduced kinetic mechanisms of gasoline surrogate that was reported as giving acceptable results in terms of pressure, heat release rate and emissions [3] were used in numerical calculations.

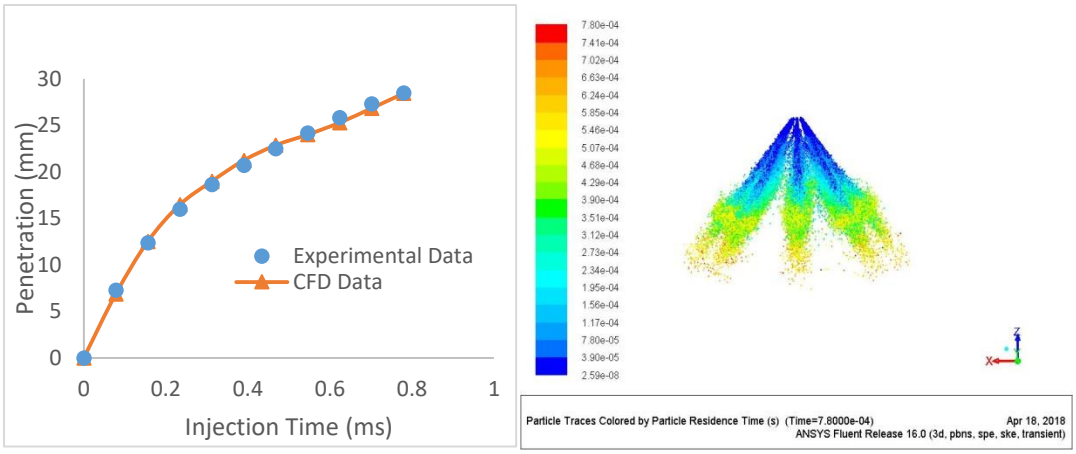

Figure 3. Comparison of experimental and numerical spray penetration length (right side) and numerical presentation of gasoline spray (left side).

The ultimate goal of this ongoing study is to put forward possible methods improving fuel consumption by using direct injection methods. In line with the expectations, the preliminary results show that air fuel mixture are almost homogenized since the fuel injected in the beginning of compression stroke rather than end of compression stroke. The rotor sweeping motion and rotational air motion inside the chamber hinders stratification. In order to obtain fuel rich and lean zones at the end of compression fuel must be injected near TDC. However due to geometrical restrictions, it may be a necessity to make a pre-combustion chamber to achieve stratified charge in the rotary engine.

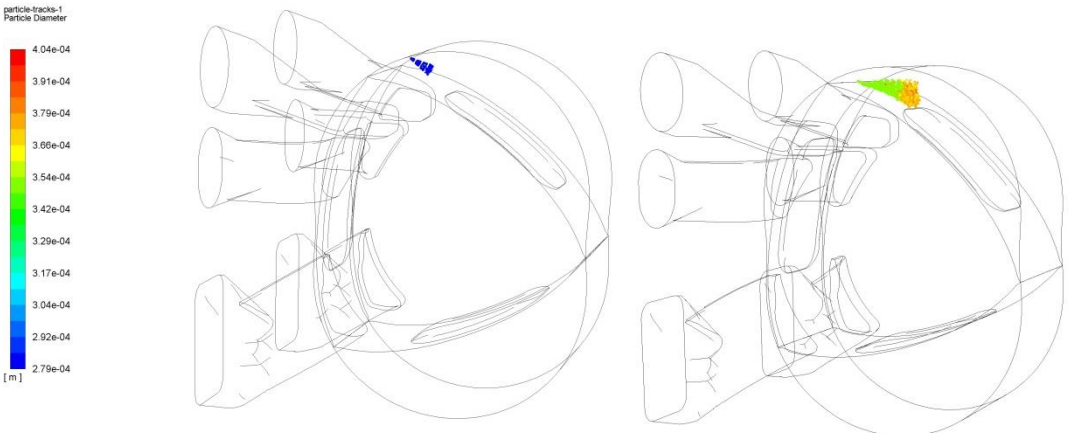

Figure 4. Early direct injections starts as the intake port is closed (right side), it is seen that there is limited time period to inject fuel into the combustion chamber since rotor edge passes injection location.

Keywords: Wankel type rotary engine, numerical modelling, direct injection.

REFERENCES

[1] Baowei Fan, Jianfeng Pan, Aikun Tang, Zhenhua Pan, Yuejin Zhu, Hong Xue, *Experimental and numerical investigation of the fluid flow in a side-ported rotary engine*, Energy Conversion and Management, Volume 95, 1 May 2015, Pages 385-397, ISSN 0196-8904.

[2] Manin, J., Jung, Y., Skeen, S. A., Pickett, L. M., Parrish, S. E., & Markle, L. (2015). *Experimental characterization of DI gasoline injection processes* (No. 2015-01-1894). SAE Technical Paper.

[3] Demir, U., Yilmaz, N., Coskun, G., & Soyhan, H. S. (2015). Evaluation of zero dimensional codes in simulating IC engines using primary reference fuel. *Applied Thermal Engineering*, *76*, 18-24.

Paper 16 **Bildiri 16**

COMBUSTION AND EMISSION CHARACTERISTICS OF ETHANOL-METHANOL-GASOLINE BLENDS IN A SPARK IGNITION ENGINE

[1]H.Enes Fil, [1]S.Orhan Akansu, [1]M.Emin Polat

[1]Department of Mechanical Engineering, Faculty of Engineering, Erciyes University, 38039 Kayseri, Turkey

E-mail: h.enesfil@erciyes.edu.tr

Abstract: Depletion of fossil fuels and environmental pollution has led researchers to foresee the need to develop bio-fuels. Alcohols are a major part of bio-fuels. This study debates combustion performance and exhaust emissions from SI engine fueled with ethanol-methanol-gasoline blends. The fuel blends contained %100 gasoline, %80 gasoline and %20 ethanol, %80 gasoline and %20 methanol and %80 gasoline, %10 ethanol and %10 methanol by volume. The excess air coefficient were kept at the lean (0.9), stoichiometric(1.0) and rich (1.1) conditions. The effects of blended fuels on engine performance were investigated and results showed that methanol-gasoline blends presents the highest volumetric efficiency; on the other hand, neat gasoline showed the lowest volumetric efficiency, torque and brake power among all test fuels. Maksimum in-cylinder pressure was occured ethanol-methanol-gasoline blend at rich condition. Results indicated that when the engine was fueled with ethanol-methanol-gasoline blends, the concentrations of CO and HC (unburnt hydrocarbons) emissions were significantly decreased, compared to the neat gasoline. Ethanol-methanol-gasoline blends presented the lowest emissions of CO and HC at stoichiometric and poor conditions but ethanol-methanol-gasoline blend was the lowest at rich conditions among all test fuels. In addition to this NOx emission increased when ethanol and/or methanol contents increased except stoichiometric condition in the fuel blends.

Keywords: Alcohols, Ethanol, Methanol, SI, Engine.

1. Introduction

Over the past several years, environmental concerns have increased importantly in the world. Excessive use of gasoline fuel in the ICE (internal combustion engine) shows that is not environmentally friendly. Gasoline cause to worldwide environmental degradation effects such as climate change, greenhouse effect, acid rain, ozone depletion etc. [1]. The increasing demands of petroleum fuels together with the greenhouse gas emission have stimulated the efforts on discovering new alternative fuels. The most substantial alternative instead of petroleum fuels in internal combustion engines are alcohols. Alcohols are an attractive alternative fuel because they can be obtained from number of sources, both natural and manufactured. Methanol and ethanol are two kinds of alcohol can be obtained from many sources both fossil and renewable these include coal, petroleum, natural gas, biomass, wood and fills and even the ocean. Ethanol can be produced from biomass such as sugar cane, sugar beet, wood, corn, and other grain. The production of ethanol from biomass sources involves fermentation and distillation of crop [2]. Ethanol is biodegradable and will evaporate quickly if spilled on land [3]. Methanol can be produced from natural gas, gasification of coal or biomass. However, coal is not preferred as a feedstock because conversion process is complex and costly

than using other feedstock in commercial methanol production [4]. Both methanol and ethanol have much higher octane number than gasoline [5]. This allows to alcohol engines to have much higher compression ratios, and so increasing thermal efficiency. Nevertheless, a significant disadvantage of methanol and ethanol relative to gasoline is that they have lower energy content [6].

Many researches have investigated the effect of ethanol and gasoline blends in petrol engines. Most of the researchers noticed, when ethanol blended gasoline was used, increase in engine brake power, engine torque, brake thermal efficiency, mean effective pressure, and volumetric efficiency, moreover, specific fuel consumption also increased. M .Al-Hasan [7] was studied a four stroke, four cylinder SI engine was used for conducting the study. This study appeared that mixing unleaded gasoline with ethanol raises the brake power, torque, volumetric and brake thermal efficiencies and fuel consumption, while it reduces the brake specific fuel consumption and equivalence air–fuel ratio. M.Abu-Zaid et al. [8] introduced an experimental work to research into the effect of methanol addition to gasoline on the performance of SI engine. The experiments were carried out, at different speed conditions, over the range of 1000 to 2500 rpm, using various blends of methanol-gasoline fuel. It was found that methanol has a significant effect on the increase the performance of the gasoline engine .The addition of methanol to gasoline increases the octane number, so engine performance increase with methanol-gasoline blend can operate at higher compression ratios. D.Balaji [9] introduced impact of isobutanol blend in SI engine performance operated with gasoline and ethanol. A four stroke, single cylinder SI engine was used for conducting this study. Experiments were conducted for fuel consumption, volumetric efficiency, brake thermal efficiency, brake power, engine torque and brake specific fuel consumption, using unleaded gasoline and additives blends with various percentages of fuel at different engine torque and fix engine speed. The result showed that blending unleaded gasoline with additives increases the brake power, volumetric and brake thermal efficiencies and fuel consumption addition of 5% isobutanol and 10% ethanol to gasoline gave the best results for all measured parameters at all engine torque values. Siwale et al. [10] studied methanol–n-butanol–gasoline blended fuels at rates of 53% methanol, 17% n-butanol and 30% gasoline on performance and emissions of SI engine. Results refered higher performance and lower emissions of fuel blends than those of neat gasoline. Nazzal [11] investigated the performance of gasoline engine using ethanol–methanol–gasoline blends at rate of 6, 6 and 88 vol% for ethanol, methanol and gasoline, respectively; the results showed important advances of engine performance at using double fuel blends. Turner et al. [12] studied the effects of ethanol–methanol–gasoline blends on SI engine emissions using five different rates from 30–42 vol% gasoline and from 70–58 vol% ethanol–methanol; results showed that the dual fuel blends have decreased carbon dioxide (CO_2) and nitric oxides (NO_x) emissions, compared to the neat gasoline.

2. Experimental Set-up and Procedure

The experimental studies were tested in the Engine Laboratory in the department of Mechanical Engineering at the University of Erciyes. The experiments were conducted in a Ford MVH418 1.8L SI engine. The SI engine was designed to generate 75kW at 5500 rpm with 10:1 compression ratio. Engine specifications are given in Table 1. Furthermore, the experimental setup is indicated in Figure 1. Engine torque and engine speed values were measured by eddy-current dynamometer. Cylinder pressure values were measured by PCB 111A22 piezoelectric pressure transducer. The cylinder pressure values were digitized at each crank angle and

indicated by averaging 80 continuous cycles. The exhaust gas constituents (CO, CO_2, HC and NO_X) were metered with a Bosch BEA 060 gas analyzer.

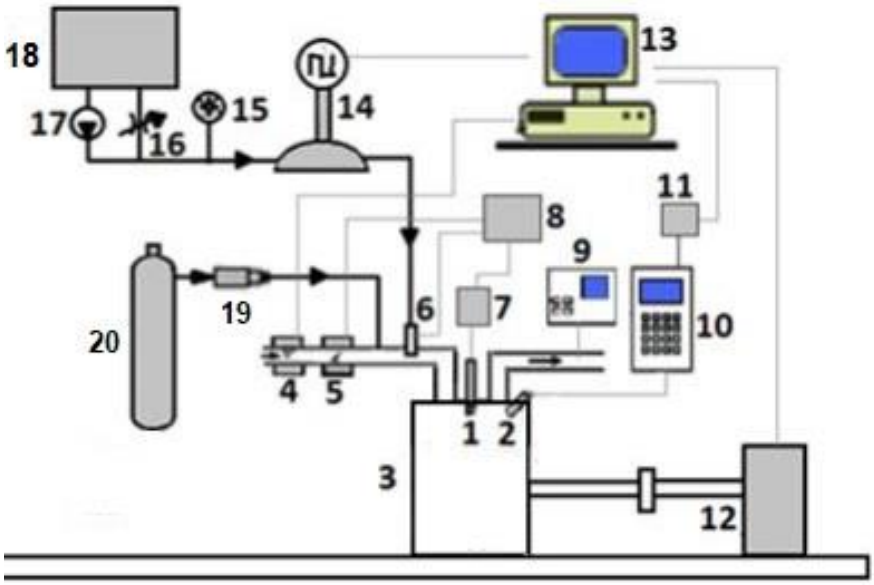

Figure 1. Experimental Setup

1.Spark Plug	11.Data Logger
2.Pressure Transducer	12.Dynamometer
3.Engine	13.Computer
4.Air Flow Meter	14.Liquid Flow Meter
5.Throttle	15.Piezometer
6.Fuel Injector	16.Reducing Valve
7.Ignition Module	17.Fuel Pump
8.Engine Control Unit	18.Fuel Tank
9.Exhaust Gas Analyser	19.Flame Arrestor
10.Charge Amplifier	20.Flame Damper

Gasoline and the other blends were pumped to fuel injectors between 2.5 and 3 bar pressure by using a fuel pump. The safety devices such as check valve, flame trap arrangement were used to quench the backfire from the engine. All blends were controlled by electronic card and software. The spark advance was measured by an oscilloscope. According to the load conditions of the test engine and the ratio of the gasoline-ethanol-methanol mixtures, the spark advances of the engine were arranged between from 21 CA before top dead centre to 2 CA after top dead centre.

Table 1. Engine Specifiations

Engine	Ford MVH418
Number of cylinders	4 in line
Stroke volume	1796 cm^3
Bore/Stroke	80.6 x 88mm
Connecting rod	137 mm
Compression ratio	10:1
Max. BMEP	10.7 bar
Max. Power	75 kW/5500 rpm
Max. Torque	150 Nm/4000 rpm
Idle/Max. Speed	800/6000 rpm
Weight	123 kg

The purpose of this study is to investigate the effects of alcohol blends on the performance of a standart SI engine. Three various types of gasoline – alcohol blends have been chosen for use in this study. They include (20%methanol-80%gasoline), (20%ethanol-80%gasoline), (10%methanol–10%ethanol-80%gasoline) and pure (%100) gasoline. Properties of the all fuels are shown in Table 2.

Table 2. Fuel Properties[13]

Property	Gasoline	Ethanol	Methanol
Chemical Formula	C_8H_{15}	C_2H_5OH	CH_3OH
Composition (C,H,O) (mass %)	86,14,0	52,13,35	37.5,12.5,50
Lower heating value (MJ/Kg)	43.5	27.0	20.1
Heat of evaporation (kJ/kg)	223.2	725.4	920.7
Stoichiometric A/F ratio (Volume %)	14.6	9.0	6.4
Oxygen content, mass%	0.0	34.7	49.9
Density (kg/m^3)	760	790	796
Saturation pressure at 38°C (kPa)	31	13.8	31.69
Flash point (°C)	-45 to -38	21.1	11.1
Auto-ignition temperature (°C)	420	434	470
Boiling point (°C)	25-215	78.4	64.5

All experiments were conducted at 1500 rpm and 25% load (Torque=30Nm) under different values of λ (0.9, 1, 1.1). So we showed that the change of engine performance values under rich,stoichiometric and lean mixture conditions.

3. UNCERTAINTIES OF INSTRUMENTS USED

Table 3. Specifications and error range of the experimental equipment and sensors

Instrument	Values	Accuracies
Cylinder pressure transducer	0 – 5000 PSI	±1 %
Hot film air mass meter	10 – 480 kg/h	≤ 3 %
Eddy Current Dynamometer	150 kW/8000 rpm	±1 rpm
Exhaust gas analyzer		
CO	0 – 10 % Vol	0.001 % Vol
CO_2	0 – 18 % Vol	0.010 % Vol
O_2	0 – 22 % Vol	0.010 % Vol
NOx	0 – 5000 ppm	1.0 ppm
HC	0 – 9999 ppm	1.0 ppm
Lambda	0.5 – 9.999	0.001

Measurement errors and uncertainties are arisen from devices used to measure the data of the experiment. Specifications and error range of the test equipment and sensors are given in Table 2. Total percentage uncertainty of the experiment has been calculated as 2.02%.

4. RESULTS AND DISCUSSION

4.1. Peak Pressure

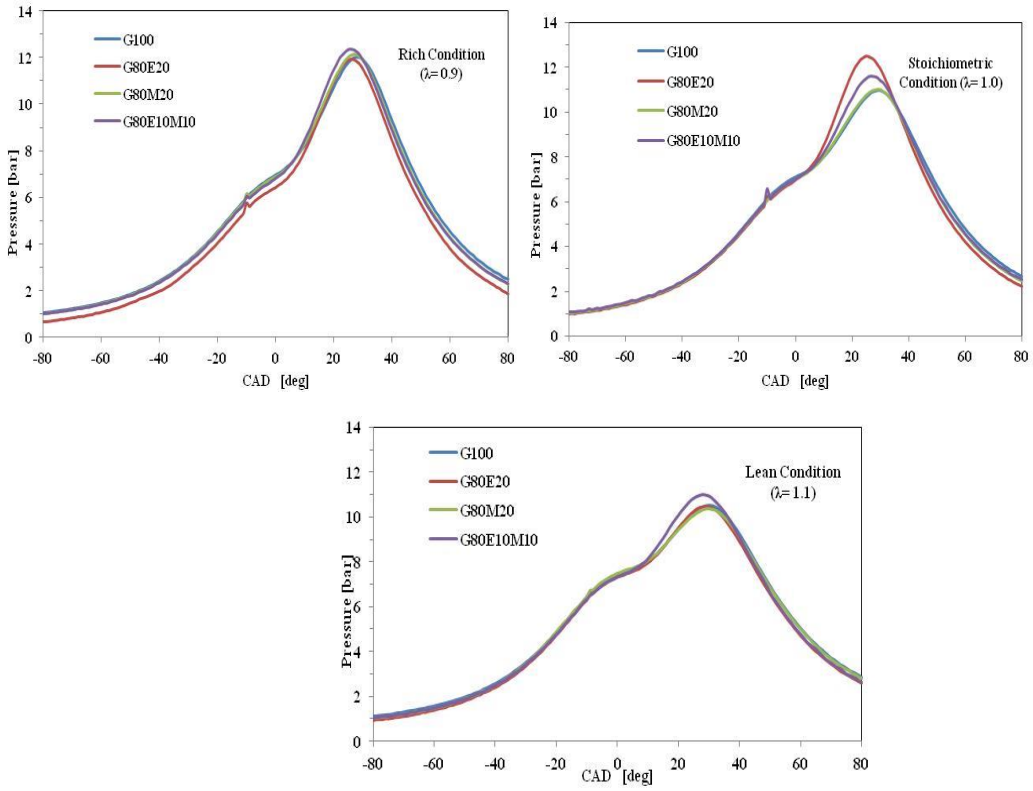

Figure 2. Variation of cylinder pressure with CA at different λ conditions

The variation of cylinder pressure with crank angle for various λ conditions have been illustrated Fig 2. The combustion characteristics of the methanol, ethanol and methanol-ethanol blends can be compared with gasoline in this figure. The peak pressure was 12,48 bar and the occurence of peak pressure angle was 25 CA ATDC in baseline gasoline-ethanol operation at stoichiometric condition, %25 load and 1500 rpm. The minimum in-cylinder pressure was 10,31 bar and the occurence of min. in-cylinder pressure angle was 31 CA ATDC in baseline gasoline-methanol operation at lean condition. Peak pressure changes were so close to each other in rich conditions. Furthermore, P_{peak} for all test fuels occured closer to top dead center (TDC). The lowest peak pressure values obtained at lean conditions for all fuels.

4.2. Heat Release Rate

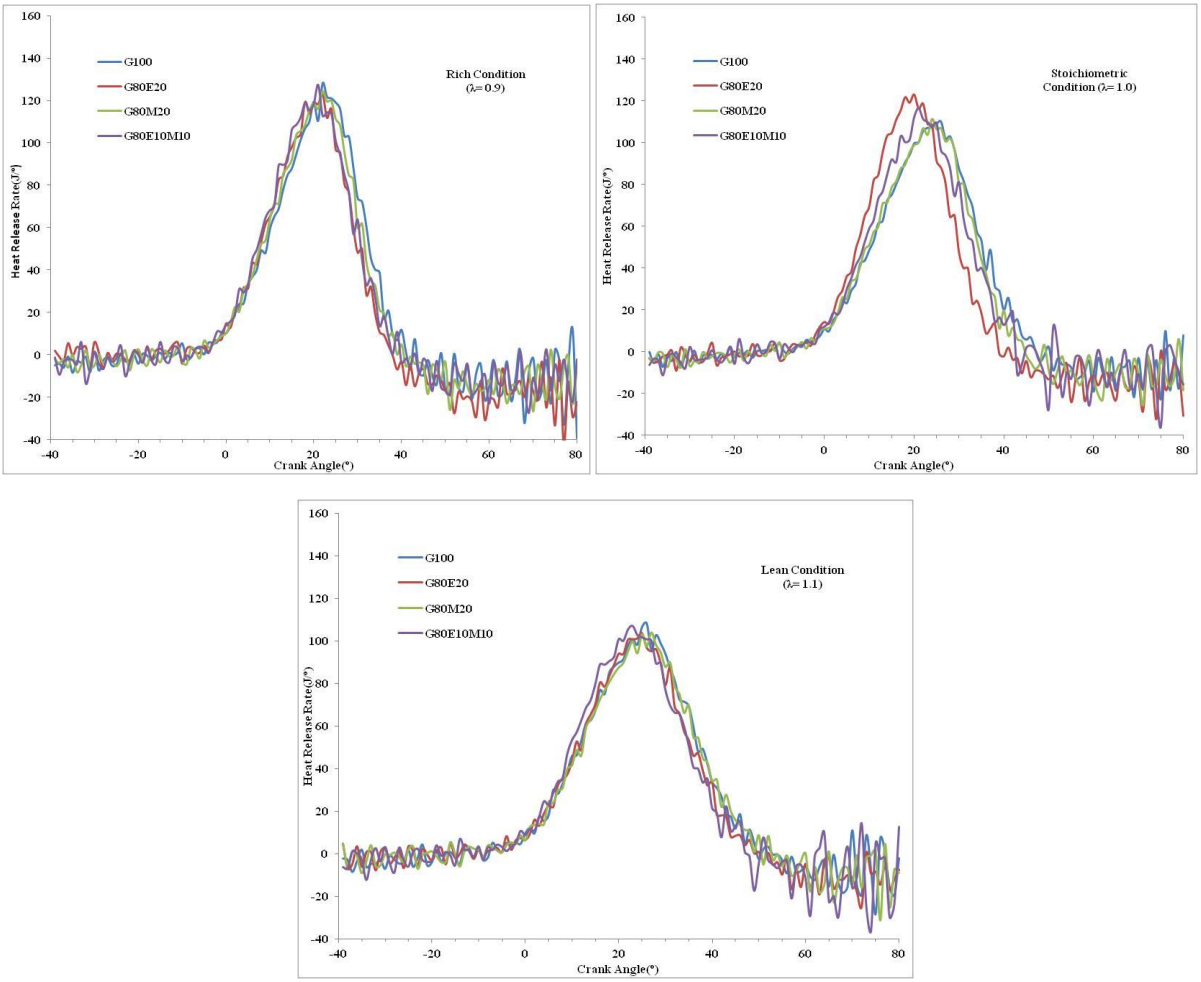

Figure 3. Variation of heat release rate with CA at different λ conditions

In internal combustion engine applications, heat release rate computes how much heat would have to be added to the cylinder contents, in order to produce the observed pressure variations [14]. A heat release analysis is normally applied to diesel engines, but it can be also applied to SI engines. The heat release rate is evaluated on a differential basis according to the following equation:

$$\frac{dQ_n}{d\theta} = \frac{\gamma}{\gamma - 1} P \frac{dV}{d\theta} + \frac{1}{\gamma - 1} V \frac{dP}{d\theta}$$

Where $dQ_n/d\theta$ is the net heat release rate, θ is the crank angles (CA) in degrees and ($\gamma=C_p/C_v$) is the ratio of specific heat of the fuel-air mixture. As seen this figures, heat release rates were so close to each other for all blends at rich conditions(λ=0.9). Because of the low evaporation pressure of ethanol, it evaporates more quickly and thus the heat release rates occured earlier than before at stoichiometric conditions (λ=1.0). The heat release rates were not vary much at lean conditions(λ=1.1).

4.3. Brake Thermal Efficiency and Brake Spesific Fuel Consumption

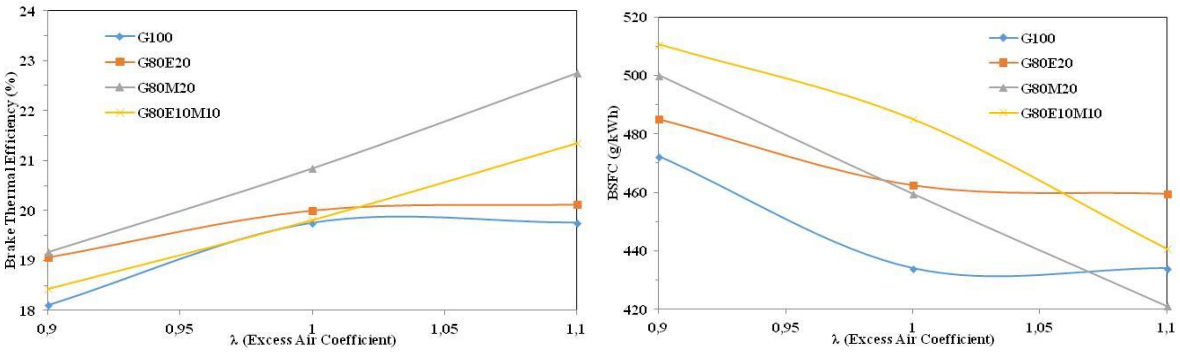

Figure 4. a) Variation of BTE with λ **b)** Variation of BSFC with λ

The variation of brake thermal efficiency (BTE) with different λ ratios is shown in Fig. 4a. The comparison of brake spesific fuel consumption (BSFC) for different λ values is shown in Fig. 4b. The highest brake thermal efficiency obtained 22,75 in baseline gasoline-methanol operation at lean condition, %25 load and 1500 rpm. The lowest brake thermal efficiency gained 18,1 in neat gasoline operation at rich condition as we expect. When methanol was added to the mixture it is seen that the brake thermal efficiency increases linearly, in addition reduces brake spesific fuel consumption. The characteristic of ethanol addition to gasoline is the same as gasoline. As we look Gasoline-Ethanol-Methanol blend, methanol did same influence because of methanol has much oxygen content as mass and its air/fuel ratio is low.

5. EMISSION PARAMETERS

5.1. Carbon monoxide(CO), Carbon dioxide (CO_2) and Hydrocarbon (HC)emissions

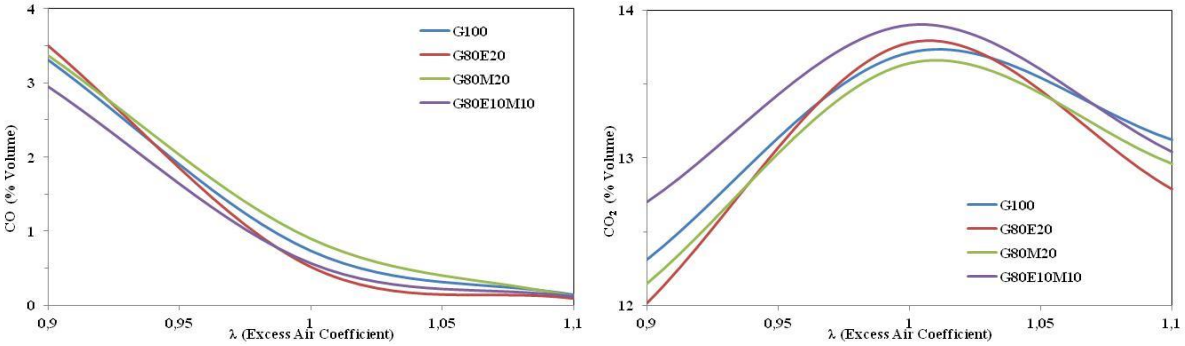

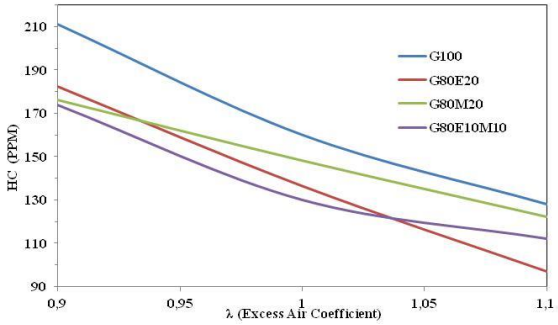

Figure 5. Variation of CO, CO_2 and HC emissions versus λ for all blends

Carbon monoxide is a colourless, odourless and very poisonous gas. Carbon monoxide is not only a harmful emission but it is also a chemical energy that cannot be converted into useful work. The emission of CO forms from incomplete combustion of HC fuel and it greatly depends on the air fuel ratio. Even though an SI engine is worked on lean conditions, there will be generated a certain amount of CO emissions due to local rich mixture zones in the combustion chamber and incomplete combustion [15]. Carbon dioxide has no direct harmful effects on the environment. However, carbon dioxide is the greenhouse gas that has the greatest effect on global warming. HC emissions are malodorous and irritating. Some of them are carcinogenic. They react with atmospheric gases to form photochemical smog. Nonstoichiometric air-fuel ratio, incomplete combustion and crevice volumes of the combustion chamber are some mainly causes of HC emissions [15].

Fig. 5 depicts CO, CO_2 and HC emissions versus λ for all blends. As seen this figure, CO, CO_2 and HC emissions for all blends showed nearly same trend. If we added ethanol and/or methanol to gasoline, they can provide more oxygen for the combustion process. Therefore, mixed fuels can be treated as partially oxidized hydrocarbons. The emissions are also significantly related to A/F (air to fuel) ratio. The stoichiometric A/F ratio for pure gasoline is about 14.8 and those for the blended fuels are lower (A/F for methanol and ethanol is 6.4 and 9, respectively, as shown in Table 2). When blended fuels are applied, the engine fuel system will supply similar fuel quantity as in gasoline condition (the gasoline engine is not tuned for the fuel blends, as mentioned early)[16]. The lowest CO, CO_2 and HC emissions (0.09, 97, 12 respectively) were gained for gasoline-ethanol blends at different λ conditions.

5.2. Nitrogen Oxide (NO)emission

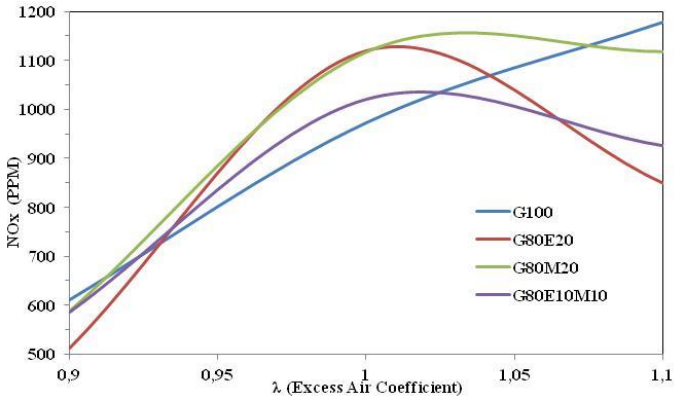

Figure 6. Variation of NO_X emissions versus λ for all blends

Most of the oxides of nitrogen comprise nitric oxide (NO), a small amount of nitric dioxide (NO_2) and traces of other nitrogen oxides. These are all grouped together and this group is called NO_X . The oxides of nitrogen tend to settle in Hemoglobin in the blood. The most undesirable toxic effect of oxides of nitrogen is their tendency to join with the moisture in the lungs to form dilute nitric acid. NO_X is one of the causes of photochemical smog [17]. NO_X formation strongly depends on the high combustion temperature and the amount of oxygen in the environment. By taking a deep look at Fig. 6, when ethanol and/or methanol contents added to gasoline, NO_X emission was decreased at rich and lean conditions except stoichiometric condition. The lowest NO_X emission obtanied for gasoline-ethanol-methanol blend at rich condition as 585 ppm.

6. CONCLUSIONS

In this study, the performance and emission characteristics of an SI engine fuelled by gasoline-ethanol-methanol mixtures have been investigated at 1500 rpm, 25% load and at different relative air to fuel ratios (λ). Experimental results of this study can be summarized as follows:

- The maximum in-cylinder pressure was 12,48 bar and the occurence of peak pressure angle was 25 CA ATDC in gasoline-ethanol operation at stoichiometric condition. The minimum in-cylinder pressure was 10,31 bar and the occurence of peak pressure angle was 31 CA ATDC in gasoline-methanol operation at lean condition.
- The highest heat release rate was 128,22 J/º at 22 CA ATDC in neat gasoline operation at rich condition.
- The highest BTE obtained 22,75 in baseline gasoline-methanol operation at lean condition. The lowest BTE gained 18,1 in neat gasoline operation at rich condition as we expect.
- The lowest BSFC obtained 421,28 g/kWh in gasoline-methanol-ethanol operation at lean mixture.
- The lowest CO, CO_2 and HC emissions (0.09, 97, 12 respectively) were gained for gasoline-ethanol blends at different λ conditions.
- The lowest NO_X emission obtanied for gasoline-ethanol-methanol blend at rich condition as 585 ppm.

7. NOMENCLATURE

CA	Crank angle (degree)
ATDC	After top dead center (CA)
BSFC	Brake specific fuel consumption (g/kWh)
BTDC	Before top dead center (CA)
BTE	Brake thermal efficiency (%)
CO	Carbon monoxide
CO_2	Carbon dioxide
EGR	Exhaust gas recirculation
HC	Hydrocarbon
NO_x	Oxides of nitrogen
SI	Spark ignition
SA	Spark advance
λ	Lambda (Excess Air Ratio)

8. References

[1] A. Elfasakhany, Modeling of Pulverised Wood Flames, PhD thesis, Fluid Mechanics Dept., Lund, Sweden, 2005. ISBN-13/EAN: 9789162864255.

[2] Demirbas A. A realistic fuel alternative for diesel engines. London: Springer; 2008.

[3] Speidel HK, Ahmed I. Biodegradability characteristics of current and newly developed alternative fuels. SAE Paper 1999; No. 1999-01-3518.

[4] Kumabe K, Fujimoto S, Yanagida T, Ogata M, Fukuda T, Yabe A, Minowa T. Environmental and economic analysis of methanol production process via biomass gasification. Fuel 2008;87:1422–7.

[5] Silva R, Cataluna R, Menezes EW, Samios D, Piatnicki CMS. Effect of additives on the antiknock properties and Reid vapor pressure of gasoline. Fuel 2005;84:951–9.

[6] Raveendran K, Ganesh A, Heating value of biomass and biomass pyrolysis products. Fuel 1996;75:1715–20.

[7] M .Al-Hasan "Effect of ethanol–unleaded gasoline blends on engine performance and exhaust emission "Energy Conversion and Management 44, 1547–1561, 2003.

[8] M .Abu-Zaid, O .Badran, and J .Yamin, Effect of methanol addition to gasoline on the performance of spark ignition engines "Energy & Fuels 18, pp(312-315), 2004.

[9] D.Balaji, Influence of isobutanol blend in spark ignition engine performance operated with gasoline and ethanol "Vol .2)7(2859-2868), 2010.

[10] L. Siwale, L. Kristóf, A. Bereczky, M. Mbarawa, A. Kolesnikov, Performance, combustion and emission characteristics of n-butanol additive in methanol– gasoline blend fired in a naturally-aspirated spark ignition engine, Fuel Proc. Technol. 118 (2014) 318–326.

[11] I.T. Nazzal, Experimental study of gasoline –Alcohol blends on performance of internal combustion engine, Eur. J. Sci. Res. 52 (2011) 16–22.

[12] J.W.G. Turner, R.J. Pearson, E. Dekker, B. Iosefa, K. Johansson, K. Bergstom, Extending the role of alcohols as transport fuels using iso-stoichiometric ternary blends of gasoline, ethanol and methanol, Appl. Energy 102 (2013) 72–86.

[13] A.K. Agarwal, Biofuels (alcohols and biodiesel) applications as fuels for internal combustion engines, Prog. Energy Combust. Sci. 33 (2007) 233– 271.

[14] Stone R. Introduction to internal combustion engine. second ed. The Macmillan press ltd; 1992.

[15] Pulkrabek, W. W. (2003). Engineering Fundamentals of the Internal Combustion Engine. 2nd edn. Prentice Hall. New Jersey.

[16] A. Elfasakhany, Investigation on the effects of ethanol-methanol-gasoline blends in a spark-ignition engine: Performance and emissions analysis, ‘Êngineering Science and Technology, and International Journal. 18 (2015) 713-719.

[17] Gupta, H. N. (1992). Fundamentals of Internal Combustion Engines. Pvt. Ltd. New Delhi.

Paper 17 **Bildiri 17**

DESIGNING AN INNOVATIVE HYBRID INDUSTRIAL COOKER

MURAT HACI[1], ZAFER KAHRAMAN[1], HAKAN SERHAD SOYHAN[2,3]

1. OZTIRYAKILER MADENI ESYA SAN. TIC. A.S – R&D TECHNOLOGY CENTER, ISTANBUL - TURKEY
2. ENGINEERING FACULTY, UNIVERSITY OF SAKARYA, SAKARYA – TURKEY
3. TEAM-SAN CO., R&D TECHNOLOGY MANAGER, SAKARYA – TURKEY

ABSTRACT

The use of biofuels has been increasing in recent years. Biofuels are also called as clean renewable energy. An increasing number of biofuels are being used in kitchens as one of the alternative energies. The aim of study is to investigate special burner designed especially for biofuel and effective combustion process for cooking. All the information obtained from this study is used to assess the feasibility in experimental and practical applications. Parametric simulations on pressures, various compositions and burner hole diameters were examined and the most suitable biofuel burner was obtained. As a result of the project, the best configuration were obtained to be used in industrial kitchen appliances.

Keywords: Biofuels, cooking burner system, simulation.

1. DESIGN PARAMETERS

The burner is vertically fired and there are 24 main fuel channels where fuel exits to ambient air, having 0.8 mm diameter each, divided into 4 packs. There are 12.95 degree between fuel channels and 25.25 degree between the channel groups which provides gaps between channel packs.

Ø	:22cm.
Water amount	:3.7 lt
Pressure	:15 mbar
Fuel consumption	:0.089 m^3
Net.cal. value	:25.895 MJ/m^3
T1	:19.7 C
T2	:91.6 C
Efficiency	: % 48.32

$$\mu = m \times Cp \times \frac{(t2 - t1)}{Vc \times Hi} \times 100$$

2. EXPERIMENTAL SETUP AND MEASUREMENTS



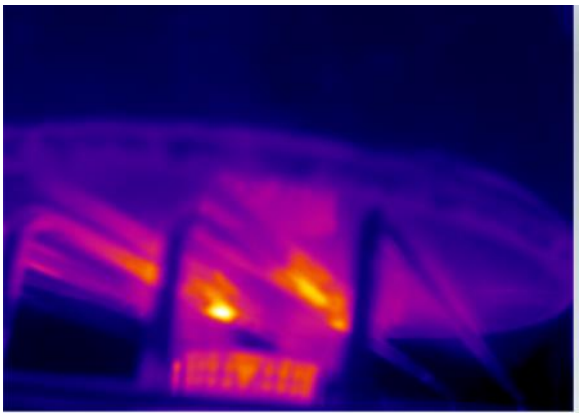
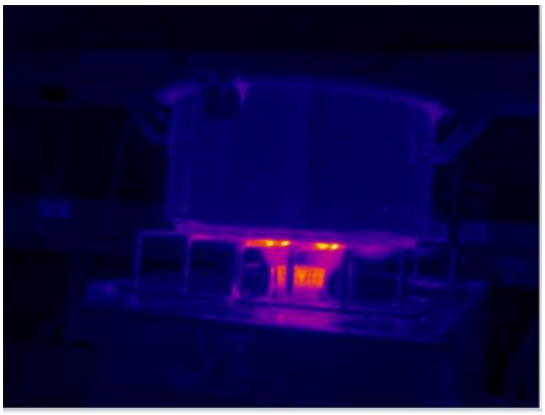

3. RESULTS AND DISCUSSION

As a result, it was observed that there was no big difference in efficiency between Ø22 cm, Ø20 cm and Ø24 cm. However, it was determined that the efficiency is increased with an increase in pot diameter (Ø30 cm). However, the increase in the percentage of CO_2 in the biofuel is adversely affected the efficiency.

Acknowledgements

Financial support from TUBITAK-TEYDEB (Project Number: 3160502) is acknowledged.

Paper 18 **Bildiri 18**

DETAILED CHEMICAL KINETIC MODELING OF THE EFFECTS OF METHANOL ADDITION ON N-HEPTANE OXIDATION

Abdalwahab Alazreg , Emre Degirmenci, Fikret Inal*

Department of Chemical Engineering, Izmir Institue of Technology, Gulbahce-Urla, Izmir,Turkey

* fikretinal@iyte.edu.tr

Absrtact

Methanol is one of the commonly used fuel oxygenate additive (i.e. oxygen containing species). In this study, the effects of methanol addition on n-heptane oxidation at atmospheric pressure, laminar, premixed, fuel-rich flame was investigated at an equivalence ratio of 2.10 using Detailed Chemical Kinetic Modeling approach. The modeling work was carried out using PREMIXED code of ChemKin package. A model validation using various available literature data for different combustion systems (i.e., laminar premixed flame and rapid compression machine) has been done. The proposed mechanism consists of 3249 reactions and 753 species. It was found that mole fraction profiles of carbon monoxide, acetylene, diacetylene, vinylacetylene and other lowmolecular-weight reaction products up to benzene were consistently lower in flame containing methanol. This mole fraction reduction is attributed to blended fuel oxygen content, oxygen remains connected to the carbon atom and carbon atom cannot participate in any other reaction. Although there are under and over estimation of species mole fractions by the model, the modeling and experimental mole fractions of species are generally in a good agreement for both n-heptane flame and n-heptane with methanol flame.

Keywords: Combustion, Methanol, n-Heptane Oxidation, Premixed Flame

INTRODUCTION

Despite the fact that combustion provides global energy support in different sectors (e.g., in transportation, electricity generation, heating, and industrial applications), the combustion products are distinctly identified as a severe source of environmental damage and are causing changes in the atmosphere [1]. The major combustion emissions can be considered as carbon monoxide (CO), nitrogen oxides (NOx), sulfur oxides (SOx), polycyclic aromatic hydrocarbons (PAH), and particulates (soot, fly ash, and aerosols). nHeptane is one of the primary reference fuels (PRF) and it can well represent the combustion characteristics of diesel and gasoline fuel.

For the better understanding of the oxidation of n-heptane fuel a number of studies have been conducted [2-7]. A modeling work was carried out by involving flow reactors, shock tubes and rapid compression machine under conditions of pressure range of 1-42 atm, temperature range of 550-1700 K, the equivalence ratio from 0.3 to 1.5 and nitrogen-argon dilution of 70-99% [2].

Species mole fractions data from variable pressure flow reactor and jet stirred reactor have been used for the low temperature part of the mechanism. Experimental results from the literature regarding ignition delay time were used to validate and developed reaction mechanism at low and high temperatures. The proposed mechanism consists of 990 species and 4060 reactions. According to the study, a very good agreement between modeling and experimental results was achieved and it was found that the vast majority of the important reaction pathways and rate expressions were reasonably correct. The ignition delay times of stoichiometric n-heptane/air mixtures have been measured at different pressures (15, 20 and 38 bar) and in the temperature range of 726– 1412 K, experimentally in shock tube [7]. Meanwhile, concentration versus time profiles of species have been measured in a jet-stirred reactor at atmospheric pressure, in the temperature range of 500–1100 K at different equivalence ratios Φ =0.25, 2.0 and 4.0. A detailed chemical kinetic model has been developed and it was claimed a good agreement between the modeling and experimental studies. Oxygenate addition on hydrocarbon fuels has been proposed as a method to reduce the combustion emissions. To gain deeper understanding many of experimental and computational studies have been conducted [8-11]. It has been found that there are many types of oxygenates including esters, ethers and alcohols, which can enhance the engines efficiency and reduce the undesired combustion products [12, 13]. Methanol has been used as a promising alternative engine fuel in recent years. A detailed chemical kinetic modeling of the oxidation of n-heptane/methanol fuel blends has been carried out to develop a chemical kinetic mechanism and create a skeletal model [14]. For the fuel blend the initial temperature range was 700–1100 K, initial pressure range was 30–100 atm and the equivalence ratio range was 0.25-1. Satisfactory predictions for both pure n-heptane and fuel blends oxidation have been achieved. The influences of methanol on premixed fuelrich n-heptane flames were studied experimentally using two laminar premixed nheptane/O2/Ar flames (Φ = 1.60, (C/O = 0.51), and Φ = 1.80, (C/O = 0.57)) and one laminar premixed n-heptane/methanol/O2/Ar flame (Φ= 1.80, (C/O = 0.51)) [15]. A modeling work was also carried out and it has been found that the concentrations of C2–C7 hydrocarbon intermediates were reduced significantly as methanol was added. The extent of the reduction in the case of constant C/O ratio was smaller than that in the case of constant equivalence ratio. It is claimed that the maximum flame temperature was reduced as equivalence ratio increased. A satisfactory prediction was achieved for the mole fraction profiles of major and intermediate species with a modified chemical mechanism. In this study, the objective was to investigate the effects of methanol addition on n-heptane oxidation using detailed chemical kinetic modeling approach.

A proposed chemical kinetic mechanism was developed and applied for laminar, premixed, fuel-rich n-heptane and nheptane/methanol flames at an equivalence ratio of 2.10.

METHOD

The detailed chemical kinetic modeling (DCKM) approach is the appropriate method to predict macroscopic phenomena from the knowledge of fundamental chemical and physical parameters, together with a mathematical model of the process. ChemKin simulation software is the commonly used one for this purpose [16]. A comprehensive and recent mechanism available in the literature, Lawrence Livermore National Laboratory LLNL (Version 3.1) mechanism [17] was selected as a base mechanism for the computational work. Since the base mechanism does not include the whole reactions of methanol oxidation and some of the reactions of C4-C6 species, Marinov's mechanism [18] and pure methanol mechanism [19] were merged with the base mechanism. Table 1 illustrates the general information of the base, donor and master mechanisms.

Table 1. Basic features of base, donor and master mechanisms

	Number of Reactions	Number of Species	Reference
Base mechanism	2827	627	[18]
Donor mechanism 1	668	154	[19]
Donor mechanism 2	1011	173	[20]
Master mechanism	3249	753	This study

The target flame was studied experimentally by Inal and Senkan [20]. The experimental conditions of the study are given in Table 2. In that study, the species were sampled from the flame by quartz microprobe. The characterization of the species concentration profiles was done by GC/TCD for major species and GC/MS for minor and trace species. The details of the experimental setup are given elsewhere [20].

Table 2. Experimental Conditions for n-heptane/methanol flame of the target study

Conditions	Premixed flame
Equivalence ratio	2.10
Pressure (atm)	1
Inlet velocity (cm/sec)	5.157
n-C7H16 mole fraction	0.0520
CH3OH mole fraction	0.0107
O_2 mole fraction	0.2803
Ar mole fraction	0.6570

RESULTS AND DISCUSSION

To investigate the capabilities of the master mechanism, model validation using various available literature data for different combustion systems (i.e., laminar premixed flame [9] and rapid compression machine [21]) was carried out. Table 3 shows the general information of the two studies that have been used for the validation work.

Table 3. General information for the studies used for validation work

Conditions	Chen 2012 [9]	Kumar 2011 [21]
System type	Premixed flame	Rapid compression machine
Temperature (K)	400 ~ 1980	850 ~ 1100
Pressure (atm)	0.04	14
Equivalence ratio Φ	1.6	1
n-C7H16 mole fraction	0.078	-
CH3OH mole fraction	0.018	0.1227
O2 mole fraction	0.549	0.184
Ar mole fraction	0.355	0.693

The species concentration profiles for H2, CO and CO2 for laminar premixed flame are shown in Figure 1. The modeling results fitted most of the experimental results of mole fractions. A good prediction has been achieved by the master mechanism. As seen from Figure 2, although there were underestimations by the master mechanism for the ignition delay time of methanol fuel, the modeling results of the master mechanism were closer to the experimental data. Kumar [21] has also used kinetic mechanism to predict the experimental ignition delay time.

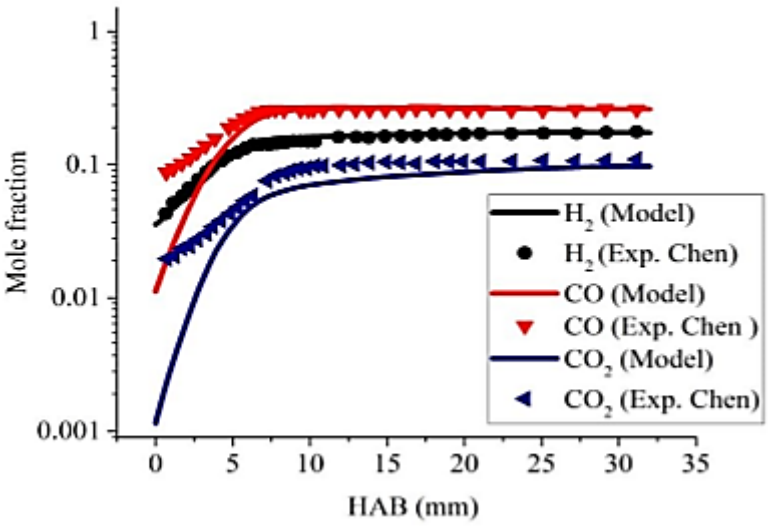

Figure 1. Validation of the master mechanism for H2, CO and CO2 mole fraction against laminar premixed flame

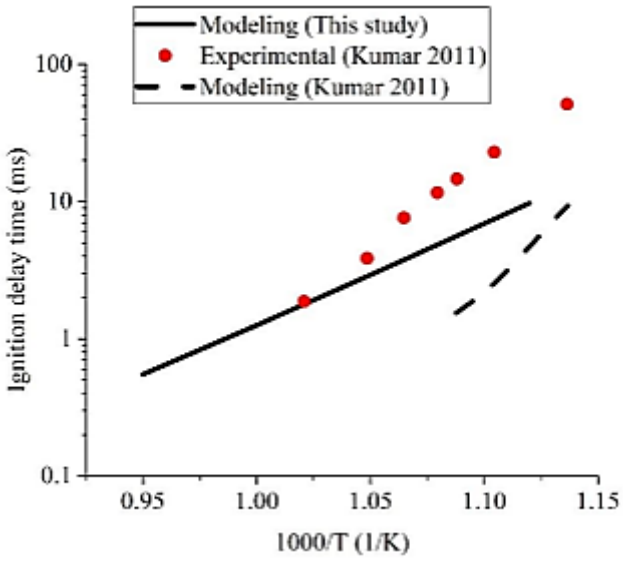

Figure 2. Validations of the master mechanism by ignition delay time

The effects of methanol addition on the oxidation of laminar, premixed, fuel-rich n-heptane flame using DCKM approach have been investigated. The modeling results of species mole fractions of n-heptane and n-heptane/methanol flames have been compared against the experimental results of the target flame [20]. The mechanism has predicted well the reduction in mole fractions of CO and C2H2 as shown in Figure 3. The CO mole fractions decreased with the addition of methanol, similar results were also found in other studies [22, 23]. For acetylene the modelling profiles showed underestimation for both flames, n-heptane and n-heptane/methanol, and the reduction was obvious as methanol was added. C2H2 is considered as one of the precursor species for first aromatic ring formation and PAH growth [20].

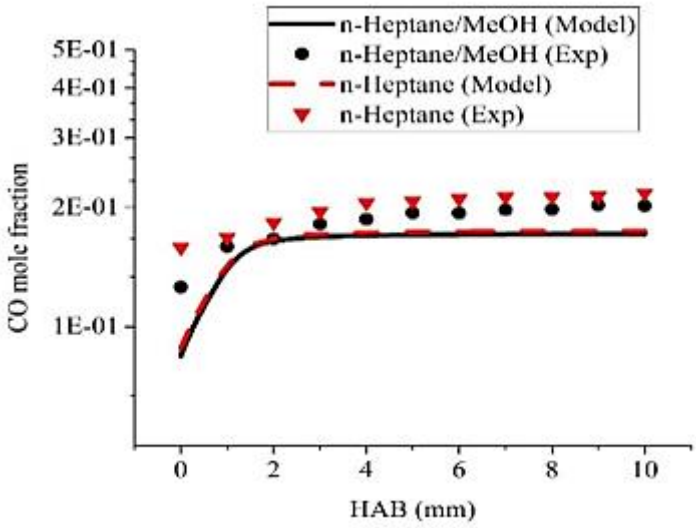

(a)

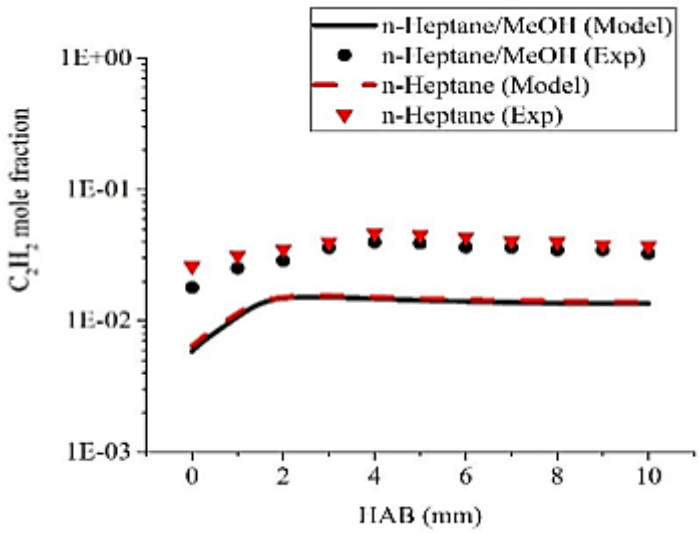

(b)

Figure 3. Species mole fractions, CO (a) and C2H2 (b) of n-heptane and n-heptane/methanol flames

For both n-heptane and n-heptane/methanol flames the prediction of propadiene (C3H4) diacetylene (C4H2) and vinylacetylene (C4H4) were underestimated by the model as shown in Figure 4. The results showed a reduction in these species mole fractions for methanol blended flame. These species were also considered as precursors for the formation of first aromatic ring. Similar extent of reduction in the mole fractions of C4–C7 species with methanol addition of the modelling results were also reported in the literature [24].

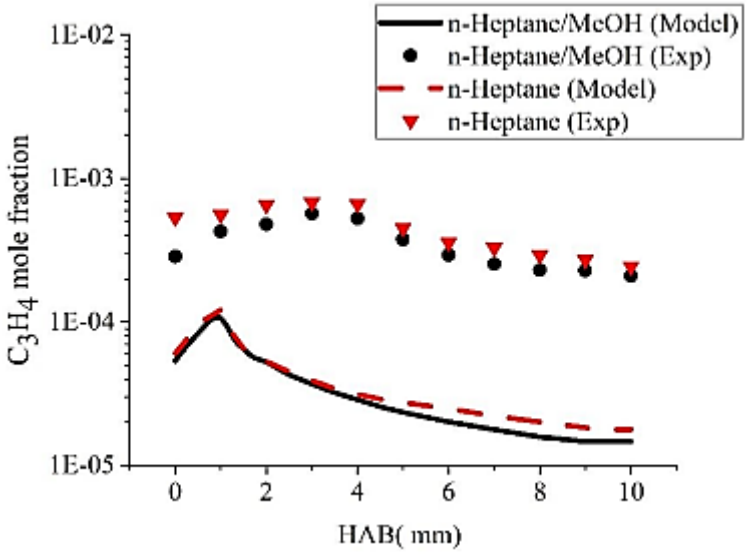

(a)

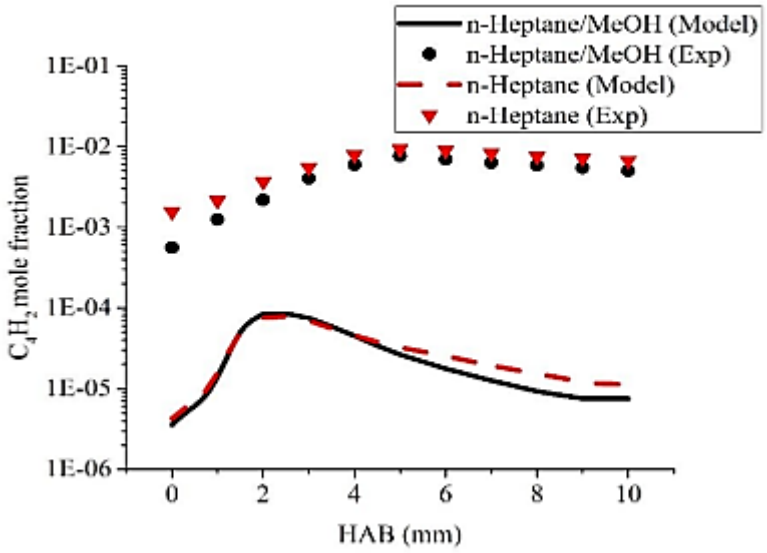

(b)

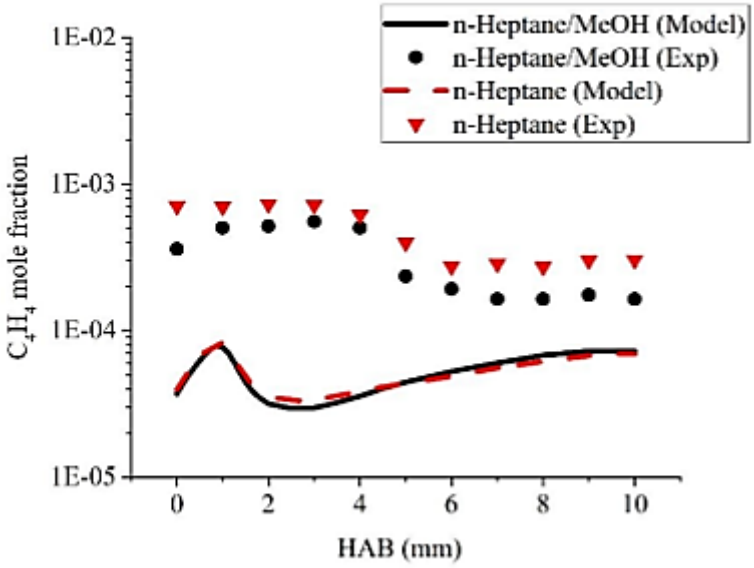

(c)

Figure 4. Species mole fractions, C3H4 (a), C4H2 (b) and C4H4 (c) of n-heptane and nheptane/methanol flames

The mole fractions of benzene decreased in the presence of methanol (Figure 5). At low height above the burner there were underestimations by the model while for heights over the 4mm above the burner there were overestimations for both of n-heptane and nheptane/methanol flames. Whereas in general, there was a good agreement between the experimental and modeling results of benzene mole fractions. According to a study conducted using two kinds of alcohols, methanol and ethanol, the maximum mole fractions of benzene decreased by 12.5% in presence of methanol, and 33.3% in presence of ethanol [24].

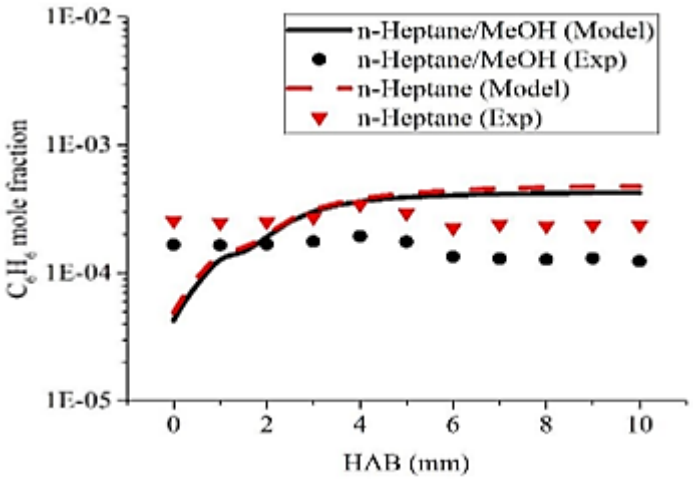

Figure 5. C6H6 mole fractions of n-heptane and n-heptane/methanol flames

The reduction of species mole fractions when methanol is added to n-heptane fuel may be attributed to, i) Methanol is oxygen containing species so oxygen remains connected to carbon atom and carbon atom cannot participate in any other reactions [20]. ii) The concentration of formaldehyde in n-heptane/methanol flame is higher than its concentration in n-heptane flame so this may play a role in the reduction of species mole fraction [14] (Figure 6). iii) The addition of methanol converts an active hydroxyl radical, OH, into inactive hydrogen peroxide, H2O2, which reduces the reactivity flame of the system [21].

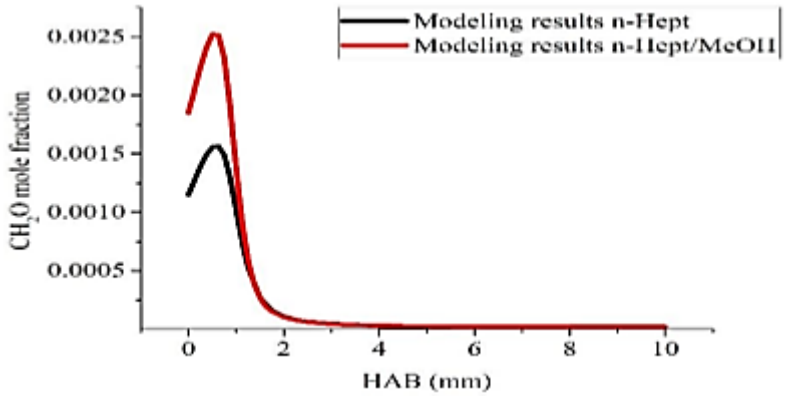

Figure 6. CH_2O mole fractions of n-heptane and n-heptane/methanol flames

CONCLUSION

A detailed chemical kinetic model of n-heptane/methanol has been developed in order to predict its effect on combustion chemistry. The mechanism consists of 3249 reactions and 753 species. It has been applied to a laminar, premixed, fuel-rich n-heptane/methanol flame at an equivalence ratio of 2.10. Although the model underpredicted the species mole fractions like acetylene, diacetylene and vinylacetylene, in general, a good agreement

between the modeling results of the proposed mechanism with the experimental data have been achieved. It has been found that methanol has reduced the mole fraction of species. The fuel oxygenates could be a reliable method for reducing toxic species mole fractions in hydrocarbon fuel combustion.

ACKNOWLEDGMENT

We would like to thank Izmir Institute of Technology Scientific Research Fund (2019 IYTE 0007) for the financial support.

REFERENCES

[1] J. Warnatz, U. Maas, and R. W. Dibble, Combustion Physical and Chemical Fundamentals, Modeling and Simulation, Experiments, Pollutant Formation. Berlin Heidelberg: Springer, 2006.

[2] H. J. Curran, P. Gaffuri, W. J. Pitz, and C. K. Westbrook, "A Comprehensive Modeling Study of n-Heptane Oxidation," Combustion and Flame, vol. 114, no. 1, pp. 149-177, 1998.

[3] L. Seidel, K. Moshammer, X. Wang, T. Zeuch, K. Kohse-Höinghaus, and F. Mauss, "Comprehensive kinetic modeling and experimental study of a fuel-rich, premixed n-heptane flame," Combustion and Flame, vol. 162, no. 5, pp. 2045-2058, 2015.

[4] T. Zeuch, G. Moréac, S. S. Ahmed, and F. Mauss, "A comprehensive skeletal mechanism for the oxidation of n-heptane generated by chemistry-guided reduction," Combustion and Flame, vol. 155, no. 4, pp. 651-674, 2008.

[5] A. Chakir, M. Belliman, J. Boettner, and C. M., "Kinetic Study of N-Heptane Oxidation," International Journal of Chemical Kinetics, vol. 24, pp. 385-410, 1992.

[6] P. Dagaut, M. Reuillon, and M. Cathonnet, "Experimental study of the oxidation of nheptane in a jet stirred reactor from low to high temperature and pressures up to 40 atm," Combustion and Flame, vol. 101, no. 1, pp. 132-140, 1995.

[7] K. Zhang, C. Banyon, J. Bugler, H. J. Curran, A. Rodriguez, O. Herbinet, F. Battin-Leclerc, C. B'Chir, and K. A. Heufer, "An updated experimental and kinetic modeling study of nheptane oxidation," Combustion and Flame, vol. 172, pp. 116-135, 2016.

[8] P. A. Glaude, F. Battin-Leclerc, B. Judenherc, V. Warth, R. Fournet, G. M. Côme, G. Scacchi, P. Dagaut, and M. Cathonnet, "Experimental and modeling study of the gas-phase

oxidation of methyl and ethyl tertiary butyl ethers," Combustion and Flame, vol. 121, no. 1, pp. 345-355, 2000.

[9] G. Chen, W. Yu, J. Fu, J. Mo, Z. Huang, J. Yang, Z. Wang, H. Jin, and F. Qi, "Experimental and modeling study of the effects of adding oxygenated fuels to premixed n-heptane flames," Combustion and Flame, vol. 159, no. 7, pp. 2324-2335, 2012.

[10] P. Dagaut and C. Togbé, "Experimental and modeling study of the kinetics of oxidation of ethanol-n-heptane mixtures in a jet-stirred reactor," Fuel, vol. 89, no. 2, pp. 280-286, 2010.

[11] C. Yao, G. Xu, and H. Xu, "Experimental and modeling study of the effect of ethanol and MTBE on the oxidation of PRF90 in low pressure premixed laminar flame," Fuel, vol. 111, pp. 131-139, 2013.

[12] E. Ajav, B. Singh, T. Bhattacharya, "Experimental study of some performance parameters of a constant speed stationary diesel engine using ethanol–diesel blends as fuel, Biomass Bioenerg," Biomass Bioenerg, vol. 17, pp. 357-365, 1999.

[13] A. Elfasakhany, "Performance and emissions of spark-ignition engine using ethanol–methanol–gasoline, n-butanol–iso-butanol–gasoline and iso-butanol–ethanol–gasoline blends: A comparative study," Engineering Science and Technology, an International Journal, vol. 19, no. 4, pp. 2053-2059, 2016.

[14] H. Xu, C. Yao, and G. Xu, "Chemical kinetic mechanism and a skeletal model for oxidation of n-heptane/methanol fuel blends," Fuel, vol. 93, pp. 625-631, 2012.

[15] G. Chen, W. Yu, X. Jiang, Z. Huang, Z. Wang, and Z. Cheng, "Experimental and modeling study on the influences of methanol on premixed fuel-rich n-heptane flames," Fuel, vol. 103, pp. 467-472, 2013.

[16] "ANSYS Chemkin Theory Manual 17.0," ed. San Diego: Reaction Desgin, 2015.

[17] M. Mehl, W. J. Pitz, C. K. Westbrook, and H. J. Curran, "Kinetic modeling of gasoline surrogate components and mixtures under engine conditions," Proceedings of the Combustion Institute, vol. 33, no. 1, pp. 193-200, 2011.

[18] N. M. Marinov, "A detailed chemical kinetic model for high temperature ethanol oxidation," International journal of chemical kinetics, vol. 31, no. 3, 1999.

[19] U. Burke, W. K. Metcalfe, S. M. Burke, K. A. Heufer, P. Dagaut, and H. J. Curran, "A detailed chemical kinetic modeling, ignition delay time and jet-stirred reactor study of methanol oxidation," Combustion and Flame, vol. 165, pp. 125-136, 2016.

[20] F. Inal and S. M. Senkan, "Effects of oxygenate additives on polycyclic aromatic hydrocarbons (pahs) and soot formation," Combustion Science and Technology, vol. 174, no. 9, pp. 1-19, 2002.

[21] K. Kumar and C.J. Sung, "Autoignition of methanol: Experiments and computations," vol. 43, no. 4, pp. 175-184, 2011.

[22] W. Yanju, L. Shenghua, L. Hongsong, Y. Rui, L. Jie, and W. Ying, "Effects of Methanol/Gasoline Blends on a Spark Ignition Engine Performance and Emissions," Energy & Fuels, vol. 22, no. 2, pp. 1254-1259, 2008.

[23] R. M. Bata and V. P. Roan, "Effects of Ethanol and/or Methanol in Alcohol-Gasoline Blends on Exhaust Emissions," Journal of Engineering for Gas Turbines and Power, vol. 111, no. 3, pp. 432-438, 1989.

[24] H. Xu, C. Yao, G. Xu, Z. Wang, and H. Jin, "Experimental and modelling studies of the effects of methanol and ethanol addition on the laminar premixed low-pressure nheptane/toluene flames," Combustion and Flame, vol. 160, no. 8, pp. 1333-1344, 2013.

Paper 19 **Bildiri 19**

YANGIN MÜHENDİSLİĞİNİN YENİ YANGIN GÜVENLİĞİ YÖNETİM MODÜLÜ ÜZERİNDEN DEĞERLENDİRİLMESİ

*[1] Orhan ODUNCU, [2] Salim TURHAN, [3,4]Gökhan COŞKUN [5,6]Hakan Serhad SOYHAN, [7] Tayfun TURNALI, [8] Selçuk KÖMCÜ, [9] Muhammet Fatih PEKŞEN, [10,11] Bülent AÇIL

[1] Sakarya Üniversitesi, Fen Bilimleri Enstitüsü, Yangın Güvenliği ve Yanma Ana Bilim Dalı, Yangın Güvenliği ve Yanma Bölümü Sakarya/Türkiye

[2] İstanbul Aydın Üniversitesi, Fen Bilimleri Enstitüsü, İş Sağlığı ve Güvenliği Ana Bilim Dalı, İSG Bölümü (Mezun) İstanbul / Türkiye

[3]Sakarya Üniversitesi Yangın güvenliği ve Yanma ABD

[4] Sakarya Üniversitesi Makina Mühendisliği Serdivan/Sakarya

[5] Sakarya Üniversitesi, Yangın Araştırma ve Uygulama Merkezi, Esentepe Kampüsü, Sakarya.

[6] Team-San, Esentepe Mah. Akademi Yolu Sok. Teknoloji Geliştirme Bölg. A Blok No:10A/B11, 54187, Sakarya.

[7,8,9,10,] Sakarya Üniversitesi Yangın güvenliği ve Yanma ABD

[11] ANDEM, Varlık Mah. 100. Yıl Bulvarı Işıldar APT. No:59/9 Muratpaşa / ANTALYA

Özet

Yangın güvenliği günümüzde ihtiyaç olmaktan çıkarak zaruriyet haline gelmiştir. Bugün dünyanın farklı ülkelerinde farklı isimler altında yangın mühendisliği lisans programları yürütülmeye devam edilmektedir. Yangınların meydana getirmiş olduğu telafisi mümkün olmayan kayıp ve yıkımlar yangın mühendisliğinin önemini her geçen gün daha da fazla artırmaktadır. Günümüzde etkin bir yangın güvenlik modülü yönetimi ile yangınların önüne geçilebilecektir. Yeni yangın güvenlik modülü ile komplike olan yangın mühendisliği özgün simülasyon çalışmaları ile daha güvenli yapıların inşa edilmesini sağlayacaktır. Bu yaklaşımın lisans seviyesinden başlanarak yüksek lisans ve doktora ile akademik bir boyuta bürünmesi programın tanınmasına katkı sağlayacaktır.

Anahtar kelimeler: Yangın Mühendisliği, Yanma Kimyası, Lisans Programı, Simülasyonlar

Abstract

Fire safety comes out of envelope today to get it from need. To be different names in different countries of the world today. Fire engineering degree programs can continue to be carried out. The unforeseeable loss and destruction of the fires have increased the importance of fire engineering even more. With today's effective fire safety module management, fires can be avoided. With the new security security module, complex manufacturing fire engineering will provide unique simulation work and more secure construction. It will assist in the recognition of the Master's and Ph.D.

Keywords: Fire Engineering, Combustion Chemistry, Undergraduate Program, Simulations

1. GİRİŞ

Maslow'un "İhtiyaçlar Hiyerarşisi" kuramında insanların temel ihtiyaçları arasında ikinci sırayı güvenlik ihtiyaçları (Şekil 1) yer almaktadır. Maslow; "Bu gereksinim için ne kadar çok doyurulursa o denli az ayak bağı olacak, ne denli az olursa da cesaret de o denli az olacaktır" diyerek insanların hayatlarının her döneminde güvenli bir çevre, güvenli bir ev, güvenli bir yaşam arzusu içerisinde olmak istediklerini ortaya koymuştur. Yangın güvenliği bu açıdan bakıldığında ihtiyaç olmaktan çıkmış zaruri hale gelmiştir [1].

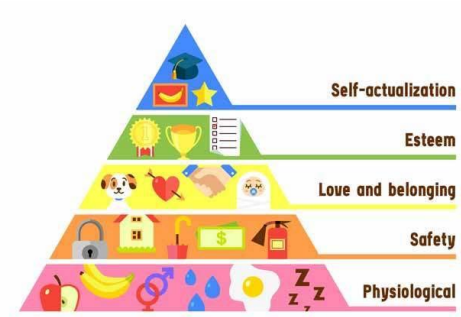

Şekil 1. Maslow'un İhtiyaçlar Hiyerarşisi [1]

Tarihte pek çok yangına sahne olan antik roma şehrinin, MS 64 yılında başlayan ve yedi gün süre ile devam eden büyük roma yangını ile üçte biri kullanılmaz hale gelmiştir. Roma'ya yeni bir çehre kazandırmaya kararlı olan imparator Neron'un şehri yeniden inşa ettirirken dayanıklı malzemeler kullanılması talimatı vermesi yangın mühendisliğinin ilk temel taşlarına yönelik rivayetler olduğu ifade edilmektedir. 1800 yıllarda sanayi devriminin başlaması ile önem kazanan yangınlar 20.yüzyılda sayıları giderek artar hale gelmiştir. 1903 yılında bir teknoloji enstitüsü tarafından kurulan ilk "yangın mühendisliği" lisans programı hayata geçirilmiştir. 1912 yılında Newyork şehri Manhattan bölgesinde bir binada halk eğitimi, yangın koruma mühendisliği ve itfaiye tekniklerinin bir arada öğretildiği ve günümüzde "Yangın Mühendisliğinin 140.Yılı" temalı etkinliklerle kutlanılan diğer bir faaliyet ise yangın mühendisliğinin tarihsel süreç içerisindeki farklı bir boyutu olmuştur. Bugün dünyanın farklı ülkelerinde farklı isimler altında yangın mühendisliği lisans programları yürütülmeye devam edilmektedir [2] [3] [4].

Tarihimiz açısından bakıldığında yangın güvenliği kavramına yönelik en dikkat çekici adımın 1579 Sultan III. Murat Han tarafından yayınlanan fermanda olduğu gözlemlenmektedir. İstanbul'da yangın sayısının artması ve büyük ziyanlar vermesi ile hayata geçirilen bildiride tüm İstanbul halkının evlerinin çatısına kadar uzanan bir merdiven bulundurması ve evlerinde yangınlara karşı içi su dolu fıçı bulundurması (Şekil 2) zorunlu kılınmıştır [5].

Şekil 2. Osmanlılarda Yangınla Mücadele [6]

Yangın güvenliği ile ilgili alınan bazı önlemlerin köklerinin bu kadar eskilere dayanmış olması meydana gelen bu kayıpların önüne geçilmesi için atılan adımlar olduğu anlaşılmaktadır

Yangın mühendisliği günümüzde pek çok tanım ile ifade edilmektedir. Yangın koruma, yangın önleme ve yangın güvenlik mühendislikleri gibi çeşitli isimlerle literatürde yer alan bu olgu aslında yangın mühendisliğidir. Kısaca şu şekilde özetlenebilir; Yapılarda meydana gelebilecek bir yangın öncesinde oluşabilecek bir zarar ile bu zararın derecesinin önceden tayin edilerek canlı ve cansız tüm yitimlerin korunmasına yönelik gerekli önlemlerin alınması ve meydana gelebilecek bir hasarın önceden tahmin edilerek kabul edilebilir bir seviyede tutulabilmesine yönelik anılan bilimsel metotlardır. Yangın mühendisliği faaliyetleri bir binanın yangın güvenliğiyle ilgili daha inşa aşamasında tüm unsurlarına uygulanabileceği gibi tamamlanmış bir binaya da uygulanabilmektedir. Bina tasarımları çizimler üzerinden incelenirken yapı içerisinde bulunan eşyalar ve bu eşyaların yana bilirlik özellikleri belirlenmeli, yapıda bulunan yaşam ve çalışma mahalleri gibi genel vaziyet planları incelenerek kullanılan yapı malzemelerini risk faktörleri belirlenerek bina tahliyesine stratejisi gözden geçirilmelidir [7].

Yangın mühendisliği pek çok belirsizlikleri ortadan kaldırılabilir. Bina tehlike sınıfına göre dizayn edilecek su sisi sistemlerinin tesisat ölçeklerinden başlanarak taşıyıcı sistemlerin yüksek sıcaklıklardaki davranış biçimine kadar pek çok teknik hesaplamaları gerektirir. Ayrıca oluşturulacak uygulama programları vasıtasıyla sanal ortamda bir yangın durumunda duman ve ısı ve toksik gazların miktarı, yangının büyüklüğü ile flashover ve patlama zamanının tahmini gibi tüm unsurlar analiz edilebilir. Daha mimari aşamada yapılacak hesaplar ile maliyeti yüksek yapılarda öngörülemeyen riskler önceden belirlenerek daha güvenli yapılar inşa edilebilir ve tanıtılabilir.

Günümüzde Uluslararası Yangın Güvenliği Bilim Derneği (IAFSS) başta olmak üzere Uluslararası Yapı Konseyi (CIB) ve pek çok standardizasyon kuruluşları yangın güvenliği mühendisliğine katkıda bulunmaktadır [7].

Kılıç, yangın mühendisliğine farklı bir bakış açısı ile değerlendirerek "Yangın Korunum Mühendisliği" kavramı üzerinde durmuştur. Binaların yangına karşı dayanımı, yangın tespit sistemleri, tahliye çıkışları gibi konular başta olmak üzere yeterli eğitim, bilgi ve deneyime sahip mühendislere ihtiyaç duyulduğunu, yanma sonucu açığa çıkan ısı ve zehirli gazlar, yangınların oluşma sebepleri, gelişim süreçleri, yangın söndürme yöntemleri, dumanını yapı içerisindeki hareketleri ve yangının diğer bölmelere yayılımı konusunda hesaplama yöntemleri ile bina taşıma yükü ve yangınlarda insan davranışlarının tahmin edilebilirliğine yönelik bilgisayar hesaplamaları konularının yangın korunum mühendisliği konuları arasında olduğunu belirtmiştir [8].

Ülkemizde yangın mühendisliği lisans programı bulunmamaktadır. Ferdi yapılan çalışmalar ise yeteri derecede ses getirememiştir. Yangınların meydana getirmiş olduğu telafisi mümkün olmayan kayıp ve yıkımlar yangın güvenliği mühendisliğinin önemini her geçen gün daha da artırmıştır. Önleme, korunma ve söndürme kavramlarından oluşan yangın güvenliği sistemi içerisinde yangın mühendisliği yeterince yer almamıştır.

Yangın mühendisliğinin dahil edildiği yeni yangın güvenlik yönetim modülü ile yangın güvenliği farklı bir boyutta olacaktır. (Şekil 3)

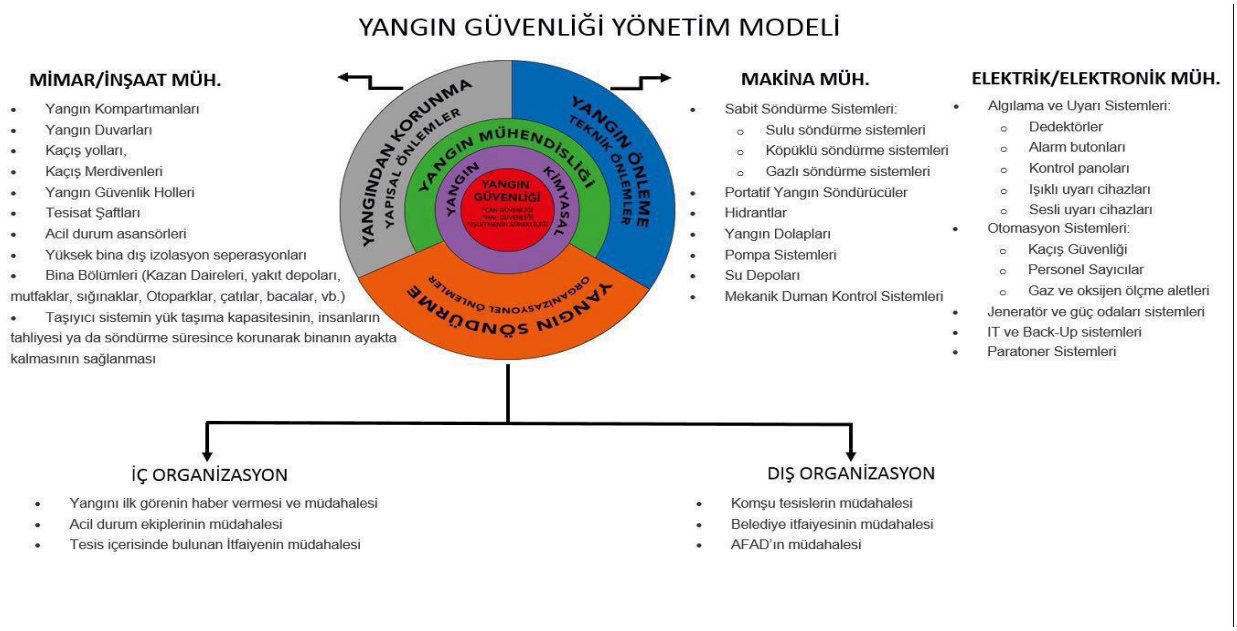

Şekil 3. Yeni Yangın Güvenlik Yönetim Modülü [8]

Yanma kimyası gibi temel faktörlerden başlanarak korunma önleme ve söndürmeye yönelik farklı disiplinlerin bir arada olduğu bu yaklaşım bir PUKO[1] döngüsü niteliğindedir. Yangın Mühendisliğinin ülkemizde yaygınlaştırılabilmesi için lisans seviyesinden başlanarak yüksek lisans ve doktora dereceleri ile akademik bir boyuta bürünmesi daha fazla tanınmasına katkı sağlayacaktır.

Farklı bilim dallarının bir araya getirilmesi ile meydana gelen yangın mühendisliği çoklu bir bilim dalı olma özelliği sergilemektedir. Ülkemizde uygulanan model; koruma, önleme ve söndürme bilimlerinin farklı mühendislik uzmanlık alanları içerisindedir. Şekil 3'deki yeni yangın güvenlik modülünde izah edildiği üzere yapısal önlemler olarak ifade edilen "Yangından Korunma" pasif önlemler niteliğini taşır. Yangın kompartımanları ve duvarları, güvenlik holleri, tesisat şaftları, yangın yükü gibi kritik mimari aşama unsurlarıdır. İnşaat mühendisliği ve mimarların sorumluluk alanındadır. Teknik önlemler ise daha çok önleme amaçlı olup sabit söndürme sistemleri, yangın pompaları, hidrantlar, seyyar söndürücüler ve yangın dolaplarının dizaynına yönelik olup makine mühendislerinin konusudur. Elektrik ve elektronik mühendisleri ise bu alanda yangın algılama ve ihbar sistemleri, otomasyon sistemleri ve jeneratör güç ünitelerinin dizayn ve projelendirme alanlarında faaliyet gösterirler. Burada tamamlanması gereken husus birbirinden ayrı gözükmekte olan bu bilim dallarına yanma ve yangın söndürme gibi kimya mühendisliği kısmının da ilave edildiği bir yapıda buluşturmaktır. Yeni oluşturulacak bu bilim dalı yangın mühendisliğidir.

[1] PUKO:Planla, Uygulama ,Kontrol Etme

Söndürme yaklaşımının en önemli temel taşı olan yangın bilimi yangın mühendisliğinin ana unsurudur. Koruma ve önlemeye yönelik mevzuat boşluklarından kaynaklanan fiili durumlar tasarım mühendisliği, yapısal mühendislik gibi isimler altında telaffuz edilerek giderilmeye çalışılmaktadır. Yanma kimyası ve yangın davranışlarının bilimsel olarak değerlendirildiği ve mühendislik kurallarının bir araya getirilerek oluşturulan bir kombinasyon yangın güvenliği alanında sorumluluk alan kimselerin ihtisaslaşmasını sağlamak için atılan bir adım olacaktır. Yangın mühendisliği ile yangın güvenliği ile ilgili yasal mevzuatların hazırlanması ve revize edilmesi, mahkemelerde süre gelen davalarda yangın bilirkişiliği alanlarında eksiklerin tamamlanması, yangın sonrası meydana gelen olay yeri incelemelerde bilimsel çalışma verileri kullanılarak daha etkin çalışma olanakları sağlanmış olacaktır. Yangın danışmanı, yangın güvenlik uzmanı, yangın müfettişliği gibi mevzuatta yeri olmayan isimlendirmeler yangın mühendisliği çatısı altında birleştirilebilir.

Gökdelenler, devasa enerji tesisleri ve geniş iş alanları burada çalışan insanları yangın riski altında bırakmakta her yıl binlerce insan yangınlarda yaşamını yitirmektedir. Yangın mühendisliği bu kayıpların önüne geçilmesidir. Güvenli bina kavramına son zamanlarda akıllı bina kavramının entegre edilmesi binaları daha emin kılsa da bu durum yangın eğitimlerinin ihmalini gerektirmemelidir. Yapılar ne kadar güvenli olursa olsun eğitimler ve tatbikatlar kati surette uygulanmalıdır. Günümüzde gökdelen yangınlarının sayısının artmış olması yangın güvenliği konusunu tekrar gözler önüne sermektedir. Ülkelerin gelişmişlik seviyeleri ile ters orantılı bir şekilde değişkenlik gösteren yangın istatistiklerinde yer alan son yıllardaki bazı veriler şaşırtıcı olmaktadır. Ekonomik yönden gelişmişlik sergileyen ülkelerdeki yangın sayıların artmış olması kaygı vericidir.

Resim 1. Batı Londra Greenfell Tower Yangını [9]

Londra'daki Grenfell Tower binasında 2017 de meydana gelen yangın seksen kişinin hayatını kaybetmesine yüzlerce insanın evsiz kalmasına sebep oldu yangının çıkış sebeplerine yönelik yapılan çalışmalar, buzdolabının derin dondurucusunda başlayan yangının tüm binayı etkisi altına almasının fazla zaman almadığı, bu kadar kısa bir zaman diliminde etkili olan yangının dış cephe yalıtımlarından kaynaklandığı belirtilmektedir. Alevlerin hızlıca ilerlemesine yakın bir zamanda değişmesine rağmen yapılan ön yangın deneylerinde başarısız olan neden izolasyon kaplamaların sebep olduğu ifade edilmektedir [10].

2. Yangın Mühendisliği ve Mimari Yaklaşım

Korkmaz, Mimarlık Eğitiminde; "Yangın Güvenlikli Tasarımın Yeri" adlı çalışmasında; Türkiye genelinde yapılan yapıların büyük bir oranında yapısal yangın güvenliği önlemlerine yönelik eksikliklerin bulunduğu bunun sebebininde eğitimlerde yaşanan yetersizlikten kaynaklandığını, ülkemizde faaliyet gösteren 90 üniversitede bulunan mimarlık bölümlerinin ders programlarının incelenmesi ve öğretim üyeleri ile yapılan anketlerde mimarlara verilen, yangın güvenliği tasarımı derslerinin yeterli bir düzeyde olmadığı belirtilmiştir. Üniversitelerde çoğu seçmeli olarak verilen bu derslerin bir yarı yıl içerisinde sadece bir veya iki ders ile yapıldığını bu durumun mesleki alanda önemli bir eksikliğe sebep olduğu, temel bilgi seviyesine ulaşmakta yeterli olmayan ders sayılarının bütün üniversitelerin mimarlık bölümlerinde zorunlu bir ders olarak işletilmesi ve konunun uzman öğretim görevlileri ile sağlanmasına dikkat çekilmektedir. Lisansüstü eğitimlere yönelik incelemede ise, yedi üniversitede bu dersin bulunmasının sayı ve içerik açısından mimarlar için yeterli olmadığı, yangın güvenliğine yönelik bütünsel tasarımların güvenli yapıların ortaya çıkmasında önemli rol alacağı ifade edilmektedir. Mimari aşamada tüm disiplinlerin bir arada olduğu ilgili yasal denetimlerin yapılarak oluşacak bir yaklaşımım gerekliliği ifade edilmektedir [11].

Pasif yangın tasarımı olarak adlandırılan yangın mühendisliği yapıların yangına olan dirençliliğinin önceden hesaplanması olarak nitelendirilir. Aktif yangın güvenliği ise yapının proje aşaması tamamlanıp ortaya çıkmasından sonra algılama ve ihbar ve sabit söndürücü sistemler gibi bir takım önlemeye yönelik tasarımlardır. Yapı elemanlarının davranış biçimini değerlendirmeden oluşturulan bu unsurlar bazı riskler taşıyabileceği gibi uzun dönemde bazı hatalar meydana getirebilir. Yapılar da meydana gelen yangınların davranışlarını incelemek için üç temel yöntem bulunmaktadır. Bunlar; yangın dinamiği, ısı transferi ve ısı-mekanik yapı sistemi analizidir [12].

Performansa dayalı yangın mühendisliği yaklaşımı bu dala geniş bir perspektiften bakılmasını sağlayabilir. Selamet, özellikle İngiltere'de sergilenen bu yaklaşım yangından korunma, yangın

kompartımanları, yangın algılama ve ihbar sistemleri, yangın söndürme, acil kaçışlar, duman yayılımı ve yangın kontrol alanlarında her yapı için önleyici bir yaklaşım sergilediğini, halihazırdaki yönetmeliğin binalar için bağımsız yangın strateji raporu oluşturmaya cevaz vermediğini ifade etmektedir [13].

Burada temel alınması lazım olan en önemli nokta ise yanma kimyasını içerisinde barındıran yangın dinamikleridir.

Bu makalede yangın dinamikleri neticesinde oluşan yanma ürünlerinin simülatör ortamında (önceden hesaplanma) yapı elemanlarına olan etkileri ile yangına dayananım, duman yayılımı ve tahliye hesaplamalarına yönelik unsurlar incelenmiştir.

2.1. Yangın Dinamikleri ve Duman Kontrolü

Yapı içerisindeki yanıcı maddelerin yanması ile meydana gelen yangın ve neticesinde kendisini gösteren ısı ve duman oluşumu gibi faktörler ile yanma mahalline gelen oksijen ile ilgilidir. Yangın davranışları pek çok yönden karmaşıklık gösterir ve ısı transferi, akışkanlar dinamiği gibi diğer unsurlara vakıf olunmasını gerektirir. Aslında bu terim yanma kimyası olarak nitelendirilebilir. Yangın ve neticesinde meydana gelen duman en tehlikeli yanma ürünüdür. İçerisinde barındırdığı toksik gazlar hem hayati tehlike hem de görüş mesafesini azaltır. Yangınlarda meydana gelen ölüm oranlarının büyük çoğunluğu duman kaynaklıdır. Kablo yollarının ve borularının iyi yalıtılmaması, tesisat boşluklarından yayılarak tüm yapıyı sarabilir. Yangın mühendisliğini diğer bilimlerden ayıran en önemli özellik bilimsel metot ve analizlerin etraflıca yapıldığı ve etkili simülasyon tekniklerinin kullanıldığı bir yaklaşım olmasıdır. Etkili simülasyon teknikleri ile bilgisayar ortamında hazırlanan simülasyonlar ile tasarım aşamasında bir mimari yapı içerisinde duman kontrolü ve yangına dayanıklılık gibi temel bina strüktürü ile ilgili hesaplamalar basitçe yapılabilmekte ve böylece daha güvenli yapıların ortaya çıkması sağlanabilmektedir.

2.1.1. Yangın Dinamikleri ile Yangın ve Tahliye Modellemesi Simülatörü

Çoklu yakıt kaynakları (poliüretan, ahşap gibi) kullanılarak sanal ortamlarda oluşturulan yangın stokiyometrisinin[2] tüm dinamiklerin aktif olarak kullanıldığı yazılımlar ile gerçekçi durumlar ortaya çıkarılmakta yangın mühendislerine potansiyel bir veri sağlanması oluşturulmaktadır.

[2] Kimyasal bir tepkimeye giren ve çıkan maddeler arasındaki kütlesel (bazen de hacimsel) hesaplamalarla ilgilenir. Kimya biliminin matematik kısmıdır.

(Resim 2.-3.-4.-5.)'de yapı geometrisini yönetmenin mümkün olduğu simülasyon yazılımları, bileşenler ve parametre girişleri yapılarak etkin bir verileme ve öngörü oluşturulmaktadır.

Aşağıdaki resimlerde bilgisayar simülatör ekranından yapının dış görünüşü görüntülenmektedir. Yapısal analizlerin yapılabilmesi için zorlu fiziki tasarımların dayanıklılık testleri grafik uygulamaları ile ara yüz kesitleri oluşturularak profesyonel yazılım imkanları ile gerçekleştirilmektedir. Böylece yangın mühendisleri ve diğer yapı teknisyenlerine güçlü görselleştirme modelleme ve tasarım imkânı sunulma imkanı sağlanmış olacaktır.

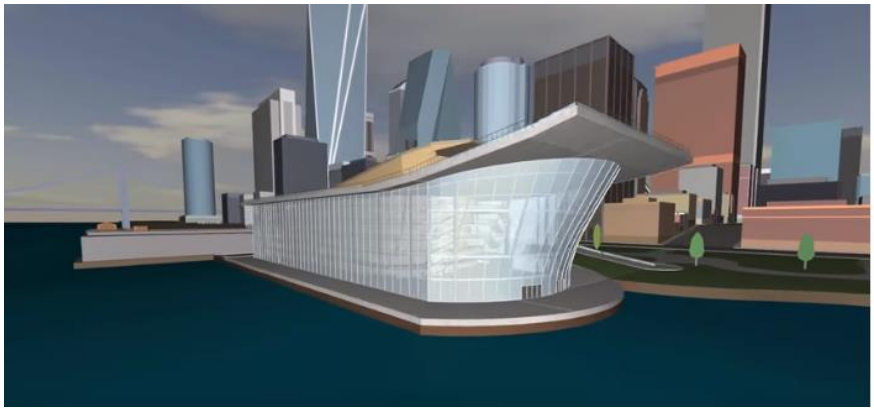

Resim 2. Bir Tiyatro Salonunun Simülatör Ortamında Dış Görüntüsü [14]

Resim 3. Bir Tiyatro Salonunun Üç Boyutlu (3D) Görüntüsü [14]

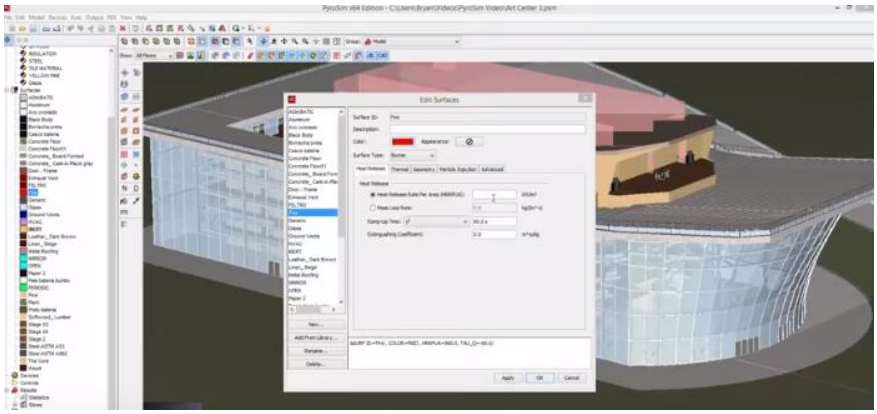

Resim 4. Veri Girişi Yapılarak Parametrelerin Oluşturulması [14]

Basit bir kimyasal reaksiyon ile simülatörde yanma olayı gerçekleştirilir. Yanma neticesinde meydana gelen karbondioksit, karbon monoksit ve diğer zehirli gazlar yanıcı madde kaynaklarının malzeme yapısına istinaden ortamdaki etkisi ve dumanın ne kadar bir alanda etkili olacağı hesaplanabilmektedir.

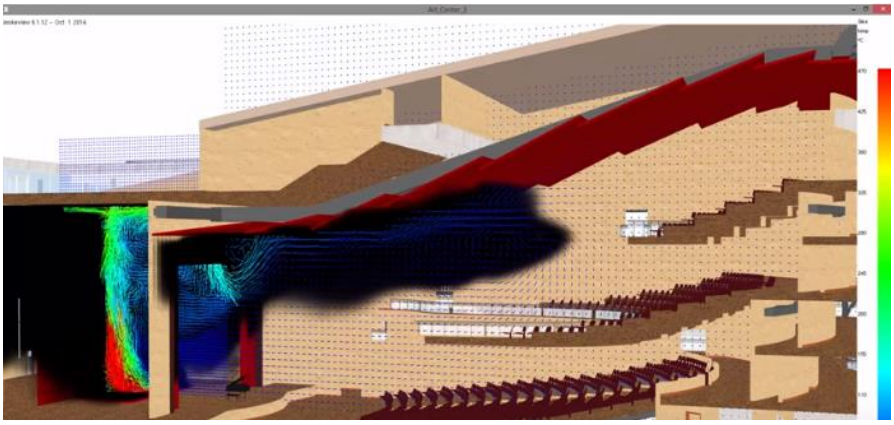

Resim 5. Yangın Neticesinde Duman İlerlemesi [14]

Dumanın hangi bölgelere ne kadar hızla ilerleyebileceği hesaplanabilir. Hesaplayıcı için gerekli olan tek şey bir diz üstü bilgisayardır. Gerekli donanımsal ve yazılım gereksinimler kullanıcı bilgisayarına yüklenir ve böylece yapıdaki büyük resim gözlenmiş olur.

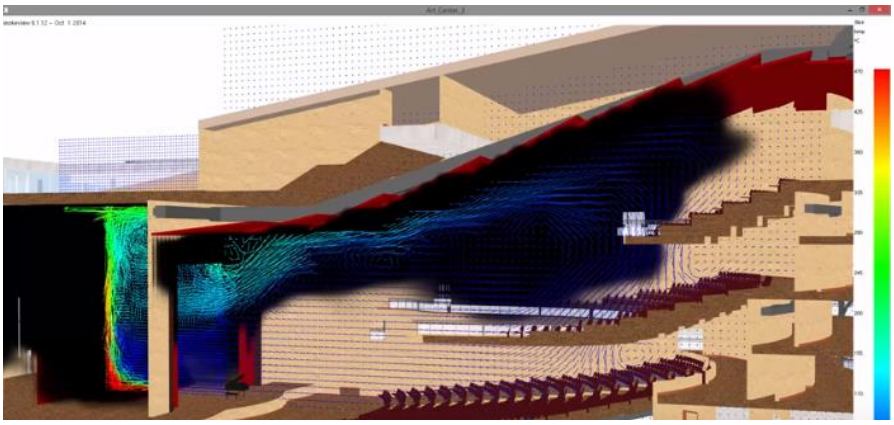

Resim 6. Duman ilerlemesinin Üç Boyutlu (3D) Görüntülenmesi [14]

Yapı içerisindeki malzemelerin özellikleri, yüzeyler, yangın ilerlemesi, sabit söndürme sistemleri kullanılarak yangının ne derece bastırılabileceği, performansa dayalı tasarım özellikleri gelişmiş atölye çalışmaları kullanılarak yangın mühendisinin karşılaşabileceği problemleri çözmek için etkin raporlama ve veri imkânı sağlanmış olunur.

(Resim 7)' de Deneysel yangın alanındaki kamera görüntüsü (Resim 8.)' de ise 3 boyutlu görünümünde duman ilerlemesi rahatlıkla görülebilmektedir.

Resim 7. Deneysel Yangın Deneyi Işık Ve Duman Yayılımı [15]

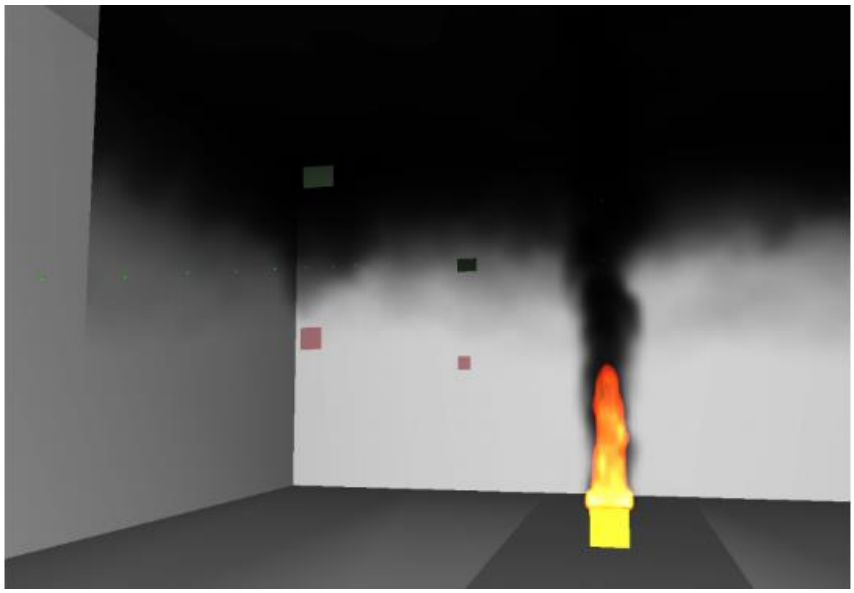

Resim 8. Yangın Deneyinin Üç Boyutlu (3D) Görüntülenmesi [15]

Modelleme ve simülasyon kapalı alanlarda duman ve yangından tahliye unsurlarının yanı sıra açık alanlardaki stadyum gibi yapılarda uygulanabildiği gibi gemi, feribot ve hava araçlarında da uygulanabilir. (Resim 6., 7., 8.)

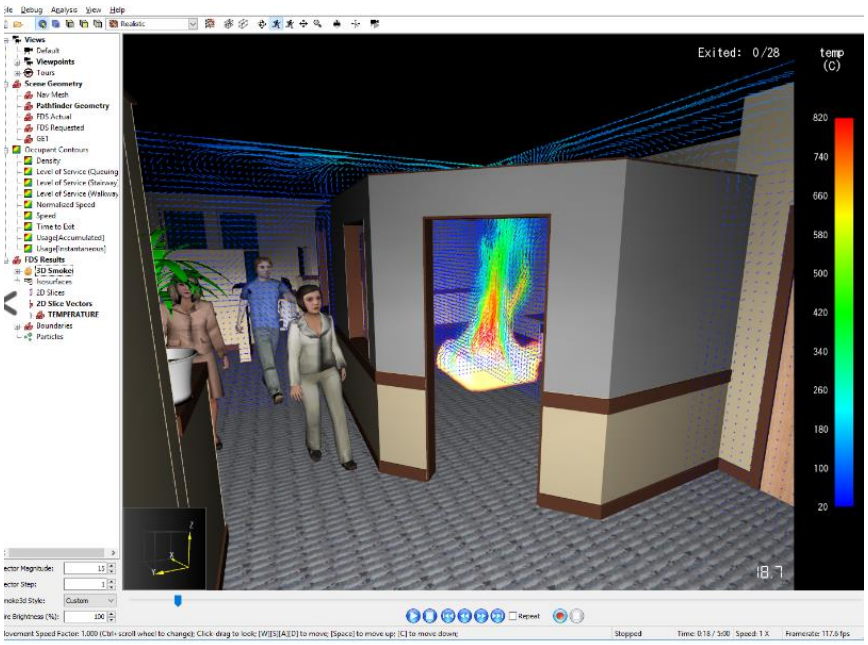

Resim 9. Kapalı Alan Yangın Ve Duman Parametreleri Girişleri Ve Isı Artışı [16]

Resim 10. Stadyumda Başlayan Bir Yangın Simülasyonu [16]

Simülasyon programları ile duman, sıcaklık, hız, toksisite ve diğer analizlerin çıktılarının görüntülenmesi sağlanır. (Resim 11.)

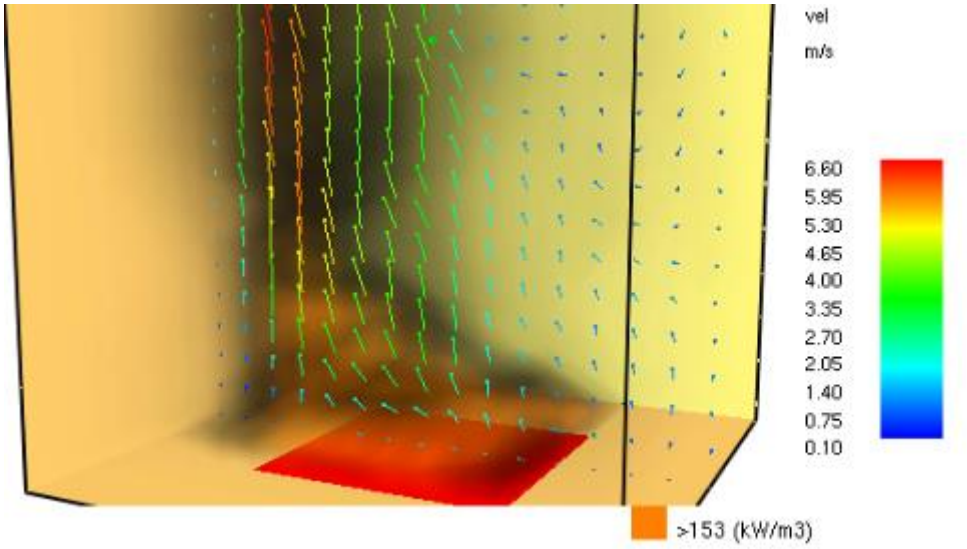

Resim 11. Duman, Isı ve Toksitite Görüntülenmesi [17]

Tasarım aşamasındaki feribot geliştirme çalışmalarında da kullanılan 3D sistem çeşitli araç ölçekleri ve belli sayıdaki yolcu kapasiteleri ile oluşabilecek yangın türlerine göre oluşturulan senaryolar ile duman yayılımı hareketleri modellenebilmektedir. Bu kadar büyük ölçekli bir gemide kuşkusuz tahliye faktörlerinin ve acil çıkış unsurlarının da diyagramlara dökülerek çalışılması ve öngörülmesi önem teşkil etmektedir. (Resim 12. ve Resim 13.)

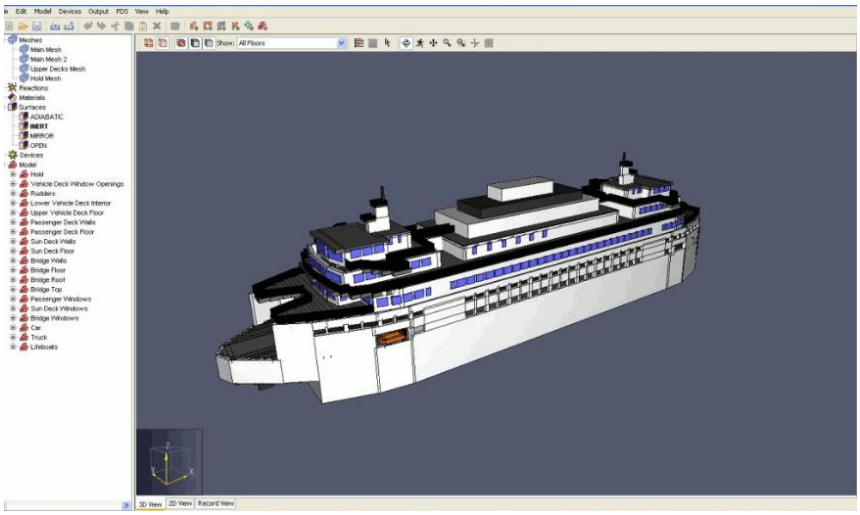

Resim 12. Feribot Dizaynında Yangın Duman Modellemesi [18]

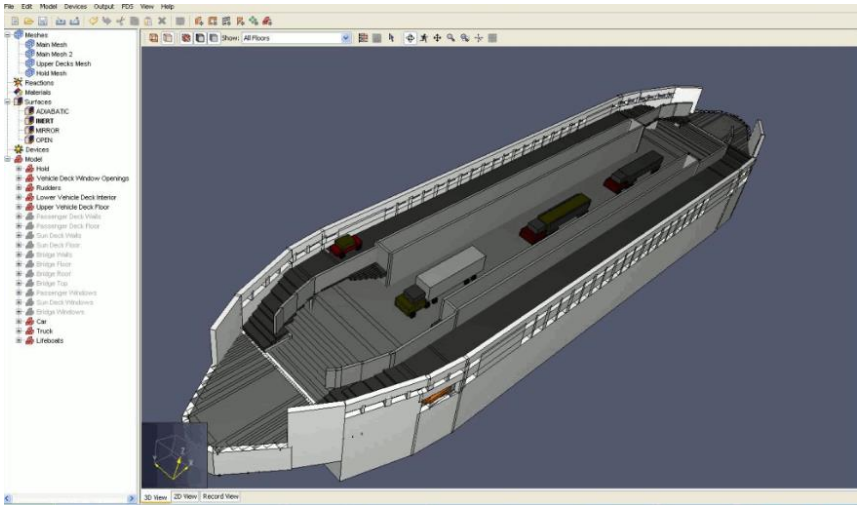

Resim 13. Feribot Dizaynı ve İç Modelleme [19]

Yeni yangın güvenlik modülü ile komplike olan yangın mühendisliği özgün simülasyon çalışmaları ile daha güvenli yapılar ve vasıtaların inşa edilmesini sağlayacaktır.

Tüm bu çalışmalar nezdinde ortaya çıkan güvenli yapılar içerisinde yangın eğitimleri aksatılmadan icra edilmeli, verilen nazari eğitimler film vb. görseller ile desteklenmeli ve eğitimler simülasyon ortamında uygulamalı olarak yapılabilmelidir [20].

3. SONUÇ

Yanma seyri çeşitli dinamikleri içerisinde barındırmaktadır. Her yangın kendine özgü bir seyirde yol alırken çevresinde bulunan fiziki ve kimyasal unsurlardan etkilenmektedir. Yangın eğitim ve tatbikatları gerçek bir yangın durumunda sayılan bu unsurlar nedeniyle yangınla mücadelede zorluklar yaşanmasına sebep olmaktadır. Mimari aşamada yapılan eksiklikler telafisi zor kayıplara sebep olabilmektedir. Yapı ve yanma davranışına yönelik önceden

yapılacak hesaplar tahliyenin etkili olmasını sağlayacaktır. Yangın mühendisliği lisans eğitimi dünyanın pek çok ülkesinde farklı isimler altında verilmektedir. Ülkemizde yangın mühendisliğine yönelik tartışmalar son zamanlarda daha sık dile getirilmeye başlanmıştır. Hem akademik alanda hem de çeşitli sempozyum ve etkinliklerde konu üzerinde çalışmalar hızlanmıştır. Bazı üniversitelerce lisans eğitimine yönelik yapılan başvurulardan sonuç alınamamıştır. Bu makalede izah olunan yeni yangın güvenlik modülü yangın mühendisliği tartışmalarına yeni bir çehre kazandırmayı amaçlamaktadır. Puko döngüsüne benzer nitelikte olan modül içerisinde yanma kimyası, koruma, önleme ve söndürme yaklaşımları bir bütüncül yaklaşım olarak sergilenmektedir. Söndürme bilimine bu yaklaşımda daha ön plana çıkmaktadır. Yangın mühendisliğini diğer bilimlerden ayıran en önemli özellik bilimsel metot ve analizlerin etraflıca yapıldığı ve etkili simülasyon tekniklerinin kullanıldığı bir yaklaşım olmasıdır. Etkili simülasyon teknikleri ile bilgisayar ortamında hazırlanan simülasyonlar ile tasarım aşamasında bir mimari yapı içerisinde duman kontrolü ve yangına dayanıklılık gibi temel bina strüktürü ile ilgili hesaplamalar basitçe yapılabilmekte ve böylece daha güvenli yapıların ortaya çıkması sağlanabilecektir. Yeni yangın güvenlik modülü ile yangın mühendisliği ve simülatör teknolojisinin entegre edileceği lisans programlarının açılması sanayisi gün geçtikçe büyüyen ülkemiz için olumlu bir gelişme olacaktır.

KAYNAKÇA

[1] https://www.guncelpsikoloji.net/kisilik-kuramlari/maslowun-ihtiyaclar-hiyerarsisi-5-temel-ihtiyac-h5577.html

[2] Soyhan, S.H., Yangın Güvenliği Ders Notları.

[3] http://www.fireengineering.com/articles/print/volume-170/issue-2/features/fire-engineering-s-140th-anniversary.html

[4] http://www.hurriyet.com.tr/roma-yi-gercekten-neron-mu-yakti-249622

[5] http://ahmetsertkan.blogspot.com.tr/2008/07/iiimurat-ferman.html

[6] https://pbs.twimg.com/media/DHx_D_kXkAAZs_d.jpg

[7] TS 13387-1 Yangın Güvenliği Mühendisliği–Bölüm 1: Yangına Karşı Performans Kavramlarının Tasarım Amaçlarına Yönelik Olarak Uygulanması.

[8] Sakarya Üniversitesi Uluslararası Yakıtlar, Yanma ve Yangın Dergisi

[9] https://www.thesun.co.uk/news/3799230/london-fire-man-waving-jumper-window-grenfell-tower-saved/

[10] https://www.staylegal.net/10-worst-skyscraper-fires/

[11] Korkmaz, E. (2016) "Mimarlık Eğitiminde Yangın Güvenlikli Tasarımın Yeri " Megaron Dergisi, Cilt 11, Sayı 2, s. 219-229.

[12] Kılıç, A**.** Yangın Korunum Mühendisliği ve Risk Değerlendirmesi, Yangın ve Güvenlik, sayı. 89, Sf. 8-9.

[13] Selamet, S. "Türkiye'de Yangın Mühendisliği" Tema Dergisi, sayı 41, s.5

[14] https://www.thunderheadeng.com/pyrosim/

[15] https://www.thunderheadeng.com/2017/06/smoke-visibility-and-obscuration-in-pyrosim/

[16] https://www.thunderheadeng.com/2017/11/results-viewer-pyrosim/

[17] https://www.thunderheadeng.com/pyrosim/pyrosim-features/

[18] https://www.thunderheadeng.com/wp-content/gallery/pyrosim gallery/pyrosim_ferry1.png

[19]https://www.thunderheadeng.com/wp-content/gallery/pyrosim-gallery/pyrosim_ferry2.png

[20] Turhan,S.,(2018). *Yangın Güvenlik Eğitimlerinin Yasal Mevzuat ve Eğitim Müfredatları Açısından Değerlendirilmesi,* İstanbul Aydın Üniversitesi,Fen Bilimleri Enstitütüsü, (Yüksek Lisans Tezi) İstanbul, sy 7

Paper 20 **Bildiri 20**

ÜÇ BOYUTLU MODELLEME İLE BENZİNLİ BİR MOTORDA FARKLI YANMA ODALARININ İNCELENMESİ

Öncel Öncüoğlu [*1] , Alper Tolga Çalık [2], Özgür Oğuz Taşkıran [3], Osman Akın Kutlar [4], Hikmet Arslan [5]

ÖZET

Bu çalışma 3 farklı yanma odası üzerinde yapılmıştır. 1. yanma odası düz pistonlu, 2. yanma odası silindirik oyuklu pistonlu, 3. yanma odası ise W tipi oyuklu ve döngü kanallı yanma odasıdır. İlk olarak deneysel verileri mevcut olan 9,1 sıkıştırma oranlı 2. tip yanma odasının verileri ile doğrulama çalışmaları yapılmış ve model parametrelerinin değerleri belirlenmiştir. Daha sonra deneyleri gerçekleşecek 10,5 sıkıştırma oranlı pistonlar için modeller oluşturulmuştur. Bu modeller ile yapılacak deneysel çalışmalar için fikir oluşturulması amaçlanmıştır.

Isı açığa çıkışı üst ölü noktadan sonra oyuklu geometrilerde daha erken olmakta, düz pistonlu yanma odasında ise ısı açığa çıkışı biraz daha gecikmektedir. Üçüncü pistonda kanal konularak amaçlanan döngü hareketi net olarak görülememiştir. Bu nedenle 3. yanma odası için oluşan sonuçlar 2. yanma odası ile benzerlik göstermiştir. Arrhenius çarpışma frekans katsayısının üç pistonda da farklı olmasından dolayı ısı açığa çıkş hızlarında farklılıklar görülmüştür.

Anahtar Kelimeler: CFD, Yanma odası, Sıkıştırma Oranı

[*] Sorumlu Yazar (ooncuoglu@itu.edu.tr)
[1] İstanbul Teknik Üniversitesi, Makina Fakültesi, İstanbul
[2] İstanbul Teknik Üniversitesi, Makina Fakültesi, İstanbul
[3] Deniz Kuvvetleri Komutanlığı, İstanbul
[4] İstanbul Teknik Üniversitesi, Makina Fakültesi, İstanbul
[5] İstanbul Teknik Üniversitesi, Makina Fakültesi, İstanbul

1. GİRİŞ

Bu çalışmada benzinli bir motorun piston kafasında yapılan değişiklikle oluşturulan üç farklı yanma odasına sahip modelinin, deneysel olarak da gerçekleştirilecek çalışmalar için bir fikir oluşturulması amacıyla üç boyutlu olarak hesaplamalı akışkanlar dinamiği analizi yapılacaktır. Motor modeli, ICEM CFD programıyla ağ yapısı oluşturulduktan sonra KIVA3V yazılımıyla çözülmüştür. Yanma odasındaki değişikliklerin motorun yanma, hava hareketleri ve ısıl değerleri üzerinde yarattığı değişiklikler incelenmiştir.

Farklı yanma odaları kullanılarak özellikle oluşacak hava hareketlerinin, yüzey alanları farklılıklarının, motor yanma parametreleri, performans, egzoz emisyonu, yakıt tüketimi, ısıl dağılım üzerine etkileri incelenmek istenmiştir. Özellikle kanallı W yanma odalı 3. tip piston [3] piyasada var olmayan yeni tasarlanmış bir piston türü olduğundan çıkacak sonuçların deneysel olarak da gerçekleştirilecek çalışmalar için fikir vermesi amaçlanmıştır.

2. YÖNTEM

KIVA yazılımı akış dinamiğini, tüm CFD çözümlerindeki gibi; Kütlenin korunumu (süreklilik denklemi), Newton'un ikinci kanunu (momentum denklemi), Termodinamiğin birinci kanununu (enerji denklemi) temel almaktadır [1]. Gaz fazı ve sıvı fazı denklemlerinin bir arada çözülmesi için Arbitrary Lagrangian Eulerian metodu kullanılmaktadır.

Yanma tarafında ise standart KIVA3Vr2 yazılımında bulunan reaksiyonlar kullanılmıştır. benzin yakıtının yanması sırasında toplam on iki bileşenden oluşan dört adet kinetik reaksiyon ve altı adet denge reaksiyonu hesaplanmaktadır. Yakıtın (C8H17) yanması için sadeleştirilmiş tek adımlı oksidasyon reaksiyonu kullanılmaktadır. NOx oluşumu için genişletilmiş Zeldovich mekanizması kullanılmaktadır. Reaksiyon hız sabiti ile sıcaklık arasındaki ilişki için Arrhenius eşitliği kullanılmaktadır.

Çizelge 1. Deney Motoru özellikleri.

Yakıt	Benzin
Zaman	4
Silindir sayısı	1
Silindir Çapı	85 mm
Strok boyu	80 mm
Sıkıştırma oranı	9,1
Emme supabı açılma zamanı	16° ÜÖN' den önce
Emme supabı kapanma zamanı	40° AÖN' den sonra
Egzoz supabı açılma zamanı	40° AÖN' den önce
Egzoz supabı kapanma zamanı	16° ÜÖN' den sonra
Biyel kolu uzunluğu	145 mm

3 boyutlu sayısal model için ağ yapıları ANSYS ICEM CFD programında oluşturulmuş ve Şekil 1'de verilmiştir. İlk olarak Çizelge 1'de özellikleri verilen 9,1 sıkıştırma oranına sahip ikinci pistona sahip benzinli motor [4] modellenip, deney-simülasyon doğrulaması yapılmış ve sonucu şekil 2 'de verilmiştir. Doğrulama çalışmaları ve devamında deneyleri yapılacak olan 10,5 sıkıştırma oranında farklı yanma odalarına sahip modeller için simülasyon matrisi çizelge 2' de verilmiştir. Yapılan kalibrasyon çalışmaları sonucunda AÖN civarında 200000 civarındakı hücre sayısının, 2 mm' nin altındaki hücre büyüklüklerinin çözüm doğruluğu ve zaman açısından uygunluğu görülerek ağ yapısının temel özellikleri belirlenmiş ve modeller oluşturulmuştur.

Çizelge 2. Simülasyon matrisi.

SİMÜLASYONLAR	**KOŞU DEVİRLERİ**		**1. DÜZ**	**2. HERON**	**3. W TİPİ KANALLI**
Kalibrasyon *(9,1 sıkıştırma oranı)*	1200 d/dk 1500 d/dk 1800 d/dk	Deney	-	+	-
		KIVA3V	+	+	+
Yeni Sıkıştırma oranlı YO *(10,5 sık. oranı)*	1200 d/dk 1500 d/dk 1800 d/dk	Deney	-	-	-
		KIVA3V	+	+	+

10,5 sıkıştırma oranı için pistonlar;

1. Düz piston, (Hücre sayısı: 198575)
2. Heron tipi silindirik oyuklu piston, (Hücre sayısı: 191976)
(Bu pistonun 9,1 sıkıştırma oranındaki motorda deneyleri ile doğrulama yapılmıştır.)
3. Kanallı W tipi piston, (Hücre sayısı: 220578)

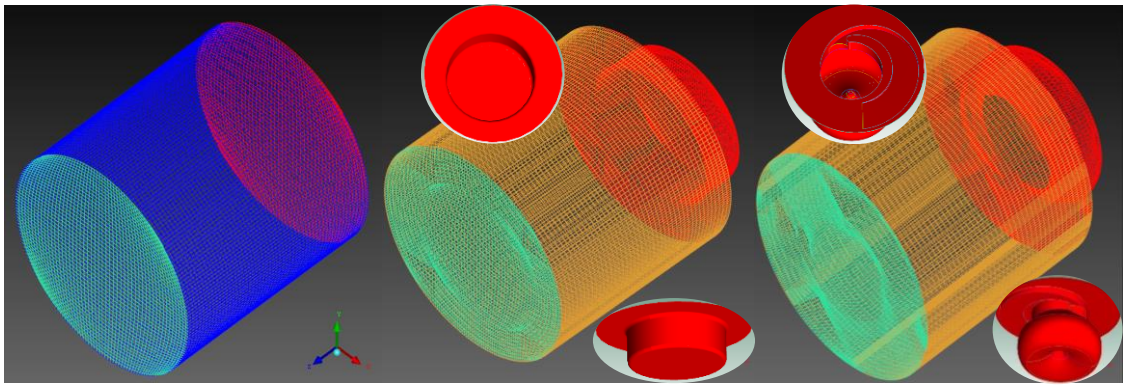

Şekil 1. Modellenen 1., 2. ve 3. pistonun ağ yapıları.

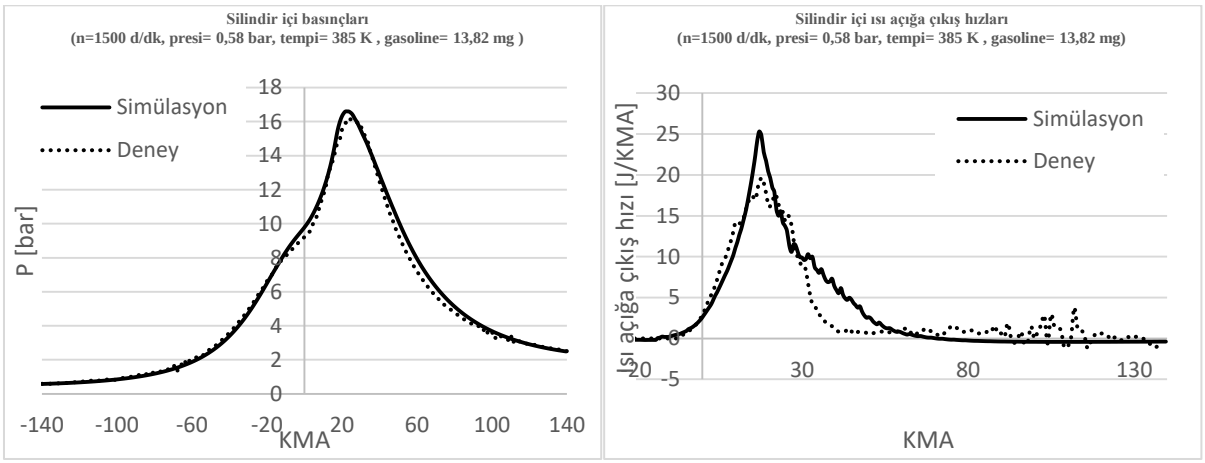

Şekil 2. 9,1 sıkıştırma oranlı 2.tip pistonun 1500 d/dk'daki deney ve simülasyon basınç değişimi ve ısı açığa çıkış hızı karşılaştırmaları.

3. BULGULAR

Doğrulama simulasyonları sonucu elde edilen veriler ışığında 10,5 sıkıştırma oranına sahip üç parklı pistonun analizi yapılmıştır. Giriş ve çalışma koşulları değiştirilmeden motor sıkıştırma oranı ayarlanarak koşular gerçekleşmiştir. 1500 d/dk için sonuçlar verilmiştir.

Yanma sırasında, deneysel veri ile doğrulanıp daha sonra sıkıştırma oranı arttırılmış 2. Yanma odası baz alınırsa, 1. Yanma odasında basıncın daha hızlı arttığı görülmektedir. Ayrıca ısı açığa çıkış hızları incelendiğinde 1. yanma odasında ısının diğer yanma odalarına göre daha hızlı olduğu görülmektedir (Şekil 2). Üst ölü noktadan sonra ısı oyuklu geometrilerde daha erken açığa çıkmakta düz pistonlu yanma odasında ise ısının yoğun olarak çıkmaya başladığı zaman biraz daha gecikmektedir. Fakat düz pistonda çarpışma frekans katsayısının en yüksek olmasından dolayı yanmanın ana evresinde ısı açığa çıkış hızı çok daha büyük olmakta, bu da basıncın daha hızlı artmasına neden olmaktadır.

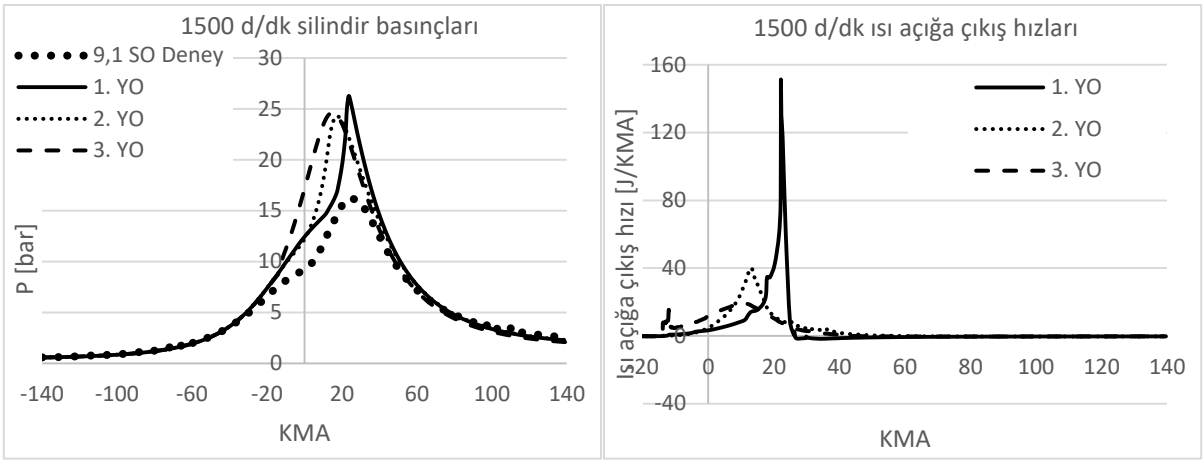

Şekil 3. 10,5 SO' lu YO'ların 1500 d/dk'daki basınç değişimi ve ısı açığa çıkış hızları.

4. SONUÇ VE ÖNERİLER

Yaklaşık 0,8-1,8 mm hücre boyutundaki 3 farklı yanma odasının simülasyonlarında kalibrasyon sonucu elde edilen değerler kullanıldığında 1. ve 3. yanma odalarında, yani daha önce deneysel verileri bulunmayan yanma odalarında, 2. yanma odasına nazaran daha farklı sonuçların çıktığı görülmüştür. Aynı reaksiyon hızı katsayıları tanımlandığında 1. yanma odasının simülasyonlarında yakıtın neredeyse yanmadığı ve çok yavaş yandığı, 3. yanma odasında ise yakıtın çok erken tutuştuğu ve anı basınç artışına sebep olduğu görülmüştür. Bunun için çarpişma frekans katsayısı ayarlanmıştır.

3. yanma odası için oluşan sonuçlar hakkında kesin bir şey söylemek pek mümkün gözükmemektedir. 3. yanma odasının, tutuşmanın erken olmasına sebep olup olmadığı, yapılacak deneylerden sonra kesin olarak belirlenebilecektir. Bunun nedeninin piston başındaki kanal nedeni ile türbülans enerjisinin daha fazla ve ağ yapısı kalitesinin diğer yanma odalarına oranla daha düşük olması gibi faktörler sayılabilir.

Bu modeller için KIVA3V yazılımının çözüm sonucunun hücre sayısına ve ağ yapısına yüksek derecede bağımlılığı teyit edilmiştir. Hücre boyutları 2 mm'den büyük olmamalıdır.
Çarpışma frekansı katsayısının ağ yapısına ve hücre sıklığına bağımlıdır ve her modelde denenerek değeri ayarlanmalıdır [2].

Asimetrik ve detaylı geometriye sahip pistonlar için daha farklı ağ yapılarında KIVA simülasyonları yapılmalı veya ağ yapısına bağımlılık azaltılmalıdır. Simülasyon sonuçları deneyler ile desteklenmelidir.

KAYNAKÇA

[1] Amsden, A.A., O'Rourke, P.J., Butler, T.D. (1989). *KIVA-2: A Computer Program for Chemically Reactive Flows witj Sprays*, LA-11560-MS, Los Alamos National Laboratory.

[2] Amsden, A.A. (1993). *KIVA-3: A KIVA Program with Block-Structured Mesh for Complex Geometries*, LA-12503-MS, Los Alamos National Laboratory.

[3] Mehdiyev R., Ogun K., Ozcan E., Arslan H., Babaoglu O., Teker H. (2011). The Twin Swirl "MR-Process" Combustion Mechanism and Conversion of Diesel Engines to Operate with Gaseous Fuels, SAE Technical paper, doi:10.4271/2011-24-0066.

[4] Kutlar, O. A., Arslan, H., & Calik, A. T. (2007). Skip cycle system for spark ignition engines: An experimental investigation of a new type working strategy. *Energy ConversionandManagement*, *48*(2),370–379. doi.org/10.1016/j.enconman.2006.07.004

Paper 21 **Bildiri 21**

KINETIC MODELING OF FUEL-RICH N-HEPTANE COMBUSTION

Emre Değirmenci, Abdalwahab Alazreg, Fikret İnal

Department of Chemical Engineering, Izmir Institute of Technology, Gulbahce-Urla, Izmir,Turkey

fikretinal@iyte.edu.tr

Abstract

The emissions resulted from the incomplete combustion of fossil fuels become one of the main issues especially in transportation sector. The aim of this study is to model onedimensional premixed, laminar, burner-stabilized, fuel-rich n-heptane flame by detailed chemical kinetic modeling technique to understand the combustion characteristics of n-heptane. A detailed chemical kinetic mechanism (DCKM) with 4185 reactions and 893 species was developed. The mechanism was validated by the experimental data of species mole fractions from jet stirred reactors and ignition delay times from shock-tubes. A detailed analysis of fuel-rich, premixed nheptane flame was carried out for species up to benzene. The model was able to predict most of the species mole-fractions in the flame with low amount of error compared to the experimental data. Pathway analysis for benzene was indicated that most of the benzene was formed from bimolecular reaction of propargyl radicals (C_3H_3) and vinyl (C_2H_3) addition to vinyl acetylene (C4H4) in the fuel-rich n-heptane flame.

Keywords: N-Heptane, Kinetic Modeling, Premixed Flame

1. INTRODUCTION

Most of the worldwide energy is generated from fossil fuel combustion. Especially in transportation sector fossil fuels are very dominant energy sources. According to projections for the next 30 years, gasoline will also be the leading fuel for transportation [1]. Gasoline contains hundreds of chemical species, mostly 4 to 12 carbons per molecule. To explain the complex combustion behavior of gasoline, n-heptane is widely used as a reference fuel.

The major emissions for internal combustion engines can be listed as CO, CO_2, unburned hydrocarbons, partially burned hydrocarbons, polycyclic aromatic hydrocarbons and soot. The products of the combustion depend on several factors such as fuel type and operating conditions. However, the chemistry behind the oxidation is the main factor that determines the products, sideproducts, and temperature-pressure behavior of the combustion. To investigate

combustion in wide range of operating conditions kinetic modeling is a must. After the development of accurate databases for thermodynamic, kinetic and transport properties of species it is possible to combine the molecular information into detailed chemical kinetic mechanisms. As a reference fuel for gasoline, n-heptane and its mixtures were studied in wide range of conditions in the literature. The stoichiometric combustion of n-heptane was studied by semi-detailed chemical mechanisms [2-4]. Detailed chemical kinetic mechanisms were also developed to understand n-heptane combustion in wider range of operating conditions [5-7]. There are also experimental studies for n-heptane combustion such as fuel rich n-heptane combustion in atmospheric [8, 9] and low pressure [10, 11] one-dimensional premixed flames, atmospheric counter-flow diffusion flames [12], jet stirred reactors [7, 13] and shock tubes [14].

In this study, the main objective is to model fuel-rich, atmospheric pressure n-heptane flame by using DCKM technique. Chemkin-Pro® [15] software was used to model the system. The main reason for selecting one-dimensional fuel-rich flame was to focus on the chemical kinetics of nheptane combustion. In such a system, species mole fractions and the temperature profile depend only on the vertical axis above the burner, the height above the burner surface (HAB).

2. METHOD

To investigate the fuel-rich n-heptane combustion, detailed chemical kinetic modeling (DCKM) approach was utilized. The mechanism development stage was initiated with the selection of the base mechanism for n-heptane decomposition. Among the considered possible base mechanisms for n-heptane combustion Lawrence Livermore National Laboratory (LLNL) n-heptane mechanism (version 3.1) [6] was chosen as the base mechanism for the mechanism development because it was the most promising mechanism at prior modeling studies for n-heptane flames [16]. The LLNL n-heptane mechanism was also validated for wide range of conditions and used as the base mechanism by various modeling studies [12, 13, 17, 18]. Decomposition reactions of nheptane explained by formation of C_1-C_2-C_3-C_4-C_5-C_6 and C_7 alkyls with almost all possible isomers in the base mechanism. After the determination of the base mechanism, donor mechanisms that include the formation of specific fuel-rich flame products such as benzene and polycyclic aromatic hydrocarbons were determined. Aromatic ring and some PAH species formation pathways with hydrogen abstraction acetylene addition (HACA) growth were involved in the Donor Mechanism 1 [19]. Additional linear PAH (anthracene), angular PAH (phenanthrene) formation and branched aromatic (indene, cyclo-penta[cd]pyrene etc.) formation pathways were involved by Donor Mechanism 2 [20]. Detailed formation and oxidation pathways of high molecular weight PAH species (anthracene,

aceanthrylene, cyclopenta [cd] pyrene, chrysene, etc.) were involved in the Donor Mechanism 3 [21]. Additional PAH and intermediate formation reactions were also added from the recent study [12]. Since the Donor and Base mechanisms used different notations to refer species, at combining base and donor mechanisms molecular structures of the species were considered. After merging these mechanisms, the resulting mechanism was called as Master Mechanism. The general information about base, Donor and Master Mechanisms are given in Table 1. This paper focuses on the formation pathways of first aromatic ring benzene in a fuel rich n-heptane flame.

Table 1. General information about base and donor mechanisms

	Number of Reactions	Number of Species	Reference
Base Mechanism	2827	627	[6]
Donor Mechanism 1	553	99	[19]
Donor Mechanism 2	672	154	[20]
Donor Mechanism 3	1110	256	[21]
Additional Reactions	74	5	[12]
Master Mechanism	4185	893	This study

As seen from Table 1, the number of reactions and species in the Master Mechanism were 4185 and 893, respectively. The number of reactions in the master mechanism is less than the total number of base and donor mechanisms since the duplicate reactions were ignored. Additionally, some reaction rate parameters were revised according to recent literature survey with the alternative rate constant parameters. The Master Mechanism was validated using the experimental data from the literature. Jet stirred reactor species mole fraction data [7, 13] and shock-tube ignition delay time data [7] were used for mechanism validation. To refer jet stirred experimental data JSR1 [13] and JSR2 [7] notations were used in Table 2 and Figures 1 and 2. The experimental conditions of jet stirred reactors used for mechanism validation are given in Table 2.

Table 2. Jet stirred reactor conditions that used for mechanism validation.

Conditions	**JSR1**	**JSR2**
Reactor Volume (cm^3)	86.5	95
Temperature (K)	550 to 1100	500 to 1100
Pressure (torr)	800	800
Residence time (s)	2	2
Equivalence Ratio (Φ)	3	2
Inlet He fraction (mol %)	0.977	0.968
Inlet O2 fraction (mol %)	0.018	0.027
Inlet n-C7H16 fraction (mol %)	0.005	0.005

Two fuel-rich jet stirred experimental data [7, 13] (Φ=2 and Φ=3) were used for the mechanism validation. The model predictions of master mechanism and experimental measurements for nheptane and benzene mole fractions are shown in Figure 1 and Figure 2, respectively.

The master mechanism slightly underestimated n-heptane mole fractions from 550 K to 700 K for both equivalence ratios but for the negative temperature coefficient region (~700 K to ~850 K) and higher temperatures, the difference between the experimental data and model predictions were smaller for n-heptane (Figure 1).

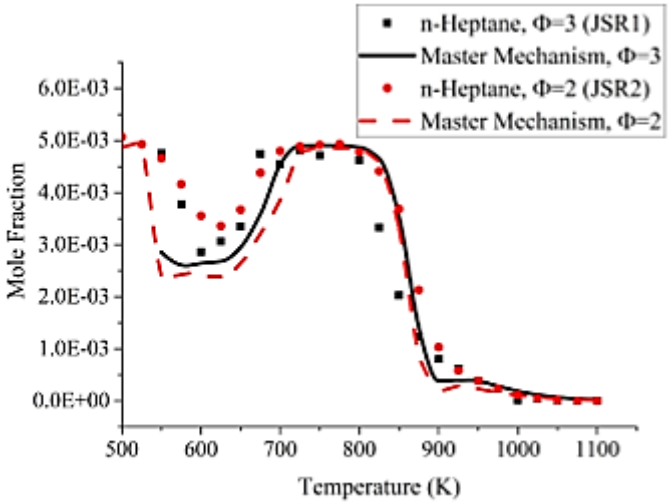

Figure 1. Validation of master mechanism by n-heptane mole fractions in jet stirred reactors

Model predictions for benzene mole fractions were consistent with the experimental data at equivalence ratio of 2. However, the master mechanism could not predict the low temperature (550 K to 850 K) formation of benzene at equivalence ratio of 3 (Figure 2).

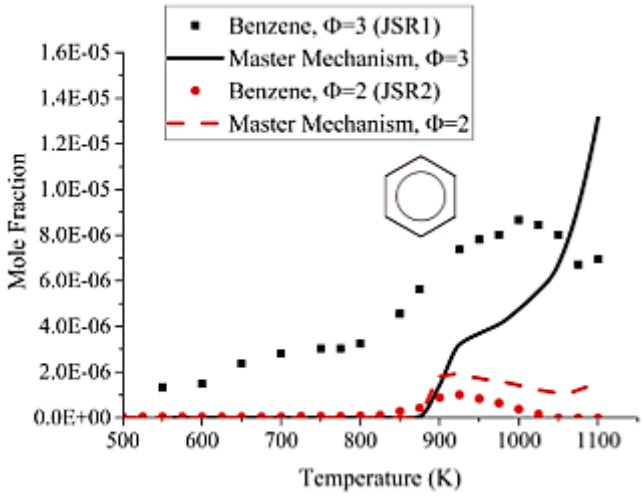

Figure 2. Validation of master mechanism by benzene mole fractions in jet stirred reactors

High pressure (20 bar), stoichiometric shock-tube data were also used to validate the mechanism in terms of ignition delay time predictions. Inlet stream properties of the shock-tube reactor experimental data [7] is shown in Table 3. The master mechanism predicted the ignition delay times with very close to the experimental data [7] at 20 bar pressure on a wide temperature range but there was an underestimation around a factor of 1.5 at the highest temperature (Figure 3).

Table 3. Inlet conditions of shock-tube experimental data.

Conditions	Shock-tube
Temperature (K)	726 to 1412
Pressure (bar)	20
Equivalence Ratio (Φ)	1
Reactant N2 fraction (mole %)	0.775
Reactant O2 fraction (mole %)	0.206
Reactant n-C7H16 fraction (mole %)	0.019

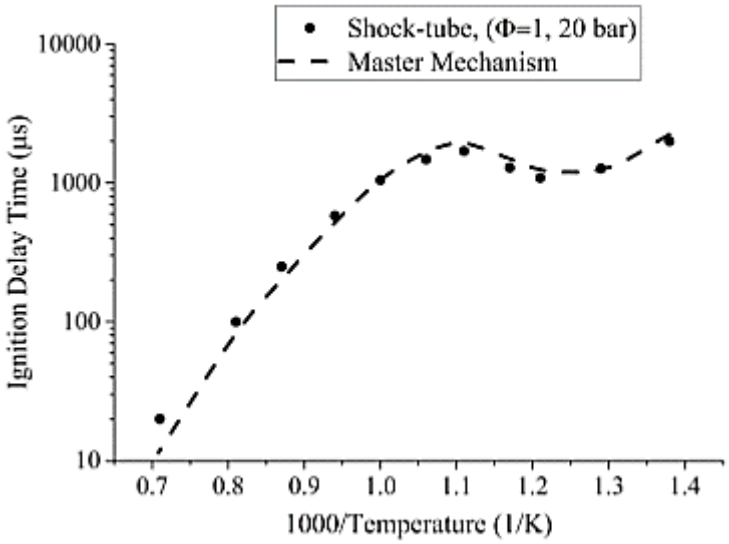

Figure 3. Validation of master mechanism in terms of ignition delay time

After the model validation, Master Mechanism was used to analyze the fuel rich n-heptane flame with an equivalence ratio of 2.1 [9]. The inlet stream properties for the flame are shown in Table 4.

Table 4. Inlet stream properties of the flame

Properties	Premixed Flame
Initial Velocity (cm/s)	5.17
Equivalence Ratio (ϕ)	2.10
n-Heptane (Mole %)	5.50
O_2 (Mole %)	28.79
Ar (Mole %)	65.71

A radiation correction for the measured flame temperatures was also carried out. Temperature measurements were done by rapid insertion technique in the experiment [9]. However, at soot rich regions the heat loss from the thermocouple junction was higher because of the soot deposition around the thermocouple junction. The energy balance around the thermocouple junction was used to apply radiation corrections to the measured temperature profile [22];

$$\varepsilon_j \sigma T_{tj}^4 = k_{g0} \times Nu_j / 2d_{tc} \times (T_{gas}^2 - T_{tj}^2)$$

where,

k_{gas}= thermal conductivity of gas (W/mK)

d_{tc}= thermocouple junction diameter

k_g0 = kg Tgas = constant; 6.54 x 10-5 (W/mK^2)

Nu_j= Nusselt number of thermocouple junction

T_{gas}= gas temperature (K)

T_{tj}= thermocouple junction temperature (K)

σ = Stefan-Boltzmann constant; 5.67x10-8 (W/m^2K^4)

ε_j= thermocouple junction emissivity

A linear correlation between recorded soot volume fractions and junction emissivity was assumed [16]. The maximum difference between measured and corrected temperature was ~280 K at 10 mm height above the burner (HAB). The soot deposition on thermocouple junction at the highest point above the burner can be assumed maximum since the experimentally measured soot volume fractions [9] were also maximum. Similar difference between measured and corrected temperatures were also reported from different flame studies in the literature [23-25].

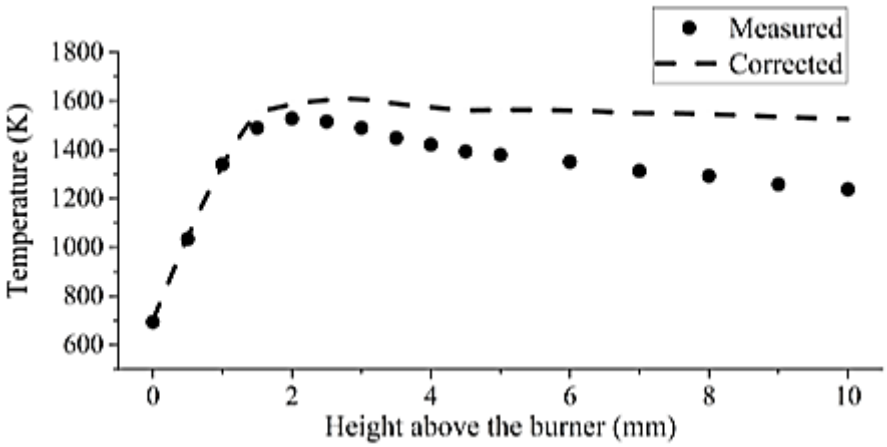

Figure 4. Measured and corrected flame temperature profiles.

The corrected temperature profile of the flame (Figure 4) was used as input parameter to predict species mole fraction profiles with the Master Mechanism.

3. RESULT AND DISCUSSION

As seen from Figure 5, the species mole fraction profiles of reactants were predicted by the master mechanism with very low error compared with experimental data [9]. In model predictions, fuel completely consumed at around 1 mm height above the burner (HAB), however in the experimental data n-heptane completely consumed at around 3 mm HAB. Experimental mole fraction profile of H_2O and model predictions were also matching with each other (Figure 6).

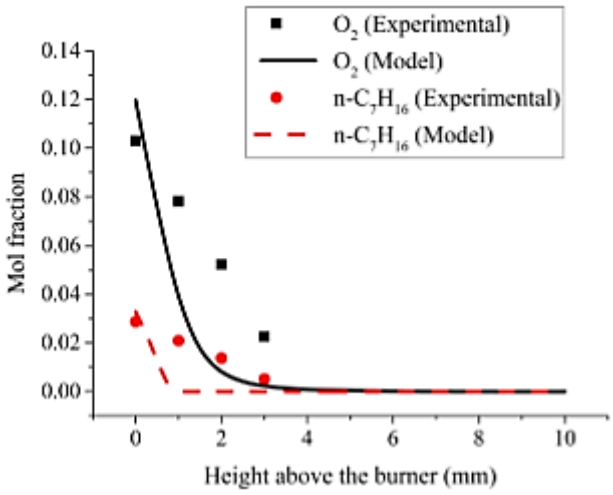

Figure 5. Comparison of measured and predicted species profiles of O2 and n-heptane.

However, the H2 profile was underestimated by a factor of about 2. Uncertainties either in the model (rate constant parameters, thermodynamic and transport properties) or in experiment might be the reason of the difference between model prediction and experimental data for H_2.

A good agreement between the model predictions and experimental data for all C1 (CO, CO_2 and CH_4) species were found (Figure 7). For CO_2 the difference between model predictions and the experimental data was less than a factor of 2. Methane mole fractions was underestimated by the model for 1 mm < HAB < 5 mm. When comparing the experimental data [9] with model predictions for C_2 species mole fraction profiles were very close to each other (Figure 8). Acetylene (C_2H_2) was considered as a precursor for first aromatic ring (benzene) formation for various fuels by the following reaction sequences [26],

$$C_2H_3 + C_2H_2 \rightarrow n\text{-}C_4H_5$$

$$n\text{-}C_4H_5 + C_2H_2 \rightarrow n\text{-}C_6H_7$$

$$n\text{-}C_6H_7 \rightarrow \text{Benzene} + H$$

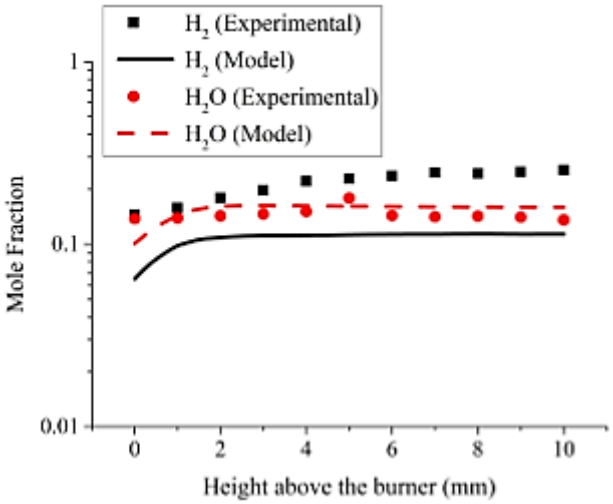

Figure 6. Comparison of measured and predicted species profiles of H_2 and H_2O.

The model predictions of ethylene (C_2H_4) was shifted to the burner surface around 1.5 mm. Ethylene was also considered as a precursor for benzene formation when it reacts with cyclopentadiene (C_5H_6) [27],

$$C_2H_4 + C_5H_6 \rightarrow \text{Benzene} + H + CH_3$$

Experimental data for ethane (C_2H_6) were available up to 3 mm HAB. The model predicted a sudden decrease for C_2H_6 mole fraction at HAB ~ 2.0 mm, up to that point measured and predicted mole fractions were very close. The mechanism predicts the trend of propene (C_3H_6) mole fraction profile, however there was a ~1.5 mm shift to the burner surface in the predictions (Figure 9).

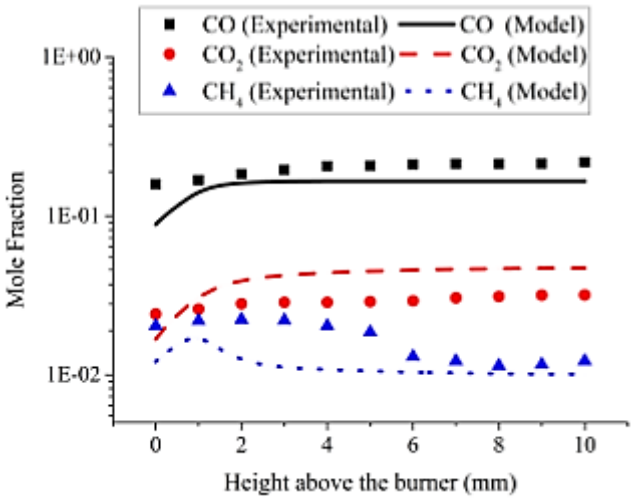

Figure 7. Comparison of measured and predicted species profiles of CO and CO_2 and CH_4.

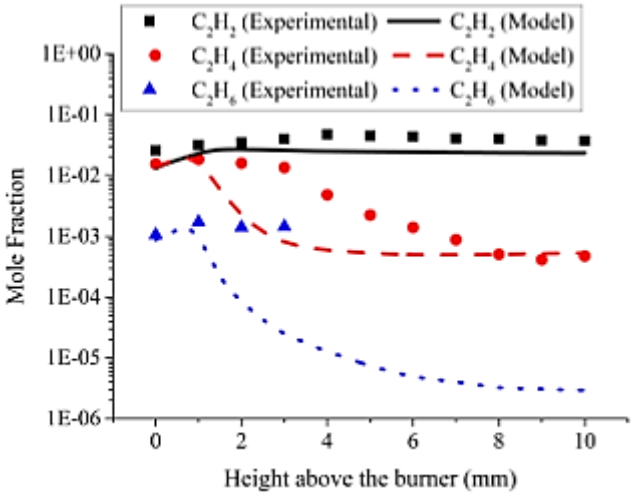

Figure 8. Comparison of measured and predicted species profiles of C2H2, C2H4 and C2H6.

The propadiene (C_3H_4) mole fraction was underestimated by the Master Mechanism by a factor of 10 for almost all HAB (Figure 9). Propadiene (allene, C_3H_4-A) was also considered as a precursor for benzene formation by reacting with propargyl radical (C_3H_3) [28],

$$C_3H_4\text{-A} + C_3H_3 = \text{Benzene} + H$$

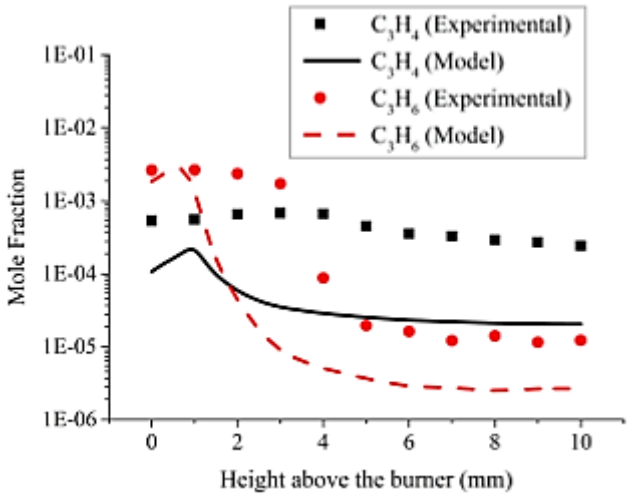

Figure 9. Comparison of measured and predicted species profiles of C_3H_4 and C_3H_6.

The comparison of model predictions and the experimental data for C_4 species are shown in Figure 10. The mechanism was capable to compute the trend for diacetylene (C_4H_2) and vinylacetylene (C_4H_4), however, the mole fractions of both species were underestimated around a factor of 10. By the following reaction route vinyl acetylene was also recognized as an important species in the benzene (C_6H_6) formation [29],

$$C_4H_4+C_2H_3 \rightarrow C_6H_6 + H$$

In experimental data there were no 1,3-butadiene (C_4H_6) HAB greater than 3 mm. In Master Mechanism predictions there was a rapid decrease for the C_4H_6 at around 2 mm HAB. 1,3butadienyl radicals (C_4H_5) that mainly formed from 1,3 butadiene was also considered as a precursor for benzene [26].

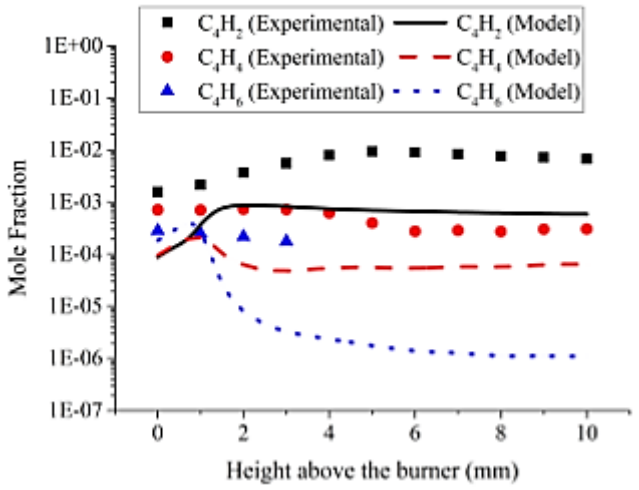

Figure 10. Comparison of measured and predicted species profiles of C_4H_2, C_4H_4 and C_4H_6.

Figure 11 shows the mole fraction of benzene along the flame. Benzene mole fraction profiles were slightly over-estimated by the master mechanism for HAB > 4 mm (Figure 11). Benzene was considered as a first aromatic ring in non-aromatic hydrocarbon flames [30].

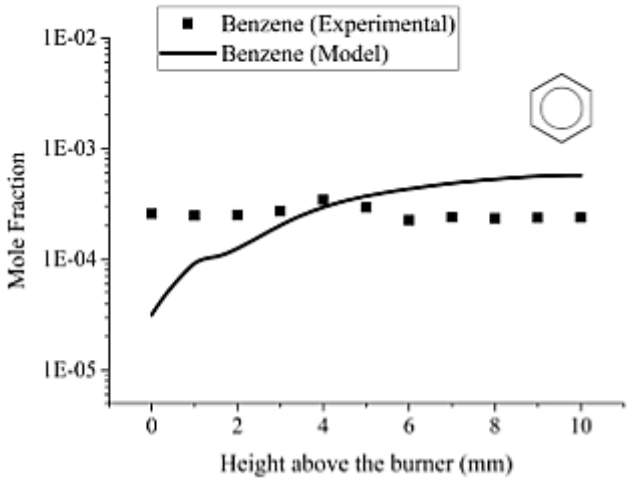

Figure 11. Comparison of measured and predicted species profiles of benzene.

Additionally, formation of benzene is also regarded as a rate limiting step for the formation of polycyclic aromatic hydrocarbons [31]. Acetylene (C_2H_2), propadiene (C_3H_4), vinyl acetylene (C_4H_4), diacetylene (C_4H_2) are generally accepted as precursor species for benzene formation in flames. However, an unstable intermediate, propargyl (C_3H_3) was also considered as a major precursor for the formation of benzene with following reactions [28, 32],

$$C_3H_3 + C_3H_3 \rightarrow \text{Benzene}$$

$$C_3H_4\text{-A} + C_3H_3 \rightarrow \text{Benzene} + H$$

There were no experimental data for the propargyl radical in the target flame study. Formation pathways for benzene on the n-heptane flame were given at the flame conditions in Figure 12. Pathways of benzene were found to be highly dependent on the HAB. Since rate of formation of benzene was found maximum at around 1.25 mm HAB, the pathway in Figure 12 was given at that distance [16]. Each line in Figure 12 shows the total production rate of multiple reactions from the specified reactant and the width of line is proportional with the formation rate.

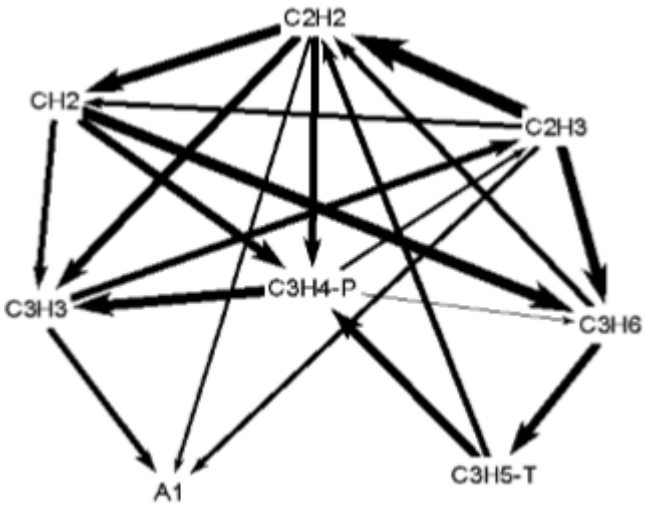

Figure 12. Simplified H and C flux to the benzene (A1) at HAB 1.25 mm.

$C_3H_3 + C_3H_3 = Benzene$ (1)

$C_4H_4 + C_2H_3 = Benzene + H$ (2)

$C_3H_4\text{-}A + C_3H_3 = Benzene + H$ (3)

$C_4H_5\text{-}N + C_2H_2 = Benzene + H$ (4)

Bimolecular reaction of propargyl radicals (reaction 1) was found as the most dominant route for the benzene formation. The vinyl addition to vinyl acetylene (reaction 2) was resulted with comparable amount of benzene production. However, the third and fourth reactions were found to be less important on the formation of benzene in considered conditions.

4. CONCLUSION

Burner stabilized, premixed, laminar, fuel-rich n-heptane flame was modeled by using DCKM. A detailed chemical kinetic mechanism was generated by merging LLNL n-heptane mechanism (version 3.1) as base mechanism and three donor mechanisms for fuel-rich hydrocarbon combustion. The Master Mechanism consists of 4185 reactions and 893 species, and it was validated by experimental data of jet stirred reactor (JSR) and ignition delay time measurements in a shock-tube. Additionally, the Master Mechanism was also used to analyze fuel-rich, premixed nheptane flame. It successfully predicted most of the stable species mole fractions up to benzene in the premixed n-heptane flame. The important reactions that forms benzene were found as bimolecular reaction of propargyl and vinyl addition to vinyl acetylene for the conditions studied using n-heptane flame by the pathway analysis.

ACKNOWLEDGEMENTS

We would like to thank Izmir Institute of Technology Scientific Research Fund (2017IYTE41) for the financial support.

REFERENCES

[1] AEO. (2018, 1 October 2018). Annual Energy Outlook 2018. Available: https://www.eia.gov/outlooks/aeo/pdf/AEO2018.pdf

[2] C. V. Callahan et al., "Experimental data and kinetic modeling of primary reference fuel mixtures," Symposium (International) on Combustion, vol. 26, no. 1, pp. 739-746, 1996.

[3] J. F. Griffiths, K. J. Hughes, M. Schreiber, and C. Poppe, "A unified approach to the reduced kinetic modeling of alkane combustion," Combustion and Flame, vol. 99, no. 3, pp. 533540, 1994.

[4] P. Dagaut, M. Reuillon, and M. Cathonnet, "Experimental study of the oxidation of nheptane in a jet stirred reactor from low to high temperature and pressures up to 40 atm," Combustion and Flame, vol. 101, no. 1, pp. 132-140, 1995.

[5] H. J. Curran, P. Gaffuri, W. J. Pitz, and C. K. Westbrook, "A Comprehensive Modeling Study of n-Heptane Oxidation," Combustion and Flame, vol. 114, no. 1–2, pp. 149-177, 1998.

[6] M. Mehl, W. J. Pitz, C. K. Westbrook, and H. J. Curran, "Kinetic modeling of gasoline surrogate components and mixtures under engine conditions," Proceedings of the Combustion Institute, vol. 33, no. 1, pp. 193-200, 2011.

[7] K. Zhang et al., "An updated experimental and kinetic modeling study of n-heptane oxidation," Combustion and Flame, vol. 172, pp. 116-135, 2016.

[8] A. E. Bakali, J. L. Delfau, and C. Vovelle, "Experimental Study of 1 Atmosphere, Rich, Premixed n-heptane and iso-octane Flames," Combustion Science and Technology, vol. 140, no. 1-6, pp. 69-91, 1998.

[9] F. Inal and S. M. Senkan, "Effects of equivalence ratio on species and soot concentrations in premixed n-heptane flames," Combustion and Flame, vol. 131, no. 1, pp. 16-28, 2002.

[10] C. Doute, J. L. Delfau, R. Akrich, and C. Vovelle, "Experimental study of the chemical structure of low-pressure premixed n-heptane-O-2-Ar and iso-octane-O-2-Ar flames," (in English), Combustion Science and Technology, vol. 124, no. 1-6, pp. 249-276, 1997.

[11] L. Seidel, K. Moshammer, X. Wang, T. Zeuch, K. Kohse-Höinghaus, and F. Mauss, "Comprehensive kinetic modeling and experimental study of a fuel-rich, premixed nheptane flame," Combustion and Flame, vol. 162, no. 5, pp. 2045-2058, 2015.

[12] S. Park, Y. Wang, S. H. Chung, and S. M. Sarathy, "Compositional effects on PAH and soot formation in counterflow diffusion flames of gasoline surrogate fuels," Combustion and Flame, vol. 178, no. Supplement C, pp. 46-60, 2017.

[13] H. M. Hakka, R. F. Cracknell, A. Pekalski, P. A. Glaude, and F. Battin-Leclerc, "Experimental and modeling study of ultra-rich oxidation of n-heptane," Fuel, vol. 144, no. Supplement C, pp. 358-368, 2015.

[14] H. K. Ciezki and G. Adomeit, "Shock-tube investigation of self-ignition of n-heptane-air mixtures under engine relevant conditions," Combustion and Flame, vol. 93, no. 4, pp. 421433, 1993.

[15] R. J. Kee, F. M. Rupley, E. Meeks, and J. A. Miller, "CHEMKIN-III: A FORTRAN chemical kinetics package for the analysis of gas-phase chemical and plasma kinetics," Sandia national laboratories report SAND96-8216, 1996.

[16] E. Degirmenci, "Detailed Chemical Kinetic Modeling of n-Heptane Flame," Chemical Engineering, Izmir Instutute of Technology, 10135797, 2018.

[17] H. Wang, M. Yao, Z. Yue, M. Jia, and R. D. Reitz, "A reduced toluene reference fuel chemical kinetic mechanism for combustion and polycyclic-aromatic hydrocarbon predictions," Combustion and Flame, vol. 162, no. 6, pp. 2390-2404, 2015.

[18] A. Raj, I. D. C. Prada, A. A. Amer, and S. H. Chung, "A reaction mechanism for gasoline surrogate fuels for large polycyclic aromatic hydrocarbons," Combustion and Flame, vol. 159, no. 2, pp. 500-515, 2012.

[19] H. Wang and M. Frenklach, "A detailed kinetic modeling study of aromatics formation in laminar premixed acetylene and ethylene flames," Combustion and flame, vol. 110, no. 12, pp. 173-221, 1997.

[20] N. M. Marinov et al., "Aromatic and Polycyclic Aromatic Hydrocarbon Formation in a Laminar Premixed n-Butane Flame," Combustion and Flame, vol. 114, no. 1, pp. 192-213, 1998.

[21] H. Richter, T. G. Benish, O. A. Mazyar, W. H. Green, and J. B. Howard, "Formation of polycyclic aromatic hydrocarbons and their radicals in a nearly sooting premixed benzene flame," Proceedings of the Combustion Institute, vol. 28, no. 2, pp. 2609-2618, 2000.

[22] C. S. McEnally, Ü. Ö. Köylü, L. D. Pfefferle, and D. E. Rosner, "Soot volume fraction and temperature measurements in laminar nonpremixed flames using thermocouples," Combustion and Flame, vol. 109, no. 4, pp. 701-720, 1997.

[23] L. R. Boedeker and G. M. Dobbs, "Soot distribution and cars temperature measuremnts in axisymmetric laminar diffusion flames with several fuels," Symposium (International) on Combustion, vol. 21, no. 1, pp. 1097-1105, 1988.

[24] Q. N. Chan, "Development of instantaneous temperature imaging in sooty flames," PhD Dissertation, Chemical Engineering, The University of Adelaide, 2011.

[25] H. Richter and J. B. Howard, "Formation and consumption of single-ring aromatic hydrocarbons and their precursors in premixed acetylene, ethylene and benzene flames," Physical Chemistry Chemical Physics, 10.1039/B110089K vol. 4, no. 11, pp. 2038-2055, 2002.

[26] J. A. Cole, J. D. Bittner, J. P. Longwell, and J. B. Howard, "Formation mechanisms of aromatic compounds in aliphatic flames," Combustion and Flame, vol. 56, no. 1, pp. 5170, 1984.

[27] M. Dente, E. Ranzi, and A. G. Goossens, "Detailed prediction of olefin yields from hydrocarbon pyrolysis through a fundamental simulation model (SPYRO)," Computers & Chemical Engineering, vol. 3, no. 1, pp. 61-75, 1979.

[28] C. H. Wu and R. D. Kern, "Shock-tube study of allene pyrolysis," The Journal of Physical Chemistry, vol. 91, no. 24, pp. 6291-6296, 1987.

[29] R. P. Lindstedt and G. Skevis, "Chemistry of Acetylene Flames," Combustion Science and Technology, vol. 125, no. 1-6, pp. 73-137, 1997.

[30] H. Richter and J. B. Howard, "Formation of polycyclic aromatic hydrocarbons and their growth to soot—a review of chemical reaction pathways," Progress in Energy and Combustion Science, vol. 26, no. 4, pp. 565-608, 2000.

[31] M. Frenklach, "Reaction mechanism of soot formation in flames," Physical Chemistry Chemical Physics, 10.1039/B110045A vol. 4, no. 11, pp. 2028-2037, 2002.

[32] C. F. Melius, J. A. Miller, and E. M. Evleth, "Unimolecular reaction mechanisms involving C3H4, C4H4, and C6H6 hydrocarbon species," Symposium (International) on Combustion, vol. 24, no. 1, pp. 621-628, 1992.

Paper 22 **Bildiri 22**

INVESTIGATION OF CYCLIC VARIATIONS OF A SPARK IGNITION ENGINE UNDER HOMOGENEOUS AND LEAN CONDITIONS FOR DIFFERENT CHAMBER GEOMETRIES

Abdurrahman Demirci[1], Osman Akın Kutlar[2], Hüseyin Emre Doğan[3], Ömer Cihan [3],

[1,3] Karamanoğlu Mehmetbey University, Mechanical Engineering Department, Karaman.

[1] arahmandemi@kmu.edu.tr (corresponding author), [3]edogan@itu.edu.tr

[2] Istanbul Technical University, Faculty of Mechanical Engineering, Istanbul.

[2] kutlar@itu.edu.tr

[4] Hakkari University, Mechanical Engineering Department, Hakkari.

[4] omercihan@hakkari.edu.tr

ABSTRACT

The tightening of emission standards and the desire to reduce fuel consumption determine direction of research on the internal combustion engines. The leaning of mixture in spark ignition engines decreases fuel consumption and NO_X emission together. Because of the fact, many researchers focused on lean combustion. The main purpose of this study is to compare the effect of different chamber geometries on combustion parameters of a spark ignition engine in lean and homogeneous mixtures. The most important variable of combustion parameters is cyclic variations. It defines the stable running of engine. Cycle to cycle variations are increased with leaning of mixture in spark ignition engines. The newly designed and manufactured combustion chamber (MR type chamber) geometry reduced the cyclic variations compared to other geometries in homogenous and lean mixtures. The lowest COV values were obtained for MR type geometry in lean mixtures for all load conditions.

Keywords: Combustion Chamber Geometry, Cyclic Variations, Lean Mixture.

INTRODUCTION

Observation of cylinder pressure enable the comparison of cycle by cycle variations. This information give us clues about combustion process. Variations in the combustion process create cyclic variations. The cycle by cycle variations are caused by the spark quality, residual gas ratio, mixture situation in spark area, air motions in cylinder. Flow motions inside of cylinder depend on the intake manifold and combustion chamber geometry. Airflow motions can be increased to certain level to obtain lower cyclic variations. Since, engine can run stably in leaner mixtures [1][2]. Because of that, a new combustion chamber geometry, which can generate more air motion in cylinder, is designed for lean operating conditions. COV values of

new combustion chamber were compared with other common used geometries in homogeneous and lean mixtures. MR type geometry has lower COV value than other type chamber geometries in lean conditions.

METHODOLOGY

Experiments were made in engine laboratory of Istanbul Technical University. They were made with a single cylinder, port fuel injection and water-cooled engine. The engine was controlled by an ECU developed in this laboratory [3]. In this experiment, the cylinder pressure was measured by using a piezo electric sensor, (AVL GU13Z-24). The signals of sensor transmitted to a charge amplifier. The output signals of amplifier were recorded on Kistler 2893A board. The crank angle was measured using trigger wheel and hall sensor. For manufacturing of chamber geometries, pistons of engine were purchased without any geometry. The desired geometries were designed and produced. The first chamber geometry is MR type, which can produce more air motions in cylinder. The other type chamber geometries are heron and disc. They are used commonly in spark ignition engines. Rough piston and manufactured geometries were shown in Figure 1. The experiments were carried out in two different relative air/fuel ratios at two different engine load and constant speed conditions.

Figure 1. Chamber Geometries: a) Rough piston (top left), b) Heron type geometry (top right), c) MR type geometry (bottom left) and d) Disc type geometry (bottom right)

RESULTS

Figure 2 shows the coefficient of variation (COV) of maximum pressure values at different engine loads for homogenous and lean mixture. The highest COV values of maximum pressure were measured at 3-bar load. Because, the decreasing of load increases residual gas ratio. The lowest maximum pressure COV values were obtained for MR type geometry, newly designed. The bowl geometry of MR type creates more air motion in cylinder. Therefore, it decreases COV values for MR type. Heron type COV values were obtained between MR and disc type.

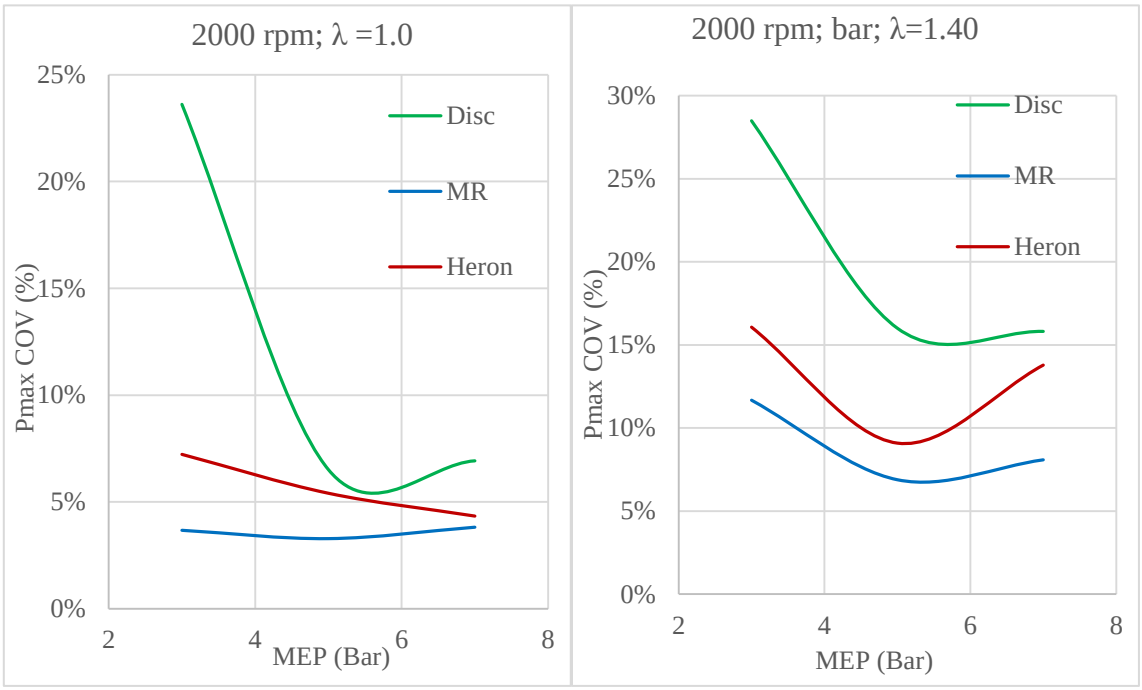

Figure 2. Maximum pressure coefficient of variation (COV) values at different engine loads for different air fuel ratios (left side λ=1.0 and right side λ=1.40).

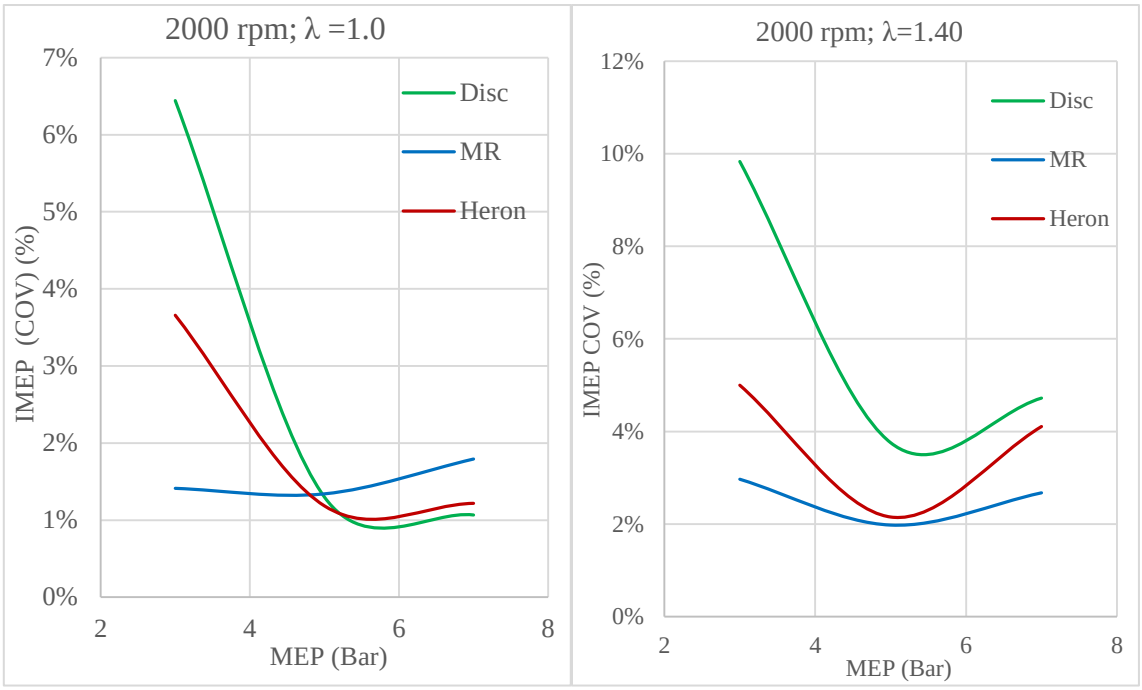

Figure 3. Indicated mean effective Pressure (IMEP) values at different engine loads for different air fuel ratios (left side λ=1.0 and right side λ=1.40)

The variation of indicated mean effective pressure (IMEP) COV values with respect to engine load was presented in Figure 3. At 3 bar load, the IMEP COV values of disc and heron type geometries were obtained higher than the desired values. One explanation for this situation could be stratified mixture for MR type through high swirl motion The COV values of IMEP for homogenous mixture lower than lean mixture condition. The leaning of mixture increases COV values as expected. The COV value of MR type geometry is higher than other geometries for IMEP values of five and seven bar at homogeneous mixture. The spark time was delayed because of knock problem at these running conditions for MR type geometry.

CONCLUSION

In this study, COV values of different combustion chamber geometries were experimentally investigated. A new combustion chamber geometry (MR type), for creating more air motion, was designed and manufactured. Two chamber geometries that are commonly used were manufactured for comparing. The results shown that the lowest COV values were obtained for MR type geometry at all load conditions for lean mixture. MR type combustion chamber geometry provides the desired COV values in lean mixtures too. Thus, the reduction in volumetric efficiency can be prevented by lean operation in the partial load conditions with the MR geometry.

REFERENCES

[1] Heywood, J.B. (1988). *Internal combustion engines*, Newyork, USA.: McGraw-Hill.

[2] Mehdiyev, R. & Wolanski, P. (2000). Bi-Modal Combustion Chamber for a Stratified Charge Engine, *SAE Technical Paper Series,* 2000-01-0196.

[3] Ö. Tekeli. (2013) *Designing and Production Ignition and Injection Units of a Gasoline Engine with Skip Cycle*, Master Thesis, Istanbul Technical University, İstanbul.

Paper 23 **Bildiri 23**

ECOFRIENDLY APPROACHES OF GASOLINE; DISTILLATION REQUIREMENTS

Cemil Koyunoglu[1]

Istanbul Technical University, Energy Institute, Ayazaga Campus, 34469, Maslak, Istanbul, Turkey, ckoyunoglu@itu.edu.tr

Abstract

The production and characteristics of fuels have been dealt with and it is appropriate at this stage to deal with the testing of combustible materials a topic of vital significance throughout the consumer and power industries. For example, it is of paramount importance that an oil refinery produces materials to a closely defined and consistent quality. A user of, say, coal in bulk must be able to carry out tests to determine the predicted performance of fuel he is purchasing, and hence be able to calculate the cost per unit energy and the efficiency of his entire process with an acceptable degree of accuracy. Due to the basic functions they play in human health, biogeochemical cycle and the world climate, it is very important to have a comprehensive understanding of the sources, changes and consequences of the surrounding organic species. Therefore, the aim of this study is to increase the awareness of the use of gasoline as environmentally friendly in the world for technical reasons. It is possible to use gasoline for determined emissions. In particular, there is a technological misperception to reduce the volatility of the gasoline. Therefore, the relationship between vapor pressure and evaporation losses of gasoline has been carefully studied in the American Auto Oil Program. At the end of this research, it was found that a drop of 0.1 psi in water pressure for gasoline samples with the same composition resulted in a evaporation loss of 4.3% in the vehicles equipped with one of the most up-to-date fuel injection systems. In fact, gasoline volatility is changed seasonally to give competent driveability because of the cooler temperature level, wintertime gasoline is a lot more volatile compared to summertime gasoline. As an example, throughout springtime and autumn, a fuel of volatility ideal for appropriate beginning at reduced environment temperature levels can trigger problems in some engines under greater ambient temperature working conditions. Subsequently, to discuss ecological impacts based upon numerous volatility specifications. In this part, Gasoline distillaiton of general requirements and methods summarized.

***** Corresponding author at: Energy Institute, Istanbul Technical University, Sariyer, 34469, Turkey.

E-mail address: ckoyunoglu@itu.edu.tr

Keywords: Eco-friendly usage; Sustainability of fuel in transportation; Gasoline specifications; Vaporization; Distillation requirements

1. Introduction

The oil companies, change the proportion of light hydrocarbons in petrol from summer to winter to give acceptable starting characteristics [1, 2].

A distillation test can be carried out to show the temperature range over which various portions of the fuel are vapourised [3-5]. It is usual to distil a 100 cm^3 sample of the fuel and to note the temperature at which the first drop of distillate is collected and also the volume of distillate collected at convenient intervals of vapour temperature [6]. The distillation is stopped when 90 % of the sample has been collected and the results plotted as shown in Figure 1. the 10 % distillation point gives an approximate indication of the starting characteristics [7-9]. Typically, 10% of the sample will have distilled over at 328 ^oK for a winter grade fuel and 338 ^oK for a summer grade [7, 8]. The range 50-70 % distillation is indicative of the warm-up and acceleration performance and the 50 % point is usually less than 378 ^oK [7, 8].

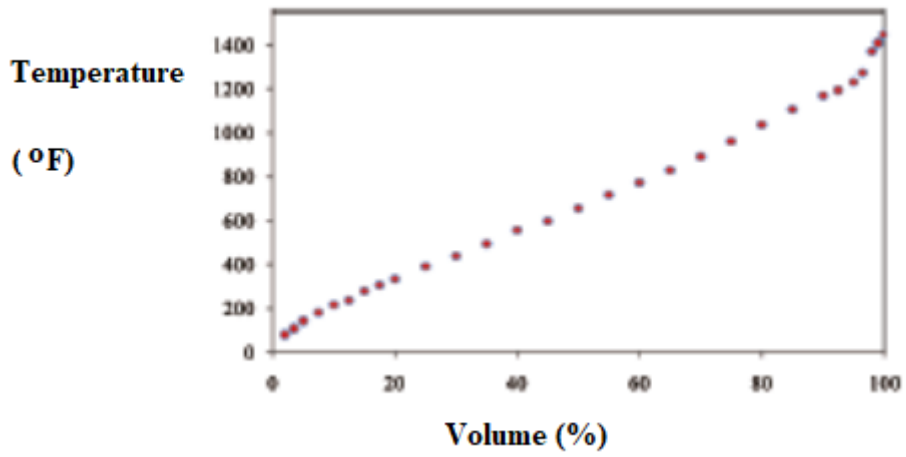

Figure 1. Typical distillation curve of petroleum products [10].

Generally flash-point is important for fuel oils since it refers to a temperature above normal room or ambient temperature, and volatility is important for gasolines whose flash-point is lower than ambient temperature [11]. Volatility is of a particular importance in the specification of a gasoline fuel for a spark ignition, internal combustion engine [12]. It is desirable that an engine should be easy to start under varying temperature conditions, ranging from a maximum in summer to a winter minimum [13]. By increasing the proportion of light hydrocarbons in a fuel ease of starting is improved but evaporation losses and problems of vapour lock are increased [14].

2. General Requirements

To match seasonal and geographic considerations with volatility requirements, the system of six classes shown in the A.S.T.M. D 4814 standard [15]. Each geographical area of the U.S. is assigned a class on a monthly basis. The selection is based on altitude and expected ambient temperature; top classes (A) are for warm weather and the bottom (E) for cold weather. Matching of the volatility to climate considerations is complicated by variations in the fuel delivery system designs and underhood temperatures [15].

Secondly, the most obvious gasoline quality parameter is octane number, because an octane index is posted [an average of research and motored number called the anti-knock index (A.K.I.)] and the driver can hear the knocking sound [16]. The true evaluation of knock is the "road octane number" which depends heavily on the particular engine-vehicle combination [17, 18]. The road octane is obtained by determining the knock limited spark advance for the test fuel under a given operating condition and then finding the octane number of the primary reference fuel that gives this same knock-limited spark advance at the same operating condition [19]. At low speeds (1000 to 1200 rpm), the road octane correlates with research octane for a given vehicle [20]. At medium engine speeds (1500 to 2500 rpm), the correlation is a combination of research and motored octane number, but engines with heated intakes (for emissions reduction) and higher specific power output can have octane requirements above the motored value [21]. Engines with incylinder deposits which insulate the chamber and cause the unburned mixture to undergo higher temperatures require higher octane fuels than the clean version of the same engine [22].

Vehicle octane requirements are lower at higher altitude, since the pressure is lower. The range over U.S.A. conditions is about 87-92 [23, 24]. Thus, fuels sold in high-altitude regions will probably cause knock at lower altitudes [25]. The use of anti-knock additives such as tetraethyl lead (T.E.L.), tetramethyl lead (T.M.L.), and methyl-cyclo-pentadiene manganese tricarbonyl after treatment devices and the adverse effects of M.M.T. on unburned hydrocarbon emissions [26, 27].

Alcohols and ethers have received attention as octane boosters [28]. Ethanol and methanol tend to decrease miles per gallon because of their lower energy content on a volume basis [28-30]. They decrease "CO" slightly but have negligible effects on "HC" and "NO" exhaust emissions [31-33]. Methanol can cause vapor lock [34-36]. Corrosion of the fuel system, and swelling of some elastomers. Cars can be designed to run on these fuels, however, and pure methanol has

received considerable attention as an alternative fuel [37]. The higher alcohols and ethers have fewer undesirable effects. Addition of 7% methyl-t-butyl ether increases research octane by 2 to 3 and motor octane by 1 to 2 with negligible side effects [37, 38]. Although octane boosting additives are the most familiar to users, many other additives are used to improve fuel quality [39, 40].

In the ongoing judicial review of ecological pollution, criminal and legal obligations relating to the impact of anthropogenic contamination on human health and welfare or environmental impact are determined. In order to determine the responsibility associated with gasoline contamination, the health-related objectives of the forensic examinations, which are due to ecological pollution of the following factors, have been determined. The first is the continuous increase in the production volume of gasoline, but the constant increase in the amount of gasoline produced from the United States for 50 years. For example, in 2001, the U.S.A. consumed 360,000 gallons of gas per day, accounting for 43% of global use (International Energy Annual, 2003). The other factor is that the fuel produced is generally consumed at the place where it is produced. For example, while there were more than 170,000 gas stations in the U.S.A. in 2002, it was observed that these stations were established in supermarkets, bulk dispensers and large warehouses. Third and most importantly, gasoline is measurable for human health and the environment [40].

Over the past 40 years, it has become even more attractive, with the work of improving the environmental impact of gasoline, making it more acceptable for the society, especially in the logistics sector, and, more recently, for the improvement of underground resources [40].

The fuel does not purposely have elements are the following

1. Tetra ethyllead,

2. Methyl tertiary butyl ether (M.T.B.E.),

3. Aromatic amines,

4. Benzene, or other carcinogens.

Also, no unwilled trace amounts of these components were located in the fuel made used of according to fuel standards requirements. The fuel and its components are not water soluble. Benzene omits by the optimum freezing point of −58 °C. A toxicology evaluation has been carried out and also exhaust emissions toxicology has not evaluated for either fuel. The fuel ought to satisfy health, safety, and environmental (H.S.E.) requirements offer for sale to the

public. Instances consist of vapor exposure, skin direct exposure the subject on cancer risk, and spill/water table contamination (that is, M.T.B.E. issue). Additional benchmarks express as below:

1. Flammability,

2. Ignition energy,

3. Auto-ignition temperature,

4. Fire-fighting media,

5. Static/conductivity,

6. Toxicity,

7. Combustion products,

8. Long-term fuel storage stability,

9. Dirt/water dropout,

10. Density,

11. Fuel distribution system, component compatibility,

12. Filtration compatibility,

13. Final-materials compatibility [41].

As an example, ecological policies prefer that all fuels including tetraethyllead must be colored to signify the presence of the lead [42].

Vehicles manufactured for sale in the U.S.A. that need to make use of unleaded fuel are required by Environmental Protection Agency policy to have long term tags on the instrument control panel and also nearby to the fuel storage tank-filler inlet reading “Unleaded Fuel Only.” The majority of 1975 and later on design passenger vehicles as well as light trucks remain in this classification [42].

Most 1971-1974 vehicles can use leaded or unleaded fuel. Pre-1971 vehicles created for leaded fuel; Nevertheless, the unleaded fuel of ideal anti-knock index may normally be made use of in these vehicles, other than that leaded fuel needs to be relied on occasionally (after a couple of tankfuls of unleaded fuel have been used). Leaded fuel may be required in some vehicles,

particularly trucks, in heavy duty service and some farm equipment. Instructions on fuel selection normally provide in publications of vehicles manufacturers (for example, owner's manuals, service bulletins, and so forth). Anti-knock agents other than lead alkyls may be used to increase the anti-knock index of fuels, and their concentrations may also limit due to either performance or legal requirements [43].

In the majority of spark ignition internal combustion engines, the fuel is metered in fluid form through the carburetor or fuel injector and is blended with air and partly vaporized before getting in the cylindrical tubes of the engine. Consequently, volatility is a very essential feature of motor fuel [43, 44].

Volatility can be considered as the evaporation of the fuel [45]. This is particularly important in that the engine is required for the first evaporation of the gasoline and therefore for the initiation of early combustion. Gasoline contains hundreds of compounds with a certain boiling point that interacts with each other [35]. The volatility of the gasoline compositions is determined by the Reid vapor pressure and distillation curve properties. The distillation curve gives an idea of the volatility of the gas along the distillation space, because the Reid vapor pressure is an important feature of the lightest part of the gasoline, the most volatile compounds [43].

The volatility of gasoline assists to car performance chiefly [9]. Initially, vaporization as well as distribution features such as preparedness to begin, habits throughout warm-up, actions during a typical procedure. Second, propensity to weaken crankcase oils and Third, level of flexibility from vapor lock in vehicles and also from a tendency to evaporate during handling or usage. It has found that in an approximate way every one of the above details of information is shown for any provided fuel by an appropriate analysis of its distillation curve when possibility conjunction with the vapor pressure [43].

The volatility of a fuel is determined by the vapor pressure, the enthalpy of evaporation and the distillation curve. The concept of volatility is the transfer of fuel from the liquid phase to the vapor phase, but also has a direct effect on the optimization of the required air / fuel mixture with respect to combustion performance [41, 43].

The volatility of the gasoline compositions can be determined based on the characteristics of the Reid vapor pressure as well as the distillation curve. Since the determination of the vapor pressure of the distillation curve, the Reid vapor pressure, means the evaporation of the lightest

component of the gasoline, it also offers a suggestion of gas volatility during the distillation. [45].

In the distillation curve, three different distillations may occur depending on the basic characteristics of the gasoline. Although these are defined as T10, T50 and T90, they represent 10%, 50% and 90% of the temperature levels at which evaporation occurs. These temperatures also characterize the variability of the light, medium and heavy fractions of the fuel. These fractions then affect the various operating routines of the motor [45].

Standard testing approaches analyze fuel high quality. For instance, the criterion for gasoline is A.S.T.M. D 4814. Gasoline top qualities are figured out regarding volatility and octane number of the hydrocarbons. A sufficient volatility needs for smooth application of petrol engines [42].

Gasoline is a challenging mixture of numerous compounds that are showed in gasoline occurs within five compound classes:

- Paraffins
- Iso-alkanes
- Aromatics,
- Naphthenes,
- Olefins,

these state to by the phrase "P.I.A.N.O."[46-48]. The significant nonhydrocarbon groups in gasolines can consist of oxygen containing ethers (e.g., M.T.B.E, tert Amyl methyl ether (T.A.M.E), and so on), alcohols, (e.g., ethanol, tert Butyl alcohol (T.B.A.). Additionally, isopropyl alcohol, methanol, sulfur- (e.g., disulfides, thianes, mercaptans, thiolanes, thiophenes), and also nitrogen containing compounds (e.g., anilines, pyrroles, indoles, etc.) [40].

More proof for the retention of obvious gasoline residues after comprehensive evaporation can note in ecological soil samples affected by gasoline several years before. For instance, some numbers in literary works show a G.C./F.I.D. chromatogram of recurring gasoline in soil that gathered from a retail gasoline terminal site that had closed greater than 25 years before the sample accumulated. The deposit leaving in this vadose area soil manages by Cg-alkylbenzene, naphthalenes, and also C_{10+} alkanes, comparable to exactly what transferred in the research laboratory vaporized gasoline [40].

The evaporation of gasoline makes significant contributions, in particular, to the acquisition of the information necessary for accessing important information on forensic issues. For this purpose, the presence of heavy hydrocarbons, which should not be present in gasoline in general, will cause significant differences in the distillation curve during the volatilization of volatiles. This particularly emphasizes the presence or absence of heavier hydrocarbons, which cannot be otherwise detected in products that are less vaporized than the gasoline sample. The presence of C_{13+} hydrocarbons which may be present at reduced levels in the gasoline is important in this respect. Although these hydrocarbons are referred to as "Alkanic tail", their exact effect properties have not been discovered. However, when the gasoline reaches the desired performance when it is burned, it is directly related to whether the hydrocarbons are stable in gasoline. In one case study, Harvey, in 1997, found a 3% by weight and 75% evaporation of an “alkane tail” from gasoline, with some "alkane tails" associated with slightly heavier oils, such as fuels. The same researcher reported that, in contrast to the gasoline mixture structure of this "alkane tail", the hydrocarbon products were due to a small mixture of gasoline and medium distillation during the pipeline transportation. Consequently, a forensic fuel analyzer that detects the "alkane tail" associated with the resulting impurity can comment on whether the "alkane tail" is associated with the nature of the gasoline or whether it increases combustion performance by mixing with a small amount of biofuel [40].

Gasoline further within the soil column might experience a various (slower) price of evaporation compared to surface area soils. However, as a basic policy, the loss of unstable compounds deeper within vadose zone area soil will certainly still be controlled by the very same procedures as evaporation in surface area soils. In the technique, the level to which subsurface gasoline vaporizes in vadose zone area soils will hardly ever change the structure of product according to will certainly confuse forensic analyses [40]. For instance, the gasoline hydrocarbons might have gone through a specific level of solubilization as a result of penetrating water. Nevertheless, the majority of the modifications kept in mind in this figure are fairly associated with evaporation, which gradually has eliminated the much more unstable substances, leaving a recurring gasoline product controlled by naphthalene, C_{3+} alkyl benzenes, alkyl naphthalenes and high molecular weight alkanes [40].

Gasoline derived N.A.P.L. recuperated from checking wells stands for the complimentary stage gasoline staying in soils at or near the water table. As a whole, these might show up much less affected by evaporation compared to the surface as well as subsurface soil samples [40].

The EPA vapor pressure policies can trigger the distillation of the fuel to be much less volatile, which for some vehicles, leads to in an even worse work out driveability efficiency [43].

Evaporation of gasoline in the subsurface generates a vapor stage that can additionally be helpful in ecological forensic examinations [40].

2.2. Motor gasoline

The motor gasoline specifications typically are just a part of the complete EN-228:2004 requirement. These properties have been highlighted, considering that they restrict the structure of the fuel and established efficiency standards that equate into needs that can associate with the molecular characteristics of the fuel. Directive 2009/30/EC23 of the European requirements changed the constraints put on oxygenated motor gasoline. The optimum oxygenates content has been boosted to 3.7 mass % O and the limitations on different oxygenates have raised correctly. For instance, the limitation on C_4 derived ethers is 15% which on C_5 and heavier ethers is 22 %. The 2009/30/EC instruction additionally consisted of distillation deprivations on motor gasoline, specifically, minimal E46 at 100 ^oC (46 vol % vaporized at 100 ^oC) and minimum E 75 at 150 ^oC. The optimum sulfur content of motor gasoline has evaluated at 10 mg/g^{-1} by the regulation [42].

Mixing estimations suggest that the paraffin needs to have an R.O.N. around 70 and an M.O.N. around 65 to satisfy motor gasoline requirements when mid range appreciates for the RON and also M.O.N. of aromatics, oxygenates and olefins are used at their corresponding blending limitations [42].

2.3. Carbon number distribution

The carbon number variety of motor gasoline is straight and also indirectly controlled. The ceiling is established the last boiling point requirements (210 ^oC; C_{11}/C_{12}) while the reduced limitation is established indirectly by the vapor pressure requirements. In the technique, motor gasoline normally covers the carbon number array C_5–C_{10}, with the quantity of C_4 identifies by the vapor pressure of the base fuel [42].

The carbon number distribution indirectly manages by both the density demands and vapor pressure restriction [42]. Also, when combined with carbon number (nC), supplies a structure for explaining the chemistry of organic types in the atmosphere, and in a certain climatic organic aerosol. These two basic amounts can make used of constraining the structure of natural aerosol

and, furthermore, to distinctly specify crucial classes of climatic responses, offering to understand into the oxidative advancement of climatic organics [49].

The structure is controlled by substance class, along with by certain substance in some circumstances. The structure should be adjusted in the refinery to follow these restrictions, also, to fulfilling the efficiency requirements of the fuel. The crucial performance standards for motor gasoline are studied octane number (R.O.N.) and also motor octane number (M.O.N.). R.O.N. and M.O.N. are actions of a fuel's resistance to autoignition under various driving as well as lots problems and straight associate with the molecular specifications of the fuel [9]. European requirements call for motor gasoline to have a minimal both R.O.N. and M.O.N. value while countries like the United States control just the roadway octane number (½ R.O.N. + ½ M.O.N.) as a solitary worth. The last is less complicated to accomplish by refining, given that there is no octane giveaway to fulfill the constricting octane number, R.O.N. or M.O.N. [42].

To discuss the refining obstacles connected to the structure of motor gasoline, it works to check out the various compound classes in connection with the octane number needs of motor-gasoline [42].

Aromatics and also fuel oxygenates are ‘‘Octane positive’’ because they have greater octane numbers compared to are needed by motor gasoline requirements. Olefins usually are practical ‘‘Octane neutral’’, being close to the octane numbers needed by motor gasoline specs. It ought to be kept in mind, however, the octane varieties of olefins are framework reliant, with straight a-olefins having reduced octane numbers compared to branched inner olefins. Aromatics oxygenates and also olefins are all controlled as well as it suggests that motor gasoline has to have a minimum of 32 % paraffin. The octane values of paraffin are quite structured vulnerable, making the top quality of the paraffin the crucial to motor gasoline refining. Paraffin octane number enhances with raising the degree of dividing and decreasing carbon number. It remains in precept feasible to make high octane paraffin, yet it calls for extremely particular conversion innovation.

Moreover, the paraffin are hardly ever separated in a refinery as well as some conversion modern technologies co produce reduced octane paraffin in combinations with high octane substances, for example, catalytic reforming. This reforming makes it difficult in technique session to attain a highoctane worth for all the paraffin in a refiner [42].

2.4. Ethanol

Ethanol has the potential to minimize the amount of carbon dioxide released at the end of combustion compared to renewable and conventional fuels [50]. For this purpose, up to 10% by volume of normal gasoline is used in today's vehicles [51]. This is an important factor in determining both the cost and the environmental impact of other fuel blending options [33, 52].

After the discovery of tetra-ethyl leads (T.E.L.), it had the ability to improve the combustion quality of the gasoline in the combustion problem with the same purpose before more than 50 years of ethanol. Finally, the negative health consequences of T.E.L. have led to the prohibition of the use of this component in gasoline in several countries. The use of alternative hydrocarbons has come to the fore with such interventions [51].

Ecological issues have resulted in the need to include oxygenates to conventional gasoline. For example, methyl tertiary butyl ether (M.T.B.E.) is an oxygenated substance put to gasoline to enhance air quality as part of the United States Federal Clean Air Act [50]. In the United States and various other parts of the world, methyl tert-butyl ether (M.T.B.E.) was approved as one of the most cost effective oxygenate [51]. Regrettably, M.T.B.E. went into groundwater in some locations of the United States, and its extremely reduced limit for taste and odor have provided the water unfavorable for human intake.

Additionally, In some locations of the United States, citizens have suffered from a range of health impacts from direct exposure to emissions from M.T.B.E blended gasoline such as sore eyes headaches, nausea, dizziness and breathing inflammation [50]. The elimination of M.T.B.E. opens up space for an ecologically appropriate high octane part for gasoline and also is a crucial driving pressure in the look for alternate elements. Ethanol is becoming as the additive to load the M.T.B.E. space as well as it is being phased right into California and the other of the U.S.A. where oxygenated fuels are called for [52, 53].

ASTM D 4814 specify the different classes of gasoline requirements for vapor pressure, distillation, and also for vapor lock security. A section of the total table from ASTM D 4814 provides a suggestion of the numerous gasoline requirements needed for various regions of the United States at various times of the year. Greater than 20 unique volatility classes see in the full ASTM 4814 table. Integrating these 20 classes with three various octane qualities returns 60 various “gasoline”. In enhancement to ASTM categories, the 1990 Clear Air Act Amendment accredits EPA as well as state federal governments to enforce policies on gasoline to minimize vehicular discharges. These ecological policies bring about an entire classification

of various gasoline: reformulated, standard, oxygenated, low R.V.P., reduced sulfur, and so on. This intricacy has resulted in the term “boutique” gasoline. The enhancement of oxygenates at numerous degrees complexes the scenario also further [52].

Ethanol appears to be the oxygenate of selection as M.T.B.E. encounters substantial pressures and also state restrictions because of the ecological threats [40]. For instance, decreases in ozone concentrations varying from 14 to 55 % were simulated. And particularly for air monitoring stations in the São Paulo city in September 2004 on examining a theoretical boost in the ethanol share of overall “gasoline+ethanol” intake from 34 % of range took a trip in the base case to 97 % in the simulated case [9].

Due to the instability of the mixture of ethanol with water, it has been shown that it should not be mixed with gasoline for various purposes. Even after a certain period of time, even if the mixture is not able to be burned in the engine after a certain period of time due to the deterioration in the homogeneity of burning problems with problems such as transport with transport trucks are mixed with gasoline. The problem of not interfering with gasoline from the beginning of ethanol is a logistical problem because of the water that is exposed to it. In the case of unconscious mixing processes, problems such as the rise of water to the surface due to phase separation from ethanol may lead to the nomenclature of gasoline, such as a fugitive, especially after the mixture [40].

The solution of the majority of refiners is to change M.T.B.E. with ethanol to satisfy the oxygen demands of Oxy fuel and also R.F.G. The using of ethanol in Oxyfuel and R.F.G. (in some markets; Chicago, California, New York) promoted extra modifications in gasoline structure by refiners. Initially, much less ethanol is required to fulfill the oxygen minimum demands. Second, changing M.T.B.E. with ethanol enhances the R.V.P. of gasoline, thus needing refiners to counter this rise by minimizing the amount of butanes and also pentanes in ethanol containing Oxyfuel and R.F.G. Third, due to simultaneous modifications in the T 50 and T 90 distillation temperature levels, refiners need to likewise decrease the percentage of larger gasoline parts (C_3 + aromatics) to satisfy these needs. In general, these adjustments lowered the volume of gasoline able to be created and enhances expenses [40].

2.5. Oxygenates

Methyl tert butyl ether (M.T.B.E., 2 methoxy 2 methylpropane) and ethanol are the most typical oxygenate used to raise octane gasoline. M.T.B.E. As in the U.S.A., it is a dominant component in Europe; In addition to its negative impact on the environment, its use is limited due to its

high solubility in water as well as the deterioration agents involved in the environmental problems [43].

Therefore, the use of ethanol-formulated gasoline is an important factor in reducing the ecological problem [43].

Excluding ethyl tertbutyl ether (E.T.B.E.), the other oxygenates were removed from the gasoline of R.V.P. and it is also known to cause a significant increase in evaporative discharge from the vehicle fueling system and during refueling. Considering that these oxygenates are high molecular weight substances, the increase of isoparaffins, such as reduced volatility, reduced the R.V.P. of gasoline. Similarly, increasing the toluene also reduced the R.V.P. of the combination. Considering high molecular weight and low steam pressure. When the oxygenates are combined with gas, they have a significant effect on the vapor pressure. In addition, oxygenates are more resistant to heating, i.e. they can be defined as compounds that produce a strong environmental effect, with larger amounts of carbon monoxide (CO) and unburned hydrocarbons (HCs) [52]. Ethanol, on the other hand, is environmentally friendly and, at the same time, capable of minimizing carbon dioxide discharges compared to conventional fuels. In addition, ethanol is available in vehicles up to 10% by volume [52].

2.6. M.T.B.E.

The most helpful forensic application of M.T.B.E. remains in regards to its concentration gradients or spatial circulation in groundwater, which can disclose several sources/releases of the M.T.B.E. [40].

2.7. T.B.A.

The use of T.B.A. became more widespread in the widespread use of gasoline after the US Environmental Protection Agency allowed it in 1979. The determination of the concentration of gasoline in the gasoline has been determined by the same agency [40].

2.8. Fuel Dyes

Identifying the existence, lack, or a combination of these dyes can be of great wonderful utility in instances where one has to separate in between or amongst possibly comparable fugitive petroleum products [54]. One constraint of dependence on fuel dye information for forensic objectives is the reported sensitivity of these dye substances to ecological weathering. Hence, the lack of noticeable dyes in a fugitive gasoline does not always imply that the compound (s) was not originally existing in the fresh fuel. Under some problems (e.g., clay rich soil and also

considerable NonAqueous Phase Liquids, N.A.P.L. mass), nevertheless, dyes can continue the subsurface environment for several years [40].

Comments

The Fuel gasoline uses for transportation yet it requires to the control of its distillation specifications commonly before and after usages. When it makes some mechanical and environmental troubles in vehicles use fuel needs to analyze in which sold. The distillation properties of gasoline which consist of some additives affect some environmental issues. This subject warns the fuel oil producers and also consumers to focus on some useful strategies to get rid of technical and also environmental problems. To do this, for every manufactured gasoline A.S.T.M. D 86 requirements should be applied, environmental effects of gasoline has to verify for A.S.T.M. D 4814 requirements.

Examination Method D 86 for distillation offers one more action of the volatility of fuels. The examination technique marks the limits for endpoint temperature and also the temperatures at which 10%, 50%, as well as 90% by volume of the fuel vaporizes. These distillation features, in addition to vapor pressure and V/L characteristics, influence the adhering to vehicle efficiency qualities: beginning, driveability, vapor lock, dilution of the engine oil, fuel economy, and carburetor icing.

References

[1] Koc AB, Abdullah M. Performance of a 4-cylinder diesel engine running on tire oil–biodiesel–diesel blend. Fuel Processing Technology 2014;118:264-9.

[2] Fang W, Kittelson DB, Northrop WF. Dilution Sensitivity of Particulate Matter Emissions From Reactivity-Controlled Compression Ignition Combustion. Journal of Energy Resources Technology 2017;139(3):032204--6.

[3] Wang H, Li C. Hydroprocessing of Coal Tar to Prepare Clean Fuel Oil A2 - Abraham, Martin A. Encyclopedia of Sustainable Technologies. Oxford: Elsevier; 2017, p. 411-22.

[4] Abbott DJ. Chapter 2 Advances in simulated distillation. Journal of Chromatography Library 1995;56:41-53.

[5] Fraser S. Chapter 4 - Distillation in Refining A2 - Górak, Andrzej. In: Schoenmakers H, editor Distillation. Boston: Academic Press; 2014, p. 155-90.

[6] Tormey HJ. The analytical distillation of gasoline. Journal of Chemical Education 1931;8(4):699.

[7] Speight JG. Handbook of Petroleum Product Analysis. Wiley; 2015.

[8] Engineers NBOC. The Complete Book On Distillation And Refining Of Petroleum Products (Lubricants, Waxes And Petrochemicals). NIIR Project Consultancy Services; 2005.

[9] Badra JA, Sim J, Elwardany A, Jaasim M, Viollet Y, Chang J, et al. Numerical Simulations of Hollow-Cone Injection and Gasoline Compression Ignition Combustion With Naphtha Fuels. Journal of Energy Resources Technology 2016;138(5):052202--11.

[10] Guerra OJ, Le Roux GAC. Improvements in Petroleum Refinery Planning: 1. Formulation of Process Models. Industrial & Engineering Chemistry Research 2011;50(23):13403-18.

[11] Asomaning J, Mussone P, Bressler DC. Two-stage thermal conversion of inedible lipid feedstocks to renewable chemicals and fuels. Bioresource Technology 2014;158:55-62.

[12] Jiménez-Espadafor FJ, Torres M, Velez JA, Carvajal E, Becerra JA. Experimental analysis of low temperature combustion mode with diesel and biodiesel fuels: A method for reducing NOx and soot emissions. Fuel Processing Technology 2012;103:57-63.

[13] Reiter MS, Kockelman KM. The problem of cold starts: A closer look at mobile source emissions levels. Transportation Research Part D: Transport and Environment 2016;43:123-32.

[14] Cañipa-Morales NK, Galán-Vidal CA, Guzmán-Vega MA, Jarvie DM. Effect of evaporation on C7 light hydrocarbon parameters. Organic Geochemistry 2003;34(6):813-26.

[15] Rodríguez-Antón LM, Gutíerrez-Martín F, Doce Y. Physical properties of gasoline, isobutanol and ETBE binary blends in comparison with gasoline ethanol blends. Fuel 2016;166:73-8.

[16] Nikolaou N, Papadopoulos CE, Gaglias IA, Pitarakis KG. A new non-linear calculation method of isomerisation gasoline research octane number based on gas chromatographic data. Fuel 2004;83(4):517-23.

[17] Jia G, Wang H, Tong L, Wang X, Zheng Z, Yao M. Experimental and numerical studies on three gasoline surrogates applied in gasoline compression ignition (GCI) mode. Applied Energy 2017;192:59-70.

[18] Laredo GC, Castillo J, Cano JL. Benzene reduction in gasoline range streams by adsorption processes using a PVDC–PVC carbon molecular sieve. Fuel 2014;135:459-67.

[19] Thomas A. Chapter Five - Automotive fuels A2 - ARCOUMANIS, CONSTANTINE. Internal Combustion Engines. Academic Press; 1988, p. 213-70.

[20] Phuangwongtrakul S, Wechsatol W, Sethaput T, Suktang K, Wongwises S. Experimental study on sparking ignition engine performance for optimal mixing ratio of ethanol–gasoline blended fuels. Applied Thermal Engineering 2016;100:869-79.

[21] Fu J, Zhu G, Zhou F, Liu J, Xia Y, Wang S. Experimental investigation on the influences of exhaust gas recirculation coupling with intake tumble on gasoline engine economy and emission performance. Energy Conversion and Management 2016;127:424-36.

[22] Yang H-H, Lee W-J, Mi H-H, Wong C-H, Chen C-B. PAH emissions influenced by Mn-based additive and turbocharging from a heavy-duty diesel engine. Environment International 1998;24(4):389-403.

[23] Stradling R, Williams J, Hamje H, Rickeard D. Effect of Octane on Performance, Energy Consumption and Emissions of Two Euro 4 Passenger Cars. Transportation Research Procedia 2016;14:3159-68.

[24] Borman G, Nishiwaki K. Internal-combustion engine heat transfer. Progress in Energy and Combustion Science 1987;13(1):1-46.

[25] Bailey RA, Clark HM, Ferris JP, Krause S, Strong RL. 6 - Petroleum, hydrocarbons, and coal. Chemistry of the Environment (Second Edition). San Diego: Academic Press; 2002, p. 147-92.

[26] Apicella B, Di Palma TM, Wang X, Velotta R, Armenante M, Spinelli N. A mass spectrometric study of gasoline anti-knocking additives. International Journal of Mass Spectrometry 2007;262(1):105-13.

[27] Maylin MV, Kirgina MV, Sviridova EV, Sakhnevitch BV, Ivanchina ED. Calculation of Gasoline Octane Numbers Taking into Account the Reaction Interaction of Blend Components. Procedia Chemistry 2014;10:477-84.

[28] Vallinayagam R, Vedharaj S, Naser N, Roberts WL, Dibble RW, Sarathy SM. Terpineol as a novel octane booster for extending the knock limit of gasoline. Fuel 2017;187:9-15.

[29] Dabbagh HA, Ghobadi F, Ehsani MR, Moradmand M. The influence of ester additives on the properties of gasoline. Fuel 2013;104:216-23.

[30] Maurya RK, Agarwal AK. Experimental Investigations of Particulate Size and Number Distribution in an Ethanol and Methanol Fueled HCCI Engine. Journal of Energy Resources Technology 2014;137(1):012201--10.

[31] Chen R-H, Chiang L-B, Chen C-N, Lin T-H. Cold-start emissions of an SI engine using ethanol–gasoline blended fuel. Applied Thermal Engineering 2011;31(8):1463-7.

[32] Yusri IM, Mamat R, Azmi WH, Omar AI, Obed MA, Shaiful AIM. Application of response surface methodology in optimization of performance and exhaust emissions of secondary butyl alcohol-gasoline blends in SI engine. Energy Conversion and Management 2017;133:178-95.

[33] Martinez-Frias J, Aceves SM, Flowers DL. Improving Ethanol Life Cycle Energy Efficiency by Direct Utilization of Wet Ethanol in HCCI Engines. Journal of Energy Resources Technology 2007;129(4):332-7.

[34] Ghadikolaei MA. Effect of alcohol blend and fumigation on regulated and unregulated emissions of IC engines—A review. Renewable and Sustainable Energy Reviews 2016;57:1440-95.

[35] Zhang C, Ge Y, Tan J, li L, Peng Z, Wang X. Emissions From Light-Duty Passenger Cars Fueled With Ternary Blend of Gasoline, Methanol, and Ethanol. Journal of Energy Resources Technology 2017;139(6):062202--8.

[36] Wei Y, Wang K, Wang W, Liu S, Yang Y. Contribution Ratio Study of Fuel Alcohol and Gasoline on the Alcohol and Hydrocarbon Emissions of a Gasohol Engine. Journal of Energy Resources Technology 2013;136(2):022201--7.

[37] Chao H-R, Lin T-C, Chao M-R, Chang F-H, Huang C-I, Chen C-B. Effect of methanol-containing additive on the emission of carbonyl compounds from a heavy-duty diesel engine. Journal of Hazardous Materials 2000;73(1):39-54.

[38] Strus B, Sobczyńska A, Wiśniewski M. Solubility of water and association phenomena in gasoline modified with hydrophilic additives and selected surfactants. Fuel 2008;87(6):957-63.

[39] den Hollander MA, Wissink M, Makkee M, Moulijn JA. Gasoline conversion: reactivity towards cracking with equilibrated FCC and ZSM-5 catalysts. Applied Catalysis A: General 2002;223(1):85-102.

[40] Stout SA, Douglas GS, Uhler AD. 18 - Automotive Gasoline A2 - Morrison, Robert D. In: Murphy BL, editor Environmental Forensics. Burlington: Academic Press; 1964, p. 465-531.

[41] Cataluña R, Dalávia D, da Silva R, Menezes E, Venturi V, Wagner R. Acceleration tests using gasolines formulated with di-TAE, TAEE and MTBE ethers. Fuel 2011;90(3):992-6.

[42] Klerk Ad. Fischer-Tropsch fuels refinery design. Energy & Environmental Science 2011;4(4):1177-205.

[43] Standard Specification for Automotive Spark-Ignition Engine Fuel. ASTM International; 2017.

[44] Bousbaa H, Sary A, Tazerout M, Liazid A. Investigations on a Compression Ignition Engine Using Animal Fats and Vegetable Oil as Fuels. Journal of Energy Resources Technology 2012;134(2):022202--11.

[45] Standard Specification for High Aromatic Content Unleaded Hydrocarbon Aviation Gasoline. ASTM International; 2016.

[46] Stout SA, Douglas GS, Uhler AD. 11 - Chemical fingerprinting of gasoline and distillate fuels. Standard Handbook Oil Spill Environmental Forensics (Second Edition). Boston: Academic Press; 2016, p. 509-64.

[47] Schifter I, González U, Díaz L, Sánchez-Reyna G, Mejía-Centeno I, González-Macías C. Comparison of performance and emissions for gasoline-oxygenated blends up to 20 percent oxygen and implications for combustion on a spark-ignited engine. Fuel 2017;208:673-81.

[48] Kiatkittipong W, Suwanmanee S, Laosiripojana N, Praserthdam P, Assabumrungrat S. Cleaner gasoline production by using glycerol as fuel extender. Fuel Processing Technology 2010;91(5):456-60.

[49] Kroll JH, Donahue NM, Jimenez JL, Kessler SH, Canagaratna MR, Wilson KR, et al. Carbon oxidation state as a metric for describing the chemistry of atmospheric organic aerosol. Nat Chem 2011;3(2):133-9.

[50] Lee CW, Mohr SN, Weisel CP. Toxicokinetics of human exposure to methyl tertiary-butyl ether (MTBE) following short-term controlled exposures. J Expo Anal Environ Epidemiol 2001;11(2):67-78.

[51] Al-Farayedhi AA, Al-Dawood AM, Gandhidasan P. Effects of Blending MTBE With Unleaded Gasoline on Exhaust Emissions of SI Engine. Journal of Energy Resources Technology 2000;122(4):239-47.

[52] French R, Malone P. Phase equilibria of ethanol fuel blends. Fluid Phase Equilibria 2005;228:27-40.

[53] Masimalai S, Nandagopal S. Combined Effect of Oxygen Enrichment and Dual Fueling on the Performance Behavior of a CI Engine Fueled With Pyro Oil–Diesel Blend as Fuel. Journal of Energy Resources Technology 2016;138(3):032206--8.

[54] Kodavasal J, Kolodziej CP, Ciatti SA, Som S. Computational Fluid Dynamics Simulation of Gasoline Compression Ignition. Journal of Energy Resources Technology 2015;137(3):032212--13.

Paper 24 **Bildiri 24**

ECO-FRIENDLY USES OF GASOLINE; SULFUR CONTENT

Cemil Koyunoglu[1]

Istanbul Technical University, Energy Institute, Ayazaga Campus, 34469, Maslak, Istanbul, Turkey, ckoyunoglu@itu.edu.tr

Abstract

Around the world, legislation mandating decreased emissions and lower levels of airborne pollutants is coming into effect. In response, refiners are implementing operational and processing changes to reduce sulfur levels in transportation fuels. New technologies are moving the downstream hydrocarbon processing industry toward cleaner, lower-sulfur transportation fuels. Sulfur-containing components exist in gasoline range hydrocarbons. A low-sulfur world doesn't come cheap, though. Refiners are investing billions of dollars in new units, upgrades/retrofits and expansions to meet new sulfur and emissions regulations. These investments will help produce high-quality fuels that meet Euro 4, Euro 5 and Euro 6 specifications. Many refiners around the globe have adopted European standards for fuel quality, as Europe has been the frontrunner on regulations for low-sulfur, "clean" transportation fuels. The total sulfur content is an important test parameter in gasoline. The most widely specified method for total sulfur content is ASTM Test Methods D5453. In this review, the importance of the total sulfur for the eco-friendly gasoline approaches is presented.

Keywords: Gasoline sulfur contents; ASTM regulations; technological advancements; sulfur reductions

---

[1]Corresponding author at: Energy Institute, Istanbul Technical University, Sariyer, 34469, Turkey. E-mail address: ckoyunoglu@itu.edu.tr

1. Introduction

Sulfur is a nonmetallic element that is chemically bound into the marine fuel [1, 2]. Sulfur originates in crude oil and is concentrated into the higher density residual fractions [3, 4]. The marine residual fuel has capped sulfur content at 4.5 weight percent to begin to control oxides of sulfur (SO_x) [5, 6]. When sulfur is burned in the diesel engine it causes several problems, primarily in promoting corrosive wear of the piston rings and cylinder liners and by causing deposits in the ring zone [7-9]. During the combustion process, sulfur dioxide and sulfur trioxide form in the cylinder [9, 10]. These sulfur compounds then combine with water vapor forming sulfuric acid and sulfurous, which can cause aggressive corrosion [11, 12]. Among the various components of FCC gasoline, Cat cracked naphtha is the largest piece of the pie and is also the primary source of sulfur (See Fig. 1.) [13].

When sulfuric acid vapor leaves the cylinder and contacts low-temperature surfaces of the heat recovery boiler, the gaseous sulfuric acid condenses and forms highly corrosive (liquid) sulfuric acid [9, 14, 15]. So, in addition to ring and liner damage [16], the sulfuric acid can attack valve guides, as well as the cooler parts of the heat recovery boiler [9, 17, 18].

Diesel engines can be designed to prevent low-temperature corrosion by maintaining surface temperatures above the sulfuric acid condensation temperature, as shown in Fig. 2. [19]. Sulfur in marine fuels is normally neutralized by using an alkaline (TBN) lube oil additive [20, 21]. The fuel sulfur level should be balanced against the lube oil TBN additives to just neutralize the sulfur [22-24]. If too much alkaline additive (TBN) is used, a harmful (abrasive) level of alkaline material is produced that can increase the wear of the cylinder liner and the piston rings [25, 26]. The average sulfur level in marine fuels today is 2.8-3.0 weight percent

Assessment assays consists of a minimal variety of examinations typically limited to the unrefined petroleum [27][27]. Based upon released information, there is little agreement regarding to what makes up an assay of evaluation [28-30]. As the information are mainly for intra-company usage, there is little driving force for a basic plan. At a bare minimum, API gravity, as well as sulfur content, are typically figured out, even though it works to likewise understand the pour point, which offers some fundamental u [31-34].

Understanding of the unrefined petroleum's aromaticity [28-30, 35-39]. A more comprehensive evaluation assay could contain the adhering to examinations: API gravity (or density or relative density), total sulfur content, pour point, viscosity, salt content, water and sediment content [28]. Private refiners might replace or include examinations (e.g., trace metals or organic

halides) that might be crucial to their procedures [28]. To combine the outcomes from these couple of examinations of a present unrefined petroleum batch with the archived information from an extensive assay, the procedure designer will have the ability to estimate typically the product slate that the crude will produce as well as any type of remarkable handling issues that might become across [28, 40, 41].

The sulfur content of an unrefined petroleum, which might differ from less compared to 0.1 to over 5 mass-%, is among its most essential quality associates [42, 43]. Sulfur compounds add to refinery devices corrosion as well as catalysts poisoning, trigger corrosiveness in refined products, and add to ecological contamination as an outcome of the fuel products burning [44-46]. Sulfur compounds might be exist throughout the boiling unrefined oils variety although, generally, they are more plentiful in the heavier fractions [47-49]. In some unrefined oils, thermally labile sulfur compounds could break down on heating to create hydrogen sulfide that is extremely harmful and also very corrosive [50-53]. Till recently, among the most commonly utilized techniques for total sulfur content decision has been a sample in oxygen combustion to transform the sulfur to sulfur dioxide [54], which is gathered as well as consequently titrated iodometrically or spotted by nondispersive infrared (ASTM Examination Technique D1552, Sulfur in Petroleum Products (High-Temperature Method)) [55]. An also older technique including burning in a bomb with succeeding gravimetric determination of sulfur as barium sulfate (ASTM Examination Technique D129 [56], Sulfur in Petroleum Products (General Bomb Method)) is not as precise as the high-temperature technique, potentially since disturbance from the sediment naturally existing in unrefined petroleum [56].

The older, classic methods are being replaced by two instrumental techniques (ASTM Examination Technique D4294, Sulfur in Petroleum Products by Energy-Dispersive X-Ray Fluorescence Spectroscopy as well as ASTM Examination Technique D2622, Sulfur in Petroleum Products by X-Ray Spectrometry) [57, 58]. D4294 has a little better repeatability and also reproducibility compared to the high-temperature technique as well as is versatile to field applications; nevertheless, this technique could be impacted by some typically existing disturbances such as halides [57]. D2622 has also much better accuracy and also the ability of fixing for disturbances, however, is presently restricted to laboratory usage, and also the devices is a lot more costly [58]. Hydrogen sulfide and mercaptans are typically identified by nonaqueous potentiometric titration with silver nitrate [59-61].

2. Methods

2.1. Sulfur Content

Total sulfur content of aviation gasoline is limited to 0.05 % mass maximum because most sulfur compounds have a deleterious effect on the antiknock effect of alkyl lead compounds [62-64]. If sulfur content were not limited, specified antiknock values would not be reached for highly leaded grades of aviation gasoline [65-67]. The sulfur content measures due to the ASTM examination for sulfur in petroleum products (lamp technique) (D1266/IP 107) or due to the ASTM examination for sulfur in petroleum products by X-Ray spectrometry (D2622/IP 447) [58, 68]. Fig. 3. reveals large reduction in sulfur from Euro 3 to Euro 4 requirements and from the base case to Euro 2 requirements [69].

In the engine system, the various metals is done a corroding action by some sulfur compounds. Effects vary via the sulfur compound chemical type present. Hydrogen sulfide and elemental sulfur are particularly implicated. Because copper is considered the most sensitive metal, fuel corrosivity toward copper is measured in ASTM Examination for detection of copper corrosion from petroleum products by the copper strip examination (D130/IP 154) [70].

In this section, various examinations techniques for total sulfur determination explained. In addition, some of the engine operating problems related sulfur content are discussed.

2.1.1. ASTM D 1266

This examination technique covers the overall sulfur in fluid oil products resolution in mass (%) concentrations from 0.01 to 0.4. In this examination, an unique sulfate evaluation treatment is explained and allows the sulfur in concentrations decision as reduced as 5 mg/kg [68].

In examination technique D2784, the similar lamp technique for the sulfur decision in liquefied oil gas is explained [71]. To use the high-temperature technique (examination technique D1552) or the high-pressure decay device technique (examination technique D129) the quartz tube method (IP 63) for the sulfur decision in larger oil products that could not be burned in a lamp, [55, 56, 68].

2.1.1.1. Summary of the D 1266

The sample is burned in a shut system, utilizing an appropriate lamp as well as an synthetic environment made up of 70 % CO_2 and 30 % oxygen avoiding nitrogen oxides development. The sulfur oxides are oxidized and are soaked up to sulfuric acid by methods of hydrogen

peroxide solution which is then purged with air to eliminate liquefied CO_2. In the absorbent sulfur as sulfate is identified acidimetrically by titration with basic sodium hydroxide solution, or gravimetrically by precipitation as barium sulfate. Additionally, the sample might be burned in air, in the absorbent, the sulfur as sulfate being identified by precipitation as barium sulfate for weighing [68].

In the lack of acid-forming or base-forming components, besides sulfur, results by the volumetric and also gravimetric finishes explained are comparable within the limits of accuracy of the technique [68].

For sulfur components below 0.01 mass %, it is required to identify the sulfate material in the absorber solution turbidimetrically as barium sulfate [68].

2.1.2. ASTM D 2622

This test technique covers overall sulfur the decision in oil and also oil products that are either liquid at ambient conditions, soluble in hydrocarbon solvents, or liquefiable with moderate warm and single-phase. These products could consists of diesel fuel, kerosene, jet fuel, residual oil, various other distillate oil, naphtha, hydraulic oil, lubricating base oil, unleaded gasoline, unrefined petroleum, biodiesel, and also gasoline-ethanol blends [58].

This test technique variety is between the 3 mg/kg total sulfur The Pooled Limit of Quantitation (PLOQ) value (computed by treatments constant with practice D6259) and the greatest level sample in the round robin, % 4.6 weight of total sulfur [58, 72].

Instrumentation covered by this examination technique could differ in sensitivity level. The examination technique applicability of at sulfur concentrations below 3 mg ⁄kg might be identified on an private basis for WDXRF tools efficient in determining lower degrees, however, accuracy in this examination technique does not use [58].

2.1.2.1. Summary of the D 2622

The sample is put in the X-ray beam, and also the sulfur Kα line top strength at 0.5373 nm is determined. The history strength, determined at a suggested 0.5190 nm wavelength (0.5437 nm for a Rh target tube) is deducted from the top strength. The resultant net checking rate is after that compared with a formerly prepared calibration curve or formula acquiring the sulfur concentration in milligrams per kilogram (mg/kg) or mass percent [58].

2.1.3. ASTM D 130

This examination technique covers the corrosiveness decision to copper of air travel turbine fuel, automobile gasoline, aviation gasoline, cleaners (e.g. Stoddard solvent), kerosene, diesel fuel, lubricating oil, natural gasoline, and also distillate fuel oil or various other hydrocarbons having a vapor pressure no higher than 124 kPa (18 psi) at 37.8°C [73]. (Some products, especially natural gasoline, might have a much greater vapor pressure compared to would typically be particular of automobile or aeronautics gasolines. Therefore, workout severe care to make sure that the pressure vessel utilized in this test examination and also including various other high vapor pressure products or natural gasoline are not put in the 100°C (212°F) bath. Samples having 124 kPa (18 psi) vapor pressures in extra might establish adequate pressures at 100°C bursting the pressure vessel. Sample for any type having more than 124 kPa (18 psi) vapor pressure, usage examination technique D1838) [74].

2.1.3.1. Summary of the D 130

A copper strip of refined is submerged in a particular the sample quantity being warmed and evaluated under temperature level conditions and also time that are particular to the material class being evaluated. At the heating duration end, the copper strip is eliminated, cleaned, the color and tarnish degree analyzed versus the ASTM copper strip corrosion regulation [70].

2.1.4. ASTM D 6334

This examination technique covers the measurable resolution of overall sulfur in gasoline-oxygenate blends and regular gasoline. PLOQ was figured out to be 15 mg⁄kg. Consequently, the useful variety for this examination technique is from 15 mg⁄kg to 940 mg⁄kg [75].

This concentration variety is based upon that utilized in the interlaboratory round robin, which reveals that the sulfur variety in the round robin samples was from 1.5 mg⁄kg to 940 mg⁄kg; nonetheless, below 15 mg⁄kg, the reproducibility comes close to 100 % of the concentration [75].

2.1.4.1. Summary of the D 6334

The sample is put in the X-ray beam, as well as the sulfur Kα line strength at 5.373 Å is determined. The strength of a corrected history, determined at a suggested wavelength of 5.190 Å, or if a rhodium tube is made use of, 5.437 Å, is deducted from this strength. The resultant net checking rate is after that compared with a formerly prepared formula or calibration curve acquiring the sulfur (in mg/kg) concentration. (Exposure to extreme X radiation amounts is

damaging to health. As a result, it is essential that the operator prevent subjecting any type of component of his/her individual, not just to main X-rays, but also to additional or scattered radiation that may be existing. The X-ray spectrometer need to be run conformity with the policies of suggestions controlling the using ionizing radiation) [75].

2.1.5. ASTM D 4294

This examination technique covers the overall sulfur resolution in oil and also oil products that are single-phase as well as either soluble in hydrocarbon solvents or liquid at ambient conditions, liquefiable with moderate warm [76-79]. These materials could consists of jet fuel, diesel fuel, other distillate oil, kerosene, naphtha, lubricating base oil, hydraulic oil, residual oil, crude oil, gasoline-ethanol blends, biodiesel, unleaded gasoline as well as comparable oil products [76, 80].

Oxygenated fuels with methanol or ethanol components surpassing the limitations provided in this requirement could be handled utilizing this examination technique, however, the accuracy and also predisposition declarations do not use (see ASTM D 4294) [76, 81].

For samples with high oxygen components (>3 % weight) sample dilution or matrix coordinating need to be carried out to guarantee precise outcomes [76, 81].

2.1.5.1. Summary of the D 4294

The sample is put in the light beam produced from an X-ray tube [76]. The resultant thrilled particular X radiation is determined, and also the built-up matter is compared to matters from formerly prepared calibration samples acquiring the sulfur concentration mass percent or in mg/kg, or both. Three groups calibration samples minimum are needed covering the concentration variety: 0.0 mass % to 0.1 mass %, 0.1 mass % to 1.0 mass %, as well as 1.0 mass % to 5.0 mass % sulfur [76]. (see technique D7343 in detail) [82].

2.1.6. ASTM D 7039

This examination technique covers the overall sulfur decision by monochromatic wavelength-dispersive X-ray fluorescence (MWDXRF) spectrometry in diesel fuel, single-phase gasoline, refinery procedure streams utilized to mix diesel and gasoline, gasoline-ethanol blends, biodiesel blends, kerosene, biodiesel, as well as jet fuel[83-86].

Volatile samples such as light hydrocarbons or high-vapor-pressure gasolines could not satisfy the specified accuracy as a result of the evaporation of light elements throughout the evaluation [83].

2.1.6.1. Summary of the D 7039

A monochromatic X-ray light beam with a wavelength appropriate thrilling the sulfur K-shell electrons is focused into an examination sampling included in a sample cell [83]. The fluorescent Kα radiation at 0.5373 nm (5.373 Å) produced by sulfur is gathered by a repaired monochromator (analyzer). The sulfur X rays strength (counts each second) is determined utilizing an appropriate detector as well as transformed to the sulfur concentration (mg/kg) in an examination sampling utilizing a calibration formula [83].

Excitation by monochromatic X rays decreases history, simplifies matrix adjustment, as well as enhances the signal/background proportion contrasted to polychromatic excitation utilized in traditional WDXRF methods [85]. (Exposure to extreme amounts of X-ray radiation is harmful to health. The operator requires taking suitable activities preventing to subject any his/her body type, not just to main X rays, however likewise to scattered radiation or additional that may be existing. The X-ray spectrometer need to be run in conformity with the policies regulating the ionizing radiation usage) [83].

2.2. Maximum Sulfur Content

Current ASTM and CGSB standards allow 0.10% mass maximum sulfur content for nonleaded gasoline, but lower levels are required by various sulfur regulations (California or Canadian Sulfur in Gasoline regulation) [87-92]. Sulfur is oxidized to SO_2 over the catalyst, so essentially competes for reactive sites that could otherwise be effective for HC, CO or NOx conversion [92].

This appears as a temporary decrease in catalyst activity at high fuel sulfur levels and leads to the requirement for ultra-low sulfur fuels to attain ultra-low emissions. Sulfur can be indirectly limited by RFC composition controls based on emission models (U.S. EPA complex model, BC TOx/NOx, and Canadian CEPA Benzene in Gasoline regulation Benzene Emission Number (BEN) requirements) (See Fig. 4.) [93-96]. The sulfur concentration in gasoline referred to in BEN must be measured in accordance with after December 31, 2003, the American Society for Testing and Materials method D 5453-00, Standard Test Method for Determination of Total Sulphur in Light Hydrocarbons, Motor Fuels and Oils by Ultraviolet Fluorescence [97].

According to Table 1, the sulfur range for gasoline must be within the range between 0 and 100 mg/kg. In addition, Fig. 5. is shown how calculate model parameters for EPA regulations as in BEN for Canada.

Both Canada and the United States have regulations in place that will reduce sulfur to 30 ppm YPA phased in between 2002 and 2010, coincident with introduction of low emission Tier 2 vehicles [98-101].

2.3. Effect of Reformulated Gasoline (RFG) on Emissions from Current and Future Vehicles

Sulfur was the only fuel property studied in Phase I whose reduction caused significant reductions (16~, 13%, and 9~) in all three exhaust emission constituents, NMHC, CO, and NOx [102-106] (See Fig. 6. and 7. for impact of RFG comparison to MTBE combustion on emissions) [107]. Fig. 6. reveals the change in the certain hydrocarbon species mass emission rates between Reformulated gasoline to contain nonoxygenated Reformulated gasoline and MTBE, based on engine-out vehicle dynamometer emission tests to use Bag 1 results and FTP composite results (1996, Auto/Oil) [107]. Fig. 7. exhibits a similar comparison between vehicle emissions for MTBE with RFG relative to nonoxygenated Reformulated gasoline, on condition for vehicle exhaust (tailpipe) emissions for Federal Tier 1 (1994 MY) vehicles [107]. Furthermore, it was observed that the sulfur effect was reversible when changing from one sulfur level to another and that the effect took place only in the catalytic converter (engine-out emissions were unaffected) [108, 109]. (See Fig. 8. and 9. for reformulated gasoline emissions and regulations) [110, 111].

Reducing fuel sulfur level improved converter efficiency [112, 113]. For NOx, reducing olefin and sulfur content caused statistically significant reductions in NOx, whereas reducing T90 caused a statistically significant increase [114-119]. Gasolines with lower sulfur content could help improve the in-use performance of catalytic emission control systems which are "poisoned" by sulfur [120-122]. Refinery catalyst performance and life may also improve if more sulfur is removed to produce low sulfur gasolines [123].

2.4. Fuel Factors to Influence Deposits in Intake Portion of Gasoline Engines Fuel System

The caustic treating processes used for sulfur removal were designed so that these compounds were allowed to remain in the finished gasoline [124]. Shortly after World War II, an epidemic of intake deposition complaints was experienced [125]. Field studies by research and

subsequent laboratory investigations indicated that these difficulties were probably attributable to the presence of acid oils [126]. In most instances, the trouble was eliminated by the application of more efficient caustic washing for the removal of phenolic material as well as some of the more acidic sulfur compounds [127, 128].

There has been a large reduction in the amount of high-sulfur and high nitrogen thermal gasoline in our total gasoline pool (real bad actors like coker and vis-breaker gasoline have in most cases been removed and are now used as charging stock for other refining units) [129, 130].

Hydrogenation processes which remove sulfur, nitrogen, oxygen, olefins and metallic impurities have come into widespread use in the past three years [131-135] (See Fig. 10. and 11. for of the first stage and quench section of gasoline hydrogenation process) [136].

Where mercaptan sulfur and unwanted oxygenated compounds have been a problem in a modest number of cases, efficient extraction processes utilizing caustic soda with solubilizing agents have been placed in operation to remove these contaminants (see Fig. 12.) [13, 137-139].

2.5. Sulfur Reduction

Sulfur will likely be reduced in reformulated gasoline because sulfur affects the efficiency of catalytic converters [112, 140]. The major source of sulfur in the gasoline pool is catalytic cracked gasoline [141, 142]. An effective way reducing sulfur is hydrotreating the catalytic cracked gasoline tail end because half of the sulfur is concentrated in the last 10% of a normal heavy catalytic cracked gasoline fraction [143-147]. A fixed bed reactor (Fig. 13(a).) was used carrying out the reduction, hydrodesulfurization, and aromatic hydrogenation tests. Catalysts were packed into the reactor column shown schematically in Fig. 13(b). [148]. Fig. 14. shows that sulfur content in the treated gasoline was less than 12 ppm for around 100 h. But, more work is must accordingly regenerate the catalyst reducing sulfur level down 1ppm or lower [148]. Ma et al. studied the removal of sulfur by using Ni-based solvent and they reported a 150 mg/L sulfur reduction in a hydrotreated naphtha at 350 ^{o}C with a few amount of hydrogen environment [149].

3. Conclusions

Due to the environmental regulations, the sulfur concentrations in gasoline should be lower than 10 ppm. Gasolines with lower sulfur content could help improve the in-use performance of catalytic emission control systems which are "poisoned" by sulfur. Refinery catalyst

performance and life may also improve if more sulfur is removed to produce low sulfur gasolines. To remove sulfur compounds and benzene from gasoline zeolite catalyst is using as an alternative solution. ExxonMobil declared to raise manufacturing ultra-low sulfur gasolines approximately 6400000L/day, the company will start to establish SCANfining flexible technology to produce according to EPA's Tier 3 for gasoline specifications by 2018 in Beaumont refinery. The new desulfurization technologies for gasoline such as pervaporation process which is based on a membrane offering a wide range variety of advantages compared to conventional separation process. This technology also presents low cost and effectively operable and offers an easy maintenance options. And the liquid phase mixtures are easily separated from the gasoline by this technique without hydrogen consumption, and lower octane reduction. Some computational methods for discovering desulfurization mechanism in gasoline are still studied.

Acknowledgements

Thanks for the people who had handled about the establishing fuel-oil laboratory called Inonu-Pal with me between 2007-2009 till it accredited. Thanks Rob Visser (Institute for Interlaboratory Studies, Manager in SGS Nederland B.V.), and Ing. Ronald Starink (Institute for Interlaboratory Studies Program Coordinator in SGS Nederland B.V.) for good cooperations and kindly understand as well as communicate with e-mail during accreditation.

REFERENCES

[1] Farahani M, Pagé DJYS, Turingia MP, Tucker BD. Storage Stability of Biodiesel and Ultralow Sulfur Diesel Fuel Blends. Journal of Energy Resources Technology 2009;131(4):041801--6.

[2] Koytsoumpa E-I, Bergins C, Buddenberg T, Wu S, Sigurbjörnsson Ó, Tran KC, et al. The Challenge of Energy Storage in Europe: Focus on Power to Fuel. Journal of Energy Resources Technology 2016;138(4):042002--10.

[3] Nishioka M, Tomich RS. Isolation of aliphatic sulfur compounds in a crude oil by a non-reactive procedure. Fuel 1993;72(7):1007-10.

[4] López L, Lo Mónaco S. Geochemical implications of trace elements and sulfur in the saturate, aromatic and resin fractions of crude oil from the Mara and Mara Oeste fields, Venezuela. Fuel 2004;83(3):365-74.

[5] D. Uhler A, A. Stout S, S. Douglas G. 10 - Chemical heterogeneity in modern marine residual fuel oils. Oil Spill Environmental Forensics. Burlington: Academic Press; 2007, p. 327-48.

[6] Uhler AD, Stout SA, Douglas GS, Healey EM, Emsbo-Mattingly SD. 13 - Chemical character of marine heavy fuel oils and lubricants. Standard Handbook Oil Spill Environmental Forensics (Second Edition). Boston: Academic Press; 2016, p. 641-83.

[7] 15 - Sulfur. Chemistry of the Elements (Second Edition). Oxford: Butterworth-Heinemann; 1997, p. 645-746.

[8] Wilbur CT, Wight DA. 24 - Fuels and fuel chemistry. Pounder's Marine Diesel Engines (Sixth Edition). Butterworth-Heinemann; 1984, p. 427-39.

[9] King MJ, Davenport WG, Moats MS. 3 - Sulfur burning. Sulfuric Acid Manufacture (Second Edition). Oxford: Elsevier; 2013, p. 19-29.

[10] Mackin MH. NINE - Chemical reactions. Study Guide to Accompany Basics for Chemistry. Academic Press; 1982, p. 165-92.

[11] Jurado N, Simms NJ, Anthony EJ, Oakey JE. Effect of co-firing coal and biomass blends on the gaseous environments and ash deposition during pilot-scale oxy-combustion trials. Fuel 2017;197(Supplement C):145-58.

[12] Hussain T, Syed AU, Simms NJ. Trends in fireside corrosion damage to superheaters in air and oxy-firing of coal/biomass. Fuel 2013;113(Supplement C):787-97.

[13] Dautzenberg FM, Angevine PJ. Encouraging innovation in catalysis. Catalysis Today 2004;93(Supplement C):3-16.

[14] Bahadori A. Estimation of combustion flue gas acid dew point during heat recovery and efficiency gain. Applied Thermal Engineering 2011;31(8):1457-62.

[15] ZareNezhad B, Aminian A. A multi-layer feed forward neural network model for accurate prediction of flue gas sulfuric acid dew points in process industries. Applied Thermal Engineering 2010;30(6):692-6.

[16] Taylor DA. 3 - Measuring instruments. Marine Control, Practice. Butterworth-Heinemann; 1987, p. 33-82.

[17] Sajjad H, Masjuki HH, Varman M, Kalam MA, Arbab MI, Imtenan S, et al. Engine combustion, performance and emission characteristics of gas to liquid (GTL) fuels and its blends with diesel and bio-diesel. Renewable and Sustainable Energy Reviews 2014;30(Supplement C):961-86.

[18] Srikanth S, Ravikumar B, Das SK, Gopalakrishna K, Nandakumar K, Vijayan P. Analysis of failures in boiler tubes due to fireside corrosion in a waste heat recovery boiler. Engineering Failure Analysis 2003;10(1):59-66.

[19] Zhang J, He K, Ge Y, Shi X. Influence of fuel sulfur on the characterization of PM10 from a diesel engine. Fuel 2009;88(3):504-10.

[20] Kumar Bose P, Banerjee R. An Experimental Investigation on the Role of Hydrogen in the Emission Reduction and Performance Trade-Off Studies in an Existing Diesel Engine Operating in Dual Fuel Mode Under Exhaust Gas Recirculation. Journal of Energy Resources Technology 2012;134(1):012601--15.

[21] Srinivasan KK, Mago PJ, Zdaniuk GJ, Chamra LM, Midkiff KC. Improving the Efficiency of the Advanced Injection Low Pilot Ignited Natural Gas Engine Using Organic Rankine Cycles. Journal of Energy Resources Technology 2008;130(2):022201--7.

[22] Choi S, Seong H. Lube oil-dependent ash chemistry on soot oxidation reactivity in a gasoline direct-injection engine. Combustion and Flame 2016;174:68-76.

[23] Di Natale F, Carotenuto C. Particulate matter in marine diesel engines exhausts: Emissions and control strategies. Transportation Research Part D: Transport and Environment 2015;40(Supplement C):166-91.

[24] Sandalcı T, Karagöz Y. Experimental investigation of the combustion characteristics, emissions and performance of hydrogen port fuel injection in a diesel engine. International Journal of Hydrogen Energy 2014;39(32):18480-9.

[25] Mignard D, Pritchard C. A review of the sponge iron process for the storage and transmission of remotely generated marine energy. International Journal of Hydrogen Energy 2007;32(18):5039-49.

[26] Ahluwalia RK, Hua TQ, Peng JK. On-board and Off-board performance of hydrogen storage options for light-duty vehicles. International Journal of Hydrogen Energy 2012;37(3):2891-910.

[27] Intake Valve Deposits in Gasoline Direct Injection Engines; Available from: http://www.aa1car.com/library/intake_valve_deposits_gdi_engines.htm. [Accessed 06.06 2017].

[28] Speight JG. Chapter 5 - Evaluation of Reservoir Fluids. Introduction to Enhanced Recovery Methods for Heavy Oil and Tar Sands (Second Edition). Boston: Gulf Professional Publishing; 2016, p. 177-250.

[29] Speight JG. Chapter 3 - Properties and Evaluation. Heavy Oil Production Processes. Boston: Gulf Professional Publishing; 2013, p. 37-62.

[30] Speight JG. CHAPTER 4 - PROPERTIES. Enhanced Recovery Methods for Heavy Oil and Tar Sands. Gulf Publishing Company; 2009, p. 95-132.

[31] Lähteenmäki-Uutela A, Repka S, Haukioja T, Pohjola T. How to recognize and measure the economic impacts of environmental regulation: The Sulphur Emission Control Area case. Journal of Cleaner Production 2017;154(Supplement C):553-65.

[32] Cao T, Lee H, Hwang Y, Radermacher R, Chun H-H. Performance investigation of engine waste heat powered absorption cycle cooling system for shipboard applications. Applied Thermal Engineering 2015;90(Supplement C):820-30.

[33] Brynolf S, Magnusson M, Fridell E, Andersson K. Compliance possibilities for the future ECA regulations through the use of abatement technologies or change of fuels. Transportation Research Part D: Transport and Environment 2014;28(Supplement C):6-18.

[34] Tse LKC, Wilkins S, McGlashan N, Urban B, Martinez-Botas R. Solid oxide fuel cell/gas turbine trigeneration system for marine applications. Journal of Power Sources 2011;196(6):3149-62.

[35] Speight JG. Chapter 1 - Heavy Oil and Tar Sand Bitumen. Introduction to Enhanced Recovery Methods for Heavy Oil and Tar Sands (Second Edition). Boston: Gulf Professional Publishing; 2016, p. 3-48.

[36] Speight JG. Chapter 9 - Chemical and Physical Properties of Hydrocarbons. Handbook of Industrial Hydrocarbon Processes. Boston: Gulf Professional Publishing; 2011, p. 325-53.

[37] Adlakha J, Singh P, Ram SK, Kumar M, Singh MP, Singh D, et al. Optimization of conditions for deep desulfurization of heavy crude oil and hydrodesulfurized diesel by Gordonia sp. IITR100. Fuel 2016;184(Supplement C):761-9.

[38] Dehkissia S, Larachi F, Rodrigue D, Chornet E. Characterization of Doba–Chad heavy crude oil in relation with the feasibility of pipeline transportation. Fuel 2004;83(16):2157-68.

[39] Snape CE, Bartle KD. Definition of fossil fuel-derived asphaltenes in terms of average structural properties. Fuel 1984;63(7):883-7.

[40] Raimondi A, Favela-Contreras A, Beltrán-Carbajal F, Piñón-Rubio A, Luis de la Peña-Elizondo J. Design of an adaptive predictive control strategy for crude oil atmospheric distillation process. Control Engineering Practice 2015;34(Supplement C):39-48.

[41] Al-Ayed OS, Matouq Md. Factors Affecting Sulfur Reactions in High Sulfur Oil Shale Pyrolysis. Journal of Energy Resources Technology 2009;131(1):012501--4.

[42] Laredo GC, López CR, Álvarez RE, Cano JL. Naphthenic acids, total acid number and sulfur content profile characterization in Isthmus and Maya crude oils. Fuel 2004;83(11):1689-95.

[43] Speight JG. Chapter 1 - Occurrence and Formation of Crude Oil and Natural Gas. Subsea and Deepwater Oil and Gas Science and Technology. Boston: Gulf Professional Publishing; 2015, p. 1-43.

[44] Speight JG. Chapter 2 - Mechanism of Acid Corrosion. High Acid Crudes. Boston: Gulf Professional Publishing; 2014, p. 31-55.

[45] Ramirez-Corredores MM. Chapter 4 - Acidity in Crude Oils: Naphthenic Acids and Naphthenates. The Science and Technology of Unconventional Oils. Amsterdam: Academic Press; 2017, p. 295-385.

[46] Singh R. 6 - Corrosion and Corrosion Protection. Pipeline Integrity Handbook (Second Edition). Gulf Professional Publishing; 2017, p. 241-70.

[47] Meriem-Benziane M, Bou-Saïd B, Boudouani N. The effect of crude oil in the pipeline corrosion by the naphthenic acid and the sulfur: A numerical approach. Journal of Petroleum Science and Engineering 2017;158(Supplement C):672-9.

[48] Cadorim HR, Pereira ÉR, Carasek E, Welz B, de Andrade JB. Determination of sulfur in crude oil using high-resolution continuum source molecular absorption spectrometry of the SnS molecule in a graphite furnace. Talanta 2016;146(Supplement C):203-8.

[49] Djokic MR, Ristic ND, Olahova N, Marin GB, Van Geem KM. Quantitative on-line analysis of sulfur compounds in complex hydrocarbon matrices. Journal of Chromatography A 2017;1509(Supplement C):102-13.

[50] Majchrowicz BB, Franco DV, Yperman J, Reggers G, Gelan J, Martens H, et al. An investigation into the changes of structure and reactivity during desulphurization of a bituminous coal. Fuel 1991;70(3):434-41.

[51] Amrani A, Deev A, Sessions AL, Tang Y, Adkins JF, Hill RJ, et al. The sulfur-isotopic compositions of benzothiophenes and dibenzothiophenes as a proxy for thermochemical sulfate reduction. Geochimica et Cosmochimica Acta 2012;84(Supplement C):152-64.

[52] Shi H, Taylor LT, Fujinari EM, Yan X. Sulfur-selective chemiluminescence detection with packed column supercritical fluid chromatography. Journal of Chromatography A 1997;779(1):307-13.

[53] Weissman JG, Kessler RV. Downhole heavy crude oil hydroprocessing. Applied Catalysis A: General 1996;140(1):1-16.

[54] Milton BE. Chapter 8 - Control Technologies in Spark-Ignition Engines A2 - Sher, Eran. Handbook of Air Pollution From Internal Combustion Engines. San Diego: Academic Press; 1998, p. 189-258.

[55] Standard Test Method for Sulfur in Petroleum Products by High Temperature Combustion and Infrared (IR) Detection or Thermal Conductivity Detection (TCD). ASTM International; 2016.

[56] Standard Test Method for Sulfur in Petroleum Products (General High Pressure Decomposition Device Method). ASTM International; 2013.

[57] Standard Test Methods for Rubber Property—Adhesion to Rigid Substrates. ASTM International; 2014.

[58] Standard Test Method for Sulfur in Petroleum Products by Wavelength Dispersive X-ray Fluorescence Spectrometry. ASTM International; 2016.

[59] Barbosa LL, Sad CMS, Morgan VG, Figueiras PR, Castro ERV. Application of low field NMR as an alternative technique to quantification of total acid number and sulphur content in petroleum from Brazilian reservoirs. Fuel 2016;176(Supplement C):146-52.

[60] Hofmann K, Hamm R. Sulfhydryl and Disulfide Groups in Meats**Dedicated to Professor Dr. Alfons Schoberl, Hannover (Germany), a pioneer in the chemistry of organic sulfur compounds. In: Chichester CO, editor Advances in Food Research. Academic Press; 1978, p. 1-111.

[61] Almasvandi MH, Rahimi M, Tagheie Y. Microfluidic cold stripping of H2S from crude oil in low temperature and natural gas consumption. Journal of Natural Gas Science and Engineering 2016;34(Supplement C):499-508.

[62] Stout SA, Douglas GS, Uhler AD. 11 - Chemical fingerprinting of gasoline and distillate fuels. Standard Handbook Oil Spill Environmental Forensics (Second Edition). Boston: Academic Press; 2016, p. 509-64.

[63] Yang C, Lambert P, Zhang G, Yang Z, Landriault M, Hollebone B, et al. Characterization of chemical fingerprints of unconventional Bakken crude oil. Environmental Pollution 2017;230(Supplement C):609-20.

[64] Speight JG. 2 - Production, properties and environmental impact of hydrocarbon fuel conversion A2 - Khan, M. Rashid. Advances in Clean Hydrocarbon Fuel Processing. Woodhead Publishing; 2011, p. 54-82.

[65] Potapenko OV, Doronin VP, Sorokina TP, Likholobov VA. Hydrogen transfer in transformations of olefin and thiophene compounds for the refining of gasoline fractions. Fuel Processing Technology 2014;128(Supplement C):251-6.

[66] Shehata MS. Emissions, performance and cylinder pressure of diesel engine fuelled by biodiesel fuel. Fuel 2013;112(Supplement C):513-22.

[67] Lin CY, Tjeerdema RS. Crude Oil, Oil, Gasoline and Petrol A2 - Jørgensen, Sven Erik. In: Fath BD, editor Encyclopedia of Ecology. Oxford: Academic Press; 2008, p. 797-805.

[68] Standard Test Method for Sulfur in Petroleum Products (Lamp Method). ASTM International; 2013.

[69] Hao J, Hu J, Fu L. Controlling vehicular emissions in Beijing during the last decade. Transportation Research Part A: Policy and Practice 2006;40(8):639-51.

[70] Standard Test Method for Corrosiveness to Copper from Petroleum Products by Copper Strip Test. ASTM International; 2012.

[71] Standard Test Method for Sulfur in Liquefied Petroleum Gases (Oxy-Hydrogen Burner or Lamp). ASTM International; 2006.

[72] Standard Practice for Determination of a Pooled Limit of Quantitation for a Test Method. ASTM International; 2015.

[73] Kamal A, Gollahalli SR. Effects of Jet Reynolds Number on the Performance of Axisymmetric and Nonaxisymmetric Gas Burner Flames. Journal of Energy Resources Technology 2000;123(2):167-72.

[74] Standard Test Method for Copper Strip Corrosion by Liquefied Petroleum (LP) Gases. ASTM International; 2016.

[75] Standard Test Method for Sulfur in Gasoline by Wavelength Dispersive X-Ray Fluorescence. ASTM International; 2017.

[76] Standard Test Method for Sulfur in Petroleum and Petroleum Products by Energy Dispersive X-ray Fluorescence Spectrometry. ASTM International; 2016.

[77] Lee S-H, Uy B, Kim S-H, Choi Y-H, Choi S-M. Behavior of high-strength circular concrete-filled steel tubular (CFST) column under eccentric loading. Journal of Constructional Steel Research 2011;67(1):1-13.

[78] Mello PA, Pereira JSF, Mesko MF, Barin JS, Flores EMM. Sample preparation methods for subsequent determination of metals and non-metals in crude oil—A review. Analytica Chimica Acta 2012;746(Supplement C):15-36.

[79] Pereira RG, de Abreu FLB, Fernandes DLT, Romeiro GA, de Andrade ET. Exhaust Emissions and Electric Energy Generation in a Stationary Engine Using Blends of Diesel and a Fuel Obtained Through the Low Temperature Conversion Process Applied to Petrochemical Residue. Journal of Energy Resources Technology 2011;132(4):044502--4.

[80] Lois E, Keating EL, Gupta AK. Fuels A2 - Meyers, Robert A. Encyclopedia of Physical Science and Technology (Third Edition). New York: Academic Press; 2003, p. 275-314.

[81] Hollebone B. Chapter 3 - Oil Physical Properties: Measurement and Correlation A2 - Fingas, Mervin. Oil Spill Science and Technology (Second Edition). Boston: Gulf Professional Publishing; 2017, p. 185-207.

[82] Standard Practice for Optimization, Sample Handling, Calibration, and Validation of X-ray Fluorescence Spectrometry Methods for Elemental Analysis of Petroleum Products and Lubricants. ASTM International; 2017.

[83] Standard Test Method for Sulfur in Gasoline, Diesel Fuel, Jet Fuel, Kerosine, Biodiesel, Biodiesel Blends, and Gasoline-Ethanol Blends by Monochromatic Wavelength Dispersive X-ray Fluorescence Spectrometry. ASTM International; 2015.

[84] Adachi G-Y, Imanaka N, Zhang F. Chapter 99 Rare earth carbides. Handbook on the Physics and Chemistry of Rare Earths. Elsevier; 1991, p. 61-189.

[85] Yang B, Wang S, Tian S, Liu L. Determination of hydrogen sulfide in gasoline by Au nanoclusters modified glassy carbon electrode. Electrochemistry Communications 2009;11(6):1230-3.

[86] Azócar L, Ciudad G, Heipieper HJ, Muñoz R, Navia R. Improving fatty acid methyl ester production yield in a lipase-catalyzed process using waste frying oils as feedstock. Journal of Bioscience and Bioengineering 2010;109(6):609-14.

[87] Mohebali G, Ball AS. Biodesulfurization of diesel fuels – Past, present and future perspectives. International Biodeterioration & Biodegradation 2016;110(Supplement C):163-80.

[88] Lin L, Zhang Y, Kong Y. Recent advances in sulfur removal from gasoline by pervaporation. Fuel 2009;88(10):1799-809.

[89] Babich IV, Moulijn JA. Science and technology of novel processes for deep desulfurization of oil refinery streams: a review☆. Fuel 2003;82(6):607-31.

[90] Desulfurising gasoline or diesel. Fuel Cells Bulletin 2001;3(29):16.

[91] Shelef M. Sulfur in gasoline in the US: On its way out? Applied Catalysis B: Environmental 1992;1(4):N34-N5.

[92] McCabe RW, Armor JN. Mechanisms of NOx removal. Applied Catalysis B: Environmental 1993;2(4):N35-N7.

[93] Shaw adds two technologies to meet environmental regulations. Focus on Catalysts 2011;2011(4):7.

[94] Laredo GC, Castillo J, Cano JL. Benzene reduction in gasoline range streams by adsorption processes using a PVDC–PVC carbon molecular sieve. Fuel 2014;135(Supplement C):459-67.

[95] Singh AP, Mukherji S, Tewari AK, Kalsi WR, Sarpal AS. Determination of benzene and total aromatics in commercial gasolines using packed column GC and NMR techniques. Fuel 2003;82(1):23-33.

[96] (EPA) EPA. Gasoline Sulfur Standards. EPA-420-B-16-004. The United States of America: EPA; 2016.

[97] Act. CEP. Benzene in Gasoline Regulations. *Application-Types and Uses of Gasoline.* SOR/97-493. Canada: Canadian Environmental Protection Act.; 1999.

[98] Chavez-Baeza C, Sheinbaum-Pardo C. Sustainable passenger road transport scenarios to reduce fuel consumption, air pollutants and GHG (greenhouse gas) emissions in the Mexico City Metropolitan Area. Energy 2014;66(Supplement C):624-34.

[99] Magyar S, Hancsók J, Kalló D. Hydrodesulfurization and hydroconversion of heavy FCC gasoline on PtPd/H-USY zeolite. Fuel Processing Technology 2005;86(11):1151-64.

[100] Graham LA, Belisle SL, Rieger P. Nitrous oxide emissions from light duty vehicles. Atmospheric Environment 2009;43(12):2031-44.

[101] Silva CM, Farias TL, Frey HC, Rouphail NM. Evaluation of numerical models for simulation of real-world hot-stabilized fuel consumption and emissions of gasoline light-duty vehicles. Transportation Research Part D: Transport and Environment 2006;11(5):377-85.

[102] Kohl AL, Nielsen RB. CHAPTER 7 - Sulfur Dioxide Removal. Gas Purification (Fifth Edition). Houston: Gulf Professional Publishing; 1997, p. 466-669.

[103] Gudaitytė I. The Research Methodology for Performance Indicators of the Transport Diesel Engine in Exploitation Conditions. Procedia Engineering 2016;134(Supplement C):256-62.

[104] Suarez-Bertoa R, Astorga C. Isocyanic acid and ammonia in vehicle emissions. Transportation Research Part D: Transport and Environment 2016;49(Supplement C):259-70.

[105] Suarez-Bertoa R, Mendoza-Villafuerte P, Riccobono F, Vojtisek M, Pechout M, Perujo A, et al. On-road measurement of NH3 emissions from gasoline and diesel passenger cars during real world driving conditions. Atmospheric Environment 2017;166(Supplement C):488-97.

[106] Olsson L. Motor vehicle air pollution control in Sweden. Science of The Total Environment 1994;146(Supplement C):27-34.

[107] Franklin PM, Koshland CP, Lucas D, Sawyer RF. Evaluation of combustion by-products of MTBE as a component of reformulated gasoline. Chemosphere 2001;42(5):861-72.

[108] Beck DD. Impact of sulfur on three-way automotive catalyst performance and catalyst diagnostics. In: Bartholomew CH, Fuentes GA, editors. Studies in Surface Science and Catalysis. Elsevier; 1997, p. 21-38.

[109] Schifter I, Díaz L, Vera M, Guzmán E, López-Salinas E. Impact of sulfur-in-gasoline on motor vehicle emissions in the metropolitan area of Mexico City☆. Fuel 2003;82(13):1605-12.

[110] Piel WJ. Transportation fuels of the future? Fuel Processing Technology 2001;71(1):167-79.

[111] Furman KC, Androulakis IP. A novel MINLP-based representation of the original complex model for predicting gasoline emissions. Computers & Chemical Engineering 2008;32(12):2857-76.

[112] Lappas AA, Valla JA, Vasalos IA, Kuehler C, Francis J, O'Connor P, et al. The effect of catalyst properties on the in situ reduction of sulfur in FCC gasoline. Applied Catalysis A: General 2004;262(1):31-41.

[113] Song C, Ma X. New design approaches to ultra-clean diesel fuels by deep desulfurization and deep dearomatization. Applied Catalysis B: Environmental 2003;41(1):207-38.

[114] Marchionna M, Di Girolamo M, Patrini R. Light olefins dimerization to high quality gasoline components. Catalysis Today 2001;65(2):397-403.

[115] Xu H, Wang C, Ma X, Sarangi AK, Weall A, Krueger-Venus J. Fuel injector deposits in direct-injection spark-ignition engines. Progress in Energy and Combustion Science 2015;50(Supplement C):63-80.

[116] Wang C, Zeraati-Rezaei S, Xiang L, Xu H. Ethanol blends in spark ignition engines: RON, octane-added value, cooling effect, compression ratio, and potential engine efficiency gain. Applied Energy 2017;191(Supplement C):603-19.

[117] Rajesh Kumar B, Saravanan S. Partially premixed low temperature combustion using dimethyl carbonate (DMC) in a DI diesel engine for favorable smoke/NOx emissions. Fuel 2016;180(Supplement C):396-406.

[118] Kim D, Bae C. Application of double-injection strategy on gasoline compression ignition engine under low load condition. Fuel 2017;203(Supplement C):792-801.

[119] Fang Z, Lin T, Xu H, Wu G, Sun M, Chen Y. Novel promoting effects of cerium on the activities of NOx reduction by NH3 over TiO2-SiO2-WO3 monolith catalysts. Journal of Rare Earths 2014;32(10):952-9.

[120] Kong Y, Lin L, Zhang Y, Lu F, Xie K, Liu R, et al. Studies on polyethylene glycol/polyethersulfone composite membranes for FCC gasoline desulphurization by pervaporation. European Polymer Journal 2008;44(10):3335-43.

[121] Antos GJ, Solari B, Monque R. Hydroprocessing to produce reformulated gasolines: The ISAL™ process. In: Froment GF, Delmon B, Grange P, editors. Studies in Surface Science and Catalysis. Elsevier; 1997, p. 27-40.

[122] Proost S, Van Dender K. Energy and environment challenges in the transport sector. Economics of Transportation 2012;1(1):77-87.

[123] Song C. An overview of new approaches to deep desulfurization for ultra-clean gasoline, diesel fuel and jet fuel. Catalysis Today 2003;86(1):211-63.

[124] Qi R, Wang Y, Li J, Zhu S. Sulfur removal from gasoline by pervaporation: The effect of hydrocarbon species. Separation and Purification Technology 2006;51(3):258-64.

[125] Henglein FA. 21 - The Chemical Technological Production of Materials. Chemical Technology. Pergamon; 1969, p. 382-695.

[126] Ramirez-Corredores MM. Chapter 6 - Emerging Technologies and Ideas with Potential. The Science and Technology of Unconventional Oils. Amsterdam: Academic Press; 2017, p. 489-676.

[127] Busca G, Berardinelli S, Resini C, Arrighi L. Technologies for the removal of phenol from fluid streams: A short review of recent developments. Journal of Hazardous Materials 2008;160(2):265-88.

[128] Burgess CE, Schobert HH. Direct liquefaction for production of high yields of feedstocks for specialty chemicals or thermally stable jet fuels. Fuel Processing Technology 2000;64(1):57-72.

[129] Boehme TR, Onder CH, Guzzella L. Dynamic model of an auto-thermal gasoline fuel processor. International Journal of Hydrogen Energy 2008;33(21):6150-64.

[130] Nagpal JM, Joshi GC, Rastogi SN. Stability of cracked naphthas from thermal and catalytic processes and their additive response. Part I. Evaluation of stability and additive response. Fuel 1995;74(5):714-9.

[131] Speight JG. Chapter 8 - Hydrotreating and Desulfurization. The Refinery of the Future. Boston: William Andrew Publishing; 2011, p. 237-73.

[132] Kilbane JJ, Le Borgne S. Chapter 2 Petroleum biorefining: the selective removal of sulfur, nitrogen, and metals. In: Vazquez-Duhalt R, Quintero-Ramirez R, editors. Studies in Surface Science and Catalysis. Elsevier; 2004, p. 29-65.

[133] Patterson HBW. Chapter 2 - Hydrogenation Process Techniques. Hydrogenation of Fats and Oils (Second Edition). AOCS Press; 2011, p. 33-48.

[134] Abstracts. Fuel and Energy Abstracts 2016;57(3):210-302.

[135] Abstracts. Fuel and Energy Abstracts 2015;56(1):2-94.

[136] Authayanun S, Pothong W, Saebea D, Patcharavorachot Y, Arpornwichanop A. Modeling of an industrial fixed bed reactor based on lumped kinetic models for hydrogenation of pyrolysis gasoline. Journal of Industrial and Engineering Chemistry 2008;14(6):771-8.

[137] Parkash S. CHAPTER SEVEN - Treating Processes. Refining Processes Handbook. Burlington: Gulf Professional Publishing; 2003, p. 210-9.

[138] Leitão A, Rodrigues A. Fixed-bed reactor for gasoline sweetening: Kinetics of mercaptan oxidation and simulation of the Merox reactor unit. Chemical Engineering Science 1990;45(3):679-85.

[139] Poe WA, Mokhatab S. Chapter 1 - Introduction to Natural Gas Processing Plants. Modeling, Control, and Optimization of Natural Gas Processing Plants. Boston: Gulf Professional Publishing; 2017, p. 1-72.

[140] Taylor KC. Automobile Catalytic Converters. In: Crucq A, Frennet A, editors. Studies in Surface Science and Catalysis. Elsevier; 1987, p. 97-116.

[141] Wang Z, Yang B, Chen C, Yuan J, Wang L. Modeling and optimization for the secondary reaction of FCC gasoline based on the fuzzy neural network and genetic algorithm. Chemical Engineering and Processing: Process Intensification 2007;46(3):175-80.

[142] Chen C, Yang B, Yuan J, Wang Z, Wang L. Establishment and solution of eight-lump kinetic model for FCC gasoline secondary reaction using particle swarm optimization. Fuel 2007;86(15):2325-32.

[143] Siddiqui MN. Conversion of hazardous plastic wastes into useful chemical products. Journal of Hazardous Materials 2009;167(1):728-35.

[144] Siddiqui MN, Redhwi HH. Pyrolysis of mixed plastics for the recovery of useful products. Fuel Processing Technology 2009;90(4):545-52.

[145] French R, Malone P. Phase equilibria of ethanol fuel blends. Fluid Phase Equilibria 2005;228(Supplement C):27-40.

[146] Coelho ST, Goldemberg J, Lucon O, Guardabassi P. Brazilian sugarcane ethanol: lessons learned[1]. Energy for Sustainable Development 2006;10(2):26-39.

[147] Farahbod F, Farahmand S. Introduction of Novel Process for Sweetening of Sour Crude Oil: Optimization of Process. Journal of Energy Resources Technology 2016;139(2):022907--9.

[148] Gupta M, He J, Nguyen T, Petzold F, Fonseca D, Jasinski JB, et al. "Nanowire catalysts for ultra-deep hydro-desulfurization and aromatic hydrogenation". Applied Catalysis B: Environmental 2016;180:246-54.

[149] Dehghan R, Anbia M. Zeolites for adsorptive desulfurization from fuels: A review. Fuel Processing Technology 2017;167(Supplement C):99-116.

Paper 25 **Bildiri 25**

EVALUATION OF CYCLE ANALYSIS IN WANKEL AND RECIPROCATING ENGINE

Ömer Cihan[a], Osman Akın Kutlar[b], Abdurrahman Demirci[c], Hüseyin Emre Doğan[b], Majid Javadzadehkalkhoran[b]
[a]Hakkari University, Engineering Faculty, Department of Mechanical Engineering, Hakkari, Turkey, E-mail: omercihan@hakkari.edu.tr
[b]Istanbul Technical University, Mechanical Faculty, Department of Mechanical Engineering, Istanbul, Turkey, E-mail: kutlar@itu.edu.tr, edogan@itu.edu.tr, javadzadehkalkh@itu.edu.tr
[c]Karamanoğlu Mehmetbey University, Engineering Faculty, Department of Mechanical Engineering, Karaman, Turkey, E-mail: arahmandemirci@kmu.edu.tr

Abstract

In this study, a single-rotor 13B-MSP (Multi Side Port) Wankel-type port fuel injection, 4-stroke and research engine and a single cylinder Antor 3LD 450, port fuel injection SI engine with three different type combustion chamber are used. Both engines were compared in same load, speed and excess air coefficient conditions. The indicator diagrams and cycle analysis were compared at 3 bar P_{me} load and 2000 rpm engine speed.
As a result; maximum pressure values were close to each other for the three combustion chamber geometries in reciprocating engine. The difference between them was due to flow and flame formation in the combustion chamber. In the Wankel engine, the maximum pressure value is lower than the others in test results and far away from the TDC. The reason for this is that the combustion speed is lower and it shifts toward the expansion stroke. This is due to low turbulence intensity during the compression process.
Keywords: Rotary engine, Wankel engine, SI engine, Indicator diagram, Cycle analysis

1. Introduction

The Wankel engines which are in the class of rotary engine, operate according to the four-stroke operating principle. Its operation is different in structure and principle compared to reciprocating engines. Only rotor and eccentric shaft act as moving parts in the Wankel engine. Compared to conventional piston engine; there is no valve assembly for intake and exhaust process. Also, the Wankel engine is provided with charge change through the ports on the side housing. The opening and closing times of the ports in side surfaces is limited by the moving rotor. The rotor provides rotational motion due to the pressure generated by the burning gases. By the way, the power is transmitted directly to the output shaft. Wankel engines can reach high rotational speeds. In addition, in evaluation of engine parts, it does not have a slider-crank mechanism compared to the reciprocating engine, therefore it has a simpler structure and less parts.
Other advantages of the Wankel engine can be listed as lighter weight, lower NOx emissions and more power production than reciprocating engine with same weight. In addition, it operates with lower vibration due to absence of reciprocating masses such as pistons and connecting rods [1-7].

2. Experimental Study

Antor 3LD 450 engine is used in reciprocating engine experiments [8-10]. General information about the engine is shown in Table 1. The engine is a single-cylinder direct-injection diesel engine in original. The process of converting the compression ignition engine to the spark

ignition engine was carried out by Kutlar [9].

The pistons with three combustion geometries (MR, cylindrical bowl, Flat) were assembled and tested in conventional piston engine (Figure 1).

a) **b)** **c)**

Figure 1. Produced MR (a), cylindrical bowl (b) and flat (c) combustion chamber geometries.

The other engine is Mazda 13B - MSP (Multi-Side Port) Wankel engine which wwas used in the experiments. The engine is originally twin-rotor. After conversion, it was transformed into a single rotor test engine [7]. The basic and geometrical properties of the engine are given in Table 2. Cylinder pressure measurement in reciprocating engine is done with AVL brand GU13Z-24 piezoelectric sensor, which was adapted to the spark plug. In Wankel engine, Kistler brand 6118BF107Q01 piezoelectric sensor has been used with a spark plug.

Table 1: General characteristics of piston engine [8].

Term	Value	Unit
Engine name	Antor 3LD 450	-
Number of cylinders	1	-
Stroke X Dimension	80X85	mm
Compression ratio	10,5	-
Stroke volume	454	cm^3
Connecting rod length	145	mm
Ratio of crank radius to connecting rod length	0,275	-
Intake valve opening advance	16	KMA
Intake valve closing delay	40	KMA
Exhaust valve opening advance	40	KMA
Exhaust valve closing delay	16	KMA

Table 2. Basic and geometric datas related to 13B MSP Wankel engine.

Term	Value	Unit
R (Rotor corner-center length)	105	mm
e (Eccentricity)	15	mm
b (Rotor width)	80	mm
ε (Compression ratio)	10	-

3. Experimental Results

The indicator diagrams and the cycle analysis of the Wankel test engine were compared with the test results of different combustion chamber geometries in the reciprocating engine. This engine has single cylinder and port fuel injection system. In the reciprocating engine experiments, different combustion chamber geometries (MR, Cylindrical bowl, Flat) with a compression ratio of 10.5 were used. The comparison was made in terms of the load and speed of the two types of engine and the selected point is the 3 bars break mean average effective pressure and 2000 rpm engine speed.

In conventional piston engine, maximum pressure values are close to each other in all three types of combustion chamber geometry. The difference in the combustion chamber geometry affects the flow and flame formation.

The maximum pressure of the Wankel test engine is much lower and is more distant from the TDC (Figure 2). This indicates that the combustion speed of the Wankel engine is lower than the conventional piston engine and shifts towards the expansion stroke. Previously, Cold flow models by Taşkıran showed that the turbulence intensity in the

combustion chamber is very low during compression [11].

When the charge change processes of engines are examined, the effect of load level was investigated on pumping losses. The pressure level remained relatively constant due to constant start of the intake after the TDC in the Wankel engine and the intake port remained fully open in most of the intake times (Figure 3).

Heat release rate is shown cumulatively for the engines at average effective pressure of 3 bar (Figure 4). The cumulative heat release rate of the three combustion chamber geometries is close to each other. The combustion velocity is lower than the others in the Wankel engine. Due to larger stroke volume of the Wankel engine, the cumulative heat release rate is by far the highest.

In order to eliminate this difference rising from the difference of the stroke volume, all engine types are normalized by converting to 1 liter stroke volume and cumulative heat release is shown in Figure 5. The Wankel engine has a significantly lower burning velocity and a cumulative amount of heat is 15-20% higher than conventional piston engines.

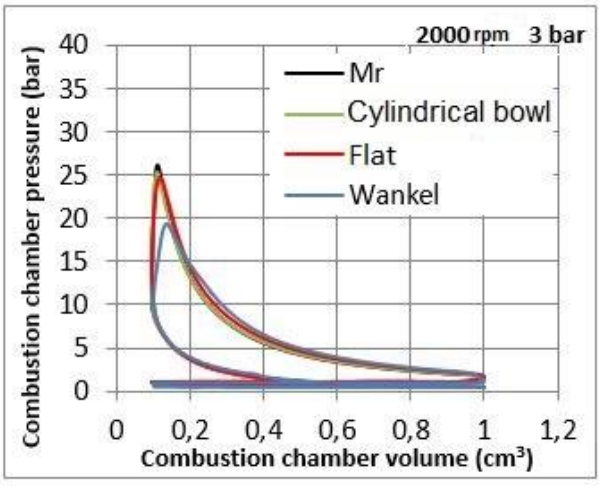

Figure 2. Comparison of p-V diagrams for Wankel engine and different combustion chamber geometries.

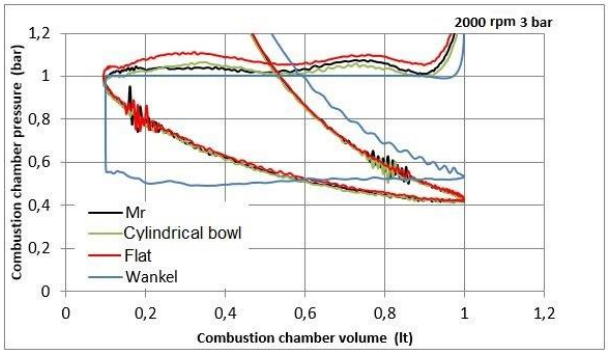

Figure 3. Comparison of charge change process for Wankel engine and different combustion chamber geometries.

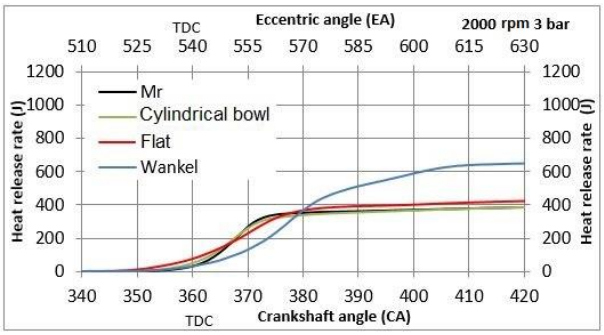

Figure 4. Comparison of cumulative heat release quantities at 3 bar load.

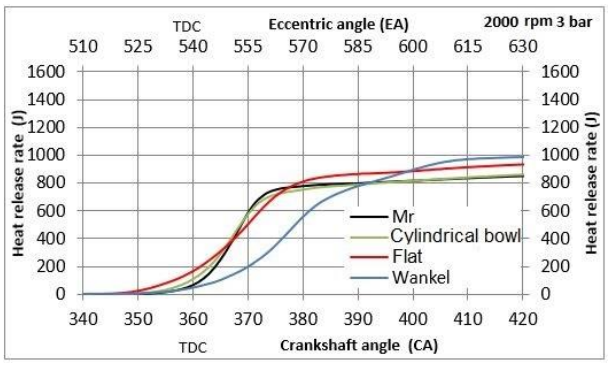

Figure 5. Comparison of the normalized amount of cumulated heat release at 3 bar load.

4. Conclusions

Three different combustion chamber geometries (MR, Cylindrical bowl, Flat) of 3LD 450 conventional piston engine with 13B MSP single rotor Wankel engine is tested and compared. Experiments are made at engine speed of 2000 rpm, 3 bar BMEP load and $\lambda = 1$ condition.

The maximum pressure values of the three different combustion chamber geometries

were close to each other. The difference between these results was due to the geometry affecting the flow and flame formation.

In the Wankel test engine, the maximum pressure values were lower than the others and more distant from the TDC. This is because of the lower combustion velocity and as a result, the process shifts toward the expansion stroke. On the other hand, the lower turbulence intensity in compression is another factor.

The pressure level remains relatively constant due to the greater opening time of the intake port in the Wankel engine.
The cumulative heat release amount for each of the three combustion chamber geometries was close to each other. Due to larger stroke volume of the Wankel engine, the cumulative heat release rate is by far the highest.

When the stroke volumes are 1 liter in both engines, the burning velocity of the Wankel engine is lower and the cumulative heat release is about 15 - 20% higher than the others.

References

[1] Ansdale, R. F., The Wankel RC Engine (1. Basım), London: Iliffe Books Ltd, p. 158, 1968.

[2] Yamamoto, K., Rotary Engine (1. Basım), Toyo Kogyo Co., Ltd, p. 147, 1971

[3] Yamamoto, K., Rotary Engine (6. Basım), Japan: Sankaido Co., Ltd, p. 67, 1981.

[4] Warner, M., Street Rotary (1. Basım), Penguin Group, p. 170, 2009.

[5] Ohkubo, M., Tashima, S. ve Shimizu, R. Developed Technologies of the New Rotary Engine (RENESIS), SAE Technical Paper Series, 2004-01-1790, p. 1-13, 2004.

[6] Froede, W. G. The Nsu-Wankel rotating combustion engine, SAE paper, 610017, p. 179-203, 1961.

[7] Cihan, Ö., Wankel motoru ve çevrim atlatma sisteminin deneysel ve sayısal olarak incelenmesi, (Doktora tezi). İstanbul Teknik Üniversitesi Fen Bilimleri Enstitüsü, İstanbul, 2017.

[8] Demirci, A., İçten yanmalı motorlarda farklı yanma odası geometrilerinin performans ve emisyonlara etkisi, (Doktora tezi). İstanbul Teknik Üniversitesi Fen Bilimleri Enstitüsü, İstanbul, 2017.

[9] Kutlar, O. A., Dört Zamanlı Otto (Rochas) Çevrimli Motorlarda Kısmi Yükte Yakıt Tüketimini Azaltmak İçin Yeni Bir Yöntem (Periyot Atlatmalı Motor). (Doktora tezi). İstanbul Teknik Üniversitesi Fen Bilimleri Enstitüsü, İstanbul, 1999.

[10] Doğru, B., Buji Ateşlemeli Motorlarda Çevrim Atlatma Yönteminin Kısmi Yüklerde İncelenmesi (Doktora tezi). İstanbul Teknik Üniversitesi Fen Bilimleri Enstitüsü, İstanbul, 2013.

[11] Taşkıran, Ö., Çalık, A.T. ve Kutlar, O.A. Effect of side ports on the flow field of a rotary engine, Sixth Conference Renewable Fuels, Fires and Combustion, in Kayseri, 2017.

Paper 26 **Bildiri 26**

HYDROTHERMAL DECOMPOSITION OF LEEK STALK INTO VALUABLE CHEMICALS IN SUBCRITICAL WATER

Nihal Cengiz*, Orkhan Nasirli, Mehmet Sağlam, Mithat Yüksel, Levent Ballice

Ege University, Engineering Faculty, Department of Chemical Engineering, 35100 Bornova, İzmir, Turkey

Abstract

Hydrothermal decomposition of leek stalk was investigated in a batch autoclave reactor system with 0.1 L of internal volume, in subcritical water with and without catalyst. Production conditions of levulinic acid (LA) and other valuable chemicals were studied to reach maximum yields. The effect of reaction time (20, 40 and 60 minutes), pH (1.0, 1.5, 2.0, 2.5), reaction temperature (140, 160 and 180 ºC), were investigated. LA production with hydrolysis, dehydration and rehydration are carried out in the presence of H_2SO_4, HNO_3 and $Zn(NO_3)_2$, $Al(NO_3)_3$, and $Cr(NO_3)_3$. The changes in gas, liquid contents according to the reaction parameters were determined by analyzes with HPLC (High Performance Liquid Chromatography) and TOC (Total Organic Carbon Analyzer). LA, formic acid, acetic acid and 5 HMF yields in g/kg biomass and LA conversions were calculated. The highest yields of LA were obtained at 180°C, and pH of 0.5 with H_2SO_4 addition at the end of 30 min of reaction time as 77.21 g LA/kg leek stalk. The yields of formic acid and acetic acid were found as 50.84 and 15.26 g/kg leek stalk, respectively.

Keywords: Hydrothermal decomposition, hydrogen, sub-critical water, biomass, levulinic acid

* Corresponding author. Tel: +90 232 3111489, Fax: +90 232 3887776

E-mail address: nihal.cengiz@ege.edu.tr

Introduction

The Lignocellulosic biomass is formed at a huge amount, approximately 1.7-2.0x10^{11} tonnes around world annually. Yearly biomass potential of Turkey is 32 million tones oil equivalent (mtoe) [1] gives present and projected biomass energy production between 1990-2030. Intensive studies are done to utilize this renewable and abundant resource as gaseous and/or liquid biofuels and valuable chemicals by thermochemical and biochemical processes and valuable chemicals. Lignocellulosic biomasses are composed of cellulose, lignin and hemicellulose as basic constituents and also include extractives. Extractives have non-structural (on-chemically bound components) components such as nitrate, nitrites, protein, ash, chlorophyll, inulin and waxes. In some plants amount of these component is about 40%. Inulin is renewable, natural fructan, which is biodegradable, and important feedstock for valuable chemicals. It is converted to HMF and LA in a molten salt hydrate medium which is appropriate for dehydration reactions [2]. Levulinic acid (LA) is one of the most versatile and significant chemical for industry as a building block produced from biomass. Various feedstocks are used to obtain levulinic acid such as monomers of carbohydretes, polysaccharides, HMF/5HMF, inuline, starch-containing wastes [3–10]. It can be found in garlic, onion, artichoke, leek stalk in different quantities. It's an ideal source of valuable chemicals.

LA is a platform chemical and can be utilized to produce a number of bio-chemicals including chemical intermediates, resins, polymers, lubricants, coatings, herbicides, pharmaceuticals and flavouring agents, solvents, anti-freeze agents and biofuels [11–14]. Manufacturing of bio-based levulinic acid is performed by hydrolysis, dehydration and rehydration by acid catalysts and bio-refining. LA is expected to play an important role in the targeted bio-refinery concept. Determination of suitable biomass for the production of LA at the lowest possible cost and high yield requires determination of suitable catalysts for hydrolysis-dehydration reactions and optimization of reaction conditions. Studies have been going on since about 15 years increasingly [15] . The main parameters affecting LA yield are; raw material type and concentration, catalyst type and concentration, solvent type, reaction time and temperature, pre-treatment of biomass and additives.

LA can be manufactured from furfuryl alcohol or maleic anhydride by hydrogenation and catalyzed hydrolysis reaction in the presence of acid catalyst. The other way of production is direct hydrolysis of lignocellosic biomass, cellulose or hexoses in acid medium [11]. The

commercial production of levulinic acid started in an autoclave by A.E. Statley Co. in the 1940s from starch with HCl [6].

Water is a suitable medium for the decomposition reaction of biomass. Particularly, if biomass contains large amount of water, it may be utilized into platform chemicals, without spending high amount of energy. Water has several interesting properties at condition close to the critical point, such as low viscosity, high solubility of organic substances. Subcritical water (SCW) is condition of above the boiling point and below the critical point (150°C - 374 °C). For processes like biomass processing, SCW act as a solvent [16].

Materials and Methods

Feedstock and catalyst

Leek stalk has an organic carbon content of 37%, in dry basis, is used as feedstock in all experiments as a real biomass. It is supplied from İzmir- Turkey and dried naturally in an open field. Dried biomass was cut small fractions and ground, sieved in basic vibrating screen shaker (AS200 Basic, RETSCH). The particle size smaller than 0.5 mm was obtained and characterized. Elemental analysis was made to identify the CHNS/O amounts in ana elemental analyser instrument (CHNS-932 by Leco, MI, USA). Basic constituents of leek stalk were determined by Van Soest method and the ratio of cellulose, lignin, hemicellulose and extractives were found [17]. The proximate, elemental analysis and composition results are given in Table 3. Amount of leek stalk has been chosen as 1.54 g due to previous studies results [18] and 20 ml of aqueous catalyst solution was fed to the autoclave reactors. In microwave reactor amount of leek stalk and catalyst solution was 0.05 g and 2.5 mL respectively. Higher amount of leek stalk caused a problem in pressure and mixing so 0.05 g was fed to microwave reactor.

H_2SO_4 (MERCK, 98%), HNO_3 (MERCK, 98%), and $Zn(NO_3)_2$ (Sigma Aldrich, in $Zn(NO_3)_2 \cdot 6H_2O$ form) , $Al(NO_3)_3$ (Sigma Aldrich, Aluminum nitrate nonahydrate, ≥ 98%) and $Cr(NO_3)_3$, (MERCK, Chromium(III) nitrate nonahydrate, ≥ 98%), were used as catalysts and the aqueous solutions of them were prepared.

Experimental procedure

Batch autoclave reactor system, consists of a reactor with an inner volume of 100 cm^3, heater and shaker which attached to the heater. The set-up was represented in a previous study [19] The construction material of autoclaves are stainless steel and can operate at pressure and temperature up to 50.0 MPa atm and 650°C respectively. The water-catalyst solution and determined amount of leek stalk is prepared, then placed in the reactor. The cap of the reactor

is sealed using a seal with no intrusion and N_2 gas is passed through the system to remove the air inside. The reactor is heated at a rate of 8–10 K/min to the desired temperature using heater and maintained at operating temperature constant with PID controllers during the chosen reaction time and shaker was turned on and was open until the reaction time ended. After the experiment is over, autoclaves were cooled in water bath and electric fans to room temperature. Solid residue was separated by means of filter paper and the aqueous product was diluted for HPLC and TOC analysis.

Microwave reactor was used at the most appropriate conditions for comparison. The similar experimental procedure was followed. Due to the small tube volumes of 9mL, used in microwave reactor, there have been used lower amount of raw materials. In microwave reactor, system was automatically cooled the tube after the reaction is finished.

The analysis of the aqueous products

The total organic carbon (TOC) content of the aqueous product was measured with a TOC analyzer (Shimadzu TOC-VCPH, Japan). Levulinic acid, acetic acid, formic acid and HMF analysis was acquired using high performance liquid chromatography (HPLC-RI Agilent Technologies, USA) equipped with a refractive index detector and the methods details were given in Table 1.

Table 1. High Performance Liquid Chromatography (Agilent 1200A) operating conditions

Column	Biorad Aminex HPX-87H (300 mm x 7.8 mm.)
Mobile Phase	0.05 % h. H_3PO_4 (pH:2,25)
Flowrate	0,6 mL/min
Dedector type	Refractive Index
Column Temperature	60°C
Dedector Temperature	30°C
P_{max}	93 bar
Injection volume	20 µL
Analysis Time	35 min

Table 2. Levulinic acid conversion and TOC results of hydrothermal decomposition reactions

Reactor type	Temperature (°C)	Catalyst	pH	Reaction Time (min)	Conversion (%) (LA)	TOC (mg/L)
Batch	120	H_2SO_4	0.5	30	6.318	7030
	140	H_2SO_4	0.5	30	13.53	8125
	160	H_2SO_4	0.5	30	19.2	7220
	180	H_2SO_4	0.5	30	20.86	12580
	200	H_2SO_4	0.5	30	17.65	7295
	180	H_2SO_4	0.5	10	9.68	11060
	180	H_2SO_4	0.5	20	18.76	12480
	180	H_2SO_4	0.5	30	20.86	12580
	180	H_2SO_4	0.5	40	20.03	12340
	180	H_2SO_4	0.5	60	9.51	11180
	180	H_2SO_4	0.5	30	20.86	12580
	180	H_2SO_4	1	30	3.25	10070
	180	H_2SO_4	1.5	30	1.45	10210
	180	$Al(NO_3)_3$	3	30	1.58	12090
	180	$Cr(NO_3)_3$	3	30	1.52	10460
	180	HNO_3	1.3	30	6.31	11930
	180	H_2SO_4	0.5	30	20.86	12580
Microwave	180	H_2SO_4	0.5	30	40.65	-

Table 3. Leek stalk characterization results

Proximate Analysis %	
Humidity	9.30
Ash	13.24
Crude Protein	16.04
Composition of Biomass %	
Extractive	56.10
Cellulose	30.80
Hemicellulose	7.90
Lignin	4.30
Elemental Analysis %	
C	37.0
H	5.76
N	2.32
S	0.48
K	3.23
Ca	1.38
Mg	0.28

Al	0.14
F	0.13
Cr	0.01
Cu	0.01
Mn	0.01
Zn	0.04

Results

To observe the effect of reaction time and find the most appropriate one, experiments have been performed during the different length of time (10, 20, 30, 40 and 60 minutes) at constant reaction temperature of 180°C and 0.5 pH in the first part. In the second part of the hydrothermal decomposition studies were carried out in subcritical water medium at the reaction temperature range of 120, 140, 160, 180 and 200°C in batch reactors at pH of 0.5 and reaction time of 30 min. Third part of experimental studies were done at various pH levels of 0.5, 1.0 and 1.5. The studies were carried out in the presence of catalyst (H_2SO_4) at a solid/liquid ratio of 1.54g leek stalk/20 mL aqueous solution in the first, second and third part at batch autoclaves. H_2SO_4 was added into water/feedstock solution to obtain pH of 0.5 for effective decomposition of the leek stalk. Various catalysts (HNO_3, $Al(NO)_3$, and $Cr(NO)_3$) are added to the subcritical reaction medium to investigate effects of catalyst on the product yields at 180°C and 30 min for comparison with H_2SO_4 in batch autoclaves. Experiments are done in microwave reactor at a solid/liquid ratio of 0.05g leek stalk/2.5 mL at 180°C of reaction temperature and 30 min of reaction time at 0.5 pH and in the presence of H_2SO_4 in the last part. At least 3 repetition were done for each experiment for accuracy. Table 1 shows reaction conditions, LA yield (%), and TOC of the aqueous product.

The liquid product yields (g product/kg biomass), for each component LA, acetic acid, formic acid and HMF were calculated on the basis of the concentration measured in HPLC expressed using the following formulas;

$$\text{Liquid product yield (g/kg biomass)} = \frac{C_i V_{liquid}}{1000 * m_{biomass}}$$

$$\text{LA yield (\%)} = \frac{C_{LA} V_{liquid}}{1000 * m_{biomass}\, TOC_{biomass}}$$

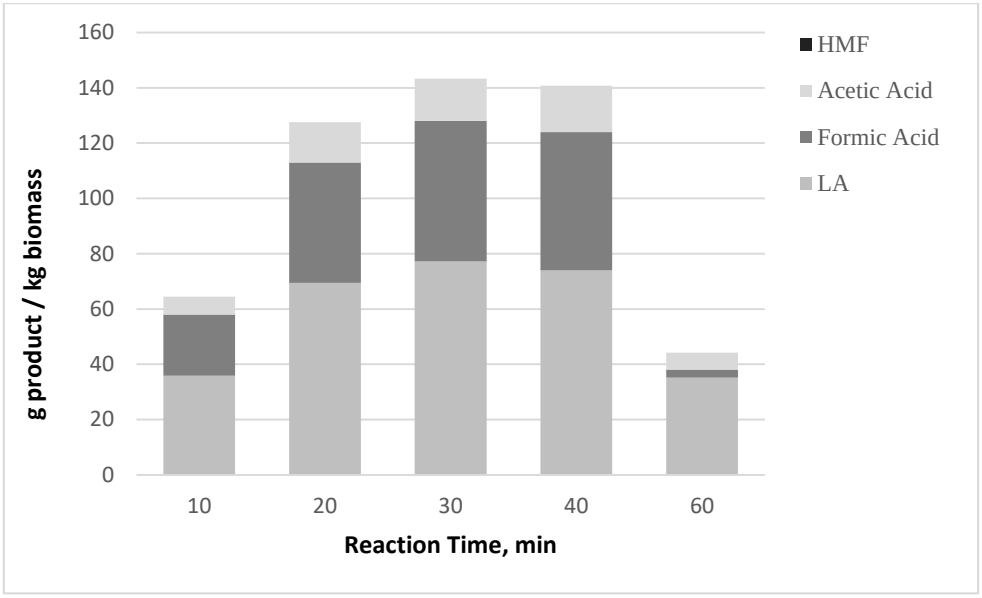

Figure 1. Variation of product yields in g product/kg biomass by reaction time (pH=0.5 and $T_{reaction}$=180°C)

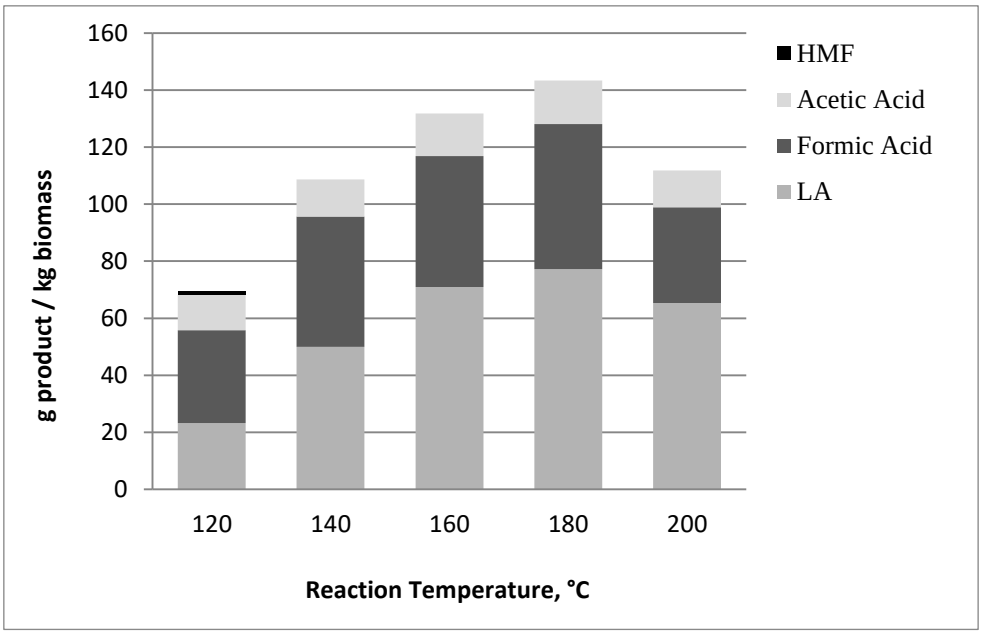

Figure 2. Variation of product yields in g product/kg biomass by reaction temperature (pH=0.5 and $t_{reaction}$=30 min)

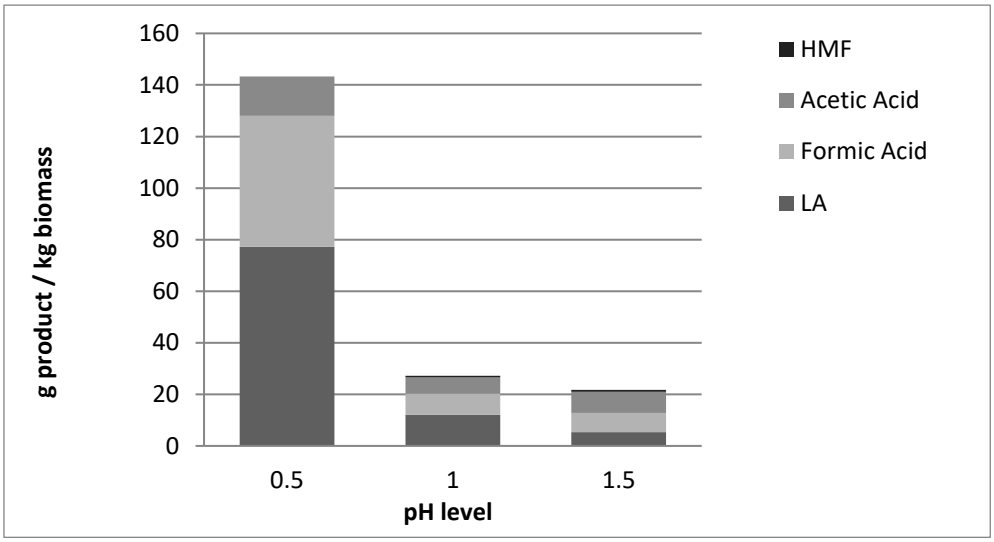

Figure 3. Variation of product yields in g product/kg biomass by pH ($T_{reaction}$=180°C and $t_{reaction}$=30 min)

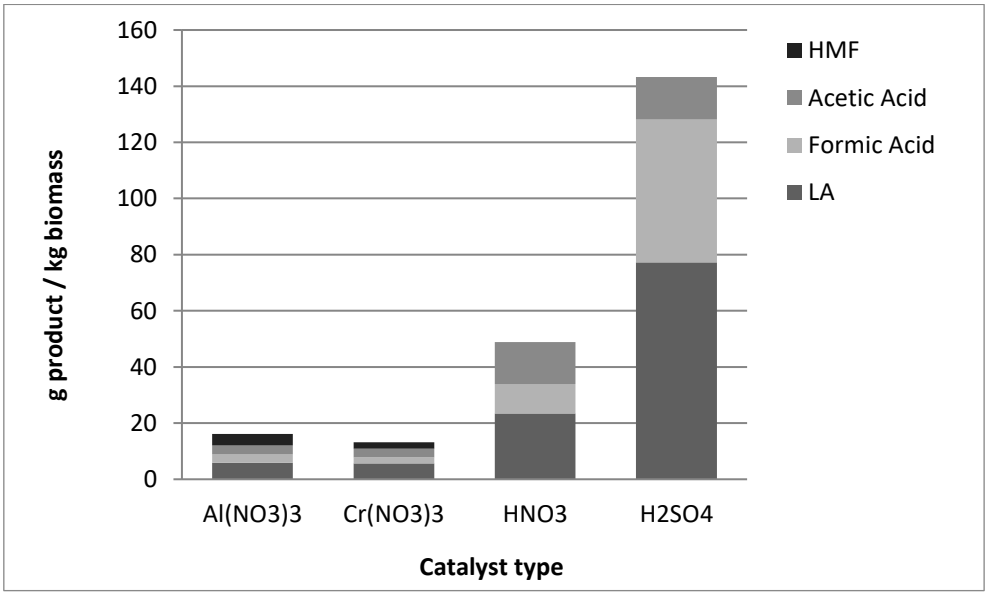

Figure 4. Variation of product yields in g product/kg biomass by different catalysts ($T_{reaction}$=180°C and $t_{reaction}$=30 min)

Effect of reaction time on the aqueous product yields

Variation of the yields of levulinic acid, acetic acid, formic acid and hydroxyl methyl furfural (HMF) in the aqueous product by the effect of reaction time is represented in Figure 1. 30 min reaction time was the most appropriate period for the leek stalk decomposition with the highest LA yield of 77.21 g/kg biomass. Up to 30 min, produced levulinic acid amount increased and

after 30 min it began to decrease. At 60 min, there is significant decrease in LA, acetic acid and formic acid. 40 min reaction time results are similar with 30 min, slightly lower yields were obtained at this condition. Acetic acid has a maximum yield at 30 and 40 min as 15 and g/kg biomass. The second most produced component is formic acid at the operated reaction times and it has a yield around 50 g/kg biomass at 30 and 40 min. HMF was not detected at this part of the studies, it may be converted to LA and formic acid totally by rehydration. Sum of the valuable chemicals obtained in this part is 140 g/kg biomass as maximum. Reaction mechanism was given in literature as [15,20,21]:

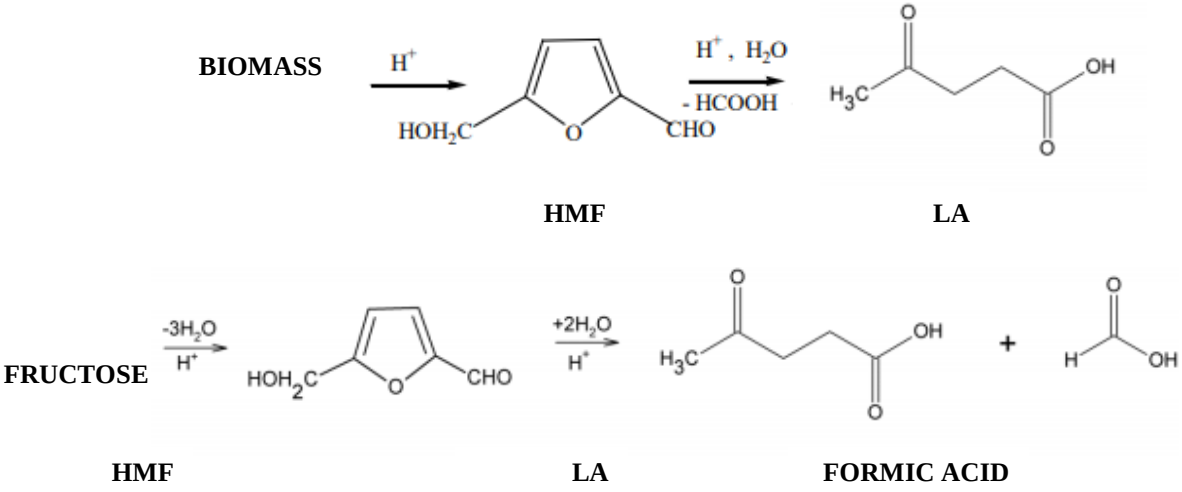

As it is seen dehydration reaction of the hexose sugars such as glucose, mannose, fructose and galactose forms HMF and yields to levulinic acid and formic acid via rehydration with 2 water molecules. HMF may be produced from inulin exist in the extractive part of the biomass. In a study of Dull et al. they achieved 5 HMF from inulin in the presence of oxalic acid by heating [22] as the first time.

LA yield was reached 20.86% at 30 min, 0.5 pH and 180°C in batch autoclave while it was 40.65% at the same conditions in microwave reactor as seen in Table 1. Total Organic Carbon in the aqueous product is changed within 11060 to 12580 ppm, results verified the maximum organic compound yield was obtained at 30 and 40 min as seen in Table 1.

Effect of temperature on the aqueous product yields

Variation of the yields of levulinic acid, acetic acid, formic acid and hydroxyl methyl furfural in the aqueous product is represented in Figure 2. As temperature increase up to 180°C, the yields of the LA promoted significantly, formic acid is slightly increased while acetic acid does

not changed remarkably. HMF is detected at 120°C only at a very low amount of 1.3 g/kg leek stalk. This can be explained HMF is converted to LA and formic acid at elevated temperatures. At the highest operated temperature of 200°C, the levulinic acid and formic acid yields were lower. The best suitable temperature was found as 180°C for the targeted compounds production in this reaction system at 30 min of reaction time and pH of 0.5. Below 200°C, there are very limited studies for the levulinic acid production in water medium from biomass or model compounds. In this study, lower reaction temperatures were selected for process economy and obtained high yields even at low pressure (2.0-3.0 Mpa) and temperatures. Mehdi et al. studied with sucrose and sulphuric acid, obtained LA yields of 40-50% at 140 °C, with a reaction time of 8 h and in a high-pressure reactor [23]. Girisuta et al. investigated water hyacinth plant (Eichhornia) decomposition into LA at various reaction temperatures, time and acid concentrations [24]. The optimization results showed that within 0-30 min with 1.0 M H_2SO_4 and at 175°C, highest LA yields were obtained as 53 mol %. Above this temperature, the yields of LA decreased that is consistent with this study. LA may further decomposed to another chemicals at elevated temperatures.

Effect of pH and catalyst type on the aqueous product yields

The pH of the medium affect the product yields too much as seen in Figure 3. While pH increased from 0.5 to 1.5, total amount of the determined aqueous product lowered from 140 to 20 g/kg leek stalk approximately. Studying at low pH levels enhance LA, formic acid and acetic acid. This results is alike found in literature that higher acid concentrations give higher LA yields [24,25].

Conclusion

Taking into consideration all the experiments, we can discuss different important points. During the experimental studies, we investigated the effect of different conditions on the LA yield. These conditions are pH, Temperature, Catalyst and Reaction time. So, what we observed after evaluated the result can be described as:

- From the experience carried out most yielding conditions were chosen as 180°C, 30 min, 1M (0.5 pH)
- Different types of catalyst are used, such as H_2SO_4, HNO_3, $Al(NO)_3$, and $Cr(NO)_3$ From the evaluated results it can be seen that the most efficient catalyst is H_2SO_4

- The lower pH the higher the LA yield
- If we compare Microwave and Batch Reactor, we can say that experiments in Microwave reactor are carried out much easier than using the Batch reactor. In addition, time dependence of yield can be easily investigated using Microwave reactor, because the experimental procedure takes shorter than that of Batch reactor.

Acknowledgments

We gratefully acknowledge for the financial support of Aliye Üster Foundation-Ege University. We appreciate to Mr. G. Serin for his support in the pre-treatment step of the leek stalk and help during the experimental studies and analysis.

Nomenclature

Ci	concentration of component 'i' in the aqueous product (mg/L)
HTG	hydrothermal gasification
$m_{biomass}$	weight of biomass in feed (g)
T	reaction temperature (°C)
t	reaction time (min)
V_{liquid}	volume of aqueous catalyst solution fed to reactor (mL)
$TOC_{biomass}$	total organic carbon content of the biomass/leek stalk (%)
LA	levulinic acid

References

[1] Kaygusuz K. Oil and Gas Production and Consumption in Turkey. Energy Exploration & Exploitation 2002;20:37–50. doi:10.1260/014459802760170394.

[2] Wang Y, Pedersen CM, Qiao Y, Deng T, Shi J, Hou X. In situ NMR spectroscopy: Inulin biomass conversion in ZnCl2 molten salt hydrate medium - SnCl4 addition controls product distribution. Carbohydrate Polymers 2015;115:439–43.

doi:10.1016/j.carbpol.2014.09.011.

[3] Morone A, Apte M, Pandey RA. Levulinic acid production from renewable waste resources: Bottlenecks, potential remedies, advancements and applications. Renewable and Sustainable Energy Reviews 2015;51:548–65. doi:10.1016/J.RSER.2015.06.032.

[4] Weingarten R, Conner WC, Huber GW. Production of levulinic acid from cellulose by hydrothermal decomposition combined with aqueous phase dehydration with a solid acid catalyst. Energy {&} Environmental Science 2012;5:7559–74. doi:10.1039/c2ee21593d.

[5] Mascal M, Nikitin EB. High-yield conversion of plant biomass into the key value-added feedstocks 5-(hydroxymethyl)furfural, levulinic acid, and levulinic esters via 5-(chloromethyl)furfural. Green Chemistry 2010;12:370–3. doi:10.1039/b918922j.

[6] Moyer WW. Preparation of levulinic acid. 2,270,328, 1942.

[7] Kang M, Kim SW, Kim JW, Kim TH, Kim JS. Optimization of levulinic acid production from Gelidium amansii. Renewable Energy 2013;54:173–9. doi:10.1016/j.renene.2012.08.028.

[8] Victor A, Pulidindi IN, Gedanken A. Levulinic acid production from Cicer arietinum, cotton, Pinus radiata and sugarcane bagasse. RSC Advances 2014;4:44706–11. doi:10.1039/c4ra06246a.

[9] Muranaka Y, Suzuki T, Sawanishi H, Hasegawa I, Mae K. Effective production of levulinic acid from biomass through pretreatment using phosphoric acid, hydrochloric acid, or ionic liquid. Industrial and Engineering Chemistry Research 2014;53:11611–21. doi:10.1021/ie501811x.

[10] Flannelly T, Lopes M, Kupiainen L, Dooley S, Leahy JJ. Non-stoichiometric formation of formic and levulinic acids from the hydrolysis of biomass derived hexose carbohydrates. RSC Advances 2016;6:5797–804. doi:10.1039/c5ra25172a.

[11] Li X, Xu R, Yang J, Nie S, Liu D, Liu Y, et al. Production of 5-hydroxymethylfurfural and levulinic acid from lignocellulosic biomass and catalytic upgradation. Industrial Crops and Products 2019;130:184–97. doi:10.1016/j.indcrop.2018.12.082.

[12] Motoki S, Odaka T. Synthesis of Glutamic Acid from Levulinic Acid. Nippon Kagaku Zassi 2011;77:401–2. doi:10.1246/nikkashi1948.77.401.

[13] Timokhin B V, Baransky VA, Eliseeva GD. Levulinic acid in organic synthesis. Russian Chemical Reviews 2002;68:73–84. doi:10.1070/rc1999v068n01abeh000381.

[14] Chang C, Chen L-L, Yang A-L. Advances in Bio-based platform chemical-Levulinic Acid. Xiandai Huagong/Modern Chemical Industry 2012;32.

[15] D.W. R, W.O. D. The conversion of lignocellulosics to levulinic acid. Biofuels, Bioproducts and Biorefining 2011;5:198–214. doi:10.1002/bbb.267.

[16] Dinjus E, Kruse A. Hot compressed water—a suitable and sustainable solvent and reaction medium? Journal of Physics: Condensed Matter 2004;16:S1161–9. doi:10.1088/0953-8984/16/14/026.

[17] H.K. Goering PJVS. Forage fiber analysis in: Agriculture Handbook No: 379, Superintendent of Documents. US Government Printing Office, Washington DC; 1970.

[18] Madenoğlu TG, Kurt S, Sağlam M, Yüksel M, Gökkaya D, Ballice L. Hydrogen production from some agricultural residues by catalytic subcritical and supercritical water gasification. The Journal of Supercritical Fluids 2012;67:22–8. doi:10.1016/j.supflu.2012.02.031.

[19] Tülay Güngören, Mehmet Sağlam, Mithat Yüksel, Hakan Madenoğlu, Rahim İşler, İsmail H. Metecan, Ahmet R. Özkan and LB. Near-Critical and Supercritical Fluid Extraction of Industrial Sewage Sludge. Ind Eng Chem Res 2007:1051–7.

[20] Amarasekara AS, Williams LTD, Ebede CC. Mechanism of the dehydration of d-fructose to 5-hydroxymethylfurfural in dimethyl sulfoxide at 150 °C: an NMR study. Carbohydrate Research 2008;343:3021–4. doi:10.1016/j.carres.2008.09.008.

[21] Kabyemela BM, Takigawa M, Adschiri T, Malaluan RM, Arai K. Mechanism and Kinetics of Cellobiose Decomposition in Sub- and Supercritical Water 1998;5885:357–61.

[22] Dull G. Action of oxalic acid on inulin. Chemiker-Zeitung 1895;19:166 and 216-7.

[23] Mehdi H, Fábos V, Tuba R, Bodor A, Mika LT, Horváth IT. Integration of

Homogeneous and Heterogeneous Catalytic Processes for a Multi-step Conversion of Biomass: From Sucrose to Levulinic Acid, $γ$-Valerolactone, 1,4-Pentanediol, 2-Methyl-tetrahydrofuran, and Alkanes. Topics in Catalysis 2008;48:49–54. doi:10.1007/s11244-008-9047-6.

[24] Girisuta B, Danon B, Manurung R, Janssen LPBM, Heeres HJ. Experimental and kinetic modelling studies on the acid-catalysed hydrolysis of the water hyacinth plant to levulinic acid. Bioresource Technology 2008;99:8367–75. doi:10.1016/j.biortech.2008.02.045.

[25] Galletti AMR, Antonetti C, De Luise V, Licursi D, Di Nasso NNO. Levulinic acid production from waste biomass. BioResources 2012;7:1824–34. doi:10.15376/biores.7.2.1824-1835.

Paper 27 **Bildiri 27**

HIZLI OTOBÜS TAŞIMA SİSTEMLERİNDE GERÇEK SÜRÜŞ EMİSYONLARI : İSTANBUL METROBUS

Orkun ÖZENER*, Muammer ÖZKAN

ÖZET

Araçların gerçek sürüş emisyonları, çevre bilincinin artması nedeniyle son yıllarda büyük ilgi görmektedir. Toplu taşıma, içten yanmalı motorlu taşıtlardan kaynaklanan kirleticilerin ana katkılardan biridir. Bu ulaşımın yolu genel olarak yoğun nüfus yoğunluğuna sahip şehir içi bölgelerden oluşmaktadır. Bu açıdan bakıldığında, bu toplu taşıma sisteminin izlenmesi ve analiz edilmesi, çevre dostu şehirler oluşturmak için gerçek sürüş emisyonları açısından önemlidir. Fosil yakıtlı toplu taşıma ekonomisi, optimize edilmesi gereken bir başka önemli husustur. Bu bağlamda, dünyanın en büyük taşıma aksı konusunda, İstanbul 24 saat çalışan Metrobüs Hızlı Otobüs Taşıma sistemi incelenmiştir. Portatif emisyon ölçüm sistemleri ve portatif yakıt tüketimi ölçüm cihazı ile donatılmış olan toplu taşıma otobüsü, Zincirlikuyu güzergahından Avcılar yönündeki ölçüm faaliyetlerinde kullanılmaktadır. Daha sonra sonuçlar işletme parametreleriyle ilgili emisyon ve yakıt tüketimi açısından analiz edilmiştir. Sonuçlar, sürüş davranışının hem emisyonlar hem de yakıt tüketimi üzerinde büyük etki yarattığını göstermiştir. Emisyonlar ve yakıt tüketimleri hem ivme hem de hız açısından analiz edilmiştir. Emisyonlar ve yakıt faktörleri geliştiriliştir. Ayrıca bazı motor işletme bölgelerinde aracın kullanılmasıyla emisyonların düşürülmesinin mümkün olduğu da analiz edilmiştir.

Anahtar Kelimeler: Gerçek sürüş emisyonları, yakıt tüketimi, toplu taşıma, dizel motor.

REAL DRIVING EMISSIONS ASSESSMENT FROM BUS RAPID TRANSPORT SYSTEMS: ISTANBUL METROBUS

ABSTRACT

The real driving emissions of vehicles are showing great interest in the last years because of increasing environmental awareness. The public transport is one of the major contributor to the pollutants arousing from combustion engine vehicles. The route of these transport are consisting generally inner city regions with huge population density. From this perspective the monitoring and analyzing of these public transport system real driving emissions is important for creating environmentally friendly cities. The economy of fossil fuelled public transportation is another major concern that should be optimized. In this context on of the biggest transport axle of the world, İstanbul city 24h working Metrobus Rapid Bus Transport system is analyzed. The public bus equipped with portable emission measurement systems and portable fuel consumption meter is used for measurement activities at the route of

Zincirlikuyu to Avcılar direction. Then the results are analyses in terms of emissions and fuel consumption regarding to the operating parameters. The results showed that the driving behavior is showing great effect on both emissions and fuel consumption. The emissions and fuel consumptions are both analyzed regarding to the acceleration and speed. The emissions and fuel factors are developed. It is also analyzed that it is possible to lower emissions with operating the vehicle some certain regions.

Keywords: Real driving emissions, fuel consumption, public transportation, diesel engine

1. INTRODUCTION

The environmental awareness increased about emissions generated from combustion engine powered public transportation at last ten year. The public transportation which mainly circulates at the inner city routes exhibits a higher priority about optimization of both emissions and fuel consumption from public transportation. Internal combustion engines used in heavy duty public transportation buses are homologated under certain (*Stationary-ESC and Transient WHTC*) engine testing cycles [1]. Also the heavy duty vehicles are know tested on the road for emission in service conformity with the regulations. The conformity factor Euro 6 regulation is 1.5 by the year 2019.

There is lots of valuable research in this area; Yu et al.[2] pollutant emissions created near bus stops and to find out the parameters that effects the pollutants emitted, Zhang et al. [3] tested 75 Beijing public buses with different propelling mechanisms for four years in Beijing. They concluded that; the average speed has big non-linear effect on fuel consumption, Wang et al.[4] measured the on board emission data of Euro III and Euro IV busses in Beijing fueled with conventional diesel and compressed natural gas. They concluded that emission and fuel factors all decreased with the increase of vehicle speed. Durbin et al.[5] measured five different heavy duty vehicles, they revealed that the emissions from these vehicles are related with the operating conditions and also with emission component, the age/certification level.

In this research one of the biggest public transportation axle of world, İstanbul's bus rapid transport- The Metrobus- line was assessed in terms of fuel consumption and emissions. The Metrobus line is a transit bus line planned by İstanbul Municipality and operated by İstanbul Public Transportation Company (IETT). Its length is about 52 km and it is crossing the city main axle from Asian side to Europe side. It is also in operation for 24 hours with ~550 busses and carries over 1 million passengers daily. The real public bus was equipped with emission and fuel consumption measurement devices are used in this research. The collected real driving emissions and fuel consumption is analyzed regarding to the operating conditions. (ie. acceleration-velocity zoned, emission generated near bus stops) .

2. EXPERIMENTAL METHODS

2.1. Test System

A Euro 5 public bus working in this route is equipped with AVL portable emissions measurement systems (PEMS) and portable fuel consumption meters (PCFM) [6, 7] was used for fuel consumption and emission monitoring. The carbon dioxide (CO_2), carbon monoxide (CO), nitrogen oxides (NO_X), Soot is monitored with PEMS. The required channels from controller area network area (CAN) line is also monitored with a can logger. Al data channels are

logged on system controller computer at same time domain. The measurement system schematic layout is given Figure 1. The test bus properties is given in Table 1.

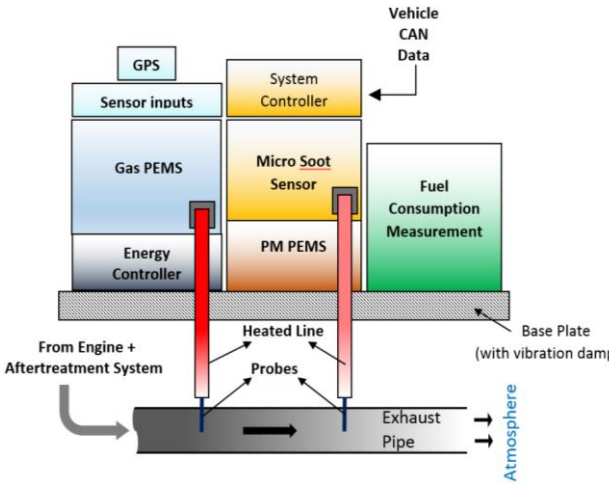

Figure 1. Test system layout

The test bus properties is given in Table 1.

Table 1. Vehicle and engine properties.

Gross Vehicle Weight	32 tones
Type	Articulated
Vehicle Length	18 m
Number of cylinders	6
Engine capacity	11.9 l
Power	260kW@2000 rpm
Torque	1600Nm@1100rpm
Compression Ratio	17.75:1
Min. Brake Specific Fuel Consumption *@Full Load-1400 rpm*	185 gr/kwh
Emission Certification Level	Euro 5

2.2. Test Route

The metrobus line is consisting of three main parts in its operation. These are i) Söğütlüçeşme to Zincirlikuyu 11 km with 8 stations ii) Zincirlikuyu to Avcılar 29 km 25 stations and iii) Avcılar to Beylikdüzü 12 km with 12 stations. The second and the longest part of this line Zincirlikuyu (Z) to Avcılar (A) is chosen for assessment. The altitude difference of the whole route is 136 meters. The analyses are carried within 6500 kg payload and 13.000 kg payload.

3. RESULTS AND DISCUSSION

The velocity change during the operation regarding to trip distance at 13.000 kg payload with the altitude and stations is pointed (in pink) is given in Figure 2. The governing authority limited the speed to 70 km/h because of safety concerns. The fuel consumption change with altitude for 6500 kg pay load and 13.000 kg payload at Z to A direction in given Figure 3. As it can be seen from the graphic the altitude has a big effect on fuel consumption rate as expected. Also the fuel cut off regions from the engine control strategy is evident. It can be analyzed that the location and acceleration limitation is important at take offs. Also it can be concluded as the locating the bus stations at high grade locations should be avoided because of high torque demands.

The exhaust emissions and also the fuel consumption generated by public bus analyzed at the takeoff sessions. The pollutants generated near bus stops are important because human health. The emission and fuel consumption graphics are given for a bus stop take off season (random chosen) at Figure 4a and Figure 4b for 13.000 kg pay load condition. It is evident that, the driver is pushing the accelerator pedal at the take off session for accelerating the vehicle. Then the fuel consumption increases harmonious with torque demand. Also it is evident that there is a huge CO, Soot and NOx peak in this region. The CO peak can be explained with air path inertia and insufficient in cylinder mixing. The soot peak can be explained with locally rich mixture formation at he take off conditions because of turbo lag. The bus is having SCR system for NOx conversion but it seems the SCR efficiency is not sufficient to convert all NOx emitted at this region. As a reason there is high emission peaks at the initial 10 second and 50 meters of take off season. From this perspective in order to prevent from these peaks the engine calibration

should be clearly considered for solving this problem.

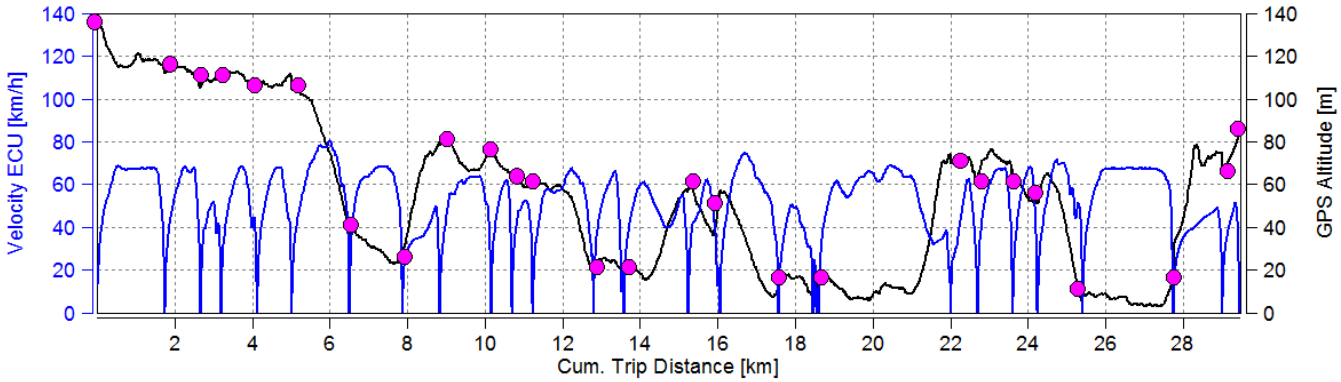

Figure 2. Velocity change regarding to distance with altitude

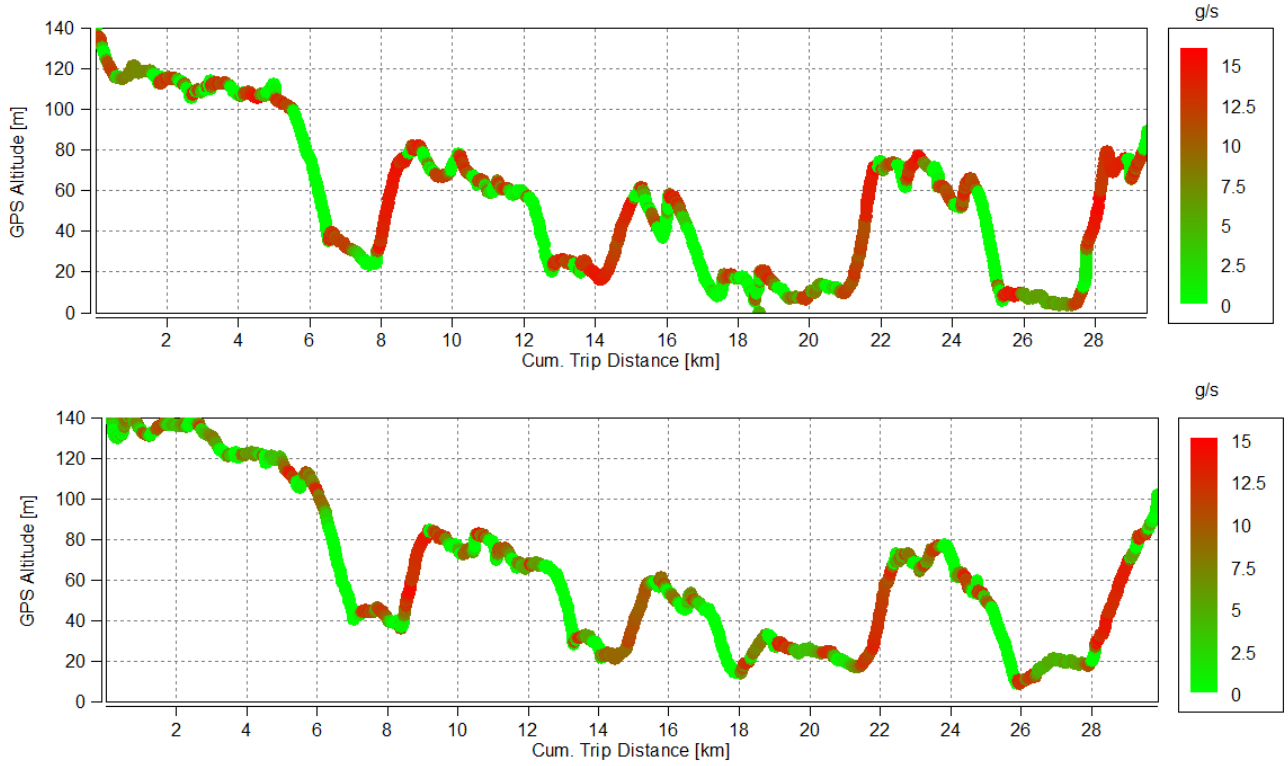

Figure 2. Fuel consumption change regarding to distance with altitude a) 13.000 kg payload b) 6500 kg payload.

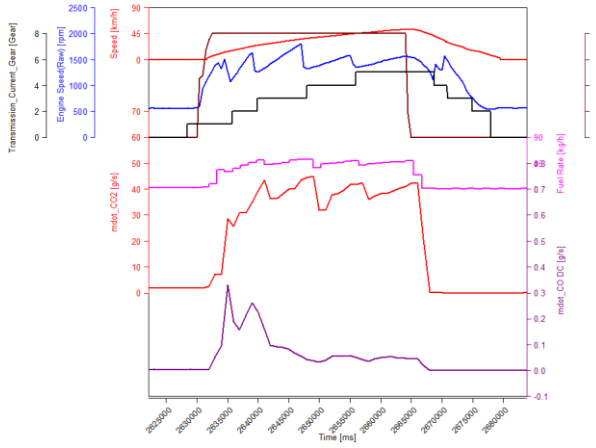

Figure 4a. Fuel consumption CO_2 and CO emissions at take offs regarding to engine speed, current gear and throttle position.

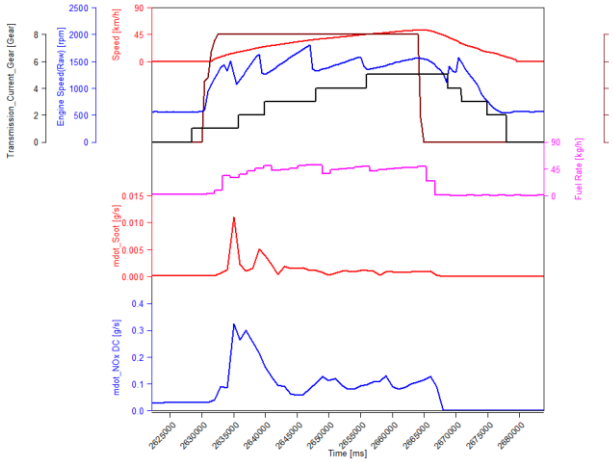

Figure 4b. Fuel consumption Soot and NOx emissions at the take offs regarding to engine speed, current gear and throttle position.

The emissions and fuel consumption contour graphics regarding to vehicle speed- acceleration are given at Figure 5. It was found that fuel consumption of the vehicle increases with the increase of vehicle speed and acceleration. (acc>0 m/s²), the significant region is over 20 km/h, effect of acceleration is higher than the velocity increase during operation, for CO and NO_X. The +0.4 m/s² acceleration level at low speeds found as critical for the emission levels from the exhaust, the CO emissions are higher when the velocity is lower from 40 km/h and acceleration level is higher than +0.4 m/s² which can be explained with insufficient mixture formation. Also the NO_X emissions was found higher especially at low speed (v<20-30 km/h) positive acceleration zones which can be explained by power demand because of acceleration demand from driver at takeoff session. It can be interpreted as the SCR conversion efficiency and calibration strategy is not sufficient for converting all NO_X

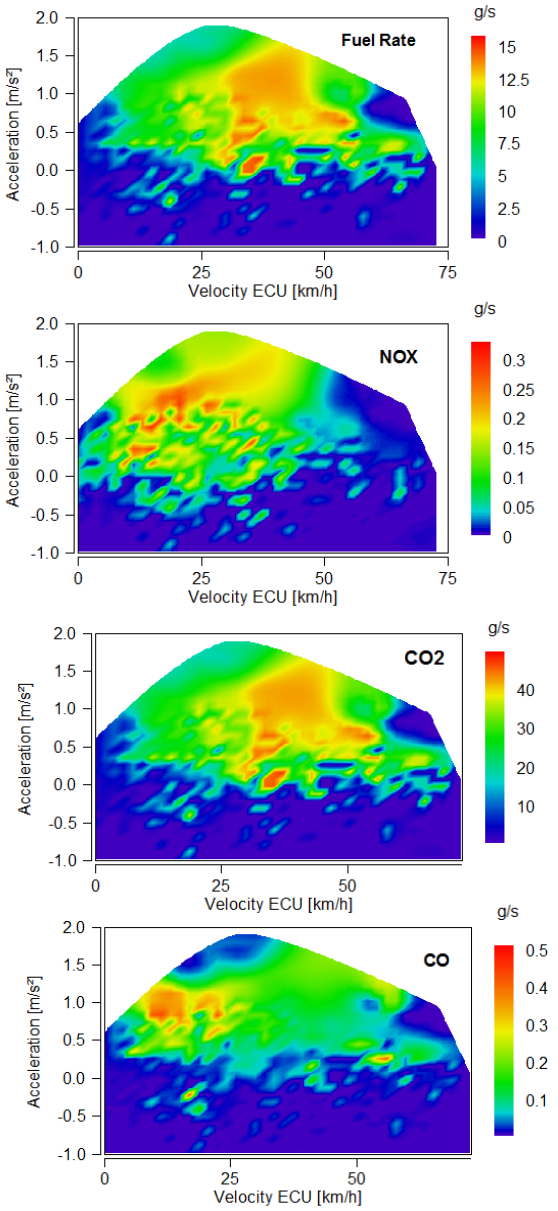

Figure 5. Fuel consumption and emission graphic regarding to the vehicle speed and acceleration at Z to A direction with 13.000 kg payload.

4. CONCLUSION

A comprehensive experimental work was carried on the one of the biggest

transportation axle of world. The results showed that it is possible to manage and operate the public transportation with the help of bus electronic control system calibration, component selection and topographic planning of the bus stops.

ACKNOWLEDGMENTS

This research was funded by the Istanbul Development Agency –ISTKA, under Information Focused Economic Development Programme, project no. BİL-86 with the partnership of Istanbul Public Transportation Company (IETT).

REFERENCES

[1] E. Union, Directive 2005/55/EC of the European Parliament and of the Council, in, 2005.

[2] Q. Yu, T. Li, H. Li, Improving urban bus emission and fuel consumption modeling by incorporating passenger load factor for real world driving, Applied Energy, 161 (2016) 101-111.

[3] S. Zhang, Y. Wu, H. Liu, R. Huang, L. Yang, Z. Li, L. Fu, J. Hao, Real-world fuel consumption
and CO2 emissions of urban public buses in Beijing, Applied Energy, 113 (2014) 1645-1655.

[4] A. Wang, Y. Ge, J. Tan, M. Fu, A.N. Shah, Y. Ding, H. Zhao, B. Liang, On-road pollutant emission and fuel consumption characteristics of buses in Beijing, Journal of Environmental Sciences, 23 (2011) 419-426.

[5] T.D. Durbin, K. Johnson, J.W. Miller, H. Maldonado, D. Chernich, Emissions from heavy-duty vehicles under actual on-road driving conditions, Atmospheric Environment, 42 (2008) 4812-4821.

[6] AVL, https://www.avl.com/-/avl-concerto-m-o-v-e, in, 2018.

[7] AVL, AVL KMA Mobile Product Description, (2013).

Paper 28 **Bildiri 28**

TEK SİLİNDİRLİ SIKIŞTIRMA ATEŞLEMELİ BİR MOTORDA POST ENJEKSİYON ZAMANLAMA VE SURECİNİN EGZOZ GAZ EMİSYONLARINA ETKİSİNİN DENEYSEL OLARAK İNCELENMESİ

Orkun ÖZENER[1], Onur GEZER[1], Muammer ÖZKAN[1],
Enishan ÖZCAN[2], Cihan BÜYÜK[2], Mustafa GÜÇLÜ[2], Abdullah KILIÇASLAN[2]

[1] Yıldız Technical University Beşiktaş/İstanbul
[2] TÜMOSAN Engine and Tractor Co. Topkapı/İstanbul

ÖZET

Dizel motorları yüksek termik verimleri ve gelişmiş yakıt ekonomisi davranışları bakımından öne çıkmaktadır. Fakat dizel motorlarında yüksek sıkıştırma oranı ve karışım teşkili karakteristiği gereğince oluşan azot oksitler ve is emisyonları kontrol altına alınmalıdır. Dizel motor yönetimi üzerine yürütülen çalışmaların hatırı sayılır bir kısmı NO_x ve is emisyonlarını kontrol altına almaya yöneliktir. Bu çalışmada su soğutmalı, common-rail yakıt enjeksiyon sistemine sahip, tek silindirli bir dizel motorda post püskürtme miktar ve zamanlamasının CO, NO_x ve is emisyonları üzerine etkisi deneysel olarak incelenmiştir. Yapılan testlerde motor hızı 1500 rpm değerinde ve püskürtme basıncı 1000 bar değerinde sabit olup post enjeksiyon başlangıcı üst ölü noktadan sonra 10-16^o KA aralığında üç farklı yakıt miktarı için denenmiştir. Yapılan çalışmanın sonucunda post enjeksiyon başlangıcı gecikmesinin artışına bağlı olarak NO_x emisyonlarında düşüş, CO emisyonlarında artış, is emisyonlarında belli bir değere kadar artış ve ardından da düşüş gözlemlenmiştir.

Anahtar Kelimeler: Dizel yanması, post enjeksiyon, emisyonlar

AN EXPERIMENTAL INVESTIGATION OF POST INJECTION TIMING AND DURATION ON EXHAUST EMISSIONS IN A SINGLE CYLINDER CI ENGINE

ABSTRACT

Today, diesel engines stand out in terms of high thermal efficiency and advanced fuel consumption behaviour. However, nitrogen oxides and particulate matter emissions are the releases that need to be controlled in diesel engines due to the mixture formation characteristics and high compression ratios. A large part of the studies on diesel engine management are carried out to control NO_x and soot emissions. In this study, water-cooled, common rail fuel injection system equipped, single cylinder diesel engine was used and the effect of post injection timing and amount on CO, NO_x and soot emissions were investigated experimentally. At 1500 rpm engine speed and 1000 bar fuel injection pressure, starting of post injection was changed between 10-16°CA after TDC and for the verification was done with three different injection quantity. As a result of the study, there was a decrease in NO_x emissions, an increase in CO emissions and an increase up to certain value then a decrease tendency in the soot emissions by delaying the post injection starting.

Keywords: Diesel combustion, post injection, emissions

1. INTRODUCTION

Internal combustion engines are showing great importance for the last century in industrial field and transportation and their usage is becoming widespread day by day. Widespread using of internal combustion engines causes decreasing of petroleum reserves and increasing environmental pollution. A certain emission regulations have been carried out in order to reducing environmentally pollution and sustainability. For these reason, researchers have focused on more efficient and less harmful combustion strategies.

Diesel engines are widely used because of their high thermal efficiency and low fuel consumption [1]. Diesel engines emit lower THC, CO and CO2 emissions than gasoline engines which are their conventional and commercial competitor. However, they are disadvantaged in terms of PM and NOx emissions. PM and NOx emissions are the most important emissions for diesel engines and many systems have been developed to control these emissions [2]. Many studies in the literature reveal that PM and NOx emissions occur in the opposite relationship [3]. In other words, an intervention on the engine management system reduces one of these emissions and increases the other. This contrast situation causes difficulties to control of diesel engine emissions.

Emissions prevention and reduction precautions in internal combustion engines can be grouped into three categories as before combustion, during combustion and after combustion. One of the precaution which taken during combustion is high pressure and multi stage injection. Multi stage injection is consist of three parts which pre-injection, main-injection and post-injection. Post-injection is the process of spraying a small amount of fuel into the cylinder after a certain period of time from the main spraying phase and provides a significant reduction in soot emissions [4]. Soot emissions occur in local fuel-rich region with high temperatures and inadequate oxygen concentration. Especially small size of particles contains great risks to human and the environment, because small particles of work can easily reach the alveoli and pass into the blood [5].

Secondary combustion, which occurs during the post-injection, burns some of the particles which raised substantially in the controlled combustion phase and reduces the soot emissions and increases the combustion efficiency. At the same time, post injection increases exhaust gas temperatures and improves the working regimes of after-treatment systems. Although many studies have been conducted with post-injection, the exact effects of post-injection on exhaust emissions and the mechanism of action are not well understood still [6]. Some studies which carried on post-injection in the literature are summarized below.

Sun et al. [7] observed that reducing engine soot emissions between 11% and 21% band with close-coupled post injection. On the other hand, NOx emissions increased by 3-5% for the relevant test matrix.

Jeftic and Zheng [8] have made experimental studies at 4-stroke, 4-cylinder, diesel engine with 90MPa injection pressure and 0.13MPa intake pressure. In this study examined the effects of post-injection, the main injection timing was kept constant at 4°CA BTDC and the post injection timing was manipulated between 20°CA ATDC and 70°CA ATDC. In this study, the behaviour of conventional diesel fuel and some alternative fuels during post-injection were investigated. According to the results, the IMEP value decreased as post-injection was delayed. It was determined that the post-injection was reduced by a significant reduction of the soot emission until the 40°CA ATDC delay then no significant reduction affect was observed with higher delay timing of post-injection. In terms of NOx emissions, NOx emissions decreased when post-injection delay increased. According to this studies

results, 30% reducing of NOx emissions was observed by withdrawing the post-injection starting point from 30°CA ATDC to 70°CA ATDC.

Li et al. [9] investigated the effects of different injection strategies on emission by using conventional diesel fuel in a 4 cylinder, four-stroke turbocharged and common rail injection engine. This study was carried out at 1450rpm engine speed and 80MPa injection pressure and three different injection strategies were examined. These are single main injection, pilot and main injection, main and post injection. In the experiments with multiple stage injection, 80% of the fuel was sent to the cylinder in the main injection phase. In the pilot-main injection application, the largest in-cylinder peak pressure was obtained. On the other hand, the single main injection strategy showed a bit higher peak pressure value than the post-main strategy. Exhaust gas temperature values were the highest in the post-main application and the lowest in the pre-main application. Nitrogen oxides are the highest in the pre-main application and lowest in the post-main application. While it is the highest value in pilot-main injection, it has the smallest value in the post-main injection in terms of soot emission. When the results obtained from the study were evaluated, it was found to be advantageous in terms of NOx in the main-post application, 3.5% compared to the single-main application and over 10% in terms of NOx compared to the pre-main application. In terms of soot emissions, the post-main application emits 4 times fewer emissions compared to the pilot main application and 40% lower emissions compared to the single main application.

Chen et al. [10], in their experimental study, examined the emission oscillations for diesel fuel and biodiesel fuels with eight cylinders turbocharged, common rail injection system diesel engine by changing the post-injection timing and post fuel injection quantity. The tests were performed at 1500 rpm engine speed and 25% engine load. Post-injection time was manipulated in a wide range of 30oCA to 150°CA after TDC. The results showed a slight improvement in the post-injection between 30-60°CA ATDC on the engine torque for equal post-injection amounts, but no significant change in engine torque was observed in post-injection with greater delay. At the same post-injection timing, THC and CO emissions increased with the increase of the post-injection quantity in both conventional diesel and biodiesel fuels, while nitrogen oxide emissions decreased in the beginning, but the NOx emissions increased with the increasing amount of post-injection.

Liu and Song [6] used turbocharged, common rail injection system a high speed diesel engine in their academic study. The experiments were performed at 1800rpm engine speed and 75% engine load. In this study, the effects of post-injection timing and the amount of fuel injected effects of during the post-injection were investigated. In the study, the main injection quantity and main injection timing were kept constant, as 22°CA BTDC and 40 mg/st. The post injection was manipulated between 10 and 30°CA ATDC and between 0 and 15 mg/st. Specific CO emissions reduced when the post-injection interval decreased with compared to other test points. While CO emissions were higher at bigger post-injection quantity, CO emissions at lower intervals were approximately independent of the post-injection quantity. A similar trend is observed in terms of specific THC emissions, but the variations depending on the quantity of post-injection also have differences in the low injection intervals. The specific nitrogen oxide emissions declined by about 10% in this study while interval increased. Soot emissions were heavily influenced by post-injection timing and showed significant decreases with the increasing interval. It was also observed that the increased interval caused very closed results for different post injection quantities.

Li et al. [11] examined pre, main and post-injection with biodiesel fuel on light-duty, direct injection, and common rail engine. The engine speed was selected at 1300 rpm, 1800 rpm, and 2300 rpm, and the total injection quantity was fixed at 58 mg/st, and the injection pressure was 130 MPa. Main injection time was selected as 1°CA BTDC and post injection was performed with a delay of 8-20°CA with reference to the main injection. According to the experimental results, CO emissions increase as the post injection quantity increases and the after injection retarding increases. This trend is even more evident at increasing engine speeds Within the post-injection times determined in the tests, THC emissions are also in the same trend with CO emissions. NOx emissions are declining both of increasing the post-injection quantity and by moving away from TDC. The study shows that engine speed is strictly dependent on NOx emissions and the significant decrease in NOx emissions is observed as engine speed increases. In terms of PM emissions, it has been observed that increasing the quantity of post-injection and away from TDC increased PM emissions.

In this study, various tests were performed on the single cylinder engine. At 1500 rpm engine speed, the main injection quantity was kept constant but the post injection quantity and timing were changed. Thus, the effects of post injection quantity and timing were investigated on CO, NOx, and soot emissions.

2. EXPERIMENTAL SETUP AND TEST CONDITIONS

The test was performed on a single-cylinder CI diesel engine equipped with a common-rail injection system. The specifications of the diesel engine and fuel injection system are shown in Table 1.

Table 1. Engine and fuel system specifications

Description	Specification
Engine Type	Single-cylinder, CI
Bore x Stroke [mm]	110*120
Total Displacement [lt]	1.14
Compression Ratio	15:1
Number of Valves	4
Injection System	Common-rail
Injector Type	Solenoid
Nozzle Hole Diameter [mm]	0.197
Nozzle of Holes per Nozzle	8

The engine was supplied with the conditioned air at 50 °C and 2,3 bar (absolute pressure). Rail pressure was set at 1000 bar and it was kept constant throughout the test. To increase the measurement accuracy, the fuel temperature was set to 38 °C in all tests. At 1500 rpm engine speed, while main injection timing and quantity was kept constant, post injection timing and quantity was changed. The main injection timing 13 °CA (BTDC) and main injection quantity 36 mg/st was selected. In addition to the main injection, post injection timing was changed between 12 °CA and 18 °CA (ATDC) one by one. Also, the post-injection was injected with different quantity which are 10 mg/st, 12 mg/st and 14 mg/st. The test was carried out with diesel fuel complying with EN590 standards.

For emission measurement, two small holes were drilled on the exhaust line. Samples were taken from these holes and sent to gas and particle matter emission measurement system. The portable measurement emission device was used for emission measurement. PEMS was equipped with NDIR analyzer for CO emission measurement, NDUV analyzer for NO_x emission measurement, and micro soot analyzer for particle matter measurements.

The detailed properties were related to test equipment were listed in Table 2.

Table 2. Test equipment

Test Equipment	Model
Dynamometer	AVL AC DynoExact
Emission Measurement	AVL Gas and PM PEMS
Indicating System	AVL IndiSmart Gigabit
Pressure Sensor	Kistler Piezoelectric
Fuel Measurement	AVL 735S
Fuel Conditioner	AVL 753C
Intake Air Conditioner	AVL Supercharging Unit
ECU	Adaptronic
Automation Software	AVL PUMA Open 2 TM

Also, the layout of the test system was shown in Figure 1.

Figure 1. The test system layout

3. RESULTS AND DISCUSSION

In this study, the quantity and advancement of the injected fuel were kept constant in the main injection phase. During the post injection, the quantity of fuel sent into the cylinder and the timing of injection were changed. The results were examined depend on changing of starting the post injection timing and post injection quantity. The effects of these post-injection parameters on CO, NO_x and soot emissions were investigated.

Graph 1 and Graph 2 reveal CO emissions depending on the post-injection starting and post-injection quantity. Post-injection was extended by 12 °CA delay to 18 °CA delay, and observed a regular increase of CO levels at all points. These values were confirmed for three different post-injection quantity and the increasing in the post-injection quantity was caused an increase in CO emissions. This can be attributed to the fact that the fuel is introduced into the combustion chamber at a thermodynamically inconvenient time and there is not enough time for the equilibrium reaction to occur due to the rapid decline of the combustion temperatures with expansion and the freezing of the reaction.

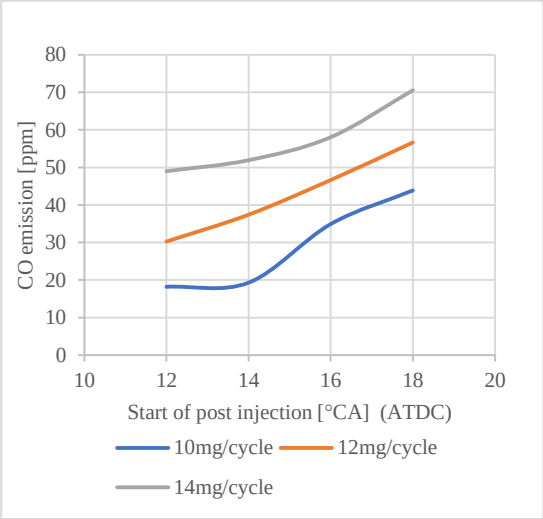

Graph 1. Changing of CO emission depending on the beginning of post injection.

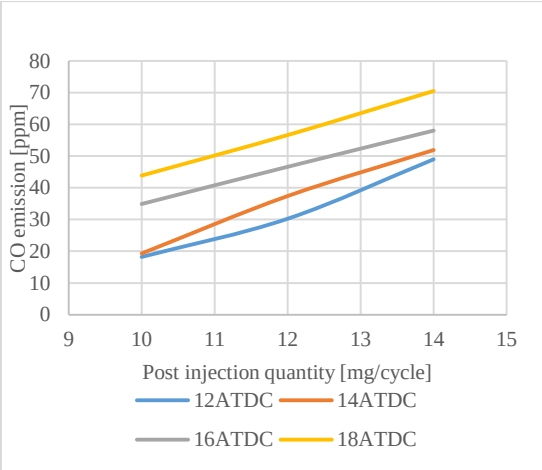

Graph 2. Change of CO emission depending on the quantity of post injection

Graph 3 and Graph 4 show the effects of post-injection beginning and post-injection quantity on NOx emissions. According to the experimental results, NO_x emissions reduce when post injection delay timing increased. This is largely due to the high cooling rate during the expansion, resulting from the high compression ratio in the diesel engine. As the post-injection was delayed, the time until the reaction was frozen prolonged, the cooling rate decreased, and the reaction rate increased accordingly. Thus, NOx emissions at engine output have shown significant reductions. A constant trend was not observed due to the change in the amount of post injection. The increase in the amount of post-injection initially increased some NO_x, then led to a decline again. The form fluctuation that took place in this spray, which is close to the TDC, was more dominant.

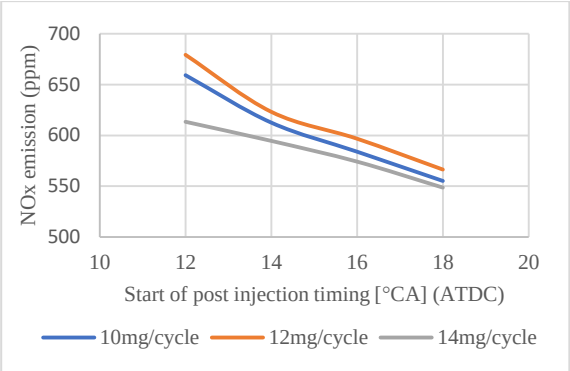

Graph 3. Change of NOx emission depending on the beginning of post injection

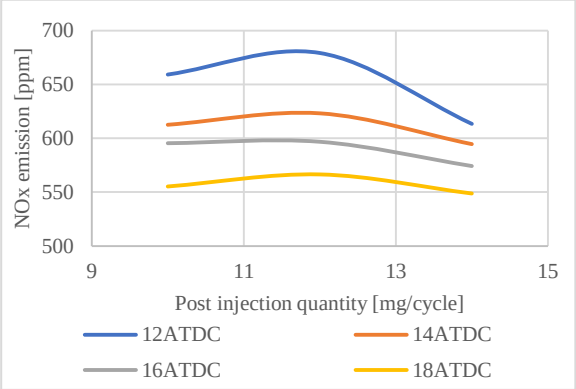

Graph 4. Change of NOx emission depending on the quantity of post injection

Graph 5 and Graph 6 demonstrate the effects of timing and quantity on soot emissions in the post-injection process. According to the results, the increasing the post-injection delay from TDC to a certain distance increased soot emissions and then this trend reversed. But this trend wasn't observed at lower amounts of post injection.

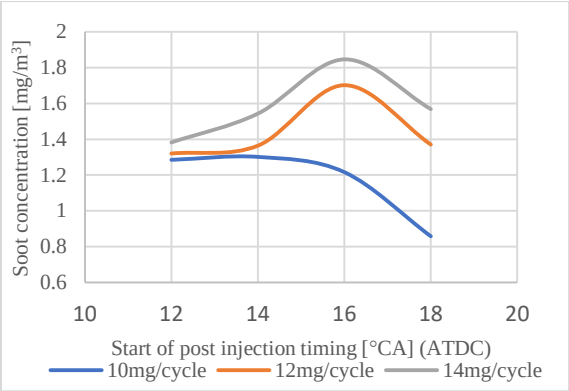

Graph 5. Change of soot emission depending on the beginning of post injection

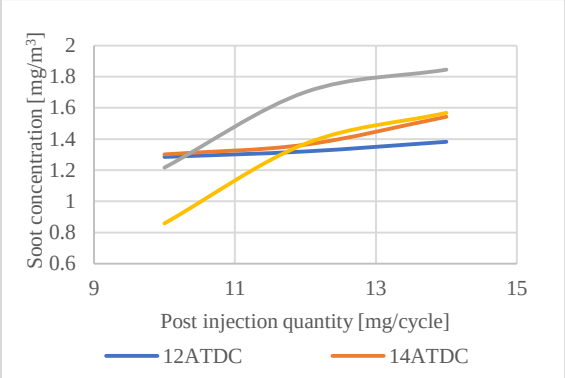

Graph 6. Change of soot emission depending on the quantity of post injection

CONCLUSION

An experimental research was carried on single cylinder research diesel engine for understanding the effect of using post injection strategy in modern diesel engines. the CO was increased with the injection retard for post injection phase for same operating condition, it was attributed to attributed to the fact that the fuel is introduced into the combustion chamber at a thermodynamically inconvenient time and there is not enough time for the equilibrium reaction to occur due to the rapid decline of the combustion temperatures with expansion and the freezing of the reaction, the NO_x emissions reduced when post injection delay timing increased. This was attributed to the high cooling rate during the expansion, resulting from the high compression ratio in the diesel engine. Also the increasing the post-injection delay from TDC to a certain distance increased soot emissions and then this trend reversed. An opposite trend was observed for lower amount of injection rates.

REFERENCES

[1] Li, X., Xu, Z., Guan, C., & Huang, Z. (2014). Effect of injection timing on particle size distribution from a diesel engine. *Fuel*, *134*, 189-195.

[2] Benajes, J., Martín, J., García, A., Villalta, D., & Warey, A. (2017). Swirl ratio and post injection strategies to improve late cycle diffusion combustion in a light-duty diesel engine. *Applied Thermal Engineering*, *123*, 365-376.

[3] Hadadpour, A., Jangi, M., Pang, K. M., & Bai, X. S. (2019). The role of a split injection strategy in the mixture formation and combustion of diesel spray: A large-eddy simulation. *Proceedings of the Combustion Institute*, *37*(4), 4709-4716.

[4] Fan, C., Song, C., Lv, G., Wei, J., Zhang, X., Qiao, Y., & Liu, Y. (2019). Impact of post-injection strategy on the physicochemical properties and reactivity of diesel in-cylinder soot. *Proceedings of the Combustion Institute*, *37*(4), 4821-4829.

[5] Mohankumar, S., & Senthilkumar, P. (2017). Particulate matter formation and its control methodologies for diesel engine: A comprehensive review. *Renewable and Sustainable Energy Reviews*, *80*, 1227-1238.

[6] Liu, W., & Song, C. (2016). Effect of post injection strategy on regulated exhaust emissions and particulate matter in a HSDI diesel engine. *Fuel*, *185*, 1-9.

[7] Sun, C., Martin, J., & Boehman, A. L. (2019). Nanostructure and reactivity of soot produced from a turbodiesel

engine using post injection. *Proceedings of the Combustion Institute*, *37*(1), 1169-1176.

[8] Jeftić, M., & Zheng, M. (2015). A study of the effect of post injection on combustion and emissions with premixing enhanced fueling strategies. *Applied Energy*, *157*, 861-870.

[9] Li, X., Guan, C., Luo, Y., & Huang, Z. (2015). Effect of multiple-injection strategies on diesel engine exhaust particle size and nanostructure. *Journal of Aerosol Science*, *89*, 69-76.

[10] Chen, P., Ibrahim, U., & Wang, J. (2014). Experimental investigation of diesel and biodiesel post injections during active diesel particulate filter regenerations. *Fuel*, *130*, 286-295.

[11] Li, H., Song, C., Lv, G., Pang, H., & Qiao, Y. (2017). Assessment of the impact of post-injection on exhaust pollutants emitted from a diesel engine fueled with biodiesel. *Renewable Energy*, *114*, 924-933.

Paper 29 **Bildiri 29**

DETAILED CHEMICAL KINETIC MODELING OF THE EFFECTS OF METHANOL ADDITION ON N-HEPTANE OXIDATION

Abdalwahab ALAZREG, Emre DEGIRMENCI, Fikret INAL

Department of Chemical Engineering, Izmir Institute of Technology, 35430, Urla, Izmir, fikretinal@iyte.edu.tr

It is not surprising that there have been many studies on the effect of fuel additives on soot and toxic species formation in hydrocarbon flames in order to improve its efficiency and performance [1, 2]. As one of the primary reference fuels (PRF), n-heptane can well represent the combustion characteristics of diesel and gasoline fuel. Thus, it is frequently used as a surrogate for diesel fuel in combustion research [3, 4]. The effects of adding methanol, ethanol and MTBE, oxygenate additives, (i.e., oxygen containing species) on laminar, premixed, fuel-rich n-heptane flames at the same equivalence ratio were investigated [5, 6]. They found that low-molecular-weight species, aromatics and soot were reduced with oxygenate addition. A shock tube study to investigate the influences of oxygenated additives (i.e. dimethyl ether, acetone and butanal) on n-heptane oxidation was conducted and a significant reduction of the combustion emissions was observed [7]. One of the commonly used oxygenate additive is methanol. Methanol has been used as an octane improver in gasoline. It also reduces exhaust carbon monoxide emissions from motor vehicles by leaning fuel-air mixture [8, 9]. Many studies investigated experimentally the addition of methanol to n-heptane and how it performed to reduce the combustion emission [10, 11]. In this study, the effects of methanol addition on n-heptane oxidation in atmospheric pressure, laminar, premixed, fuel-rich flame was investigated using Detailed Chemical Kinetic Modeling approach.

Generally, the objective of this effort is to predict macroscopic phenomena from the knowledge of fundamental chemical and physical parameters, together with a mathematical model of the process. The computation work was conducted using PREMIXED code [12] of ChemKin package [13]. ChemKin is one of the most commonly used software; it is used worldwide for combustion, chemical processing and automotive industries. In defining the chemistry set in a ChemKin simulation, users must first supply the thermodynamic data and transport data for each species in the chemical system and definitely reaction rate parameters. A model validation using various available literature data for different combustion systems (i.e. laminar premixed flame and rapid compression machine) was also carried out. In addition, the effects of adding

oxygenate, methanol, to n-heptane flame on the formation of combustion products were investigated using Inal and Senkan's experimental study [5]. The experimental conditions are given in Table1.

Table.1. Experimental Conditions for n-heptane and methanol of the target study

Equivalence ratio	2.10
Pressure	1 atm
Inlet velocity	5.157 cm/sec
Initial mole fractions	
n-heptane	0.0520
Methanol	0.0107
Oxygen	0.2803
Argon	0.6570

A comprehensive and recent mechanism available in the literature, Lawrence Livermore National Laboratory (LLNL) n-heptane mechanism (version 3.1) [14], was selected as the base mechanism for the modeling work. Marinov's mechanism [15] and pure methanol mechanism [16] were merged with the base mechanism. The proposed mechanism consists of 3249 reactions and 753 species.

It was found that, the mole fraction profiles of carbon monoxide, acetylene, diacetylene, vinylacetylene, other low-molecular-weight reaction products and species up to benzene were consistently lower in flame containing methanol. Figure.1 shows model predictions and experimental data for CO mole fractions for n-heptane and n-heptane/ methanol flames.

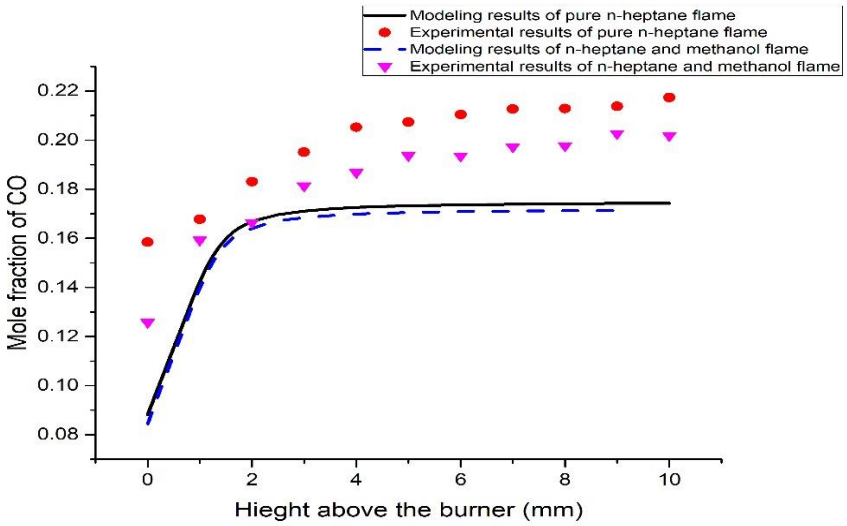

Figure 1. Experimental and modeling results of CO mole fraction of both n-heptane and n-heptane with methanol

The addition of methanol to n-heptane fuel reduced the mole fractions of combustion products. By comparing the experimental and modeling results of both n-heptane flame and n-heptane with methanol flame there were a good agreement between mole fractions of species.

References:

1. Raj, A., et al., A reaction mechanism for gasoline surrogate fuels for large polycyclic aromatic hydrocarbons. Combustion and Flame, 2012. 159(2): p. 500-515.

2. Wang, H., et al., A reduced toluene reference fuel chemical kinetic mechanism for combustion and polycyclic-aromatic hydrocarbon predictions. Combustion and Flame, 2015. 162(6): p. 2390-2404.

3. Ra, Y. and R.D. Reitz, A reduced chemical kinetic model for IC engine combustion simulations with primary reference fuels. Combustion and Flame, 2008. 155(4): p. 713-738.

4. Westbrook, C.K., W.J. Pitz, and H.J. Curran, Chemical Kinetic Modeling Study of the Effects of Oxygenated Hydrocarbons on Soot Emissions from Diesel Engines. The Journal of Physical Chemistry A, 2006. 110(21): p. 6912-6922.

5. Fikret INAL , S.S., Effects of oxygenate additives on polycyclic aromatic hydrocarbons(pahs) and soot formation. Combustion Science and Technology, 2002. 174(9).

6. Inal, F. and S.M. Senkan, Effects of oxygenate concentration on species mole fractions in premixed n-heptane flames. Fuel, 2005. 84(5): p. 495-503.

7. Hong, Z., et al., The effect of oxygenates on soot formation in rich heptane mixtures: A shock tube study. Fuel, 2009. 88(10): p. 1901-1906.

8. Dagaut, P. and C. Togbé, Experimental and modeling study of the kinetics of oxidation of ethanol-n-heptane mixtures in a jet-stirred reactor. Fuel, 2010. 89(2): p. 280-286.

9. Sayin, C., A.N. Ozsezen, and M. Canakci, The influence of operating parameters on the performance and emissions of a DI diesel engine using methanol-blended-diesel fuel. Fuel, 2010. 89(7): p. 1407-1414.

10. Chen, G., et al., Experimental and modeling study of the effects of adding oxygenated fuels to premixed n-heptane flames. Combustion and Flame, 2012. 159(7): p. 2324-2335.

11. Chen, G., et al., Experimental and modeling study on the influences of methanol on premixed fuel-rich n-heptane flames. Fuel, 2013. 103: p. 467-472.

12. Kee RJ, R.F., Smooke MD, Miller JA., PREMIX: a fortran program formodeling steady one-dimensional premixed flames. Livermore,CA: Springer, 1985.

13. Kee RJ, R.F., Miller JA, CHEMKIN-II: a fortran chemical kinetic package for the analysis of gas phase chemical kinetics. Livermore,CA: Sandia National Laboratories1989.

14. Mehl, M., et al., Kinetic modeling of gasoline surrogate components and mixtures under engine conditions. Proceedings of the Combustion Institute, 2011. 33(1): p. 193-200.

15. Marinov, N. M., W. J. Pitz, C. K. Westbrook, A. M. Vincitore, M. J. Castaldi, S. M. Senkan, "Aromatic and Polycyclic Aromatic Hydrocarbon Formation in a Laminar Premixed n-Butane Flame," Combustion and Flame114, 192-213 (1998).

16. U. Burke, W.K. Metcalfe, S.M. Burke, K.A. Heufer, P. Dagaut, H.J. Curran A Detailed Chemical Kinetic Modeling, Ignition Delay time and Jet-Stirred Reactor Study of Methanol Oxidation Combustion and Flame (2016) 165 125–136

Paper 30 **Bildiri 30**

INVESTIGATION OF HYDROGEN BLENDING EFFECTS ON TURBULENT METHANE FLAME PROPERTIES USING PDF-MONTE CARLO METHOD AND FGM CHEMISTRY TABULATION APPROACH

Meryem Alaya[#1], Ridha Ennetta[*2], Rachid Said[#3]

 # Ionized and Reactive Media Study (EMIR), Monastir Preparatory Institute for Engineering Studies (IPEIM), University of Monastir, 15 Street Ibn al-Jazzar, 5019 Monastir, Tunisia

[1]meryem_alaya@live.fr ; corresponding author

[3]rachid.said@ipeim.rnu.tn

[*] *Mechanical Modeling, Energy & Materials (M²EM), National School of Engineers of Gabes (ENIG), Gabes University, Avenue of Omar Ib-Elkhattab, 6023, Zrig, Gabes, Tunisia*

[2]ridha_ennetta@yahoo.fr

ABSTRACT

This In this work, a computational investigation of the impacts of hydrogen blending on the fundamental properties of spherical propagating methane-air flames was performed in an adiabatic constant vessel at different conditions of equivalence ratios and turbulence intensities.

Due to the spherically symmetric of the problem, a one-dimensional simulation was considered and an ignition in the middle of the domain was occurred. The turbulence was supposed to be isotropic and homogenous.

The combustion chemistry was described by the tabulated detailed kinetic mechanism GRIMech. Tabulation has been performed, in a pre-processing step, using the Chem1D code based on the FGM chemistry tabulation approach.

Numerical simulations of the flame evolutions were based on PDF-Monte Carlo method. The emphasis is placed on the mean flame radii, flame brush thickness, turbulent propagating velocity and the minimum ignition energy. Computed results were compared to measured data in literature and good agreements were observed. We notice that the mean flame radii, the flame brush thickness and the flame speed increase monotonically with the increase of the content of hydrogen in the fuel. However, the minimum ignition energy (MIE) decreases as the added hydrogen fraction increases.

***Keywords*— Hydrogen, methane, turbulent velocity, flame radius, flame thickness, MIE**

INTRODUCTION

Ecological and economical regulations produce an urgent need to found clean alternative fuels.

Natural gas (NG) represents a clean alternative. In fact, thanks to methane, its main component, it offers important environmental and economic advantages. Its pollutant emissions are lower compared with other fuels [1].

Unfortunately, the low flame speed, the high sensitivity to cyclic variations and the low flammability limits of methane pose great challenges [2].

One of the effective strategies to solve this problem is to associate methane with a more reactive fuel.

The hydrogen is considered as an excellent candidate by improving efficiency and enhancing the NG combustion process thanks to its low ignition energy and high flame speed [3].

In order to study the combustion characteristics of hydrogen enriched methane flames, several numerical and experimental researches have been carried out.

A number of recent studies [4-6] have already demonstrated that hydrogen addition to NG enhances flame speed and combustion stability for the very poor mixing zones that reduce emissions of green house effect gases and improve the engine thermal efficiency.

Navarro et al. [4] showed that hydrogen blending helps to decrease CO2 emissions.

Askari et al. [5] found that adding hydrogen can significantly improves HCCI combustion performances and decreases pollutant emissions.

According to Guo et al. [6] hydrogen blending of methane/air flame has a great effect in extending the flammability limits and improving operation under ultra lean conditions.

Others studies [7-12] have been conducted to present a clearer understanding of the benefits of the utilization of hydrogen in blended form on NG combustion properties.

In this, study we will focus on the effect of adding hydrogen on expanding methane/air flames as is the case in internal combustion engines.

By analogy with laminar flames, turbulent flame speed has been considered as the basic characteristic of premixed turbulent combustion, thus it has been the main focus of several theoretical and experimental researches for decades [13].

To achieve the goal of such studies, a large number of computational models and approaches have been developed: Reynolds Averaged Navier-Stokes (RANS) approach [14], Bray-Moss-Libby (BML) model [15, 16] , Large Eddy Simulation (LES) [17] and Direct Numerical Simulation (DNS) [18] are some examples.

DNS, LES and RANS are considered as the three principal approaches in modeling turbulent combustion [19].

In order to describe turbulent premixed flames, numerous models have been developed.

Due to their effectiveness and accuracy, probabilistic approaches are the most utilized in this regard [20], [21].

This model is inspired from the definition of the fine grained density function [22]. The ensemble average of the fine grained density function is considered and is termed the PDF: Probability Density Function. [23]

This stochastic description has many advantages: i) PDF may be defined in many turbulent reacting flow fields, ii) it includes all information to describe unsteady reacting flow fields and iii) it is applicable to premixed as well as non-premixed flames.

However, the PDF changes at every point in the flow field [24], thus the difficulty is to determine the PDF.

Two principal paths have been proposed: to presume the PDF shape [25,26] or to solve a PDF–transport equation [27,28].

Within the Monte Carlo solution algorithm development, PDF has been able to be calculated from a variety of flame configurations [29].

Thus, for few decades, many authors used Monte Carlo solution to simulate ignition and to study the flame characteristics in turbulent combustion conditions [30, 31].

Also, in this work we adopted Monte Carlo scalar PDF transport to simulate a premixed turbulent flame in a constant volume vessel.

Monte Carlo algorithm developments continue and it becomes more and more efficient. Nowadays it allows characterizing flame propagation taking in consideration turbulence as well as chemistry interaction.

In the present study, turbulence is supposed to be homogenous and isotropic and its characteristics are those of the frozen k-ε model [32]. In addition, we consider that the calculation domain is an open space and there are no flame-walls interactions. By the way, turbulence does not present any decay or dissipation rate decrease. The turbulent velocities are spatially correlated that makes difference between our study and classical PDF methods.

Mostly, chemistry is described by reduced chemical kinetic mechanisms [33,34]. A question arises; a reduced chemistry is it sufficient to describe the physics of methane-hydrogen mixture combustion?

The experiment shows that a reduced scheme does not allow to adequately predicting all the flame propagation characteristics. As an example, the one-step model of Marinov et al. [35] shows that from certain equivalence ratio, the speed and thickness of the flame cannot be obtained correctly.

The fine prediction of the evolution of the spherical propagation characteristics of the turbulent hydrogen-enriched methane flame requires the use of detailed chemical kinetics.

Despite the continual progress on storage capacity and calculation speed that modern computers and computational methods (CFD) have experienced, simulating turbulent combustion using detailed chemistry remains a high-flying challenge. Indeed, the models of turbulent flames are extremely complex because of the large scales of time and length involved. On the other hand, it is easier to model a laminar flame because of its relatively simple flow.

How can we then follow and understand the chemistry of turbulent combustion and at the same time maintain a reasonable computing time?

To answer this question, various alternatives have been proposed during the last decade. Recently, the method of chemistry tabulation has attracted great interest in modeling premixed combustion.

This technique consists in tabulating the chemical kinetics according to the key parameters.

The three best known and commonly used tabulation approaches are: ILDM [36], ISAT [37] and FGM [38].

In this work, we used the FGM method integrated in the Chem1D code to tabulate the detailed reaction mechanism GRIMech3.0. Then, the obtained tables are used, in the PDF-MC code, to study the effect of hydrogen addition one the methane-air flame propagation characteristics.

The computed results are confronted with measured data in literature and a reasonable agreement was observed. We have notice that mean flame radii, flame brush thickness as well as turbulent flame velocities increase monotonically with the increase of the amount of hydrogen blending.

However, the minimum ignition energy (MIE) decreases as the hydrogen content in the fuel increases.

COMBUSTION MODELLING FORMULATION

The equations used in our problem are:

- The mass conservation equation: used in spherical coordinates form. Its solution gives the expansion velocities provoked by the temperature gradient between hot products and fresh gas:

$$\frac{\partial \bar{\rho}}{\partial t}+\frac{1}{r^2}\frac{\partial\left(r^2\bar{\rho}\boldsymbol{u}_r\right)}{\partial r}=0 \tag{1}$$

- The Lagrangian joint PDF transport equation:

$$\begin{aligned}&\frac{\partial}{\partial t}\left(\rho(\underline{\psi})\, f_{\underline{u},\Phi}(\underline{v},\underline{\psi})\right)+\sum_{i=1}^{3}\frac{\partial}{\partial_{xi}}\left(\rho(\underline{\psi})Vif_{\underline{u},\Phi}(\underline{V},\underline{\psi})\right)=\\&-\sum_{i=1}^{3}\frac{\partial}{\partial_{vi}}\left(\rho(\underline{\psi})\left\langle A_i\middle|\underline{V},\underline{\psi}\right\rangle f_{\underline{u},\Phi}(\underline{v},\underline{\psi})\right)\\&-\sum_{i=1}^{3}\frac{\partial}{\partial_{vi}}\left(\rho(\underline{\psi})\left\langle A_i\middle|\underline{V},\underline{\psi}\right\rangle f_{\underline{u},\Phi}(\underline{v},\underline{\psi})\right)\\&-\sum_{i=1}^{N}\frac{\partial}{\partial_{\psi\alpha}}\left(\rho(\underline{\psi})\left\langle\theta_\alpha\middle|\underline{V},\underline{\psi}\right\rangle f_{\underline{u},\Phi}(\underline{v},\underline{\psi})\right)\end{aligned} \tag{2}$$

Where

$$A_i\frac{1}{\rho}\left(\frac{\partial\tau_{ij}}{\partial x_j}-\frac{\partial P}{\partial x_j}\rho F_i\right);i,j=1,3$$

And

$$\theta_\alpha=\frac{1}{\rho}\left(\frac{\partial J_k^{\alpha}}{x_k}+\rho\omega_\alpha+S_\alpha\right);\alpha=1,N$$

- The Perfect gas equation:

$$\bar{P}=\bar{\rho}\frac{RT}{M} \tag{3}$$

Where:

ρ :the density

u_r : The Favre averaged radial velocity corresponding to the expansion velocity provoked by the temperature gradient between fresh gas and hot products.

$\underline{\Phi}$, $\underline{u}$: are respectively , a scalar vector and a velocity vector in the physical space and to which correspond respectively the vectors of random values, $\underline{\Psi}$ and V in the conditional space.

$F_{\underline{u},\underline{\Phi}}$: The PDF of velocities and scalars.

A_i, θ_α: The change terms that characterize the stochastic process

τ_{ij} The strain tensor

F_i: The stirred force per volume unity

P : The pressure

J_k^α: The diffusive fluxes

ω_α: The reaction rate

S_α: The source term

T : The Favre averaged temperature

M : The molar mass of the mixture

PDF-MONTE CARLO METHOD

This method is used in the case of turbulent reactive flow with fluctuation terms that need to be statically treated.

The basic idea of the PDF Monte Carlo simulation consists in calculating the displacement in the space of a certain number of probabilistic particles. This is done by simulating the different terms of the PDF equation by interactions of these particles after random walk. The simulation can be based on Eulerian balance equations or Lagrangian equations.

The type of PDF used in this present work is the transported PDF called Pope's method [30]. Monte Carlo method properties have been well studied by Pope [39], [40].

Ennetta et al [41] tested the accuracy of this method in predicting methane propagating flame characteristics using reduced chemical kinetic scheme. They found that, the current model predict, correctly, the effect of increasing turbulence intensity and equivalence ratio on methane-air premixed flame properties such as the mean radius and the turbulent velocity. The main blame of this method is its slow convergence.

In this method, the calculation domain is divided into Nc cells. Each cell contains a given number of Ni particles. The displacement of these elements (particles) in the whole domain is due to the gas expansion velocity, provoked by the temperature gradient between burned and unburned gases, and to the turbulent diffusion, where a correlation velocity deduced from turbulence spectrum is respected.

Simulation parameters

In this work, the computational environment considered is a 1D one dimensional spherically symmetric domain. The changes are considered only in the radial direction.

At first, the premixed fuel (CH4 or CH4+H2)-air mixture is at rest. Then a hot source is used to generate a localized deposit of thermal energy. This energy triggered the flame initiation and highly increased the temperature in this region [32] as well as in the case of internal combustion engine.

The computational domain considered is in the radial direction and is composed of

NC =500 cells each one with a given size Δr and contain initially, Ni particles.

Each particle is specified with a velocity and some thermo-chemical variables (concentrations, T,..). The calculation was done at a constant pressure P=1 atm.

In order to account for convective transport assured by the mean flow and turbulence (in space and time), each fluid particle is tracked by the numerical process during each time step.

Chemical reaction and molar mixing change the chemical and thermal composition of each element that are calculated in a pre-processing step using Chem1D code based on FGM method.

The cell size and the calculation time step chosen from literature are respectively Δr=0.25mm and Δt=0.1 ms which remain constant during the calculation. These parameters allow more precise detection of the flame front evolution.

Some numerical tests were performed by Raman et al. [42] to find the optimal time and space steps. For the methane-air mixture a time step equal to 1.10^{-4}s provides acceptable results [42].

Turbulent length and time scales are given by the following formulas:

$$l_t = 0.164 \frac{k^{3/2}}{\varepsilon} \; ; \qquad \tau_k = 0.3$$

These parameters values are equal to those used in experimental cases.

The input values required and used for the simulation are the following:

Δr : Cell size

Δt : Time step

k : Turbulent kinetic energy

ε : Dissipation of turbulent kinetic energy

x : Ignition energy

c_{finit} : normalized mean fuel concentration

t_{ignit} : Ignition time

r_{ignit} : Ignition gap

N_i : Initial number of particles in each cell

T_{ini} : Initial temperature

T_{adiab} : Adiabatic flame temperature

P : Pressure

Chemical kinetics

The combustion chemical kinetics of the H2+CH4-air flames was obtained by a detailed chemistry tabulation approach called FGM.

The FGM technique is used to simplify the chemical kinetic model taking into account the local flamelet structure. It has already proven to be accurate for modeling both premixed and partially premixed flames in LES, DNS and RANS calculations [43],[44].

The simulations have been performed using the code CHEM1D [45], based on the FGM method, to tabulate the detailed reaction mechanism GRIMech3.0 [46]. This mechanism is considered as a standard in modeling NG combustion. [47]

In a previous work [48] this detailed scheme was used to study the effect of hydrogen addition on the laminar speed of methane flame. It has been shown that GRIMech3.0 gives very satisfactory results.

Different fuel mixtures are considered: pure methane and methane-hydrogen mixture. These fuels are burnt at standard conditions with equivalence ratio from 0.9 to 1.1.

FGM Approach

Detailed chemistry can be more accurate than reduced one, but unfortunately, also computationally very expensive. In order to reduce computing times and costs an approach with tabulated chemistry is applied.

In this study, we used the so-called Flamelet-Generated Manifold (FGM) approach developed by Van Oijen [49] for laminar premixed flames. It allows using 1D laminar flamelet data for the tabulation of composition, temperature, density, etc, as function of local control variables.

This innovative method follows from some of other methods available in literature such as "ILDM (Intrinsic Low Dimensional Manifold) [36].

This laminar flamelet concept considers a turbulent flame as a set of thin laminar freely propagating one-dimensional flames. These flamelets are produced using CHEM1D [45] the code for detailed chemistry.

In a pre-processing step, control variables are defined, flamelet system is calculated with detailed chemistry and tables are generated, reflecting the thermo-chemical variables as a function of one or more control variables.

Then the manifold is computed. All the thermal properties (diffusivity, density, temperature,..) are stored in a tabulated form in the FGM data base.

A better description of the different phenomena can be achieved by increasing the number of independent control variables. [35] [38] [50]. In the case of simple fuel such as the CO/H2 mixture, two control variables are sufficient, but for a more precise reproduction of the combustion rate of the methane/air mixture at least three degrees of freedom are necessary. [38]

Thanks to this approach a great reduction of the computational costs of combustion simulation can be made [38][51][52] and high levels of accuracy can be kept.

FGM technique has been proven to be appropriate for highly stretched premixed counter flow flames [53] , laminar premixed benzene flames with heat losses [38], confined triple flames [54] and preferential diffusive effects[55].

Furthermore, this approach performed well also for turbulent partially premixed flames [56], [57] as well as for turbulent flames with heat losses.[52].

The application of premixed FGM including heat loss, turbulence and high pressure has never been studied in literature [58].

In this research the FGM method is applied for the simulation of turbulent methane/hydrogen combustion in a constant volume vessel.

The question which is addressed in this work is how well premixed flames are reproduced when premixed flamelet-based FGM database are used to represent combustion chemistry.

RESULTS AND DISCUSSION

In this section, flame mean radius, flame turbulent velocity, flame-brush thickness and the minimum ignition energy are studied. In fact these turbulent flame front characteristics represent a great challenge for decades in the turbulent combustion field. Our numerical values are compared to experimental results available in literature and a reasonable agreement was found. This study was done for parallelepiped vessel geometry with a constant volume. Ignition starts in the middle of the domain then a flame kernel propagates spherically.

1. Effect of hydrogen addition on the flame mean radius

Lecordier [59] defined the flame radius R_f in 2D configuration as the radius of the circle that contains the same surface of burned gas S_b by: $R_f = \sqrt{\frac{1}{\pi} S_b}$

In a 1D configuration (our case), the flame mean radius represents the distance that exists between the flame front position and the ignition center. The flame front position is determined in a region where the temperature is around 600 K. This value corresponds to the experimental temperature of silicon oil vaporization.

Figure 1 gives the variations of the flame radius function of time for three hydrogen fraction (%H2) in the mixture: 20, 80 and 100% at stoichiometric conditions (Φ=1) and with turbulent intensity level u'= 3.

Curves show that flame radius increases with time at fixed hydrogen fraction.

Numerical results are in good agreement with experimental curves found by Huang et al [60].

Huang et al [60] found that a linear relationship between flame radius and time for each mixture is demonstrated at stoichiometry which is also approved by our simulation.

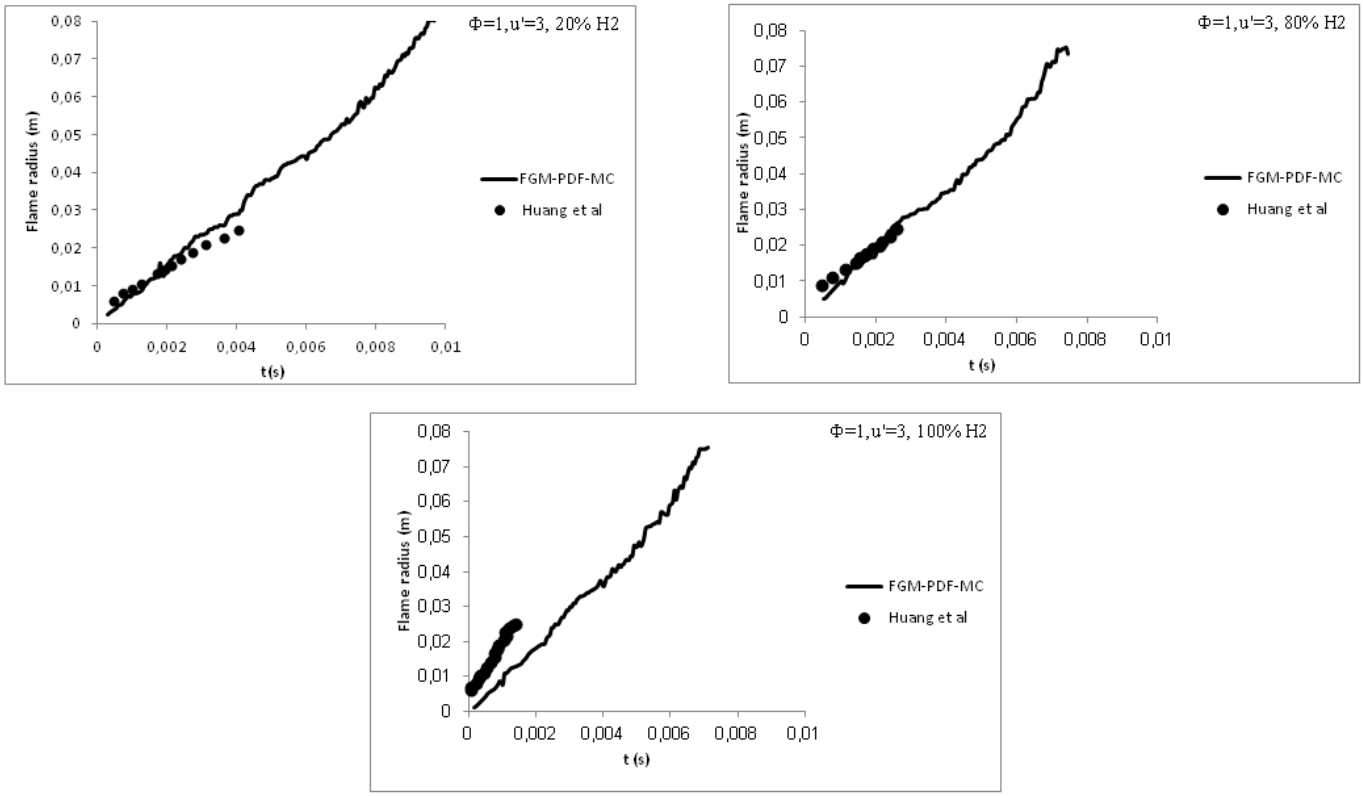

Fig. 1 Evolution of mean flame radius versus time at Φ=1, u'=3

Also, it was shown in Figure 2 that, at fixed time, the flame mean radius increases with the increase of hydrogen content in the mixture; therefore the flame develops more rapidly when the fuel becomes more hydrogenated.

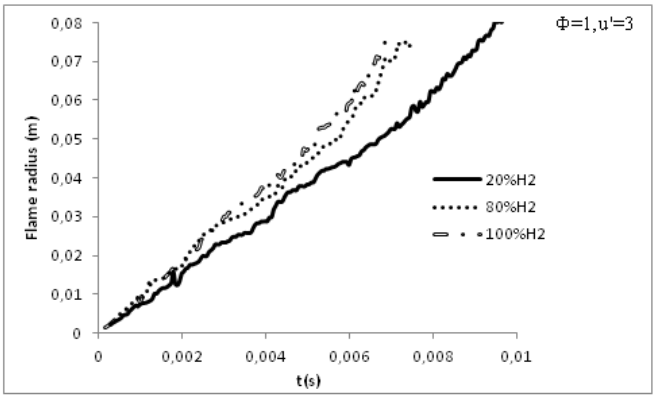

Fig. 2 Effect of hydrogen addition on flame mean radius

Effect of hydrogen addition on the flame brush thickness

Many relations were proposed in order to define the flame brush thickness also called flame width.

It is often defined by: $\delta_t = \frac{1}{\max|\nabla c|}$ where $c = \frac{T - T_f}{T_b - T_f}$ is the progress variable defined as a normalized temperature ; (b: burned, f: unburned) gas

Figure 3 displays the flame brush thickness variation versus hydrogen fraction at constant equivalence ratio (Φ=1).

It's noted that hydrogen addition provokes an increase in the flame brush thickness at a similar turbulence intensity and a constant equivalence ratio.

According to Hongsheng et al. [61], the variation in preferential diffusion is the first origin of this increase in the flame brush thickness. In fact, the fuel Lewis number is reduced with the addition of hydrogen. This decrease in Lewis number yields an increase of the local flame instability and then an increase in the flame brush thickness.

In addition Hongsheng et al. [61] affirmed that this increase might be the result of the increase in turbulent burning velocity at same equivalence ratio and turbulent level.

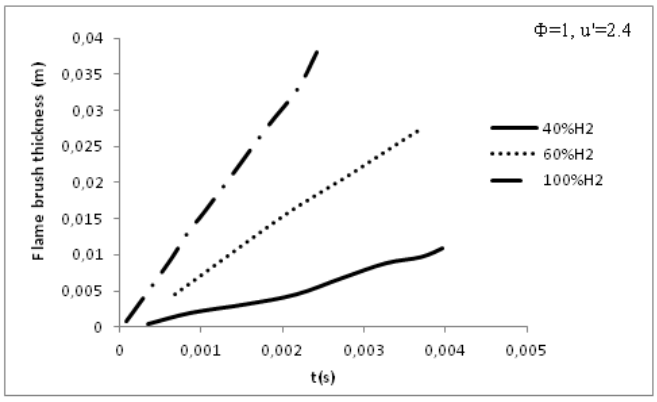

Fig. 3 Effect of hydrogen addition on flame brush thickness

2. Effect of hydrogen addition on turbulent flame velocity:

The flame velocity is described as the differential of the flame mean radius versus time.

In order to study the effect of hydrogen addition on the turbulent flame velocity we plotted the turbulent flame velocity versus hydrogen fraction for stoichiometry and for two fixed levels of the turbulence intensity: u '= 2 and u' = 2.4.
For both turbulent intensity levels, the turbulent burning velocity increased non-linearly with the increase of hydrogen content and the combustion becomes faster.

A satisfactory agreement is found between our simulation and experiment data of Fairweather et al [62] and Ekenechukwu [63].

Experimental results showed that the rises were modest with the addition of 10 and 20% of hydrogen and it becomes significant by 40%.

According to Ekenechukwu [63], this increase in the turbulent burning velocity could be a result of the increase in burning velocity of laminar flamelets that constitute the turbulent structure.

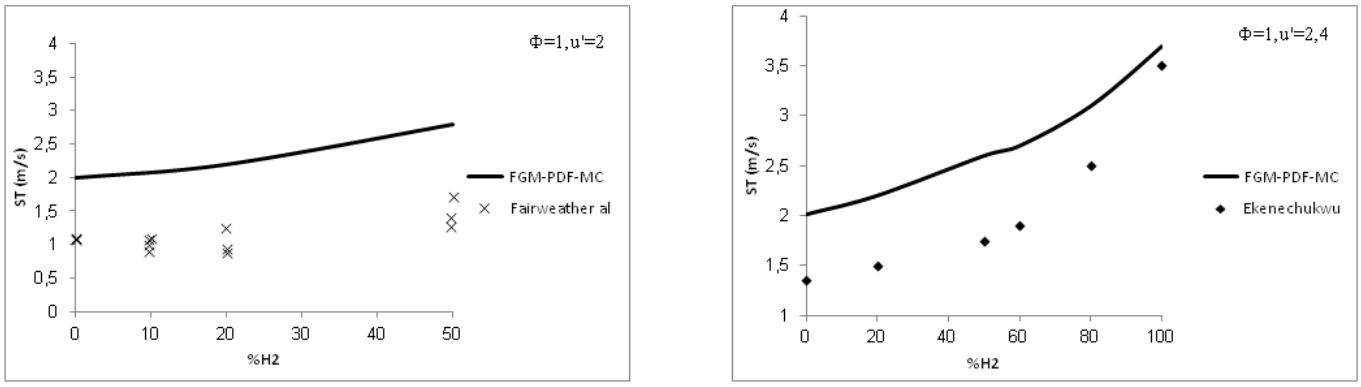

Fig. 4 Effect of hydrogen addition on turbulent flame velocity.

Effect of hydrogen addition on lowest ignition energy

The minimum ignition energy (MIE) represents the lowest energy necessary for the ignition achievement.

Figure 5 display the minimum ignition energy against equivalence ration for different methane-hydrogen mixtures (0%, 50% and 100% of hydrogen). One can see that the minimum of ignition energy is found close to stoichiometry.Our results are compared with data presented by Lewis & Von Elbe [64], Hankinson et al [65] Gexcon [66] and D.W.V [67]. A reasonable agreement was observed.

As expected, Figure 5 shows that the MIE decreased as hydrogen content in the fuel increases due to the low ignition energy required by hydrogen. This observation confirmed by Hankinson et al [65] is obvious in Figure 6.

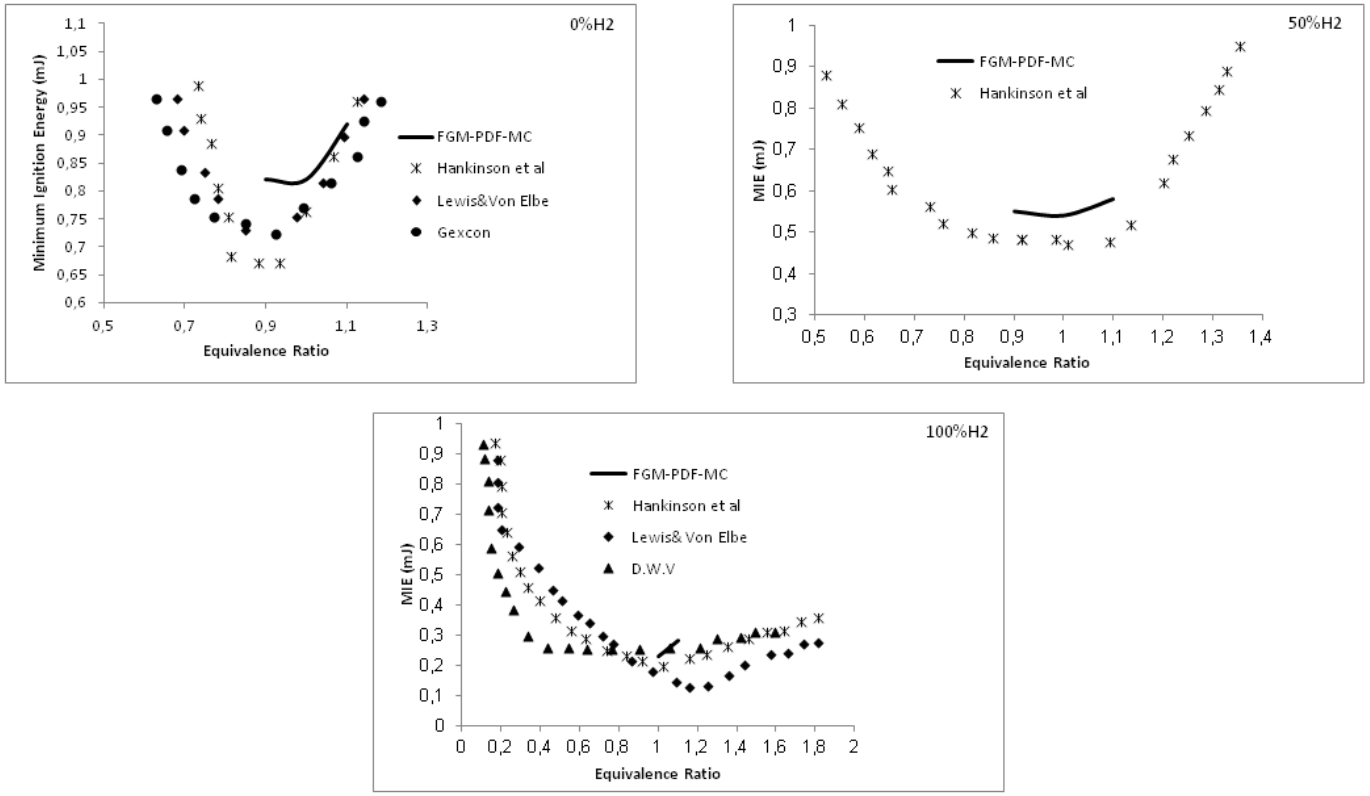

Fig. 5 MIE versus Equivalence Ratio, u'=2.

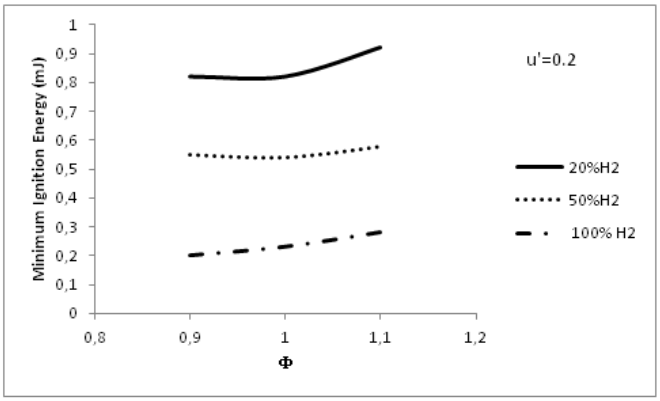

Fig. 6 Effect of hydrogen on MIE, u'=2

CONCLUSIONS

Spherical propagation of methane-air turbulent flames with different hydrogen blending levels was numerically simulated in an adiabatic constant volume vessel.

Numerical simulations were based on the PDF-Monte Carlo method using FGM approach for tabulating chemistry described by the standard detailed mechanism GRImech3.0. Turbulence was supposed to be homogeneous and isotropic.

The effects of hydrogen blending on the mean flame radii, flame brush thickness, turbulent propagating velocity and minimum ignition energy are investigated.

The computed results are confronted with measured data in literature and reasonable agreements were observed.

Simulations show that the mean flame radii, the flame brush thickness and the turbulent flame speed increase monotonically with the increase of the amount of hydrogen blending.

However, the minimum ignition energy, which represents the lowest energy necessary for achieving ignition, decreases as the hydrogen content in the fuel increases as a consequence of the low ignition energy of hydrogen. The lowest values of minimum ignition energy are found close to stoichiometry.

Good agreements, in mean flame radius, turbulent flame speed and minimum ignition energy measured by several researchers and predicted numerically by this study, were achieved. Therefore, PDF-Monte Carlo method associated with FGM approach for tabulating detailed chemistry could be an attractive numerical tool to predict hydrogen addition effects on turbulent methane-air propagating flame characteristics.

Funding: This research did not receive any specific grant from funding agencies in the public, commercial, or not-for-profit sectors.

References

[1] Boumeddane B., Investigations numériques de l'auto inflammation des mélanges méthane/air en mode HCCI, 19ème Congrès Français de Mécanique, Marseille, 24-28 August, 2009.

[2] Fotache C.G. and Kreutz T.G., Law. C.K., Ignition of hydrogen enriched methane by heated air. Combustion and Flame 1997; 110: 429–40.

[3] Yu G., Law C.K. and Wu C.K., Laminar flame speeds of hydrocarbon+ air mixtures with hydrogen addition. Combustion and Flame 1986;63: 339–47.

[4] Navarro E., J Leo, T. and Corral R.., C02 emissions from a spark ignition engine operating on natural gas-hydrogen blends (HCNG). *Applied Energy*, 101, 112-120, (2013).

[5] Askari M.H., Hoseinalipour S.M., Jazayeri S.A. and Baghsheikhi M., Effect of hydrogen addition to natural gas on homogeneous charge compression ignition combustion engines performance and emissions using a thermodynamic simulation. *International Journal of Automotive Engineering*, 1:2, 43-52, (2011).

[6] Guo H., Smallwood G.J., Liu F., Ju Y. and Gülder Ö.L., The effect of hydrogen addition on flammability limit and NOx emission in ultra-lean counter flow CH4/air premixed flames. *Proceedings of the Combustion Institute*, 30, 303–311, (2005).

[7] Sierens R., Variable composition Hydrogen/Natural gas mixtures for increased engine efficiency and decreased emissions. *Journal of Engineering for Gas Turbines and Power*. 122:1, 135-140, (1999).

[8] Nabhani N. and Sharifi V., Investigation on the Combustion of Hydrocarbon Fuel Enriched by Hydrogen for a Cleaner Environment. *International Conference on Chemical, Environmental Science and Engineering, ICEEBS'2012*, Pattaya, Thailand, July 28-29, (2012).

[9] De Sanctis S., Grimolizzi L., Ogliari S. and Galler D., Hydrogen enrichment of natural gas: Impact on the internal combustion engine emissions. *Energy: production, distribution and conservation*, Milan, Italy, (2006).

[10] Gersen S., *Experimental study of the combustion properties of methane/hydrogen mixtures*. PhD Thesis, University of Groningen, the Netherlands, (2007).

[11] Hernández-Pérez F.E., Groth C.P.T. and Gülder Ö.L., Large-eddy simulation of lean hydrogen-methane turbulent premixed flames in the methane-dominated regime. *International Journal of Hydrogen Energy*, 39, 7147-7157, (2014).

[12] Hora T.S. and Agarwal A.K., Experimental study of the composition of hydrogen enriched compressed natural gas on engine performance, combustion and emission characteristics. *Fuel*, 160, 470-478, (2015).

[13] Lipatnikov A.N. and Chomiak J., Turbulent flame speed and thickness: phenomenology, evaluation, and application in multi-dimensional simulations, Progress in energy and combustion science 28 (2002) 1-47.

[14] Pope S. B., Advances in PDF Methods for Turbulent Reactive Flows.In *Advances in Turbulence X*; Andersson, H. I., Krogstad, P. A. Eds.; CIMNE: (2004); pp 529-536.

[15] Bray K.N.C., Turbulent transport in flames, Proc. R. Soc Lond 1995, A451:231.

[16] Bray K.N.C. and Libby P.A., In: Libby P.A., Williams F.A. editors. Turbulent reacting flows, vol. 2. London: Academic press, 1994.p. 115-51.

[17] Weller H.G., Tabor G., Gosman A.D. and Furbey C., Application of a flame-wrinkling LES combustion model to a turbulent mixing layer, Porc, combust, Inst 1998; 27:899.

[18] Poinsot T., Using direct numerical simulations to understand premixed turbulent combustion, Porc, Combust, Inst, Vol: 26, pp: 219–232, 1996.

[19] Givi P., Spectral and Random Vortex Methods in Turbulent Reacting Flows. In *Turbulent Reacting Flows*; Libby, P. A., Williams, F. A. Eds.; Academic Press: London, UK, 1994; Ch 8, 475-572.

[20] Pope S. B., Computations of turbulent combustion: Progress and challenges, *Proc. Combust. Inst.* 1990, Vol: 23, 591–612.

[21] Givi P., Filtered Density Function for Subgrid Scale Modeling of Turbulent Combustion, *AIAA J.* 2006, *44* (1), 16–23.

[22] Lundgren T.S., Distribution functions in the statistical theory of turbulence, The Physics of Fluids, Vol. 10, pp. 969-975, 1967.

[23] O'Brien E. E., The Probability Density Function (PDF) Approach to Reacting Turbulent Flows. In *Turbulent Reacting Flows, Topics in Applied Physics*; Libby, P. A., Williams, F. A., Eds.; Springer-Verlag: Heidelberg, 1980; Ch 5, *44*, 185-218.

[24] Poinsot T. and Veynante D., Theoretical and numerical combustion, R. T. Edwards, 2001, ISBN: 1930 217056.

[25] Libby P.A. and Williams F.A., Turbulent combustion: Fundamental aspects and areview, In: Libby P.A. and Williams F.A , editor Turbulent Reacting Flows, London Academic Press, 1994, p.2 – 61.

[26] Borghi R. and Moreau P., Turbulent combustion in a premixed flow, Acta astronautica. Vol 4, pp. 321–341, 1977

[27] Pope S.B., PDF methods for turbulent reactive flows, Progress in Energy and Combustion Science, Vol. 11, Issue 2, Pages 119-192, 1985.

[28] Dopazo C., Recent Developments in PDF Methods, Turbulent Reacting Flows, Libby P.A., Williams F.A., Eds, Academic Press, 1994.

[29] Bilger R.W., Pope S.B. and Bray K.N.C., Driscoll J.F., Paradigms in turbulent combustion research, *Proc. Combust. Inst.* 2005, *30*, 21–42.

[30] Haworth D. C. and Pope, S. B., Monte Carlo solutions of a joint PDF equation for turbulent flows in general orthogonal coordinates, *J. Comput. Phys.* 1987, *72*, 311–346.

[31] Borghi R., Champion, M. *Modélisation et théorie des flammes*; TECHNIP: Paris, France, 2000.

[32] Fruchard N., L'allumage dans les moteurs a essence: une modélisation et des applications, Thèse, Université de Rouen, 1995.

[33] Ren Z. and Pope S. B., An investigation of the performance of turbulent mixing models, *Combust. Flame* 2004, *136*, 208–216.

[34] Garrick S. C. and Interante V., Stochastic Modeling and Simulation of Turbulent Reacting Flows, *9th Int. Symp. Flow Visualisat.*, Heriot-Watt University: Edinburgh, 2000; 1-10.

[35] Bastiaans R.J.M., Verman A.W. and Pitsh H., DNS of lean hydrogen combustion with flamelet-generated manifolds, Center for Turbulence Research, Annual Research Briefs, 2007

[36] Pera C., Colin O.and Jay S., Development of a FPI Detailed Chemistry Tabulation Methodology for Internal Combustion Engines, *Oil & Gas Science and Technology – Rev. IFP*, Vol. 64, No. 3, pp. 243-258, 2009.

[37] Gicquel O., Darabiha N. and Thevenin D., Laminar premixed hydrogen/air counterflow flame simulations using flame prolongation of ildm with differential diffusion, Proceedings of the Combustion Institute 28 (Part 2) (2000) 1901–1908.

[38] Van Oijen J. and de Goey, L., Modelling of Premixed Laminar Flames using Flamelet Generated Manifolds, Combust. Sci. Technol. 161 (2000) 113–137.

[39] Pope S.B., Transport equation for the joint probability density function of velocity and scalars in turbulent flow, The Physics of Fluids, Vol. 24, pp. 588-596, 1981.

[40] Pope S.B., A Monte Carlo method for the pdf equations of turbulent reactive flow, The Physics of Fluids, Vol. 25, pp. 159-174, 1981.

[41] Ennetta R., Lâjili M. and Said R. Study of Methane Propagating Flame Characteristics Using PDF-Monte Carlo Model and Reduced Chemical Kinetic Scheme, *Energy & Fuels* 2009, *23*, 2903–2907

[42] Raman V., Fox R.O. and Harvey A.D., Hybrid finite-volume/transported PDF simulations of a partially premixed methane–air flame, Combustion and Flame, Vol., 136, pp.327-350, 2004

[43] Van Oijen J. A., Groot G. R. A., Bastiaans R. J. M. and de Goey L. P. H., A flamelet analysis of the burning velocity of premixed turbulent expanding flames, Proc.Combust. Inst. 30:657-664 (2005).

[44] Vreman A. W., Albrecht B. A., van Oijen J. A., de Goey L. P. H., and Bastiaans R. J. M., Premixed and nonpremixed generated manifolds in large-eddy simulation of Sandia flame D and F, Combust. Flame 153:394-416 (2008).

[45] CHEM1D, A one-dimensional laminar flame code, Eindhoven University of Technol-ogy. http://www.combustion.tue.nl/chem1d/

[46] Smith G.P., Golden D.M., Frenklach M., Moriarty N.W., Eitneer B., Goldenberg M., Bowman C.T., Hanson R.K., Song S., Gardiner Jr.W.C., Lissiauski V.V. and Qin Z., GRIMech 3.0. Retrieved from http://www.me.berkeley.edu/gri_mech.

[47] Ennetta R., Hamdi M. and Said, R., Comparison of Different Chemical Kinetic Mechanisms of Methane Combustion in an Internal Combustion Engine Configuration, Thermal Science, 12(1), pp. 43-51, 2008.

[48] Ennetta R., Alaya M. and Said R., Numerical study of laminar flame velocity of hydrogen-enriched methane flames using several detailed reaction mechanisms, Arab J Sci Eng, DOI 10.1007/s13369-016-2275-3.

[49] Van Oijen J.A., *Flamelet-Generated Manifolds:Development and Application to Premixed Laminar Flames*. PhD thesis, Eindhoven University of Technology,Combustion Technology, 2002.

[50] van Oijen J. A., Bastiaans R. J. M. and de Goey L. P. H., Modeling preferential diffusion effects in premixed methane-Hydrogen-Air flames by using Flamelet Generated Manifolds, V European Conference on Computational Fluid Dynamics ECCOMAS CFD 2010, Eindhoven University of Technology.

[51] Van Oijen J. A., Lammers F. and de Goey, L. P. H., Modeling of complex premixed burner systems by using flamelet-generated manifolds, Combust. Flame, 127, pp. 2124–2134, (2001).
[52] Donini A., Martin S.M., Bastiaans R.J.M., van Oijen J.A.and de Goey L.P.H., Numerical simulations of apremixed turbulent confined jet flame using the flamelet generated manifold approach with heat loss inclusion, Proceedings of the ASME Turbo Expo, GT2013-94363, (2013).
[53] Van Oijen J. and de Goey L., Modelling of premixed counterflow flames using the flamelet-generated manifold method, Combust. Theor. Model., 6, pp. 463–478, (2002).
[54] Van Oijen J. and de Goey L., A numerical study of confined triple flames using a flamelet-generated manifold, Combust. Theor. Model, 8, pp. 141–163, (2004).
[55] Donini A., Bastiaans R.J.M., van Oijen J.A. and de Goey L., Differential diffusion effects inclusion with flamelet generated manifold for the modeling of stratified premixed cooled flames, Proc. Combust. Inst., DOI:10.1016/j.proci.2014.06.050, (2014).
[56] Vreman A.W., Albreht B.A., van Oijen J.A. and de Goey L., Premixed and nonpremixed generated manifolds in large-eddy simulation of Sandia flame D and F" Combust. Flame, 153, pp. 394–416, (2008).
[57] Ramaekers W.J.S., van Oijen J.A. and de Goey L., Stratified turbulent Bunsen flames: flame surface analysis and flame surface density modeling, Combust. Theor. Model, 16, pp. 943–975, (2012).
[58] Donini A., Bastiaans R.J.M., van Oijen J.A. and de Goey L., Numerical Simulations of a Turbulent High-Pressure Premixed Cooled Jet Flame With the Flamelet Generated Manifolds Technique, (2015).
[59] Lecordier B., Etude de l'interaction d'une flamme prémélangée avec le champ aérodynamique, par association de la tomographie Laser et de la P.I.V. Ph.D. Thesis, University of Rouen, France, 1997.
[60] Huang Z., Zhang Y., Zeng K., Liu B., Wang Q. and Jiang D., Measurements of laminar burning velocities for natural gas–hydrogen–air mixtures, Combustion and Flame, 146, 302–311, (2006).
[61] Hongsheng G., Cédric G. and Escudié D., Burning Rates and Surface Characteristics of Hydrogen-Enriched Turbulent Lean Premixed Methane-Air Flames, Article in International Journal of Hydrogen Energy October 2010 DOI: 10.1016/j.ijhydene.2010.07.066.
[62] Fairweather M., Ormsby M.P., Sheppard C.G.W. and Woolley R., Turbulent burning rates of methane and methane–hydrogen mixtures, Combustion and Flame 156 (2009) 780–790
[63] Ekenechukwu C.O., Effects of Hydrogen Concentration on Stoichiometric H2/CH4/Air Premixed Turbulent Flames, Conference Paper in SAE Technical Papers, October 2013,DOI:10.4271/2013-01-2563.
[64] Lewis B. and Von Elbe G., Combustion, Flames and Explosions of Gases, third ed., Academic Press, New York, 1987.
[65] Hankinson G. Mathurkar H. and Lowesmith B.J., Ignition energy and ignition probability of methane-hydrogen–air mixtures, Loughborough University, Leicestershire, LE11 3TU.
[66] Bjerketvedt D., Bakke J.R. and van Wingerden K., Gas explosion handbook, Gexcon, Journal of Hazardous Materials, Vol: 52, pp: 1-150, 1997.
[67] D.W.V, German Hydrogen Association, 2002.

Paper 31 **Bildiri 31**

INVESTIGATION OF THE APPROPRIATE OPERATING CONDITIONS OF NATURAL GAS AND GASOLINE FUELS IN THE LEAN MIXTURE REJIME

Hüseyin Emre Doğan[1], Osman Akın Kutlar[2], Majid Javadzadehkalkhoran [3], Abdurrahman Demirci[4]

[1,3] Istanbul Technical University, Graduate School of Science, Engineering and Technology, Istanbul.
[1]edogan@itu.edu.tr (corresponding author), [3] javadzadehkalkh@itu.edu.tr
[2] Istanbul Technical University, Faculty of Mechanical Engineering, Istanbul.
kutlar@itu.edu.tr
[4] Karamanoğlu Mehmetbey University, Mechanical Engineering Department, Karaman.
arahmandemi@kmu.edu.tr

ABSTRACT

There are different opinions about the future of internal combustion engines due to excessive air pollution caused by the increasing use of fossil fuels in engines. However, an alternative power system that is more efficient, economical, environment friendly and widely used as internal combustion engines haven't been invented. For this reason, many studies on the widespread use of alternative fuels are carried out. In this study, the results of experiments with both gasoline and natural gas fuel in a single cylinder test engine were evaluated. The main objective of this study is to compare exhaust gas emissions and effective efficiency at the operating limits in lean mixture conditions. At the same time, cycle to cycle variation in these operating conditions should not exceed an acceptable value. In the lean mixture condition, gasoline fuel has exceeded this determined limit previously from natural gas. Therefore, the reduction in NO emission was not at desired levels. In case of working with natural gas, NO emission has decreased to very low levels since it reaches to the cycle to cycle variation limits in more lean mixtures ($\lambda = 1.70$). At all experiment points, natural gas is more efficient than gasoline. As a result, it has been observed that NO emissions can meet the standards without a loss of efficiency for this engine in case of the natural gas and lean mixture.

Keywords: Lean burn, Natural gas, Nitrogen oxide emission, Low temperature combustion.

INDRODUCTION

There are different methods to obtain emission standards in ICE's. Alternative fuels must be used instead of gasoline and diesel engines to provide this easily [1]. NO, THC, PM emissions are the major problems to be solved today. PM problem could be eliminated in engine with a homogeneous mixture. In order to reduce NO emissions, it is necessary to reduce in-cylinder temperatures. Working with extremely lean mixture is a method used to reduce the temperature. For this purpose, acceptable operating conditions in the lean mixing regime of CNG and gasoline fuels have been investigated in this study. It is aimed to reduce NO emissions below 200 ppm in the lean mixture conditions for both fuels. For these operating parameters, which are suitable for NO emission, the cycle to cycle variation values are also investigated for compliance with the desired limits.

EXPERIMENTAL METHOD

The experiments were carried out on a single cylinder test engine with spark ignition and manifold injection system. In addition, a mini ECU and software has been developed in our laboratory for the control of this engine [2]. AVL GU21D piezoelectric transducer was used to

measure the cylinder pressure and this data was recorded over 200 cycles. A precise scale has been used for the measure of CNG fuel consumption. Emission measurements were made with Horiba Mexa 7500 and Bosch BEA 350 devices. The experiments were carried out in three different relative air/fuel ratios in two different engine speed and load conditions. For both fuels; efficiency, NO emission and cycle to cycle variation (net indicated pressure changes) values were compared under the same operating conditions.

RESULTS

According to the results obtained for both fuels, the CNG is more efficient (5-12%) than gasoline fuel at all operating points. Gasoline fuel is not suitable to work with lean mixture when the mean effective pressure is 1bar. As could be seen in Figure 1, it is possible to operate in the lean mixing regime in both fuels under 3 bar engine load conditions. In this study, we call it the extremely poor mixture ($\lambda > 1.6$), the cycle to cycle variation of natural gas fuel is less than that of gasoline. Essentially, the NO emission values in both fuels are about 250 ppm under the R/A = 1.6. Although the gasoline fuel in terms of NO emissions provides the desired conditions, it does not meet the criteria for the cycle to cycle variations. The gasoline engine usually exceeds this limit after R/A =1.45. So, even if NO emission is about 10 times less than the stoichiometric mixture, stable operation under these conditions is not a concern for gasoline. As seen from Figure 2, the natural gas is still better than gasoline even if it works with the leaner mixture. In addition, NO emissions decreased to around 150 ppm caused by decrease in cylinder temperature due to the further leaner mixture for CNG.

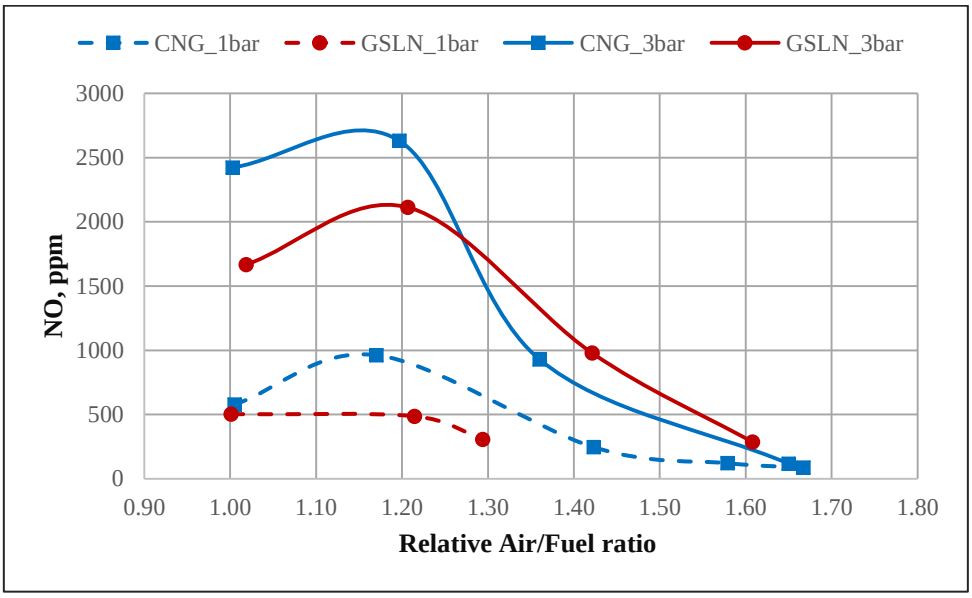

Figure 1. NO emission changes for gasoline and natural gas (n = 1500 rmp, p_{me} = 1 - 3 bar, ε = 12).

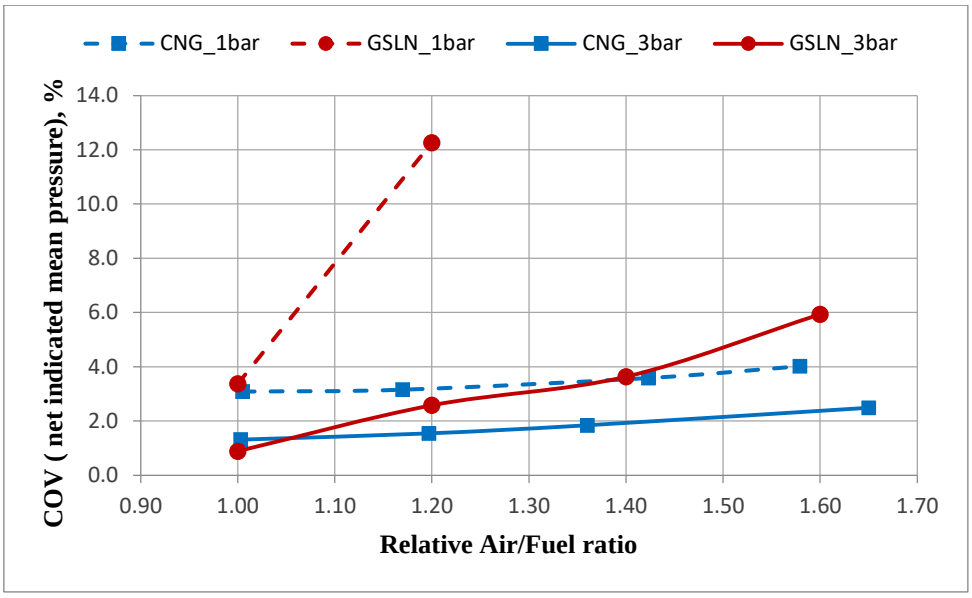

Figure 2. Coefficient of variation (COV) value for net indicated mean effective pressure under same operating conditions in figure 1.

CONCLUSION

As described in the Results section, CNG fuel provides the desired limits in the extremely lean mixing regime. Besides, the effect of working with a more lean mixture on the effective efficiency value should be examined. Furthermore, contrary to our expectations, THC emissions remained almost the same as gasoline. CNG can be 20% more efficient than gasoline under ideal conditions [3]. If THC emissions do not meet the required standards, it can be solved easily by using a simple and inexpensive method of oxidation catalyst.

REFERENCES

[1] Hora, T. D., Agarwal A. K. (2015). Experimental study of the composition of hydrogen enriched compressed natural gas on engine performance, combustion and emission characteristics, *Fuel*, 160(2015), 470 - 478doi.org/10.1016/j.fuel.2015.07.078.

[2] Ö. Tekeli. (2013) *Designing and Production Ignition and Injection Units of a Gasoline Engine with Skip Cycle*, Master Thesis, Istanbul Technical University, İstanbul.

[3] Khan, M. I., Yasmin, T., Shakoor, A. (2015). Technical overview of compressed natural gas (CNG) as a transportation fuel, *Renewable and Sustainable Energy Reviews, 51(2015) 785-797*doi.org/10.1016/j.rser.2015.06.053.

Paper 32 **Bildiri 32**

THE HEATING, EVAPORATION AND COMBUSTION OF KEROSENE DROPLETS IN A GAS-TURBINE COMBUSTOR: CFD MODELLING USING THE DISCRETE COMPONENT APPROACH

Mansour Al Qubeissi[1,2], Geng Wang[1], Nawar Al-Esawi[2], Oyuna Rybdylova[3], Sergei Sazhin[3]

[1]Faculty of Engineering, Environment and Computing, Coventry University, UK
[2]Institute for Future Transport and Cities, Coventry University, UK
[3]Advanced Engineering Centre, School of Computing, Environment and Mathematics, University of Brighton, UK

The modelling of heating, evaporation and combustion processes in a combustion system is crucial to its design and advancement [1,2], and essential to the assessment of the suitability of kerosene as an aviation fuel [3]. In this study, we have conducted a detailed analysis of kerosene fuel droplet heating and evaporation, using the previously developed discrete component model (DCM). Kerosene fuel composition (approximated by 44 components of the full composition reported in [4]) is replaced with 2 surrogate components to reduce the computational time. In contrast to the classical industrial analyses of aviation fuel (e.g. the distillation curve method [5]), the DCM takes into account gradients of species mass fractions in droplets. It is based on the analytical solutions to the heat transfer and species diffusion equations subject to appropriate boundary and initial conditions [6]. Numerical codes using these solutions were extensively verified and validated in [7–9]. The effective thermal conductivity and effective diffusivity approaches for moving droplets are used in the model.

The DCM was implemented in the commercial CFD software of ANSYS-Fluent which was applied to study the processes in a combustor. The computational domain is shown in Figure 1. A polyhedral mesh was used for the hydrodynamic model, as shown in Figure 2. This opened opportunities for the simulation of the full combustion cycle. The influence of droplet evaporation on the combustion process was investigated.

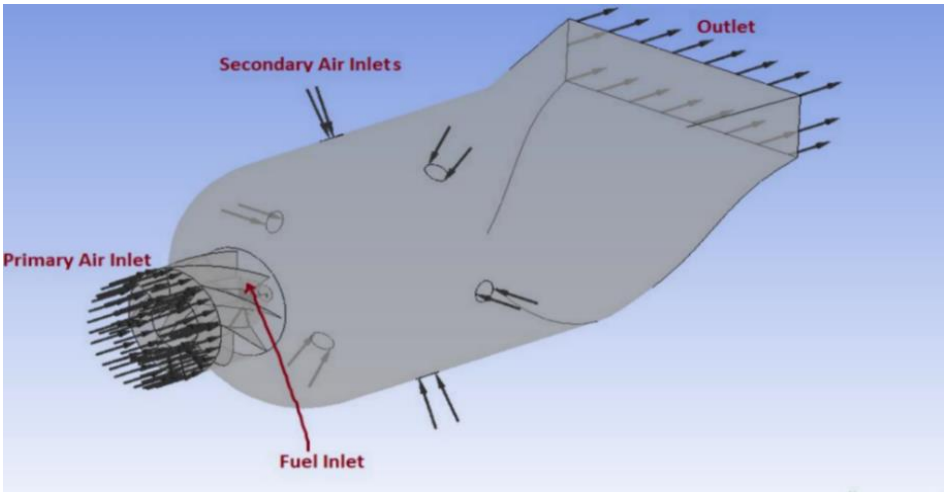

Figure 1. The can combustor geometry used in our CFD simulation.

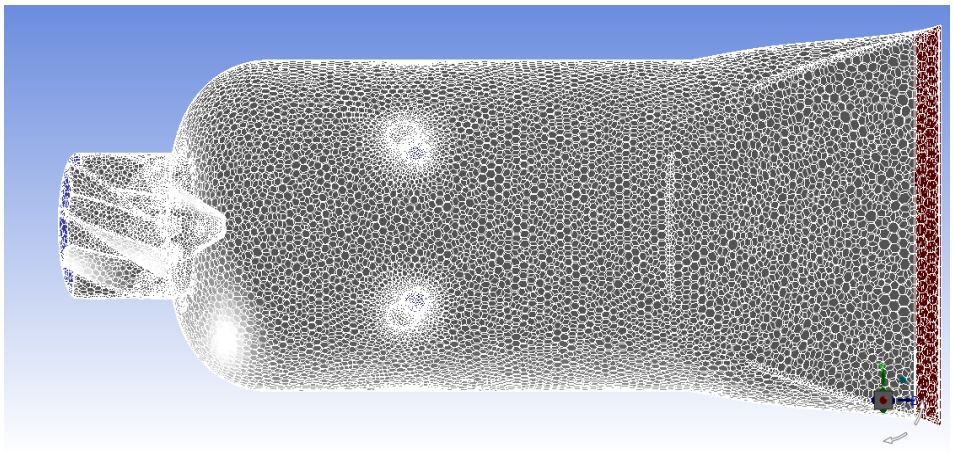

Figure 2. The mesh used for the combustor simulation.

The analysis was applied to a balanced mixture of kerosene and diesel fuels, represented in the ANSYS-Fluent database by $C_{12}H_{23}$ and $C_{10}H_{22}$, respectively. The initial droplet diameter and temperature were 100 µm and 375 K, respectively. The ambient gas temperature and pressure were 800 K and 4 bar, respectively. A co-axial air-blast atomizer was used with air and fuel mass flowrates of 0.175 kg/s and 0.003 kg/s, respectively, and an injection speed of 1 m/s. As shown in Figure 3, the evolution of droplet radii with time was predicted using three approaches, namely: 1) the results predicted by standard ANSYS Fluent software using constant properties; 2) the results predicted by ANSYS Fluent with the implementation of transient properties of fuel composition using the user defined function (udf), but without the DCM; and 3) ANSYS Fluent results with full implementation of the DCM and transient thermodynamic and transport properties.

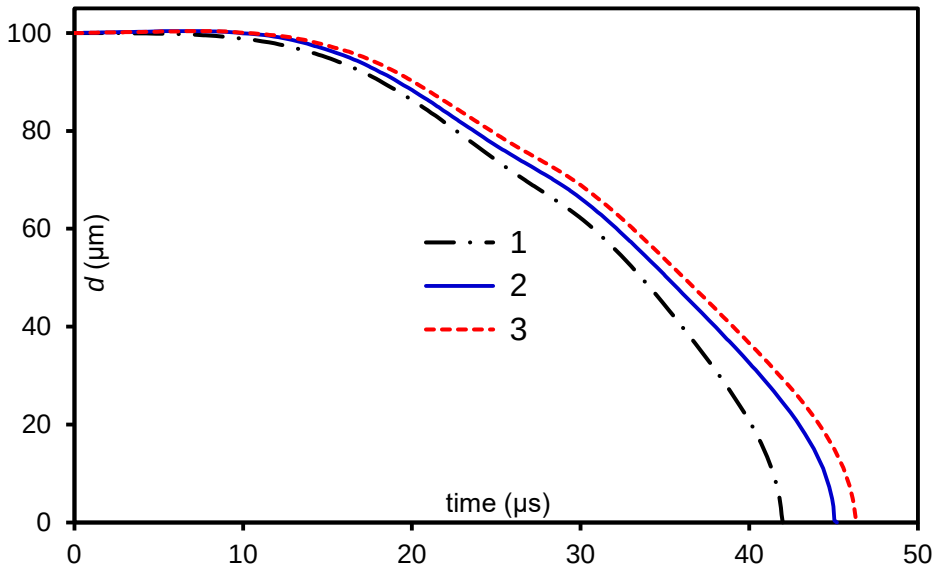

Figure 3. The evolutions of droplet diameter using the three modelling approaches: 1 refers to Standard ANSYS Fluent results, with constant properties, 2 refers to ANSYS Fluent results, with in-house properties using udf, and 3 refers to ANSYS fluent results with the in-house developed DCM using udf.

The preliminary results show that the maximal impact of incorporating the DCM into the ANSYS-Fluent prediction of droplet evaporation is up to 10.4% compared to the case when a standard ANSYS-Fluent model is used. Also, our results indicate that the fuel composition and

temperature gradient inside droplets, which are ignored in the standard ANSYS Fluent model, can lead to noticeable impact on the spray formation and combustion processes. The new results have been compared with those reported in the literature [12] (see Figure 4) for kerosene droplets of 1.8 mm initial diameter.

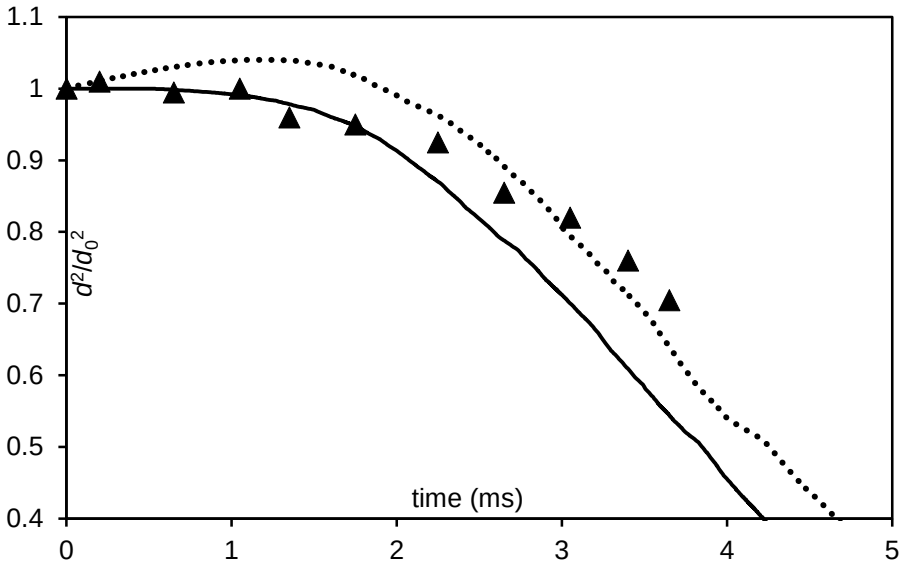

Figure 4. The validation of the models for the normalised droplet diameters squared predicted by the standard ANSYS-Fluent (solid curve), and ANSYS-Fluent with the DCM udf (dotted curve), using data reported in [12] (bold triangles) for kerosene fuel.

As can be seen from Figure 4, general agreement between the numerical results and experimental data was found. In our analyses, we considered the impact of thermal-swelling on droplet evaporation. Finally, the combustion of the blended fuel droplets was simulated, and the influence of fuel evaporation and species diffusion on flame properties was investigated and will be presented in the full paper.

Keywords: Aviation fuel, CFD model, Combustion, Droplet evaporation, Gas turbine, Kerosene

Acknowledgement

The authors are grateful to the Institute for Future Transport and Cities – Coventry University (Grant No. ECR019), and the EPSRC (Grant No. EP/R012024/1) for providing financial support for this project.

References

[1] Al Qubeissi, M., 2018, "Predictions of Droplet Heating and Evaporation: An Application to Biodiesel, Diesel, Gasoline and Blended Fuels," Applied Thermal Engineering, 136(C), pp. 260–267.
[2] Sazhin, S. S., 2014, *Droplets and Sprays*, Springer, London.
[3] Jones, E. G., and Balster, L. M., 1997, "Impact of Additives on the Autoxidation of a Thermally Stable Aviation Fuel," Energy & Fuels, 11(3), pp. 610–614.
[4] Lissitsyna, K., Huertas, S., Quintero, L. C., and Polo, L. M., 2014, "PIONA Analysis of Kerosene by Comprehensive Two-Dimensional Gas Chromatography Coupled to Time of Flight Mass Spectrometry," Fuel, 116, pp. 716–722.
[5] Lovestead, T. M., and Bruno, T. J., 2009, "Application of the Advanced Distillation Curve Method to the Aviation Fuel Avgas 100LL," Energy & Fuels, 23(4), pp. 2176–2183.
[6] Sazhin, S. S., 2017, "Modelling of Fuel Droplet Heating and Evaporation: Recent Results and Unsolved Problems," Fuel, 196, pp. 69–101.
[7] Al Qubeissi, M., Al-Esawi, N., Sazhin, S. S., and Ghaleeh, M., 2018, "Ethanol/Gasoline Droplet Heating and Evaporation: Effects of Fuel Blends and Ambient Conditions," Energy & Fuels, 32(6), pp. 6498–6506.
[8] Sazhin, S. S., Elwardany, A. E., Krutitskii, P. A., Deprédurand, V., Castanet, G., Lemoine, F., Sazhina, E. M., and Heikal, M. R., 2011, "Multi-Component Droplet Heating and Evaporation: Numerical Simulation versus Experimental Data," International Journal of Thermal Sciences, 50(7), pp. 1164–1180.
[9] Elwardany, A. E., Sazhin, S. S., and Im, H. G., 2016, "A New Formulation of Physical Surrogates of FACE A

Gasoline Fuel Based on Heating and Evaporation Characteristics," Fuel, 176, pp. 56–62.
[10] Al Qubeissi, M., 2015, *Heating and Evaporation of Multi-Component Fuel Droplets*, WiSa, Stuttgart.
[11] Sazhin, S. S., Al Qubeissi, M., Kolodnytska, R., Elwardany, A. E., Nasiri, R., and Heikal, M. R., 2014, "Modelling of Biodiesel Fuel Droplet Heating and Evaporation," Fuel, 115, pp. 559–572.
[12] Wang, F., Liu, R., Li, M., Yao, J., and Jin, J., 2018, "Kerosene Evaporation Rate in High Temperature Air Stationary and Convective Environment," Fuel, 211, pp. 582–590.

Paper 33 **Bildiri 33**

EXPERIMENTAL INVESTIGATION OF ACETYLENE IN AN SI ENGINE AT PARTIAL LOAD

Reyhane Doğan[1*], Mehmet İlhan İlhak[2], Selahaddin Orhan Akansu[3], Nafiz Kahraman[4]

1. Erciyes University Engineering Faculty Department of Mechanical Engineering, Kayseri, Turkey email: reyhanedgn@gmail.com
2. Phd. Erciyes University Engineering Faculty Department of Mechanical Engineering, Kayseri, Turkey email: ilhanilhak@gmail.com
3. Phd. Erciyes University Engineering Faculty Department of Mechanical Engineering, Kayseri, Turkey email: akansu@erciyes.edu.tr
4. Phd. Erciyes University Aeronautics and Astronautics Faculty Department of Aerospace Engineering, Kayseri, Turkey
email: nafiz@erciyes.edu.tr

ABSTRACT

Because of the increase in energy demand in the world and decreasing fossil fuel reserves, alternative fuel search studies are one of the research topics of today. In addition to liquid fuels, gas fuels are also investigated as an alternative to internal combustion engines. In this study, the effect of acetylene gas gasoline and ethanol on the emission parameters and engine performance of a spark-ignition engine was investigated. The experiments have been carried out under 25% constant load at 1500 rpm and in different air excess ratios. The engine used in the experiment is a four-cylinder, four-stroke and water-cooled internal combustion engine. As a result of the experiments, it was observed that the thermal efficiency of acetylene was higher than that of ethanol and gasoline. Acetylene (for higher lambda values) at emission values gives better values than ethanol and gasoline.

Keywords: Acetylene,Ethanol,Gasoline, Emissions, Internal combustion engine

1. INTRODUCTION

Acetylene gas; It is a gas that is colorless, garlic-smelling, highly flammable, lighter than air, has no toxic effect, but can cause a suffocating effect by reducing the oxygen of the air. Acetylene gas has an important place in the manufacturing industry. Acetylene gas is a gas that achieves high flame speed and flame temperature with minimal oxygen consumption compared to other fuel-gases [1].It has a very wide flammability range and minimum ignition energy required for ignition[2]. Acetylene was added by researchers to different fuels and their effects have been investigated.

In a research at Erciyes University, the performance of acetylene was added to the overall performance of the engine. Experiments have been carried out in an SI engine under stoichiometric conditions. In the tests, performance and emission parameters have been examined by changing the load from 25% to full load. While hydrocarbon emissions decreased in all engine loads, NO emissions increased in low emissions compared to

gasoline [3].Lakshmanan and Nagarajan have chosen a four-stroke, 4.4 kW diesel engine with a slight modification of the intake manifold to hold the gas injector controlled by an electronic control unit (ECU), and experiments have been conducted for various gas flow rates.As a result, they observed that performance was nearer to diesel at the full load and a safe operation of acetylene replacement up to 24% was possible to reduction in emission parameters [4,5,6].

Brusca at al. Performed a theoretical and experimental analysis of an acetylene and alcohol-driven internal combustion engine. A standard 8 kW spark ignition engine with carburettor was modified with electronic injection control system (ECU) and two standard commercial injectors. As a result of the experiment, exhaust emissions were decreased by CO, HC and NOx compared to gasoline and acetylene and alcohol fuel [7]. Kumar et al. in their study, a single cylinder was tested with pure petrol and gasoline - acetylene double fuel mode with diethyl ether (DEE) as an oxygen additive in a direct injection (DI) and spark ignition (s) engine. As a result of the studies, it was concluded that the mixing ratio of DEE20 showed better performance[8].

2. EXPERIMENTAL SETUP AND TEST PROCEDURE

The experiments were conducted in the Motors Laboratory of Erciyes University Mechanical Engineering department. The experiments were performed on a four-cylinder, four-stroke and water-cooled Ford MVH418 1.8L SI engine designed to improve the nominal power output of 75 kW at 5500 rpm.The engine specifications are given in Table 1.Acetylene ratio was measured by Alicat M100 SPLM gas flowmeter.Cylinder pressure values were measured with PCB 111A22 piezoelectric pressure transducer and Bosch BEA 060 gas analyzer was used to measure exhaust gas components (CO, CO2, HC and NO).

Experiments have been performed under different air excess ratio at 1500 rpm and 25% constant load using pure gasoline, ethanol and acetylene. The properties of fuels are given in Table 2.

Table 1: Engine specifications

Engine	Ford MVH418
Cylinders	4 in line
Weight	123 kg
Bore/Stroke (mm)	80.6/88
Compression ratio	10:1
Max. power	75 kW
Max. BMEP	10.7 bar
Max. Torque	150 Nm/4000 rpm
Engine stroke volume (L)	1.796 L
Idle/max. speed	800/6000 rpm

Table 2: The properties of fuels [1][3]

Properties	Acetylene	Ethanol	Gasoline
Formula	C_2H_2	C_2H_5OH	C_8H_{18}
Dentinsy (kg/m^3)	1.092	785	720-775
Ignition energy (MJ)	0.019	0.7	0.24
Auto ignition temperature (°C)	305	558	246-280
Adiabatic flame temperature (K)	2500	1920	2270
Lower calorific value (MJ/kg)	48.23	26.9	43
Flammability limits (vol.%)	2.5-81	3.3-19	1.4-7.6
Flame speed (m/s)	1.5	0.61	0.4
Stoichiometric air fuel ratio	13.2	8.93	14.7

3. RESULTS AND DISCUSSIONS

3.1 Brake Thermal Efficiency

The variation of brake thermal efficiency for acetylene gas, ethanol and gasoline in various excess air ratio is shown in Figure 1.As seen this figure the brake thermal efficiency of gasoline and ethanol are lower than acetylene. The experiment engine can be operated with gasoline and ethanol in rich and poor mixing conditions, but with acetylene it can only work under very poor mixing conditions.It is seen that the maximum brake thermal efficiency is obtained for all fuels in poor mixture conditions. The maximum brake thermal efficiency is 21.3% at λ=1.29 for gasoline operation, 21.8% at λ=1.45 for ethanol operation and 24.5% at λ=2.27 for acetylene operation.

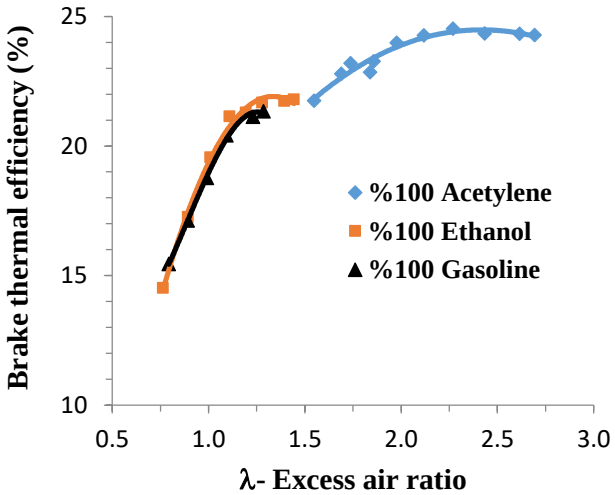

Figure 1. Variation of brake thermal efficiency by excess air ratio

3.2 Hydrocarbon Emissions

Unburned hydrocarbon emissions or organic matter are the result of incomplete combustion of hydrocarbons [9].The graph showing the HC emissions of acetylene according to the increased excess air excess ratio is given in Figure 2.As can be seen from Figure 2, HC emission values in different excess air ratio have not changed much for acetylene.Whenwe

compare acetylene, gasoline and ethanol, it is seen that the lowest emission rate belongs to acetylene.

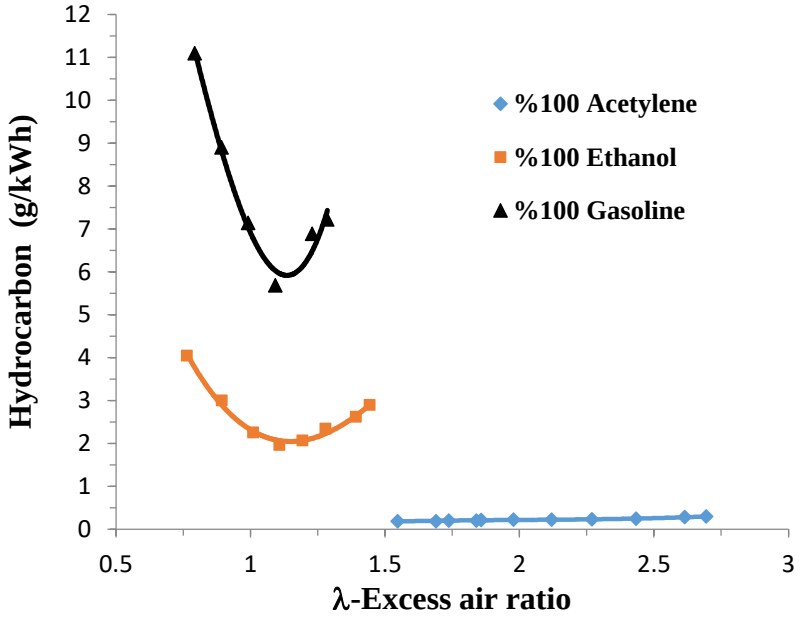

Figure 2. Variation of HC emissions by excess air ratio

3.3 Nitrogen Oxides (NOx) Emissions

NO, NO_2, N_2O_2 and similar compounds are all defined as nitrogen oxides (NOx).The NO_X emission varies depending on the excess air ratio [10]. The Bosch BEA 060 Gas Analyzer equipment used to measure emission values only measures the NO value from the NOx values. Figure 3 shows the variation of nitrogen monoxide emissions with the excess air ratio obtained as a result of experiments performed with acetylene gas,ethanol and gasoline at 1500 rpm engine speed and 25% engine load.

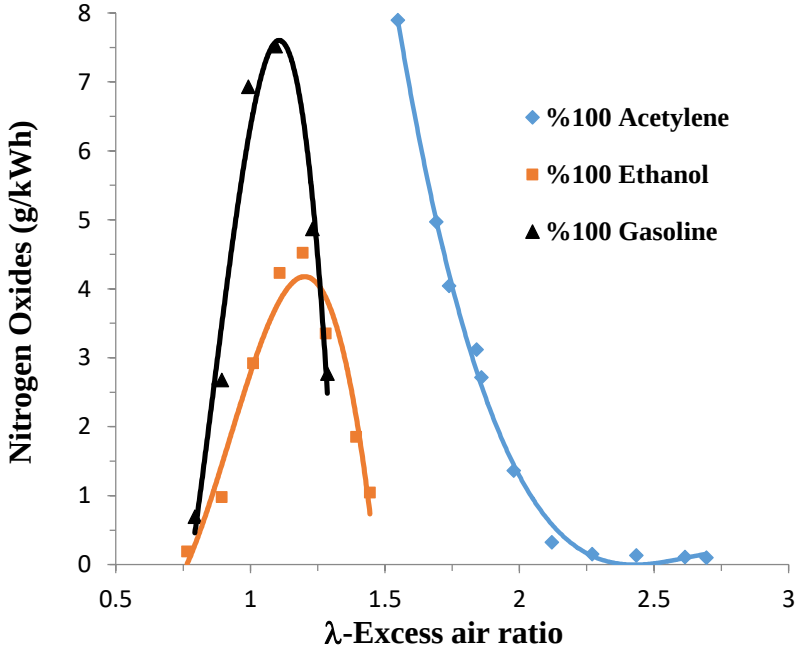

Figure 3. Variation of NO emissions by excess air ratio

4. CONCLUSION

This study investigated the effect on the emissions and performance of a spark ignition engine at 1500 rpm and 25% constant load using acetylene gas, ethanol and gasoline. The results of the investigation are presented below.

- The maximum thermal efficiency of acetylene is 15% higher than gasoline operation and 12% higher than ethanol operation.
- The UHC emission of ethanol is lower than that of gasoline and the UHC emission of acetylene is lower than that of ethanol and gasoline.
- It has been observed that NO emission is almost never occurred in acetylene operation at very high excess air ratios.

ACKNOWLEDGE

The authors would like to acknowledge to Erciyes University Scientific Research Projects Coordination Unit.

REFERENCES

[1] Vural E., Özer S., 2014, 'Buji Ateşlemeli Motorlarda Yakıta Asetilen Gazı İlavesinin Egzoz Emisyonlarına Etkisinin Deneysel Analizi ', BEU Journal of Science, 3(1), 24-34
[2]Sharma P.K., Kuinkel H., Shrestha P., Poudel S., 'Use of Acetylene as an Alternative Fuel in IC Engine', Rentech Symposium Compendium, Vol.-1, March 2012.
[3] İlhak M.İ., Akansu S.O., Kahraman M., Ünalan S., 2018, ' Experimental study on an SI engine fuelled by gasoline/acetylene mixtures' , Energy, 151, 707-714
[4] T. Lakshmanan, G. Nagarajan. Experimental investigation on dual fuel operation of acetylene in a DI diesel engine. Fuel Processing Technology 91 (2010) 496–503
[5] T. Lakshmanan, G. Nagarajan.Experimental investigation of timed manifold injection of acetylene in direct injection diesel engine in dual fuel mode. Energy 35 (2010) 3172-3178
[6] T. Lakshmanan, G. Nagarajan. Experimental investigation of port injection of acetylene in DI diesel engine in dual fuel mode. Fuel 90 (2011) 2571–2577
[7] S. Brusca, R. Lanzafame,m A. Marino Cugnu Garrano, M. Mesina, 2014 ' On the Possibility to Run an Internal Combustion Engine on Acetylene and Alcohol', Energy Procedia, 45, 889-898
[8]Anshu Kumar , Dr. Keshavendra Choudhary and Raji N Mishra, 2016, 'Acetylene used as alternative fuel in petrol engine',International Journel of Engineering Ssıences&Research., ISSN: 2277-9655
[9]T. Sandalcı.Taşıt ve Çevre Ders Notları ., http://www.yildiz.edu.tr/~sandalci/dersnotu/TC/TC3.pdf Accessed: 2018.12.27
[10]Kelen F., 2014, ' Motorlu Taşıt Emisyonlarının İnsan Sağlığı ve Çevre Üzerine Etkileri', Journal of The Institute of Natural & Applied Sciences, 19(1-2),80-87

Paper 34 **Bildiri 34**

USING MICROWAVE TECHNOLOGY IN COMMERCIAL BIODIESEL PRODUCTION: A REVIEW

Veli Gokhan Demir[a,*], Nadir Ilten[a], Hakan Serhad Soyhan[b]

[a]Balıkesir University, Mechanical Eng. Dep., Balikesir, Turkey 10100,
veligokhandemir@balikesir.edu.tr
[b]Sakarya University, Mechanical Eng. Dep., Sakarya, Turkey 54100

Biodiesel production has been remaining as one of the most popular research topics because of the environmentally friendly nature of biodiesel. Transesterification reaction performed with methanol (methanolysis) and a base catalyst is commonly preferred technique in biodiesel production due to the relatively lower production cost. However, higher production cost is an important drawback for spreading commercial biodiesel against petroleum based diesel. In this respect, alternative productions methods such as microwave assisted biodiesel production have increasingly become the focus to decrease production cost by minimizing reaction time and energy consumption in production processes. In the literature, the superior advantages of microwave irritation were proved and exhibited by numerous studies. However, these studies have been performed in small/laboratory scales, and any large scale microwave assisted biodiesel production has been found out. In this review study, "microwave technology" in biodiesel production is examined, and the base-catalyzed transesterifications carried out under microwave are compared with similar conditioned ones using conventional systems. In addition, the pilot scale microwave assisted biodiesel reactor (60 L) designed by us is introduced as an initial model of large scale microwave assisted biodiesel production systems, and the results of base catalyzed methanolysis results are presented.

Keywords: Biodiesel, Transesterification, Base Catalysts, Microwave, Production Cost.

Paper 35 **Bildiri 35**

THEORETICAL INVESTIGATION ON COMBUSTION CHARACTERISTICS OF ETHANOL-FUELED DUAL-PLUG SI ENGINE

İsmail ALTIN[1], Atilla BİLGİN[2], İsmet SEZER[3]

[1]Karadeniz Technical University, Department of Naval Architecture and Marine Engineering, TURKEY

[2]Karadeniz Technical University, Department of Mechanical Engineering, TURKEY

[3]Gümüşhane University, Department of Mechanical Engineering, TURKEY

ABSTRACT

Spark ignition (SI) engines have been especially important power plants to drive the light-duty vehicles. Numerous methods have been executed to develop all outputs of the SI engines. Dual-plug ignition system is one of the best tools to improve combustion, engine performance and exhaust emission characteristics of the SI engines. Alternative fuels, such as ethanol, have been also extensively used to contribute engine characteristics in SI engines since few last decades. Effects of equivalence ratios, spark timings and spark plug locations on combustion characteristics have been theoretically investigated in ethanol-fueled dual-plug SI engine in this study.

Keywords: SI engine, Dual-plug, Ethanol, Combustion characteristics

MODEL VALIDATION AND CASE STUDY

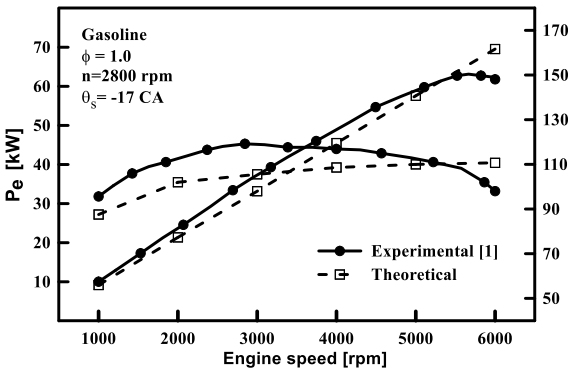

Figure 1. Validation of the model

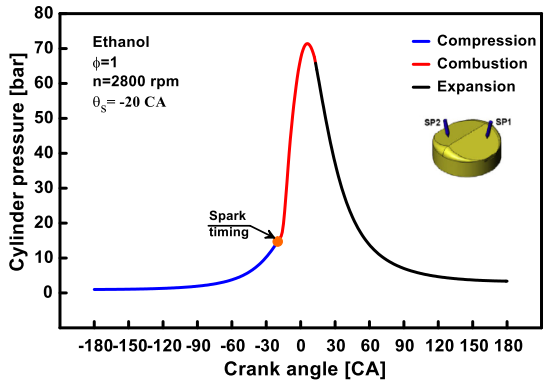

Figure 2. History of cylinder pressure at dual- plug configuration

REFERENCE

1. H. Migita, T. Amemiya, K. Yokoo and Y. Iizuka, The new 1.3-liter 2-plug engine for the 2002 Honda Fit, *JSAE Review*, Vol. 23, pp. 507-511, 2002.

Paper 36 **Bildiri 36**

EVALUATION OF THE PARTIALLY PREMIXED COMPRESSION IGNITION COMBUSTION WITH DIESEL AND BIODIESEL BLENDED DIESEL AT PART LOAD CONDITION

Tolgahan Kaya*[1], Osman Akın Kutlar[1], Özgür Oğuz Taşkıran[2]

[1] Istanbul Technical University, Faculty of Mechanical Engineering, Istanbul, Turkey

[2] Design Project Office, Istanbul Naval Shipyard, Istanbul, Turkey

Abstract

European Commission announced stringent emission limits for vehicles that run with diesel engine [1]. Moreover, countries in Europe will prohibit the sales of internal combustion engine vehicles starting from 2025 [2]. Researchers and automotive companies started to investigate alternative methods to achieve low emissions without sacrificing the efficiency of diesel engines. Researchers focused on advanced combustion methods, which enable the advantages of gasoline and diesel engines by achieving homogenous fuel-air mixture in the combustion chamber that ignite itself [3]. Besides, alternative fuels were also utilized under developed advanced combustion methods to improve the disadvantages of the advanced combustion phenomena. The disadvantages advanced combustion methods, which need to be improved, are the lack application at high load conditions and increased fuel consumption [4]. Although experimental studies were performed to improve advanced combustion with pure diesel, there are limited number of study about partially premixed combustion with biodiesel blended diesel, that modify fuel parameters to improve performance and emissions. In this study, advanced combustion method, which can be named as Partially Premixed Compression Ignition (PPCI), was studied experimentally with pure diesel and biodiesel blended diesel, by adjusting fuel injection parameters and exhaust gas recirculation (EGR) rate. During the experiments, combustion data, performance and emission data were acquired to investigate and correlate the relation of combustion parameters with emission and performance.

Experiments were performed in the engine dynamometer at part load condition, which were selected from operation points of the New European Driving Cycle (NEDC) and the Worldwide Harmonized Light Vehicles Test Cycle (WLTC), of a 1.5 liter diesel engine. Injected fuel quantity kept constant during the experiments to be able to evaluate the reaction of same amount of fuel in the combustion chamber. 7 mg of fuel injected at one time into the cylinder at 630 bar during all experiments. Start of Injection (SOI) time and EGR rate was adjusted during the experiments of the pure diesel (B00) and biodiesel blended diesel (50% biodiesel + 50% diesel in volume = B50). First, experiments of the B00 were conducted. Experiments started with the sweep of the SOI from -5 CA to -70CA by keeping the EGR-60%. After, EGR was swept from 10 to 70% by keeping the SOI at -15 and -30CA. During the experiment, 60 seconds were waited after modifying an engine parameter to start the data acquisition. Average of 120 seconds were calculated by the operation system of the engine dynamometer during the measurement. Two set of experiments were performed for each condition. Once completing the experiments of pure diesel, fuel filter of the engine was replaced with a new one. Then, experiments of the B50 were conducted at same operation conditions in same sequence.

Power, NO_x, HC, Opacity, and Burn Duration (BD) results of the experiments were compared as shown in Figure 1. Biodiesel improve HC, opacity while worsening power and NO_x. However, power of B00 and B50 was similar at SOI -25 CA. Besides, B50 burned faster compared to B00, moreover, SOC of B50 is earlier than B00 as can be seen in Figure 2. For the

selected operation point maximum power was observed at SOI of -15CA. However, NO_x and opacity of -25CA were better than -15CA, whereas power of both point was almost same. Combustion of SOI at -25CA can be named as partially premixed combustion as injected fuel create more homogenous charge before SOC compared to the SOI -15CA condition.

Thus, premixed mixture has potential to improve opacity and NO_x emission while keeping the power of the engine. Biodiesel may also be utilized to reduce the size of diesel particulate filter.

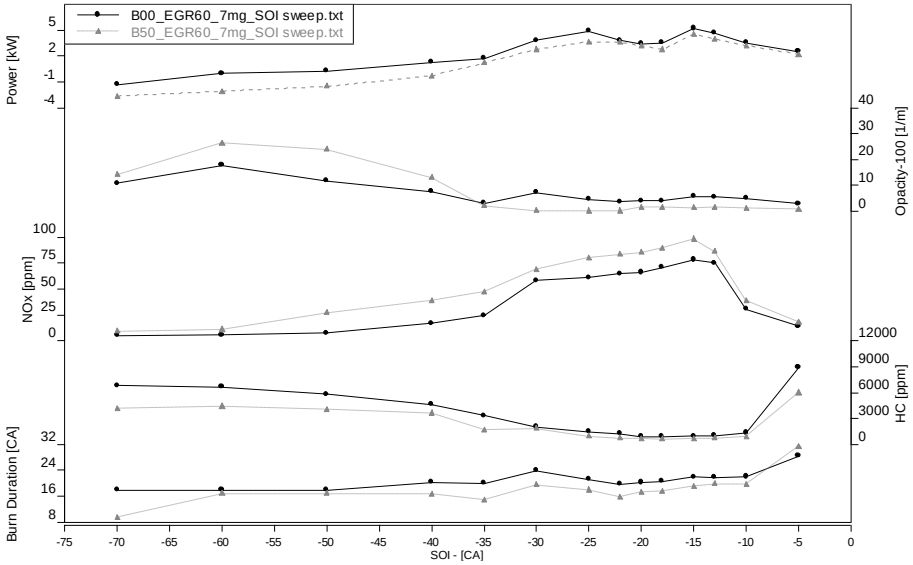

Figure 1. Sweep of SOI from -5 to -60 CA at 60% EGR Rate.

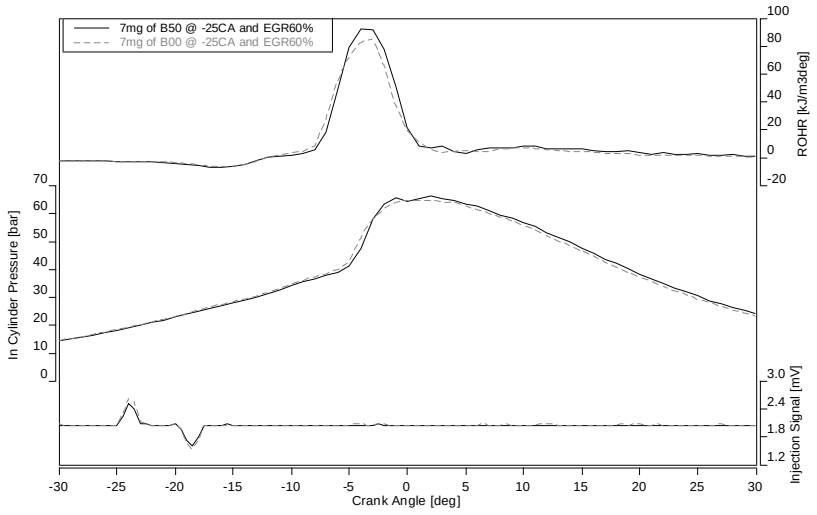

Figure 2. Combustion data of 7mg B00 and B50 at -25CA

REFERENCES

[1] Pacheco AF, Martins MES, Zhao H. New European Drive Cycle (NEDC) simulation of a passenger car with a HCCI engine: Emissions and fuel consumption results. Fuel 2013;111:733–9. doi:10.1016/j.fuel.2013.03.060.

[2] International Energy Agency. Global EV Outlook 2018 Towards Cross-Modal Electrification. Paris: 2018.

[3] Turkcan A, Ozsezen AN, Canakci M, Coskun G, Soyhan HS, Demir U. An experimental and modeling study to investigate effects of two-stage direct injection variations on HCCI combustion. Combust Sci Technol 2015;187:642–58. doi:10.1080/00102202.2014.960562.

[4] Imtenan S, Varman M, Masjuki HH, Kalam MA, Sajjad H, Arbab MI, et al. Impact of low temperature combustion attaining strategies on diesel engine emissions for diesel and

biodiesels: A review. Energy Convers Manag 2014;80:329–56. doi:10.1016/j.enconman.2014.01.020.

Paper 37 **Bildiri 37**

A COMPARISON OF THE VARIOUS MOTOR TYPE FOR USAGE AT FUEL CELL VEHICLES

İsmet Tikiz[1], Anil Can Turkmen[2], Cenk Celik[2], Hakan Serhad Soyhan[3], Halil Ibrahim Sarac[2]

[1]Department of Mechanical Engineering, Kirklareli University, 39100 Kirklareli, Turkey

[2]Department of Mechanical Engineering, Kocaeli University, 41040 Kocaeli, Turkey

[3]Department of Mechanical Engineering, Sakarya University, 54050 Sakarya, Turkey

Abstract

Nowadays, efforts are underway to get electric vehicles to replace internal combustion engines. At this point, the power supplies of electric vehicles have emerged as a problem. As an alternative to batteries, the studies on the use of fuel cells in the vehicles are continuing. In this study, various parameters of two fuel cell vehicles using AC induction and permanent magnet motor are investigated. The study was performed using the ADVISOR software. As a fuel cell, a 50 kW hydrogen-oxygen fuel cell made by the Argonne National Laboratory and a 25 kW NiMH battery of Ovonic brand were used as batteries. The motor powers are set at 50kW and 80kW. All other vehicle-related components are kept constant. As a driving cycle, a cycle representing the semi-dense suburbs of New York City, previously created by Ford Motor Company, was used.

The results of the study are compared with the output torque of the motor, the temperature of the battery module, the power loss of the battery, the maximum torque vector, the motor temperature, the power loss of the motor, the driving torque of the rotor and the fuel consumption are compared with two different power for both the permanent magnet motor and the AC induction motor. As a result of this study, the technical superiority of permanent magnet motors against AC induction motors is clearly seen. When the higher powers are reached, the superiority of permanent magnet motor compared to AC induction motor is seen more clearly. In particular, the motor output torque is close to twice the AC induction motor, the maximum torque vector is affected less in moments of acceleration and deceleration, and because of the low heat loss during operation, the low engine temperature makes the permanent magnet motors advantageous in the vehicles.

Keywords: Fuel cell vehicle, permanent magnet motor, AC induction motor, Advisor, electric vehicle

Paper 38 **Bildiri 38**

CALCULATION OF WIND ENERGY POTENTIAL AND PERFORMANCE ANALYSIS

Ipek Caglayan[1,*], İsmet Tikiz[2], Anil Can Turkmen[1], Cenk Celik[1], Hakan Serhad Soyhan[3]

[1]*Department of Mechanical Engineering, Kocaeli University, 41040 Kocaeli, Turkey*

[2]*Department of Mechanical Engineering, Kirklareli University, 39100 Kirklareli, Turkey*

[3]*Department of Mechanical Engineering, Sakarya University, 54050 Sakarya, Turkey*

Abstract

In this study, a technical feasibility study was carried out for a wind turbine in Kocaeli University campus. For this purpose, the location of the wind turbine was installed on the map. By using Windographer software, the wind speed of the selected point is taken with 1 hour resolution and the energy and turbine output power can be produced according to the selected turbine.

In order to confirm the accuracy of the data received from the software, the error rate was calculated by re-calculating the data received from the General Directorate of Meteorology. Daily average of 1 hour data was obtained and then monthly wind speed data were obtained and seasonal addition was taken. The turbine was constructed according to the hub height of 10-90 m. In addition, the study showed that the turbine would work with high efficiency in winter months due to power output. It was observed that the yield was higher than the wind in winter.

In this study, the output power of the selected turbine calculated using the software for modeling the wind speed at working altitude of the wind turbine. Thus, the producing power of turbine calculated as 195 kW and energy in terms 1,704,959 kWh/year with considering the losses. Due to the selected point, the efficiency of obtained energy of the wind turbine is 13.2% without losses and 10,9% with losses. The installation of the wind turbine at the selected point appears to be suitable.

Keywords: MERRA, Windographer, Wind, Wind Energy, Data Analysis, Mean Wind Speed, Mean Power Density.

Paper 39 **Bildiri 39**

THE INVESTIGATION OF ENGINE PERFORMANCE OF CR_2O_3 AND AL_2O_3 +% 13 TIO_2 COATINGS APPLIED AT DIESEL ENGINE

Erdinç VURAL[1], Serkan ÖZEL[2]*

[1]*Adnan Menderes University, Germencik Yamanturk Vocational School, Aydın, Turkey*

[2*]*Bitlis Eren University, Department of Mechanical Engineering, Bitlis, Turkey*

ABSTRACT

In combustion engines, the combustion chamber elements are coated with ceramic materials in order to increase the material quality of the components forming the combustion chamber, heat resistance of the hot parts of the metal components, engine efficiency and performance. In this study, the piston surface of a diesel engine, NiCr with bond coat and without bond coat with Cr_2O_3, Al_2O_3 13% TiO_2, Cr_2O_3 + 25% Al_2O_3 ceramic coating powders were coated by using plasma spraying method to increase engine efficiency and performance. Compared to coated engine and standard engine performance values; engine power, engine torque, exhaust gas temperatures and brake thermal efficiency increased while decrease was observed in specific fuel consumption.

Keywords: Diesel engine, performance, coating, Cr_2O_3, Al_2O_3 +13% TiO_2

Paper 40 **Bildiri 40**

OPTIMIZATION OF EFFECT OF THERMAL BARRIER COATING (TBC) CERAMIC LAYERS ON DIESEL ENGINES PERFORMANCE BY TAGUCHI METHOD

Serkan ÖZEL[1*], Erdinç VURAL[2], Murat BİNİCİ[3]

[1*]*Bitlis Eren University, Department of Mechanical Engineering, Bitlis, Turkey*

[2]*Aydın Adnan Menders University, Germencik Yamantürk Vocational School, Aydın, Turkey*

[3]*Bitlis Eren University, Department of Industrial Engineering, Bitlis, Turkey*

ABSTRACT

In this study, thermal barrier layers were coated on piston surface using plasma spray method. The effects of coated layers were investigated experimentally and statistically using Taguchi optimization method on Torque. Coating materials used in this study were Al_2O_3 +13% TiO_2, Cr_2O_3, and Cr_2O_3+ % 25 Al_2O_3. Each coating material was tested at different speeds, which are 1400 rpm, 2000 rpm, 2600 rpm and 3200 rpm. The results showed that Torque value at the speed of 2600 rpm was increased with the use of Al_2O_3 +13% TiO_2. The results of the experiment were also tested using Taguchi optimization method with coating material and speed parameters. The design of Taguchi analysis was carried out with $L_{16}(4^2)$ orthogonal array. It was statistically determined that the coating material (P= 0,004 < 0,005) and speed (P= 0,000 < 0,005) parameters were statistically significant on the Torque value. Also, the highest value of Torque was observed to be with the coating material of Al_2O_3 +%13 TiO_2 and the speed of 2600 rpm.

Keywords: Thermal Barrier Coating, Diesel engine, Torque, Taguchi optimization

Paper 41 **Bildiri 41**

CHACTERIZATION OF SOLID PRODUCTS FROM APPLE TREE PRUNING WASTE TORREFACTION

Berrin SAYGI YALÇIN[1,2*], Cemil KOYUNOĞLU[3], Jale GÜLEN[2]

[1]Yalova University, Engineering Faculty, Department of Chemical and Process Engineering, 77200, Yalova, Turkey.

[2]Yildiz Technical University, Chemical and Metallurgical Engineering Faculty, Chemical Engineering Department, 34210, Istanbul, Turkey.

[3]Yalova University, Engineering Faculty, Department of Energy Systems Engineering, 77200, Yalova, Turkey.

*berrin.yalcin@yalova.edu.tr

Abstract:

In Turkey 122.317 tons of apple tree pruning waste (ATPW) is composed per year. However, direct use this waste as a solid fuel is hindered by its intrinsic fuel characteristics, such as low bulk density, low energy yield and hygroscopic nature. Torrefaction is a promising process to enhance the fuel characteristics of the ATPW. The benefit of this process is that energy value of torrefaction products are nearly equal to coal. In addition torrefaction products are renewable energy sources and could be co-fired with coal thereby reducing greenhouse gases and global warming. In this study, the effect of different parameters such as temperature, particle size and residence time were investigated on ATPW. Temperature, particle size and residence time was respectively varied from 150 to 350ºC, 1-5mm, and 10-50 min. Torrefaction process was conducted in inert atmosphere with a heating rate of 15ºC/min. Calorific value, mass yield, and energy yield were computed and used to determine the quality of the resulting biochar. Response surface methodology was used for determination of influence of each factors. The results showed that the temperature and residence time were significant factors effecting the heating value, mass yield and energy yield ratio in torrefaction of the ATPW. From the results of data, 250 °C torrefaction temperature, 30 min residence time and 3mm particle size was found to be suitable for torrefaction of ATPW. In tis conditions heating value, mass yield and energy yield of torrefied ATPW was found 22.08 MJ/kg, %63.27 and %69.62, respectively.

Keywords: Biomass, torrefaction, apple tree pruning waste

Paper 42 **Bildiri 42**

INVESTIGATION OF WASTE COOKING OIL-BIODIESEL AND DIESEL FUEL PARTICULATE MATTER USING FTIR, TEM AND ELEMENTAL ANALYSES

Yahya Ulusoy

Department of Agricultural Machinery, Uludağ University, Bursa, Turkey

yahyau@uludag.edu.tr

Abstract

This study investigated the use of a methyl esterified waste vegetable oil (MEWV)-diesel fuel blend in a diesel tractor engine by comparing the resulting particulate matter (PM) collected on a filter with that of diesel fuel. MEWV is originating from domestic, commercial and food industry sources collected from the Marmara region (Turkey) by a waste oil collection organization. Testing of the MEWV was conducted in engine test laboratories where particles were collected in emission filters and these filters were analysed in the laboratory environment to evaluate the results. The study also investigated the overall morphology of soot particles from a blend of 75% biodiesel + 25% diesel (B75) in a diesel engine at three different loads (75%, 50% and 10%) as compared with those from diesel fuel (B0).

Fourier transform infrared (FTIR) and elemental analyses were carried out and the exhaust emissions collected on the filters were examined via transmission electron microscopy (TEM). The FTIR (JASCO Model FT / IR 6800-ATR) analyses were performed on the samples with a maximum scan rate in the range of 500 cm^{-1} to 4000 cm^{-1}. For the FTIR spectroscopy of the smoke emission (SE) from the combustion chamber collected on the filter. The samples were scanned 500 to 4000 cm^{-1} wavenumber and the spectra were recorded. FTIR spectra analyses of diesel fuel and MEWV fuels at three different loads were shown below.

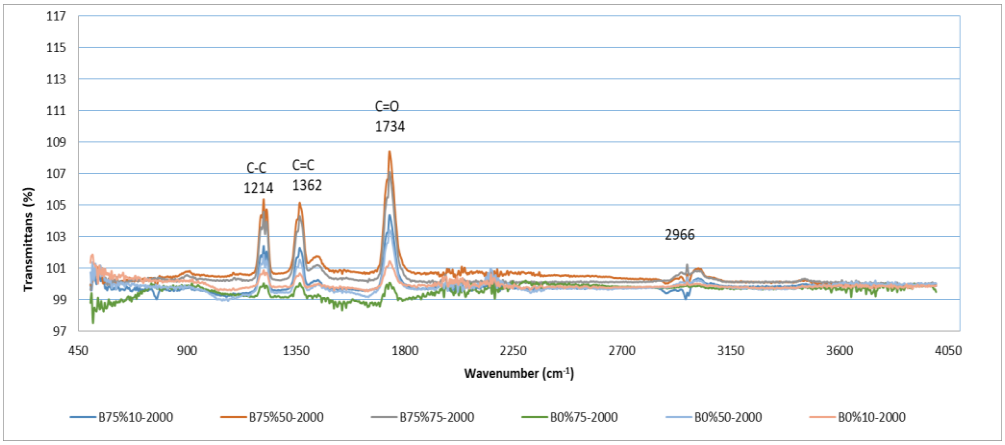

Data on the size and morphology of the SE were obtained using the Quanta 650 FEG HV / LV / ESEM-STEM detector. The results showed the importance of the TEM analyses of the B75 fuel SE for internal structural changes during the oxidation process. The change in diameter in the oxidized SE was experimentally observed.

The study results are summarized as follows:

• The FTIR spectra of the B75 fuel blend of biodiesel obtained from WCO and diesel fuel showed characteristic regions of oxygen bonds. No significant peak of permeability was observed for the B0 fuel due to low sulphur concentration, while the B75 fuel showed no sulphur peak points in the spectrum. The presence of long carbon chains was confirmed by the vibration of the C-H bonds.

• As a result of the clean and complete combustion of the B75 fuel, it produced fewer SE than the B0 fuel. Within the loading rates, it was observed that the amount of SE decreased as a result of the operation of the engine regime at 50% and 75% loading rates and the more efficient combustion of the fuel.

• The size distribution of the B0 fuel SE did not follow the same trend as the B75 fuel. Compared to B0, in the B75 fuel, due to the high biodiesel ratio, the initiation of soot precursors was reduced and the oxygen present in the biodiesel was seen to reduce the size and number of SE through further oxidation (Lapuerta et al., 2012; Omidvarborna et al., 2015a).

• The laboratory results confirmed that the degree of unsaturation was related to the oxygen content of the biodiesel fuels. The B75 unsaturated biodiesel fuel obtained from WCO formed smaller soot particles, as shown in the TEM images.

Keywords: Waste cooking oil, biodiesel, emissions, PM, FTIR, TEM

Paper 43 **Bildiri 43**

CALCULATED EXHAUST EMISSIONS OF EURO 6 CLASS GASOLINE, DIESEL AND LPG FUELLED PASSENGER CAR ON DEFINED RDE (REAL DRIVING EMISSION) ROUTE

Muhammet AYDIN*, Cem SORUŞBAY

Faculty of Mechanical Engineering, Istanbul Technical University
Maslak, 34469 İstanbul Turkey

Abstract

Due to the insufficient representation of chassis dynamometer test for emission regulation, European Commission put into the force a new procedure, which contain both laboratory test and real driving test. In this new test procedure, even though WLTC replace with NEDC, it is needed to test the vehicle on real traffic conditions, which contain urban, rural and highway road parts. Due to the new emission regulation, lots of academic investigations focus on creation of RDE (Real Driving Emission) routes and RDE test. In this study, we introduce a new methodology for creating RDE routes and compare calculated CO, HC and NO_x emissions of gasoline, diesel and LPG fuelled passenger car on defined RDE route as a case study. RDE routes were created by a code in MATLAB with using Istanbul road map data and half hour traffic flow data. This code, firstly, create all RDE routes starting from defined coordinates and then analyse all routes with respect to traffic flow rate and RDE boundary conditions identified by European Commissions. Obtained outputs of this model were used for GPS test to get real time vehicle speed, acceleration, deceleration, engine speed, engine coolant temperature and engine load rate. After verification of GPS test and RDE model, half-hour traffic data and GPS test outputs were used to calculate exhaust emissions by IPCC third approach (Tier III), which consider mean vehicle speed, fuel type, engine size and ambient air temperature, for our case study.

Keywords: Real Driving Emission, Emission calculation, Gasoline vehicle, Diesel vehicle, LPG vehicle.

Paper 44 **Bildiri 44**

EVALUATION OF PERFORMANCE, COMBUSTION AND EMISSIONS OF SOYBEAN BASED BIODIESEL FUEL BLENDS IN A CI ENGINE

Mehmet Reşit Seraç[a], Selman Aydın[a], Sinan Erdoğan[b], Mustafa Kemal Balki[c], Cenk Sayın[d]

[a]*Department of Automotive Engineering, Faculty of Technology, Batman University, Batman, Turkey*
[b]*Institute of Pure and Applied Sciences, Marmara University, Istanbul, Turkey*
[c]*Department of Mechanical Engineering, Sinop University, Sinop, Turkey*
[d]*Department of Mechanical Engineering, Faculty of Technology, Marmara University, Istanbul, Turkey*

ABSTRACT

In this paper, engine tests were performed using ultra-low sulfur diesel fuel (ULSD), soybean-based biodiesel and mixtures thereof. Performance, combustion, and exhaust emissions tests were carried out with a 4 stroke, 4-cylinder, water-cooled, and direct injection NWK22 diesel engine generator. The maximum power output of the engine is 18 kW and a compression ratio of it is 17:1. All test fuels were prepared by blending 90% ultra-low sulfur diesel fuel- 10% soy-based biodiesel this blend is named SOB10 and 50% ultra-low sulfur diesel fuel- 50% soy-based biodiesel blend is named SOB50. They were tested under 10.8 kW load conditions and a constant engine speed of 1500 rpm. The density, viscosity, thermal value and cetane number of ULSD are 0.832 g/cm^3, 2.79 mm^2/s, 44.8 Mj/kg, and 54.3, respectively. The properties of B10 are 0.828 g/cm^3, 2.76 mm^2/s, 43.6 Mj/kg, and 56.5, respectively. The properties of B50 are 0.853 g/cm^3, 3.30 mm^2/s, 41.4 Mj/kg, and 54.3, respectively. Specific fuel consumption of soy-based biodiesel and their mixtures was measured higher than that of ULSD. The cylinder gas pressure values of biodiesel and their mixtures are higher than that of ULSD. The heat release rate and average gas temperature values of biodiesel and their mixtures are lower than that of ULSD due to their low thermal values. CO_2 emissions of biodiesel and mixtures are higher than those of ULSD due to the oxygen content of biodiesel. The rapid decline in oil resources has increased the search for new sources as an alternative. In this study, it has been found that soybean-based biodiesel can be used as an alternative energy source as a generator fuel.

Keywords: Soybean-based biodiesel; Power generator diesel engine; Combustion; Performance; Emission

Paper 45 **Bildiri 45**

ELEKTROMEKANİK SUPAP MEKANİZMASI KULLANILMASI DURUMUNDA EGZOZ SUPAP ZAMANLAMASININ DEĞİŞİMİNİN HAVA AKIŞ PARAMETRELERİNE ETKİSİNİN MODELLENMESİ

Usame Demir[1,*], Gökhan Coşkun[1], Hakan S. Soyhan[1,2]

[1] Sakarya Üniversitesi Mühendislik Fakültesi, Makine Mühendisliği Bölümü, Sakarya, Turkey
[2]Team-SAN Ltd. Şti., Sakarya Üniversitesi Teknokent, Sakarya, Turkey

ÖZET

Bu çalışmada buji ateşlemeli tek silindirli bir motorun klasik kam mekanizması yerine elektromekanik supap mekanizması kullanılması durumunda hava akış parametrelerine olan etkiler 3 boyutlu Hesaplamalı Akışkanlar Dinamiği (HAD) yazılımı ile incelenmiştir. Analiz çalışmaları için ANSYS FORTE yazılımı kullanılmıştır. Bu yazılım sadece içten yanmalı motor simülasyonu yapabilmektedir. Forte yazılımı kullanılarak silindir içi akış simülasyonları gerçekleştirilmiştir. Analizlerde kullanılan modelde emme ve egzoz manifoldları dahil olan silindir iç kısmınında bulunduğu hacimler yani tam akış modeli kullanılmıştır. Yanma verimliliğine etkisi olan yatay kütlesel hava debisi silindir içi basınç gibi değerlere devirin etkisi analiz sonuçları ile ortaya konmuştur. Analiz çalışmasında elektromekanik supap profili için literatür araştırması yapılmış ve en ideal supap açılma süresi belirlenmiş ve bu süreye göre elektromekanik supap profilleri farklı devirler için oluşturulmuştur. Egzoz supapının erken yada geç kapanma durumları Elektromekanik supap kullanılması durumunda motorun volumetrik verimine dolaylı yoldan yanma verimliliğine olumlu etkilerin olduğu bu çalışmayla ortaya konmuştur.

Anahtar Kelimeler: Hesaplamalı Akışkanlar Dinamiği, Silindir İçi Akış Modellenmesi, Buji Ateşlemeli Motor, Elektromekanik Supap Mekanizması

MODELING BY USING ELECTROMECHANICAL SUPPORT MECHANISM EFFECT OF EXHAUST VALVE TIMING ON THE AIR FLOW PARAMETERS

Usame Demir[1,*], Gökhan Coşkun[1], Hakan S. Soyhan[1,2]

[1] Department of Mechanical Engineering, Sakarya University, Sakarya, Turkey
[2]Team-SAN Co, Technocity at Sakarya University, Sakarya, Turkey

ABSTRACT

In this study, using electromechanical valve mechanism instead of conventional cam mechanism affects on air flow parameters were investigated by 3D Computational Fluid Dynamics (CFD) software for single cylinder spark ignition engine. ANSYS FORTE software was used for analysis studies. This software can only simulate an internal combustion engine. In-cylinder flow simulations were performed using CFD software. In the 3-D model used for the analyses, the full flow model was used in the interior of the cylinder including the suction

and exhaust manifolds. The effects of mass air flow, horizontal vortex, such as horizontal vortex, which have an effect on combustion efficiency, are determined with the results of analysis. In the analysis study, literature search was made for electromechanical valve profile and the optimum valve opening time was determined and electromechanical valve profiles were created for different RPM. In the case of the use of electromechanical valve mechanism, early or late closure of the exhaust valve has a positive effect on the volumetric efficiency of the engine and has an indirect effect on combustion efficiency.

Paper 46 **Bildiri 46**

DEĞİŞKEN EMME SUPAP ZAMANLAMASI VE ELEKTROMEKANİK SUPAP MEKANİZMASI KULLANILMASININ HAVA AKIŞ PARAMETRELERİNE ETKİSİNİN HAD İLE İNCELENMESİ

Usame Demir[1,*], Gökhan Coşkun[1], Hakan S. Soyhan[1,2],

[1] Sakarya Üniversitesi Mühendislik Fakültesi, Makine Mühendisliği Bölümü, Sakarya, Turkey

[2]Team-SAN Ltd. Şti., Sakarya Üniversitesi Teknokent, Sakarya, Turkey

ÖZET

Bu çalışmada buji ateşlemeli tek silindirli bir motorun klasik kam mekanizması yerine elektromekanik supap mekanizması kullanılması durumunda hava akış parametrelerine olan etkiler 3 boyutlu Hesaplamalı Akışkanlar Dinamiği (HAD) yazılımı ile incelenmiştir. Analiz çalışmaları için ANSYS yazılımının alt modülü olan ve içten yanmalı motor simülasyonu yapabilen Forte yazılımı kullanılarak silindir içi akış simülasyonları gerçekleştirilmiştir. Analizlerde kullanılan modelde emme ve egzoz manifoldları dahil olan silindir iç kısmının da bulunduğu hacimler yani tam akış modeli kullanılmıştır. Yanma verimliliğine etkisi olan yatay girdap, dikey girdap gibi değerlere devirin etkisi analiz sonuçları ile ortaya konmuştur. Analiz çalışmasında standart supap profiline göre öncelikle supap profilleri oluşturulmuştur. Ardından elektromekanik supap mekanizması için gerekli profil için literatür araştırması yapılmıştır. Literatürde en ideal supap açılma süresi belirlenmiş ve bu süreye göre elektromekanik supap profilleri her farklı devir için oluşturulmuştur. Emme supabının açılma zamanın erkene alınma durumlarının etkisi incelenmiştir. Elektromekanik supap mekanizması kullanılması durumunda motorun volumetrik veriminin düşük devirlerde düştüğü fakat devir yükseldikçe volümetrik verimde artış olduğu görülmüştür.

Anahtar Kelimeler: Hesaplamalı Akışkanlar Dinamiği, Silindir İçi Akış Modellenmesi, Buji Ateşlemeli Motor, Elektromekanik Supap Mekanizması

Paper 47 **Bildiri 47**

MODELING OF USING ELECTROMECHANICAL VALVE MECHANISM BY CFD EFFECT OF EXHAUST VALVE TIMING ON THE AIR FLOW PARAMETERS

Usame Demir[1,*], Gökhan Coşkun[1], Hakan S. Soyhan[1,2],

[1] Department of Mechanical Engineering, Sakarya University, Sakarya, Turkey

[2]Team-SAN Co, Technocity at Sakarya University, Sakarya, Turkey

ABSTRACT

In this study, using electromechanical valve mechanism instead of conventional cam mechanism affects on air flow parameters were investigated by 3D Computational Fluid Dynamics (CFD) software for single cylinder spark ignition engine. In the experimental study, the cylinder pressure, intake and exhaust air temperatures at different cycles and the air entering the cylinder from the intake manifold were measured by the conventional cam mechanism. In-cylinder flow simulations were performed using Forte software, which is a sub-module of ANSYS software and can simulate internal combustion engine for analysis studies. In the model used in the analyses, the volumes in the interior of the cylinder including the intake and exhaust manifolds, ie the full model, are used. The values such as swirl and tumble ratio, which have an effect on combustion efficiency, have been observed with the results of analysis. In the analysis study, valve profiles were formed according to the standard valve profile. A literature search was carried out for the required profile for the electromechanical valve mechanism. In the literature, the ideal valve opening time has been determined and according to this time electromechanical valve profiles have been performed for each different cycle. The effect of early opening of the intake valve has been investigated. It is seen that the engine volumetric efficiency decreases when using electromechanical valve mechanism at low RPM compared to the standard valve profile but the volumetric efficiency increases with the increase of the RPM.

Keywords: Computational Fluid Dynamics, In-Cylinder Flow Modeling, Spark Ignition Engine, Electromechanical Valve Mechanism

Paper 48 **Bildiri 48**

AN ENERGY EFFICIENCY STUDY FOR AN ATMOSPHERIC NATURAL GAS BOILER: A CASE STUDY

Cemil Koyunoğlu[1], Fikret Yüksel[1,*]

[1]Department of Energy Systems Engineering, Yalova University, 77200, Yalova, Turkey

ABSTRACT

Turkey's primary electricity supply is still coal and natural gas cycle power plants meets the majority. In 2010 153.190 GWh producing both technologies, Turkey is created 72.5's % of the total electricity production of natural gas and 26.1% of which 46.5% of coal is known to be sourced from power plants. The next largest electricity generation was provided by hydroelectric power at 24.5% at the same year. To help meet the rapidly growing national energy demand in the next 10 years the need for studies to be an example of energy efficiency in natural gas power plants, which constitute an important part of electricity generation, is increasing day by day. In this study, it is aimed to contribute to energy efficiency studies with case studies in atmospheric natural gas boilers.

Keywords: Natural gas boilers, Energy Efficiency, Fuel/Air ratio, Research & Development

Paper 49 **Bildiri 49**

MICROWAVE IGNITION OF MUNICIPAL WASTE, MANURE AND SIRNAK ASPHALTITE SLIME PELLETS FOR COMBUSTION IN FLUIDIZED BED COMBUSTION CHAMBER

Yıldırım İsmail TOSUN

Şırnak University, Engineering Faculty, Mining Engineering Dept., Şırnak

(yildirimismailtosun@gmail.com)

ABSTRACT

Low quality fuels are used in power generation as potential contributions to rural economic development on the contrary to reduce reliance on high quality fuels, as an additional demand centre for electricity commodities and as a way to urbanization.

Especially cold start in coal incineration pro combustion cause hard emission control may cost higher prices on use of diesel such as 60-90$/ton in fluidized bed. The microwave ignition may decrease cold start cost to lower such as 3-5$/ton. Biomass waste pellets are produced in two different forms in size. One type of manure wastes is in nut size and easily be evaluated in agricultural industry and other may be evaluated as animal feed filling materials in fine size under 20 microns as which collected following solid-liquid separation thickeners. That incinerated waste in finer size may deteriorate environment near urbanization and water contamination in streams. Beneficiate from that finer bio-mass carbon in toxic gas emission control during combustion can efficiently be evaluated in microwave combustion. However, fluidized combustion are carried out with cold start of pellets 5mm containing 100 microns Şırnak asphaltite as solid fuel ignited combustion. In order to avoid this disturbing flow manner of that waste material, waste pellets were used in combustion chamber. Fine Şırnak asphaltite slime below 100 micron may also be evaluated as fuel material without washing for filling material in pelletizing such as binder paper and manure waste. 40%, 60% and 80% bio-waste pellets were used in our combustion experiments at 5 mm sized pellets.

Keywords: Microwave Ignition, Municipal Waste, Manure, Şırnak Asphaltite Slime, Pellet Combustion, Fluidized Bed Combustion, Bubbling Chamber

Paper 50 **Bildiri 50**

CA FERRITE PELLETS FOR COMBUSTION IN FLUIDIZED BED COMBUSTION CHAMBER

Yıldırım İsmail TOSUN

Şırnak University, Engineering Faculty, Mining Engineering Dept., Şırnak

(yildirimismailtosun@gmail.com)

ABSTRACT

One type of manure Ca ferrite wastes is pelletized in nut size and easily be evaluated in power industry and similar pellet may be evaluated as animal feed filling materials in fly ash waste post combustion at finer size under 20 microns as which collected following solid-liquid separation thickeners. That incinerated waste in finer size may deteriorate environment near urbanization and water contamination in streams. Beneficiate from that finer bio-mass carbon and Ca ferrite control toxic gas emission during combustion can efficiently be evaluated in microwave combustion. However, in fluidized bed combustion microwave radiation are carried out at cold start with pellets 5mm containing Şırnak asphaltite as solid fuel ignited combustion. In order to avoid this disturbing flow manner of that waste material, waste pellets were used in combustion chamber. Fine iron slime below 100 micron may also be evaluated as ignition material without binding material in pelletizing such as binder paper and manure waste. 4%, 6% and 8% ferrite pellets were used in our combustion experiments at 5 mm sized pellets.

Keywords: Ca Ferrite, Waste Pellets, Microwave Ignition, Şırnak Asphaltite Slime, Pellet Combustion, Fluidized Bed Combustion, Bubbling Chamber

Paper 51 **Bildiri 51**

TAM ÖLÇEKLİ STANDART BİR YANGIN ODASI TEST DÜZENEĞİ VE YANGIN TESTLERİNDEN ISI YAYILIM ORANININ TESPİTİ

Cemil SAĞLAM[1], Gökhan COŞKUN[1,2], Hakan S. SOYHAN[1,2,3]

[1] Sakarya Üniversitesi, Yangın ve Yangın Güvenliği EABD

[2] Sakarya Üniversitesi, Makine Mühendisliği Bölümü

[3] Sakarya Üniversitesi, Yangın Uygulama ve Araştırma Merkezi

Özet

ISO, ASTM gibi çeşitli standartlarda tanımlanmış yangın odası test düzeneğinin temel amaçlarından biri oda içerisinde yanan bir cismin ısı yayılım oranının tespit edilmesidir. Elde edilen ısı yayılım oranı çıktısı cisim yanması hakkında önemli bir veri olması yanında yangın modellemesi yapabilen yazılımlar içinde gerekli bir girdi verisidir. Literatürde çeşitle cisimler, mobilyalar, konfeksiyon ürünleri, elektronik cihazlar gibi karmaşık malzemelerden oluşan cisimler yangın odasında deneye tabi tutulup ısı yayılım oranı verileri elde edildiği bilinmektedir. Fakat bu veriler sınırlı sayıda cisim için yapılmıştır, yetersizdir ve zenginleştirilmesi gerekmektedir. Bu amaçla Sakarya Üniversitesi Yangın ve Yangın Güvenliği EABD programı kapsamında yapılan bir tez çalışması ile standartlara uygun bir yangın odası kurulmuştur ve veri almak için gereken ekipmanlar hazırlanmaktadır. Bu çalışmada yangın odası için yapılan çalışmalar ve ısı yayılım oranı tespiti için kullanılacak ekipman ve hesaplama yöntemlerinden bahsedilmiştir.

Paper 52 **Bildiri 52**

KÜTÜPHANE BİNALARINDA TAHLİYE SÜRESİNİ UZATAN FAKTÖRLERİN DENEYSEL VE BİLGİSAYAR DESTEKLİ SİMÜLASYON YÖNTEMLERİYLE İNCELENMESİ

Gökhan COŞKUN, Bülent AÇIL, Hakan S. SOYHAN

Acil durumlarda tahliyeyi etkileyen yapısal, teknik ve yönetimsel tedbirlere bağlı olarak gelişen çevresel faktörlerin yanı sıra insanın biyolojik, fizyolojik ve psikolojik yapısından kaynaklı faktörler de bulunmaktadır. Bu çalışmada bir üniversitenin kütüphane binası temel alınarak acil durumlarda tahliyeyi etkileyen faktörler etraflıca incelenmiştir.

Çalışma esnasında kütüphane binasında tahliyeyi etkileyen tüm çevresel faktörler detaylandırılmış ve deneysel bir tahliye tatbikatı gerçekleştirilmiştir. Aynı şartlar altında bir de bilgisayar simülasyonu gerçekleştirilmiştir. Bütün çevresel şartlar ve tahliyeye konu kişi sayısı ve dağılımı aynı olmasına rağmen simülasyon çalışmasında tahliye hızının deneysel tahliye tatbikatından 1 dakika daha hızlı gerçekleştiği tespit edilmiştir. Bu süre farkının bütün literatür çalışmalarına paralel olarak insan faktöründen kaynaklandığı değerlendirilmektedir. Tatbikata katılanların sağlıklı birey oldukları düşünüldüğünde bu süre farkının fizyolojik nedenlerden ziyade tahliye bilinç seviyesindeki farklılıktan kaynaklandığına kanaat getirilmiştir. Çünkü deneysel tatbikatta çıkan tahliye reaksiyon süresi dahi farklılık arz etmektedir ve bu çıkarımın en yakın göstergelerinden biridir.

Sonuç olarak kütüphane binalarının tahliyeye elverişli hale getirilmesinin yanında kişilerin tahliye konusunda bilinçlendirilmesinin de çok büyük bir öneme sahip olduğu yapılan çalışma neticesinde net bir şekilde ortaya konmuştur.

Paper 53 **Bildiri 53**

ACİL DURUM TAHLİYESİ EĞİTİMİNİN TAHLİYE DAVRANIŞLARINA VE SÜRELERINE ETKİLERİNİN DENEYSEL VE BİLGİSAYAR DESTEKLİ SİMÜLASYON YÖNTEMLERİYLE İNCELENMESİ

Gökhan COŞKUN, Recai AKSOY, Üsame DEMİR, Hakan S. SOYHAN

Bu çalışmada okul öncesi, ortaöğretim ve lise öğrencilerinin ve öğretmenlerinin bulunduğu bir eğitim binasında acil durum anında gerçekleşmesi gereken tahliye davranışları ve süreleri incelenmiştir. İlk aşamada bireylerin tahliye konusunda özel bir eğitim almadığı koşul göz önüne alınarak tahliye deneyi yapılmıştır. Daha sonra öğrencilere yaş gruplarına göre tahliye anında nasıl davranmaları gerektiğine dair özel bir eğitim verilmiştir. Ayrıca öğretmenler de acil durum anında öğrencileri nasıl yönlendirmeleri gerektiğini ve hangi yolları izleyerek binayı terk etmeleri gerektiğini anlatan özel bir tahliye eğitimine tabi tutulmuşlardır. Eğitimden sonra tekrar tahliye deneyi yapılmıştır. Yapılan deneyler aynı koşullarda bilgisayar ortamında modellenmiştir. Bir eğitim kurumda olası bir tahliyenin kişilerin eğitimli ve eğitimsiz olması durumuna göre farklı girdi parametrelerinin kullanılması gerektiği yapılan modelleme çalışmalarından anlaşılmıştır. Tahliye simülasyonlarının acil durum tahliye planlarının oluşturulmasında gelecek yıllarda daha sık kullanılacak bir yöntem olacağı öngörülmektedir. Yapılan çalışmada elde edilen veriler sayesinde her bir eğitim kurumu için deneysel çalışma yapmadan doğrudan simülasyonların yapılması için önemli bir kaynak oluşturacağı düşünülmektedir.

Paper 54 **Bildiri 54**

INVESTIGATION OF EMISSIONS AND COMBUSTION DATA OF BIODIESEL USAGE IN CERAMIC COATED DIESEL ENGINE BY MULTIPLE CRITERIA DECISION-MAKING METHODS

Sinan Erdoğan[a], Selman Aydın[b], Mustafa Kemal Balki[c], Cenk Sayın[d]

[a]*Institute of Pure and Applied Sciences, Marmara University, Istanbul, Turkey*
[b]*Department of Automotive Engineering, Batman University, Sinop, Turkey*
[c]*Department of Mechanical Engineering, Sinop University, Sinop, Turkey*
[d]*Department of Mechanical Engineering, Marmara University, Istanbul, Turkey*

ABSTRACT

The fossil fuels used in internal combustion engines are rapidly depleted and the environmental consciousness of people is increasing. Along with these, the importance of modification studies in alternative motor vehicles and the search for alternative fuels is increasing. Although the interpretation of experimental data is a scientifically important method, it has become even more important to determine the best option for engine manufacturers or R&D engineers nowadays when technology is rapidly changing. In this study, the performance, emission and combustion characteristics of biodiesel obtained from cotton oil-based waste frying oil were investigated in a diesel engine coated with thermal barrier. The experimental results were evaluated using multi-criteria decision-making methods and the operating conditions that give the best engine performance, emission and combustion characteristics were determined. This paper demonstrates that MCDM techniques can also be applied to engineering issues to enable decision makers, such as engine manufacturers and R&D engineers, to make the best decision to strengthen fuel economy and an environmentally friendly approach. In this way, decision-making processes will be facilitated and will provide both economic and time savings to decision makers.

Paper 55 **Bildiri 55**

COMBUSTION DEVELOPMENT OF HEAVY DUTY DIESEL ENGINE IN SINGLE CYLINDER RESEARCH ENGINE

Cengizhan Cengiz[1], Nurettin Dasdemir[2], Arda Coşkun[3]

[1]*Ford Otosan A.Ş. İnönü Ar-Ge Test Merkezi, Eskişehir, TURKEY, ccengiz@ford.com*

[2]*Ford Otosan A.Ş. İnönü Ar-Ge Test Merkezi, Eskişehir, TURKEY, ndasdemi@ford.com*

3Ford Otosan A.Ş. Sancaktepe R&D Center, Istanbul, TURKEY, acoskun5@ford.com.tr

Abstract

Combustion development of diesel engine is a complex process. Combustion chamber design, injector parameter and thermodynamic selections are the main parts of this development. Piston bowl shape design, compression ratio definition and injector related parameters such as spray angle, nozzle tip protrusion and flow rate parameters assesments should be performed. In the first step, simulation methods are used to develop the combustion chamber design and optimize the parameters to reduce the design space where test have been performed. In the second step, test methods are used to develop the combustion chamber. Test activity is used to correlate simulating activities, compare the most possible hardware options. A precise controlled measuring system, well defined test platform and repeatable conditions are required. For this purpose, single cylinder research engine platforms are used for simulation validation, hardware assesment and performance & emissions calibrations of the combustion system. In this work, combustion development activities in Single Cylinder Engine is explained.

Paper 56 **Bildiri 56**

DPF AGING TESTS ON COMMERCIAL AUTOMOTIVE CATALYST

İsmail Hakkı SAVCI*, Hande BEZCİ ZEREN**

* Ford OTOSAN Flow Performance and Durability Laboratory

isavci@ford.com

** Ford OTOSAN Flow Performance and Durability Laboratory

hzeren@ford.com.tr

With stringent diesel engine emission regulations at recent years, the DPF systems have become the one of the main technology to remove soot particles from tailpipe of the diesel engines. Fresh catalyst parts become aged after certain miles and their characteriztion is decreased significantly. To understand emission performance of the catalyst aging is crucial due to emission legistration. One of the main characterization of the catalyst aging is thermal aging. To address this issue, flow burner systems may be used to increase exhaust temperature to get aged catalysy by the high temperature.

A burner-based aging system offers an alternative solution that provides higher exhaust temperatures, with lower fuel consumption compared to a diesel engine bench aging system. This paper presents a natural burner based aging system that addresses the technical challenges of using a burner to simulate diesel exhaust and the validation of aging equivalency between the burner-based system and a diesel engine dynanometer. The operational cost effectiveness of burner systems compared to diesel systems is also explored.

Paper 57 **Bildiri 57**

PERFORMANCE AND COMBUSTION CHARACTERISTICS OF A CRDI DIESEL ENGINE FUELED WITH TERNARY MICROEMULSIFICATION FUELS

Huseyin Sanli [1, 2]

[1] Ford Otosan Ihsaniye Automotive Vocational School, Kocaeli University, 41680, Golcuk, Turkey

[2] Alternative Fuels R&D Center, Kocaeli University, 41275 Izmit, Turkey

Global energy consumption has been increasing each year and the energy requirement is predicted to be raised in all sectors. Transportation is one of the prominent sectors in energy consumption. Very big portion of the energy used in transportation sector is still met by fossil fuels, especially petroleum-based diesel fuel. This situation causes some critical problems such as high energy import bills for the countries whose do not have own fossil energy sources, energy dependency and environmental damages caused by exhaust emissions. Thus, biofuels are very important alternative energy sources for sustainable transportation and lower emissions.

When the current situation of the automotive industry is considered, it is seen that liquid biofuels (biodiesel and bio-alcohols) have various technical and economical superiorities over the other alternative energy sources. For example, they are compatible with the existing fuel distribution infrastructure and require no modification in engines and fuel injection systems. Among the biofuels, bio-alcohols (especially bioethanol) have higher consumption amount than biodiesel in the USA and South America, while biodiesel is the leader biofuel in European Union.

Biodiesel fuels have lots of technical advantageous compared to petroleum-based diesel fuel and they emit less exhaust emissions except for NO_x emissions. If the feedstock types used in biodiesel production is examined, it is realised that very big portion of global biodiesel production is produced from high quality, food-grade vegetable oils. This feedstock choice increases the biodiesel cost inevitably and so makes it an economically unfavourable fuel. Moreover, this situation causes to increases in the prices of vegetable oils used in food industry due to problems in supply and demand balance. Because of these reasons, food-grade, high-quality and expensive vegetable oils should not be used in biodiesel industry as feedstock. In this context, waste frying oils have a big potential that should not be ignored.

Another issue that needs to be taken into consideration in terms of high biodiesel unit price is the transesterification reaction in which biodiesel fuel is produced. Considering in industrial scale, transesterification reaction requires infrastructure investment, energy consumption, chemical and water usage, labour and time all of those increase the biodiesel cost.

Microemulsification is one of the four chemical methods (transesterification, microemulsification, dilution, and pyrolysis) used for decreasing the extremely high viscosities of crude vegetable oils, which is the biggest technical hurdle against their direct usage as fuel in diesel engines, to an acceptable value.

In the current study, ternary microemulsification fuels consisting of waste frying oil (without converting biodiesel), petroleum-based diesel fuel and alcohol were prepared. As the alcohol constituents of the microemulsification fuels, 1-butanol (n-butanol) and 2-propanol (iso-propanol) were used. When preparing the test fuels, the viscosity of the ternary fuels was kept below 5 $mm^2.s^{-1}$ which is the viscosity upper limit given in European Biodiesel Standard (EN-14214). Test fuels used in the engine tests were coded as following: "D" for petroleum-based diesel fuel, "D50W30B20" for 50% petroleum-based diesel fuel-30% waste frying oil-20% n-butanol (on volume basis, v/v) ternary microemulsification fuel, "D50W30IP20" for 50% petroleum-based diesel fuel-30% waste frying oil-20% iso-butanol (v/v) ternary microemulsification fuel.

Engine tests were performed in a four-cylinder, four-stroke, water-cooled, turbocharged-intercooled, common rail direct injection diesel engine. During engine tests, engine speed was kept fixed at 2000 rpm, while the engine load was increased from 50 Nm to 150 Nm with the increments of 25 Nm. The influences of the ternary microemulsification fuels on the performance and combustion characteristics of the test engine was determined and compared with those of D as the reference fuel.

D has lower brake specific fuel consumption and higher brake thermal efficiency values than those of microemulsification fuels at all engine loads tested. However, this difference increased with increasing engine load. D50W30IP20 has relatively better performance characteristics than D50W30BU20.

Higher in-cylinder pressures were attained with D at low loads; however, this situation has changed at higher engine loads. Microemulsification fuels had very similar in-cylinder pressures up to 100 Nm, but D50W30BU20 produced relatively higher pressures than D50W30IP20 at the engine loads of 125 Nm and 150 Nm. Despite their comparatively lower cetane numbers, ignition delay periods were lower for microemulsification fuels (apart from 50 Nm). Combustion durations of microemulsification fuels were shorter compared to those of D at all operating conditions; even though their fuel consumption amounts were higher.

Keywords: Biodiesel, Microemulsification, Engine Test, Performance, Combustion

Paper 58 **Bildiri 58**

COMPARISON OF COMBUSTION AND EMISSION CHARACTERISTICS OF OUTPUT SYNTHETIC GAS COMPOSITIONS OF TWO DIFFERENT POWER STATIONS

[1*]Harun Yilmaz, [1]Omer Cam, [2]İlker Yilmaz

[1] Erzincan Binali Yildirim University, Ali Cavit Çelebioğlu Civil Aviation College, Department of Airframes and Powerplants, Erzincan, 24002, Turkey
[2] Erciyes University, Faculty of Aeronautics and Astronautics, Department of Airframes and Powerplants, Kayseri, 38030, Turkey

* E-mail: hyilmaz@erzincan.edu.tr

Abstract

In this study, combustion and emission characteristics of output synthetic gas compositions of two different power stations, namely Schwarze Pumpe and Fife, were investigated in a swirl stabilized combustor. For this purpose, an experimental test rig which is equipped with a premixed burner that can combust synthetic gases in a wide gas composition range was built and utilized. Tested synthetic gas mixtures are 61.9%H_2-26.2%CO-6.9%CH_4-5.0%CO_2 (Schwarze Pumpe - H_2/CO: 2.36) and 34.4%H_2-55.4%CO-5.1%CH_4-5.1%CO_2 (Fife - H_2/CO: 0.62). Actually, these gas mixtures contain slight amount of N_2 and Ar. Therefore, right amount of CO_2 was added to each mixture to represent these inert constituents. The comparison of combustion behavior of respective synthetic gas mixtures was conducted via examining axial and radial temperature values throughout the combustor. Besides, emission behavior was interpreted by analyzing measured CO, CO_2 and NO_x values at combustor chimney. Results of this study showed that output synthetic gas of Schwarze Pumpe station performs better with respect to temperature distribution and emitted CO and NO values.

Keywords: Synthetic Gas, Combustion And Emission.

Introduction

Synthetic gas is derived from gasification of any carbon containing raw material, and its composition controlled by many parameters such as type of reactor and gasifying agent, temperature during gasification process, residence time, and feedstock. The main purpose of the gasification process is to maximize conversion rate of feedstock into the gas product. Primarily, feedstock is exposed to high temperature, and then thermal degradation starts. Unlike pyrolysis, feedstock is in contact with gasifying agent. At sufficiently high temperatures, carbon oxides and other hydrocarbons are formed as result of the reactions between the gasifying agent and feedstock [1].

Synthetic gas is mainly composed of H_2 and CO, and can be used for electricity and liquid fuel production as an environment friendly option [2]. This positive aspect of synthetic gas have promoted gasification technology and many researchers conducted both experimental and numerical studies on synthetic gas combustion.

Arroyo et al. investigated combustion behavior of two different synthetic gas blends obtained from biogas, and compared results with those acquired from combustion of gasoline, CH_4 and biogas (which is used from synthetic gas production) in tested spark ignition engine. Results of their study showed that hydrogen constituent in synthetic gas blend increases peak pressure value in cylinder, and moves peak pressure closer to top dead position than CH_4 and biogas. Lastly, it was concluded that synthetic gas enables higher combustion performance albeit its inert constituents at leaner conditions [3].

Lee et al. conducted experimental studies on a model gas turbine engine (GE7EA). They used H_2/CO mixture as fuel and add varying amount of N_2, CO_2 and steam to analyze effects of these diluents on pollutant emissions, flame stability, flame shape and temperature distribution. As expected, it was found that emission of NO_x decreases as the amount of diluents increase. They also detected no combustion instabilities, and confirmed that tested diluents are efficient in reducing NO_x emission while providing effective operation [4].

Ning et al. simulated hydrogen carbon monoxide mixture flames in a one dimensional micro-flow reactor model. They used oxygen/nitrogen, oxygen/carbon monoxide or oxygen/water vapor mixtures as oxidant, and analyzed ignition behavior of tested syngas under various combustion atmosphere conditions. Results of their study showed that CO_2 and H_2O increase ignition temperature more than N_2, and this increment is more intense when the oxidant is mixture of O_2 and H_2O [5].

Yu et al. performed experimental studies on premixed synthetic gas/air flames to examine propagation behavior of such flames in a half open duct. They varied equivalence ratio and hydrogen amount in gas mixture, and evaluated propagation behavior via examining flame structure and flame tip dynamics. Depending on the equivalence ratio and hydrogen amount, various flame structures were observed. It was also found that characteristics of synthetic gas/air flames hydrogen significantly affected by hydrogen amount [6].

As mentioned before, composition of synthetic gases is controlled by many parameters. This situation brings many challenges to synthetic gas combustion with respect to flame stability issues. Because, synthetic gas constituents such as H_2, CO and CH_4 have very different transport, physical and chemical properties. For example, H_2 causes flame instabilities such as flashback, dynamic flame instabilities etc. Regarding these, many researchers studied synthetic gas flame instabilities [7-10].

In this study, combustion and emission characteristics of two different synthetic gas blends which are obtained from Schwarze Pumpe and Fife power stations were compared. To this end, an experimental test rig was built, and premixed 61.9%H_2-26.2%CO-6.9%CH_4-5.0%CO_2 and 34.4%H_2-55.4%CO-5.1%CH_4-5.1%CO_2 mixtures were tested under the same boundary and

physical conditions. The reason for these mixtures to be chosen is that the difference in volumetric heating values of these synthetic gas blends is as low (76 kJ/m^3) as can eliminate inlet effects. During experiments, equivalence ratio was also varied between the values of 0.6, 0.8 and 1.0, and its effects also evaluated. Comparison of combustion and emission characteristics was conducted via examining temperature and pollutant emission profiles.

Experimental Apparatus

In figure 1, schematic of the experimental test rig is given. Tested synthetic gas mixtures were composed by precisely metering (via a digital mass flow controller) the amount of each synthetic gas constituent (depending on the thermal power) supplied from an external tank. These gases are then directed to a gas collector, mixed with combustion air in a static pre-mixer, inclined to the burner and combusted. Reader may refer to Ref. [11] for detailed explanation of the experimental apparatus.

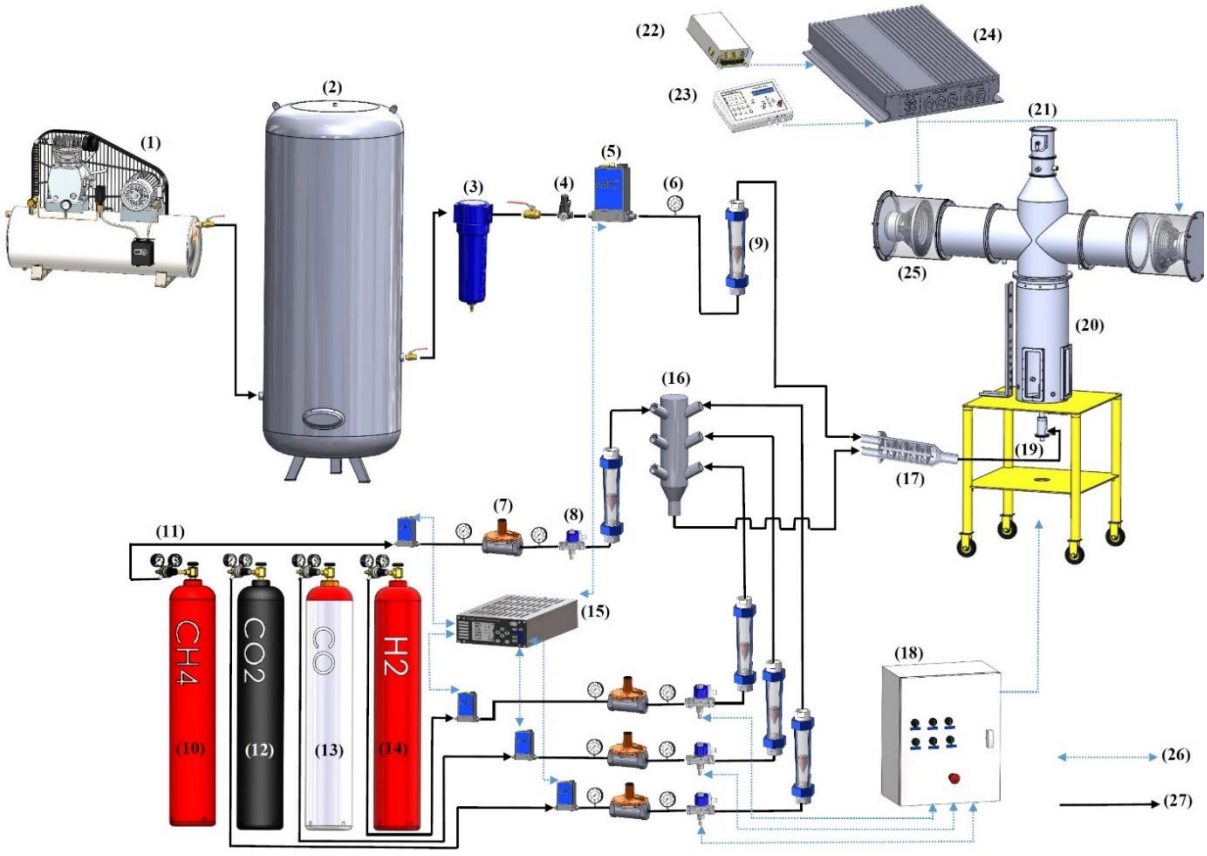

Figure 1. Layout of the overall combustion system.

1. Air compressor (5.5 hp, 500 lt)	10. CH_4 tank	19. Burner
2. External air tank (1 m^3)	11. Pressure regulator	20. Combustion chamber
3. Filter (for steam and oil removal)	12. CO_2 tank	21. Flue
4. Pressure regulator (1 MPa to 0.3 MPa)	13. CO tank	22. Power source
5. Mass Flow Controller	14. H_2 tank	23. Function generator
6. Manometer	15. Vacuum system controller	24. Audio amplifier
7. Pressure Regulator	16. Gas collector	25. Loudspeaker
8. Solenoid Valve	17. Fuel/air pre-mixer (static)	26. Electrical connections
9. Float type flowmeter	18. Control panel	27. Gas supply lines

Operating Conditions

All experiments have been performed at local atmospheric conditions of city of Kayseri, Turkey. Mixing of fuel gases and air, and combustion took place at room conditions. During combustion tests, thermal power of the combustor and swirl number were set as 5 kW and 0.2, respectively, and the amount of air was varied in accordance with equivalence ratio (0.6, 0.8 and 1.0). In Table 1, some properties of the tested synthetic gas mixtures are given.

Table 1. Some properties of tested synthetic gas mixtures.

	Composition (%)						
	H_2	**CO**	**CH_4**	**CO_2**	**N_2+Ar**	**H_2/CO**	**Heating Value (kJ/m^3)**
Schwarze Pumpe	61.9	26.2	6.9	2.8	1.8	2.36	12492
Fife	34.4	55.4	5.1	1.6	3.1	0.62	12568

Results and Discussions

For axial temperature measurements, B and K type thermocouples were located at a fixed radial (combustor centerline), and 9 different (63, 113, 163, 213, 263, 313, 413, 513 and 613 mm away from burner outlet) axial locations. Measured temperature values at these axial locations were plotted against distance from burner outlet, and presented in Figure 2.

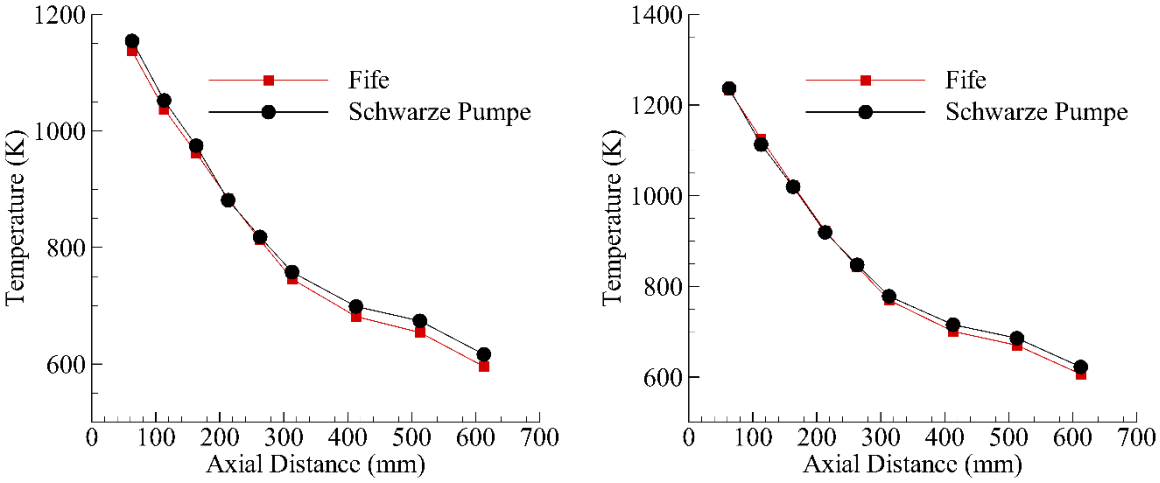

Figure 2. Axial temperature profiles at different equivalence ratios.

Because of the intrinsic properties of hydrogen (such as high burning rate, high reaction kinetics and diffusion ability etc.), synthetic gas mixture with high H_2/CO ratio, namely Schwarze Pumpe, flashed back at stoichiometric conditions and consequently, we could not attain a stable flame. This is why temperature profiles are not presented at 1.0 equivalence ratio. As clearly seen in Figure 2, temperature profiles are in a good agreement with each other in terms of both trend and value in and near the flame region. At 0.6 equivalence ratio, temperature values of 61.9%H_2-26.2%CO-6.9%CH_4-5.0%CO_2 mixture are slightly higher than that of 34.4%H_2-55.4%CO-5.1%CH_4-5.1%CO_2 mixture in the flame region. However, this agreement diminishes further downstream of the combustor and mixture with the higher H_2/CO ratio forms higher exit temperature value. Although volumetric heating values of tested mixtures are very

close, gravimetric heating value of 61.9%H_2-26.2%CO-6.9%CH_4-5.0%CO_2 mixture is higher (almost twice). This situation is attributed to this phenomenon. At 0.8 equivalence ratio, temperature profiles of both gas mixture are nearly coincident from burner outlet till the axial distance of 300 mm. As a conclusion, it can be inferred that gas composition variation of tested gas mixtures doesn't significantly affect temperature distribution. Nevertheless, equivalence ratio effects on temperature values are more profound. As expected, temperature values increase as equivalence ratio rises irrespective of the gas composition (Figure 3).

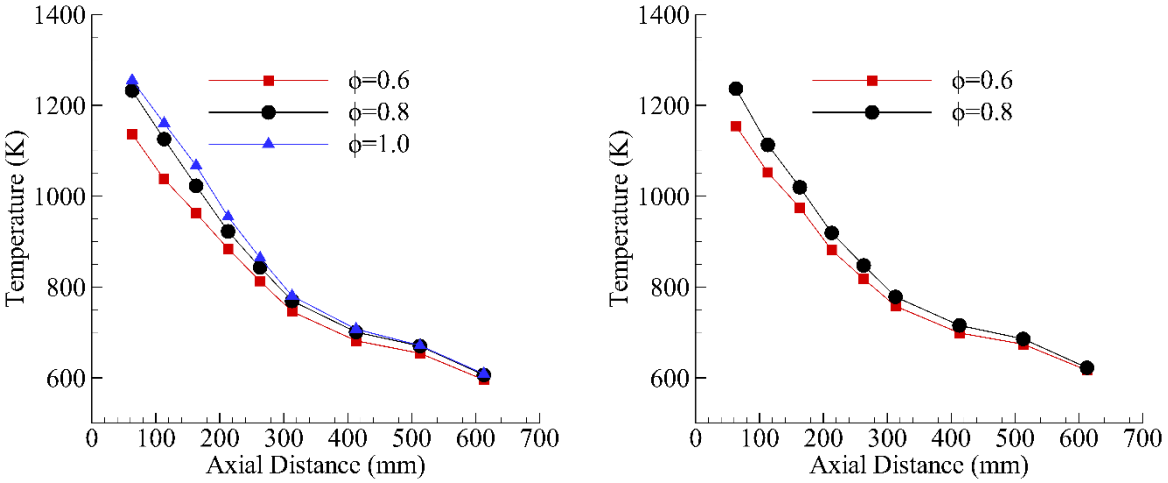

a) Schwarze Pumpe b) Fife

Figure 3. Axial temperature profiles of tested gas mixtures at different equivalence ratios.

Radial temperature measurements are performed at 3 different axial (113, 213, 313 mm away from burner outlet) and radial (5, 10 and 16 cm away from combustor centerline) locations. Consistent with the axial temperature profiles, radial temperature values do not considerably vary with gas composition (Figure 4). In the radial distance range of 0-10 cm, temperature values are very close for both mixtures. However, further increments in radial range (10-16 cm) causes 61.9%H_2-26.2%CO-6.9%CH_4-5.0%CO_2 mixture to form higher temperature values than its counterpart. Except for the centerline temperature values, radial temperature values increase as axial distance increases. This is because of the homogenously propagation of post combustion gases into the combustor. The tendency of radial temperature profiles doesn't effectively change with equivalence ratio (Figure 5). The conformity between temperature profiles of tested gas mixture increases and nearly same temperature values form irrespective of the axial and radial locations (except for the radial distance range of 0-5 mm at 113 mm axial location).

Likewise, radial temperature values increase with equivalence ratio (Figure 6). This increment is more distinct in the radial range of 0-5 cm and decreases as radial distance increases (at 113 mm axial distance). At 213 mm axial distance, temperature increment with equivalence ratio increment is profound at all radial locations. At 313 mm axial location, temperature values are nearly insensitive to radial distance (in the radial distance range of 10-16 cm).

Emission measurements were performed at a fixed location at combustor chimney by awaiting at least 3 minutes to reach thermal equilibrium, and results are tabulated in Table 2. Emissions of CO and NO are given in ppm unit, while CO_2 and O_2 are presented as the percentage of the total exhaust gases.

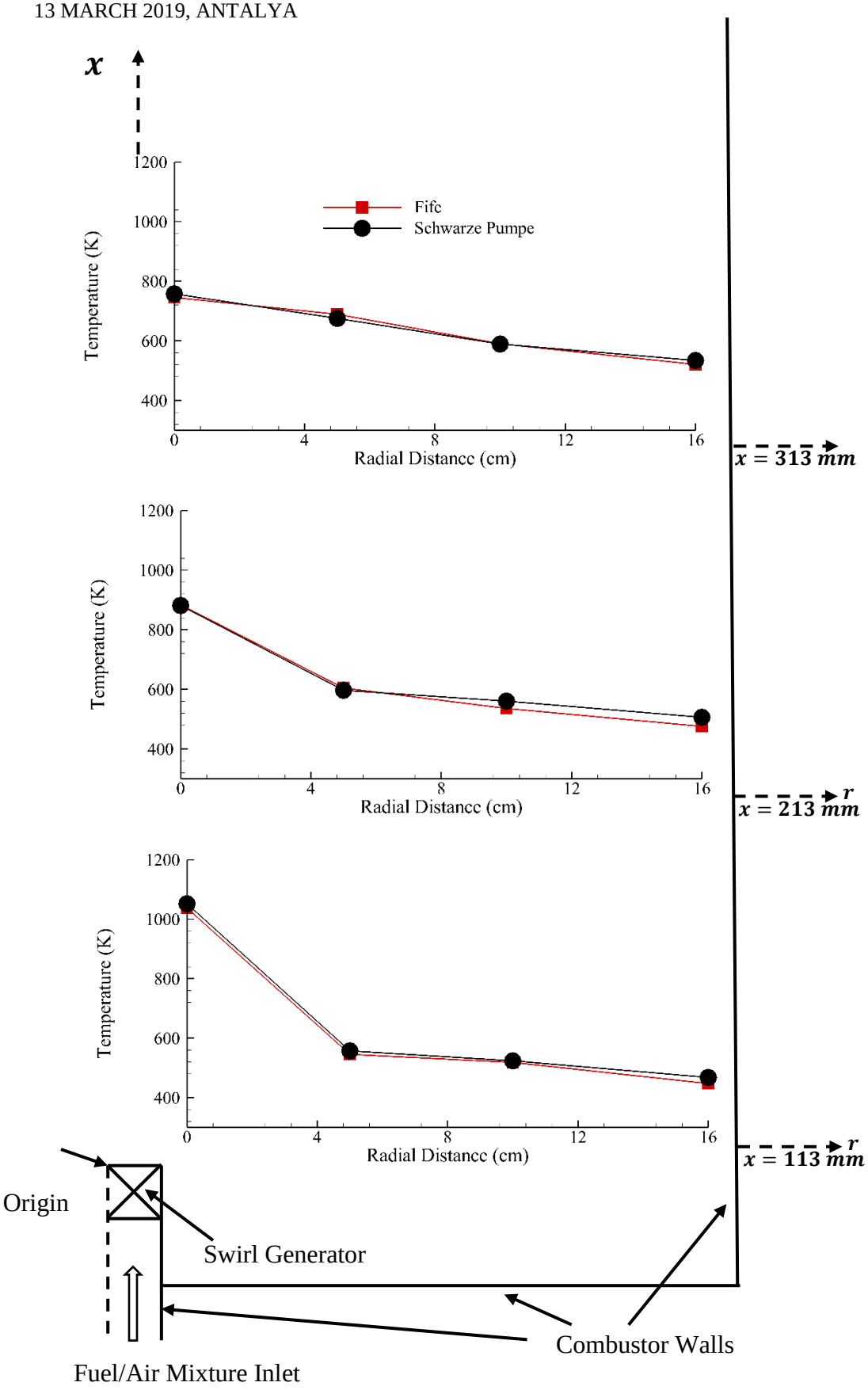

Figure 4. Radial temperature profiles of tested gas mixtures at 0.6 equivalence ratio.

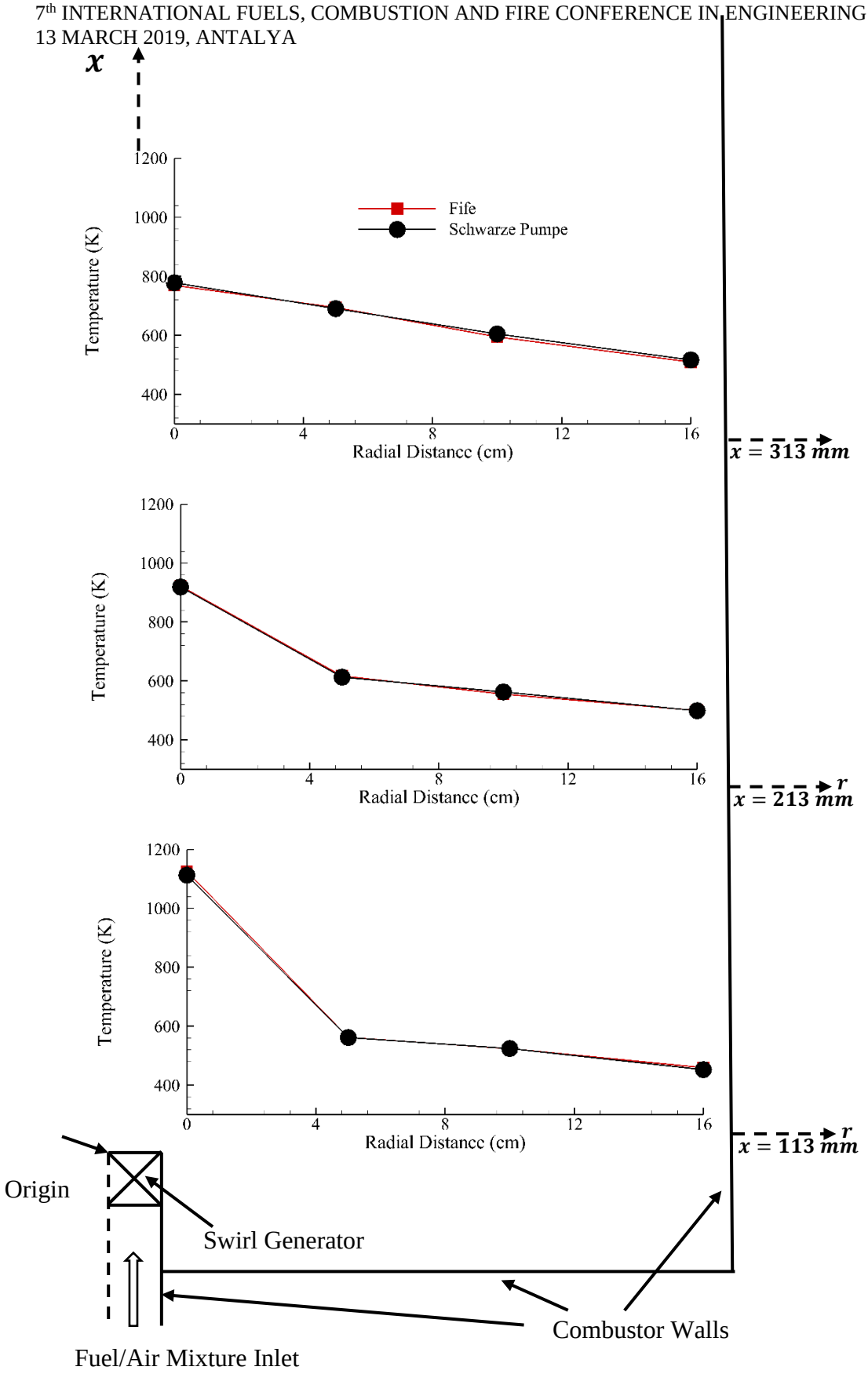

Figure 5. Radial temperature profiles of tested gas mixtures at 0.8 equivalence ratio.

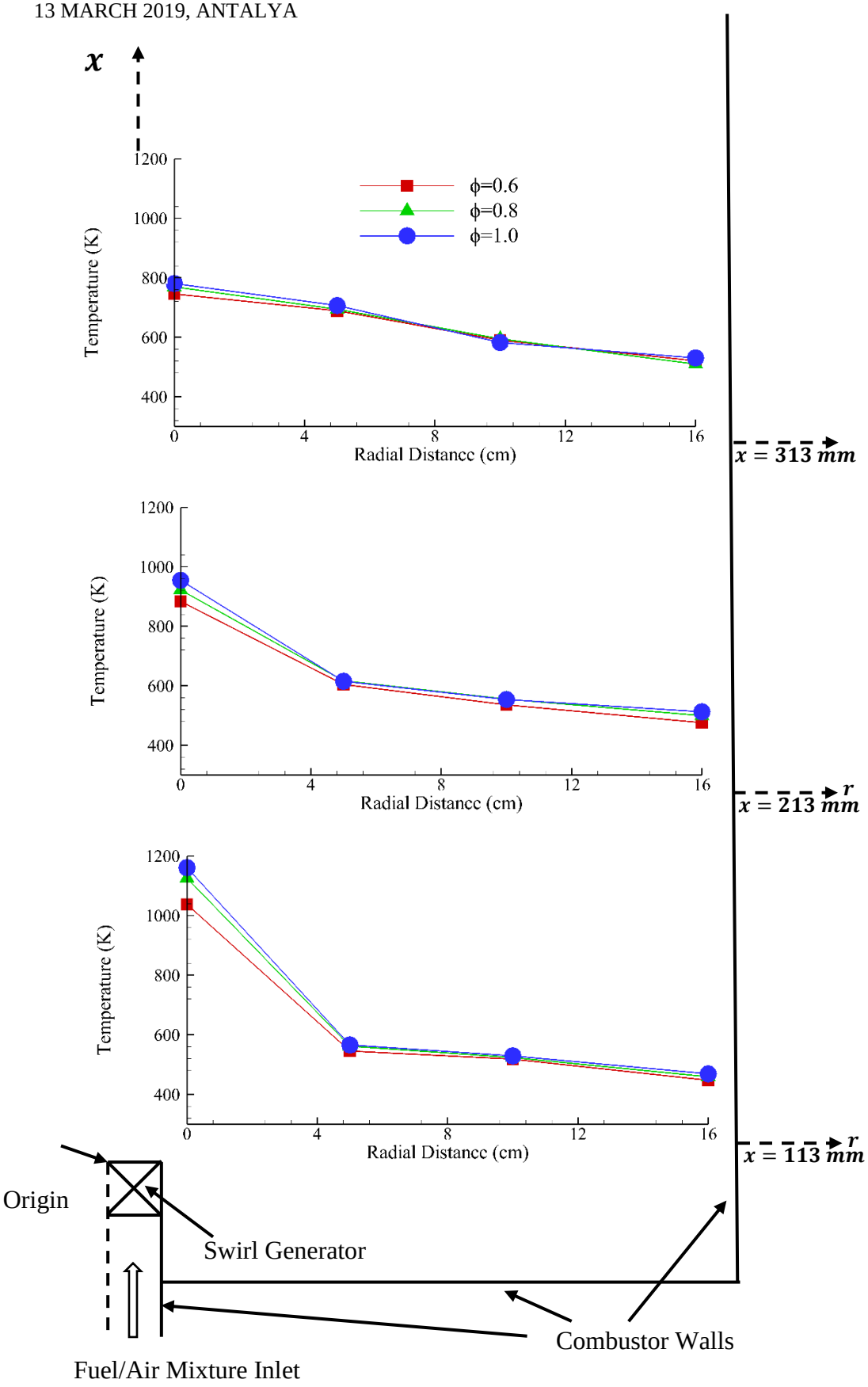

Figure 6. Radial temperature profiles of tested gas mixtures at 0.8 equivalence ratio.

Table 2. Measured emission values at combustor chimney.

Equivalence Ratio	0.6				0.8				1.0			
	O_2	CO	NO	CO_2	O_2	CO	NO	CO_2	O_2	CO	NO	CO_2
Schwarze Pumpe	12.7	124	2	3.9	10.8	1	14	4.9	-	-	-	-
Fife	12.2	1604	12	4.2	10.4	31	15	5.1	8.6	33	55	5.9

Considering emitted pollutant emissions, 61.9%H_2-26.2%CO-6.9%CH_4-5.0%CO_2 mixture performs better at both equivalence ratios tested. High hydrogen content of this mixture activates fast oxidation pathways of CO and forms very low CO levels even at 0.6 equivalence ratio. It is 1604 ppm for its counterpart. This situation also causes emissions of CO_2 of respective mixture to increase (despite its low CO content). Although exit temperature values of 61.9%H_2-26.2%CO-6.9%CH_4-5.0%CO_2 mixture is higher, it evolves less NO than 34.4%H_2-55.4%CO-5.1%CH_4-5.1%CO_2 mixture. At 0.8 equivalence ratio, emission of NO increases depending on the temperature increment. On the other hand, CO emissions largely decrease, and CO_2 emissions increase since CO oxidation kinetics favor at elevated temperatures. At 1.0 equivalence ratio, further increments in CO_2 and NO emissions are present for 34.4%H_2-55.4%CO-5.1%CH_4-5.1%CO_2 mixture.

Conclusions

In this study, combustion and emission characteristics of output gas mixtures of two different power stations were compared. Combustion tests were conducted in a swirl stabilized premixed combustor, and during experiments, equivalence ratio was varied while swirl number and thermal power of the combustor were set as invariable. A brief of important results are as follow:

- Temperature distribution throughout the combustor is not significantly affected by gas composition since volumetric heating values of tested gas mixtures are very close, while pollutant emissions are highly related to gas composition.
- With respect to pollutant emissions and exit temperature values, output synthetic gas of Schwarze Pumpe station favors.

Acknowledgement

We would like to thank the Scientific and Technological Research Council of Turkey (TÜBİTAK-MAG-215M821) for its financial support.

References

[1] Rosendahl, L. (Ed.). (2013). Biomass combustion science, technology and engineering. Elsevier.

[2] Kalogo, Y., & Monteith, H. (2012). Energy and resource recovery from sludge. IWA Publishing.

[3] Arroyo, J., Moreno, F., Muñoz, M., Monné, C., & Bernal, N. (2014). Combustion behavior of a spark ignition engine fueled with synthetic gases derived from biogas. Fuel, 117, 50-58.

[4] Lee, M. C., Seo, S. B., Yoon, J., Kim, M., & Yoon, Y. (2012). Experimental study on the effect of N_2, CO_2, and steam dilution on the combustion performance of H_2 and CO synthetic gas in an industrial gas turbine. Fuel, 102, 431-438.

[5] Ning, D., Wang, S., Fan, A., & Yao, H. (2018). A numerical study of the effects of CO_2 and H_2O on the ignition characteristics of syngas in a micro flow reactor. International Journal of Hydrogen Energy, 43(50), 22649-22657.

[6] Yu, M., Yang, X., Zheng, K., Zheng, L., & Wan, S. (2018). Experimental study of premixed syngas/air flame propagation in a half-open duct. Fuel, 225, 192-202.

[7] Lee, M. C., Yoon, J., Joo, S., Kim, J., Hwang, J., & Yoon, Y. (2015). Investigation into the cause of high multi-mode combustion instability of H_2/CO/CH_4 syngas in a partially premixed gas turbine model combustor. Proceedings of the Combustion Institute, 35(3), 3263-3271.

[8] Choi, O., & Lee, M. C. (2016). Investigation into the combustion instability of synthetic natural gases using high speed flame images and their proper orthogonal decomposition. International Journal of Hydrogen Energy, 41(45), 20731-20743.

[9] Park, J., & Lee, M. C. (2016). Combustion instability characteristics of H_2/CO/CH_4 syngases and synthetic natural gases in a partially-premixed gas turbine combustor: Part I—Frequency and mode analysis. International Journal of Hydrogen Energy, 41(18), 7484-7493.

[10] Lapalme, D., Halter, F., Mounaïm-Rousselle, C., & Seers, P. (2018). Characterization of thermodiffusive and hydrodynamic mechanisms on the cellular instability of syngas fuel blended with CH 4 or CO 2. Combustion and Flame, 193, 481-490.

[11] Yilmaz, H., & Yilmaz, I. (2019). Combustion and Emission Characteristics of Premixed CNG/H_2/CO/CO_2 Blending Synthetic Gas Flames in a Combustor with Variable Geometric Swirl Number. Energy.

Paper 59 **Bildiri 59**

THE INVESTIGATION OF ENGINE PERFORMANCE OF CR_2O_3 AND AL_2O_3+TIO_2%13 COATINGS APPLIED AT DIESEL ENGINE

Erdinç VURAL[1], Serkan ÖZEL*[2]

[1]Aydin Adnan Menderes University, Germencik Yamantürk Vocational School, Aydin, Turkey
*[2]Bitlis Eren University, Department of Mechanical Engineering, Bitlis, Turkey

ABSTRACT

In combustion engines, the combustion chamber elements are coated with ceramic materials in order to increase the material quality of the components forming the combustion chamber, heat resistance of the hot parts of the metal components, engine efficiency and performance. In this study, the piston surface of a diesel engine, NiCr with bond coat and without bond coat with Cr_2O_3, Al_2O_3+13%TiO_2, Cr_2O_3+25%Al_2O_3 ceramic coating powders were coated by using plasma spraying method to increase engine efficiency and performance. Compared to coated engine and standard engine performance values; engine power, engine torque, exhaust gas temperatures and brake thermal efficiency increased while decrease was observed in specific fuel consumption.

Keywords: Diesel Engine, Performance, Coating, Cr_2O_3, Al_2O_3+13%TiO_2.

1. INTRODUCTION

In order to improve the performance of internal combustion engines, the researchers provide combustion chamber and engine elements with excellent surface properties, and use advanced technological materials to manufacture more efficient engines [1-3]. Thermal barrier coating (TBC) is the coating of combustion chamber elements of internal combustion engines with ceramic materials with low thermal conductivity coefficient. TBC motors are defined as low-temperature motors (LHR). In these engines, the insulation of combustion chamber elements reduces the heat transfer between the gas and cylinder liners inside the cylinder, preventing the heat from the combustion chamber from going to the cooler and keeping it under control and ensuring that the combustion chamber can recover the energy in a useful way [4, 5].

In internal combustion engines, plasma spray coating method is one of the methods applied to make ceramic material coating on the surfaces of combustion chamber elements. Plasma spray coating method, high coating thickness, low cost, ease of applicability and can be applied quickly is one of the most applied methods in surface coatings[6, 7]. For this reason, researchers today cover engine parts with thermal barrier materials using plasma spray coating method, but continue to work to improve engine performance [8].

In this study, the piston and valve surfaces of an internal combustion diesel engine were coated with NiCr bond coat and without bond coat, Cr_2O_3, Al_2O_3+13%TiO_2, Cr_2O_3+25%Al_2O_3 powder coated, and the performance of the coated engines were

measured. When the previous studies were examined, thermal barrier coating materials used frequently in the market were used, two different ceramic materials were used on the piston surface, and an adequate study was not found to improve engine performance without covering and intercooling. For this reason, it is aimed to improve engine performance by creating thermal barrier coating of Cr2O3 and Al_2O_3+13%TiO_2 ceramic layers which are coated on pistons and valve surfaces.

Nomenclature

BSFC Brake Specific Fuel Consumption

BTE Brake Thermal Efficiency

CE0 Standard Engine

CE1 Coated Engine with Cr_2O_3

CE2 Coated Engine with Al_2O_3+13%TiO_2

CE3 Coated Engine with Cr_2O_3+ 25%Al_2O_3

CE4 Bond Coated (NiCr) Engine with Cr_2O_3

CE5 Bond Coated (NiCr) Engine with Al_2O_3+13%TiO_2

CE6 Bond Coated (NiCr) Engine with Cr_2O_3+ 25%Al_2O_3

EGT Exhaust Gas Temperature (^oC)

LHR Low Heat Rejection

min-1 Engine Revolution Per Minute NiCr Bond Coat

rpm Revolution Per Minute

SEM Scanning Electron Microscopy

TBC Thermal Barrier Coating

μm Micron Meter

2. MATERIALS AND METHOD

In the experiments, single cylinder, four stroke, air cooled diesel engine was used. The technical specifications of the test engine are given in Table-1. diesel engine pistons and valves, with plasma spray coating method with NiCr bond coat and without bond coat Cr_2O_3, Al_2O_3+13%TiO_2, Cr_2O_3+25%Al_2O_3 were coated powder. The schematic picture of the coated piston is given in Figure 1, and the powder and ratios to be coated on the surface are given in Table 2. In order to keep the compression ratio of the standard engine constant with the value in the catalog, the chip has been removed from the piston and valve surfaces as much as the coating thickness. For Pistons and valves (suction, exhaust), 200-300 μm thick coatings were obtained in CE1, CE2 and CE3 samples and for CE4, CE5 and Ce6 samples, 350-450 μm thick (80-150 μm thick for NICR bond coat). Total coating thickness varies depending on the tension limitations of the sprayed material [9, 11].

Table 1. Technical feature of the test engine.

Engine Types	4-stroke direct injection, diesel engine
Number of cylinders	1
Cylinder diameter (mm)	78
Stroke (mm)	62
Cylinder Displacement (cc)	296
Compression ratio	20/1
Maximum power (kW)	4
Valve regulation	Top cam, 2 valves
Maximum engine speed (rpm)	3600
Warehouse volume (L)	3,5
Krank Açısı (CA)	31^0
Enjeksiyon Basıncı (bar)	200

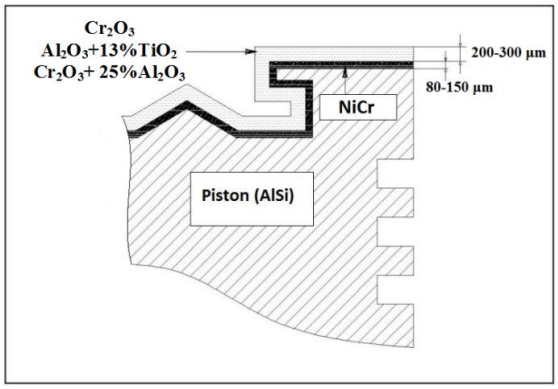

Figure 1. Schematic picture of the piston that has been coated.

Table 2. Powder and proportions that will be coated on the surface.

Specimens	Coating Materials	Boand Coat
CE 0	Standart Engine	-
CE 1	Cr_2O_3	-
CE 2	Al_2O_3+13%TiO_2	-
CE 3	Cr_2O_3+ 25%Al_2O_3	-
CE 4	Cr_2O_3	NiCr
CE 5	Al_2O_3+13%TiO_2	NiCr
CE 6	Cr_2O_3+ 25%Al_2O_3	NiCr

In the experiments, diesel fuel which is given in Table-3 is used. Diesel fuel meets EN590 standards. For the measurement of internal combustion engine speed, torque, power and specific fuel consumption and exhaust gas temperature in experiments Netfren brand, 26 kW power based on the principle of the Föttinger hydrodynamic dynamometer was used. The measured data is recorded on the computer in real time. Experiment test parameters were carried out at full load at 7 different engine speeds and the engine was operated for 10 minutes, to bring the engine to operating temperature before the test was started. The engine has been brought to operating temperature and the test engine has been loaded at different speeds and measurements have been taken. The experiments were repeated three times and were used to transfer the average to the graphs. The experiments were repeated three times and were used to transfer the average to the graphs. Schematic picture of the experimental setup was given in Figure-2.

Table 3. Diesel fuel properties.

Fuel Specification	Diesel
Chemical Structure	C13H28
Lower heating value (kJ/kg)	42,500
Autoignition temperature (°C)	240
Boiling point (°C)	160–370
Cetane index	52
Viscosity-kinematic @ 40 °C	3
Density (15 °C) (kg/L)	0.83
Latent heat of evaporation (MJ/kg)	0.260
Carbon/Hydrogen Ratio (C/H)	~0.47

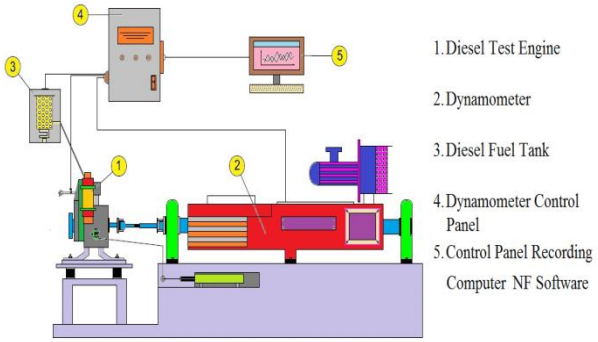

Figure 2. Engine test mechanism schematic view.

3. RESULTS AND DISCUSSION

3.1 The Coating Layer

SEM photos of samples CE2 and CE5 are shown in Figure 3. Figure 3 shows that there is no gap between the coating layer and the substrate material.

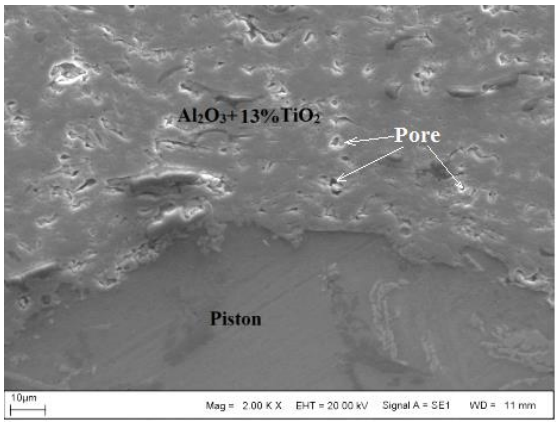

(a)

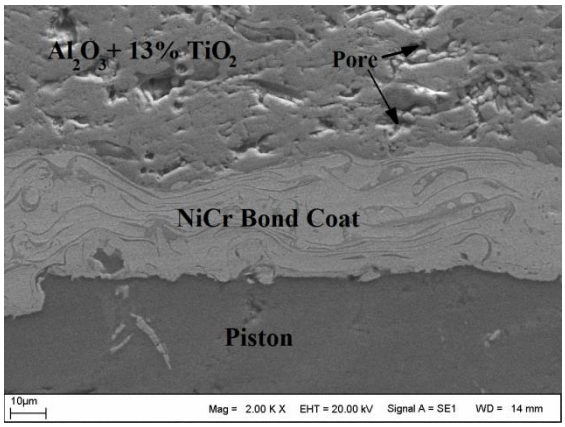

(b)

Figure 3. a) CE2 and b) SEM microstructure appearance of samples CE5.

The thermal conductivity of Al_2O_3+13%TiO_2 ceramic material is low [12]. In the samples CE2 and CE5, it was observed that the porosity was less. For this reason, thermal barrier properties are thought to yield higher results than other samples. The amount of pore in plasma spray coatings affects thermal conduction coefficient [5].

3.2 Engine Performance

Figure 4 shows the effect of coatings on engine power. In internal combustion engines, the engine power of the active cylinder is obtained as a result of burning of the fuel in the unit time is useful work. The combustion reaction in diesel engines starts with the spraying of the fuel. The fuel must reach the ignition temperature in order to burn. The duration of fuel injection from the injector to the combustion reaction of the fuel is slow and full of fuel for it to burn in the first place, it must undergo a certain period of time. For this reason, diesel engines are given the advance of ignition, so during the delay of ignition is more fuel consumption into the cylinders. Therefore, the temperature of the fuel and ignition advance in the cylinder, it is observed that ignition temperature is an important parameter [13, 14]. Fuel consumption in the range of the most efficient burning of both fuel consumption, according to the unit fuel consumption is thought to be maximum engine power. The results obtained in Figure 4 and Figure 6 show that it supports this situation. Figure 4 shows that motor power increases with increasing engine speed for all coating types. Depending on the number of cycles, the number of cycles in the unit time has also increased. With the increase in the number of cycles, the air flow in the cylinder at absorption time by affecting the fuel/air mixture has increased homogeneity. Motor power up to 2600 rpm as quickly as, and then slowly increased. This is because the engine speed is too high, so there is not enough time to burn the whole of the fuel that is sprayed into the cylinder. When the increase in engine power was examined for all test engines, it was observed that the thermal barrier effect resulting from ceramic coating improved combustion efficiency and the coated engine work produced better engine power in the same conditions as the non-coated diesel engine.

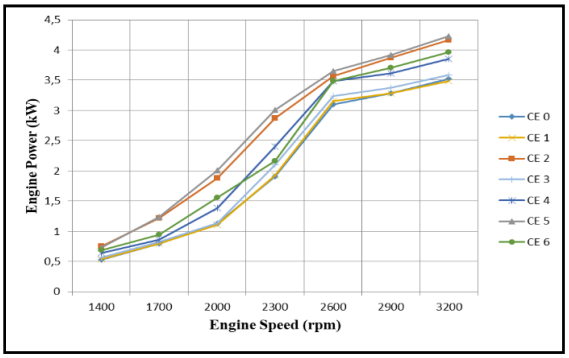

Figure 4. Engine power changes under different speed.

The highest engine power in standard and coated engines was found to be at 3200 rpm. This is due to the increase in engine speed, the amount of fuel increases, so the increased fuel density causes the engine power to increase [15]. Thermal barrier coated Motors increased motor power by 1.72% in ce1 sample, 4.84% in CE3 sample, 10.86% in CE4 and CE6 samples, 12.97% in CE2 and 14.92% in CE5 sample when compared to standard engine.

Figure 5 shows the effect of coatings on the engine torque. In internal combustion engines, torque can be called the rotational force from the cylinder arm as a result of the pressure obtained at the end of the combustion of the fuel inside the cylinder affects the piston surface. Torque is an important measure of the motor's ability to do work, but its size depends on the characteristics of the engine [16].

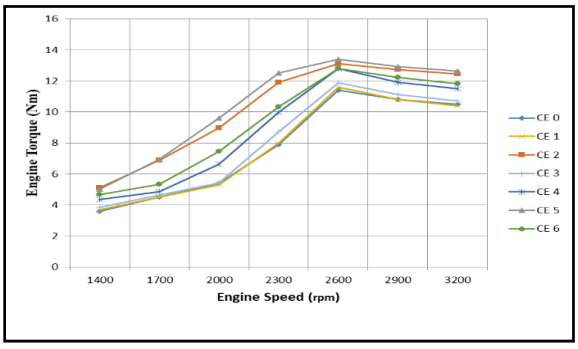

Figure 5. Engine torque changes under different speed.

It is seen in Figure 5 that the coatings increase torque throughout all engine cycles. As the engine speed increases in internal combustion engines, the increase in engine torque is seen, and this increase is seen again by passing a maximum point [17]. The increase in torque with increased engine speed, after 2600 rpm, is thought to reduce engine torque due to the increase in cylinder walls and gas temperatures resulting from the increase in volume efficiency and increased friction losses at high speeds as a result of thermal barrier coating. Thermal barrier coated engines are known to have high combustion end temperature. As we mentioned earlier, the reaction time decreases with the injection of fuel into the cylinders, so the ignition time decreases [13]. However, the air/fuel ratio is fully met each other and has formed a homogeneous mixture because the spraying time is reduced. Thus, volumetric efficiency is increased, so it is thought to increase the torque of the engine. In addition, increasing the temperature in the cylinder causes the pressure coming to the piston surface to increase. This is why the thermal barrier coating provides more heat in the cylinder and thus increases the pressure. Therefore, all thermal barrier-coated engines have increased torque compared to the standard engine. Thermal barrier coated Motors increased by 1.52% in CE1 sample, 3.63% in CE3 sample, 8.61% in CE4 and CE6 sample, 10.73% in CE2 and 12.35% in CE5 sample when compared to standard engine. In internal combustion engines, torque and power are terms that change in connection with each other. The net torque generated by combustion can be increased by increasing the average effective pressure or by decreasing the losses in the cylinder block. Figure 5 shows that the torque obtained from the engine is increased due to the increased engine speed. The heat losses in the cylinder block in the engine operated by thermal coating were reduced and more of the heat energy resulting from combustion was converted into mechanical energy. This has led to higher engine torque

in the coated engine compared to the non-coated standard engine. However, the engine torque is a slight decrease as the high speed goes up. The reason for this is thought to be the negative effect of temperature rise in cylinder block and combustion gases on volumetric efficiency at high speeds.

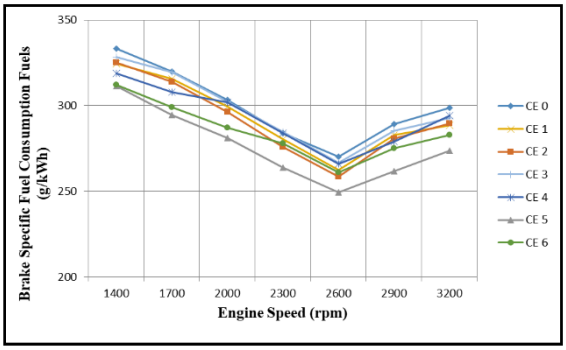

Figure 6. BSFC changes under different speed.

Figure 6 shows the effect of coatings on brake specific fuel consumption. It is known that more pressure is applied to the piston surface with the increase in combustion end temperature in coated engines [18]. This means more useful work with the same amount of fuel. In general, the thermal barrier-coated engines have less fuel consumption than the standard engine [19, 20]. However, as the engine goes up to high speeds, the volumetric efficiency decreases, combustion time decreases and the fuel injection range decreases because the fuel inside the cylinder is not fully burned, causing the moment to decrease, and the BSFC increases. Thermal barrier coated Motors were found to have decreased by 1.07% in CE1 sample, 2.34% in CE3 sample, 2.82% in CE4 sample, 4.34% in Ce6 sample, 11.82% in CE2 and 14.96% in CE5 sample compared to standard engine. It is observed that BSFC falls due to the increased engine speed for all test engines. The high turbulence of the air swept into the cylinder with the increase of engine speed helps to create a homogeneous mixture within the cylinder following the fuel spraying process. This improves combustion efficiency and reduces fuel consumption. However, the increase in the engine speed of the cylinder reduces the time required to burn the entire mixture of fuel in the cylinder, 2600 rpm motor speed after the decline in BSFC has lost its effect. Thermal barrier coating in the engine cylinder with increased gas temperature in the ignition delay time is shortened, this situation improves combustion efficiency.

Figure 7 shows the effect of coatings on exhaust gas temperature. The exhaust gas temperature can be called the temperature of the burning fuel in the cylinders as the combustion products at the end of the combustion [21]. Exhaust gas temperature is an indication of the combustion end temperature present in the cylinder.

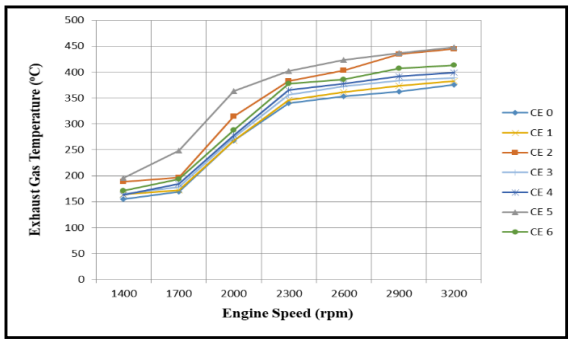

Figure 7. EGT changes under different speed.

The experiments show that the applied coatings form a thermal barrier and increase exhaust gas temperatures. The increase in exhaust gas temperatures at all engine speeds has been detected. This is due to the increase in the combustion temperature of thermal barrier coated engines, as well as combustion products increase the temperature and exhaust gas temperature is thought to affect. Thermal barrier coated engines compared to standard engine exhaust gas temperatures, CE1 sample 2.21%, CE3 sample 5.1%, CE4 sample 6.61%, Ce6 sample 8.54%, CE2 sample 12.4% and CE5 sample 16.54% were observed to increase. Figure 7 shows that EGT has increased due to the increase in engine speed for all test engines. This is due to the increase in the engine cycle and the increase in the amount of fuel burned in the cylinder at the time of the unit and the increase in the heat energy produced at the

end of combustion can be explained. Therefore, increasing engine speed increases both exhaust gas temperature and flow rate. The heat energy that is prevented from passing to the cooler fluid and cylinder walls in thermal coating engines increases the EGT by passing to exhaust gases. In addition, high internal temperatures shorten the duration of ignition delay ensures a good combustion. This is to help improve fuel consumption.

In Figure 8, the brake thermal efficiency change of the thermal barrier coated engines and the standard engine is given. It has been observed that brake thermal efficiency increases in engines covered with thermal barrier. Important parameters affecting the thermal efficiency of the brake ignition delay, combustion temperature, the chemical and physical properties of the fuel are. The increase in combustion temperature with thermal barrier coating has been observed to increase the thermal efficiency of brake and it has been determined that this situation is in harmony with the literature [20, 22-24].

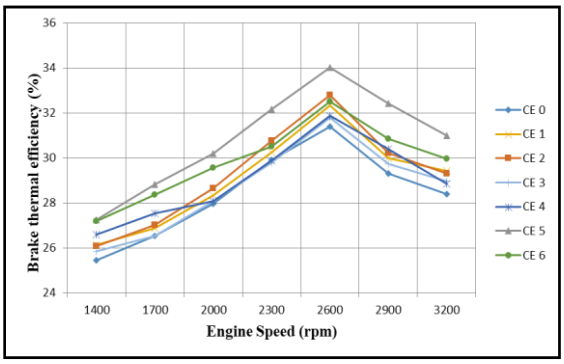

Figure 8. Thermal efficiency changes under different speed.

The highest thermal efficiency was found in the CE5 coated motor. With the decrease in porosity in the coating, the coating formed a good thermal barrier to the Pistons and Valve surfaces, causing the brake thermal efficiency to increase. Thermal barrier coated Motors have increased brake thermal efficiency by 0.89% in CE1 sample, 2.66% in CE3 sample, 3.39% in CE4 sample, 4.84% in Ce6 sample, 8.73% in CE2 and 10.17% in CE5 sample compared to standard engine. With the increasing engine speed, BTE has also increased. This shows that a more efficient combustion occurs in the cylinder due to the increase in engine speed. However, in high engine speed, the combustion efficiency decreases with the shorter time required for combustion and the cooling of the engine block. In addition, the excessive temperature increase of combustion gases reduces volumetric efficiency and causes BTE to decrease. In general, thermal coatings at all engine speeds and better performance values were achieved in BTE compared to the standard diesel engine.

4. CONCLUSIONS

The results of the experimental study showed that when compared to standard engine and thermal barrier coated engines, motor power, torque, brake thermal efficiency and exhaust gas temperature increase and decrease in specific fuel consumption were observed in thermal barrier coated engines.

In this experimental study, it was determined that the ceramic powders used can be easily coated to the piston surface by plasma spray coating method, and the motor performance results were examined, the best results were obtained in the samples coated with intermediate bond coating and coated with Al_2O_3+13%TiO_2 powder. The samples covered with Al_2O_3+13%TiO_2 powder are considered to be the best thermal barrier due to the fact that they are found in the pores. In addition, since the thermal conductivity coefficient of Al_2O_3+13%TiO_2 thermal barrier coating is lower than Cr_2O_3, it has been found that the samples covered with Al_2O_3+13%TiO_2 powder added to Cr_2O_3 powder have improved engine performance.

Thermal barrier coatings at all engine speeds were found to increase 14% in

engine power compared to standard engine, 12% in engine torque, 16% in exhaust gas temperatures and 10% in brake thermal efficiency. 14% reduction in specific fuel consumption was measured.

ACKNOWLEDGMENTS

This work was supported by Scientific Research Project Unit of Bitlis Eren University under project-No: BEBAP-2014.15. The authors would like to thanks the Bitlis Eren University Science and Technology Research and Application Center for tests of specimens.

REFERENCES

[1] R. Thirunavukkarasu, M. Mahendran, R. Tamilselvan, S. Periyasamy, "Investigation on Single, Four And Five Holes Fuel Injector Nozzle on Performance And Emission Characteristic of Diesel on A VCR Engine by Using Ceramic Coating Material on The Piston Crown", *Materials Today: Proceedings, Volume 5, Issue 2, Part 2, Pages 7577-7585,* 2018.

[2] P. Ramaswamya, V. Shankar, V.R. Reghu, N. Mathewd and M. Kumar, "A Model to Predict the Influence of Inconsistencies in Thermal Barrier Coating (TBC) Thicknesses in Pistons of IC Engines", *Materials Today: Proceedings 5, 12623–12631,* 2018.

[3] A.Thibblin, S.Jonsson, "Ulf Olofsson, Influence of microstructure on thermal cycling lifetime and thermal insulation properties of yttria-stabilized zirconia thermal barrier coatings for diesel engine applications", *Surface and Coatings Technology, Volume 350, 25 September, Pages 1-11,* 2018.

[4] B.R.Prasath, P.Tamilporai, M.F.Shabir, "Analysis of combustion, performance and emission characteristics of low heat rejection engine using biodiesel", *International Journal of Thermal Sciences, Volume 49, Issue 12, Page 2483-2490,* 2010.

[5] E.Vural, "The Investigation Of Effect On Engine Performance And Exhaust Emissions Of Ceramic Coatings Applied To Single Cylinder Diesel Engine", *Ph.D. Thesis, Graduate School of Natural and Applied Sciences, Karabuk University, Turkey,* 2014.

[6] M.Bounazef, S.Guessasma, G.Monta von, C.Coddet, "Effect of APS process parameters on wear behaviour of alumina-titania coatings", *Mater. Lett. 58, pp. 2451-2455,* 2004.

[7] H.R.Sichani, M.Salehi, H.Edris, M.T. Farani, "The effect of APS parameter on the microstructural, mechanical and corrosion properties of plasma sprayed Ni-Ti-Al intermetallic coatings", *Surface and Coatings Technology, Volume 309, Pages 959-968,* 2017.

[8] H.Hazar, H.Sevinc, "Investigation of the effects of pre-heated linseed oil on performance and exhaust emission at a coated diesel engine", *Renewable Energy, Volume 130, Pages 961-967,* 2019.

[9] B.A.Phillips, and J.K.Knapp, "Thermal spray coatings reduce wear and corrosion on calender rolls", *Tappi Journal, 197-205,* 1995.

[10] P.Ramaswamy, S.Seetharamu, K.B.R Varma. and K.J.Rao, "Thermo mechanical fatigue characterization of zirconium ($8\%Y_2O_3$ - ZrO_2) and mullite thermal barrier coatings on diesel engine components: effect of coatings on diesel engine performance", *Proceedings of the institution of mechanical Engineers, ProQuest Science Journals, 214, 729,* 2000.

[11] A.Parlak, H.Yaşar, B.Şahin, "Performance and exhaust emission characteristics of a lower compression ratio LHR diesel engine", *Energy Conversion and Management, 44,163-175,* 2003.

[12] P.Bagde, S.G.Sapate, R.K.Khatirkar, N.Vashishtha, "Friction and abrasive wear behaviour of Al_2O_3-13TiO_2 and Al_2O_3 -13TiO_2 +Ni Graphite coatings", *Tribology International, Volume 121, Pages 353-372,* 2018.

[13] B.Safgonul, H.E.Arslan, M.Ergeneman, C.Sorusbay, "Internal combustion engines book", *Istanbul,* 1995.

[14] H.Hazar, U.Ozturk, "The effects of Al_2O_3-TiO_2 coating in a diesel engine on performance and emission of corn oil methyl ester", *Renewable Energy, 35, 2211-2216,* 2010.

[15] T.Sandalcı, O.Işın, S.Galata, Y.Karagöz, I.Güler, "Effect of hythane enrichment on performance, emission and combustion characteristics of an CI engine, International Journal of Hydrogen Energy", *Volume 44, Issue 5, Pages 3208-3220,* 2019.

[16] E.Vural, S. Ozel, "The effect of Cr_2O_3 thermal barrier coatings on engine performance of internal combustion diesel engine", *14 th International Conference of Combustion, p.p 374-378, Karabuk/Turkey,* 2018.

[17] H.Gurbuz, "An experimental study on the effects of the thermal barrier plating over diesel engine performance and emissions", *M.Sc. Thesis, Graduate School of Natural and Applied Sciences, Department of Mechanical Engineering, Karabük University,* 2011.

[18] C.Yao, J.Hu, P.Geng, J.Shi, D.Zhang, Y.Ju, "Effects of injection pressure on ignition and combustion characteristics of diesel in a premixed methanol/air mixture atmosphere in a constant volume combustion chamber", *Fuel, 206, 593-602,* 2017.

[19] V.Gnanamoorthi,M.Jayaram, "Experimental investigation of Al_2O_3/8YSZ and CeO_2/8YSZ plasma sprayed thermal barrier coating on diesel engine". *Ceramics International,Available,https://doi.org/10.1016/j.ceramint.2018.10.218,* 2018.

[20] P.S. Jena, K.S.Acharya, H.C.Das, P.P.Patnaik, S.Bajpai, "Investigation of the effect of FeCl3 on combustion and emission of diesel engine with thermal barrier coating", *Sustainable Environment Research, Volume 28, Issue 2, March, Pages 72-78,* 2018.

[21] U.Asad, M.Zheng, "Exhaust gas recirculation for advanced diesel combustion cycles", *Applied Energy, 123, 242-252,* 2014.

[22] M.Celik, Y.O.Ozgoren, "The determination of effects of soybean and hazelnut methyl ester addition to the diesel fuel on the engine performance and exhaust emissions", *Applied Thermal Engineering, 124, 124-135,* 2017.

[23] C.Zhang, A.Zhou, Y.Shen, Y.Li, Q.Shi, "Effects of combustion duration characteristic on the brake thermal efficiency and NOx emission of a turbocharged diesel engine fueled with diesel-LNG dual-fuel", *Applied Thermal Engineering, Volume 127, Pages 312-318,* 2017.

[24] S.Karthikayan,S.Ganesan, P.Vasanthakumar, G. Sankaranarayanan, M.Dinakar, "Innovative research trends in the application of thermal barrier metal coating in ınternal combustion engines", *Materialstodays: proceedings, 4/8, 9004-9012,* 2017.

Paper 60 **Bildiri 60**

OPTIMIZATION OF EFFECT OF THERMAL BARRIER COATING (TBC) ON DIESEL ENGINE TORQUE BY TAGUCHI METHOD

Serkan ÖZEL*[1], Erdinç VURAL[2], Murat BİNİCİ[3]

*[1]Bitlis Eren University, Department of Mechanical Engineering, Bitlis, Turkey
[2]Aydın Adnan Menders University, Germencik Yamantürk Vocational School, Aydın, Turkey
[3]Bitlis Eren University, Department of Industrial Engineering, Bitlis, Turkey

ABSTRACT

In this study, thermal barrier layers were coated on piston and valve surfaces using plasma spray method. The effects of coated layers were investigated experimentally and statistically using Taguchi optimization method on engine torque. Coating materials used in this study were Al_2O_3 +13% TiO_2, Cr_2O_3, and Cr_2O_3+ 25% Al_2O_3. Each coating material was tested at different speeds, which are 1400 rpm, 2000 rpm, 2600 rpm and 3200 rpm. The results showed that the highest torque value was achived with the use of Al_2O_3 +13% TiO_2 at the speed of 2600 rpm. The results of the experiment were also tested using Taguchi optimization method with coating material and engine speed parameters. The design of Taguchi analysis was carried out with L_{16} (4^2) orthogonal array. The highest S/N ratio of the engine torque was observed to be with the coating material of Al_2O_3 +13% TiO_2 at the speed of 2600 rpm. In order to determine the statistical significance of experimental parameters on engine torque, ANOVA and F-test were carried out. The results of the statistical analysis showed that the coating material ($P= 0.003 < 0.05$) and engine speed ($P= 0.000 < 0.05$) parameters were statistically significant on the engine torque value.

Keywords: Thermal Barrier Coating, Diesel Engine, Torque, Taguchi optimization, ANOVA

INTRODUCTION

Diesel engines have an important role in the automotive industry. They are widely used in both transport and agriculture industries because they have higher fuel saving and lower fuel consumption than other types of engines [1]. However, due to the increases in fuel costs, decreases in supplying the high-quality fuels to the markets and concerns for environmental issues, researchers in the industries have begun to research on more productive engines [2].

Efficiency and emissions of engines are crucial. There are two ways to make a diesel engine more productive and efficient with lower emission levels. First one is the reduction of losses like heat loss from the cylinder, wall, cooling water and friction losses in order to make the engine more efficient mechanically and indicatively. Using a suitable alternative fuel in the engine is the second way [3]. Regarding the first way, thermal barrier coating (TBC) is one of the most commonly used technologies so as to keep the heat inside the engine so that it can improve the thermal efficiency of the engines. TBC has been used to make improvements on the efficiency and performance of different types of machine tools for a long time and it can be applied to the areas having high temperatures or heat transfer surfaces of gas tribunes. TBC technology can be applied by insulating the engine with ceramic-based coating [4-7].

There are some advantages of using TBC in diesel engines. Besides keeping the heat inside the engine, thermal fatigue and shocks can be prevented. It can also reduce the emission levels of Hydrocarbon and Carbon Monoxide. Moreover, a piston can be protected from corrosion attack, thermal stress, and high heat emissions by reducing heat flux into the piston and fuel consumption. Additionally, due to the high increase in fuel prices and decreasing quality of fuels, TBC can be an advantage to get more efficient engine performance. In relation to the low-quality fuels, TBC can keep much more heat inside the engine even though the fuel is low quality [1-8].

Taguchi design method, which is one of the experimental methods, is successful in solving optimization problems as it increases processing performance with a lower number of experiments and less cost. Using Taguchi, the number of experiments can be decreased significantly and thus the loss of time and cost can be prevented. In addition to solving the problems with a few experiments, Taguchi supports developing high-quality process and product from every angle. It has minimum sensitivity to the process or manufacturing conditions of products and uncontrollable factors. Therefore, both the necessary tolerances can be provided with the lowest cost and Taguchi lost function can bring a new understanding to the quality process [9-12]. The Taguchi optimization method has previously been used in many experimental design studies [13-16].

In this study, thermal barrier layers were coated on a piston surface by using plasma spray method. The effects of coated materials and engine speeds were investigated experimentally, and statistically using Taguchi optimization method on engine torque.

MATERIALS AND METHOD

Coating Materials

Ceramic powders were coated on piston and valve by using the plasma spraying method. Al_2O_3 +13% TiO_2**,** Cr_2O_3, and Cr_2O_3+ % 25 Al_2O_3 were used as ceramic coating powders.

Table 1. The powders coated on piston and valve surfaces

Coating Materials	Substrate
Standard Engine	Piston and Valve
Al_2O_3 +13% TiO_2	
Cr_2O_3	
Cr_2O_3+ 25% Al_2O_3	

Engine Tests

The combustion chamber elements (piston and valve) of a single-cylinder, 4-stroke air-cooled diesel engine are coated with using Cr_2O_3, Al_2O_3 + 13% TiO_2, Cr_2O_3 + 25% Al_2O_3 powders with plasma spray coating method. The schematic illustration of the plated plunger is shown in Table 1. The engine torque values of the standard engine and other coated engines were measured with the use of experimental setup shown in Figure 1. The technical features of test engine used in the experimental setup are illustrated in Table 2.

Table 2. The powders coated on piston and valve surfaces

Brand	Diesel engine
Number of cylinders	1
Cylinder diameter (mm)	70
Stroke (mm)	57
Cylinder Displacement (cc)	219
Compression ratio	20/1
Maximum power (kW)	3.72
Max. Torque (N.M / rpm)	13
Valve regulation	Top cam, 2 valves
Maximum engine speed (rpm)	3600
Warehouse volume (L)	2.2
Fuel Consumption (g / Hp.hour)	185
Oil Capacity (L)	0.75

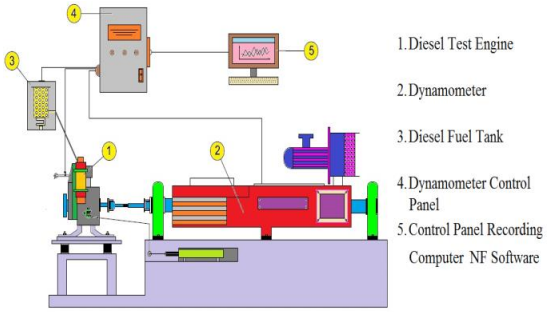

Figure 3. A schematic view of the test setup

Statistical Method

Taguchi method is a very useful technique for improving the design of experiments. In an analysis, the response of the experimental trials can be obtained using signal-to-noise (S/N) ratios, which are very significant. Concepts for analyzing data are given below.

- Higher the better,
- Nominal to better,
- Lower the better,

Information of each parameter can be retrieved using Analysis of Variance (ANOVA) [17].

In this study, L_{16} (4^2) orthogonal array was employed for the robust design of the experimentations. The parameters presumed to affect engine torque is coating materials and engine speeds. Table 2 gives the standard engine, Al_2O_3 + 13% TiO_2, Cr_2O_3, and Cr_2O_3 + 25% Al_2O_3 coating materials levels; 1400, 2000, 2600 and 3200 engine speed levels.

Table 3. Control factors and levels

Control Factors	Level 1	Level 2	Level 3	Level 4
Coating Material	Standard	Al_2O_3 + 13% TiO_2	Cr_2O_3	Cr_2O_3 + 25% Al_2O_3
Engine Speed	1400rpm	2000rpm	2600rpm	3200rpm

Model employed for the experiment of this research is "higher the better". Signal to Noise ratios (S/N) can be obtained using the equations underneath.

Higher the better S/N = $-10\ x\ log_{10}\left(\frac{1}{n}\sum_{i-1}^{n}\frac{1}{Y_i^2}\right)$

Nominal the better S/N = $-10\ x\ log_{10}\ (s\text{^}2)$

Lower the better S/N = $-10\ x\ log_{10}\left(\frac{1}{n}\sum_{i-1}^{n}Y_i^2\right)$

Where Y_i = the result of the each experiment, i = number of repetitions

RESULTS AND DISCUSSIONS

The experiments were carried out with four different types of diesel engine at four different speeds. One of the engine type was standard engine and the other three were the coated engines mentioned in Section 2. Coated powders were Al_2O_3+13%TiO_2, Cr_2O_3 and Cr_2O_3+25%Al_2O_3. The purposes of these experiments were to measure and define the optimum value of the engine torque.

Experimental Results

Torque values measured on the engine are given in Table 4, depending on the coating

materials and engine speeds. The highest torque values were observed with the coating material of Al_2O_3+13%TiO_2 at each speed. In addition, the highest torque value was obtained as 13.1 at the speed of 2600 rpm with the coating material of Al_2O_3+13%TiO_2. On the other hand, the standard engine has the lowest torque values at each speed and the lowest one is 3.6 at the speed of 1400 rpm. When we look at Figure 2, which is created using the values of Table 4, the engine torque increases as the engine speed increases in each type of coating materials. However, there is a slight decrease after the speed of 2600 rpm in each coating material. As the engine speed increases in internal combustion engines, an increase in motor torque is observed and this increase decreases again at a maximum point [18]. The reason for this decrease in engine torque might be because of the decrease in volumetric efficiency caused by the increase in cylinder walls and gas temperatures as a result of thermal barrier coating and increasing friction losses at high speeds. Engines which are coated with a thermal barrier is generally known with their high combustion and temprature. Also, as a result of spraying fuel into the clyinders, reaction time decreases and this makes firing time very short [19]**.** However, short spraying time causes an increase in the amount of air falling on the fuel and this makes volumetric efficiency high as a result of the complete combustion of the fuel. As a result, the engine torque increases.

Table 4. Experimental results of coating materials and engine speeds on engine torque at different levels

	Standard Engine	Al_2O_3+13%TiO_2	Cr_2O_3	Cr_2O_3+25%Al_2O_3
1400rpm	3.6	5.1	3.7	3.86
2000rpm	5.4	8.97	5.3	5.44
2600rpm	11.4	13.1	11.6	11.88
3200rpm	10.5	12.43	10.4	10.7

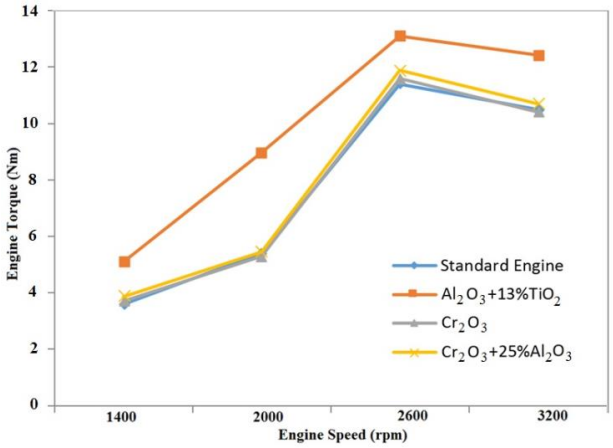

Figure 2. Effects of the coating materials and engine speed on engine torque

Statistical Results

The experiments mentioned in previous section were performed using Taguchi design method and ANOVA and F-test were carried out in order to define the statistical significance of the test parameters.

Table 5 in this section shows the S/N ratios determined for the experimental control parameters mentioned in Section 2.3. This table records figures maximizing the results under the influence of the test parameters. Furthermore, these figures are employed to plot the influence of the parameters of coating material and engine speeds on the engine torque in Figure 3.

Statistical analysis, which has two independent parameters as coating material and engine speeds, depicts the result that the variations in coating material and engine speed are statistically significant on the engine torque. Table 6 demonstrates that the engine torque is significantly affected at different levels of coating materials and engine speeds.

Table 5. S/N ratios of factor levels for engine torque

Control Factors	Engine Torque			
	Level 1	Level 2	Level 3	Level 4
Coating Material	16.83	19.36*	16.87	17.13
Engine Speed	12.09	15.73	21.57*	20.81

*Levels which are maximazing the results

The S/N ratios of engine torque are revealed by Table 5. Level 2 for the coating materials and level 3 for the engine speed have the highest ratios. In contrast, level 1 for the coating material and engine speed has the lowest ratios.

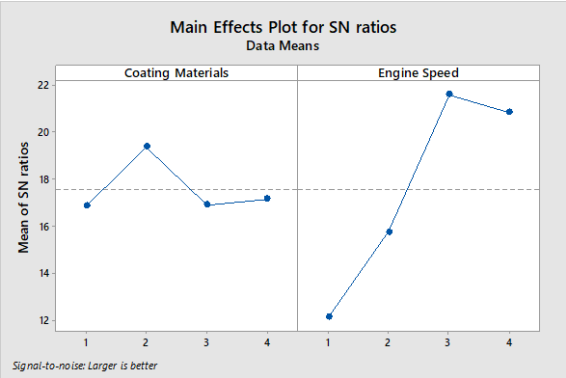

Figure 3. S/N ratio graph of experimental parameters for engine torque

The S/N ratios of engine torque are revealed by Table 5 and Figure 3. Level 2 for Coating Materials and level 3 for engine speed have the highest ratios. In contrast, level 1, which is standard engine, for coating materials and engine speed have the lowest ratios.

Table 6. Analysis of variance (ANOVA) for Torque

Source	DF	Seq SS	MS	F	P
Coating Material	3	17.712	5.9042	9.85	0.003
Engine Speed	3	239.494	79.8313	133.18	0.000
Error	9	5.395	0.5994	-	-
Total	15	262.601	-	-	-

Finally, the results from Figure 3 depicts that the engine torque reaches its maximum point with the coating material of Al_2O_3+ 13% TiO_2 at the speed of 2600 rpm. Also, P-values for the coating material and engine speed are below 0.05, which means they are both statistically significant parameters on the engine torque.

CONCLUSIONS

- Experimental study demonstrates that a better engine torque can be obtained with the use of different types of coating material and engine speed.

- The highest experimental engine torque value was measured as 13.1 Nm with the use of Al_2O_3 + 13% TiO_2 at the speed of 2600 rpm.

- According to the results of Taguchi analysis, the maximum S/N ratios of coating material and engine speed were measured as 19.36 at Level 2 and 21.57 at Level 3 respectively.

- Taguchi design method showed that maximum engine torque value was achieved using the coating material of Al_2O_3 + 13% TiO_2 at the speed of 2600 rpm.

- The statistical study points out that both the P values of coating material and engine speed parameters are smaller than 0.05 and this means that they are statistically significant on the engine torque.

ACKNOWLEDGMENTS

This study was supported by Bitlis Eren University Scientific Research Projects Coordination Unit. Project Number: BEBAP-2014.15. The authors would like to thanks the Bitlis Eren University Science and Technology Research and Application Center for tests of specimens.

REFERENCES

[1] G. Sivakumar, and S. S. Kumar, ‘‘Investigation on effect of Yttria Stabilized Zirconia coated piston crown on performance and emission characteristics of a diesel engine,’’ *Alexandria Engineering Journal*, vol.53 no. 4, pp. 787-794, 2014.

[2] A. Kumar, S. Kumar, A. Veeresh Babu, ‘‘Effect of Mahua Methyl Ester on Performance & Emission Characteristics on Di Diesel Engine with Mullite as a Thermal Barrier Coating (TBC),’’ *International*

Research Journal of Engineering and Technology (IRJET), vol. 05, no. 04, pp. 1973-1977.

[3] V. Goel, N. Kumar, and P. Singh, ‘‘Impact of modified parameters on diesel engine characteristics using biodiesel: A review,’’ *Renewable and Sustainable Energy Reviews*, vol. 82, pp. 2716-2729, 2018.

[4] R. Gehlot and Brajesh Tripathi, ‘‘Thermal analysis of holes created on ceramic coating for diesel engine piston,’’ *Case Studies in Thermal Engineering*, vol. 8, pp. 291-299, 2016.

[5] V. Garud, S. Bhoite, S. Patil, S. Ghadage, N. Gaikwad, D. Kute, and G. Sivakumar, ‘‘Performance and combustion characteristics of thermal barrier coated (YSZ) low heat rejection diesel engine,’’. *Materials Today: Proceedings*, vol. 4 no. 2, pp. 188-194, 2017.

[6] M. Durat, M. Kapsiz, E. Nart, F. Ficici, and A. Parlak, ‘‘The effects of coating materials in spark ignition engine design,’’ *Materials & Design (1980-2015)*, vol. 36, pp. 540-545, 2012.

[7] H. Hazar and H. Sevinc, ‘‘Investigation of the effects of pre-heated linseed oil on performance and exhaust emission at a coated diesel engine,’’ *Renewable energy*, vol. 130, pp. 961-967, 2019.

[8] A. Thibblin, S. Jonsson, and U. Olofsson, ‘‘Influence of microstructure on thermal cycling lifetime and thermal insulation properties of yttria-stabilized zirconia thermal barrier coatings for diesel engine applications,’’ *Surface and Coatings Technology*, vol. 350, pp. 1-11, 2018.

[9] M. Yao, T. Ma, H. Wang, Z. Zheng, H. Liu, and Y. Zhang, ‘‘A theoretical study on the effects of thermal barrier coating on diesel engine combustion and emission characteristics,’’ *Energy*, vol. 162, pp. 744-752, 2018.

[10] E. Şirin, Ş. Şirin, Y. Turgut, and İ. Korkut, ‘‘Optimization of surface roughness using the taguchi method in milling of aisi d2 cold work tool steel,’’ *Düzce Üniversitesi Bilim ve Teknoloji Dergisi*, vol. 3, no. 1, 2015. (in Turkish)

[11] A.B. Naik and A. C. Reddy, ‘‘Optimization of tensile strength in TIG welding using the Taguchi method and analysis of variance (ANOVA),’’ *Thermal Science and Engineering Progress*, vol. 8, pp. 327-339, 2018.

[12] S. Özel, H. Turhan, and E. Gönel, ‘‘Optimization of effect of production parameters on wear resıstance of coated layer on the surface of copper alloy by taguchi method,’’ *Internation Journal of Advance Research and Innovative Ideas in Education*, vol. 3 no. 4, pp. 1517-1523, 2017.

[13] I. C. Park and S. J. Kim, ‘‘Cavitation erosion behavior in seawater of electroless Ni-P coating and process optimization using Taguchi method,’’ *Applied Surface Science*, 2018.

[14] R. Tabaraki and A. Nateghi, ‘‘Application of taguchi L16 orthogonal array design to optimize hydrazine biosorption by Sargassum ilicifolium,’’ *Environmental Progress & Sustainable Energy*, vol. 35 no. 5, pp. 1450-1457, 2016.

[15] C. Moganapriya, R. Rajasekar, K. Ponappa, R. Venkatesh and S. Jerome, ‘‘Influence of coating material and cutting parameters on surface roughness and material removal rate in turning process using taguchi method,’’ *Materials Today:*

Proceedings, vol. 5 no. 2, pp. 8532-8538, 2018.

[16] H.K. Trivedi and D.V. Bhatt, ‘‘An experimental investigation on friction and wear test parameters of cylinder liner and piston ring pair using Taguchi technique,’’ *Industrial Lubrication and Tribology*, vol. 70, no. 9, pp. 1721-1728, 2018.

[17] D.C. Montgomery, ‘‘Design and Analysis of Experiments,’’ 9th Edition, 1 review, *Publisher: Wiley*, Release Date: May 2017. ISBN: 978-1-119-11347-8.

[18] H. Gürbüz, ‘‘An experimental study on the effects of the thermal barrier plating over diesel engine performance and emissions, *M.Sc. Thesis, Graduate School of Natural and Applied Sciences, Department of Mechanical Engineering, Karabük University*, January 2011.

[19] B. Safgönül, M. Ergeneman, H.E. Arslan, C. Soruşbay, ‘‘Internal combustion engines,’’ *Birsen Yayınevi*, Istanbul, p. 218, 2008.